DO URINE VESICLES OFFER A FINGERPRINT OF CHRONIC KIDNEY DISEASE PROGRESSION?

Melanie Tepus Petrsoric

A thesis submitted in partial fulfilment of the requirement of Nottingham Trent University for the degree of Doctor of Philosophy

January 2025

Copyright Statement

The work presented, including the generation of data and its analysis, was carried out by the author. A portion of the content in Chapter 1, along with parts of the introductions in Chapters 4 and 5, has been previously published by the author as an open access review article:

Tepus, M., Tonoli, E. and Verderio, E.A.M., 2023. Molecular profiling of urinary extracellular vesicles in chronic kidney disease and renal fibrosis. *Frontiers in Pharmacology,* 13, 1041327.

To my family

Abstract

Diabetic nephropathy (DN) is the most prevalent form of chronic kidney disease (CKD), with symptoms typically appearing in the later stages. As a result, it frequently progresses to renal fibrosis and kidney failure. Despite an increasing number of studies is focusing on biomarkers for DN and other types of CKD, there is still a pressing need to discover non-invasive markers for monitoring the progression of DN. Urinary extracellular vesicles (uEVs) are a promising source of kidney disease biomarkers since they are secreted from kidney cells, play a role in inter-cellular communication, and carry molecular cargo that reflects pathophysiological conditions. The primary aim of this study was to use a multi-omics approach to identify a multi-marker panel of DN progression employing uEVs as a source of biomarkers (proteins, miRNAs) and chemical-physical features such as surface charge. Exploring the interaction between uEVs miRNA and protein markers of DN was a further key objective expected to uncover new regulatory mechanisms involved in DN.

Cell-free urine samples of DN (n=53), diabetes with no CKD (n=20), and healthy (n=20) cohorts were sourced from Sheffield Kidney Institute (UK) and Patras University Hospital (Greece) with uniform standardised criteria and informed consent. DN cohorts were stratified in stable and progressive disease based on rate of eGFR loss, respectively <2 ml/min/year (n=28) and >5 ml/min/year (n=25). uEVs were isolated and characterised with adherence to MISEV. Protein uEVs markers were identified through quantitative proteomics of uEVs lysates for each subject and a selection validated using single EV analysis directly in biofluids (pooled samples). miRNA markers were detected via miRNA sequencing on individual samples and by NanoString digital profiling (in pool) and validated by TaqMan Advanced qPCR. uEVs surface charge was measured in individual subjects uEVs preparations.

Quantitative proteomics revealed 72 proteins with differential expression in progressive versus stable DN when normalised to equal uEVs protein (46 proteins when normalised to equal volume of starting urine). The differential expression of five proteins was confirmed in progressive DN (Vasorin, Podocalyxin, Mucin 1, Ganglioside GM2 activator,

and Argininosuccinate synthase). Transcriptomic analyses identified four miRNAs with differential expression in progressive versus stable DN of which three (miR-99a-5p, miR-223-3p, miR-3613-5p) exhibited the same expression trend when validated. Moreover, a panel of proteins and miRNAs (L-lactate dehydrogenase C chain, Muscleblind-like protein-1, miR-891a-5p, miR-432-5p, miR-890, miR-892a) was found significantly altered in DN compared to diabetes. As miR-99a-5p and miR-223-3p were predicted to directly target and regulate the expression of Muscleblind-like protein 1, their direct interaction was confirmed by 3'UTR luciferase reporter system in transfected HK2 cells. Quantification of uEVs surface charge revealed a significantly less negative charge in diabetes without CKD than in DN uEVs (p<0.05), suggestive of glycomics changes.

In conclusion, this study has identified and validated a novel panel of uEV markers for DN progression, which could assist in stratifying DN, particularly patients who are at risk of progressing to the advanced progressive stage. The crosstalk between uEV miRNAs and proteins dysregulated in DN raises new research questions that could help uncover mechanisms of DN pathogenesis and increased severity.

Acknowledgements

I can hardly believe that I've reached the end of my PhD journey. However, I wouldn't have made it here without the support of all the important people who were part of it.

First and foremost, I would like to express my sincere gratitude to my director of studies Prof Elisabetta Verderio Edwards. Dear Eli, thank you for choosing me to be part of your team and for all your guidance and advice for the past 5 years. Although you were always very busy, you still made time for me, as well as for every other member of your team, and I never felt alone or lost. Above all, thank you for believing in me even when I didn't believe in myself, and for being not only professional and upholding high standards, but also kind and caring at the same time. I truly feel fortunate to be a part of your team, and I couldn't have asked for a better supervisor.

I would also like to thank my co-supervisors: Prof Tim Johnson from Mestag, Dr Maria Hernandez-Fuentes from UCB, and Dr David Bocoock from NTU, for your invaluable guidance. You were always prompt in responding to my requests, and your kindness and encouragement made my journey easier and more motivating.

Furthermore, I would like to thank Dr Clare Coveney for great support with proteomics and for always granting me access to the HTA freezers whenever I needed to collect or return my samples (which happened quite often). I also appreciate Dr Jayakumar Vadakekolathu Narayanan for valuable assistance with Nanostring, as well as your availability and patience during all the discussions we had. A huge thank you to Dr Christos Polytarchou for providing me with a letter of recommendation to join the PhD program, and for your support with molecular biology in the final experimental phase of my PhD. The experience I gained during my Master's in your group, along with the support you provided during my PhD, and the lab materials you generously supplied, were all crucial in helping me successfully complete a full chapter of my thesis.

Sincere thanks to my dear friends and colleagues Dr Maria Pia Savoca, Dr Elisa Tonoli, Dr Amalia Luce, Suraj Lama and Dr Grace Atobatele for making my PhD journey so much easier and more enjoyable. Sharing all the laughs, tears, frustrations and challenges with you was truly a blessing.

A big thank you as well to all my IBRC friends. Sharing the ongoing issues of IBRC with you made everything feel less stressful.

Now, I would like to express special thanks to my wonderful and supportive family. Thank you, my dear Ivica, for standing by me through these challenging years, for all the sacrifices you've made for me, and for your incredible support with childcare, household responsibilities, finances, and more. You know how much of a role you've played in this journey. You are an amazing husband and father, and I love you deeply! Thank you, my dear Antonio, for showing me the true meaning of life and for giving me even more motivation to finish my PhD. I love you with all my heart. I also want to thank my second baby boy, who is on the way, for inspiring me to stay focused and keep up with my thesis writing. Thank you to my dear mum and dad for their unwavering support throughout my education and for always being there for me. Your belief in me, along with taking care of Antonio so I could have more time to work, has meant so much. Thank you for constantly encouraging me to keep going. Thank you, Paula, for being the best sister in the world. Whenever I'm upset, you always help me see the brighter side of things and calm me down. I truly appreciate your positivity and optimism. Thank you to my grandparents and my aunt Tanja for your constant love, care and interest in my work. Also, I want to thank all my in-laws for their care and belief in me and my work, especially my mother-in-law, who moved in with us and provided invaluable help with household tasks and childcare during the most critical times.

Nevertheless, thank you to all my friends in Croatia who stayed in touch, cheered me on, and were eager to see me as soon as I returned. I'm so grateful to have you in my life!

Finally, I thank Almighty God for designing this entire journey for me and making all the miracles in my life happen. From a girl who was not very ambitious and preferred a quiet,

steady life, hesitant to leave her hometown to start university, and struggled with speaking in English, somehow this girl managed to complete both a master's and a PhD in the UK while raising a family. Once again, I have to cite one of my favourites Bible quotes:

„I am able to do all things through him who strengthens me! "

Philippians 4,13

Publications

Tepus, M., Tonoli, E. and Verderio, E.A.M., 2023. Molecular profiling of urinary extracellular vesicles in chronic kidney disease and renal fibrosis. *Frontiers in Pharmacology,* 13, 1041327.

Manuscripts in preparation

Tepus, M., Savoca, M.P., Maamra, M., Goumenos, D., Johnson, T. and Verderio, E.A.M. *Application of surface charge of urinary extracellular vesicles to distinguish diabetes-associated conditions*

Tepus, M., Boocock, D., Coveney, C., Vadakekolathu, J., Polytarchou, C., Hernandez-Fuentes, M., Maamra, M., Goumenos, D., Johnson, T. and Verderio, E.A.M. *Multi-omics of urinary extracellular vesicles revealing fingerprint of diabetic nephropathy progression*

Conferences

Melanie Tepus Petrsoric, Maria Pia Savoca, Elisabetta Verderio. *Surface charge of urinary extracellular vesicles. Is it useful for patient stratification?* Matrix and Messengers: The collaborative Roles of EVs and ECM in the Extracellular Space. 16 September 2024, Nottingham, UK. Oral presentation

Amalia Luce, Melanie Tepus Petrsoric, Elisa Tonoli, Silvia Zappavigna, Michele Caraglia, Gabriella Misso and Elisabetta Verderio Edwards. *Transglutaminase II gene silencing to unravel the cancer progression mechanisms in glioblastoma*. FEBS 2024 Advanced Course: Transglutaminases in human disease processes. 19th-23rd May 2024, Bertinoro, Italy. Poster presentation by Amalia Luce

Melanie Tepus Petrsoric, Clare Coveney, David J Boocock, Dimitris Goumenos, Maria Hernandez-Fuentes, Timothy S Johnson and Elisabetta Verderio. *Proteins and miRNAs from urinary extracellular vesicles as candidate biomarkers of diabetic nephropathy progression.* ISEV EV-based Biomarkers Meeting, 12th-14th October 2023, Aalborg, Denmark. Session chair. Selected for participation in this small competitive workshop

Melanie Tepus Petrsoric, Clare Coveney, David J Boocock, Dimitris Goumenos, Maria Hernandez-Fuentes, Timothy S Johnson and Elisabetta Verderio. *Urinary extracellular vesicles cargo and surface charge are promising tool for detecting diabetic nephropathy (progression).* 2023 UCB PhD Studentship Day, 11th July 2023, Slough, UK. Oral presentation

Melanie Tepus Petrsoric, Clare Coveney, David J Boocock, Dimitris Goumenos, Timothy S Johnson and Elisabetta Verderio. *Exploring protein cargo and surface charge of urinary extracellular vesicles (uEVs) in the detection of diabetic nephropathy progression*. UK Kidney Week 2023, 5th-7th June 2023, Newport, UK. Poster presentation

Melanie Tepus Petrsoric, Timothy S Johnson, David J Boocock, Graham Ball and Elisabetta Verderio Edwards. *Do urine vesicles offer a fingerprint of Chronic Kidney Disease progression?* 2022 UCB PhD Studentship Day, 14th July 2022, virtual. Poster presentation

Elisabetta Verderio, Elisa Tonoli, Melanie Tepus, Clare Coveney, Maria Pia Savoca, David Boocock, S Watson, Dimitris Goumenos, Timothy S Johnson. *Large and small urinary extracellular vesicles (uEV): a source of progressive biomarkers for diabetic nephropathy.* UK Kidney Week 2021 Virtual Conference, 4th-7th October 2021, virtual. Oral presentation by Elisabetta Verderio Edwards

Melanie Tepus Petrsoric, Timothy S Johnson, David J Boocock, Graham Ball and Elisabetta Verderio Edwards. *Do urine vesicles offer a fingerprint of Chronic Kidney Disease progression?* PGR STAR Conference, 8th-9th June 2021, virtual. Oral presentation

Table of contents

List of abbreviations

2-ME	β-Mercaptoethanol
3'UTR	3' untranslated region
5'UTR	5' untranslated region
α-SMA	α-smooth muscle actin
Abs	Absorbance
ABCB1	ATP-dependent translocase ABCB1
ACE	Angiotensin-converting enzyme
ACR	Albumin to creatinine ratio
ADPKD	Autosomal dominant polycystic kidney disease
AER	Albumin excretion rate
AGEs	Advanced glycation end-products
AGO2	Argonaute RISC catalytic component 2
AIDA	Advanced Image Data Analyzer
AKI	Acute kidney injury
AKT1	Akt serine/threonine kinase
ALIX	Apoptosis-linked gene-2-interacting protein X
AMPE	Glutamyl aminopeptidase
ANAG	Alpha-N-acetylglucosaminidase
Ang I / Ang II	Angiotensin I / II
APN	Aminopeptidase-N
APS	Ammonium Persulfate
AQP1/2	Aquaporin-1/-2
ASSY	Argininosuccinate synthase
BCA	Bicinchoninic acid
BH	Benjamini–Hochberg
bp	Base pair
BSA	Bovine Serum Albumin
BUN	Blood urea nitrogen
CARM1	Co-activator associated arginine methyltransferase 1
CCL2	Chemokine (C-C motif) ligand 2
CD44	CD44 antigen
CD59	CD59 glycoprotein
CD133	Prominin-1
cDNA	Complementary DNA
CDS	Coding sequence
CKD	Chronic kidney disease
CKD-EPI	Chronic Kidney Disease Epidemiology Collaboration

CTGF	Connective tissue growth factor
CTL2	Choline transporter-like protein 2
CTR	Control
CV	Coefficients of variation
DALYs	Disability-adjusted life-years
DAVID	Database for Annotation Visualization and Integrated Discovery
DDA	Data Dependent acquisition
DIA	Data Independent acquisition
DKD	Diabetic kidney disease
DM1	Type 1 diabetes mellitus
DM2	Type 2 diabetes mellitus
DN	Diabetic nephropathy
DNA	Deoxyribonucleic acid
dNTPS	Deoxynucleotide Triphosphates
DTT	1,4-Dithiothreitol
E2F1	E2F transcription factor 1
ECL	Enhanced Chemiluminescence
ECM	Extracellular matrix
EGF	Epidermal growth factor
EGFR	Epidermal growth factor receptor
eGFR	Estimated glomerular filtration rate
EMT	Epithelial to mesenchymal transition
EnMT	Endothelial-to-mesenchymal transition
ERK	Extracellular signal-regulated kinase
ESCRT	Endosomal sorting complex required for transport
ESKD / ESRD	End stage kidney disease / End stage renal disease
EVs	Extracellular Vesicles
FBS	Fetal Bovine Serum
FC	Fold Change
FGF	Fibroblast growth factor
FLOT-2	Flotillin-2
FSGS	Focal segmental glomerulosclerosis
GBM	Glomerular basement membrane
GFR	Glomerular filtration rate
HCl	Hydrochloric acid
HK2	Human kidney epithelial cell line
HPLC	High Performance Liquid Chromatography
HRP	Horseradish Peroxidase
HS	Heparan sulphate

Hsp70/Hsp90	Heat shock proteins 70/90
ICAM-1	Intercellular adhesion molecule-1
IgA1	Immunoglobulin A1
IgAN	Immunoglobulin A nephropathy
IPSP	Plasma serine protease inhibitor
ISEV	International Society of Extracellular Vesicles
kDa	kilodalton
KDIGO	Kidney Disease: Improving Global Outcomes
KIM-1	Kidney injury molecule-1
LAMP1/2	Lysosome-associated membrane glycoprotein 1/2
LBPA	Lyso-bisphosphatidic acid
LDHC	L-lactate dehydrogenase C chain
L-FABP	Liver-type fatty acid-binding protein
LN	Lupus nephritis
LNIV	Type IV lupus nephritis
LNIV-CC	LNIV with cellular crescent
log$_2$(FC)	Logarithm base 2 of Fold change
LOX	Lysyl oxidase
MAPKs	Mitogen-activated protein kinases
MBNL1	Muscleblind-like protein 1
MCD	Minimal change disease
MDRD	Modification of Diet in Renal Disease
MIgG	Mouse immunoglobulin G
miRNA	Micro RNA
miR-NC	miR-negative control
MISEV	Minimal information for studies of extracellular vesicles
MMP	Matrix metalloproteinase
MS	Mass Spectrometry
mTOR	mammalian target of rapamycin
MUC1	Mucin-1
MVBs	Multivesicular body
µg	Microgram
µl	Microliter
NaCl	Sodium Chloride
NAG	N-acetyl-β-D-glucosaminidase
NaOH	Sodium Hydroxide
NCBI	National Center for Biotechnology Information
ND	Not determined
NDRD	Non-diabetic renal disease

ng	Nanogram
NGAL	Neutrophil gelatinase associated lipocalin
Nkd-2	Naked cuticle homolog 2
nM	Nanomolar
NPH-RC	Nephronophthisis-related ciliopathies
NS	Nephrotic syndrome
NTA	Nanoparticle Tracking Analysis
NTU	Nottingham Trent University
PAGE	Polyacrylamide Gel Electrophoresis
PAI	Plasminogen activator inhibitor-1
PANTHER	Protein ANalysis Through Evolutionary Relationships
PBS	Phosphate Buffered Saline
PCR	Polymerase Chain Reaction
PDGF	Platelet derived growth factor
PDGFR	Platelet derived growth factor receptor
PEDF	Pigment epithelium-derived factor
Pen/Strep	Penicillin-Streptomycin
PI3K	Phosphoinositide 3-kinase
PODXL	Podocalyxin
PTEN	Phosphatase and tensin homolog
qPCR	Real Time PCR
RAAS	Renin-angiotensin-aldosterone system
Rab proteins	Retinoic acid-binding proteins
RAB-10	Ras-related protein Rab-10
RIPA	Radio Immunoprecipitation Assay
RISC	RNA-Induced Silencing Complex
RNA	Ribonucleic acid
RT	Reverse transcription
RT	Room temperature
RT-PCR	Reverse-transcription Polymerase Chain Reaction
SAP3	Ganglioside GM2 activator
SD	Standard deviation
SDS	Sodium Dodecyl Sulphate
SLC7A5	Solute carrier family 7 member 5
SLE	Systemic lupus erythematosus
SN1	Supernatant 1
SN2	Supernatant 2
SNAREs	Soluble N-ethylmaleimide-sensitive factor attachment protein receptors
SnoN	Ski-related novel protein N

STAT3	Signal transducer and activator of transcription 3
STD	Standard
SWATH-MS	Sequential Window Acquisition of All Theoretical Mass Spectra
TAE	Tris-acetate-EDTA
TBMN	Thin basement membrane nephropathy
TBS	Tris Buffered Saline
TBST	Tris Buffered Saline - Tween 20
TCA	Trichloroacetic acid
TEC	Tubular epithelial cells
TEM	Transmission electron microscopy
TEMED	Tetramethylethylenediamine
TFA	Trifluoroacetic acid
TGF-β	Transforming Growth Factor- β
TGM2, TG2	Transglutaminase 2 /Type-2 transglutaminase
THAS	Thromboxane–A synthase
TNF	Tumour necrosis factor
TOF-MS	Time Of Flight Mass Spectrometry
TP53	Tumour protein p53
TRIS	Tris(Hydroxymethyl) Aminomethane
TSG101	Tumour susceptibility gene 101
VASN	Vasorin
VEGF	Vascular endothelial growth factor
WB	Western Blotting
WT 1	Wilms' tumor-1
ZP	Zeta potential

CHAPTER 1:

General Introduction

1.1 Chronic Kidney Disease (CKD)

The uniform definitions of chronic kidney disease (CKD) and its staging system were originally described in international guidelines in 2002 (National Kidney Foundation, 2002), which were reviewed and updated in 2012 (Levin et al., 2013), and more recently in 2024 (Stevens et al., 2024) by which CKD is general term of long-lasting heterogeneous disorders defined as irreversible damage and abnormalities of kidney structure or function with health consequences. Kidney damage is caused by the gradual loss of essential kidney functions which is shown by glomerular filtration rate (GFR) of less than 60 mL/min per 1.73 m², or markers of kidney damage such as albuminuria, persistent haematuria, abnormalities with urine sediment or abnormalities detected by imaging or histology, that last longer than 3 months (Levin et al., 2013; Webster, A.C., *et al*., 2017; Stevens et al., 2024).

CKD can affect various components of the nephron, the functional unit of the kidney. Each nephron is structured from the glomerulus and tubules. The primary functions of the nephron are to filter the blood (via the glomerulus), reabsorb essential substances into the blood, as well as to eliminate waste (through the tubules) (Meltzer, 2019). More details of the nephron's structure and function are provided in Figure 1.1

For individualized management and prognosis of CKD, CKD classification considers parameters of cause, GFR category (G1-G5), and albuminuria category (A1-A3) abbreviated as CGA which enables accurate evaluation of severity and risk. However,

regular classification system is based on two categories: GFR and albuminuria (Levin et al., 2013; Stevens et al., 2024).
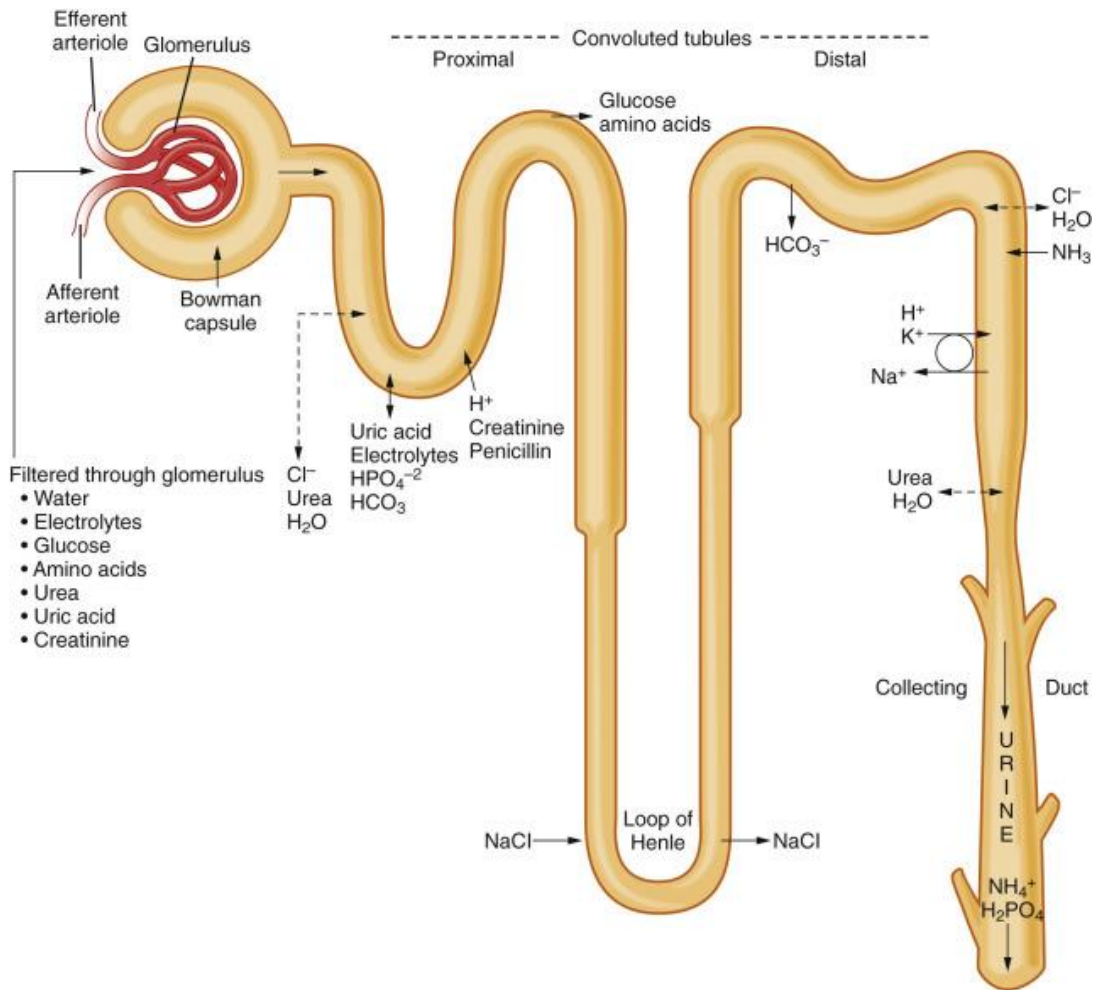
Figure 1.1: The structure and function of the nephron. The glomerulus consists of a complex network of branching capillaries surrounded by the Bowman's capsule. Its function is to filter water, amino acids, free ions, etc. from the blood, which enter through the afferent arteriole and exit via the efferent arteriole. The filtered fluid then moves from the Bowman's capsule into the proximal tubule. The proximal tubule is responsible for reabsorbing substances such as Na^+, water, bicarbonate, Cl^-, glucose, amino acids, phosphate, urea etc. This is followed by the loop of Henle, which establishes an osmolarity gradient and facilitates the reabsorption of Ca^{2+} and Mg^{2+}. The distal tubule is responsible for secreting ammonia and urea, regulating K^+, Na^+, and Ca^{2+}, and reabsorbing water, which results in the formation of concentrated urine. This urine then flows into the collecting duct, where NH_4^+ production, reabsorption of Na^+, K^+, Cl^-, water and bicarbonate, as well as secretion of K^+ and H^+ take place. Image was taken from Meltzer, 2019

1.1.1 Glomerular filtration rate (GFR)

Glomerular filtration rate is still considered the best index for measuring kidney function and diagnosing and staging CKD. It is a measure of total fluid filtered through all functional nephrons per unit of time. GFR cannot be measured directly in humans but using urinary and plasma clearance measurements which includes the use of a filtration marker, either exogenous or endogenous. The requirements of an ideal exogenous substance are: to freely pass the glomerular capillary wall without interfering with plasma proteins or being affected by its size or charge, must not be altered during its filtration meaning it shouldn't be reabsorbed, secreted, synthesized or metabolised by tubular cells, must not affect the kidney function and should be easily quantitated (Elwood and Sigman, 1967; Stevens et al., 2019). Urinary clearance of inulin is considered the gold standard filtration marker for measurement of GFR (mGFR) (Shannon and Smith, 1935), however requires the complex protocol of constant intravenous infusion and timely urine collections due to which urinary clearance of iothalamate, or plasma clearance of iohexol (Griep and Nelp, 1969; Gaspari et al., 1995), ethylene-diaminetetraacetic acid (EDTA) or diethylene triaminopenta-acetic acid (DTPA) are used as alternatives (Rehling et al., 1984) all of which highly correlate with urinary clearance of inulin. However, the procedure of GFR measurement by exogenous substances is laborious, expensive, not broadly available, and not simple to perform in clinical practice, therefore the more convenient measurement of the GFR level is estimation of GFR from the serum/plasma level of endogenous filtration markers such as creatinine, cystatin C, and urea (Inker and Titan, 2021).

1.1.1.1 Creatinine

Creatinine is a 113-Da amino acid derivative which originates from muscles and is produced directly by conversion from creatine in the nonenzymatic reaction, or it can be converted from phosphocreatine into phosphocreatinine which is followed by dephosphorylation to creatinine (Pottel et al., 2024). Kidneys are the main route of creatinine elimination, since it has a small molecular diameter and does not bind to the plasma proteins, it can freely pass glomerular capillary wall and be secreted by the tubules. Under normal physiological conditions rates of creatinine production and excretion are quite constant which is why it is commonly used as endogenous indicator to measure GFR and hence assess kidney function (Pottel et al., 2024). Although few studies suggested that endogenous creatinine clearance compared with inulin clearance is favourable in terms of accuracy and reliability (Brod and Sirota, 1948; Tobias et al., 1962), and nowadays creatinine is still the most widely used endogenous filtration marker to estimate GFR worldwide, there are a few limitations and problems with its measurements (Perrone et al., 1992; Porrini et al., 2019). One example is that levels of serum creatinine are reliable under stable conditions such as in CKD, however in cases of sudden changes in GFR, for example in acute kidney injury or kidney recovery, there is lack of precision and accuracy because serum creatinine takes time to stabilize (Chen and Chiaramonte, 2019). Next, a portion of creatinine is secreted from tubules and because of this creatinine clearance measurements result in overestimation of the true GFR, which is also unpredictable among different individuals (Kim et al., 1969; Shemesh et al., 1985; van Acker et al., 1992). Furthermore, the levels of serum creatinine and urine

creatinine are influenced by differences in age, gender, race or ethnicity, but also muscle mass, especially correlated with lean (fat-free) mass and physical activity which makes renal interpretation complicated in populations with very low or high muscular mass, as well as in children and elderly among who muscle mass is extremely variable (Perrone et al., 1992; Baxmann et al., 2008). In addition, it can also be influenced by diet as food rich in proteins such as cooked meat increase serum creatinine levels (Jacobsen et al., 1979; Mayersohn et al., 1983), or similar example is by taking some drugs (Andreev et al., 1999). Finally, the increased concentrations of serum creatinine are easy to detect in severe kidney dysfunction, however, the approach is not very sensitive in the earlier stages of mild and moderate kidney damage. It has been found that serum creatinine gets elevated after GFR capacity declines by about 50%, indicating that creatinine alone is an insufficient biomarker for detecting early kidney impairment, but only when glomerular filtration function is irreversibly disrupted (Shemesh, O., *et al*., 1985).

1.1.1.2 Cystatin C

To increase the accuracy of the CKD diagnosis, concentration of cystatin C in serum is used as an alternative or additional endogenous marker to estimate GFR. It is a small 13 kDa protein that belongs to the cystatin family of cysteine proteinase inhibitors and is produced by all human nucleated cells (Kyhse-Andersen et al., 1994; Newman et al., 1995). Cystatin C is completely filtered at the glomerulus, and after it passes through the glomerular membrane it is degraded by proximal tubular cells without returning to the blood, so very small amount of cystatin C is lost by urine, and its serum level is used as the indicator of GFR. However, in the kidney disease, tubular cells are damaged due to

which reabsorption of cystatin C after filtration is impaired, so its concentration in urine increases, in which case even urinary cystatin C can reflect on GFR (Jiang et al., 2022). Compared to creatinine, cystatin C is less dependent on muscle mass and diet, its production rate is stable and does not alter in inflammatory conditions, and is eliminated exclusively by glomerular filtration, so it is not surprising that several studies, which applied different methodologies in measuring serum cystatin C, have suggested that cystatin C is a superior endogenous filtration marker to creatinine, or at least as good as creatinine (Grubb et al., 1985; Pergande and Jung, 1993; Kyhse-Andersen et al., 1994; Newman et al., 1995). Despite its advantages, serum cystatin C is variable in certain conditions for example during the use of corticosteroids, in thyroid disease and cancer, but also influenced by certain factors not related to renal function such as serum level of C-reactive protein (CRP), obesity, and smoking, therefore neither creatinine nor cystatin C is perfect marker when used alone, but the combination of the two provide more accurate eGFR (Knight et al., 2004; Stevens et al., 2024).

1.1.1.3 Urea

Urea is the nitrogenous end product of protein catabolism, produced in the liver, freely filtered at the glomerulus and reabsorbed by the renal tubules. During kidney disease, urea excretion is reduced and consequently its blood concentration increased (Stevens et al., 2010).

The nitrogen component of serum urea, known as blood urea nitrogen (BUN), is used as an additional indicator of renal function as it inversely correlates with decreased eGFR,

however it is not very strong indicator since urea production is affected by protein intake, but also variables such as dehydration, fever, pregnancy, heart failure etc (Mitchell and Kline, 2006).

Despite its imperfection, increased level of BUN was proposed as prediction marker of adverse kidney disease outcomes because was found to be linked with poor CKD prognosis in patients with moderate to severe CKD stages (Seki et al., 2019).

Furthermore, a higher level of the blood urea nitrogen to creatinine ratio (UCR) was found to be significantly associated with an increased risk for all-cause mortality, infection-related death, and coronary heart disease incidence in haemodialysis patients, and was proposed as independent predictor of poor CKD prognosis due to increased catabolic burden and inflammation (Oksa et al., 1987; Tanaka et al., 2017).

More recently, a high blood urea nitrogen to serum albumin ratio (BAR) has been shown to be significantly associated with worse CKD prognosis and increased mortality in CKD patients with type 2 diabetes mellitus admitted to the intensive care unit (ICU). It is therefore believed that high BAR, which is caused either by high BUN or low albumin, is a new indicator of poor prognosis in such patients (Liu et al., 2024).

1.1.1.4 Equations used to estimate GFR

For about 20 years, several equations have been used to calculate eGFR.

Modification of Diet in Renal Disease (MDRD) Study 1999 equation (Levey et al., 1999) considers serum creatinine concentration, demographic characteristics such as age, sex,

and ethnicity, serum measurements of urea nitrogen and albumin concentrations. It showed better accuracy compared to some older prediction equations most common of which was the Cockcroft-Gault equation (Cockcroft and Gault, 1976).

MDRD Study 2006 equation (Levey et al., 2006) is an updated version of the original MDRD equation which involves the use of a standardized serum creatinine assay. In addition, instead of 6 variables (age, sex, ethnicity, serum levels of creatinine, urea, and albumin) re-expressed MDRD equation from 2006 contains 4 variables (age, sex, ethnicity, and serum creatinine levels) which simplifies its use in clinical practice without affecting accuracy and precision.

Chronic Kidney Disease Epidemiology Collaboration (CKD-EPI) 2009 equation showed further improvement in accuracy of estimating GFR compared to the previous MDRD equations, particularly at higher eGFR levels (Levey et al., 2009). The variables included in this equation are the standardized measurement of serum creatinine, age, race, and sex, as in the MDRD Study equation, however GFR and serum creatinine were transformed into natural logarithms to reflect their inverse relationship and to stabilize the variance in the range of GFR. In addition, new variables of diabetes status, prior organ transplant, and weight were included if significant.

CKD-EPI equation from 2012 brought another improvement. Compared to previous equations based exclusively on serum creatinine as an endogenous marker, this equation uses a variable of serum cystatin C, both alone and in combination with serum creatinine.

The combination of serum creatinine and serum cystatin C in this equation resulted in better performance with a higher accuracy of GFR estimation (Inker et al., 2012).

The most recently published CKD-EPI 2021 creatinine and cystatin C equation reports eGFR without using the parameter of race as it was recognized that race is a social rather than a biologic construct (Inker et al., 2021). Development of the new CKD-EPI 2021 equation was followed by the formation of the National Kidney Foundation and the American Society of Nephrology Task Force, which provided recommendations for clinical laboratories, including the implementation of CKD-EPI 2021 equation with an eliminated rase parameter when calculating eGFR in order to standardize laboratory reporting (Miller et al., 2022).

1.1.1.5 GFR classification

GFR levels are classified into 6 categories from G1 to G5 (Table 1.1) that provide information about the progression stage of CKD (Stevens et al., 2024):

Table 1.1 CKD classification based on GFR

GFR category	GFR [ml/min/1.73 m^2]	Terms
G1	≥ 90	Normal or high
G2	60 - 89	Mildly decreased
G3a	45 - 59	Mildly to moderately decreased
G3b	30 - 44	Moderately to severely decreased
G4	15 - 29	Severely decreased
G5	< 15	Kidney failure

GFR glomerular filtration rate

1.1.2 Albuminuria & proteinuria

The term albuminuria refers to the condition when an excessive amount of albumin is excreted in the urine. Proteinuria on the other hand refers to the abnormal amount of urinary total protein. Unlike in healthy conditions where very low amounts of protein, including albumin, are filtered and excreted in the urine, in almost all renal diseases protein levels are persistently increased, which is why proteinuria is used as an additional and early sign of kidney damage, but also marker of kidney disease progression. The pore size of the glomerular barrier in a healthy state has been reported to range from 2.5 to 2.8 nm, whereas in diabetic nephropathy (DN), it can increase to 10-80 nm, which may explain the elevated levels of albuminuria and proteinuria (Ota et al., 1995).

Processes leading to albuminuria/proteinuria were recently reviewed by Comper et al., 2022, where was explained that all plasma proteins with molecular weights ranging from 30 to 150 kDa can leak to varying degrees across the glomerular filtration barrier. However, the development of albuminuria and proteinuria is primarily driven by the inhibition of two key processes at the nephrotic level: degradation of plasma proteins and retrieval of plasma proteins (Comper et al., 2022). In diabetic conditions plasma proteins were found to remain intact, while in healthy states are degraded into peptides (Osicka et al., 2000). Furthermore, now it is known that along with water and NaCl proximal tubules also reabsorb excreted plasma proteins, however inhibition of retrieval pathways leads to nephrotic proteinuria accompanied with hypoproteinaemia (Russo et al., 2007). Another key cause of albuminuria/proteinuria is the breakdown of the size- and charge-

selective glomerular capillary wall (GCW) barrier in the glomerulus, which normally prevents the filtration of plasma proteins. The primary component of this GCW barrier is the glomerular endothelium (Butler et al., 2020; Ballermann et al., 2021).

Although proteinuria had long been used in clinical laboratories as an early measure of renal disorders, measurement of urinary albumin has been proven to be a more accurate approach than measurement of total protein in urine, and it has therefore been suggested to replace proteinuria by albuminuria (Shihabi et al., 1991; Newman et al., 1995). Urinary albumin is considered more specific and sensitive measure for assessment of glomerular permeability compared to total urinary protein for several reasons: increased urinary loss of albumin might occur without having significant measurable effect on total protein loss making the measure of total urinary protein imprecise and insensitive (Newman et al., 1995). In particular, total urinary proteins also involve Tamm-Horsfall glycoprotein, also known as uromodulin, which is a primary constituent of urinary casts secreted by renal tubules and therefore is not measure of glomerular permeability, however it can make up to 50% of total proteins in urine (Hoyer and Sailer, 1979). There was also documented large variation and imprecision in amount and composition of total proteins between samples, as well as the lack of standardized method for total urinary protein measurements (McElderry et al., 1982; Dube et al., 2005). For the above reasons and also because albumin is the major plasma protein found in urine in most kidney diseases, the KDIGO 2012 clinical practice guidelines changed the clinical terminology to focus on albuminuria rather than proteinuria (Levin et al., 2013). The measure of albuminuria has been particularly shown to be sensitive for indication of

kidney disease in patients with diabetes mellitus and hypertension. Quantification and testing for albuminuria can be done by 24-hour urine collection and measuring albumin (or protein) excretion in mg, which is considered gold standard despite being inconvenient approach for the patients and often with unreliably collected samples. However, more convenient but still satisfactory approach is collection of "spot" urine samples and measuring albumin (in mg) to creatinine (in g or mmol) ratio, found to be accurate prediction of 24h albumin excretion. However, it is important that urines are collected under standardized conditions including first voided, morning, clean mid-stream sample (Keane and Eknoyan, 1999).

Even if albuminuria was accepted as more accurate method than proteinuria to indicate CKD, there were also reported some biological and analytical variabilities in albumin measurements and therefore diagnostic limitations (Howey et al., 1989). As an example, factors that can lead to the variability in albuminuria calculation and estimation are the period during which the samples were collected (days, weeks, months), the collection type of urine samples (24 h, timed overnight, first morning, second morning, random), sample clarity (influence of physical contaminants such as menstrual or urinary bleeding, seminal fluid etc.), study design, urinary albumin concentration, health condition of subjects (influence of fever, orthostasis, exercise, hydration status) and pre-analytical handling and storage of urine samples (storage temperature and length, or adsorption to the surface of storage container) (Miller et al., 2009). Moreover, even different analytical methods can cause variability or underestimation of urinary albumin measurements. In particular, it has been widely recognized that urine contains modified or fragmented

forms of albumin like glycated albumin or C-terminal truncation product because of albumin exposure to urinary environment including possible presence of various proteases, increased amounts of nitrite, increased concentration of glucose and urea, aerobic oxidizing conditions etc. However, urine albumin assays are calibrated using serum albumin, therefore, there is a lack of data on the influence of albumin fragments on urine albumin tests (Sviridov et al., 2008). All this points to the importance of repeating and confirming positive tests of increased urinary albumin (Stevens et al., 2024).

1.1.2.1 Albuminuria classification

Albuminuria, referring to urinary albumin levels, is classified into 3 categories from A1 to A3 (Table 1.2) which like eGFR provides information about the CKD stage (Stevens et al., 2024). Although the different stages of albuminuria were historically referred to as normoalbuminuria (for A1), microalbuminuria (A2), and macroalbuminuria (A3), such terminology was discouraged by the 2012 Clinical Practice Guidelines for the Evaluation and Management of Chronic Kidney Disease and changed to normal, moderately increased, and severely increased albuminuria (Levin et al., 2013).

Table 1.2 CKD classification based on albuminuria

Albuminuria category	AER [mg/24h]	ACR [mg/mmol]	ACR [mg/g]	Terms
A1	< 30	< 3	< 30	Normal to mildly increased
A2	30 - 300	3 - 30	30 - 300	Moderately increased
A3	> 300	> 30	> 300	Severely increased

AER albumin excretion rate; ACR albumin-to-creatinine ratio

1.1.3 Kidney biopsy

Native kidney biopsy is an important and often crucial examination in the diagnosis of CKD, but also in acute kidney disease, which provides more precise and accurate diagnosis of the disease cause, activity and severity because it shows the morphological changes of the kidney tissue such as the presence and amount of arteriosclerosis, glomerulosclerosis, interstitial fibrosis and tubular atrophy, increased nephron size and decreased nephron number. In addition, kidney biopsy can be useful for providing information about CKD prognosis and guiding treatment strategies which is why it is considered the gold standard method in the diagnosis of kidney diseases (Asghar et al., 2024). On the other hand, kidney biopsy is an invasive procedure, so chances of complications cannot be excluded, especially in patients with severe renal dysfunction where the risk of bleeding is increased and although rarely, the procedure can threaten organs or life (Alkadi et al., 2022). In addition, there are a few contraindications for kidney biopsy such as coagulopathy, hypertension which increases the risk of bleeding, small kidneys indicating chronic irreversible damage and likely unspecific fibrotic changes with limited benefit for specific diagnosis, kidney asymmetry suggesting that kidneys were affected differently by the condition, having only one kidney which increases the risk of renal failure in a scenario of biopsy-associated complications (Hull et al., 2022). Moreover, it was showed that kidney biopsy related removal of piece of tissue caused fibrotic scars during biopsy, appearance of haematoma, and disruption of distant nephrons, can lead to the damage of about 8,000 nephrons which consequently results in GFR reduction of 0.7 mL/min (Dattani et al., 2020). It is also important to note that histological samples do

not always provide a definitive answer and that their interpretation can still be affected by sampling error, too small tissue sample with too few glomeruli taken, the lack of specificity like in interstitial fibrosis and tubular atrophy where signs show chronic damage rather than suggesting diagnosis (Hull et al., 2022). Despite possible contraindications, consequent reduction in GFR and higher risks of complications in CKD patients with impaired renal function, it has been proven that even in such patients performing a renal biopsy leads to better long-term renal outcomes compared to a group of patients who did not undergo a renal biopsy, which indicates its important role for accurate and timely diagnosis and further treatment (Zhang, T., et al., 2023b).

The incidence of reported complications associated with renal biopsy was reported in a recent meta-analysis that reviewed the literature published from 1983 to 2018. The highest frequency of 11% was reported for the adverse event perinephric hematoma, followed by pain 4.3%, gross haematuria 3.5%, need for red blood cell transfusion 1.6%, need for intervention to stop bleeding 0.3%, and the lowest incidence was reported for the most serious side effect - death 0.008% (Poggio et al., 2020). Analysis of the Transforming Research in Diabetic Nephropathy (TRIDENT) study done from 2017 to 2019 showed that biopsy-associated complications in patients with diabetic kidney disease are overall rare (7%) and involved prolonged hospital stay (4%), hematoma >5 cm (4%), gross haematuria (2%), or requirement for blood transfusions (2%) (Hogan et al., 2020). However, due to potential harm and lack of recognition of potential utility, the procedure of kidney biopsy is often delayed or declined by patients. Moreover, some CKD patients cannot afford the kidney biopsy procedure or time away from work required for it. Even

if data from native kidney biopsy complications are heterogeneous, the overall conclusion is that complications are rare, and therefore the most recent KDIGO 2024 Clinical Practice Guidelines recommended kidney biopsy as safe and acceptable diagnostic test to evaluate the cause of CKD and guide treatment decisions when clinically suitable (Stevens et al., 2024).

1.1.4 The CKD burden

CKD is a highly prevalent non-communicable disease that contributes to morbidity and mortality worldwide and is also an important independent risk factor for cardiovascular disease. It represents a significant global health problem, with a rising incidence and burden, and is a serious threat to people's life and health (Ke et al., 2022). Based on information and findings summarized for the 2017 Global Burden of Disease, Injury and Risk Factor (GBD) Study, the number of people with CKD at all stages of the disease was nearly 700 million in 2017, while 1.2 million people died from CKD, which is projected to rise to 2.2 to 4 million by 2040. Renal replacement techniques are the only life-saving treatments for the patients with end-stage kidney disease (ESKD), but also very costly treatments, and many countries are in shortages of such services, which is why many more people die prematurely (Bikbov, et al., 2020; Jha, et al., 2013). CKD burden can be also expressed as the number of years of life lost to disease and the number of years lived with disability due to disease, which is called Disability-adjusted life-years (DALYs) (Stevens et al., 2024). It has been estimated that in 2017 CKD was responsible for 35.8 million DALYs, which increased to 41.5 million in 2019 (Stevens et al., 2024). Moreover,

according to the GBD study, from 1990 to 2019, DALYs for CKD has risen from 29th to 18th (Vos et al., 2020) and is predicted to become the 5th most common cause of years of life lost worldwide by 2040 (Foreman et al., 2018).

Diabetic cause of CKD (type 1 and type 2) was responsible for one third of all CKD DALYs (30.7%) in 2017, and in general diabetes mellitus together with hypertension is the greatest risk factor of CKD (Bikbov, et al., 2020).

1.2 Diabetic kidney disease and diabetic nephropathy

Diabetic kidney disease is the most common aetiology of CKD and the leading cause of CKD progression to ESKD as well as cardiovascular events, subsequently being the main contributor to increased CKD burden globally (Alicic et al., 2017; Fenta et al., 2023). It develops in about 30% of patients with type 1 diabetes mellitus (DM1) and 40% with type 2 diabetes mellitus (DM2), in whom presents the main risk factor of increased mortality (Alicic et al., 2017; Afkarian et al., 2013). The worldwide incidence of CKD as a result of DM2 increased for 74% from 1990 to 2017 (Li et al., 2021). With the increasing prevalence of diabetes which is projected to affect 643 million people by 2030 and 783 million people by 2045 (Magliano and Boyko, 2021), also rises the DKD (Ogurtsova et al., 2017). Although the exact cause of DKD is still unknown, there are many known risk factors, apart from diabetes mellitus, that can promote its development and/or progression such as hypertension, hyperglycaemia, hyperlipidaemia, obesity, aging, family history of kidney disease, smoking, heavy alcohol drinking, lack of physical activity, consumption of nephrotoxic medications, HIV infection etc. (Fenta et al., 2023).

The term of DKD is often used interchangeably with DN, however DKD refers to pathologic structural and functional changes of the affected kidneys caused by diabetes mellitus, while DN refers to specific histological findings on kidney biopsy from DKD patients (Hull et al., 2022), so even if all DN cases are part of DKD, not all DKD have definition of DN. From the studies using kidney biopsies from diabetic CKD patients, it has been shown that DKD patients can manifest DN, but also non-diabetic renal disease

(NDRD), either alone or superimposed on DN (Sharma et al., 2013). In comparison to DN which is usually diagnosed in DM1 patients living with diabetes for >10 years, accompanied by proteinuria as well as retinopathy or neuropathy, NDRD is predicted by shorter duration of diabetes mellitus, absence of diabetic retinopathy or neuropathy, high levels of haemoglobin, and non-nephrotic proteinuria (Amoah et al., 1988; Mak et al., 1997; Tone et al., 2005; Chang et al., 2011). Albuminuria is a strong predictor of DN, but in NDRD albuminuria can present low levels or regress (Kramer et al., 2003). Another important difference is that DN is irreversible condition while some cases of NDRD are treatable (Amoah et al., 1988; Chang et al., 2011). The pathophysiological mechanisms and the morphological features of kidney abnormalities, for instance diabetic renal lesions are similar in DM1 and DM2 (Alsaad and Herzenberg, 2007).

1.2.1 Characterisation of diabetic nephropathy (DN)

The first clinical sign of DN is moderately increased albuminuria, followed by a progressive decrease in eGFR and hypertension (Said and Nasr, 2016). However, an autopsy-based study has reported that before the onset of moderately increased albuminuria and other clinical signs, affected kidneys may have already undergone glomerular and tubulointerstitial damage such as the development of characteristic DN lesions (Klessens et al., 2016). Multiple sections of the kidney undergo structural alterations in DN which can be characterised morphologically and histologically by mesangial expansion as a result of increased deposition of mesangial matrix and hypertrophy of mesangial cells, followed by the thickening of the glomerular basement

membrane (GBM), but also capillary and tubular basement membranes, leading to diffuse and nodular glomerulosclerosis, then tubulointerstitial fibrosis and atrophy which occur proportionally to the severity of glomerulosclerosis, but also variable degrees of efferent hyaline arteriolosclerosis and arterial sclerosis, as well as loss of endothelial fenestrations and drop in podocyte (Alsaad and Herzenberg, 2007; Alicic et al., 2017). Podocytes can experience both functional and structural damage early in the pathology of DN. A reduction in their number and density is linked to the onset of proteinuria and the progression of DN (Su et al., 2010). Additionally, DN in both insulin-dependent (Parving et al., 1988) and non-insulin-dependent (Parving et al., 1992) diabetic patients can present as proliferative retinopathy and blindness, neuropathy, arterial hypertension, and is linked to higher morbidity and mortality rates.

1.2.2 Markers of DN

Monitoring DN using plasma or urine protein fingerprints has been explored through various proteomics techniques, although it is hindered by the abnormal albumin levels commonly seen in this condition (Hung et al., 2011; Coca et al., 2017; Van et al., 2017). The tubular injury marker kidney injury molecule-1 (KIM-1), detectable in both blood and urine, has been suggested as a factor contributing to the progression of DN (Sabbisetti et al., 2014; Schrauben et al., 2021; Vaidya et al., 2011). Another marker of tubular injury, N-acetyl-β-D-glucosaminidase (NAG), has been associated with DN in patients with DM1 (Vaidya et al., 2011), while haptoglobin has been identified as a strong predictor of DN in patients with DM2 (Bhensdadia et al., 2013). A meta-analysis of urinary liver-type fatty

acid-binding protein (L-FABP) has demonstrated its potential to detect all stages of DN

and predict the severity and progression of the disease in patients with both type 1 and

type 2 diabetes (Zhang L et al., 2022). A protein fingerprint of DN progression has been

proposed by the Chronic Renal Insufficiency Cohort (CRIC) Study (Schrauben et al., 2021).

1.3 CKD aetiologies

In addition to DN, various other nephrotic syndromes and renal diseases can lead to the development of CKD and are therefore associated with increased rates of mortality and morbidity (Kolb et al., 2021).

1.3.1. Autosomal dominant polycystic kidney disease

Autosomal dominant polycystic kidney disease (ADPKD) is an inherited kidney disease caused by mutations in genes PKD1 and PKD2 encoding for proteins polycystin-1 (PC-1) and polycystin-2 (PC-2). PC-1 has features of an ion channel and G-protein coupled receptor (GPCR) whereas PC-2 is a calcium-permeable non-selective cation channel which in healthy conditions form a complex in the primary cilia that is important for intracellular calcium regulation (Ta et al., 2020). When the function of polycystin is lost, this in turn leads to a decreased intracellular calcium and increased cyclic adenosine monophosphate (cAMP) levels, which is linked with the activation of protein kinase A, abnormal aerobic glycolysis, and accumulation of intracellular ATP, subsequently activating downstream mTOR signalling responsible for impaired tubulogenesis, cell proliferation, increased fluid secretion and interstitial inflammation (Mise et al., 2018; Chebib and Torres, 2016). The formation of fluid-filled cysts disrupts the renal parenchyma and often progresses to ESKD (Ong et al., 2015).

1.3.2 Immunoglobulin A nephropathy

Immunoglobulin A nephropathy (IgAN) is the most common type of glomerulonephritis, which can manifest from asymptomatic hematuria to rapidly progressive kidney disease. There are four recognized processes in IgAN that cause kidney damage: aberrant glycosylation of immunoglobulin A1 (IgA1), synthesis of galactose-deficient IgA1 antibodies, formation of immune complexes by binding of the galactose-deficient IgA1 and the anti-glycan/glycopeptide antibodies, and accumulation of the immune complexes in the glomerular mesangium (Rodrigues et al., 2017, Suzuki et al., 2011). Dysregulation of mucosal IgA production has been reported to cause IgAN and an inflammatory response to the immune complexes resulting in the proliferation of mesangial cells, expansion of ECM, release of pro-inflammatory cytokines and growth factors, damage to podocytes and tubular cells, all of which leads to deterioration of renal function (Radford et al., 1997; Lai et al., 2009).

1.3.3 Thin basement membrane nephropathy (TBMN)

Thin basement membrane nephropathy (TBMN) is a hereditary, non-progressive disorder characterized by structural changes in the glomerular basement membrane (GBM), which is uniformly thinned in most glomerular capillaries (Tryggvason and Patrakka, 2006). It has been established that the thickness of GBM in normal individuals ranges between 330 and 460 nm (Dische et al., 1990), while GBM thickness in TBMN patients ranges from 121 nm to 227 nm (Haas 2006). TBMN usually shows normal renal function without proteinuria but has a similar initial clinical presentation to IgAN and Alport

syndrome, including persistent microscopic haematuria (Tryggvason and Patrakka, 2006). At the genetic level, TBMN is associated with mutations in the type IV collagen genes *COL4A3* and *COL4A4* with the consequences of reduced cross-linking of type 4 collagen network, reduced content of new type 4 collagen chains in the GBM, and ultimately reduced thickness and stability of the GBM (Badenas et al., 2002).

1.3.4 Focal segmental glomerulosclerosis (FSGS) and minimal change disease (MCD)

Focal segmental glomerulosclerosis (FSGS) and minimal change disease (MCD) are types of podocytopathies, both characterized by the appearance of primary lesions of podocytes or visceral epithelial cells, proteinuria and minimal immune deposits. Although the pathologies are similar, FSGS and MCD are separate conditions that differ in prognosis and treatment (Mariani et al., 2023; Rosenberg and Kopp, 2017). FSGS can be characterized by tubulointerstitial scarring and glomeruli showing segmental solidification of the glomerular tuft. MCD, on the other hand, can be diagnosed by extensive podocyte injury at the ultrastructural level with an appropriate number of normal-looking glomeruli and scar-free tubulointerstitium (Rosenberg and Kopp, 2017). In addition, unlike MCD, FSGS frequently recurs after kidney transplantation, in ~25% of patients, and often progresses to ESKD (Cravedi, et al., 2013).

Based on genetic susceptibility, pathophysiologic drivers, clinical history, and response to therapy FSGS can be classified into six forms: 1. primary (idiopathic) for example due to circulating factors such as cardiotrophin-like cytokine-1 (CLC-1), apoA1b, anti-CD40

antibody, or serum urine–type plasminogen activator receptor (suPAR), 2. adaptive or post-adaptive which arises as a consequence of single nephron hyperfiltration and glomerular hypertension after conditions such as congenital cyanotic heart disease, sickle cell anaemia, obesity, androgen abuse, sleep apnea, and high-protein diet, 3. genetic due to podocyte-specific gene mutations including *NPHS1*, *NPHS2*, *WT-1*, *LAMB2*, *CD2AP*, *TRPC6*, *ACTN4* and *INF2*, 4. virus-associated, for instance, HIV or parvovirus B19, 5. medicine-induced like interferon-α, lithium, and pamidronate, and 6. APOL1 risk allele-associated FSGS (D'Agati et al., 2004; Rosenberg and Kopp, 2017; Chen and Liapis, 2015).

1.3.5 Lupus nephritis

Lupus nephritis (LN) is a severe glomerulonephropathy that occurs as a frequent complication of systemic lupus erythematosus (SLE), a chronic polygenic autoimmune disorder characterized by pathological processes that reinforce themselves by establishing and maintaining chronic inflammation. Some of the abnormalities in SLE are altered apoptosis and clearance of cellular debris, altered antigen presentation, aberrant frequency, phenotype, and molecular signalling for multiple immune cell subsets, and dysfunctional production of soluble immune mediators (Ferretti and La Cava, 2016). Based on pathogenic mechanisms, there are two aetiologies of LN: extrarenal and intrarenal. In the extrarenal aetiology of LN, multiple genetic variants compromise the mechanism that normally ensures immune tolerance to nuclear autoantigens, which becomes evident by the presence of anti-nuclear antibodies. Some examples of genetic variants leading to LN are polymorphisms in genes *FAS* and its ligand *FASL* which are

responsible for the activation of caspases, then polymorphisms in autophagy gene *ATG5* and the autophagy initiator and phosphatase gene *MTMR3,* or in polymorphisms in *DNASE1* resulting in impaired degradation of neutrophil extracellular traps (NETs) (Munroe and James, 2015). Intrarenal LN occurs because of the binding of antibodies to multiple intrarenal nuclear autoantigens followed by the development and deposition of anti-nuclear autoantibodies-containing immune complexes bound within the glomerulus. Such immune complexes in the kidney induce inflammation leading to the recruitment of immune cells which further enhances inflammatory reactions (Munroe and James, 2015). Furthermore, intrarenal LN also involves complement activation and the formation of tertiary follicles within the kidney, the proinflammatory effects of B cells, and the secretion of autoantibodies by plasma cells (Lech and Anders, 2013). A complication that worsens the prognosis of the disease and often leads to renal failure is the appearance of a cellular crescent, severe active vascular, glomerular and tubulointerstitial lesions, that manifest in up to 50% of patients with LN. The higher proportion of crescents increases the risk of adverse outcomes (Zhang, W., et al., 2016a).

1.3.6 Paediatric nephrotic syndrome

Paediatric nephrotic syndrome (NS) is a chronic childhood glomerular disease associated with glomerular podocyte dysfunction due to primary T-cell disorder and may be accompanied by medical complications such as thromboembolism and bacterial infections. It is usually preceded by minimal-change nephrotic syndrome and FSGS but can also be caused by genetic disorders or secondary diseases such as infections and

neoplasia. Children with refractory FSGS may develop end-stage renal disease (Eddy and Symons, 2003).

1.3.7 Nephronophthisis-related ciliopathies

Nephronophthisis-related ciliopathies (NPH-RC) are a group of autosomal recessive cystic kidney diseases associated with impairments in the structure and function of the primary cilia and a common genetic cause of ESKD. Apart from the mutations in nephrocystin genes *NPHP1, NPHP2, NPHP3, NPHP4, NPHP5,* and *NPHP6* (Hildebrandt and Zhou, 2007), another discovered genetic cause of NPH-RC is mutations in ADAM Metallopeptidase With Thrombospondin Type 1 Motif 9 (*ADAMTS9*) which, although known to be secreted in the extracellular space, also localizes near the basal bodies of primary cilia in the cytoplasm (Choi et al., 2019). The characteristics of nephronophthisis are normal or reduced kidney size, cysts on the corticomedullary junction, and dominant tubulointerstitial fibrosis (Hildebrandt and Zhou, 2007).

1.3.8 Fabry nephropathy

Progressive impairment of renal functions can also occur as a consequence of Fabry nephropathy, a rare X-linked recessive disorder caused by deficient activity of the hydrolase α-galactosidase A due to which glycosphingolipids systemically deposit within lysosomes in various organs (Desnick et al., 2001). Patients with Fabry disease have reduced life expectancy due to renal failure, cardiomyopathy, and cerebrovascular disease (Waldek et al., 2009).

1.4 Renal fibrosis

Renal fibrosis is the primary underlying factor in all progressive kidney diseases and represents the final stage of CKD as it advances to ESKD. Renal fibrosis may be defined as unsuccessful wound-healing of kidney tissues which have undergone chronic and sustained injury. A dynamic system, renal fibrosis involves extracellular matrix (ECM) components and renal and infiltrated cell types. This topic has been thoroughly reviewed over the past decade, for example by Webster et al., 2017; Boor et al., 2010, and the most common events associated with renal fibrosis were schematically shown in Figure 1.2.

1.4.1 Epithelial to mesenchymal transition (EMT) and myofibroblasts

Renal fibrosis is characterized by the excessive accumulation of connective tissue in the kidney parenchyma, accompanied by the epithelial-to-mesenchymal transition (EMT) of tubular epithelial cells (TEC) into myofibroblasts, which are the key mediators in the remodelling of fibrotic tissue. EMT is a tightly regulated process marked by the loss of epithelial cell adhesion, as evidenced by a reduction in epithelial markers like E-cadherin, the de novo expression of α-smooth muscle actin (α-SMA), and an increased expression of mesenchymal markers such as vimentin and desmin. This process also involves disruption of the tubular basement membrane, along with enhanced cell migration and invasion (Yang and Liu, 2001). Yang et al. (2020) published recommendations on the criteria for defining EMT, suggesting that EMT status should be characterized by changes in cellular phenotype, such as the loss of apical-basal cell polarity, weakening of cell-cell

adhesion, cell individualization, acquisition of cell motility, cytoskeleton remodelling, or basement membrane invasion. These phenotypic changes should be evaluated alongside a range of molecular markers, most common which are E-cadherin and vimentin, and the assessment of transcription factors linked to EMT, for example Slug, E47, Twist1, Zeb1, and Zeb2. They emphasized that EMT should not be defined by just one or a few molecular markers (Yang, J. et al., 2020). Markedly increased activation of interstitial myofibroblasts is a common manifestation of fibrosis which plays a central role in its pathogenesis and progression and is also used as prediction of chronic renal failure (Tang et al., 1996; Essawy et al., 1997; Roberts et al., 1997). These scar-forming cells progressively produce ECM components and exhibit increased expression of α-SMA; however, they can be also identified by naked cuticle homolog 2 (Nkd2), which is specifically expressed in terminally differentiated myofibroblasts which was shown to be required for collagen expression in human kidney (Kuppe et al., 2021). Even though non-specific and imperfect, a few more markers of myofibroblasts have been suggested: fibroblast specific protein–1 (FSP-1) also called S100A4, vimentin, platelet-derived growth factor receptor, 5'-nucleotidase (NT5E) also known as CD73, and production of fibrillar collagen protein (Campanholle et al., 2013; Falke et al., 2015). The origin of myofibroblasts varies, and in renal fibrosis, their primary source is populations of perivascular fibroblasts and pericytes that adopt the myofibroblast phenotype (Lin et al., 2008; Kuppe et al., 2021). It has been reported that half of the accumulated myofibroblasts arise from the local proliferation of resident fibroblasts, while the other half originates from either the differentiation of bone marrow-derived mesenchymal

stem cells or through cell transformations like EMT or endothelial-to-mesenchymal transition (EndMT) (LeBleu et al., 2013).

1.4.2 Transforming growth factor-beta (TGF-β)

Various growth factors, cytokines, stress molecules and metabolic toxins were found to contribute to the pathogenesis of renal fibrosis. The cytokine transforming growth factor-beta (TGF-β) is the primary regulator of EMT, and its overactive signalling through the SMAD pathway is a key driver of profibrotic events. It is a member of a superfamily consisting of three isoforms: TGF-β1, TGF-β2, and TGF-β3 of which TGF-β1 is the most studied member in renal fibrosis (Yuan et al., 2022). TGF-β promotes the migration of mesenchymal fibroblasts to the surrounding interstitial parenchyma, thereby enhancing ECM production and accumulation, which contributes to the decline in renal function (Sato et al., 2003). Pro-fibrotic biological effects of TGF-β are stimulated upon binding of TGF-β to serine/threonine kinase TGF-β receptor type II (Tgfbr2 or TβRII), which subsequently activates TGF-β receptor type I, leading to phosphorylation and activation of the downstream Smad signalling. Activation of receptor-regulated Smad2 and Smad3 induces the recruitment of its common-partner Smad4, also known as Co-Smad, forming a heteromeric complex which translocate to the nucleus where Smad3 acts as a transcription factor and therefore regulates the transcription of target genes (Itoh et al., 2000). Even though both Smad2 and Smad3 members are responsible for pro-fibrotic and pro-inflammatory responses, in renal fibrosis, Smad3 is a critical mediator (Lan, 2011). Interestingly, while active TGF-β is known to promote progressive renal fibrosis,

its latent form was shown to have protective anti-inflammatory and anti-fibrotic effects (Wang et al., 2005; Huang et al., 2008). One proposed mechanism is the association of latent TGF-β with overexpression of renal Smad7, an inhibitor of downstream TGF-β signalling, which subsequently mediates inhibition of the NF-κB inflammatory pathway via induction of IκBα expression (Wang et al., 2005; Lan, 2011).

In addition, homeodomain interacting protein kinase 2 (HIPK2) plays a crucial role in regulating various profibrotic pathways, including the TGFβ/Smad3 pathway, with Smad3 acting as its downstream effector. Inhibiting HIPK2 has been shown to reduce renal fibrosis by suppressing downstream signaling of Smad3 (Liu, R. et al., 2017; Xiao et al., 2020).

Furthermore, Kayhan et al. (2023) demonstrated some beneficial roles of TGF-β signalling in renal remodelling and pathogenesis of CKD. Deletion of the TβRII receptor in the proximal tubule led to an impaired proximal tubule response to chronic injury with the effects of enhanced renal remodelling, mitochondrial injury and dysfunction associated with oxidative stress, and an enhanced and exacerbated Th1 inflammatory response (Kayhan et al., 2023).

1.4.2.1 Signalling pathways in renal fibrosis and CKD

TGF-β signalling interacts with other cell signalling pathways such as the renin-angiotensin-aldosterone system (RAAS), Wnt/β-catenin, and mitogen-activated protein kinases (MAPKs) p38, JNK and ERK, however there are a few other key developmental signalling pathways which contribute to renal fibrosis such as Notch and Hedgehog

signalling, but even mammalian target of rapamycin complex 1 (mTORC1), p53 and epidermal growth factor receptor (EGFR) signalling (Edeling et al., 2016; Meng et al., 2016; Yuan et al., 2022). RAAS is a critical pathway leading to CKD, where renin stimulates the production of angiotensin I (Ang I), which is then converted to Ang II by the angiotensin-converting enzyme (ACE) (AlQudah et al., 2020). Treatment of mesangial cells with Ang II, a pro-fibrotic mediator of RAAS, triggers the synthesis and secretion of TGF-β, leading to an increase in ECM components such as biglycan, fibronectin, and collagen I, contributing to glomerulosclerosis (Kagami et al., 1994). Ang II was found to induce renal inflammatory injury and fibrosis by binding to its well-known receptor AT1R (Zhang, H., et al., 2015) and to myeloid differentiation protein-2 (MD2) (Xu et al., 2017). In addition to the classical RAAS pathway of fibrosis, there exists an alternative RAAS pathway in which ACE2 plays a crucial role in converting Ang II to Ang I-VII, counteracting the pathological effects of the classical pathway (Liu, Z., et al., 2012). In addition to TGF-β-dependent mechanism, Smad signalling pathway can be activated, and thus ECM production stimulated in a TGF-β-independent manner via ERK/p38 MAP kinase-Smad cross talk pathway. For example, in hypertensive condition, Ang II can be involved by binding to its AT1 receptor (Yang et al., 2009) and similarly, during diabetic complications, advanced glycation end-products (AGEs) are able to activate Smad2 and Smad3 after binding to RAGE receptors (Li, J.H., et al., 2004). Both Ang II and AGEs were shown to promote renal fibrosis by inducing expression of connective tissue growth factor (CTGF) (Yang et al., 2009; Chung et al., 2010b).

Wnt/β-catenin signalling is known to be essential for regulating nephron formation during embryogenesis and injury repair. However, by targeting many downstream targets of β-catenin such as RAAS, plasminogen activator inhibitor-1 (PAI) or matrix metalloproteinase MMP-7, it is also involved in fibrosis development, which is promoted by TGF-β and contributes to fibroblast activation and ECM production (Akhmetshina et al., 2012). Its continuous activation is accompanied by activation of interstitial myofibroblasts, development of renal fibrotic lesions, excessive ECM deposition, and accelerated senescence of tubular epithelial cells, thus leading to progressive CKD (Xiao et al., 2016; Luo et al., 2018). β-catenin was even reported to target exosomal osteopontin (OPN) and by controlling communication between tubular epithelial cells and fibroblasts through exosomal OPN-CD44 axis signalling, it mediates fibroblast activation, and promotes renal fibrosis and CKD (Chen, S., et al., 2022).

Both ligands and receptors from Notch signalling were reported upregulated in different CKD pathologies, as well as in animal CKD models, promoting overexpression of fibrotic markers collagen 1α1/3α1, fibronectin, and α-smooth muscle actin and leading to CKD progression (Xiao et al., 2014; Edeling et al., 2016). The Notch3 receptors are critical in renal fibrosis and inflammation as their deficiency was shown associated with reduced deposition of collagen and protective effect from tubular injury and cell loss (Djudjaj et al., 2012). Furthermore, it was found that abnormal activation of Notch proteins induces severe albuminuria, and positively correlates with glomerulosclerosis, tubulointerstitial fibrosis, and kidney dysfunction in general (Murea et al., 2010; Li, L., et al., 2021). Moreover, it has been demonstrated that increased epithelial expression of Notch

facilitates development of renal fibrosis through activation of TGF-β/Smad signalling and myofibroblast activation (Xiao et al., 2014).

Another signalling pathway that plays a role in fibrotic CKD is Hedgehog signalling whose ligands were reported to be expressed in tubular epithelial cells, and effectors in adjacent interstitial pericytes and perivascular fibroblasts, positive for platelet-derived growth factor receptor suggesting a paracrine signalling loop (Fabian et al., 2012). Different study reported that Hedgehog signalling induced the expression of α-SMA, desmin, fibronectin, and collagen I, suggesting its role in promoting myofibroblast activation, extracellular matrix production, and the development of renal interstitial fibrosis (Ding et al., 2012). In fact, it has been shown *in vivo* and *in vitro* that fibroblasts are the principal targets of renal Hedgehog signalling causing fibroblast proliferation, but not proliferation of TECs (Zhou et al., 2014). Recent study demonstrated that by targeting the Hedgehog receptor Smoothened (SMO) and downstream Hedgehog signalling, exosomes derived from umbilical cord mesenchymal stem cells inhibit renal fibrosis in DN (Zhang, K. et al., 2024).

1.4.3. Other growth factors

In addition to TGF-β, multiple other factors are involved in the complex interplay leading to renal fibrosis: platelet derived growth factor (PDGF), vascular endothelial growth factor (VEGF), epidermal growth factor (EGF), and connective tissue growth factor (CTGF) (Falke et al., 2015). Platelet-derived growth factor (PDGF), involving PDGF-A, PDGF-B, PDGF-C, and PDGF-D ligands (Li et al., 2000; LaRochelle, et al., 2001), induces extensive

fibroblasts and myofibroblasts proliferation and ECM synthesis through binding to the receptor tyrosine kinases PDGF α-receptor (PDGFR-α) or PDGF β-receptor (PDGFR-β) (Tang et al., 1996; Andrae et al., 2008). Upon PDGF ligand binding, PDGFRs undergo dimerization and subsequent activation through autophosphorylation (Kelly et al., 1991). PDGF, but also fibroblast growth factor (FGF), induce activation of phosphoinositide 3-kinase (PI 3-kinase) and ERK signalling and stimulate focal adhesion kinase (FAK) phosphorylation (Hunger-Glaser et al., 2004). More recently, PDGF-C has emerged as a promising target in progressive CKD, as it has been shown to contribute to both renal fibrosis and hypertension, with its antagonism alleviating both conditions (van Roeyen et al., 2019).

CTGF, a fibroblast chemoattractant and mitogen (Bradham et al., 1991), was found to be significantly overexpressed at sites of chronic tubulointerstitial damage, mainly by fibroblastic cell types (Ito et al., 1998). In connective tissue cells, it is selectively induced by TGF-β where it acts by stimulating fibroblastic cell proliferation and ECM synthesis (Frazier et al., 1996). Also, the increased expression of CTGF correlated with the degree of tubulointerstitial damage, all of which indicates its role in the development and progression of glomerulosclerosis and tubulointerstitial fibrosis (Ito et al., 1998). Furthermore, CTGF has been shown to control fibrotic and proliferative processes through the EGFR signalling pathway (Rayego-Mateos et al., 2018).

VEGF is an endothelium-specific growth factor that is highly expressed in glomerular podocytes and tubular epithelial cells in the kidneys, while its VEGF receptors are mainly found on preglomerular, glomerular and peritubular endothelial cells. Key roles of VEGF

include endothelial cell proliferation, differentiation, and survival, mediating endothelium-dependent vasodilation, inducing microvascular hyperpermeability, and interstitial matrix remodelling, all of which is mediated by nitric oxide synthase (eNOS). Interestingly, in different CKD aetiologies, VEGF can exert either deleterious or recovery effects (Schrijvers et al., 2004). In DN, for example, VEGF was found to be overexpressed, and its expression was linked with detrimental roles while its inhibition led to improvement of diabetes-related renal changes (De Vriese et al., 2001; Flyvbjerg et al., 2002). Furthermore, in cystic kidney diseases, VEGF has been suggested to have an angiogenic role thus favouring the growth of cyst cells (Bello-Reuss et al., 2001). On the other hand, in various forms of glomerulonephritis, reduced synthesis of VEGF, as a result of podocyte injury, can cause the loss of endothelial cells and thus promote the development of glomerulosclerosis (Ostendorf et al., 1999; Schrijvers et al., 2004). Vascular growth factors, such as VEGFA, also regulate endoplasmic reticulum stress-induced activation of the unfolded protein response. When this response persists, it contributes to vascular remodelling, cell death, and tissue degradation in kidney disease (Ricciardi and Gnudi, 2020). Targeted VEGF therapy resulted in renal recovery, primarily driven by the modulation of renal macrophages towards a VEGF-expressing M2 phenotype, which restored VEGF signalling and supported the improvement of renal function and microvascular integrity in CKD (Engel et al., 2020).

Another factor that plays a role in renal fibrosis development is EGF, firstly detected in human urine in 1975 (Starkey et al., 1975), which is one of the ligands that binds to receptor tyrosine kinase EGFR. EGFR activation in proximal tubular epithelial cells and

podocytes was reported to be associated with DN development and progression (Saad et al., 2005; Chen, J., et al., 2015). Likewise, inhibition of EGFR signalling has shown therapeutic potential in autosomal-dominant polycystic kidney disease (Torres et al., 2003). In a recent study, EGFR signalling has been shown to be increased in interstitial myofibroblasts and responsible for renal fibrosis development by inducing pericyte and fibroblast migration and proliferation which are later transformed into myofibroblasts by the influence of other pro-fibrotic cytokines or growth factors such as TGF-β (Cao et al., 2023). Moreover, EGFR-dependent ERK signalling has been reported to be responsible for sustained TGF-β expression in renal fibrosis (Chen, J., et al., 2012).

1.4.4 Crosslinking in renal fibrosis

Irreversible crosslinking of ECM components causes increased ECM production and its decreased degradation due to resistance to proteolytic enzymes, leading to renal scarring and fibrosis. This is achieved by the formation of ε(γ-glutamyl) lysine dipeptide bonds within ECM (Johnson et al., 2003). A key enzyme that has a pathological role in renal scarring is transglutaminase 2 (TG2) (Prat-Duran et al., 2021), a member of a large enzyme family responsible for Ca2+-dependent transamidation, it is considered the most abundant member in the kidney (Burhan et al., 2016). TG2 is a known marker of kidney fibrosis progression, acting by cross-linking and stabilizing the ECM, as well as activating TGF-β through a heparan sulfate/syndecan-4 interaction (Scarpellini et al., 2014; Verderio et al., 2016; Burhan et al., 2016). TG2 is externalized in experimental models of CKD and found secreted in urine (Da Silva Lodge et al., 2022) and in urinary vesicles (Furini et al.,

2018). Interestingly, TG2 in its closed conformation has been suggested to have anti-fibrotic effects (Prat-Duran et al., 2024). While TG2 protein expression was found downregulated in fibrotic CKD, TG2 mRNA level along with transaminase activity were increased (Prat-Duran et al., 2024).

Another group of ECM cross-linking enzymes whose increased activity is mediated by TGF-β and associated with renal fibrosis is the lysyl oxidase (LOX) family (Goto et al., 2005). Furthermore, a study on human samples found elevated serum LOX levels in patients with renal fibrosis, suggesting that serum LOX could serve as a diagnostic marker for the condition (Zhang, L., et al., 2020; Zhang, X., et al., 2022).

1.4.5 Dysregulation of lipid metabolism

Renal fibrosis has also been associated with lipid metabolism disorders, characterized by abnormal lipid accumulation in kidney tissue and the dysregulation of signalling pathways (Yuan et al., 2022). In DN patients, there is extensive accumulation of lipid droplets in TECs, podocytes, mesangial cells, and fenestrated endothelial cells, along with downregulation of acyl-CoA oxidase 1 (ACOX1), carnitine palmitoyltransferase 1 (CPT1), and peroxisome proliferator-activated receptors (PPAR-α and -β), as well as upregulation of the LDL receptor and the fatty acid transporter CD36 (Herman-Edelstein et al., 2014). Genome-wide unbiased transcriptome analysis confirmed the downregulation of key enzymes and regulators involved in fatty acid oxidation (FAO) in the fibrotic kidney (Kang et al., 2015).

In summary, renal fibrosis is linked to the loss of renal function, particularly evident in the pathology of DN (Qian et al., 2008). The outcome of CKD can differ between individuals and is closely associated with the progression of fibrosis. CKD can be classified into three forms based on its progression over time: "stable CKD," where patients maintain stable eGFR levels; "reversible CKD," where eGFR levels improve; and "progressive CKD," where eGFR levels decrease irreversibly over the years, a stage reached by the majority of CKD patients (Zhong et al., 2017).
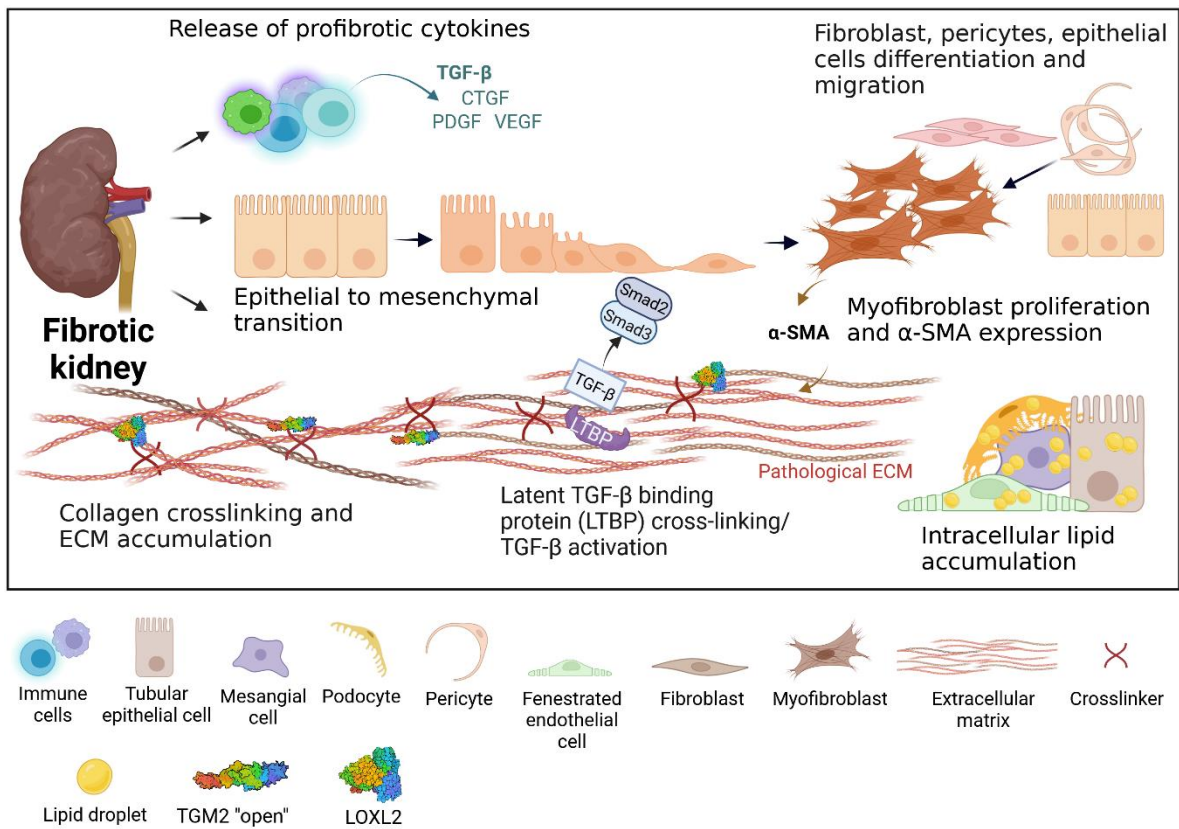
Figure 1.2: Schematic illustrating the key events in renal fibrosis. The primary processes contributing to renal fibrosis in the context of CKD include epithelial-to-mesenchymal transition, increased activation of myofibroblasts, TG2- and LOX-mediated crosslinking of ECM components, secretion of profibrotic cytokines by activated immune and other renal cells, and lipid accumulation in kidney tissue. Figure is modified from Tepus et al., 2023

1.5 Extracellular vesicles (EVs)

1.5.1 Discovery of EVs

Particles that are now known as extracellular vesicles (EVs) were initially detected in the

blood, already in 1899, and described as „dancing bodies" or „blood dust" in the plasma,

or „blood granules" that are identical to the „dancing bodies" but were initially

constituents of the leukocytes from which were extruded and dispersed in the plasma

(Horder, 1899). This particulate material, also named "platelet dust", was sedimented by

ultracentrifugation at 100,000xg and characterised as rich in phospholipid composition.

It also showed coagulant function when released from platelets (Wolf, 1967). Pan and

Johnstone showed in 1983 that vesicles containing transferrin receptor and cell surface-

bound antibody are externalized into the cellular environment during sheep reticulocyte

maturation in vitro, and the process of vesicle formation was not dependent on the

presence of the anti-transferrin-receptor antibodies. Furthermore, the same group

showed that the transferrin receptor was released intact from the cells, suggesting there

is no receptor degradation during its externalization in vesicular form (Pan and

Johnstone, 1984), which is an early indication of the role of EVs in molecular transport

and intercellular communication. In fact, it was suggested that vesicles are specific to the

cells they are arising from (Johnstone et al. 1987). In addition, in these particles it had

been found that the transferrin receptor and antibody binding sites faced the

extracellular medium suggesting that two membrane inversions had occurred prior to

vesicle formation: initial endocytosis and later intra-cellular budding. Following the

fusion of endosomes into a larger vesicle structure, inward budding of the small vesicles occurred forming multivesicular bodies which fused with the cell membrane and eventually released vesicles by exocytosis. This was an early and the first description of the biogenesis of the small, about 50-nm in size, vesicles (Johnstone et al. 1987). On the other hand, Allan et al., 1976 isolated and characterised microvesicles, which are the larger fraction of extracellular vesicles. They showed by electron microscopy the spherical shape of these 100-nm vesicles with similar electron density characteristics to the erythrocytes from where they are secreted. Furthermore, the mechanism of microvesicles release into extracellular milieu was described as outward vesiculation or "budding" from the cell membrane (Allan et al., 1976). Microvesicles were also detected in various normal and neoplastic mammalian cell lines where it was reported that 70% of cell membrane enzymatic activity (5'-nucleotidase activity) was accumulated in ectosomes in the medium after 24 hours incubation, suggesting highly efficient packaged transfer of the cellular components (Trams et al., 1981). Apart from being produced and secreted by eukaryotic cells, EVs were found in plants (Robinson et al., 2016), bacteria, archaea, fungi, and parasites (Deatherage and Cookson, 2012) meaning they have been conserved throughout evolution. Although EVs were initially proposed to eliminate unneeded products from the cells into the medium or fluids, it is now well established that EVs are small membrane-bound carriers of proteins, nucleic acids, and lipids with the important role in intercellular communication (Van Niel et al., 2018).

1.5.2 Different types of EVs

The generic term of extracellular vesicles refers to all membrane particles secreted from the cell that contain cytosol but not nucleus, therefore cannot replicate. Based on their biogenesis, there are two main categories of EVs: exosomes and ectosomes (van Niel et al., 2018; Théry et al., 2018) (Figure 1.3). According to their origin, size and morphology, both types of vesicles are often named by different names such as: intraluminal vesicles (ILVs), exosome-like vesicles, nanoparticles or nanovesicles, tolerosomes, dexosomes, prostasomes (referring to exosomes), and microparticles or microvesicles, shedding vesicles, blebbing vesicles, oncosomes, migrasomes, neurospheres, apoptotic bodies (referring to ectosomes) (Cocucci and Meldolesi, 2015; van Niel et al., 2018). Exosomes were firstly described in 1980s as vesicles from endosomal origin (Johnstone et al. 1987) with the diameter range of 30-100 nm, or slightly larger (up to 150 nm) (Colombo et al., 2014). Ectosomes are 50–1000 nm in size and their biogenesis is based on outward budding and fission of the plasma membrane from where are released in the extracellular space (Heijnen et al., 1999, van Niel et al., 2018). Moreover, the composition of the exosomes should be closer to those from the endosomes than plasma membrane, while composition of the ectosomes should be closer to the plasma membrane (Colombo et al., 2014). Even if much effort has been put to identify specific exosomal or ectosomal content from various sample types (Gonzales et al., 2009; Rai et al., 2021; Lischnig et al., 2022), both exosomes and ectosomes are recovered in the extracellular environment, with no consensus on particular exosomal or ectosomal markers to track their origin, so it is still very challenging to demonstrate with certainty that vesicular fraction is 100%

exosomes or ectosomes. Therefore, the International Society for extracellular vesicles has proposed to refer to them according to their size, as "small extracellular vesicles" and "large extracellular vesicles" (Théry et al., 2018; Welsh et al., 2024). Despite differences in size and origin, ectosomes and exosomes are believed to have analogous functions in inter-cellular communication, thus playing important roles in cell physiology and pathology by targeting and fusing with the target cells (Cocucci and Meldolesi, 2015).

Furthermore, Zhang, H. et al., 2018 demonstrated by asymmetric-flow field-flow fractionation (AF4) analytical tool the existence of two subpopulation of exosomes: large exosomes that were 90-120 nm in size, and small exosomes that were 60-80 nm in size that differ in their functional cargo. The same group identified a new type of nanoparticles, not previously described, that are actively secreted from the cultured cells, and they called them "exomeres". Characterisation of exomeres showed they are about 35 nm in size, without external membrane structure, positive for heat-shock protein 90 (Hsp90) which is one of the EV markers used for EV characterisation, and with the least negative surface charge (-2.7 to -9.7 mV) when compared to small and large exosome fractions (-9.0 to -12.3 mV and -12.3 to -16.0 mV respectively). It was also shown that exomeres are carriers of selective protein, nucleic acid, lipid, and glycan cargo. In fact, by proteomic, genomic, lipidomic and glycomic studies it has been revealed that each of the three EV subpopulations have distinct molecular signature (Zhang, H., et al., 2018). Two exomere cargos, β-galactoside α2,6-sialyltransferase 1 (ST6Gal-I) and amphiregulin (AREG), were shown to be biologically active in recipient cells implying their role in transporting functional cargo (Zhang, Q., et al., 2019).

Very recently, another new type of EVs was discovered, EV-like migrasome-derived nanoparticles (MDNPs) (Ma, Y., et al., 2023) which were described as nanoparticles with a membranous structure with a typical round morphology containing characteristic markers of migrasomes, a subtype of large vesicles formed as a result of cell migration (Ma, L., et al., 2014), but without protein or miRNA markers characteristic of known EVs.

1.5.3 Biogenesis of EVs

The formation of both exosomes and ectosomes involves the accumulation of components in small membrane domains that undergo membrane budding while still in continuity with the original membrane. The biogenesis of exosomes and ectosomes occurs at different locations within the cell, but both processes involve membrane trafficking.

1.5.3.1 Biogenesis of exosomes (small EVs)

Generation of exosomes includes complex processes that vary according to the cell type, stimuli received by the cells and the cargo. The mechanism starts with the process of endocytosis where transmembrane proteins or extracellular ligands are uptaken, trafficked and enclosed in early endosomes. This is followed by the maturation of early endosomes into late endosomes (Stoorvogel et al., 1991), during which small intraluminal vesicles accumulate in the lumen of the endosome by inward budding of the early endosomal membrane, segregating specifically sorted endosomal proteins, lipids, and cytosolic components, thus forming a multivesicular body (MVB) (Figure 1.3). There are two possible outcomes for the MVB content, either discharge and digest if MVB fuses

with lysosomes for the degradation pathway, or release into the extracellular milieu after fusing MVB with the plasma membrane for the exocytosis pathway (Cocucci and Meldolessi, 2015; Colombo et al., 2014). However, the two MVB fates are now known to rely on different MVB populations that even if coexist in the cell and are morphologically the same, contain different biological components (Raposo and Stoorvogel, 2013). For example, MVBs destined for exosome secretion as opposed to those destined for degradation are rich in cholesterol (Mobius et al., 2002) and lack lyso-bisphosphatidic acid (LBPA) (White et al., 2006), a marker of late endosome (Kobayashi et al., 1998). MVBs destined for exosome release contain surface proteins such as tetraspanin CD63, the lysosome-associated membrane proteins LAMP1 and LAMP2, and molecules from late endosomes such as MHC class II, while MVBs destined for degradation contain small GTPase Rab7 (Colombo et al., 2014; Guerra and Bucci, 2016). In addition, it has been reported that production of intraluminal vesicles in MVBs positive on EGFR requires activation of phosphatidyl inositol (PI) 3-kinase (Futter et al., 2001), whereas inhibition of phosphatidyl inositol (PI) 3-kinase has been shown elsewhere to have no effect on the accumulation of internal lumenal membranes within LBPA-containing MVBs/late endosomes (Bright et al., 2001). Several proteins were found to be involved in the sorting and transport functions of the endosomal system: *N*-ethylmaleimide-sensitive factor (NSF)/Sec18p and its soluble associated proteins (SNAPs) are required for mediating docking/fusion events during transport from early to late endosomes (Robinson et al., 1997), components of soluble N-ethylmaleimide-sensitive factor attachment protein receptors (SNAREs), also known as vesicle-associated membrane protein (VAMP) that

play a role in defining the specificity of vesicular trafficking (Prekeris et al., 1999), and Rab proteins such as Rab5 which was suggested to act as a timer that determines the frequency of membrane docking/fusion events (Rybin et al., 1996).

Furthermore, sorting and incorporation of the cargo into exosomes and secretion of exosomes involves special sorting machineries - subunits of endosomal sorting complex required for transport (ESCRT) (Hessvik and Llorente, 2017), classified into four protein complexes: ESCRT-0 consisting of Hrs (*h*epatocyte growth factor-*r*egulated tyrosine kinase *s*ubstrate) and STAM1/2 (*s*ignal *t*ransducing *a*daptor *m*olecule1/2) subunits (Asao et al., 1997), ESCRT-1 formed by the class E Vps proteins Vps23 (or TSG101 mammalian gene), Vps28 (or VPS28 mammalian gene), and Vps37 (or VPS37A, B, C, D mammalian gene) (Katzmann et al., 2001), ESCRT-2 composed of Vps22 (EAP30 mammalian gene), Vps25 (EAP25 mammalian gene), and Vps36 (EAP45 mammalian gene) (Babst et al., 2002a), ESCRT-3 formed by Vps2 (CHMP2A, B mammalian gene), Vps20 (CHMP6 mammalian gene), Vps24 (CHMP3 mammalian gene), and Snf7 proteins (CHMP4A, B, C mammalian gene) (Babst et al., 2002b), but also AAA ATPase Vps4 (VPS4A, B mammalian gene) that was initially discovered in yeast as vacuolar protein sorting (vps) genes which are now known to be necessary for delivering transmembrane cargo into endosomes, sorting the cargo within internal vesicles and thus converting endosomes into MVBs (Babst et al., 1997; Henne et al., 2013; Babst, 2005). The ESCRT-dependent process of cargo sorting and formation of MVB vesicles starts with the initial recruitment of the ESCRT-1 components to endosomes mediated by ESCRT-0 complex (Bache et al., 2003; Raiborg and Stenmark, 2009). ESCRT-1 protein complex then binds to ubiquitinated

endosomal cargo and activates ESCRT-2 protein complex. Activated ESCRT-2 then initiates recruitment of the small coiled-coil proteins from cytoplasm to endosomes followed by their oligomerization and ultimately formation of the ESCRT-3 complex whose role is to concentrate and sort MVB cargo, and to cleave intraluminal vesicles into the lumen of MVB (Babst et al., 2002b; van Niel et al., 2018). The final step is binding the multimeric AAA-type ATPase Vps4 to ESCRT-III and disassembling the ESCRT-III complex in an ATP-dependent manner (Babst et al., 1998; Lottridge et al., 2006; Obita et al., 2007). Along with the ESCRT machinery, there is involvement of the specific proteins associated with each of the ESCRT component, such as apoptosis-linked gene-2-interacting protein X (ALIX) and tumour susceptibility gene 101 (TSG101). Colombo et al., 2013 showed that inhibition of ESCRT-0 proteins HRS and STAM1, and ESCRT-1 protein TSG101 resulted in reduced exosome secretion, while inhibition of ESCRT-3 proteins CHMP4C, VPS4B, VTA1, and ALIX caused an increase in exosome secretion. In addition, the same group showed that loss of function of selected ESCRT components also affects the nature and protein contents of vesicles. For example, depletion of VPS4B increased secretion of exosome-associated markers (CD63, MHC II, HSC70), while depletion of ALIX increased the amount of MHC II in cells and secreted vesicles but also increased the proportion of medium-sized and large-sized vesicles (Colombo et al., 2013). However, now is known that cargo clustering and membrane budding can occur in both ESCRT-dependent and ESCRT-independent manners since simultaneous silencing of all four ESCRT components did not block accumulation of intraluminal vesicles into MVBs (Stuffers et al., 2009).

An alternative, ESCRT-independent pathway has been shown to be promoted by the generation of ceramide through the activation of neutral sphingomyelinase 2, phosphatidic acid via the activation of phospholipase D2, or lipid-raft formation in a Rab31-flotillin-dependent manner (Arya et al., 2024). Trajkovic et al, (2008) showed that sphingolipid ceramide is involved in the formation of intraluminal vesicles destined for secretion by imposing the spontaneous negative curvature on membranes, probably due to its conical shape. Also, ceramide can induce coalescence of microdomains into larger domains that cause domain-induced budding. Inhibition of neutral sphingomyelinase, which hydrolyses sphingomyelin to ceramide, resulted in reduced exosome secretion (Trajkovic et al., 2008). Accordingly, Chairoungdua et al., (2010) suggested that tetraspanins CD9 and CD82 can stimulate vesicular secretion of β-catenin via the ceramide-dependent pathway showing that neutral sphingomyelinase inhibition resulted in a decrease in vesicle-associated β-catenin secretion. This was confirmed by Matsui et al. (2021), who demonstrated that ceramide plays a specific role in basolateral exosome release, while the release of apical exosomes is regulated by ALIX in conjunction with Syntenin1 and Syndecan1 (Matsui et al., 2021). The Syntenin-ALIX-mediated exosome biogenesis and budding into MVBs are regulated by the small GTPase ADP ribosylation factor 6 (ARF6) and its effector phospholipase D2 (PLD2), which converts phosphatidylcholine into phosphatidic acid and choline (Ghossoub et al., 2014). Furthermore, an additional ESCRT-independent pathway of exosomal packaging and cargo release was revealed showing that exosomal release of β-catenin induced by CD82 expression requires E-cadherin which forms a complex with β-catenin and functions as a

negative regulator of canonical Wnt signaling (Chairoungdua et al., 2010). Tetraspanin CD63 was also shown to directly participate in ESCRT-independent cargo sorting mechanism. In particular, CD63 is responsible for the sorting of the luminal component of the PMEL protein into intraluminal vesicles of melanocytes, which is essential for the formation of melanosome precursors and consequently for melanosome maturation (van Niel et al., 2011). Moreover, RAB31 has been shown to play dual roles in exosome biogenesis: promoting the formation of ILVs via FLOT proteins (RAB31-FLOT exosome pathway) and preventing the degradation of MVEs by recruiting the GTPase-activating protein TBC1D2B (RAB31-TBC1D2B exosome pathway) (Wei et al., 2021). Besides the canonical pathways of MVB biogenesis, it has been identified and reviewed in Arya et al. (2024) that specialized, non-canonical exosomes are derived from the nuclear envelope, mitochondria, autolysosomes, and autophagosomes.

1.5.3.2 Biogenesis of ectosomes (large EVs)

As mentioned earlier, large vesicles or ectosomes originate directly from the plasma membrane by outward budding (Figure 1.3). As reviewed in Dixson et al. (2023), ectosomes of varying sizes may be formed through different biogenesis mechanisms. The formation of smaller ectosomes closely resembles exosome biogenesis, involving ESCRT proteins and tetraspanins, and can also be shed from membrane protrusions such as filopodia, cilia, and microvilli. In contrast, the formation of larger ectosomes relies on rearrangements of the actin cytoskeleton, which drive plasma membrane blebbing and scission to release large EVs (Dixson et al., 2023). This process involves several molecular rearrangements at specific sites of the plasma membrane where budding occurs, such as

changes in protein and lipid composition and Ca^{2+} levels (Minciacchi et al, 2015). The plasma membrane is known to have a specific arrangement and content of phospholipids, which is necessary to maintain its dynamic asymmetric state. Phosphatidylcholine and sphingomyelin are located on the outer side of the membrane, while phosphatidylserine and phosphatidylethanolamine are located on the inner side of the membrane (Verkleij et al., 1973). Increased intracellular Ca^{2+} levels affect the distribution of these phospholipids on the plasma membrane through modulation of the enzymatic activities of translocase, scramblase, floppase, and protease calpain. For example, elevated cytoplasmic Ca^{2+} induces inhibition of translocase and activation of scramblase which consequently results in the inability of phosphatidylserine and phosphatidylethanolamine to return to the inner side of the membrane (Piccin et al., 2006; Pap et al., 2009), but also activation of the protease calpain leading to proteolysis and disruption of cytoskeletal proteins, causing cytoskeletal rearrangement and consequently membrane budding (Pasquet et al. 1996). Phosphatidylserine exposed on the surface of large vesicles binds annexin V, which plays a role in phospholipid-dependent procoagulant activity, but a subpopulation of platelet-derived large vesicles was found to be unable to bind annexin V, suggesting that generation of large vesicles can occur even when membrane asymmetry is maintained (Connor et al., 2010; van Niel et al., 2018). In addition, it has been shown that large vesicles derived from activated or apoptotic cells have distinct antigenic profile. Vesicles released from activated endothelial cells were positive for CD62E, CD54, or CD106, while vesicles released from apoptotic cells contained CD31 and CD105 (Jimenez et al., 2003). Cholesterol-rich lipid

rafts have been reported to play an important role in the production of large vesicles since membrane cholesterol depletion significantly reduced their secretion from monocytes (del Conde et al., 2005). In addition, in different cancer cell types of formation of large vesicles was shown to be regulated by small GTPase RhoA which triggers specific signalling pathway involving Rho-associated coiled coil-containing kinases 1 and 2 (ROCK1 and ROCK2) and downstream LIM-kinase (LIMK) responsible for cytoskeletal remodelling and dynamics (Li et al., 2012). Furthermore, another GTP-binding protein ARF6 has also been shown to be implicated in the shedding and release of large vesicles from cancer cells by facilitating actomyosin-based vesicle neck contractions. This is achieved via AR6-dependent activation of the chain of reactions involving phospholipase D that promotes the recruitment of the extracellular signal-regulated kinase (ERK) to the plasma membrane, then ERK phosphorylates and activates myosin light chain kinase which induces exchange between myosin and actin. This ultimately allows the plasma membrane to detach from the cytoskeleton, resulting in vesicle release (Muralidharan-Chari et al., 2009; Pap et al., 2009). The key role of actin-myosin cytoskeletal processes in the generation and release of large vesicles was also confirmed after pharmacological inhibition of actin polymerization and myosin function, which resulted in the inhibition of vesicle release (Muralidharan-Chari et al., 2009).
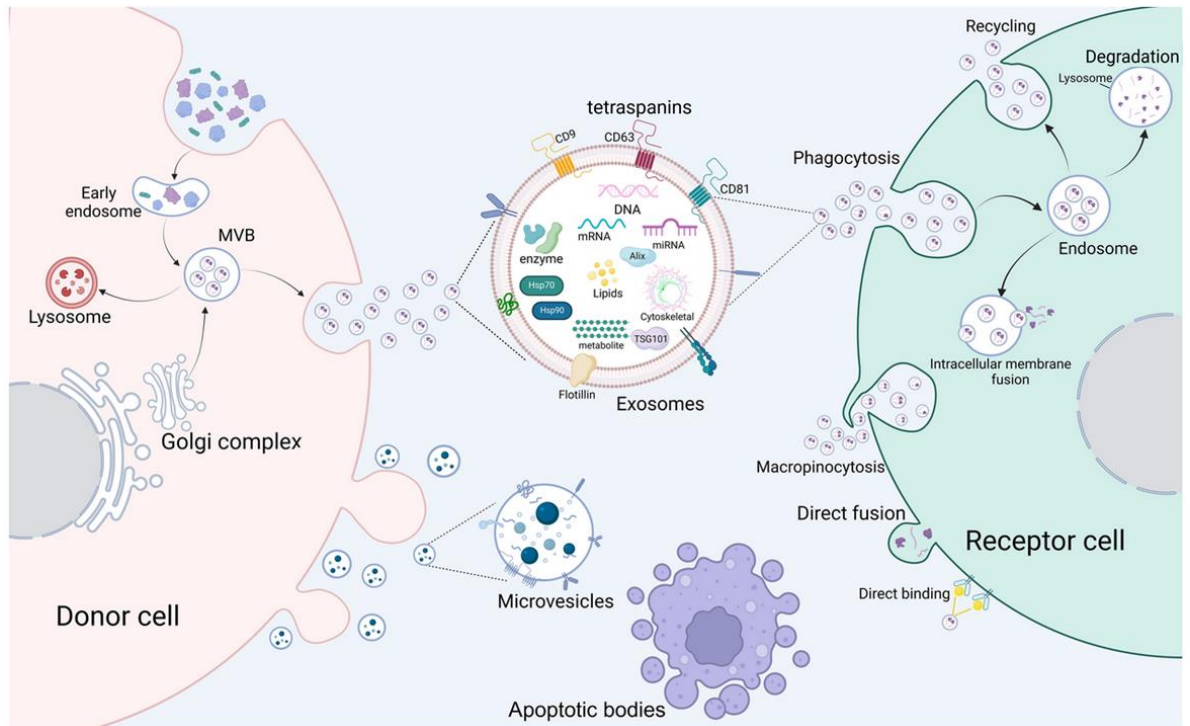
Figure 1.3: Classification, biogenesis, and uptake of EVs. Two main types of EVs are exosomes and ectosomes. Exosomes are derived from the endosomal compartment and are secreted by inward budding, whereas ectosomes originate from outward budding of the cell membrane. Uptake mechanisms of EVs by recipient cells include clathrin-mediated endocytosis, membrane fusion, phagocytosis, pinocytosis. Figure is taken from Li, B. et al., 2024.

1.5.4 EVs targeting and uptake by recipient cells

The main function of EVs in both normal physiological condition and disease is cell-to-cell communication which includes cell targeting, EV cargo releasing in the recipient cells and transmission of the signal (Liu and Wang, 2023). In order to be able to deliver the molecular cargo to the recipient cells and induce their phenotypic changes, which consequently enable the appearance of their physiological or pathophysiological effect, secreted EVs must target and adhere to the plasma membrane of the recipient cell. This can be followed either by fusion of EVs with the plasma membrane, or their uptake by

the recipient cell (Tian et al., 2013) via various endocytic pathways including specific protein interactions, endocytosis, cell surface membrane fusion, and cell-specific EV uptake, as schematically shown in Figure 1.3 (Mulcahy et al., 2014).

Even if some studies indicated that EVs can be integrated into recipient cells in a non-selective way (Horibe et al., 2018), substantial evidence showed that EV size and receptor-ligand interactions play an important role in the EV-target cell binding specificity (Mathieu et al., 2019).

Proteins, lipids and glycans interactions between EVs and recipient cells' plasma membranes greatly influence EVs' internalisation (Liu and Wang, 2023). Thus, EV attachment to the cell surface and endocytosis depends on the constituents on the surface of EVs and the appropriate ligands on the recipient cells, such as tetraspanins, integrins, lipids, lectins, heparan sulphate proteoglycans and components of extracellular matrix (Mulcahy et al., 2014). The first group of proteins involved in binding and uptake of EVs are tetraspanins, proteins that are highly represented in EVs, some of them even markers of EVs, which together with their associated molecules play a key role in cell adhesion (Andreu and Yáñez-Mó, 2014). Tetraspanin Tspan8 selectively recruits CD49d to small vesicles, creating a Tspan8-CD49d complex, which promotes the internalization of such vesicles by endothelial cells (Nazarenko et al., 2010). It has also been shown that Tspan8 internalizes separately from CD9 and CD151 suggesting that individual tetraspanins follow different internalization pathways (Rana et al., 2011). In addition, the diversity of the tetraspanin complexes affects target cell selection, for example EVs containing the complex of tetraspanin Tspan8 and alpha4 integrin chain are selectively

taken up by endothelial and pancreas cells, with intercellular cell adhesion molecule-1 (ICAM-1 or CD54) as a main ligand (Rana et al., 2012). Furthermore, it was shown that EV uptake by dendritic cells is mediated by tetraspanins CD9 and CD81, integrin CD11a with its ligand CD54, and phosphatidylserine on vesicles, and integrins αv (CD51) and β3 (CD61), as well as CD11a with CD54 on dendritic cells since their inhibition or blockade significantly reduced vesicle internalization (Morelli et al., 2004). It was also shown that β1-integrin (CD29) and hyaluronan receptor CD44 are required for the integration of mesenchymal stem cell-derived large vesicles into tubular epithelial cells as anti-CD29 and anti-CD44 blocking antibodies prevented their uptake (Bruno et al., 2009). The next important molecules for EV internalization are heparan sulphate (HS) proteoglycans such as syndecan and glypican whose presence is necessary on the surface of recipient cells where they have been found to serve as internalizing receptors for small EVs originating from cancer cells (Christianson et al., 2013; Christianson et al., 2014). The function of HS proteoglycans in EV internalization was confirmed by their enzymatic depletion on the cell surface, but also by treatment of cells with HS mimetic heparin, both of which resulted in significantly reduced EV uptake. Interestingly, vesicular uptake was shown to be dependent on HS proteoglycan sulfation since cell mutants lacking 2-O-sulfation and N-sulfation significantly attenuated EV uptake, just as desulphated heparin did not achieve an inhibitory effect (Christianson et al., 2013). Furthermore, lectins were also suggested as molecular factors that have an impact on EV uptake: selectins, siglecs and galectins (Johannes et al., 2016; Barrès et al., 2010).

After binding to the recipient cells, EVs uptake occurs via various mechanisms (Liu and Wang, 2023). The most experimentally reported mechanism of vesicular internalization into endosomal compartments is endocytosis, which is now well-known to be energy dependent mechanism (Escrevente et al., 2011; Christianson et al., 2013) that can occur through distinct endocytic pathways involving clathrin-mediated endocytosis, caveolin-dependent endocytosis, macropinocytosis, involvement of lipid rafts, and phagocytosis (Mulcahy et al., 2014; van Niel et al., 2018).

As the name suggests, clathrin-mediated endocytosis depends on clathrin, a polygonal structure called triskelion because it consists of three heavy chains and three light chains. The mechanism occurs with a high concentration of transmembrane receptors and their associated ligands in vesicular buds also called 'coated pits' located on the plasma membrane, followed by coated pits maturation, invagination and pinching off into the intracellular space which requires involvement of clathrin and its associated internal adapter protein AP2 which binds clathrin with high affinity and also controls binding to membranes (Wang et al., 1993). By encapsulating coated pits, clathrin and AP2 are so responsible for the vesicle formation, which after internalization undergo clathrin dissociation or 'un-coating', after which fuse with endosomes where they release their content (Conner and Schmid, 2003; Wang et al., 1993). In addition to clathrin and its accessory protein, a large GTPase dynamin plays an essential role in vesicle reformation and scission during endocytosis (Takei et al., 1996; Orth et al., 2002), and its inhibition was proven to block vesicle endocytosis (Newton et al., 2006). Several studies showed internalization of EVs via clathrin-mediated endocytosis, for example small EVs from

ovarian cancer cells taken up by the same cells (Escrevente et al., 2011), small EVs from pheochromocytoma cell line taken up by the same cells (Tian et al., 2014), and oligodendroglial small EVs taken up by neurons (Frühbeis et al., 2013).

Similar to the clathrin mediated mechanism, caveolin- or caveolae-dependent endocytosis involves the formation of caveolae (˝little caves˝), flask-like invaginations of the plasma membrane that can be internalized into the cell. Caveolae consist of caveolins, integral membrane proteins (Rothberg et al., 1992), and are subdomains of glycolipid rafts, plasma membrane microdomains enriched in cholesterol and sphingolipids (Nabi and Le, 2003). Caveolin-1 is a cholesterol-binding protein (Murat et al., 1995) which together with the cholesterol is responsible for the caveolae formation (Anderson, 1998). Nanbo et al. (2013) showed that small vesicles derived from Epstein-Barr virus (EBV)-infected B cells, but also EBV-uninfected B cells, are internalized by the EBV-negative two different cell lines of human nasopharyngeal carcinoma, human gastric carcinoma, and human lung adenocarcinoma recipient cells via caveolin-dependent endocytosis. EV internalization was significantly repressed after cell treatment with dynamin inhibitor or caveolin-1 knockdown (Nanbo et al., 2013). Interestingly, in another study caveolin-1 has been found to negatively regulate lipid raft-mediated endocytosis of EVs (Svensson et al., 2013). This was presented by significantly decreased EV uptake after caveolin-1 overexpression in different cell lines: glioblastoma cells (U87 MG), human cervix adenocarcinoma cells (HeLa), mouse embryonic fibroblasts (MEF), and chinese hamster ovary cells (CHO-K1). Moreover, caveolin-1 knock-out or stable knock-down resulted in significant increase of EV uptake. In addition, the mechanism of

caveolin-1 regulation of the lipid raft-mediated EV uptake was discovered to be through reducing the levels of phosphorylated extracellular signal-regulated kinases (ERK1/2) and hence suppressing their signalling (Svensson et al., 2013). Although the mechanism of caveolae-dependent endocytosis includes common features of other lipid raft-dependent endocytosis pathways, for instance, lipid composition, clathrin independence, dynamin dependence, or sensitivity to cholesterol depletion, caveolae-dependent endocytosis is considered a separate category of EV internalization due to its specific morphology and association with caveolins (Nabi and Le, 2003). In addition to caveolae, small lipid raft structures can localize to flat regions of the plasma membrane and include various molecular actors, such as flotillins, which have been found to play a role in clathrin- and caveolin-independent vesicular trafficking (Frick et al., 2007). Coexpression and clustering of flotillin-1 and flotillin-2 at the plasma membrane in a 1:1 ratio was found to generate flotillin microdomains and membrane invagination morphologically similar to that of caveolae, resulting in the production and accumulation of flotillin-positive intracellular vesicles (Frick et al., 2007). Flotillin microdomain internalization has been shown to be regulated by tyrosine-kinase-endocytic process, in particular by Src kinase-mediated phosphorylation of flotillin 2 (Babuke et al., 2009) and Fyn kinase-mediated phosphorylation of both flotillins (Riento et al., 2009) upon epidermal growth factor (EGF) stimulation of the cells.

The endocytosis process of macropinocytosis is defined by the formation of the large organelles called macropinosomes formed from actin-rich extensions of the plasma membrane, also known as membrane ruffles. Such membrane ruffles protrude from the

cell surface and collect fluid and components from the surrounding extracellular area, followed by their fusion with the plasma membrane or themselves and internalization into the intracellular space (Mulcahy et al., 2014). This process requires activation of the receptor tyrosine kinases EGFR and PDGFR, but also Src family kinases, leading to increased actin polymerization at the cell surface and actin-mediated ruffling, ultimately resulting in increased macropinosome formation, but also Rac1 GTPase activity and Na^+/H^+ exchanger function (Kerr and Teasdale, 2009). In terms of EVs, macropinocytosis was reported to be the mechanism of small EV uptake which were secreted by oligodendrocytes and taken up by microglia cells. Blocking the functions of Na^+/H^+ exchanger, Rac1 or dynamin by pharmacological inhibitors resulted in suppressed EV uptake (Fitzner et al., 2011). Furthermore, Tian et al. (2014) showed that in addition to clathrin-mediated endocytosis of EVs, macropinocytosis was also involved in internalization of EVs secreted by rat pheochromocytoma PC12 cells because the use of inhibitors of phosphoinositide 3-kinase (PI3K) and Na+/H+ exchangers, associated with macropinocytosis, significantly reduced EV uptake (Tian et al., 2014). Nakase et al. (2005) showed that activation of macropinocytosis-related receptors (C-X-C chemokine receptor type 4 and EGFR) by their ligands, as well as expression of oncogenic Ras protein enhanced the efficiency of cellular EV uptake.

Although phagocytosis is considered a mechanism for internalizing larger particles, pathogens or other contents such as cellular debris (Conner and Schmid, 2003), it has been reported that EVs can be internalized by phagocytosis, for example by dendritic cells (Morelli et al., 2004). In another study was shown that EVs secreted from two

leukaemia cells lines were more efficiently internalized by phagocytic cells - macrophages compared to non-phagocytic cells and were colocalized with phagolysosomal markers (Feng et al., 2010). These studies therefore imply that phagocytosis is involved in the uptake of some EVs.

In addition to the internalization of EVs by cells, EVs can release their contents in the recipient cell even by fusion with the plasma membrane of the cell. This is achieved by merging the outer leaflets of the lipid bilayers of the vesicle and the cell in an aqueous environment which is followed by reversible opening of small aqueous pores spanning two opposing membranes which expands to complete the fusion process (Jahn and Südhof, 1999; Chernomordik and Kozlov, 2008). Several specific fusion proteins/protein families are involved in this process initially with the role of recognizing the two membranes to be merged but also destabilizing the water/lipid interface to allow the membranes to fuse, for example SNAREs, Rab proteins, and Sec1/Munc-18 related proteins (SM-proteins) (Jahn and Südhof, 1999; Jahn and Scheller, 2009). The mechanism of the fusion of EVs with the cell membrane was shown by Parolini and others (2009) who discovered that fusion of EVs with malignant cells was enhanced in an acidic environment (Parolini et al., 2009). Another study demonstrated that the mechanism of membrane fusion/hemifusion is the mode of EV-mediated transfer of functional miRNA cargo between dendritic cells by tracking EVs labelled with a lipophilic dye in a fluorogenic de-quenching assay (Montecalvo et al., 2012).

1.5.5 Urinary EVs (uEVs)

In urine, "membrane-bound vesicles" with procoagulant activity were first identified in a 100,000 x g precipitate and characterized as 100 nm to 1.1-micron particles by scanning and transmission electron microscopy (Wiggins et al., 1986). Following initial observations in normal urine, analysis of urine samples from patients with renal injury revealed that the proximal tubule releases enzymes from the brush border into the urine shortly after injury. Notably, patients with glomerulonephritis were found to excrete "blebs" ranging from 100 to 300 nm. It was reported that glomerular podocytes release vesicles coated with complement receptor 1, which has been suggested as a potential marker for podocyte injury (Pascual et al., 1994). The first comprehensive characterization of extracellular vesicles (EVs) in human urine (uEVs) was reported in 2004 (Pisitkun et al., 2004). In this study, uEVs were isolated using an ultracentrifugation protocol and examined through immunogold electron microscopy. Proteomic profiling of uEVs revealed their protein cargo, identifying the presence of endosomal pathway proteins and shedding light on how certain proteins, like aquaporin-2 (AQP2), are released into urine. This paved the way for the concept that uEVs could serve as a valuable tool for disease biomarker discovery. It is now established that uEVs can be released by cells from the kidneys, bladder, and the urogenital tract as a whole (Erdbrügger and Le, 2016) as shown in Figure 1.5. Although it has been discovered that some EVs may pass through the glomerular barrier (Bellucci et al., 2021), and thus urine may contain some portion of circulating EVs from the serum, more than 99% of uEVs are shown to originate from the urogenital tract, with the majority coming from renal cells

(Svenningsen et al., 2020; Nørgård et al., 2022). This is likely due to the mechanical and charge barrier of the glomerulus, which prevents serum EVs from easily passing through under normal physiological conditions (Pisitkun et al., 2004; Gildea et al., 2014). Interestingly, EVs containing kidney-specific antigens, particularly α8 integrin from mesangial cells, have been detected in plasma, indicating the presence of kidney-derived EVs in the bloodstream (Komatsu et al., 2024).

Small and large uEVs are thought to serve similar functions to circulating EVs in facilitating cell-to-cell communication and intercellular signal transmission. Their cargo is anticipated to reflect the physiological and pathophysiological states of renal cells (Gildea et al., 2014; Street et al., 2011).

1.5.6 Functions of uEVs

It is now widely recognized that the primary function of uEVs is intra-nephron communication, linking the upper nephron segments with the distant lower segments, thereby transmitting signals and promoting both proximal-to-distal communication and glomerular-to-tubular cross-talk (Grange et al., 2023). Moreover, uEVs intra-nephron communication involves intra-glomerular and intra-tubular crosstalk (Grange and Bussolati, 2022). In addition to transporting and delivering their cargo to target cells, EVs can alter the phenotype of the host-cells by transferring various populations of proteins and nucleic acids (Quesenberry et al., 2014). This ability makes them a potent mechanism for disease dissemination. For instance, it has been shown that TGF-β-containing EVs secreted by injured epithelial cells can, upon uptake by target cells, induce

profibrotic effects. These include stimulating cell proliferation, type I collagen production, and the expression of α-SMA and F-actin in the same cell type from which the EVs were secreted (Borges et al., 2013). Similarly, podocyte-derived EVs have been shown to crosstalk with proximal tubular epithelial cells inducing expression of collagen IV and fibronectin, activation of MAPK and TGF-β receptor-dependent signalling pathways and thus contributing to pro-fibrotic responses by proximal tubular epithelial cells (Munkonda et al., 2018). On the other hand, EVs released from different cell types such as mesenchymal stem cells have shown renal protective and pro-survival effects in acute kidney injury both in vitro and in vivo once taken up by TECs (Bruno et al., 2012). Another example is CD133, a glycoprotein also known as prominin-1, which serves as a marker for kidney progenitor cells involved in tissue repair. EVs containing CD133, released by this stem cell population, have been shown to promote renal regeneration following injury (Ranghino et al., 2015).

The roles of uEVs in both physiological conditions (such as bacteriostatic and bacteriocidal functions in innate immunity, coagulation, oxygen consumption, and aerobic glucose metabolism) and pathological conditions (including the exacerbation of AKI, CKD, and kidney stones) have been reviewed by Grange et al. (2023) and shown in Figure 1.4. Given these growing discoveries, there is significant interest in detecting proteins, nucleic acids, and lipids isolated from uEVs for potential use as diagnostic, prognostic, and therapeutic biomarkers for CKD (Cocucci and Meldolesi, 2015; Zhang, W., et al., 2016a). In addition to serving as a source of biomarkers, the cargo within EVs is thought to aid in tissue repair when derived from therapeutic cells. This is due to their

advantageous properties compared to parent cells, including greater stability, lower immunogenicity, longer storage potential, better tissue penetration due to their small size, and a reduced risk of embolization following intra-arterial injection of EVs as opposed to cells (Huang, W., et al., 2022). Therefore, there is increasing research interest in the development of synthetic particles, such as loading synthetic cargo into EV membrane-coated particles or creating artificial EV mimics (Grange and Bussolati, 2022).
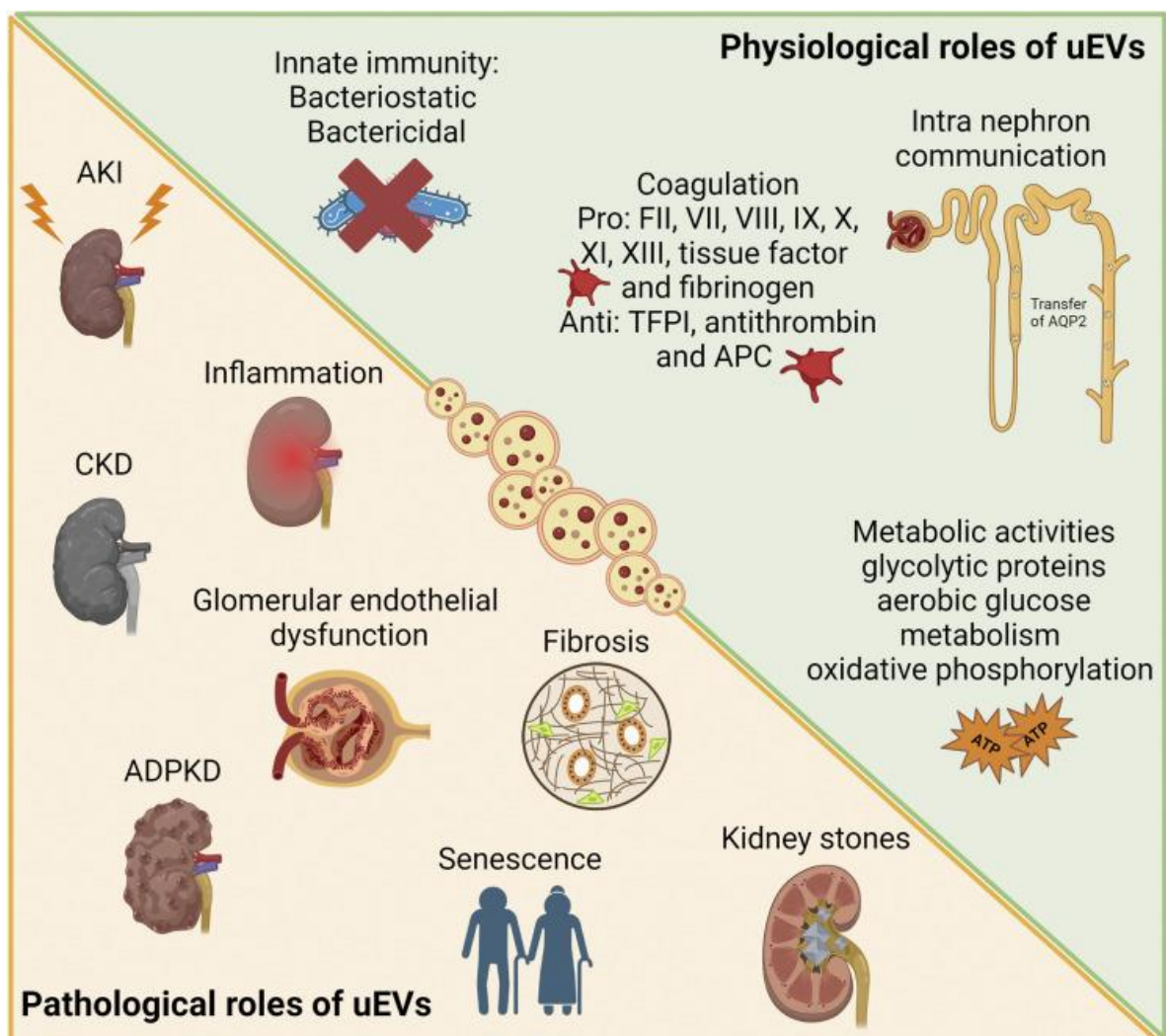
Figure 1.4: Summary of the established roles of uEVs in health and disease. Figure was taken from Grange et al., 2023

1.5.7 EV markers and tracking the cell origin of uEVs

The most widely recognized vesicular markers are tetraspanins (CD9, CD63, CD37, CD81, and CD82), which are the most abundant proteins in the membranes of small EVs. These proteins play key roles in cell adhesion, motility, membrane fusion, protein transport, and signalling (Andreu and Yáñez-Mó, 2014). TSG101, ALIX, and clathrin are EV markers linked to MVB biogenesis, while annexins and small GTPases, such as retinoic acid-binding (Rab) proteins, are involved in membrane transport, docking, and fusion with target cells. Additionally, heat shock proteins Hsp70 and Hsp90 are also associated with exosomal biogenesis (Reddy et al., 2018). Membrane receptor integrins and lipid raft flotillins are also key markers (Merchant et al., 2017; Cricrì et al., 2021). In addition to general markers, EVs carry cargo specific to the cell type from which they originate, which can be used to track the source of isolated EVs and identify the cell type undergoing pathological changes (Figure 1.5). The International Society of Extracellular Vesicles (ISEV) has compiled a list of protein markers specific to various cell types and segments within the kidney, based on evaluations using flow cytometry and Western blotting (reviewed by Erdbrugger et al., 2021). TECs are a source of CD24-containing uEVs, also referred to as cluster of differentiation-24 or heat-stable antigen CD24. The presence of uEVs from podocytes can be identified by markers such as podocin, podocalyxin (PODXL), nephrin, Wilms' tumor-1 (WT1), complement receptor-1 (CR1), and canonical transient receptor potential-6 (TRPC6). Urinary EVs from proximal tubular cells typically contain megalin, cubilin, aminopeptidase-N (APN), sodium/glucose cotransporter-2 (SGLT2), carbonic anhydrase (CAIV), Na+/H+ exchanger isoform-3 (NHE3), and urate transporter-

1 (URAT1) (Turco et al., 2016). To identify uEVs from the descending limb of Henle's loop, markers such as solute carrier family-14 member 2 (SLC14A2) and aquaporin-1 (AQP1) can be used, while uromodulin and epidermal growth factor receptor (EGFR) are indicative of the ascending limb origin. The type-2 Na+-K+-2Cl- cotransporter (NKCC2) serves as a marker for the Henle's loop (Turco et al., 2016). Furthermore, it has been previously noted that progenitor tubular cells release EVs displaying CD133 (Erdbrugger et al., 2021). uEVs from collecting duct cells are characterized by the presence of mucin-1, a glycoprotein that activates protective pathways in TECs following hypoxia in acute kidney injury (Pastor-Soler et al., 2015), as well as AQP2 and V-ATPase (Turco et al., 2016). Distal tubule-derived uEVs typically express prominin-2, thiazide-sensitive Na-Cl cotransporter (NCC), and solute carrier family 12 member 3 (SLC12A3) (Pomatto et al., 2017; Erdbrugger et al., 2021; Turco et al., 2016). The beta-1 adrenergic receptor (β-1 AR) has been identified as a marker for juxtaglomerular cells in uEVs, while transgelin (SM22 alpha) marks mesangial cell origin. Additionally, claudin-1 and cytokeratin 8 are markers for uEVs from parietal cells (Bowman's capsule), and cytokeratins 19–20 serve as markers for uEVs originating from the transitional epithelium (renal pelvis) (Turco et al., 2016Some uEV markers are common to multiple cell types, such as ACE, which has been detected in uEVs from both the glomerulus and proximal tubules, AQP1 in uEVs from the proximal tubules and Henle's loop, and AQP2 in uEVs from both the distal tubules and collecting duct (Erdbrugger et al., 2021). Although specific EV markers for fibroblasts are not yet identified, PDGFRβ and CD73, which are highly expressed on the plasma membrane of fibroblasts, are used as markers for interstitial and cortical

fibroblasts, respectively. However, these markers may also identify pericytes or proximal tubular cells (Asada et al., 2011; Schiessl et al., 2018; Perry et al., 2019; Arai et al., 2021). Recently, naked cuticle homolog 2 (NKD2), a negative regulator of Wnt/β-catenin signaling, has been proposed as a marker of myofibroblasts and a potential therapeutic target. Its knockdown has been shown to significantly reduce the expression of ECM components, independently of TGF-β (Kuppe et al., 2021).
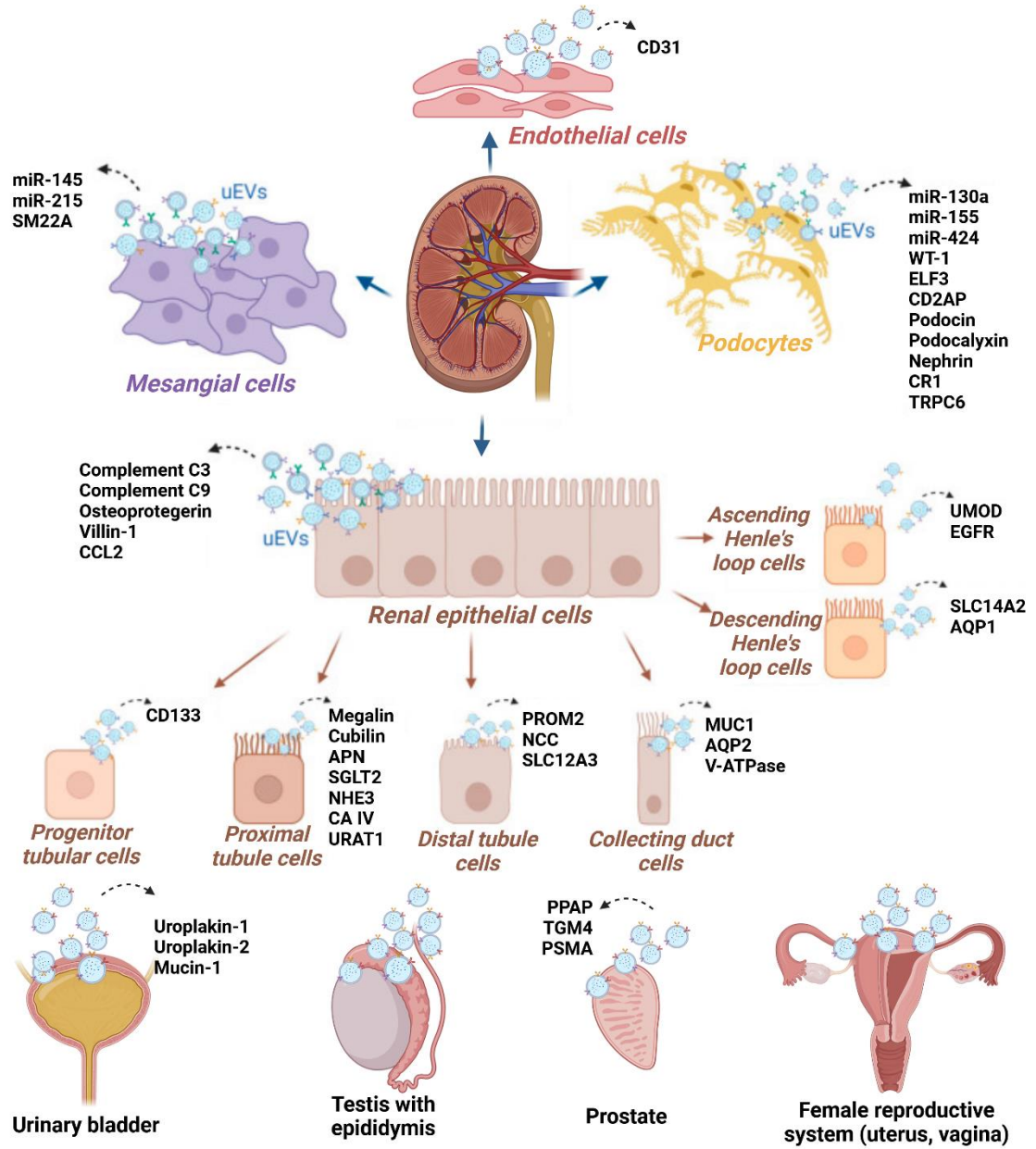
Figure 1.5: The origin of uEVs in the urogenital tract, along with protein and miRNA markers used to trace the cellular/organ source. Figure is modified from Tepus et al., 2023

All cell types that are present in the kidney, with specific genetic markers of each epithelial, endothelial and immune cell type, were detected by a revolutionary single-cell RNA sequencing approach from mouse kidneys (reviewed by Balzer et al., 2022). Similarly, single-cell RNA sequencing approach was applied on human samples using urines from healthy and DKD patients, which revealed that almost all kidney cell types can be detected from urine samples. Another finding was that healthy and DKD samples with more preserved kidney function had very few cells in their urines, which can suggest that total cell number in urine can be another indicator of kidney function (Abedini et al., 2021). Assuming that all types of kidney cells secrete extracellular vesicles, at greater or lesser extent, which have a known role and function of intercellular communication and can carry cell-specific markers that enable tracking of their origin, but also molecules specific to CKD pathology that indicate the stage and type of CKD, not surprisingly, urinary EVs are becoming an increasingly popular source of information in biomarker discovery studies.

1.6 Significance of studying uEVs as a source of biomarkers for DN progression

Several uEV biomarkers for various types of CKD have been proposed (Tepus et al., 2023; Li, B. et al., 2024), however the progression stage of CKD that ultimately leads to kidney fibrosis, ESKD and kidney failure (Zhong et al., 2017) has not been thoroughly explored. Identifying the progressive stage of DN is crucial for developing effective new treatments that not only prevent renal failure but also potentially promote regression of DN (Hovind et al., 2001). Moreover, the urgent need for new non-invasive markers that can indicate DN progression with improved accuracy continues to be emphasized (Lee and Lam, 2015; Barutta et al., 2021; Kammer et al., 2023; E et al., 2024).

Furthermore, despite the ongoing advancement of EV research, no EV product has received approval from regulatory agencies to date (Grange and Bussolati, 2022).

The hypothesis of this PhD project was that uEVs could serve as a valuable tool for diagnosing and/or predicting the progression of DN, as they provide enhanced protection and stability for their molecular cargo while also reflecting pathophysiological events in renal cells. Therefore, the main aim was to identify a multi-marker panel of proteins and miRNAs from uEVs which can be used as accurate, specific and non-invasive biomarkers of DN progression, the stage which largely requires more exploration.

CHAPTER 2:

Materials and methods

2.1 Materials

2.1.1 Laboratory reagents and chemicals

Table 2.1. List of chemicals and reagents; RT = room temperature

Name	Product code	Company	Storage temperature (°C)
1,4-Dithiothreitol (DTT)	MB1015	Melford	4°C
1 kb DNA ladder	N3232S	New England Biolabs	-20°C
2-Mercaptoethanol	M3148-25ML (102343186)	Sigma	RT
10x Buffer for T4 DNA Ligase with 10 mM ATP	B0202S	New England Biolabs	-20°C
Acetic acid glacial	10394970	Fisher Scientific	RT
Acetonitrile	34967-2.5L	Fluka	RT
Agar	LP0012	Oxoid	RT
AGE-BSA	121800-10MG	Sigma	-80°C
Alexa Fluor™ Antibody Labelling Kits AF488 green	A20181	Invitrogen	4°C
Alexa Fluor™ Antibody Labelling Kits AF647 far-red	A20186	Invitrogen	4°C
Alexa Fluor™ Antibody Labelling Kits AF555 orange	A20187	Invitrogen	4°C
Ammonium Persulfate (APS)	215589-100G	Sigma	RT
Ampicillin sodium salt	A0166-5G	Sigma Aldrich	4°C
BCA reagent A [1% (w/v) BCA, 2%(w/v) Na2CO3, 0.16% (w/v) NaK tartrate, 0.4%(w/v) NaOH, 0.95%(w/v) NaHCO3]	B9643-1L-KC	Sigma	RT
BCA reagent B [4% (w/v) CuSO4]	C2284-25ML-KC	Sigma	RT
Bio-Rad Protein Assay Dye Reagent Concentrate, 450 ml	5000006	Bio-Rad	4°C
Bovine Serum Albumin (Purity 96%)	A4503-50G	Sigma	4°C
Bovine Serum Albumin	A7030-100G	Sigma	4°C
cOmplete EDTA-free Protease Inhibitors	11836170001 Roche	Sigma	4°C
DH5 alpha competent cells	EC0112	Invitrogen	-80°C

Dimethyl sulfoxide	D2438-10ML	Sigma	RT
DMEM/F12 (with L-glutamine and 15mM HEPES)	10-092-CV	Corning	4°C
dNTP mix	N0447S	New England Biolabs	-20°C
Dual-Glo luciferase assay system	E2920	Promega	-20°C
Dulbecco's Modified Eagle's Medium - high glucose	D6546-500ML	Sigma	4°C
Ethanol, Absolute (200 Proof), Molecular Biology Grade	16606002	Fisher Scientific	RT
Ethylenediaminetetraacetic acid disodium salt solution	03690-100ML	Sigma	4°C
ExoView Human Tetraspanin Kit with Cargo	EV-TETRA-C-CAR	NanoView Biosciences	4°C
EZ-Chemiluminescence Detection Kit for HRP	K1-0170	Geneflow	4°C
EZ-PCR Mycoplasma Detection Kit	20-700-20	Biological Industries	-20°C
Foetal Bovine Serum	35-079-CV	Corning	-20°C
Foetal Bovine Serum, exosome-depleted	A2720803	Gibco	-20°C
Formic Acid Optima LC/MS	A117-50	Fisher Chemical	4°C
Gel Loading Dye Blue 6x	B7021S	New England Biolabs	-20°C
Gel Loading Dye Purple 6X	B7024S	New England Biolabs	-20°C
GelRed Nucleic Acid Stain	41003-T	Biotium	RT
Geneticin (G-418)	11811-031	Gibco	RT
Iberose High Specification Agarose for Electrophoresis	AGR-100	Web Scientific	RT
InstantBlue – A Coomassie Based Staining Solution for Protein Gels	ISB1L	Expedeon	4°C
Iodoacetamide	I1149-25G	Sigma	4°C
LB Broth Lennox	BP1427-500	Fischer Scientific	RT
Leprechaun Exosome Human Tetraspanin Kit	251-1044	UnChained Labs	4°C
Luciferase Assay System	E1500	Promega	-20°C
Methanol gradient grade for liquid chromatography LiChrosolv® Reag. Ph Eur	1.06007.2500	Supelco	RT
miRCURY LNA miRNA Mimic_miR-99a-5p	339173	Qiagen	-20°C

miRCURY LNA miRNA Mimic_miR-223-3p miRCURY LNA miRNA Mimic_negative control			
Nitrocellulose membrane	1620115	Bio-Rad	RT
N,N,N',N'-Tetramethylethylenediamine (Temed)	T9281	Sigma	RT
*Not*I-HF restriction enzyme	R3189S	New England Biolabs	-20°C
NucleoSpin Gel and PCR clean-up	740609.50	Macherey-Nagel	RT
Opti-MEM (1x) + GlutaMAX 500 ml	51985-026	Gibco	4°C
Penicillin-Streptomycin	P4333-100ml	Sigma	-20°C
Plasma/Serum RNA Purification Mini Kit	55000	Norgen	RT
Phosphate Buffered Saline	LZBE17-516F / 15313581	Lonza / Corning	RT
Phosphoric acid	345245-100ML	Sigma	RT
Ponceau S	P3504	Sigma	RT
Prestained Protein Ladder – Broad molecular weight (10-245 kDa)	ab116028	Abcam	-20°C
Propan-2-ol	P749017	Fisher	RT
ProteaseMAX surfactant	V2071	Promega	-20°C
Proteinase K	P8107S	New England Biolabs	-20°C
ProteoSpinTM Abundant Serum Protein Depletion Kit	17300	Norgen	4°C
Protogel – 30% Acrylamide/Bis-acrylamidesolution (37.5:1 ratio)	A2-0072	Geneflow	RT
PsiCHECK-2 reporter plasmid	C8021	Promega	-20°C
Q5® High-Fidelity DNA Polymerase	M0491	New England Biolabs	-20°C
QIAamp DNA Mini Kit	51304	Qiagen	RT
QIAprep Spin Mini prep kit	27104	Qiagen	RT
Recombinant human TGFβ active protein	ab50038	Abcam	-80°C
RNaseZAP	R2020-250ML	Sigma	RT
Sequencing Grade Modified Trypsin	V5111	Promega	-20°C
Sodium Hydroxide (NaOH)	10010650	Fisher	RT

SuperSignal West Femto ECL	34094	Thermo Scientific	4°C
SYBR Safe DNA Gel Stain	S33102	Invitrogen	RT
T4 DNA Ligase	M0202S	New England Biolabs	-20°C
Total exosome Isolation (from urine) reagent	4484452	Invitrogen	4°C
Triethyl ammonium bicarbonate (TEAB)	T7408-100ML	Sigma	4°C
Trypan Blue stain 0.4%	T10282	Invitrogen	RT
Trypsin 10x	59427C-100ML	Sigma	-20°C
Trypsin Gold, Mass Spectrometry Grade	V5280	Promega	-20°C
Ultrapure DNase/RNase-Free Distilled Water	10977-835	Invitrogen	RT
*Xho*I restriction enzyme	R0146S	New England Biolabs	-20°C

2.1.2 Primary antibodies

Table 2.2. List of primary antibodies; Rb = rabbit, Ms = Mouse

Antigen	Antibody	Code	Company	WB dilutions
Alix	Rb polyclonal	Pab0204	Covalab	1:1000
Argininosuccinate synthetase 1 (ASS1)	Rb polyclonal	16210-1-AP	Proteintech	
CD63	Ms monoclonal	ab193349	Abcam	1:1000
Entactin (Nidogen 1)	Rb polyclonal	13766-1-AP	Proteintech	1:1000
Flotillin-2	Ms monoclonal	610383	BD Transduction Laboratories	1:5000
Ganglioside GM2 activator	Rb polyclonal	10864-2-AP	Proteintech	1:500
Glutamyl aminopeptidase (anti-ENPEP)	Ms monoclonal	CF504251	Origene	1:500
GS28 (E-7)	Ms monoclonal	Sc-133148	Santa Cruz Biotechnology	1:500
Mucin 1 (Anti-Hu CD227) Alexa Fluor 488	Ms monoclonal	53-9893-80	eBioscience (Invitrogen)	NA
Mucin 1	Rb monoclonal	ab109185	Abcam	1:1000
Muscleblind Like Splicing Regulator 1 (MBNL1)	Ms monoclonal	66837-1-Ig	Proteintech	
Podocalyxin	Rb polyclonal	18150-1-AP	Proteintech	1:500
Thromboxane A-Synthase	Rb polyclonal	PA5-102542	Invitrogen	1:500
Titin	Rb polyclonal	PA5-100211	Invitrogen	1:500
TOM20 (F-10)	Ms monoclonal	Sc-17764	Santa Cruz Biotechnology	1:100
Transglutaminase-2 (TG2) (CUB 7402)	Ms monoclonal	MA5-12739	Thermo Fisher	1:500
Vasorin	Rb polyclonal	PA5-98236	Invitrogen	1:1000

2.1.3 Secondary antibodies

Table 2.3. List of secondary antibodies; HRP = horseradish peroxidase

Secondary antibody for WB	Code	Company	Dilution
Goat anti-mouse IgG HRP	P0447	Dako	1:2500
Goat anti-rabbit IgG HRP	P0448	Dako	1:2500

2.1.4 Laboratory equipment

Table 2.4. List of laboratory equipment

Instrument	Company
AccuSpin Micro 17 centrifuge	Fisher Scientific
CLARIOstar plate reader	BMG LABTECH
Concentrator plus	Eppendorf
Countess 3 Automated Cell Counter	Invitrogen
Eppendorf refrigerated centrifuge 5417R, fixed-angle rotor FA-45-30-11	Eppendorf
Eppendorf refrigerated centrifuge 5804R, fixed-angle rotor FA-45-6-30	Eppendorf
EutechTM Elite pH Spear	Thermo Scientific
ExoView R200 reader	NanoView Biosciences / Unchained Labs
Grant QBT4 Heating Block	Grant
LAS4000 imaging system	GE Healthcare
Mini PROTEAN Gel casting system	Bio-Rad
Mini PROTEAN Tetra Cell	Bio-Rad
MSE Soniprep 150 Plus Ultrasonic Disintegrator & Continuous Flow, 120v	MSE
NanoDrop 8000	Thermo Scientific
Optima XPN-100 Ultracentrifuge, rotor 70.1 Ti	Beckman Coulter
Slimline LED Blue Light Transilluminator	Syngene
Thermo-Shaker PHMT-PSC24N	Grant-bio
U:Genius 3 Gel imaging system	Syngene
Water bath	Grant
ZetaView PMX 120	Particle Metrix

2.1.5 Plastic wares

Sterile tissue culture plastic (TCP) wares were supplied by either Sarstedt, Sartorius, StarLab, or Nest.

Sealing covers used for qPCR were supplied by Appleton Woods

S-trap columns were supplied by Protifi.

2.1.6 Companies

Table 2.5. List of companies

Company	Address
Abcam	Cambridge, UK
BD Biosciences	Oxford / Workingham, UK
Beckman Coulter	High Wycombe
Bio-Rad	Hemel Hempstead, UK
Covalab	Cambridge, UK
Dako	Glostrup, Denmark
Eppendorf UK	Stevenage, UK
Fisher Scientific	Loughborough, UK
Geneflow	Lichfield, UK
Invitrogen	Paisley, UK
Life Technologies	Paisley, UK
Lonza	Wokingham, UK
Melford	Ipswich, UK
New England Biolabs	Hitchin, UK
PlasmidsNG	Birmingham, UK
Promega	Southampton, UK
Proteintech	Manchester, UK
QIAGEN	Manchester, UK
Sarstedt	Leicester, UK
Sartorius Stedim	Epsom, UK
Scientific Laboratory Supplies	Nottingham, UK
Sigma-Aldrich	Dorset, UK
Thermo Scientific	Paisley, UK
Unchained Labs	Malvern, UK

2.2 Methods

This study adhered to high standards of safety practices, such as wearing personal protective equipment, including gloves and lab coats at all times during laboratory experiments, and safety glasses and masks when necessary. Furthermore, all chemicals, as well as biological materials used in this study, were carefully assessed in accordance with the Control of Substances Hazardous to Health (COSHH) and BioCOSHH regulations, and appropriate control measures were implemented. All work was carried out in a controlled environment (concerning biosafety levels 1 and 2).

2.2.1 Protein quantification

2.2.1.1. Bio-Rad protein quantification

Estimation of protein quantification from urinary extracellular vesicles was performed by Bio-Rad protein quantification assay, the colorimetric assay based on the Bradford method where the dye Coomassie brilliant blue G-250 binds to basic and aromatic amino acid residues and changes sample colour accordingly (Bradford, M.M., 1976). A standard curve of known protein concentrations was prepared by serial dilutions of bovine serum albumin (BSA) to 0.5 mg/ml, 0.4 mg/ml, 0.3 mg/ml, 0.2 mg/ml, 0.1 mg/ml and 0 mg/ml in RIPA lysis buffer, pH 7.2. Protein quantification was performed using the commercially available Bio-Rad Protein Assay Dye Reagent Concentrate (5000006, Bio-Rad), diluted in distilled water 1:5 and filtered through the 0.45 µl filter (Sartorius / Starlab). 200 µl of Bio-Rad Protein Assay Dye Reagent Concentrate was incubated with BSA standards and samples diluted in RIPA buffer to a final volume of 10 µl per well in a 96-well plate. After 5-10 minutes incubation at room temperature, the absorbance was measured at 595 nm on CLARIOstar plate reader. BSA standards and samples were measured in duplicates. The standard curve obtained from BSA standards was used to calculate the protein concentrations of unknown samples.

2.2.1.2. BCA protein quantification

Protein quantification from cell medium extracellular vesicles was estimated by copper-based Bicinchoninic acid (BCA) protein assay. This assay is based on monitoring the production of cuprous (Cu^+) ions as a result of the interaction of proteins with Cu^{2+} ions,

known as the biuret reaction. Bicinchoninic acid forms a complex with Cu^+ in an alkaline environment resulting in an intense purple colour that increases proportionally with the increasing protein concentration (Smith et al., 1985). Like the Bio-Rad assay, unknown protein concentrations were calculated from a BSA standard curve with known protein concentrations prepared by serial dilutions to 1 mg/ml, 0.75 mg/ml, 0.5 mg/ml, 0.25 mg/ml, 0.125 mg/ml and 0 mg/ml in RIPA lysis buffer, pH 7.2. BCA working solution consisting of BCA reagent A [1% (w/v) BCA, 2%(w/v) Na_2CO_3, 0.16% (w/v) NaK tartrate, 0.4%(w/v) NaOH, 0.95%(w/v) $NaHCO_3$] and BCA reagent B [4% (w/v) $CuSO_4$] in 50:1 ratio was prepared fresh just before applying to the standards and samples diluted in RIPA lysis buffer 1:5 to a final volume of 25 µl per well in a 96-well plate. 200 µl of BCA working solution was incubated with samples and standards for 30 minutes at 37°C covered from light. The absorbance was measured at 562 nm on CLARIOstar reader.

2.2.2 Western blot

2.2.2.1 Sample preparation

Protein samples were solubilised in 6x Laemmli buffer (360 mM Tris-HCl pH 6.8, 60% (v/v) glycerol, 12% (v/v) Sodium Dodecyl Sulphate (SDS), 30% (w/v) β-mercaptoethanol, 0.006% (w/v) bromophenol blue), boiled 10 minutes at 97°C in a heating block, cooled on ice and centrifuged for 14 seconds (short run) to collect all the proteins. Until the next day, the samples were stored at -20°C, and the following day heated again for 5 minutes before loading onto the gel. Laemmli buffer is usually used due to its several roles: to denature proteins into their individual polypeptide chains and make them all negatively charged by adding SDS to amino acid residues in order to separate proteins only according to their molecular weight (SDS component), to reduce intra- and inter-molecular disulfide bonds and so disrupt protein cross-links (2-mercaptoethanol component), to increase the density of the samples so that samples layer into the loading wells (glycerol component), to provide dye that runs ahead of the proteins and make the sample loading easier (bromophenol blue component), and to work in conjunction with the discontinuous buffer system (Tris-HCl pH 6.8 component) (Laemmli, U.K., 1970).

2.2.2.2 Sodium dodecyl sulphate – polyacrylamide gel electrophoresis (SDS-PAGE)

Protein samples were separated according to their size by denaturing SDS-PAGE. Gels which were 1.5 mm thick were prepared on a Bio-Rad Mini PROTEAN gel casting system. 10% resolving gel was prepared according to Table 2.6 and poured between Mini PROTEAN III glass plates until ~2 cm from the top. About 200 µl of 100% isopropanol was

added on top of the resolving gel in order to make a straight line after which the gel was left to polymerase until it was completely solid (~10 minutes). Isopropanol was then removed, and gel washed with distilled water. 5% stacking gel was prepared as described in Table 2.7 and poured on top of the resolving gel. A 10-well comb was immediately inserted to form the wells, and the gel was left for another 10 minutes to polymerise after which was moved to an electrophoresis chamber.

Table 2.6. Composition of one SDS-PAGE 10% resolving gel of acrylamide

Stock solution	Volume for 10% gel
30% Protogel (30% acrylamide/bisacrylamide solution – 37.5:1 ratio)	2.9 ml
4x Protogel resolving buffer (1.5 mM Tris HCl, 0.4% SDS, pH 8.8)	2.2 ml
Distilled water	3.5 ml
10% (w/v) ammonium persulphate (APS)	87.7 µl
N,N,N',N'-Tetramethylethylenediamine (TEMED)	12.5 µl

Table 2.7. Composition of one SDS-PAGE 5% stacking gel of acrylamide

Stock solution	Volume for 5% gel
30% Protogel (30% acrylamide/bisacrylamide solution – 37.5:1 ratio)	0.37 ml
4x Protogel stacking buffer (0.5 mM Tris-HCl, 0.4% SDS, pH 6.8)	0.57 ml
Distilled water	1.27 ml
10% (w/v) ammonium persulphate (APS)	22.5 µl
N,N,N',N'-Tetramethylethylenediamine (TEMED)	3.27 µl

The gel was placed in the buffer tank filled with running buffer (25 mM Tris-HCl, 192 mM glycine, 0.1% (w/v) SDS). The total amount of samples (40 µl), together with 3 µl of pre-stained protein ladder with known molecular weights (ab116028, Abcam), were loaded into the gel, and a voltage of 100 V was applied until the samples reached the stacking

gel after which the voltage was increased to 150 V. Electrophoresis run until the dye front reached the bottom of the gel (~1:30h).

2.2.2.3 Transfer

Following the protein separation by SDS-PAGE, proteins were transferred electrophoretically from the gel onto a nitrocellulose membrane with 0.45 µm pores (1620115, Bio-Rad) using a Bio-Rad Mini Trans-Blot wet blotting system (Bio-Rad). The transfer "sandwich" was assembled starting from the negative electrode side in the following order: fibre pad, 2 pieces of filter tissue, polyacrylamide gel, nitrocellulose membrane, 2 pieces of filter tissue, fibre pad. Prior to assembling the "sandwich", fibre pads, filter tissues and nitrocellulose membrane were pre-soaked in the transfer buffer (48 mM Tris, 39 mM Glycine, 0.0375% (w/v) SDS, 20% (v/v) Methanol). The "sandwich" was then placed in an appropriate tank filled with transfer buffer and containing the ice unit for cooling the system during the transfer. The constant current of 180 mA was applied and the transfer run for 70 minutes.

2.2.2.4 Ponceau red staining

After the transfer, the nitrocellulose membrane was immersed in red Ponceau S stain (0.1% (w/v) Ponceau S, 5% (v/v) glacial acid) for 10 minutes to visualise the protein bands. The excess Ponceau S stain was removed by rinsing with distilled water and completely washed in TBS-T (25 mM Tris-HCl, 150 mM NaCl, 2 mM KCl, 0.1% (v/v) Tween-20) before blocking. Ponceau S is an anionic diazo dye that reversibly stains proteins by binding to

positively charged protein amino groups as well as to nonpolar regions in the protein producing reddish pink protein bands with a clear background (Al-Amoudi et al., 2015).

2.2.2.5 Blocking and Immunoprobing

The membranes containing the transferred proteins were blocked by blocking solution (5% (w/v) fat-free milk powder in TBS-T) for 1 hour at room temperature on a shaker to prevent non-specific antibody binding. After the blocking step, the membranes were then probed with appropriate primary antibodies diluted in the blocking solution (Table 2.2). The incubation of membranes with primary antibodies was performed overnight at 4°C on the shaker. The following day, the membranes were washed 3 times with TBS-T (10 minutes each) and incubated for 2 hours with adequate HRP-conjugated secondary antibodies, diluted in the blocking solution (Table 2.3) at room temperature under constant shaking, and washed again 3 times with TBS-T.

2.2.2.6 Enhanced Chemiluminescence (ECL)

Immunoreactive bands on the membrane were detected using the EZ-Chemiluminescence Detection Kit for HRP (K1-0170, Geneflow) or SuperSignal West Femto ECL (34094, Thermo Fisher). Reagents A and B were mixed together in equal volumes depending on membrane size and incubated for 5 minutes in the dark. After placing the membrane on a dark tray in the LAS4000 imaging instrument (GE Healthcare), with the proteins facing up, the EZ-ECL mixture was uniformly applied on the membrane and left for 1 minute in the dark before measurement. Chemiluminescent images were

obtained with the LAS software, with exposure times ranging between 10 seconds and 16 minutes, depending on the experiment.

2.2.2.7 Stripping and re-probing

In order to remove antibodies, bound to specific proteins on the nitrocellulose membranes and to re-probe the same membranes with different antibodies, the nitrocellulose membranes were stripped with 0.5 NaOH for 8 minutes at room temperature with constant shaking. After 8-minute stripping, the membranes were washed 3 times with TBS-T (5 minutes each) and re-blocked in blocking solution for 1 hour, after which the membranes were immunoprobed as described in section 2.2.5.5.

2.2.2.8 Protein quantitation in Western blotting - Densitometric analysis

Intensities of immuno-reactive bands were measured and quantified using the image analysis software 2-D Densitometry AIDA (Advanced Image Data Analyzer) version 3.44. The principle of the software algorithm is to determine the signal density over the selected area, which in this case is the protein band. Then relative quantification is calculated by comparing the measured density to the background area, usually adjacent to the target band. The formula used to calculate the intensity of bands against loading control is:

Normalised protein expression = <u>Intensity/Area-bkg [a.u. / mm2] of protein of interest</u>

Intensity/Area-bkg [a.u. / mm2] of loading control

with bkg = background.

Normalised protein expressions were normalised to one control in each blot, to allow the comparison of blots performed at different times.

2.2.3 Coomassie staining

To assess the efficiency of abundant protein depletion from urine samples, samples were loaded (20 µg full urine and 20 µl depleted urine) on a 10% (v/v) polyacrylamide gel and run on the SDS-PAGE. Gel was stained with InstantBlue – A Coomassie Based Staining Solution for Protein Gels (ISB1L, Expedeon) for ~30 min and washed with dH2O for ~16 hours. While in acidic conditions, Coomassie dye binds to basic and hydrophobic residues of proteins, showing an intense blue colour. The gel image was taken on ImageQuant LAS 4000 biomolecular imager (GE Healthcare).

2.2.4 Mass spectrometry

2.2.4.1 MS analysis in two modalities: data-dependent acquisition (DDA) and data-independent acquisition (DIA)

Proteome is complex and requires pre-processing step followed by high-resolution separation which is coupled with high-resolution analyser instruments. Since proteins cannot be easily analysed, they must be digested by proteases such as trypsin to smaller peptides. The generated peptides are usually separated by chromatography, such as liquid chromatography (LC), which reduces the complexity of the sample (Escher et al., 2012).

All pre-processed samples were resuspended in the same volume of 30 µl of 5% (v/v) acetonitrile / 0.1% (v/v) formic acid, transferred to high-performance liquid chromatography (HPLC) vials and analysed by reverse-phase HPLC-electrospray ionization tandem mass spectrometry (RP-HPLC-ESI-MS/MS) using the TripleTOF 6600 mass spectrometer SCIEX (Canada). Liquid chromatography coupled to tandem mass spectrometry (LC-MS/MS) is the widely used and preferred method to identify and quantify proteins (Gillet et al., 2012). The data output of chromatographic separation is retention time (RT) specific to every peptide/protein which is used to support peptide identification by aligning LC peaks across acquisitions (Escher et al., 2012).

The mobile phases for the RP-HPLC were solvent A [2% (v/v) acetonitrile, 5% (v/v) DMSO in 0.1% (v/v) formic acid in LC/MS grade water] and solvent B [LC/MS grade acetonitrile containing 5% (v/v) DMSO and 0.1% (v/v) formic acid].

All MS instruments analyse a mass/charge ratio (m/z) therefore generation of ions is required for the analysis. Peptides are eluted into an electrospray ion source where they are dispersed in small, highly charged droplets. After the evaporation of solvent from the charged droplets, multiple charged ions of the analyte are produced and enter the mass spectrometer (Aebersold and Mann, 2003). Sequential use of ionization processes such as time-of-flight (TOF) technique enables obtaining information about peptide sequences and it is called tandem mass spectrometry (MS/MS). The first MS instrument filters the mass, collecting only the ions with mass of interest ("parent ions") and the second MS instrument analyses fragmentation products ("daughter ions") generated by collision with an inert gas, known as collision-induced dissociation (CID) (Yinon, 1990; Domon and Aebersold, 2006).

The mass spectrometer was used in two different modalities: shotgun data-dependent acquisition (DDA) employed for spectral library construction, and Sequential Window Acquisition of all Theoretical Mass Spectra (SWATH) - data-independent acquisition (DIA) employed for the acquisition of quantitative data. Because thousands of proteins and even more peptides after trypsin digestion can be eluted at a given time during HPLC separation, protein detection by shotgun proteomics requires mass spectrometer scheduling peptide fragmentation events based on the peptide mass and intensity information in the MS spectra (Graumann et al., 2012). This results in creating MS/MS scans reflecting on precursor isolation and fragmentation events. The software operating the mass spectrometer sorts precursor ions detected in each MS scan by intensity. To select precursors for fragmentation, the software applies certain filters for example

minimum signal intensity, charge state, avoidance of already fragmented precursors, as well as inclusion and exclusion lists of certain peptide masses (Graumann et al., 2012). The principle of the DIA method is based on collecting accurate high-resolution mass fragment ion spectra throughout the user-defined chromatographic retention time (elution range) by sequentially cycling through 40 discrete 25-Da wide precursor isolation windows (swats) in the user-defined space, for example, 400 – 1200 m/z range. (Gillet et al., 2012).

For the construction of a spectral library using DDA the single injection of 4 µl of each sample was injected by autosampler (Eksigent nanoLC 425 LC system) at 5 µl/min onto a YMC Triart-C18 column (25 cm x 2µm, 300 um i.d pore size), using an increasing linear gradient elution of solvent B over solvent A going from 2% to 40% in a total time of 120 min. This was followed by single injection of 4 µl per sample and linear gradient elution in a total time of 60 min for SWATH/DIA analysis. Regeneration and re-equilibration of the column were performed by loading 90% solvent B for 10 min and 5% solvent B for 10 min. Auto calibration was performed by the MS every 4 samples using an injection of a standard of 25 pmol β-Galactosidase digest. The electrospray ionisation, then, was carried out using PicoTip® nanospray emitters uncoated SilicaTips™ (New Objective Inc., USA), with voltage set to +2400 V.

The spectral library was constructed on all samples singularly and a pool of all samples together, with the high sensitivity setting, by using the output from ProteinPilot 5.01 (SCIEX, Canada) searching against the Swissprot human database (June 2021). All generated DDA files were pooled together and aligned to the SWATH data file using

PeakView 2.1 SWATH microapp (SCIEX, Canada) as an ion library and spiked in indexed retention time (iRT) peptide standards (Biognosys, Switzerland), after filtering for false discovery rate (FDR) of 1% and excluding shared peptides. The false discovery rate (FDR) was set to 1% and the peptide length was set to 7-30 amino acids.

Spectral alignment and targeted data extraction from the SWATH data was performed in PeakView 2.0 using the reference spectral library generated by DDA. SWATH data was processed using an extraction window of 5 min and applying the following parameters: maximum 6 peptides/protein, maximum 6 transitions, peptide confidence of >99%, exclude shared peptides, and XIC width set at 75 ppm.

All MS runs were performed by Dr David Boocock and Dr Clare Coveney at NTU proteomic facility in John Van Geest Cancer Research Centre. This thesis' author carried out sample processing and data analysis.

2.2.4.2 Processing and bioinformatic analysis of proteomic data

Venn diagrams were created using the Venny 2.0 online resource (https://bioinfogp.cnb.csic.es/tools/venny/index.html) in order to compare the numbers and content of uniquely identified and matched proteins from shotgun proteomics between the comparable groups.

Proteins detected in uEVs samples were compared against the Vesiclepedia database which contains an updated list of all proteins already reported in EVs. This was done using the feature in FunRich (Functional Enrichment Analysis Tool) software (http://www.funrich.org/).

Volcano plots, graphically showing the amount and/or identity of significantly overexpressed and underexpressed proteins, were created using ggplot2 package in R statistical software.

Heat maps, like Volcano plots, show all proteins significantly increased or decreased in tested groups but with the expression of each protein shown per individual sample. These were created in Morpheus versatile matrix visualization and analysis software (Morpheus, https://software.broadinstitute.org/morpheus).

Cellular compartment analyses were done using PANTHER (Protein Analysis THrough Evolutionary Relationships, http://pantherdb.org) online resource, and pie charts of the analyses were created in Excel.

Protein-protein interaction network of significantly differentially expressed proteins in one over the other comparable group (for example progressive DN vs stable DN) was visualized by String: Functional protein association network (free access at https://string-db.org). Pathway enrichment analysis in uEVs sample type was done by Kyoto Encyclopedia of Genes and Genome Pathways (KEGG) system, integrated within the String database.

2.2.5 Cell culture

2.2.5.1 Cell line and culture growth conditions

In-vitro experimental work was performed using the commercially available human kidney cell line HK-2 (human kidney 2), immortalized by transduction with human papilloma virus 16 (HPV-16), therefore it is classified as biosafety level 2.

HK-2 cells were grown in Dulbecco's modified Eagle's medium with Ham's F-12 Nutrient Mixture (DMEM/F12) 1:1, containing 4.5 g/L glucose and L-glutamine with or without 15 mM HEPES, and supplemented with 10% (v/v) filtered (0.2 μm) heat-inactivated Foetal Bovine Serum (FBS), 2 mM L-glutamine (if the opened bottle is older than 1 month), 100 IU/mL penicillin and 100 μg/mL streptomycin (1%). Such medium composition is considered and referred to as complete medium.

2.2.5.2 Cell passaging and counting

All sterile solutions used for cell culture were pre-warmed at 37°C. Cells were usually passaged at 70-90% confluency. Cell monolayers were washed with sterile PBS pH 7.4 [137mM NaCl, 2.7 mM KCl, 10 mM Na_2HPO_4, 1.8mM KH_2PO_4] and incubated with filter sterilised (0.2 μm) trypsin/EDTA [0.25% (w/v) trypsin, 2 mM EDTA in PBS] for 5 min at 37°C. After 5 minutes of incubation, cell detachment was facilitated by gently tapping the flask. Three to four volumes of complete medium were then added to the flask to inactivate the trypsin and to resuspend and collect as many as possible cells from the flask. Cell suspension was transferred to a 15 ml tube and cells were pelleted by centrifugation at 300 x g for 5 min. Cell pellet was resuspended in 1 ml complete medium

and the desired dilution of cells was re-seeded in a new flask containing fresh culture medium.

Cells were counted by staining homogeneously mixed cell suspension with 0.4% Trypan blue (T10282, Invitrogen) 1:1 and loading 10 µl of the stained cell suspension in each side of the Countess cell counting chamber slide (through capillary action), which was then inserted into the Countess 3 Automated Cell Counter (Invitrogen) set on a brightfield count in order to be able to distinguish live from dead cells. The mean value of the live cells was calculated from the live cell counts on each side of the counting slide.

2.2.5.3 Cryopreservation of cells and resuscitation of frozen cells

A cell pellet of ~1-2 million cells was cryopreserved by centrifuging the cell suspension at 300 x g for 5 min after trypsinization, as described in 2.2.5.2. The entire supernatant was carefully removed, and the pellet resuspended in 1 ml of freezing media consisting of sterile FBS and 10% dimethyl sulfoxide (DMSO). Cells resuspended in freezing medium were transferred to sterile cryovials and slowly frozen by wrapping the cryovials in a thick layer of tissue roll and placing at -80°C before transferring to liquid nitrogen for long-term storage in order to limit cell death due to thermal shock.

Thawing of frozen cells, on the other hand, was done quickly by placing the frozen cryovial directly at 37°C. Once defrosted, cells were recovered by transferring the volume of cell suspension into 5 ml of pre-warmed complete medium and centrifuging at 300 x g for 5 min. The medium was removed, and the cell pellet was resuspended in fresh

complete medium and transferred to a T25 or T75 flask with medium. The medium was changed the day after to completely remove DMSO.

2.2.5.4 Mycoplasma detection

Mycoplasma test was done using EZ-PCR Mycoplasma Test Kit (Biological Industries) following the protocol instructions. Briefly, 1 ml of conditioned cell medium was collected from the cell culture that stayed in culture for at least 48 hours after the last media change and centrifuged at 200 x g for 1 min to pellet cell debris. The supernatant was transferred to a new tube and centrifuged at 20,000 x g for 10 min. The pellet (which could be invisible) was resuspended in 25 μL of provided buffer solution and heated to 97°C for 3 min using a heating block. At this point, samples were stored at -20°C until ready for PCR processing (1-3 days). The PCR reaction mixture was prepared for the samples and positive control, which was provided by the kit, as well as for a negative control where distilled H2O was used instead of sample/positive control. PCR was performed on the T100 Thermal Cycler (Bio Rad) using the program shown in table 2.8.

Table 2.8 PCR program for mycoplasma amplification

Step	Temperature	Duration	
Initial denaturation	94°C	30 sec	
Denaturation	94°C	30 sec	⎫
Annealing	60°C	120 sec	⎬ 35 cycles
Extension	72°C	1 min	⎭
Denaturation	94°C	60 sec	
Annealing	60°C	120 sec	
Final extension	72°C	5 min	

Amplified PCR products were run on gel electrophoresis using 2% (w/v) agarose in TAE buffer (40 mM Tris, 20 mM 100% glacial acetic acid, 1 mM EDTA, pH 8) agarose gel containing 1:10,000 1X SYBR Safe (Invitrogen) and loading 20 µl of the unstained samples together with 100 bp DNA ladder (Promega). Electrophoresis ran at constant voltage of 120 V for about 30-45 min. The result was visualized on the UV transilluminator (Syngene).

Mycoplasma test was interpreted as negative when samples showed only one 357 bp band compared to positive control that showed double bands: at 357 bp and 270 bp where mycoplasma would appear. No bands were present in negative control.

2.2.5.5 Cell lysate preparation

Cell lysate preparation was done for the purpose of immunoblotting for the proteins from HK2 cells. Confluent cell monolayers or about 1 million cells were trypsinized and spun down as explained in 2.2.5.2 and cell pellet was resuspended in 100 µl RIPA lysis buffer, supplemented with 1:100 protease inhibitors (Sigma) and sonicated three times for 30 s with 1 minutes break on ice, using a probe sonicator to lyse the cells. Upon sonication, cell pellets were incubated on ice for 20 minutes followed by centrifugation at 1,000 x g for 5 min to pellet cells debris. The total proteins were recovered from the supernatant. Protein quantification was done by BCA assay as explained in 2.2.1.2, and the desired amount of protein was diluted in 6x Laemmli buffer, boiled for 10 min at 97°C and stored at -20°C until the electrophoresis.

2.2.6 Molecular biology

2.2.6.1 In-house method of gDNA extraction from human kidney epithelial cells (HK2)

Genomic DNA was extracted from the human cell line to be used as a template for PCR amplification of the 3'UTR sequence of the MBNL1 gene. All used solutions were freshly prepared and sterilized by autoclaving.

Cells from the one confluent T175 flask were washed with sterile PBS, trypsinized, and counted as explained in 2.2.5.2. Cell pellet containing 1.125×10^7 cells was washed with PBS and resuspended in 3 ml of lysis buffer [10 mM Tris-HCl pH 8.2, 400 mM NaCl, 2 mM EDTA pH 8.2], 0.2 ml of filter-sterilized 10% SDS, and 0.5 ml of molecular biology grade proteinase K (P8107S, New England Biolabs). Resuspended cell pellet was then incubated overnight at 37°C. At the end of incubation, 1 ml of saturated NaCl (~5 M) was added, vortexed for 15 seconds and centrifuged at 1200 x g for 15 minutes. After centrifugation, the supernatant was transferred into a new 15 ml tube and 2 volumes of 100% ethanol (molecular biology grade) was added. Tube was slowly inverted several times, and a thread of DNA appeared which was collected with a tip and placed in an Eppendorf tube. DNA was dissolved in 200 µl TE buffer [10 mM Tris-HCl, 0.2 mM EDTA pH 7.5, final pH 8.2] and incubated at 37°C overnight.

2.2.6.2 Commercial method of gDNA extraction

As an additional approach, genomic DNA was extracted using the commercial QIAamp DNA Mini Kit (51304, Qiagen) according to the QIAamp DNA Mini Blood Mini handbook. Briefly, cell pellet from 5×10^6 HK2 cells was resuspended in 200 µl PBS, and

supplemented with 20 µl proteinase K. The provided lysis buffer was pre-warmed at 56°C and 200 µl was added to the sample, after which sample was vortexed for 15 seconds and incubated in a water bath at 56°C for 10 minutes to increase DNA yield.

Following lysis, 200 µl of 100% molecular biology grade ethanol was added to the sample, which was then transferred to QIAamp Mini spin column, and centrifuged at 6000 x g for 1 min. Samples were washed with 500 µl of provided buffers AW1 and AW2 which were removed by centrifuging again at 6000 x g for 1 min. To dry the column, empty column was centrifuged at full speed for 1 min.

DNA was incubated for 5 min with the provided elution buffer AE, and eluted in 200 µl by centrifuging at 6000 x g.

Quality control and concentration of the extracted gDNA was assessed by NanoDrop 8000 spectrophotometer.

2.2.6.3 Amplification of 3'UTR sequence from gDNA by classic PCR

Having designed primers for the 3'UTR sequence from MBNL1 gene (2618 bp), this product was amplified by classic PCR using T100 Thermal Cycler (Bio Rad) for the purpose of cloning it as an insert into the reporter plasmid for the downstream luciferase reporter assay. The PCR reaction consisted of 50 ng of gDNA used as a DNA template, 0.5 µM forward and reverse primers, 200 µM dNTPs (N0447S, New England Biolabs), 0.02 U/µl Q5 High Fidelity DNA Polymerase (M0491, New England Biolabs) with supplied 1x Q5 reaction buffer, in a total reaction volume of 50 µl. The thermocycling program is shown in table 2.9. The annealing temperature of designed primers was determined using the

Tm Calculator on the New England Biolabs website which considers type of the polymerase, concentration of the primers, and primer sequences. Only the part of primer sequence complementary to DNA template was considered for determining the annealing temperature (without added sequence for the restriction enzyme binding site and dummy bases). The formula used was Ta = Tm_lower + 1°C, where Ta stands for annealing temperature and Tm_lower for the melting temperature of the primer which has lower value.

Table 2.9: PCR program for amplifying 3'UTR sequence of MBNL1 gene

Step	Temperature	Duration	
Initial denaturation	98°C	2 min	
Denaturation	98°C	10 sec	
Annealing	64°C	30 sec	35 cycles
Extension	72°C	1.5 min	
Final extension	72°C	2 min	
Hold	4°C		

Amplified PCR products were loaded onto 1% (w/v) agarose (AGR-100, Web Scientific) gel in 1x TAE (Tris-acetate-EDTA) buffer (40 mM Tris, 20 mM 100% glacial acetic acid, 1 mM EDTA pH 8) containing 1:10,000 GelRed Nucleid Acid Stain (41003-T, Biotium). Both 1kb DNA ladder (N3232S, New England Biolabs) and PCR samples were mixed with Gel Loading Dye Blue 6x (B7021S, New England Biolabs) and nuclease-free water and loaded onto a gel: 6 µl of ladder (1 µl ladder, 1 µl dye, 4 µl water) and 12 µl of samples (5 µl PCR

product, 2 μl dye, 5 μl water). The electrophoresis ran for ~1 hour at 80-100 V. The result was visualized on the UV transilluminator (Syngene).

2.2.6.4 Gel excision and purification

Once the desired PCR product was amplified and its molecular weight was confirmed by diagnostic agarose-gel electrophoresis, the entire remained PCR product from 50 μl PCR reaction was run again on the 1% agarose gel electrophoresis for 1.30 h in order to be purified from the remaining reaction components (polymerase, primers, dNTPs, unspecific products). In order to be able to load entire PCR product into the same well, 3 wells of the comb were connected to create a larger well in the gel. All the equipment for agarose gel electrophoresis was washed with 1% SDS prior to running the PCR sample. A strong DNA bend at the right molecular weight was visualized using the Syngene Slimline LED Blue Light Transilluminator and was excised with a newly open scalper. The bend was purified from the gel using the NucleoSpin Gel and PCR clean-up kit (740609.50, Macherey-Nagel) according to the provided protocol. In brief, the sample was mixed with 200 μl of NTI buffer (30-60% guanidinium thiocyanate) per 100 mg of sample and incubated at 50-60°C until gel was fully melted (~10 min). Melted sample was then added to the column and centrifuged at 11,000 x g for 1 min. This was followed by the two wash steps with ethanol-based NT3 buffer, at the same centrifugation speed. Sample was eluted twice with EB buffer (5mM Tris/HCl pH 8.5). The first elution was in total volume of 20 μl, and the second elution in 15 μl. Concentration and purity of the gel-purified PCR product were measured by NanoDrop 8000 spectrophotometer.

2.2.6.5 Digestion of the 3'UTR insert and psi-CHECK2 plasmid

PsiCHECK-2 reporter plasmid (C8021, Promega) was kindly donated by Dr Christos Polytarchou. Both 3'UTR insert, and the reporter plasmid were digested using the restriction enzymes *Not*I_HF (R3189S, New England Biolabs) and *Xho*I (R0146S, New England Biolabs). Digestion reactions for both insert and plasmid are shown in table 2.10. In both reactions, the amount of total glycerol from restriction enzymes did not exceed 5% in order to avoid star activity. Digestion reactions were performed for 1.5 h at 37°C in water bath after which reactions were immediately loaded on 1% agarose gel and run for 1.5 h. Two wells of the comb were joined together to load entire volume of samples (60 µl insert and 30 µl plasmid) and bends were excised and purified as explained before in 2.2.6.4.

Table 2.10: Digestion reactions for insert and plasmid

Digestion reaction of 3'UTR insert	Digestion reaction of psiCHECK2-reporter plasmid
• 0.6 µg insert (29 µl) • 2 µl *Not*I_HF restriction enzyme • 2 µl *Xho*I restriction enzyme • 5 µl rCutSmart buffer • 12 µl nuclease free water	• 1 µg plasmid (0.35 µl) • 1 µl *Not*I_HF restriction enzyme • 1 µl *Xho*I restriction enzyme • 2.5 µl rCutSmart buffer • 20.15 µl nuclease free water
Total volume = 50 µl	**Total volume = 25 µl**

2.2.6.6 Ligation of the 3'UTR insert into the psi-CHECK2 plasmid

Digested and gel-purified sequences of 3'UTR MBNL1 insert and psiCHECK-2 plasmid underwent ligation reaction in a molar ratio 1:3 (plasmid:insert). The molar ratios were calculated using the NEBioCalculator from the following formula:

Moles dsDNA = mass of dsDNA (g) / MW of dsDNA (g/mol) from where MW of dsDNA is calculated as:

MW dsDNS = (number of bp of dsDNA x average molecular weight of a base pair) + 36.04 g/mol. The average molecular weight of a base pair is 615.96 g/mol, excluding the water molecule removed during polymerization and assuming deprotonated phosphate hydroxyls. The 36.04 g/mol accounts for the 2 -OH and 2 -H added back to the ends. So, the final formula is:

Moles dsDNA (mol) = mass of dsDNA (g) / ((length of dsDNA (bp) x 615.96 g/mol/bp) + 36.04 g/mol).

To calculate the mass of the insert needed for the ligation reaction, the following formula was used:

Required mass insert (g) = desired insert/vector molar ratio x mass of vector (g) x ratio of insert to vector lengths

The volume of ligation reaction was 20 μl of which 13 μl was insert (corresponding to 187.8 ng and 0.2329 pmol), 4 μl was plasmid (corresponding to 150 ng and 0.077 pmol), 2 μl T4 ligase buffer (10x) and 1 μl T4 ligase (M0202S, New England Biolabs). Ligation

reaction was performed overnight at ~16°C in a water bath after which reaction was stored at -20°C.

2.2.6.7 Bacterial transformation

Bacterial transformation was performed in order to produce multiple copies of a recombinant plasmid DNA. Fresh LB agar petri plates were prepared using 2% Luria-Bertani (LB) Broth Lennox (BP1427-500, Fisher Scientific) [1% (w/v) tryptone, 0.5% (w/v) yeast extract, 0.5% (w/v) NaCl] and 1.5% agar (LP0012, Oxoid) in Miliq DI water, as well as 2% LB medium without agar. Both preparations were autoclaved. Fresh Ampicillin (A0166-5G, Sigma Aldrich) stock was prepared in concentration 100 mg/ml in Miliq water, and filter sterilized close to the bunsen. Soon after autoclaving finished, LB media were collected, allowed to cool to ~55°C and supplemented with Ampicillin in a total concentration 100 µg/ml, and poured in petri-dish, 25 ml LB agar per 100 mm petri plate. Bacterial transformation work was performed close to the bunsen. DH5α *E. coli* bacterial competent cells (EC0112, Invitrogen) were taken from -80°C immediately before using them and kept on ice. From one ligation product which was in volume of 20 µl, two transformation reactions were conducted:

- 5 µl of ligation reaction in 50 µl DH5α bacterial cells

- 10 µl of ligation reaction in 100 µl DH5α bacterial cells

The mixtures of ligated product (recombinant plasmid DNA) with bacterial cells were kept on ice for 30 min, followed by a heat-shock at ~42°C in water bath for 40 seconds, and then transferred again on ice for 2 minutes. Transformed reactions were

supplemented with pre-warmed (at 37°C) LB medium without ampicillin to final volume of 1 ml and incubated for 1 hour at 37°C with shaking at 200 rpm.

Each transformed bacteria preparation was plated in 3 conditions:

- 50 μl plated without centrifuging

- 200 μl plated without centrifuging

- Remained 750 μl centrifuged at 2000 rpm for 5 min, 500 μl removed and 100 μl concentrated product plated

Transformed reactions were distributed on the solid agar plates using sterile glass beads close to the Bunsen. Plates were kept at 37°C without shaking for ~40 min and then turned upside down (lid at the bottom) to avoid condensation and incubated for ~24 hours.

2.2.6.8 Miniprep

Total of eight colonies appeared on the Petri dish. All of them were collected with a tip and added to 50 ml tubes containing 5 ml of pre-warmed LB medium supplemented with freshly prepared ampicillin to a final concentration of 100 μg/ml. Lids were not very tightly closed to allow some air. Tubes with bacteria were incubated at 37°C with shaking at 250 rpm overnight (~17 h). The following day plasmids were isolated from the bacteria using QIAprep Spin Mini prep kit (27104, Qiagen) according to the manufacturers protocol, which is based on alkaline lysis of bacterial cells using RNase A-containing buffer P1 and buffer P2, then neutralizing buffer N3. The alkaline lysis principle was explained in Bimboim and Doly, 1979. Basically, high molecular weight chromosomal

DNA is denaturised while plasmid DNA remains double stranded. In the neutralization step with acidic sodium acetate, chromosomal DNA renatures and forms an insoluble network which is removed by centrifugation, while plasmid DNA stays in the supernatant. Bacterial lysis is followed by selective adsorption of plasmid DNA onto silica in the presence of high salts. Salts are removed with washing steps using ethanol-containing buffer PE and the plasmid DNA was eluted in 50 µl of a low-salt buffer EB. All centrifugation steps were done at 13,000 rpm (17,900 x g).

Concentration and purity of the eluted recombinant plasmid DNA from 8 mini preps were assessed by NanoDrop 8000 spectrophotometer.

2.2.6.9 Diagnostic digestion

Recombinant plasmid DNAs from all 8 colonies were tested by diagnostic digestion in order to confirm if the molecular cloning was successful. Digestion of recombinant plasmid DNA with the restriction enzymes *Not*I and *Xho*I should result in 2 bends: 1 corresponding to the insert (2618 bp) and 1 corresponding to the plasmid vector (6273 bp). Digestion reaction consisted of 1 µg of recombinant plasmid DNA, 0.5 µl of *Not*I_HF restriction enzyme, 0.5 µl of *Xho*I restriction enzyme, 1 µl rCutSmart buffer and the MiliQ water to the total reaction volume of 10 µl. Digestion reaction was performed for 1h at 37°C in a water bath. After digestion, 500 ng of DNA (5 µl of reaction) from all 8 preparations were loaded on the 1% agarose gel and run for ~2 h at 80-90 V.

2.2.6.10 Recombinant plasmid DNA sequencing

Recombinant plasmid DNA from two miniprep preparations, selected based on the highest DNA concentration were sent for sequencing to PlasmidsNG, UK company to verify the recombinant sequence. Before sending, DNA samples were diluted in nuclease-free water to a final concentration of 100 ng/μl in a total volume of 15 μl, pipetted into the strip PCR tubes which were labelled with a given registered project code, and placed in 50 ml tube in which were shipped the same day at RT. In the company, the long-read sequencing using the latest R10.4.1 chemistry from Oxford Nanopore Technologies was performed, which is a single molecule sequencing based on nanopores. The reaction is carried out in a flow cell which contains membrane with nanopores. On each side of the membrane is solution with applied cathode or anode. DNA molecules are placed in the side with a cathode and after applying electrophoretic force, DNA passes through the nanopores. Single nucleotides are captures and analysed on a computer-linked tools (Lin et al., 2021).

Sequenced data were received in fastq format. SnapGene software was used to open and download the sequence in fasta format. The sequence of the recombinant plasmid was aligned to the sequence of the 3'UTR MBNL1 insert using BLAST NCBI online tool to check for the potential mutations within 3'UTR insert.

2.2.6.11 Transient co-transfection of the HK2 cells with recombinant plasmid and miRNAs

For the purpose of 3'UTR luciferase reporter assay, recombinant reporter plasmid containing the 3'UTR sequence of MBNL1 gene was co-transfected with miRCURY LNA miRNA Mimic_miR-99a-5p (339173, Qiagen) and miRCURY LNA miRNA Mimic_miR-223-3p (339173, Qiagen) targeting the 3'UTR region of MBNL1 gene, as well as with miRCURY LNA miRNA Mimic_negative control (339173, Qiagen) into HK2 cells. Transient co-transfection was done by liposome-based method using Lipofectamine 3000 (L3000-008, Invitrogen). Cells were trypsinized, counted and 10-15,000 cells were seeded into 96-well plate 24 hours prior transfection. After 24h media was changed to 65 µl fresh DMEM/F12 containing 10% FBS, 1% GlutaMAX, but no antibiotic to avoid increased cytotoxicity during transfection, and co-transfection was done directly on the adherent cells. 0.3 µl/well of Lipofectamine 3000 reagent was mixed with 5 µl/well OptiMEM media (51985-026, Gibco). In a separate tube, 10 µl OptiMEM media was mixed with 100 ng/well recombinant plasmid DNA and 5 nM/well miRNA mimic. Two tubes were mixed 1:1 ratio and incubated for 10-15 minutes after which 10 µl of DNA-lipid complex was added in each well, making total volume of 75 µl/well. The principle is based on cationic lipid forming a complex – Lipoplex with negatively charged nucleic acids. Such complex then interacts with negatively charged cell membrane, enters the cell via endocytosis, and free the nucleic acid inside the cell (Vegas and Anderson, 2012; Akinc et al., 2008). Transfected cells were incubated for 24 hours before proceeding with the 3'UTR luciferase reporter assay.

2.2.7 Power analysis

In order to decide on the cohort size for the experiment, the *A priori* power analysis was conducted using the G*Power 3.1 software (Erdfelder et al., 1996) and applying the One-way ANOVA statistical test. The input parameters were: α error probability also known as type I error probability = 0.05, power (or 1 - β error) also known as Type II error probability = 0.95, number of groups = 2 to 4 (depending on an experiment), and the effect size value was calculated based on the data from the previous small cohort size pilot experiments, using the weighted mean values of each group and standard deviation within each group. Standard deviation within each group was calculated by the following formula (Kang, 2021):

$$S_{pooled} = \sqrt{\frac{(n_1 - 1)S_1{}^2 + (n_2 - 1)S_2{}^2 + (n_3 - 1)S_3{}^2 + (n_4 - 1)S_4{}^2}{((n_1 - 1) + (n_2 - 1) + (n_3 - 1) + (n_4 - 1) - 4)}}$$

where n is number of samples in each group and S is standard deviation of each group.

However, due to the limited availability to patient samples, 95% power couldn't be achieved, therefore the *Post hoc* power analysis was applied with the effect sizes calculated from the main experiment's data to determine the actual power of an experiment when the maximum possible sample sizes were used.

2.2.8 Statistical analysis

Statistical analysis was performed using GraphPad Prism 8 and 9 software (GraphPad, Inc, USA). Data are represented as mean ± SD from at least three independent experiments. In general, data were normally distributed which was determined by running normality test, so parametric statistical tests were applied: two-tailed t-test for comparing two groups, one-way ANOVA when comparing more than two groups, or two-way ANOVA when comparing more than two groups with two different parameters. Tests for multiple comparison correction were applied where indicated, usually when the risk of false negative findings was low. Usually default recommended multiple comparison test was selected (Tukey or Sidak). For omics data, Benjamini Hochberg adjustment of p-values was applied. A difference was considered significant if $p < 0.05$ or adjusted $p < 0.05$ and showed by asterisks.

CHAPTER 3:

Comparison of urine and uEVs proteomics for biomarker discovery

3.1 Introduction

3.1.1 What is an ideal biomarker?

There are various definitions of the term biomarker (biological marker). The "National Institutes of Health (NIH) Biomarkers Definitions Working Group" define a biomarker as "A characteristic that is objectively measured and evaluated as an indicator of normal biological processes, pathogenic processes, or pharmacologic responses to a therapeutic intervention" (Biomarkers Definitions Working Group, 2001). However, the question is, what makes a good, if not ideal, biomarker? From the pharmaceutical industry point of view, a good biomarker must be present in peripheral body tissue or fluid, must be easily detectable and quantifiable by affordable and robust tests, and must be as specific as possible within a damaged tissue (Biomarkers on a roll, 2010). An ideal biomarker must be also highly sensitive enabling early diagnosis, should produce rapid results, and be unaffected by comorbid conditions. Ideally, the levels of biomarkers should rapidly change upon treatment to allow application in drug development/clinical trials and provide insight into the underlying mechanism of the disease (Bennett and Devarajan, 2017).

3.1.2 Urine as a source of biomarkers

Urine is an attractive source of biomarkers because it mirrors body changes and can be collected non-invasively in large quantities (Harpole et al., 2016). Among urinary proteins proposed as biomarkers of kidney disease, uromodulin (Prajczer et al., 2010), kidney

injury marker 1 (KIM1) (van Timmeren et al., 2007), and neutrophil gelatinase associated lipocalin (NGAL) (Viau et al., 2010) have been named in the early days. Further advances in high-throughput technologies and mass spectrometry techniques have enabled improvements in urine proteome analysis (Fliser et al., 2007; Van et al., 2017), resulting in an increased number of studies reporting panel of urinary proteins significantly differentially expressed in CKD compared to healthy controls (Vivekanandan-Giri et al., 2011; Jin et al., 2012; Fan et al., 2021). However, the urinary proteome can be very variable as affected by many physiological factors such as age, gender, nutrition, exercise (Shao et al., 2019; Feng et al., 2023). A number of studies has reported intra- and inter-individual variation in the urinary proteome (Shao et al., 2019; Guo et al., 2015; Nagaraj and Mann, 2011). However, urinary peptide detection can be robust, reproducible and promising for clinical implementation (Mavrogeorgis et al., 2021). A urinary biomarker panel known as CKD273 peptide classifier, consisting of 273 naturally occurring peptides from 30 proteins in human urine, was discovered by capillary electrophoresis–mass spectrometry and used for discriminating CKD from unaffected individuals (Good et al., 2010). The CKD273 peptide classifier, as well as more recently developed CKD273 sub-classifier (Rodríguez-Ortiz et al., 2018) has shown potential utility and application for predicting CKD progression (Roscioni et al., 2013; Critselis and Lambers, 2016). When CKD273 peptide classifier was compared with urinary albumin excretion rate (UAE) in terms of identifying progressing patients, in the early stage of CKD it outperformed UAE measure for estimation of disease progression, however in the late CKD stages with significant kidney damage, UAE was more effective (Pontillo et al., 2017). In addition,

CKD273 could identify diabetic patients likely to progress to CKD, independently on albuminuria and eGFR (Zürbig et al., 2019). The composition of the CKD273 panel is mostly made of peptides from collagens and abundant plasma proteins (Good et al., 2010; Rodríguez-Ortiz et al., 2018), so the prediction of progressing patients is based on attenuated degradation of collagens leading to fibrosis, which is a hallmark of CKD, and increase of plasma proteins in urine as a result of kidney damage in DN type of CKD (Zürbig et al., 2019).

Urinary proteins (Santiago-Hernandez et al., 2021), as well as urinary N-glycoproteins (Santiago-Hernandez et al., 2024), can predict early renal and vascular damage, discriminating patients with higher cardiorenal risk, a stage that requires active therapy. A set of urinary proteins have also been shown to discriminate patients with severe focal segmental glomerulosclerosis (FSGS) from mild FSGS and minimal change disease (MCD) (Chebotareva et al., 2022). A study on diabetic kidney disease (DKD) has shown urinary proteins that could distinguish DKD from diabetes, stage 3 from stage 4 of DKD, and early stage 3 DKD from diabetes (Fan et al., 2021). These were albumin, afamin, annexin A7, apolipoprotein D, complement C9, Plasma serine protease inhibitor, vacuolar protein sorting-associated protein 4A, ceruloplasmin, and serotransferrin.

Clearly among the potential biomarkers emerged from these studies many were abundant plasma proteins, which do not reflect much on pathological changes of kidney cells and kidney tissue and hence could not provide insights into mechanisms of disease.

3.1.3 uEVs as a source of biomarkers

It is highly important to determine whether urinary molecules can be detected with sensitivity and specificity to aid in the early diagnosis and prognosis of kidney disease. As most urinary proteins such as albumin and IgG are filtered from the blood, they are qualitatively similar to the abundant plasma proteins (Spahr et al., 2001). Due to their high concentration in pathology, they significantly interfere with the detection of other rare urinary biomarkers (Filip et al., 2015), greatly reducing the sensitivity of the approach. Instead, EVs, which can be isolated from urine and reflect cellular changes in pathology, may provide a more sensitive platform for biomarker discovery. Therefore, EVs molecules may better meet the definition of "good biomarker" (Bennet and Devarajan, 2017).

Unlike in urine, a longitudinal study, consisting of 9 timepoints over 6 months of uEVs proteome from four female and four male healthy donors showed that the majority of uEVs proteome was stable over prolonged time (Erozenci et al., 2021), which makes uEVs an attractive source of diagnostic and prognostic protein biomarkers. In terms of reproducibility, 40% of proteome was the same in all uEVs of the individuals analysed and 90% was the same in more than 1 individual at all timepoints (Erozenci et al., 2021). Furthermore, uEVs proteome profile has shown potential to predict non-CKD patients with a high cardiorenal risk to develop CKD, as the uEVs protein profile was evident before the occurrence of pathological albuminuria which makes uEVs a useful tool in early diagnosis of CKD (Anfaiha-Sanchez et al., 2024). Unlike uEVs protein profile,

concentration, size and tetraspanin content of uEVs were not affected in individuals with subclinical albuminuria level (Anfaiha-Sanchez et al., 2024).

Even in the prediction of kidney transplantation outcome, the protein signature of uEVs and serum EVs have shown to be highly accurate in discriminating rejecting patients based on receiver operating characteristic curve analysis, and uEVs signature was found to be correlated with eGFR, creatinine, and proteinuria, which were associated with patient outcomes based on univariate analysis (Burrello et al., 2023).

Urine and uEVs proteome were quantified and compared in a prostate cancer pathology where 190 men were recruited for translational and biomarker study (Khoo et al., 2024). Even though the synergistic value of urine and uEVs proteome was suggested, in cases where a longitudinal study is not possible, uEVs more faithfully recapitulated aspects of a disease due to their cellular origin. A positive correlation of uEVs proteome with kidney proteome was reported in studies using rat model (Wu et al., 2021; van Heugten et al., 2022). However, this was challenged by Sabaratnam et al. (2019) who found no correlation in uEVs tubular transport protein abundance with kidney specimens. An explanation was provided in Blijdorp and Hoorn (2019) suggesting that correlation of uEVs proteome with kidney tissue proteome might be reliable in CKD, and less reliable in healthy status (Blijdorp and Hoorn, 2019).

It has been shown that uEVs excretion depends on the nephron mass; for example, female individuals were shown to have significantly lower total kidney volume and subsequently 49% reduced uEVs excretion compared to male individuals (Blijdorp et al.,

2022). The authors therefore implied that for the inter-individual comparison of uEVs biomarkers, nephron mass or uEVs excretion rate should be measured.

Despite growing interest, there is still a gap in understanding whether urine or uEVs are a better or complementary for biomarker detection in CKD, particularly in DN progression. The main scope of this study was to explore this by comparing uEVs samples with unfractionated urine samples of DN progression and by applying qualitative and quantitative mass spectrometry (SWATH-MS/MS) as a robust high-throughput technique. Stable and progressive DN cohorts from three urine sample preparations (urine, urine depleted of abundant plasma proteins, and uEVs) were employed to identify urinary candidate biomarkers of DN progression and to compare the size and quality of proteome that can be identified from each sample type.

3.2 Aims of the chapter

The aims of this chapter were:

1) To stratify diabetic nephropathy (DN) patients into stable and progressive groups, based on their loss of estimated glomerular filtration rate (eGFR).

2) To isolate and characterise urinary EVs (uEVs).

3) To evaluate the advantage of uEVs proteomics versus total urine proteomics in exploring markers of diabetic nephropathy (DN).

3.3 Methods

3.3.1 Study Participants

Human cell-free urine samples were provided by UCB Biopharma through two industrially sponsored biorepositories: 1) The Department of Nephrology and Transplantation, University Hospital Patras University, Greece which was approved by the Ethics Committee of the University Hospital of Patras under 228/15-07-2015, by the Council of the University Hospital of Patras 39/21-10-2015 and by the Research Committee of the University of Patras 453/15-02-2016), and 2) Sheffield University / Sheffield Teaching Hospitals NHS Foundation Trust, UK which was approved by the Ethics Committee reference number 08/H1305/649 (Yorkshire - South Humber) until October 2012 and 12/YH/0297 (Yorkshire-Bradford) after this date. All work was performed under NHS R&D number STH16448.

3.3.1.1 Urine collection from study participants

Spot urine samples were collected into 200 ml sample pots and placed immediately on ice. To make cell-free samples, urines were centrifuged at 800 x g for 10 minutes at 4°C, aliquoted in 20 ml aliquots and then frozen and stored at -80°C. Entire sample processing was done within 2 hours. No protease inhibitors were added at the time of collection. From the collection clinic samples were shipped on dry ice and stored at -80°C until further use.

3.3.2 Isolation of uEVs by differential centrifugation

To isolate extracellular vesicles (EVs) from urines, complete human urine samples were thawed and centrifuged for 10 minutes at 500 x g in order to pellet cells. For cell-free urine samples, this step was omitted. All cell-free urine samples were diluted with particle-free phosphate-buffered saline (PBS) (LZBE17-516F, Lonza / 15313581, Corning) and supplemented with 50x cOmplete™ EDTA-free protease inhibitors (11836170001 Roche, Sigma). The isolation of the uEVs was performed from 2 ml, 5 ml or 10 ml of starting urine by differential centrifugation protocol published in Furini et al., 2018. Entire procedure was performed on ice and all centrifugation steps were done at 4°C. The pellet of cell debris and apoptotic bodies was discarded while the pellets from the following steps were collected. The first pellet of large EVs was resuspended with 100 µl of 200 mg/ml 1,4-Dithiothreitol (DTT) (MB1015, Melford) in particle-free PBS and incubated for 10 min at 37°C, with vortexing every 2 minutes or shaking at 300 rpm on the thermo-shaker, in order to break THP (Tamm-Horsfall protein / Uromodulin) fibres and release vesicles. The volumes were then supplemented with 1 ml of particle-free PBS, followed by the next centrifugation step, after which the supernatants were pooled together with the supernatants from the previous step. Supernatants were then filtered through the 0.22 µm filter and ultracentrifuged. The pellets of large and small uEVs fractions were resuspended in 40 µl of the radioimmunoprecipitation assay (RIPA) lysis buffer (25 mM Tris pH 7.4, 150 mM NaCl, 1 mM EDTA, 1% NP40, 5% glycerol) or urea-based proteomics lysis buffer (9.5 M urea, 2% (w/v) DTT, 1% (w/v) N-Octyl-Beta-Glucopyranoside (OGP)) + freshly added protease inhibitor (PI) (Roche 50x, 1 tablet in 1 ml of water), except the

samples for uEVs characterization by nanoparticle tracking analysis, which were resuspended in 100 µl of particle-free PBS.

3.3.3 Isolation of uEVs by commercial exosome isolation reagent

"Total exosome isolation (from urine) reagent" (4484452, Invitrogen) was used as an additional method to isolate urinary vesicles. The purpose of commercial method was to lower down the starting volume of urine, as well as to enable simpler and less laborious process of EV isolation. Therefore, starting cell-free urine material was 2 ml. The procedure was done according to the manufacturer's instructions. Briefly, cell-free urine samples from healthy donors were centrifuged at 2000 x g for 30 min at 4°C to remove cell debris. Clarified supernatants were transferred to the new tubes and topped up with one volume (2 ml) of the "Total exosome isolation (from urine) reagent" and the mixtures were well mixed by vortexing and inverting the tubes. The samples were then incubated for 1 h at RT, followed by centrifugation at 10,000 x g for 1 h at 4°C. After centrifugation, the supernatants were aspirated by pipetting and then discarded, while the pellet contained uEVs which were resuspended in either RIPA lysis buffer or PBS, depending on the further downstream application. The principle of this reagent is based on precipitation, so the reagent binds water molecules, hence forcing less soluble components such as vesicles out of solution. Short centrifugation at a low speed allows vesicles to be collected.

3.3.4 Concentration and protein depletion of urine samples

3.3.4.1 Concentration and desalting

Cell-free urine samples were centrifuged at 5000 x g for 5 minutes at 4°C using centrifuge 5804R (Eppendorf) with fixed-angle rotor (FA-45-6-30) to ensure cell debris were removed, followed by filtration through 0.45 µm syringe filters (Sartorius / Starlab) directly into 5 KDa MWCO Vivaspin 15R ultrafiltration tubes (Sartorius). Urine samples were concentrated and desalted by centrifuging Vivaspin ultrafiltration tubes at 6000 x g for 45 minutes at 4°C until urine volume reached 0.75 - 1 ml. This was followed by purification of remaining salts by diluting concentrate with 5 ml of milliQ distilled water into the Vivaspin ultrafiltration tubes and centrifuging at the same speed until volume reached 0.3 - 0.75 ml. Concentrated and desalted urine samples were resuspended at the bottom of the concentrate pocket of Vivaspin tubes and recovered into eppendorf tubes. The principle of concentration and desalting is based on vertical membrane technology also known as tangential flow filtration (TFF), a rapid method for the liquid-phase separation and purification of biomolecules which operates in a pressure-dependent flux by utilizing ultrafiltration membranes such as Hydrosart modified regenerated cellulose membrane present in Vivaspin columns. While fluid is forced through the pores of the membrane, proteins above the certain molecular weight of size are retained (van Reis and Saksena, 1997; van Reis and Zydney, 2001).

3.3.4.2 Protein depletion

Concentrated cell-free urine samples (300 – 400 µg) were depleted of abundant plasma proteins: albumin, α-antitrypsin, transferrin and haptoglobin using the "ProteoSpinTM Abundant Serum Protein Depletion Kit" (Norgen) and following the manufacturer's instructions. Briefly, samples were diluted in wash solution G to a final volume of 500 µl and washed in the same solution 3x by centrifugation at 6,600 x g for 1 minute. Proteins were eluted twice with Elution buffer C in the elution tube supplemented with protein neutralizer.

3.3.4.3 Acetone precipitation

Proteins from depleted cell-free urines were precipitated twice with 5 volumes of 100% acetone at -20°C. First time for 16 hours followed by centrifugation at 15,000 x g for 30 minutes at 4°C and pellet resuspension in 1 volume of dH$_2$O. Second time for 1 hour 40 minutes followed by 10 minutes centrifugation at the same speed. Supernatants were discarded and pellets were left open (covered with parafilm with holes to avoid dust contamination) to dry and then resuspended in 100 mM triethyl ammonium bicarbonate (TEAB) buffer.

3.3.5 Sample processing for mass spectrometry (MS)

3.3.5.1 Generation of peptides for MS from urine samples

Following urine concentration, 100 µg of proteins, which was the maximum protein amount that could be applied to mass spectrometer, were resuspended in 100 mM TEAB and used for proteomic analysis. Process of peptide generation included protein reduction with 0.5 M DTT (MB1015, Melford) in dH2O for 20 min at 56°C, protein alkylation with 0.55 M iodoacetamide (IAA) (I1149-25G, Sigma) in dH2O for 15 min at RT and protected from light, and finally protein digestion with sequencing grade modified trypsin (V5111, Promega) resuspended in trypsin resuspension buffer (V542A, Promega) for 16-17 hours at 37°C in a water bath. The ratio trypsin:sample proteins was 1:40.

The procedure was the same for the urines depleted of plasma proteins, however since protein amount was limited, entire samples were used for proteomic analysis, and 0.5 µl of trypsin was added at the minimum.

Upon overnight trypsinization, samples were vacuum concentrated to dryness at 60°C (set to V-AQ) (Concentrator plus, Eppendorf) for 90 min and stored at -20°C until ready for MS analysis.

3.3.5.2 Generation of peptides for MS from uEVs when using urea-based lysis buffer

Small and large uEVs pellets were resuspended in 30 µl of urea-based proteomics lysis buffer (9.5 M urea, 2% (w/v) DTT, 1% (w/v) N-Octyl-Beta-Glucopyranoside (OGP)), of which 6.6 µl was used for Bio-Rad protein quantification assay (1:3 dilution of sample, in

duplicates), while the remaining volume was topped up with 50 mM TEAB to 95 µl. This step of sample dilution in TEAB was important to reduce urea concentration down to 2 M before trypsin digestion, as otherwise, a high concentration of urea would markedly decrease trypsin activity (Harris, 1956). Proteins were then subjected to reduction by heating samples at 56°C for 20 min, however without DTT addition since samples already contained 26 mM DTT as a component of proteomics lysis buffer. After reduction, proteins underwent alkylation by incubating samples with 15 mM IAA for 15 min at RT, in the dark. Finally, proteins were digested using Trypsin Gold, Mass Spectrometry Grade (V5280, Promega) in a final protease:protein ratio of 1:20 (w/w) dissolved in 50 mM acetic acid, and 0.01% (w/v) ProteaseMAX Surfactant (V2071, Promega) which is trypsin enhancer that solubilizes proteins, including difficult membrane proteins, and improves protein digestion by providing a denaturing environment. Incubation of samples with trypsin was done overnight (14-16 h) at 37°C in a water bath. The total volume of samples at the point of trypsinization was 100 µl. The next day trypsin was inactivated by the addition of 0.5% trifluoroacetic acid (TFA) and samples were vacuum-dried and resuspended in 30 µl of 5% (v/v) acetonitrile/0.1% (v/v) formic acid for qualitative (DDA shotgun) and quantitative (DIA-SWATH) MS analysis.

3.3.5.3 Generation of peptides for MS from uEVs when using RIPA lysis buffer

The Suspension trapping (S-trap) micro spin column (Protifi) digestion protocol was used to remove interfering lysis buffer components such as SDS from RIPA lysis buffer according to the manufacturer's instruction. The protocol consists of a few main steps: protein solubilization, reduction and alkylation, protein trapping, protein cleaning, and

protein incubation and digestion, leading to final product of peptides ready for MS analysis. Briefly, samples were solubilized in 5% (w/v) SDS, 100 mM TEAB at pH 7.55, sonicated in bath sonicator (Cole-Parmer) for 10 min to improve protein dissolving and to recover adherent proteins, reduced with 0.5 M DTT at 56°C for 20 min, and alkylated with 0.5 M IAA at RT for 15 min protected from light. To completely denature proteins and trap them efficiently, samples were treated with phosphoric acid to a final concentration of 1.2% (v/v) and S-trap binding/wash buffer (90% (v/v) methanol in 100 mM TEAB at pH 7.1) and centrifuged at 4,000 x g for 45 seconds. The S-trap columns with samples were manually rotated for 180° between three washes with S-trap buffer. Samples were digested with digestion buffer consisting of 1:10 (w/v) sequencing grade modified trypsin in 100 mM TEAB pH 7.55 and incubated for 1 hour 30 min at 47°C. Peptide samples were eluted with 40 μl of 100 mM TEAB, followed by 40 μl of 0.2% (v/v) formic acid, and 50 μl of 50% (v/v) acetonitrile + 0.2% (v/v) formic acid to recover hydrophobic peptides. All the centrifugation steps were run at 4,000 x g for 45 seconds. Eluted peptides were pooled together, and samples were vacuum dried at 60°C (set to V-AQ) for 90 min and stored at -20°C until ready for MS analysis.

3.3.6 Quantitative MS data analysis

Quantitation and fold change (FC) analysis between the compared groups were performed using the OneOmics cloud processing software (SCIEX), employing weighted average of proteins spectral results among the different biological replica to calculate FC and relative significance. The outcome of the experiment is a list of protein identification

names (IDs), with FC values expressed as logarithm on base 2 (log2FC), and confidence level of FC calculated by the software. The confidence score in the OneOmics software is a score based on a proprietary algorithm that serves as an alternative to a traditional p-value (Lambert et al., 2013). It incorporates fragment data and peptide fold change, rather than relying solely on proxy protein abundance, since mass spectrometers measure peptides and fragments, not proteins directly. The word "significant" is a stretch for 50-65% confidence. While the software defaults to a 75% confidence threshold, in datasets with high variability or low replicate numbers, lowering this threshold to 50% may be acceptable to avoid missing potentially relevant changes. This approach essentially creates a ranked list of proteins where a higher confidence percentage corresponds to a greater likelihood that the observed change is real (Lambert et al., 2013). In summary, fold changes with a confidence higher than the 0.80 (80%) are considered as highly significant, confidence between 0.80 and 0.5 (50%) acceptable but less significant, and confidence values below 0.5 not considered significant. In this thesis, data were regarded as significant above 55% confidence.

3.4 Results

3.4.1 Patient stratification

3.4.1.1 Patient stratification

Cell-free urine samples from DN patients, stable and progressive, diabetic patients with no CKD and healthy controls were sourced from two biorepositories (Sheffield Kidney Institute, UK and Patras University Hospital, Greece), as described in the Methods 3.3.1.

Stratification of DN patients into stable and progressive groups was based on eGFR loss over time, also known as eGFR slope, calculated from the longitudinal measurements of eGFR [ml/min] from the patients over the years (range 1-8 years). The criteria for the selection of stable DN patients was the eGFR loss not greater than 2 ml/min/year (value of eGFR change or slope above -2 ml/min/year) and of progressive DN patients, eGFR loss greater than 5 ml/min/year (eGFR slope value of -5 ml/min/year or below). Another criterion for sample selection was that the eGFR value at the time of sample collection [ml/min] had to be in the range of 30-44 ml/min according to moderate stage of CKD (stage 3b). Therefore, all samples of stable and progressive groups were within the same CKD stage, except for three samples which were under that threshold. A table with individual eGFR and eGFR slope values for each individual stable and progressive DN patient is provided in Appendix.

Furthermore, selection was focused on patient samples with tight linear progression representing fibrosis while the patient samples with acute exacerbations possibly

induced by drugs or inflammatory response were avoided. An example of selected stable and progressive DN patients is in Figure 3.1.

Cell-free urine samples from diabetics with no CKD and healthy controls were selected randomly. A summary of the clinical information of the selected patient samples is shown in Table 3.1.

Table 3.1: Clinical information of patient samples

	Stable DN	Progressive DN	Diabetic	Healthy
Number of subjects	28	25	20	20
Gender (Female/Male)	8/20	5/20	10/10	7/4 (ND=9)
Age (mean ± SD)	70.3 ± 11 (ND=5)	64.7 ± 10.2 (ND=4)	57.4 ± 13.7 (ND=10)	41.9 ± 27.4 (ND=8)
BMI (mean ± SD)	28.8 ± 4.9 (ND=17)	30.3 ± 8.4 (ND=12)	30.1 ± 6.6 (ND=10)	25.9 ± 4.2 (ND=10)
Serum creatinine (mg/dL) (mean ± SD)	1.83 ± 0.2 (ND=6)	2.07 ± 0.3 (ND=5)	0.98 ± 0.2 (ND=10)	0.8 ± 0.2 (ND=10)
eGFR (ml/min) (mean ± SD)	36.68 ± 4.5	33.92 ± 4.5	80.2 ± 15.4 (ND=10)	ND
eGFR change (ml/min/year) (mean ± SD)	2.25 ± 3.7	-9.53 ± 4.6	NA	NA
CKD stage	CKD 3b	CKD 3b	NA	NA

*ND = not determined (not provided information), NA = not applicable

eGFR over time
Slope = 1.98 ml/min/year → Stable

Stable patient SKI961

eGFR over time
Slope = -9.05 ml/min/year → Progressor

Progressive patient PDN154
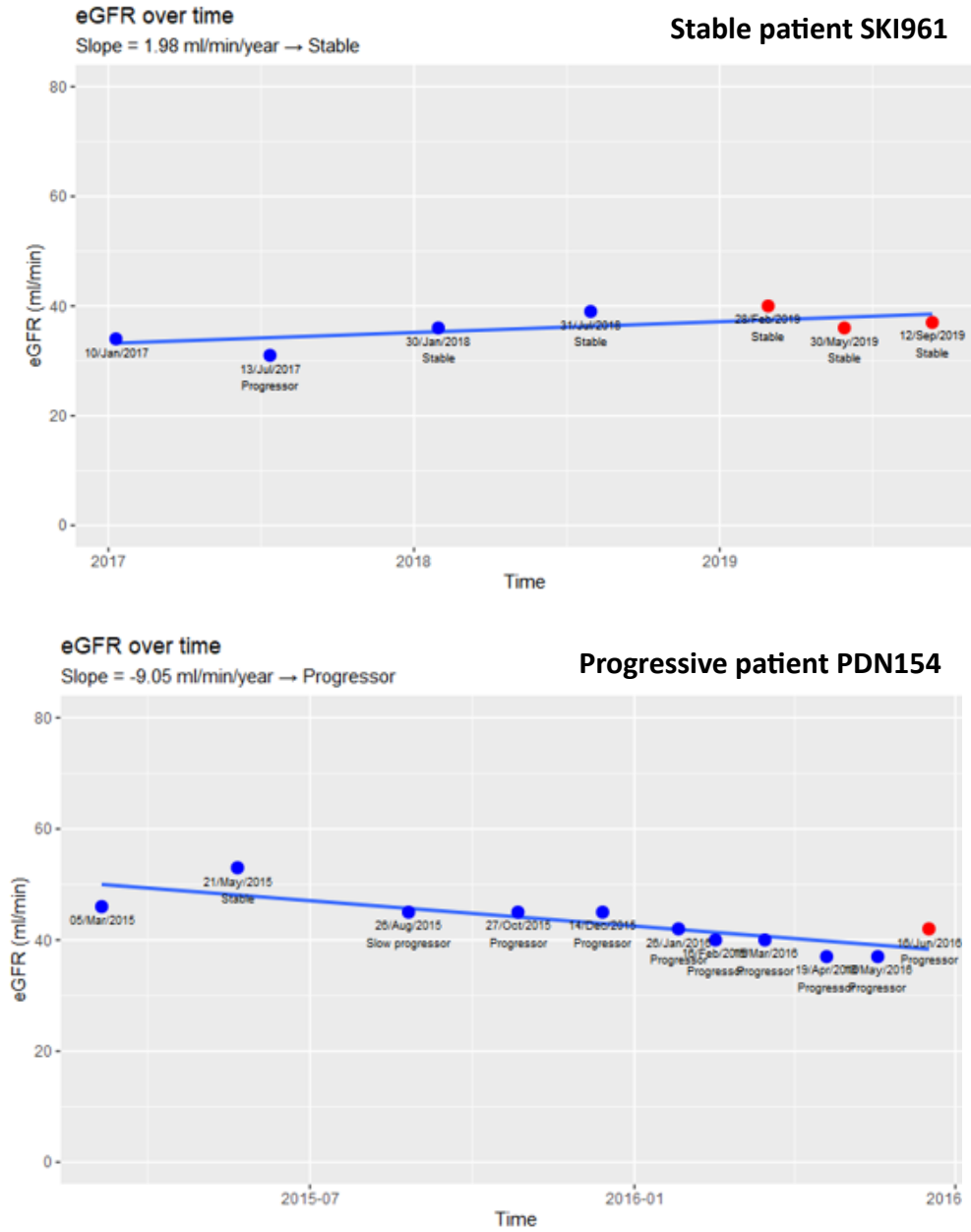
Figure 3.1: Examples of regression plots showing stability or progression of chronic kidney disease based on eGFR decline (eGFR slope). Samples were considered stable if eGFR decline was less than 2 ml/min/year, and progressive if eGFR decline was greater than 5 ml/min/year. The dots indicate when eGFR was measured for a given patient. Red dots indicate that samples were also stored when eGFR was measured.

3.4.2 Urinary EV isolation and characterisation

The uEVs were isolated based on the differential centrifugation protocol previously developed by the Verderio group, study from cell-free urine samples (Furini et al., 2018). As shown in Figure 3.2, population of large uEVs was isolated by low-speed centrifugation, whereas small uEVs were isolated by ultracentrifugation.
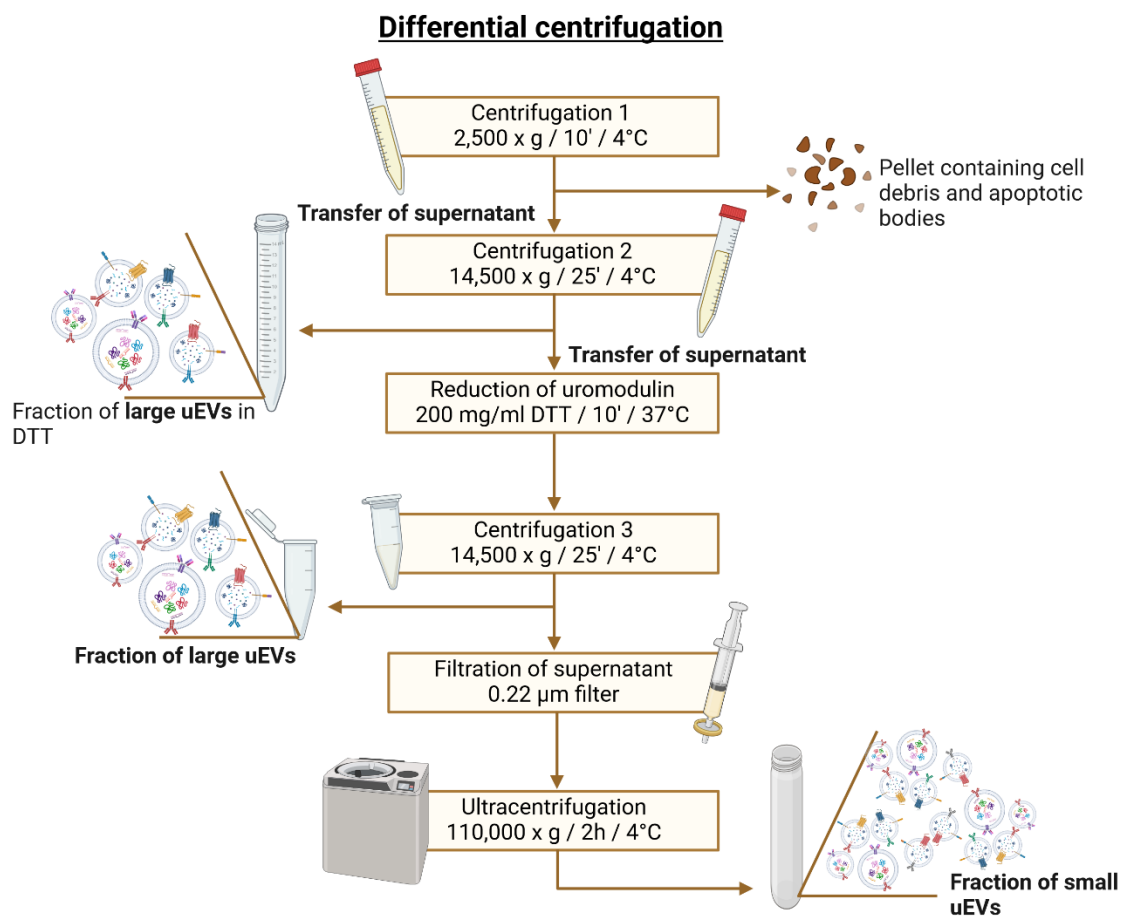
Figure 3.2: Differential centrifugation method for uEVs isolation, developed from Furini et al., 2018. In the first centrifugation step, cell debris and large apoptotic bodies are discarded. The second centrifugation step yields fraction of large uEVs which is then treated with reducing agent DTT in order to untrap vesicles from uromodulin. The next round of subseparation is to collect and resuspend large uEVs pellet. Supernatant is filtered through 0.22 nm filter and then in the last step of ultracentrifugation small uEVs are recovered.

The isolated uEVs were characterised following the minimal information for studies of extracellular vesicles (MISEV) guidelines for EV characterisation which recommends using different independent methods that do not have the same measurement limitations (Welsh et al., 2024) and employing healthy control subjects.

By immunoblotting (Figure 3.3), the presence of small uEVs (S) and large uEVs (L) was shown by the expression of EV markers either cytoplasmic (ALIX, FLOT2, HSP70) or of transmembrane origin (LAMP1), and the absence of negative control Golgi marker (GS28). EV markers were detected from uEVs fractions isolated from 2 ml, 5ml, and 10 ml of healthy urine, showing increase in the signal of EV markers with the increasing volume of urine.
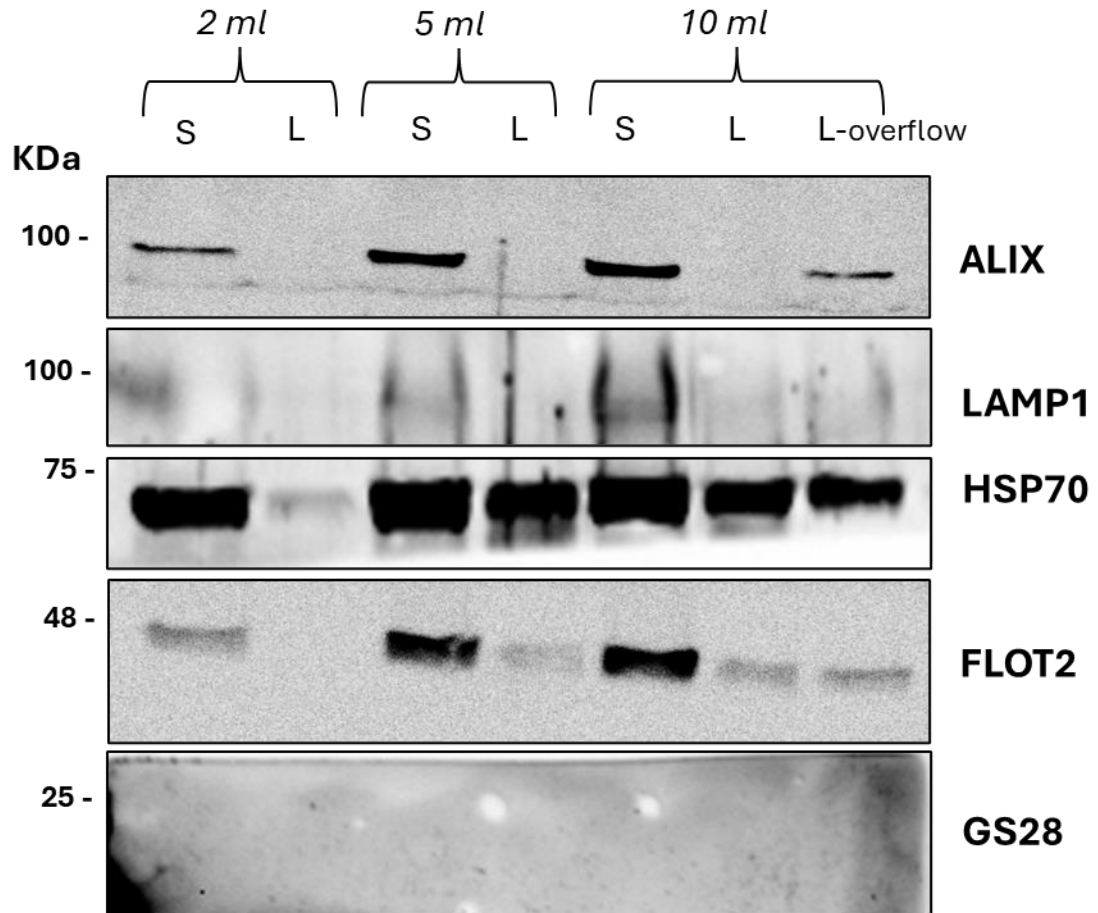
Figure 3.3: Western blot characterization of small (S) and large (L) uEVs isolated from 2 ml, 5 ml, and 10 ml of urine from a healthy subject. Positive EV markers Alix, LAMP1, HSP70, FLOT2, and negative marker GS28 were analysed in uEVs lysates separated by 10% SDS-PAGE and immunoblotted. Experiments were performed in three independent replicas (one shown).

Size distribution of small and large uEVs population was measured by nanoparticle tracking analysis (NTA). Figure 3.4 shows that the peak size of small EVs was 120 nm, and for large 194 nm in a healthy sample. Furthermore, the small uEVs population was 1000-fold more concentrated compared to large uEVs using this approach. However, the concentration estimated by NTA should be interpreted with caution, as the particles counted may include not only EVs but also co-isolates like lipoproteins, large protein complexes, and aggregates.

Small uEVs   **Large uEVs**

Peak diameter: 120.3 nm
Concentration: 1.2×10^9 particles/ml

Peak diameter: 194 nm
Concentration: 1.1×10^6 particles/ml
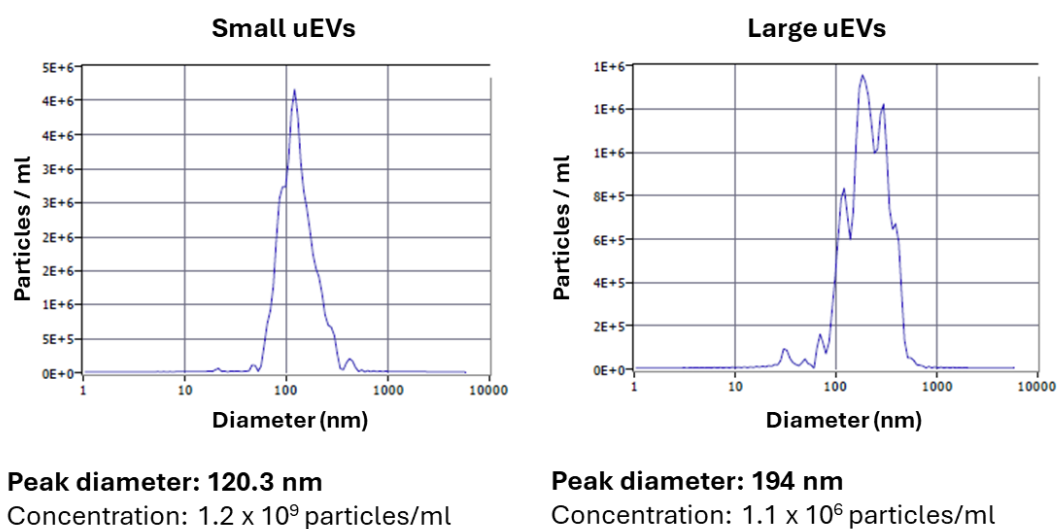
Figure 3.4: Size distribution of uEVs from a healthy control subject measured by nanoparticle tracking analysis (NTA). uEVs were isolated from 2 ml of healthy control urine and EV pellets were resuspended and diluted in particle-free PBS pH 7.4. Data show the peak size of small uEVs being close to 100 nm while the size of large uEVs was close to 200 nm.

UEVs morphology was investigated by transmission electron microscopy (TEM) negative staining. As shown in Figure 3.5, the uEVs displayed the characteristic membranous and round-shaped morphology. The size of the small uEVs was confirmed to be about 100 nm, and of the large about 200 nm, which is consistent with NTA measurements (Figure 3.4).
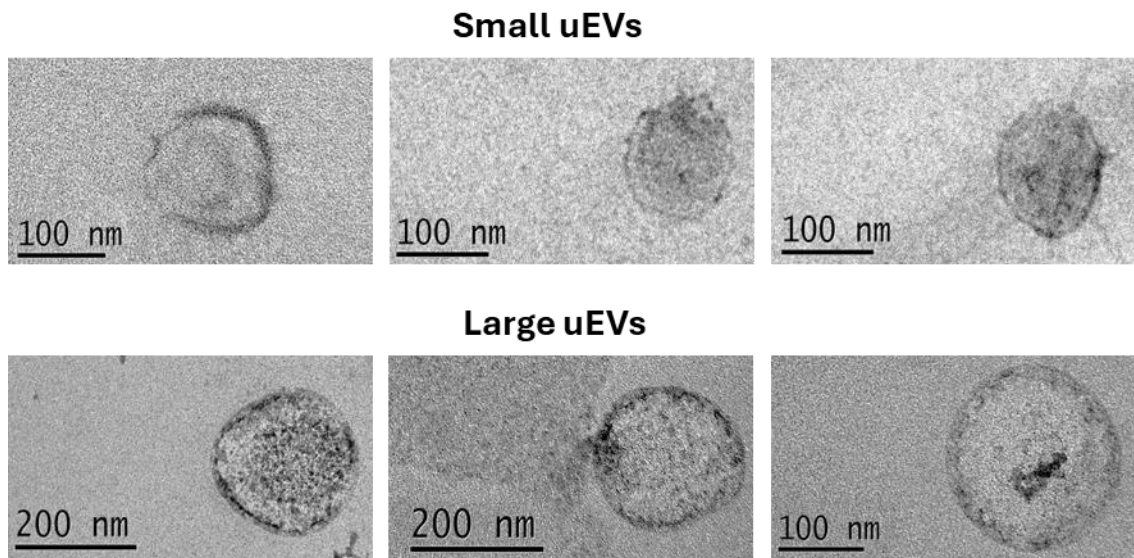
Figure 3.5: Transmission electron microscopy (TEM) of uEVs. The characteristic membranous and round-shape morphology of small and large uEVs is shown. uEVs were isolated from healthy control urine and resuspended in particle-free PBS pH 7.4. Isolation of uEVs was performed by this thesis author, while the processing of samples for microscopy and acquiring images was carried out by Dr Maria Pia Savoca.

In summary, the presence of small and large uEVs isolated by differential centrifugation method was confirmed by showing the presence of four EV markers by Western blot, size distribution by NTA and characteristic morphology by TEM. The next question asked how the chosen "in-house" EV isolation method compared to a common commercially available method.

3.4.2.1 Comparison of uEVs isolation approaches

The differential centrifugation method for EV isolation is regarded as a gold standard approach (Tian et al., 2020), generally being efficient and providing high EV yield (Chen, M. et al., 2023; Zhang, M., et al., 2018). However, it is laborious and time-consuming compared to commercial precipitation or column-based methods, it has compromised purity of the yield due to possible presence of protein aggregates, and is not always compatible with clinical practice, because it requires large starting volumes of sample material (Zhang, M., et al., 2018; Ciftci et al., 2023). To explore whether uEVs could be efficiently isolated by a method more applicable in clinical settings, uEVs were isolated by a commercially available "Total Exosome Isolation (from urine) reagent" from Invitrogen requiring only 2 ml of starting urine material. Firstly, uEVs were isolated by both differential centrifugation and the commercial method from 2 ml of starting urine material from the same healthy control individual. The uEVs yield was compared by western blotting by detecting two positive EV markers (Alix and Flotillin-2). As shown in Figure 3.6, Alix and Flotillin-2 could be detected only in the fraction of small uEVs isolated by differential centrifugation and not from the commercial method. The large uEVs

fraction did not display these markers regardless of the approach when using 2 ml of urines. Figure 3.6 shows that differential centrifugation is significantly more efficient method than the reagent, at least when analysed by western blotting.

To gain more insights on the quality of the two preparations, mass spectrometry proteomic analysis was performed to compare proteomes of uEVs fractions isolated by the two methods. Study from 2 ml of healthy control urine, as before, from small and large uEVs fractions isolated by differential centrifugation were joined together into a common fraction of uEVs.

In Figure 3.7 it can be seen that by proteomic data-dependent acquisition (DDA) analysis more proteins were detected in the uEVs isolated by differential centrifugation compared to uEVs from the commercial reagent. Only about 12% of identified proteins were common between the two preparations. Although 35% of proteins were uniquely found only in the uEVs obtained by the commercial reagent, the uEVs obtained by "in-house" differential centrifugation had all together a higher number of detected proteins and 53% were uniquely found by differential centrifugation.
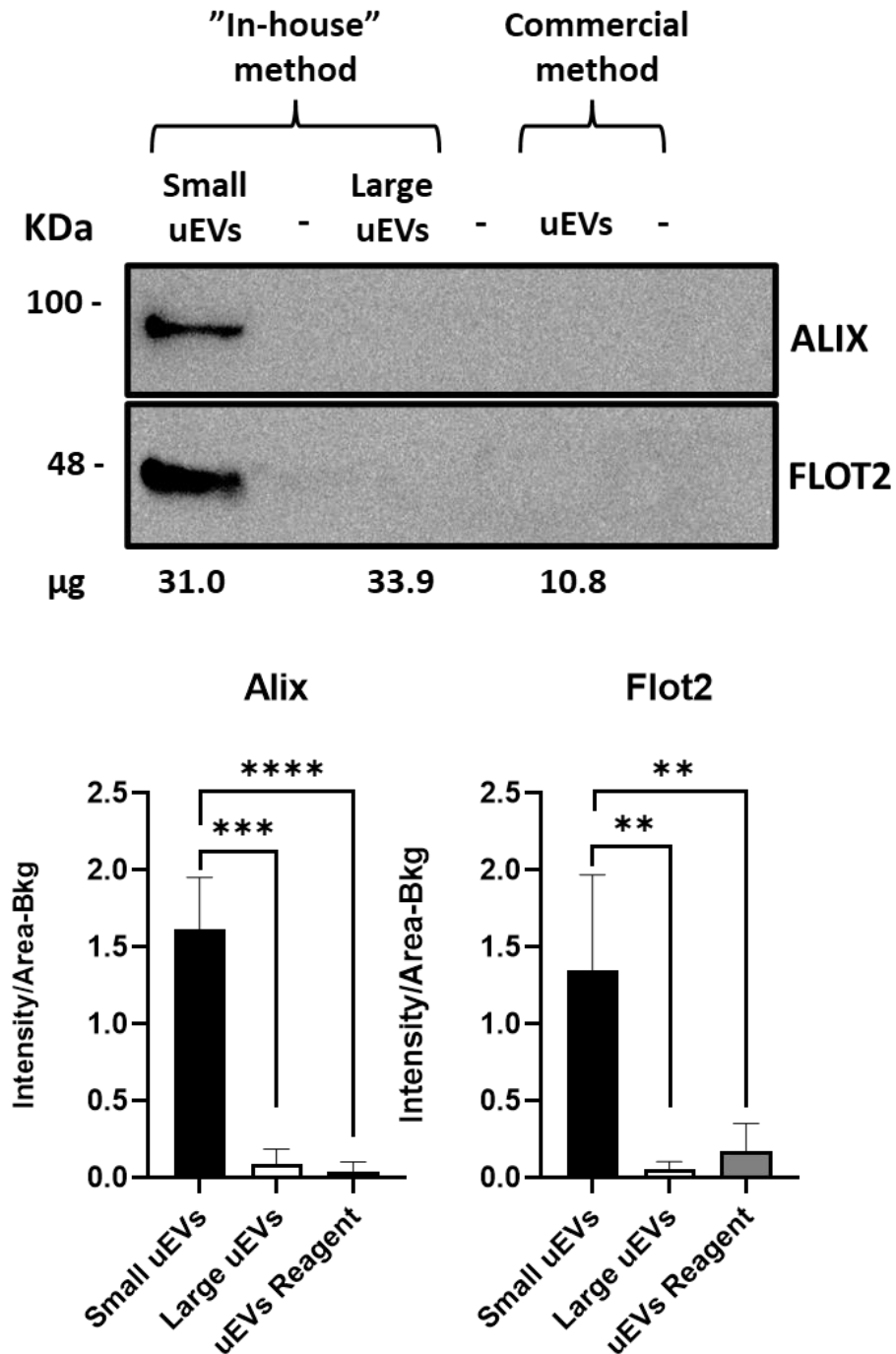
Figure 3.6: Western blot comparison of two EV isolation methods: "In-house" centrifugation and a commercial reagent. uEVs were isolated from 2 ml of healthy control urine and processed as described in Figure 3.3 legend. Experiment was performed in three independent replicas. Densitometric analysis was done by AIDA software and graphs were created in GraphPad Prism. Statistical test used was One-way ANOVA, ****p < 0.0001, ***p < 0.001, **p < 0.01. "-" indicate empty wells.
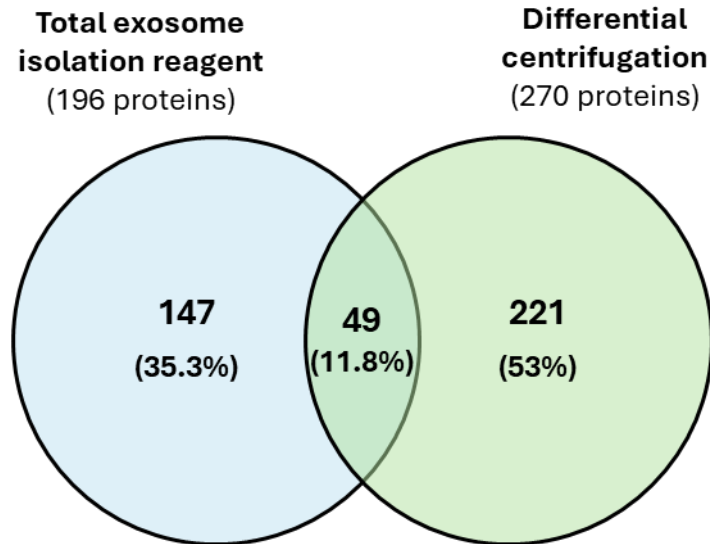
Figure 3.7: Data dependent acquisition (DDA) of uEVs isolated from 2 ml of healthy control urine by Total exosome isolation reagent and differential centrifugation showing difference in number of total proteins detected. Higher number of proteins was identified in uEVs isolated by differential centrifugation approach. Venn diagrams were created in Venny 2.1 and PowerPoint.

Both data from the western blotting analysis of the uEVs lysates and DDA proteomics led to conclude that the type of EV isolation method is critical for the proteomic composition, but the differential centrifugation approach is a more efficient approach in terms of quantity and uEVs proteome size for EV isolation than Total exosome isolation (from urine) reagent.

3.4.2.2 Optimisation of uEVs lysate for proteomics analysis

It is known that selection of lysis buffer can impact the overall proteomic detection and sequence coverage (Helm et al., 2024). In the attempt to further improve the proteome size of uEVs, the lysate preparation was optimised by changing the lysis buffer. Urea-based lysis buffer is the widely used denaturant in proteomic studies (Betancourt et al., 2018), therefore it was compared with the RIPA buffer used to generate uEVs lysates (Figure 3.7) which is also a common buffer for total protein denaturation from cells and tissues in proteomics (Gomes et al., 2024; Subedi et al., 2019). UEVs were isolated from a healthy individual and small and large uEVs fractions were combined into a common uEVs fraction and resuspended in either urea or RIPA lysis buffer. To maximise yields 5 ml were the starting urine volume. For each analysed lysis buffer, three independent uEVs isolations were done to have triplicates from each group, as shown in the Figure 3.8 workflow.

Healthy control urine

Aliquots of 5 ml urine

Pellets of <u>large</u> uEVs

+

Pellets of <u>small</u> uEVs

Small + large uEVs resuspended in **RIPA** buffer

Small + large uEVs resuspended in **urea** buffer

Sample processing for MS and LC-MS/MS analysis
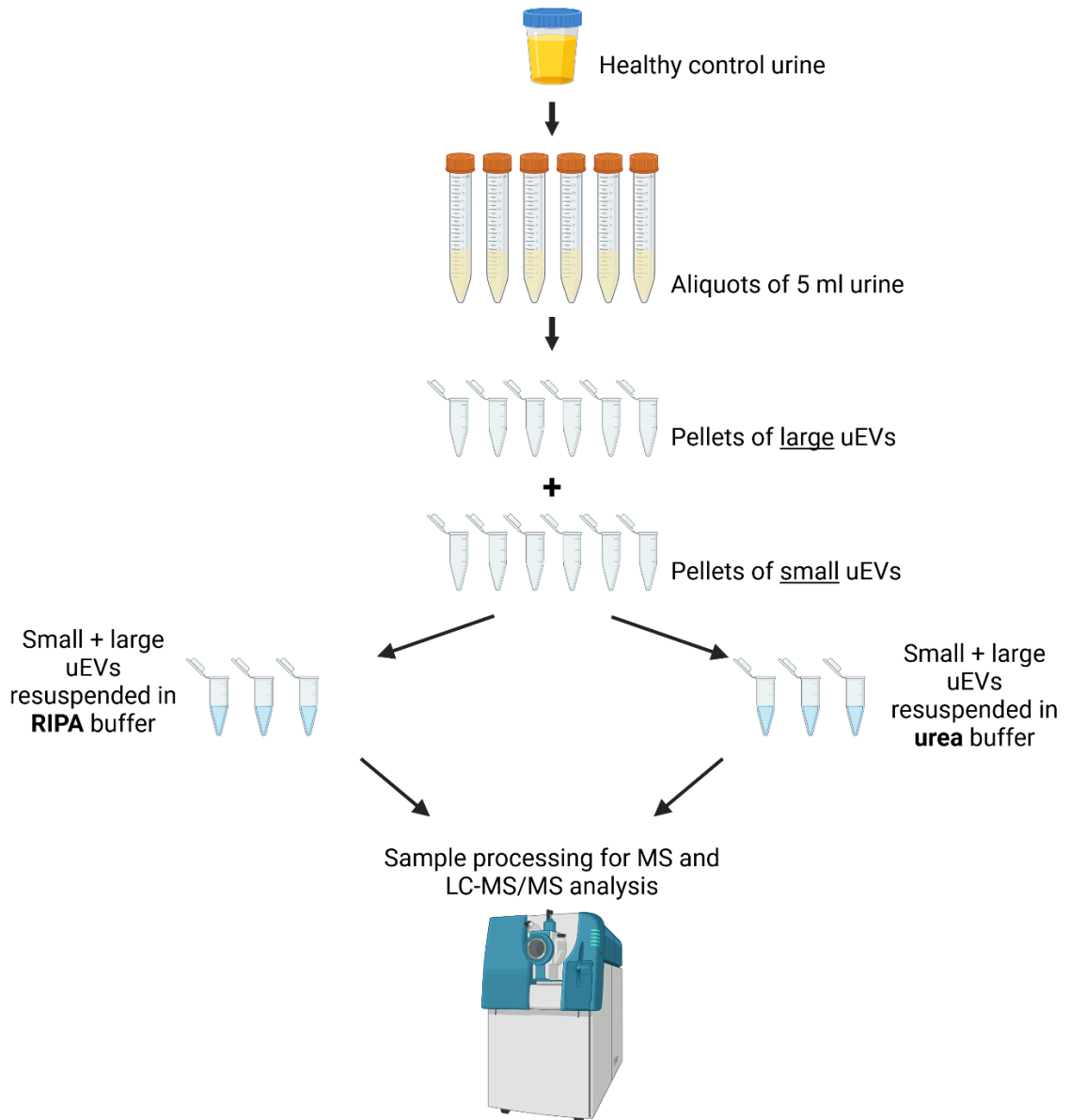
Figure 3.8: Workflow of the comparison between uEVs samples preparations with RIPA and urea-based lysis buffer for proteomic analysis.

Both qualitative and quantitative proteomic analyses were conducted to explore the difference in proteome from the uEVs preparations in different buffers. For the qualitative proteomics, a peptide library was created by DDA from all the samples in both comparing groups. As can be seen from Venn diagram in Figure 3.9, qualitative proteomics revealed that the proteome size was larger in the RIPA-based uEVs preparations and with four folds more unique proteins than in the urea-based uEVs preparations. However, about 66% of all identified proteins were in common to both uEVs preparations (in RIPA and urea-based lysis buffers).
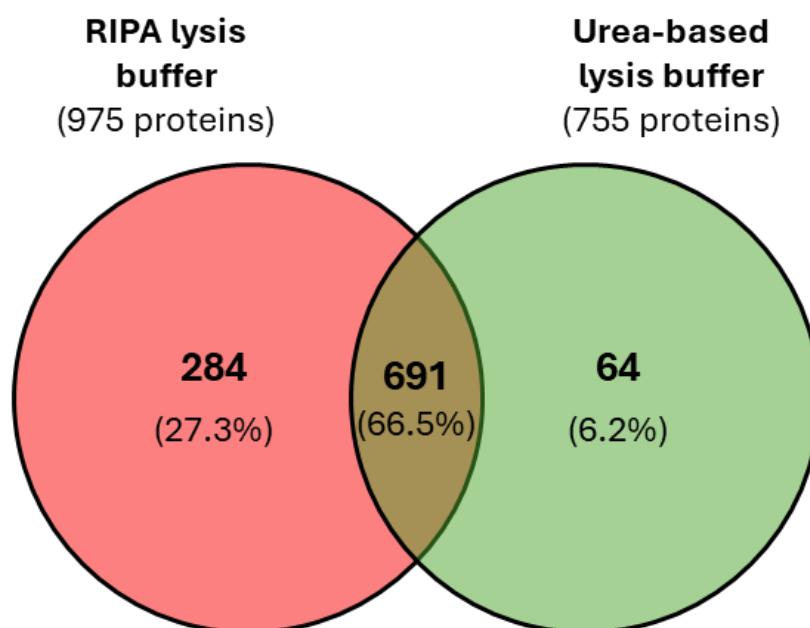
Figure 3.9: Venn diagrams showing the number of proteins detected by DDA from uEVs lysed by RIPA lysis buffer and urea-based lysis buffer. Qualitative proteomic analysis showed that more than 66% of detected proteins were in common, however 4x more unique proteins were identified in uEVs prepared in RIPA lysis buffer.

Quantitative proteomics was done by SWATH data independent acquisition (DIA) to explore significantly differentially expressed proteins in uEVs with RIPA lysis buffer versus uEVs with urea-based lysis buffer. As shown in Table 3.2, for the same proteins there were generally more quantity in the RIPA-based uEVs lysates than urea-based with confidence level > 65% (29 proteins significantly increased and only 5 proteins significantly decreased in uEVs lysed with RIPA compared to uEVs lysed with urea). Among the significantly increased proteins, only apolipoprotein D, serotransferrin, and albumin were highly abundant plasma proteins, whereas the others were likely cell proteins which are generally interesting disease biomarkers.

In summary, this proteomic analysis showed that using RIPA lysis buffer for uEVs samples increases protein library in qualitative proteomics and yield in quantitative proteomics. This suggests that RIPA is a more suitable detergent than urea for uEVs studies.

Table 3.2: Significantly differentially changed proteins in uEVs lysed with RIPA compared to uEVs lysed with urea lysis buffer. SWATH data quantification was done using SCIEX OneOmics software with 1% FDR. Differential expression was expressed as fold change (RIPA vs urea). Out of 1039 proteins detected; 34 were significantly changed in RIPA-based uEVs vs urea-based uEVs lysed (confidence level > 65%)

Protein ID	Protein name	Fold change (RIPA / urea)	Confidence
Increased proteins			
WFDC2_HUMAN	WAP four-disulfide core domain protein 2	8.456	74%
IBP3_HUMAN	Insulin-like growth factor-binding protein 3	7.819	66%
DEFB1_HUMAN	Beta-defensin 1	7.326	81%
APOD_HUMAN	Apolipoprotein D	6.812	85%
IBP2_HUMAN	Insulin-like growth factor-binding protein 2	6.704	81%
COFA1_HUMAN	Collagen alpha-1(XV) chain	6.190	85%
CGB3_HUMAN	Choriogonadotropin subunit beta 3	6.126	79%
MA1A1_HUMAN	Mannosyl-oligosaccharide 1,2-alpha-mannosidase IA	5.506	72%
FOLR1_HUMAN	Folate receptor alpha	5.252	74%
VASN_HUMAN	Vasorin	5.098	80%
CLUS_HUMAN	Clusterin	4.979	86%
PRG2_HUMAN	Bone marrow proteoglycan	4.853	68%
CD59_HUMAN	CD59 glycoprotein	4.153	84%
H14_HUMAN	Histone H1.4	3.660	81%
ITA3_HUMAN	Integrin alpha-3	3.473	87%
CRCT1_HUMAN	Cysteine-rich C-terminal protein 1	3.444	79%
FBLN3_HUMAN	EGF-containing fibulin-like extracellular matrix protein 1	3.371	71%
DEF3_HUMAN	Neutrophil defensin 3	3.238	83%
4F2_HUMAN	4F2 cell-surface antigen heavy chain	3.050	73%
KNG1_HUMAN	Kininogen-1	3.040	70%
TRFE_HUMAN	Serotransferrin	2.579	72%
UROK_HUMAN	Urokinase-type plasminogen activator	2.556	67%
ALBU_HUMAN	Serum albumin	2.310	71%
IPSP_HUMAN	Plasma serine protease inhibitor	2.158	82%
TSN1_HUMAN	Tetraspanin-1	2.107	68%
ALDOB_HUMAN	Fructose-bisphosphate aldolase B	2.052	74%
GBB1_HUMAN	Guanine nucleotide-binding protein G(I)/G(S)/G(T) subunit beta-1	2.028	81%
EGF_HUMAN	Pro-epidermal growth factor	1.999	78%
G3P_HUMAN	Glyceraldehyde-3-phosphate dehydrogenase	1.710	66%
Decreased proteins			
S10A9_HUMAN	Protein S100-A9	-7.727	87%
SPRR3_HUMAN	Small proline-rich protein 3	-4.773	83%
CALB1_HUMAN	Calbindin	-4.662	71%
S10A8_HUMAN	Protein S100-A8	-4.482	76%
CYTB_HUMAN	Cystatin-B	-3.533	80%

3.4.3 Comparing urine proteomics with uEVs proteomics

The size and quality of the urine proteome was compared to that of the uEVs proteome. In this study, urines from four stable and four progressive DN patients were used, whose clinical characteristics are shown in Table 3.3. The mean eGFR slope of the stable DN patients was -1.24 ±0.70, and that of progressive DN patients -10.93 ±3.64.

Table 3.3: Clinical information of stable and progressive DN patient samples

Sample ID	DN cohort	CKD stage	eGFR collection point [ml/min]	eGFR slope [ml/min/year]	Age	Gender	BMI	Serum creatinine [mg/dL]
PDN209	Stable	CKD 3b	31	-1.75	83	Male	27.689	2.2
PDN266	Stable	CKD 3b	38	-0.22	83	Male	33.897	1.8
PDN162	Stable	CKD 3b	32	-1.35	70	Male	25.826	2.2
PDN300	Stable	CKD 3b	42	-1.64	70	Male	ND	1.7
PDN17	Progressive	CKD 4-3b	25	-5.92	66	Male	31.070	2.7
PDN22	Progressive	CKD 4-3b	26	-11.82	78	Male	29.069	2.6
PDN194	Progressive	CKD 3b	31	-14.62	69	Male	23.723	2.26
PDN348	Progressive	CKD 4-3b	29	-11.34	54	Female	39.556	1.9

A *Post hoc* power analysis was performed using GPower v3.1.9.7 software and applying two-tailed t-test. When the effect size was determined from the intensity values of the top 10 upregulated proteins in uEVs from progressive DN, with the confidence level above 65%, the analysis gave experimental power of 29.54%.

Cell-free urines were either filtered and concentrated or further depleted of abundant plasma proteins (such as albumin, α-antitrypsin, transferrin and haptoglobin), followed by acetone precipitation as described in the Methods 3.3.4 and shown in Figure 3.10. UEVs were isolated as explained earlier in Results 3.4.2.

Total amount (μg) of proteins used for downstream mass spectrometry from each urinary sample type, stable (n=4) and progressive (n=4) cohort is shown in Table 3.4.

Table 3.4: Protein quantities used for mass spectrometry analysis. The maximum possible amount of protein was used for each urinary sample type from stable (n=4) and progressive (n=4) subjects. Values are expressed as mean ± SD.

	Protein amount in stable DN	Protein amount in progressive DN
Urine	100 μg	100 μg
Depleted urine	1.94 ± 2.32 μg	4.21 ± 2.05 μg
Urinary EVs	35.50 ± 12.46 μg	47.36 ± 15.27 μg
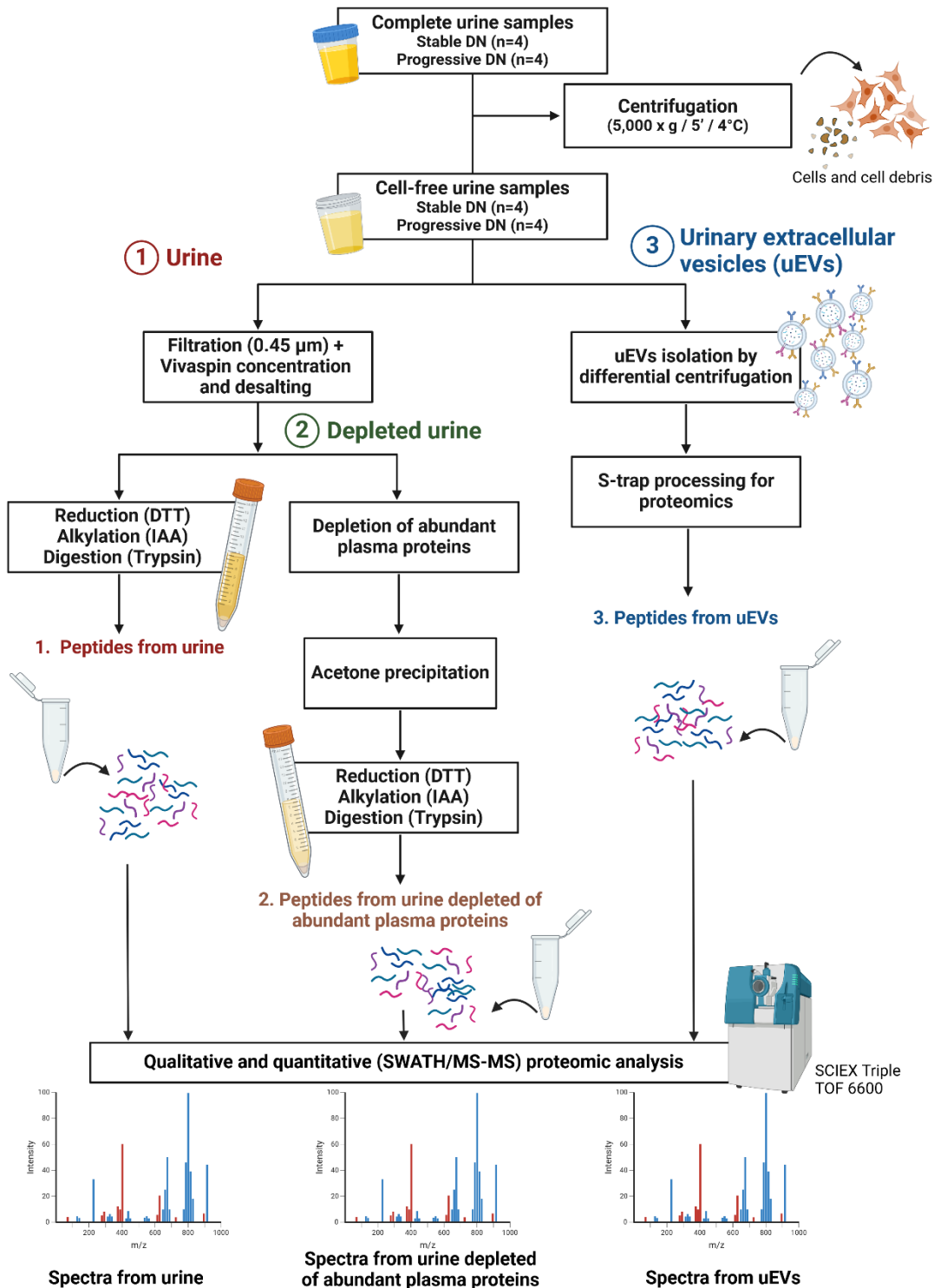
Figure 3.10: Workflow of the proteomic analysis of three urinary sample types: urine, urine depleted of abundant plasma proteins, and uEVs obtained as described in the Methods 3.3.2 and 3.3.4. Study from 5 ml urine. In all cases urine was from 4 stable and 4 progressive DN patients. Image created with BioRender.com

To assess the efficiency of the depletion, depleted urine sample lysates and non-depleted lysates were analysed by SDS-PAGE and stained with Coomassie blue as shown in Figure 3.11 which revealed that the abundant proteins were depleted in all four patients. The best depletion can be observed for albumin (66.5 kDa), followed by haptoglobin (alpha subunit 16-23 kDa, beta subunit 35-40 kDa). Depletion can also nicely be seen for transferrin (80 kDa), and a little bit less efficient for alpha-antitrypsin (54 kDa).
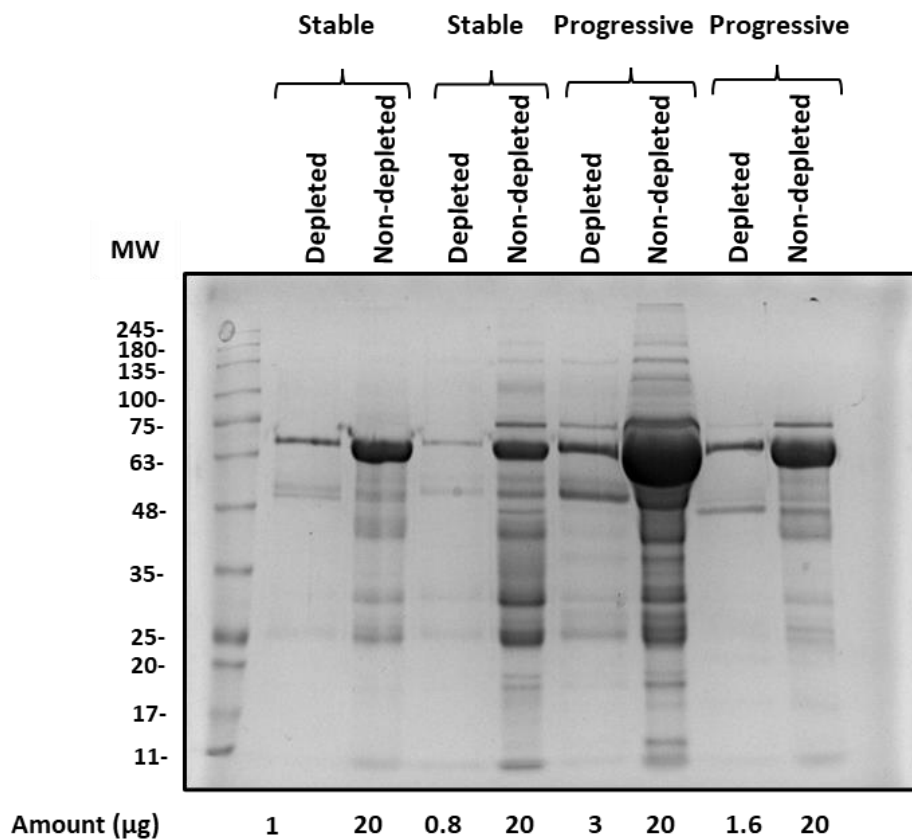
Figure 3.11: Coomassie staining of 10% SDS-PAGE showing the efficiency of urine depletion of abundant plasma proteins. Equal amount (20 µg) of non-depleted urines and equal volume (20 µl) of depleted urines, corresponding to 1 µg and 0.8 µg in stable DN samples and 3 µg and 1.6 µg in progressive DN samples, were loaded on each lane.

To compare the number of proteins that can be identified from the library of urine, depleted urine and uEVs, qualitative mass spectrometry was performed. A spectral library was created by DDA (746 proteins in total). When the proteome size of the three urine sample types was compared, uEVs displayed the largest proteome with 4-6 folds more proteins being identified than in urine or depleted urine in both the stable and progressive DN samples (Figure 3.12). Furthermore, above 70% of unique proteins were found in uEVs from both stable DN and progressive DN cohorts (black areas in Figure 3.12), and only 12% of proteins were in common to all three sample types (central grey areas in Figure 3.12) in stable DN, and 11% in progressive DN.
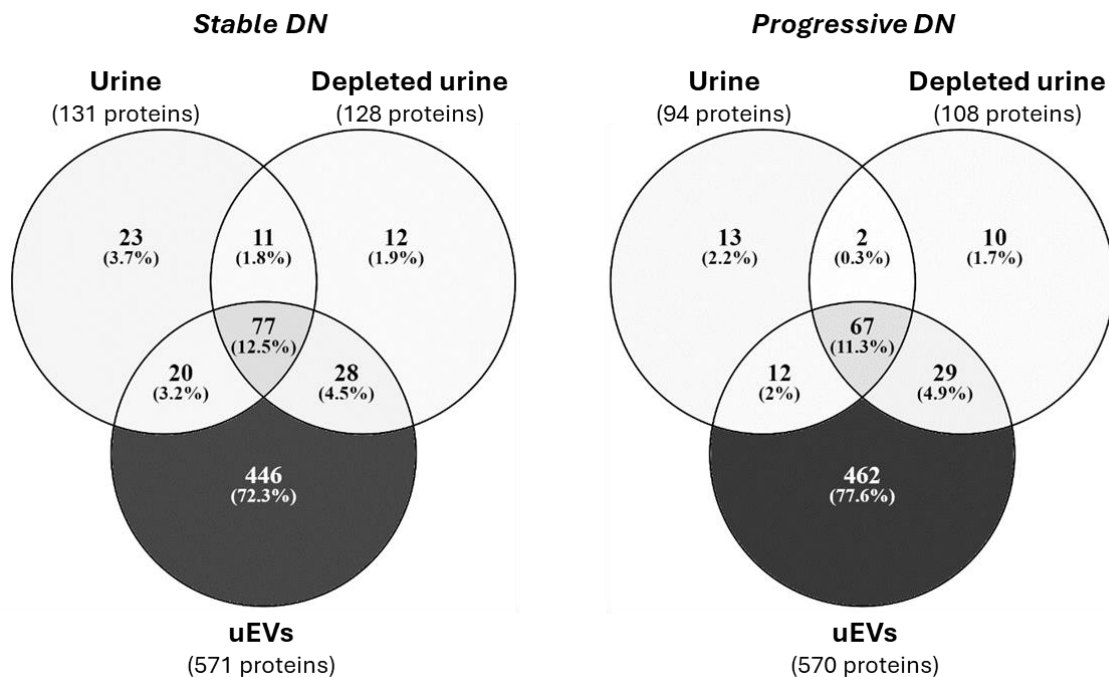
Figure 3.12. Venn diagrams showing the number of proteins detected by DDA from stable (n=4) and progressive (n=4) DN cohorts in three urinary sample preparations. Comparison of the urine, depleted urine and uEVs within stable DN and progressive DN cohorts showed uEVs sample preparation as the richest in number of detected proteins.

Following qualitative proteomics, comparative quantitative proteomics was also carried out to evaluate the three urine sample types. Proteins were considered significantly differentially expressed if the confidence level was above 55% with fold change ≤ -1.5 for downregulated and fold change ≥ 1.5 for upregulated proteins. This result suggests that analysis of uEVs leads to identify an increased level of differences between stable and progressive CKD by urinary proteomics. Quantitative mass spectrometry revealed 10 significantly downregulated proteins in progressive (n=4) compared to stable (n=4) DN as shown in Table 3.5. and Figure 3.13A. In the depleted urine, 5 proteins were found significantly upregulated of which three were abundant plasma proteins (albumin, immunoglobulin, beta-2-glycoprotein) and 2 proteins significantly downregulated in progressive DN, of which one was immunoglobulin (Table 3.6., Figure 3.13B). Quantitative proteomics of the uEVs samples revealed 39 proteins significantly differentially expressed in progressive compared to stable DN of which 20 were upregulated and 19 downregulated (Table 3.7, Figure 3.13.C).

Table 3.5: Significantly differentially expressed proteins between progressive (n=4) and stable (n=4) DN <u>full urine</u>

Protein ID	Protein name	Fold change (Prog / Stab)	Confidence
Decreased proteins			
SULF2_HUMAN	Extracellular sulfatase Sulf-2	-7.821	76.3%
DAF_HUMAN	Complement decay-accelerating factor	-5.429	72.7%
SAP3_HUMAN	Ganglioside GM2 activator	-5.039	69.1%
EPCR_HUMAN	Endothelial protein C receptor	-4.951	59.5%
KVD40_HUMAN	Immunoglobulin kappa variable 2D-40	-4.680	58.8%
CD44_HUMAN	CD44 antigen	-4.656	62.2%
CAD13_HUMAN	Cadherin-13	-3.950	60.6%
KV315_HUMAN	Immunoglobulin kappa variable 3-15	-3.745	56.7%
UTER_HUMAN	Uteroglobin	-3.327	60.7%
LEAP2_HUMAN	Liver-expressed antimicrobial peptide 2	-1.826	65.3%

Table 3.6: Significantly differentially expressed proteins between progressive (n=4) and stable (n=4) DN <u>urine depleted of abundant plasma proteins</u>

Protein ID	Protein name	Fold change (Prog / Stab)	Confidence
Increased proteins			
HMCN1_HUMAN	Hemicentin-1	10.199	63.5%
PEPC_HUMAN	Gastricsin	8.329	55.3%
HV226_HUMAN	Immunoglobulin heavy variable 2-26	8.015	68.1%
ALBU_HUMAN	Serum albumin	3.296	71.5%
APOH_HUMAN	Beta-2-glycoprotein 1	2.886	68.4%
Decreased proteins			
KV113_HUMAN	Immunoglobulin kappa variable 1-13	-8.143	66.3%
PPIC_HUMAN	Peptidyl-prolyl cis-trans isomerase C	-5.529	59.7%

Table 3.7: Significantly differentially expressed proteins between progressive (n=4) and stable (n=4) DN <u>uEVs</u>

Protein ID	Protein name	Fold change (Prog / Stab)	Confidence
<td colspan="4" align="center">**Increased proteins**</td>
PEDF_HUMAN	Pigment epithelium-derived factor	9.681	74.5%
ABCF1_HUMAN	ATP-binding cassette sub-family F member 1	8.399	69.5%
HEP2_HUMAN	Heparin cofactor 2	8.012	70.4%
RET4_HUMAN	Retinol-binding protein 4	7.938	72.6%
FBLN5_HUMAN	Fibulin-5	6.907	57.2%
THRB_HUMAN	Prothrombin	6.817	84.2%
CO2_HUMAN	Complement C2	6.222	69.6%
ANT3_HUMAN	Antithrombin-III	6.213	73.7%
CO9_HUMAN	Complement component C9	5.765	74.3%
HEMO_HUMAN	Hemopexin	5.584	61.8%
HPT_HUMAN	Haptoglobin	5.243	78.1%
IGHM_HUMAN	Immunoglobulin heavy constant mu	5.015	78.1%
CO1A1_HUMAN	Collagen alpha-1(I) chain	4.449	59.1%
APOA4_HUMAN	Apolipoprotein A-IV	4.109	73.1%
ANGT_HUMAN	Angiotensinogen	4.015	61.1%
KAIN_HUMAN	Kallistatin	3.907	57.5%
AFAM_HUMAN	Afamin	3.834	74.4%
HGFA_HUMAN	Hepatocyte growth factor activator	3.656	56.2%
CO8G_HUMAN	Complement component C8 gamma chain	3.559	74.2%
TRFE_HUMAN	Serotransferrin	3.274	76.4%
<td colspan="4" align="center">**Decreased proteins**</td>
PEPA5_HUMAN	Pepsin A-5	-7.492	55.4%
K22E_HUMAN	Keratin, type II cytoskeletal 2 epidermal	-5.732	67.2%
CUBN_HUMAN	Cubilin	-4.195	87.5%
ANAG_HUMAN	Alpha-N-acetylglucosaminidase	-3.834	75.2%
AMPE_HUMAN	Glutamyl aminopeptidase	-3.801	69.8%
NU133_HUMAN	Nuclear pore complex protein Nup133	-3.712	67.3%
NAPSA_HUMAN	Napsin-A	-3.495	67.1%
SAP3_HUMAN	Ganglioside GM2 activator	-3.463	81.3%
CD44_HUMAN	CD44 antigen	-3.226	55.4%
ASAH1_HUMAN	Acid ceramidase	-3.023	77.5%
NEP_HUMAN	Neprilysin	-2.946	77.2%
PCP_HUMAN	Lysosomal Pro-X carboxypeptidase	-2.810	68.7%
DPEP1_HUMAN	Dipeptidase 1	-2.759	64.0%
SC5A1_HUMAN	Sodium/glucose cotransporter 1	-2.723	56.9%
AMPN_HUMAN	Aminopeptidase N	-2.717	79.8%
BHMT1_HUMAN	Betaine--homocysteine S-methyltransferase 1	-2.471	58.3%
IPSP_HUMAN	Plasma serine protease inhibitor	-2.430	79.6%
TSN1_HUMAN	Tetraspanin-1	-2.287	57.7%
GNAI3_HUMAN	Guanine nucleotide-binding protein G(k) subunit alpha	-1.739	68.5%

A

B
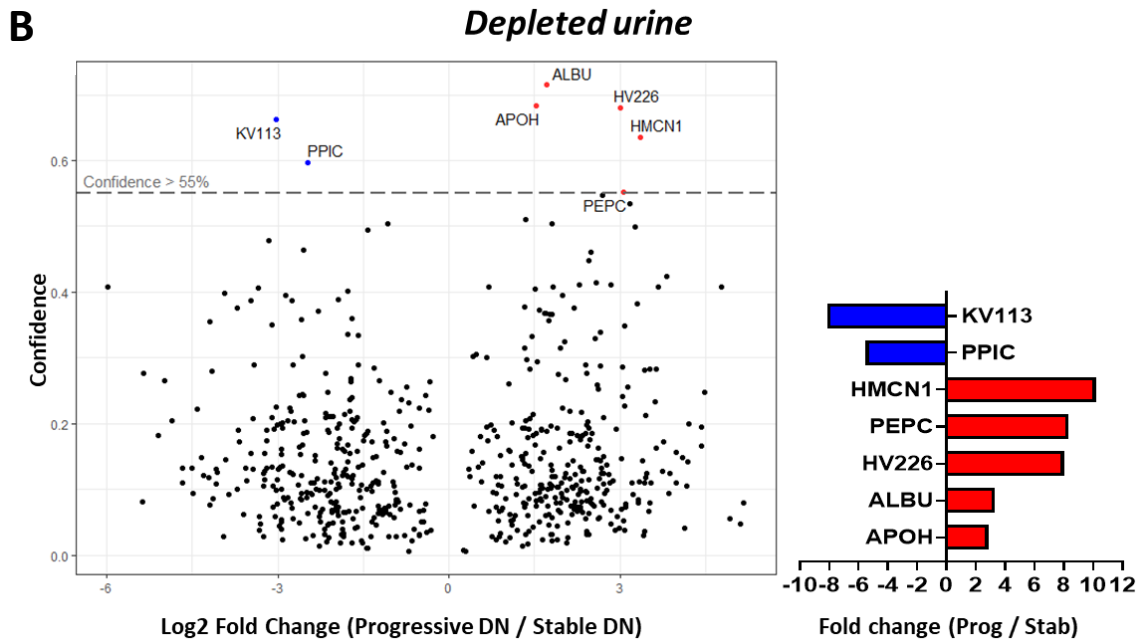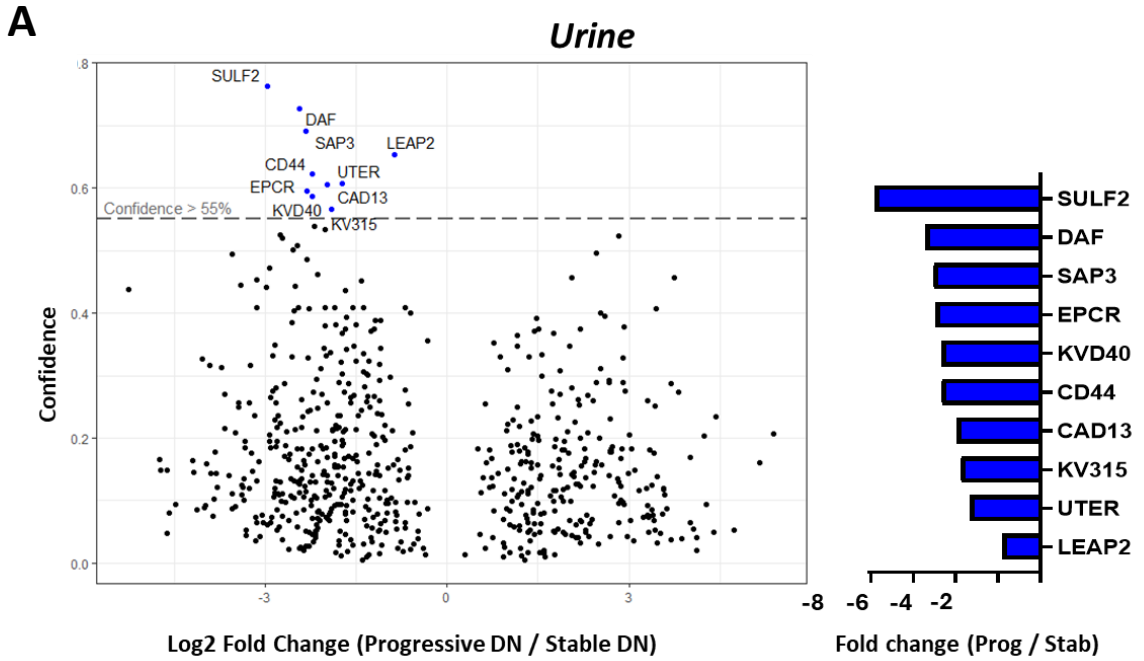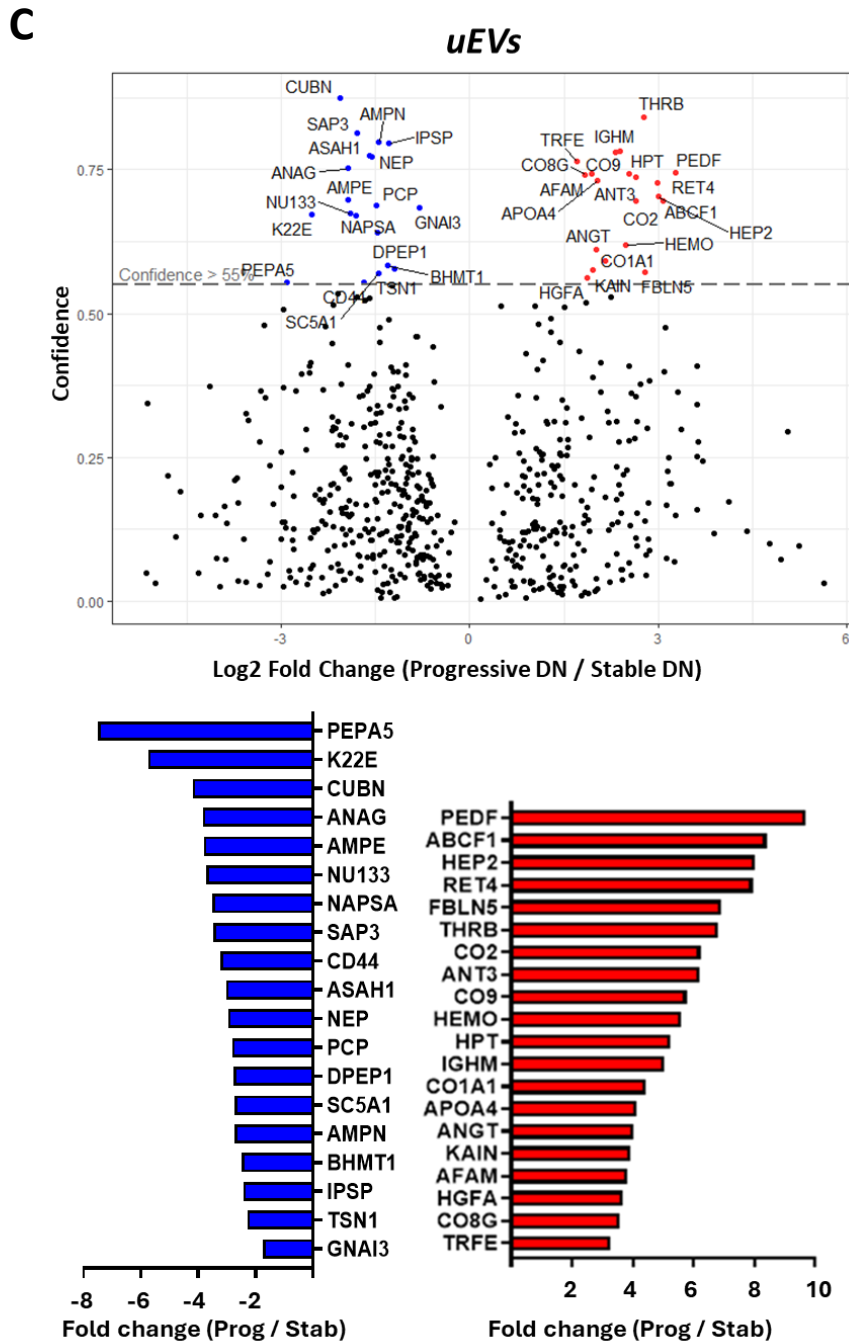
Figure 3.13: Proteins significantly differentially changed in progressive compared to stable DN cohorts in urine (A), depleted urine (B) and uEVs (C). Differential expression was expressed as fold change (prog DN/stab DN) which was transformed into log2 for volcano plots presentation with blue representing downregulation and red upregulation. Dotted line shows 55% confidence and all proteins above were considered significantly changed. In histograms proteins are listed according to fold change ratios from the most differentially expressed (in either down- or up-direction) on top to the least differentially expressed at the bottom. Volcano plots were created using ggplot2 package in R statistical software.

To view the expression of each protein in the individual urine samples, heat maps were created as shown in Figure 3.14. There was a clear separation of underexpression in progressive DN shown as a prevalence of blue colour, and overexpression in stable DN shown as a prevalence in red colour. Depleted urine and uEVs showed more variability among individuals. When the two proteins, Ganglioside GM2 activator (SAP3) and CD44 antigen (CD44), which appeared significantly changed in both urine and uEVs (marked with arrows in Figure 3.14) were observed per individual sample, it can be seen that even if both proteins were overall significantly downregulated in progressive DN from both sample types, in uEVs this difference was less sharp.
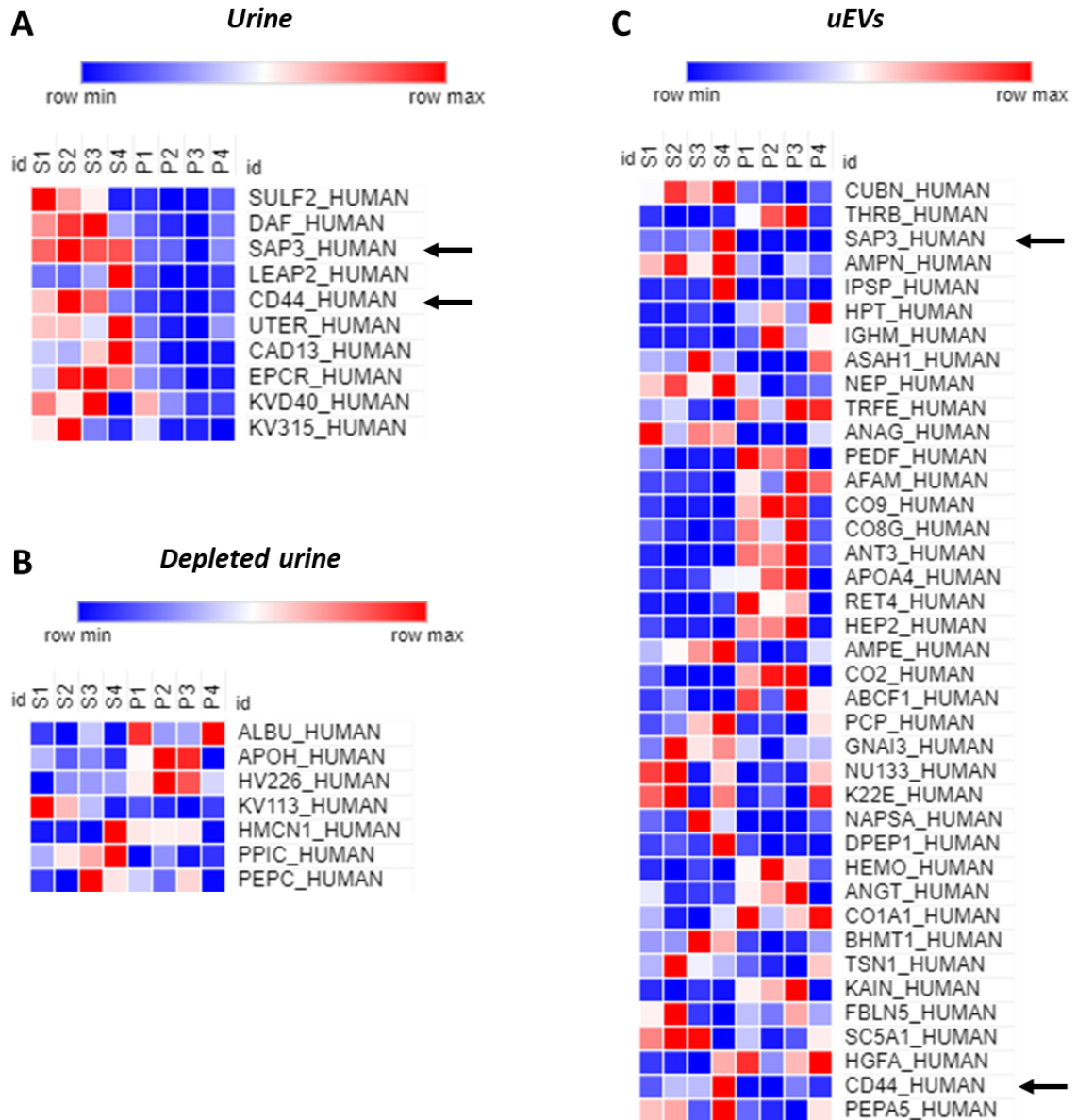
Figure 3.14: Heat maps showing expression of significantly differentially changed proteins between progressive and stable DN cohort in urine (A), depleted urine (B) and uEVs (C). Proteins are listed from the most significant on top to the least significant at the bottom, according to confidence level. Bright blue colour represents minimum expression, and bright red colour represent maximum expression. S1-4 (stable patients), P1-4 (progressive patients). Heat maps were created in Morpheus versatile matrix visualization and analysis software.

Cellular compartment analysis of the significantly changed proteins, done using PANTHER (Protein Analysis THrough Evolutionary Relationships, http://pantherdb.org), showed that the majority of proteins in all urinary sample types were localized in the extracellular space/region or extracellular matrix and in exosomes, followed by plasma membrane or cell surface, and cytoplasm or cytosol (Figure 3.15). However, higher percentages of proteins located in intracellular compartments other than cytoplasm and cytosol, such as nucleus, endoplasmic reticulum, Golgi apparatus, lysosome, and endosome are present in the uEVs sample type compared to urine and depleted urine. This may suggest that since uEVs are originating from kidney cells, they are enriched in intracellular protein content compared to urine, and therefore uEVs can be more informative on pathophysiological changes.
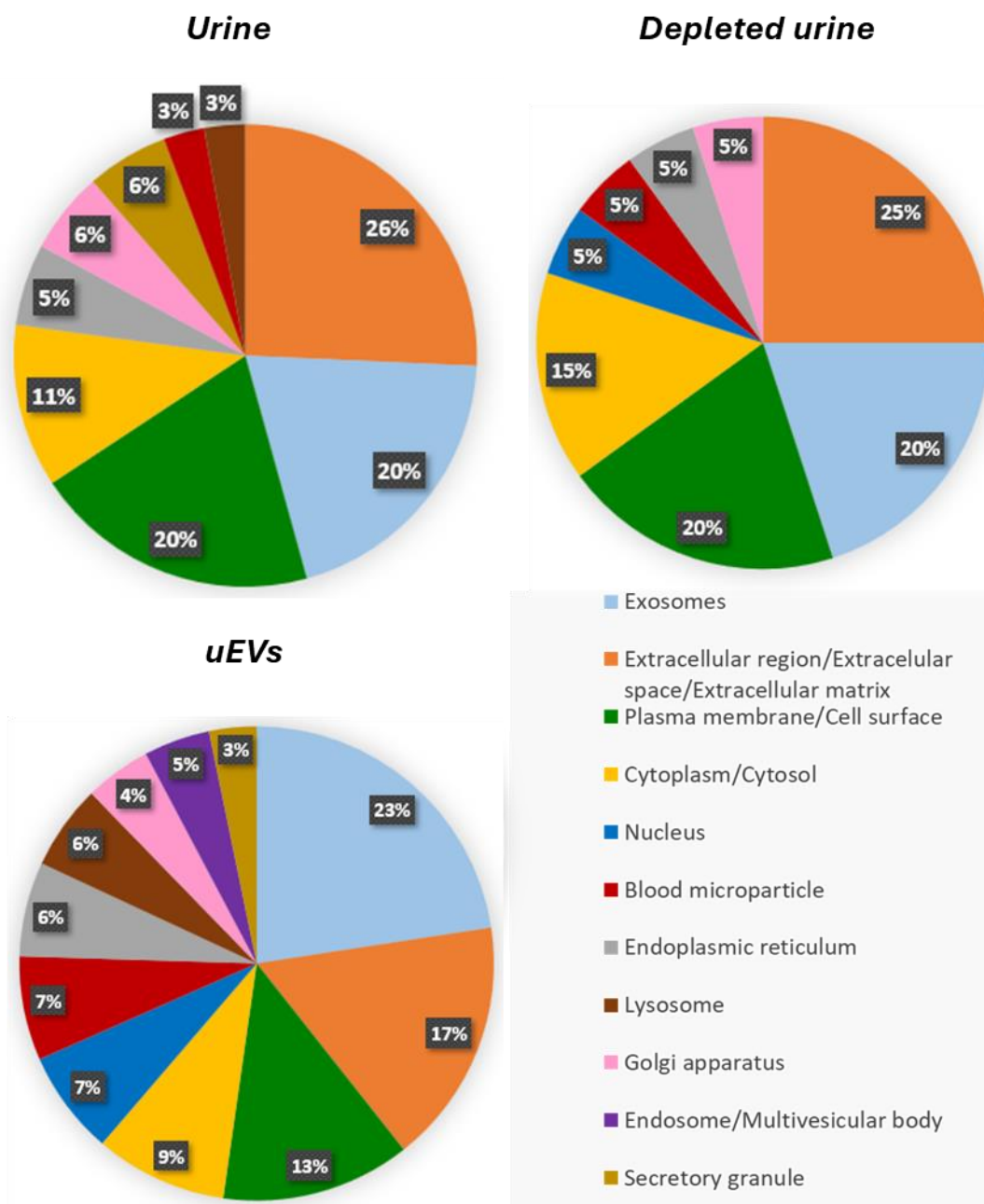
Figure 3.15: Subcellular localization of proteins identified as significantly differentially changed in progressive compared to stable DN in urine, depleted urine and uEVs. Cellular compartment analysis was done using PANTHER online resource (http://pantherdb.org), and pie charts created in Excel.

The analysis of functional protein interaction network (Figure 3.16) and pathway enrichment of significantly differentially expressed proteins in the three analysed urinary sample types showed no clusters of protein functions and/or common pathways formed in urine (A) or depleted urine (B) (Figure 3.16). In uEVs instead (C), protein network from significantly changed proteins consisted of 37 proteins and 82 interactions from which pathway enrichment analysis showed three significantly enriched pathways: Complement and coagulation cascades pathway (purple), Renin-angiotensin system pathway (red), and Lysosome pathway (green).

Taken together, this data show that uEVs compared to urine or depleted urine offer enriched protein discovery, both qualitative and quantitative. Higher number of detected proteins, especially of cellular origin, make uEVs stronger source of biomarkers compared to urines.
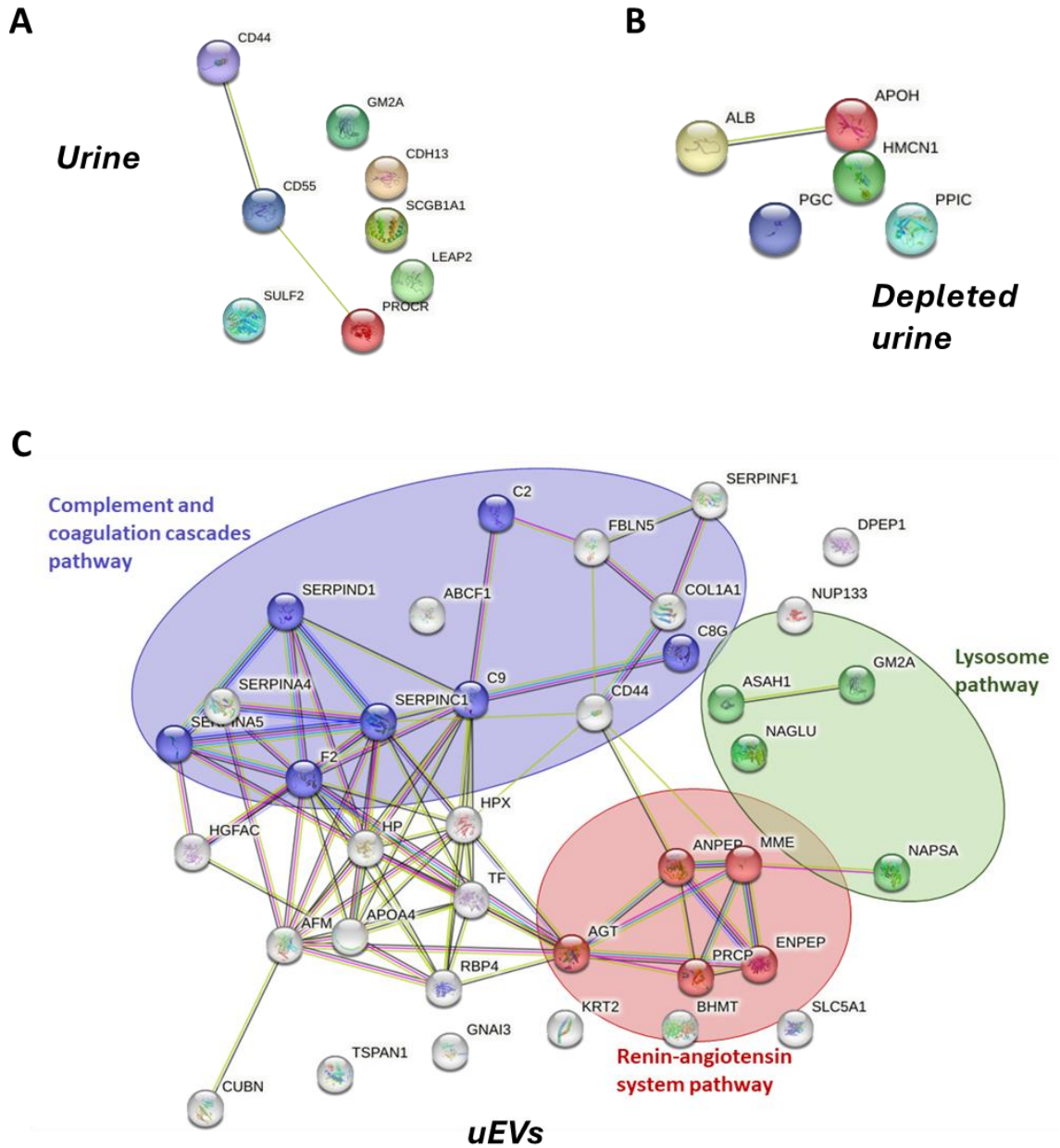
Figure 3.16: Protein-protein interaction network of significantly differentially expressed proteins in progressive DN compared to stable DN in urine (A), depleted urine (B), and uEVs (C). Protein-protein interaction network was visualized by String: Functional protein association network (https://string-db.org). Pathway enrichment analysis was done by Kyoto Encyclopedia of Genes and Genome Pathways (KEGG) system, integrated within the String database.

3.5 Discussion

The main aim of this chapter was to compare urine and uEVs sample types in terms of biomarker discovery by exploring the size and quality of the respective proteomes. Because urinary proteomics can be challenging due to the highly abundant plasma proteins that leak through the glomeruli in kidney disease and therefore mask the rare cell-derived proteins that could be potential early markers of disease and disease progression (Prikryl et al., 2021), the study presented in this chapter was based on urine sample depleted of abundant plasma proteins. It was also based on uEVs isolated from urine, usually deprived of the same abundant plasma proteins. The two sample types were compared in terms of resulting proteomes, as task rarely accomplished before.

Gudehithlu et al. (2016) reported that in DN, uEVs ceruloplasmin and gelatinase correlated with pathological changes of the renal tissue but not the urine counterparts, suggesting that uEVs better reflect the cellular pathological phenotype than urine. Prikryl et al. (2021) suggested that uEVs proteomes were significantly less complex to analyse than that obtained from urine with lower effect of background plasma proteins on pathological insights.

In addition, although there is accumulating number of studies on urinary candidate diagnostic biomarkers of different kidney diseases, kidney disease progression is still not a much explored area (Takizawa et al., 2022; Anfaiha-Sanchez et al., 2024; Tepus et al., 2023). This chapter was focused on profiling proteins for candidate biomarkers of DN progression from non-invasive liquid biopsies urine and uEVs.

Qualitative proteomics revealed remarkably more distinct proteins identified in uEVs compared to two urine samples, in both stable DN and progressive DN cohorts (Figure 3.12). Although qualitative proteomics does not reflect on protein abundancies, but rather on library dimension, uEVs were richest in number of identified proteins. A similar finding was reported in a parallel study where proteomic profiling of uEVs and urine was performed using patients with breast cancer and healthy controls showing that the uEVs protein library was almost 10 times more enriched compared to urine (Jeanmard et al., 2023).

Quantitative proteomics of uEVs revealed a higher number of significantly differentially expressed proteins in progressive DN compared to stable DN than found in either urine or depleted urine samples (Figure 3.13). Interestingly, uEVs contained more proteins of intracellular compartments origin such as nucleus, endoplasmic reticulum, lysosome, or endosome/multivesicular body compared to urines (Figure 3.15). Proteins of intracellular origin were of greater interest than abundant plasma proteins because they are more likely to reflect the state and stage of kidney disease. It cannot be excluded the possibility that plasma proteins or even some of the extracellular proteins, localized in extracellular region/space or ECM could be present in urine as a product of filtration due to kidney injury and a damaged glomerular barrier and therefore these are likely less specific in reflecting pathophysiological condition.

Of those proteins discovered as significantly differentially changed in progressive vs stable DN, few urine or depleted urine unique markers were previously reported as linked with type 2 diabetes. These were cadherin-13 (CAD13), ganglioside GM2 activator

(SAP3), uteroglobin (UTER), and serum albumin (ALBU) (Jin et al., 2012). Although urinary SAP3 and UTER were found upregulated in moderate albuminuria compared to mild albuminuria state of type 2 diabetes patients, here the same proteins were found downregulated in progressive versus the stable stage of DN. It can be concluded that the expression of the two proteins increases with progression of albuminuria in diabetes, however not with progression of diabetes with CKD component. This suggests that diabetes and DN do differ in terms of markers of disease and therefore the two conditions are indeed separate.

From the list of significantly differentially changed proteins in progressive vs stable DN identified in uEVs (Table 3.7), four identified proteins were previously reported as uEVs biomarkers of CKD, however not of DN type. Complement C9 (CO9) was increased in uEVs from autosomal dominant polycystic kidney disease (Salih *et al.,* 2016), while dipeptidase 1 (DPEP1) was decreased in uEVs from patients with focal segmental glomerulosclerosis and its decrease correlated with the CKD stage (Stokman *et al*., 2019). Aminopeptidase N (APN) was decreased in uEVs isolated from immunoglobulin A nephropathy (Moon et al., 2011) compared with healthy controls. In addition, cubilin (CUBN) which is a known hereditary glomerular disease protein (Storm et al., 2011), was reported to be significantly increased in urine from moderate albuminuria compared to mild albuminuria condition (Jin et al., 2012), and together with APN is known to be a marker of uEVs originating from proximal tubular cells (Hogan et al, 2014; Tepus et al.,2023).

Moreover, seven proteins that were found significantly changed in uEVs from progressive DN were reported in a "urine study" done by Jin et al. (2012): afamin (AFAM),

serotransferrin (TRFE), hemopexin (HEMO), and haptoglobin (HPT) which were increased in moderate compared to mild albuminuria in urine but increased in uEVs from progressive compared to stable DN in the work from this chapter. Plasma serine protease inhibitor (IPSP) and alpha-N-acetylglucosaminidase (ANAG) were decreased in moderate albuminuria stage (Jin et al., 2012) and here these markers were also found decreased in uEVs from advanced stages of DN. Fibulin-5 (FBLN5), on the other hand, was decreased in moderate albuminuria urine, while in this study was found increased in the uEVs progressive stage of DN. The study by Jin et al. (2012) focused on urine proteins associated with DN, though not its progression, however the identification of similar dysregulated proteins in uEVs from progressive DN in this chapter supports their role in disease development and progression.

Despite efforts in this project, it must be recognised that differences in sample preparation of urine on one hand and uEVs on the other hand may limit a direct comparison of the urine and uEVs proteome; unfortunately, methodological variation between different urinary sample types cannot be avoided. Despite methodological differences, the comparison of the proteome from urine, depleted urine and uEVs in terms of biomarker discovery has given a valuable information about the range of protein discovery and protein content which can be found from each of the analysed sample. Another potential limitation of this study is the relatively small sample size (n=4), which led to low experimental power for the proteomic comparison of full urine and uEVs.

In conclusion, qualitative and quantitative proteomics of uEVs revealed a greater proteome size and quantities compared to urine featuring proteins of intracellular origin

rarely seen in urine, suggesting that uEVs is a strong alternative source of DN biomarkers.

Despite its small size, this pilot investigation highlighted the importance of uEVs proteomics in CKD biomarkers discovery.

CHAPTER 4:

Discovery of uEVs protein candidate

biomarkers of DN progression

4.1 Introduction

4.1.1 Diabetic nephropathy (DN) development and progression

Diabetic nephropathy (DN) is the most common type of CKD and the leading cause of the end stage kidney disease (ESKD) and kidney failure (Himmelfarb et al., 2013), also associated with increased cardiovascular morbidity and mortality in either diabetes type 1 (Groop *et al*., 2009) or diabetes type 2-linked kidney disease (Afkarian *et al*., 2013). It is characterised by the progressive decline in renal function, decreased estimated glomerular filtration rate (eGFR), the presence of persisting severely elevated albuminuria, and diabetic renal lesions (Alsaad and Herzenberg, 2007). There are also co-existing heterogeneous clinical features of DN such as retinopathy, neuropathy, and arterial hypertension (Parving *et al*., 1988; Parving *et al*., 1992). It has been proven that kidney inflammation is involved in DN development and progression (Jin et al., 2024) including accumulation of macrophages and T cells in glomerulus and interstitium, production of pro-inflammatory cytokines such as IL-1, TNF-α, INF-γ and chemokines such as CXCL8, CXCL10, MCP-1, CCL3, CCL5 which might be stimulated by high glucose or advanced glycation end products (AGEs), but also production of reactive oxygen species, all of which promotes cell injury and the development of fibrosis (Lim and Tesch, 2012). Furthermore, in addition to plasma and urinary levels of cytokines, chemokines and cell adhesion molecules are increasingly expressed in DN, and their levels correlate with albuminuria (Shikata et al., 2013).

Diagnosis and prediction of DN progression are based on measurements of eGFR [ml/min/year] and albuminuria measured as albumin to creatinine ratio (ACR [mg/g or mg/mmol]) or albumin excretion rate (AER [mg/24h]) in urine, categorised in different progression stages (Inker *et al*., 2014). However, the drop in eGFR is not always accompanied by an increased amount of albumin in the urine, which means that when albuminuria is observed for the first time, kidney function may already be impaired (Krolewski *et al*., 2014; Tsalamandris *et al*., 1994). Without biopsy, the gold standard for definitive diagnosis of renal fibrosis and CKD, that can show histopathological changes characteristic of diabetic glomerulopathy, the accurate and early diagnosis of DN remains a challenge (Selby and Taal, 2020). However, tissue biopsy is an invasive procedure that can lead to complications such as bleeding, perinephric hematoma, gross haematuria etc. (Whittier *et al*., 2004). In addition, it is prone to interobserver variation, which consequently results in inconsistent feedback (Furness and Taub, 2001) and is not always specific to a particular pathology (Bleyer *et al*., 2017). Moreover, renal biopsy is rarely done repeatedly, therefore, finding non-invasive, sensitive and specific biomarkers of early renal injury but also DN progression, that also allow longitudinal follow-up, are of great importance and interest.

Even if early diagnosis of DN is very important for timely treatment in order to prevent or slow down the progression, identification of the progressive stage of DN is critical for the development of new powerful treatment options that prevent renal failure but also potentially induce regression of DN (Hovind et al., 2001). In a 3-year longitudinal study, elevated levels of multiple factors were shown to be promoters of DN progression such

as albuminuria, serum cholesterol or hyperlipidaemia in general, glomerular lesions, blood pressure, blood glucose as well as declining eGFR (Hovind et al., 2001). In addition, cystatin C, fibroblast growth factor 23 (FGF23) and 21 (FGF21), solute tumour necrosis factor (TNF) receptors, pigment epithelium derived factor in serum, and liver-fatty acid binding protein (L-FABP) in urine are all considered prognostic markers of DN progression. However, despite this existing list of prognostic markers of DN progression obtained from serum or urine, there is still a great need for new markers that can predict DN progression with high sensitivity and specificity (Lee and Lam, 2015).

More recently, consideration of signalling pathways such as ferroptosis, autophagy/mitophagy, apoptosis/necroptosis, and lipid metabolism pathways have emerged as critical to determine the rate of DN progression, based on full-length transcriptome sequencing using serum samples (E et al., 2024).

4.1.2. uEVs biomarkers of DN

As reviewed in Tepus et al., 2023 and summarised in Table 4.1, some protein markers of DN have been proposed. Most of them are markers of early or late stage of DN. Two studies have reported protein markers with the potential to stratify different DN stages (Musante et al., 2015; De et al., 2017), however disease-stratifications were only based on differences in albuminuria levels, and not on longitudinal eGFR decline. Musante et al., (2015) showed that uEVs cathepsins were most increased in the moderate-to-severe albuminuria groups, while kallikrein 13 and proteinase-3 were predominantly expressed in the mild-to-moderate albuminuria groups, with a decrease observed in the severe albuminuria group (Musante et al., 2015). Furthermore, C-megalin (gp330) has been linked to the progression of albuminuria when detected in uEVs from DN subjects. It was found to correlate with albumin-creatinine ratio (ACR) and negatively correlate with eGFR (De et al., 2017).

In an early ELISA-based study, the expression of dipeptidyl peptidase IV (DPP IV) was explored in DN compared with controls and was positively correlated with ACR in diabetic patients with T2D, indicating that DPP IV in large uEVs may be associated with the severity of DN (Sun et al., 2012). Another early investigation involving a larger cohort found higher levels of Wilm's Tumor-1 (WT1) in the uEVs of T1D patients with proteinuria compared to those without proteinuria, whereas WT1 expression was absent in the non-diabetic control group. Because WT1 in uEVs could be detected earlier than proteinuria and glomerular damage, it was considered as a biomarker of early renal injury in

diabetics (Kalani et al., 2013). Zubiri et al. (2014) identified three potential markers of DN in uEVs, though in a small cohort of DN patients. These were α-microglobulin/bikunin precursor (AMBP) and histone-lysine N-methyltransferase (MLL3), both of which were upregulated in DN, and voltage-dependent anion-selective channel protein 1 (VDAC1), which was downregulated in the DN uEVs. However, due to its presence in most cell types, VDAC1 is regarded as a non-selective marker of kidney disease in DN. Next, in the rat model of early DN, downregulation of the regucalcin protein (or senescence marker protein-30) was observed. A pilot study examining regucalcin in the uEVs confirmed the same trend in both DN rats and humans (Zubiri et al., 2015). Furthermore, comparative proteomics between whole urine samples and small uEVs in a large study on patients with DN identified uEVs ceruloplasmin and gelatinase as early biomarkers of kidney disease (Gudehithlu et al., 2015). The levels of uEVs gelatinase and ceruloplasmin were found to correlate with their changes in renal tissue, suggesting that they could potentially serve as biomarkers of DN (Gudehithlu et al. 2015). However, uEVs ceruloplasmin was not exclusively associated to DN, as it also emerged as a potential early biomarker of membranous nephropathy (MN), IgA nephropathy (IgAN), lupus nephritis (LN), and focal segmental glomerulosclerosis (FSGS). In all these conditions, uEVs ceruloplasmin levels were consistently higher in CKD compared to control subjects (Gudehithlu et al., 2019). More recently, a connection between EVs ETS-related transcription factor Elf-3 (ELF3) with TGF-β signalling was established. Additionally, ELF3 was found to be specific for DN, as it was present in the uEVs of DN patients but not in the uEVs of other CKD patients. Given its correlation with eGFR decline, ELF3 was

proposed as an early marker of DN. CD73, an early target of the profibrotic TGF-β pathway and a detectable marker of progressing DN, was enriched in uEVs from DN patients, while it was found very low in healthy controls and in diabetics with no renal impact (Cappelli et al., 2020). Alpha1-antitrypsin, which was found deregulated in IgAN as shown in Table 4.2, was also found to be significantly increased in DN patients with severe albuminuria compared to DN patients with moderate or mild albuminuria, pre-diabetic cohort and healthy individuals. The study, however, was done by western blotting without further validation (Ning et al., 2020).

In addition to the DN type of CKD, all known uEVs protein markers for CKD other than DN are summarised in Supplementary table 2.

As discussed, all currently known uEVs protein markers of DN do not reflect on stability or progression of DN, and most studies were carried out by immunoblotting or ELISA, whereas the only high-throughput MS-based analysis involved a small sample size (Zubiri et al., 2014). The focus of this chapter was to identify uEVs protein markers associated with DN progression, which is an area that remains little explored.

Table 4.1: Proteins isolated from human uEVs, proposed to be biomarkers of DN

uEV protein	CKD type	Expression in CKD vs CTL	Sample size	Method of analysis	Source
Dipeptidyl peptidase-IV (DPP IV)	DN	↑	Mild albuminuria = 43 Moderate albuminuria = 50 Severe albuminuria = 34	ELISA	Sun et al., 2012, Diab Vasc Dis Res
Wilms's tumor 1 transcription factor (WT1)	DN	↑	DM1 = 48 Control = 25	Immunoblotting	Kalani et al., 2013, PLoS ONE
α-microglobulin / bikunin precursor (AMBP)	DN	↑	DN = 5 Control = 5	LC-MS/MS + SRM	Zubiri et al., 2014, Journal of Proteomics
Histone-lysine N-methyltransferase (MLL3)		↑			
Voltage-dependent anion-selective channel protein 1 (VDAC1)		↓			
Gelatinase	DN	↓	DN = 82 Control = ND	Fluorometric assay using FITC-gelatin as a substrate	Gudehithlu et al., 2015, Am J Nephrol
Ceruloplasmin		↑		Sandwich ELISA	
Regucalcin	DN	↓	DN = 4 Control = 3	Immunoblotting	Zubiri et al., 2015, Transl Res.
Cathepsin A, C, D, L, X/Z/P	DN	↑	DN = 37 Control = 12	Proteome profiler human protease array kit + inhibitor array kit	Musante et al., 2015, J Diabetes Res
Kallikrein 13					
Proteinase 3					
Cystatin B					
C-megalin	DN	↑	DM2 = 33 Control = 11	Immunoblotting	De et al., 2017, Diabetes
ETS-related transcription factor Elf-3 (ELF3)	DN	↑	DN = 25 MCD = 25 Control = 5	Immunoblotting	Sakurai et al., 2019, PLoS ONE
CD73	DN	↑	DN = 10 DM = 48 Control = 10	Immunoblotting	Cappelli et al., 2020, BBA Mol Basis Dis

↑ - increased expression; ↓ - decreased expression; DN - Diabetic Nephropathy; CTL - control

4.2 Aims of the chapter

The aims of this chapter were:

1) To discover uEVs protein markers of DN progression.

2) To select a set of most interesting uEVs proteins identified as candidate progression markers for further validation steps.

3) To validate selected uEVs protein markers of DN progression.

4) To identify candidate uEVs protein markers of DN by focusing on comparison between progressive DN and diabetic control.

4.3 Methods

4.3.1 Library-free DIA-NN MS analysis

The raw SWATH data were extracted directly from the human proteome FASTA-file using the library-free DIANN-software algorithm. DIA-NN approach offers significant improvement of the quantification precision and outperforms other existing DIA-MS analysis workflows. Raw data can be processed either by using a spectral library or in a library-free way where a protein sequence database (Uniprot, Swissprot, NCBI) is used. Library-free workflow consists of *in silico* digestion of the proteins and the prediction of the fragmentation spectra of the resulting peptides and the respective retention times by relying on deep neural networks (DNNs), artificial intelligence methods which are considered the preferred machine learning approach for analysis of complex data (Demichev et al., 2020). Library-free analysis was carried out by searching against the Swissprot human database (June 2021).

Differential expression of detected proteins between the analysed cohorts was performed using the open-source software for differential expression analysis StatsPro, developed by R shiny (Version 1.3.2). In the raw SWATH data, there was frequent occurrence of missing values of certain proteins in certain patient samples. These missing values are usually imputed by StatsPro. Because the interest for potential biomarker detection was in proteins with real protein intensity values rather than those with majority of imputed values based on approximations, the set criterion for differential expression analysis was to include only proteins with less than 40% missing

values meaning that the real protein intensity values had to be present in at least 60% of all analysed patient samples (stable and progressive individuals). Therefore, pre-processing data settings included number of missing values among individual samples being set at 0.4. Furthermore, the coefficients of variation (CV) threshold was set at 1.5 meaning that proteins with CV higher than 1.5 were excluded from the analysis. The false discovery rate (FDR) was estimated based on the Linear Models for Microarray Data (Limma) statistical test, which is a parametric test from an R/Bioconductor software package used for analysing gene expression data from various high-throughput experiments (Ritchie et al., 2015). The Benjamini-Hochberg (BH) method was used to correct p-values for multiple testing. Proteins were considered differentially expressed with the fold change (FC) ± 1.5, hence proteins with adjusted p < 0.05 and relative FC of 1.5 (i.e., the absolute logarithmic fold changes with base 2 |Log2(FCs)| > 0.585) were considered differentially expressed proteins.

4.3.1.1 Normalization approaches of the proteomic data

Proteomic data were normalized using two approaches: one based on an equal amount of EV protein, referred to as "equal amount," and the other based on an equal volume of starting urine used to isolate EVs, referred to as "equal volume". Before injecting the samples into the mass spectrometer, all lyophilized samples were resuspended in a volume matching their total protein mass prior to lyophilization, ensuring a concentration of 1 µg/µl for all samples. By applying an equal volume of 40 µl per sample, which corresponded to an equal protein amount (40 µg), the original dataset was considered normalized to "equal amount". To generate a dataset that represents the

scenario where equal volumes of EV suspension were injected despite variations in total protein mass, specifically in case of resuspending all lyophilized samples in the same volume, regardless of variations in protein quantification, all MS intensity values were multiplied by the EV total protein mass measured before lyophilization. This adjustment resulted in new intensity values that were considered normalized to "equal volume."

4.3.1.2 Data analysis of the differential expression data

Volcano plots were created using ggplot2 package in R statistical software. Heat maps were created in Morpheus versatile matrix visualization and analysis software. Classification of significantly differentially changed proteins in progressive DN based on their subcellular localization was performed using GeneCards (The Human Gene database) and focusing on compartments with only high confidence (levels 5 and 4). The confidence of each protein localization is ranked from 5 as the highest to 1 as the lowest and is derived from integrated evidence from database annotations, automatic text mining of the biomedical literature, and sequence-based predictions. Five subcellular localization categories were created: intracellular proteins, extracellular proteins, proteins that are localized intracellular / plasma membrane / extracellular proteins, proteins localized at plasma membrane / extracellular proteins, and plasma proteins listed in Anderson, 2002. Localization of significant proteins was individually checked before classifying proteins in certain categories.

Protein-protein interaction network of significantly upregulated and downregulated proteins in progressive compared to stable DN was visualized by String: Functional

protein association network v12.0. Network analysis was based on known and predicted

interactions, with confidence level 0.4 (medium confidence) which was default setting.

4.3.2 Antibody labelling

The antibodies used for the ExoView validation of uEVs protein expression were

conjugated with fluorophores using Alexa Fluor 488 (A20181, Invitrogen), 555 (A20187,

Invitrogen), and 647 (A20186, Invitrogen) antibody labelling kits. Before purchasing

antibodies, their composition was checked to ensure compatibility with Alexa Fluor

antibody labelling kit and thus conjugation efficiency. In particular, antibodies had to be

free from ammonium ions or primary amines, not resuspended in unsuitable Tris and

glycine buffers, but instead in PBS, also free from BSA or gelatin and with sodium azide

concentration lower than 3 mM. In addition, if possible, the antibodies with

concentration of about 1 mg/ml or above were selected.

The principle of the antibody conjugation using Alexa Fluor products is based on a

reactive dye, which contains a succinimidyl ester group, which binds to the primary

amine group of the protein, forming dye-protein conjugates with a very stable amide

bond.

All the procedure was done as per recommended protocol. Briefly, antibodies were

diluted in MilliQ water with 1/10th of 1M sodium bicarbonate in a total volume of 100

µl. Such protein solution was transferred to the vial with reactive dye, pipetted up and

down to fully dissolve, and incubated at RT for 1h covered from light. The spin column

was assembled as guided by the protocol and placed in a 12 x 75 mm polystyrene round-

bottom Falcon tube (352054, BD) as an alternative to recommended 13 x 100 mm glass tube. Purification resin was vortexed, and 1.5 ml added to the column. Pressure was applied for the drops of buffer to elute after which column with resin was centrifuged for 3 minutes at 1100 x g at RT using the AccuSpin Micro 17 centrifuge (Fisher Scientific) with a fixed angle rotor. After antibody-dye incubation, 100 µl of reaction was loaded dropwise to the centre of column and centrifuged for 5 minutes at the same speed.

4.3.2.1. Determination of the degree of labelling (DOL)

Degree of labelling was measured using NanoDrop 8000 spectrophotometer, blanked with nuclease free water, and set to Proteins and Labels protocol. Measures were taken in triplicates and mean values of protein absorbance (A280) and respective dye absorbance (Adye) were used for the calculations of protein concentration (M) and degree of labelling (moles dye per mole protein) by the following equations:

Protein concentration (M) = ([A280-(Adye x CF280)] x dilution factor) / 203,000

where CF280 value is a correction factor for the fluorophore's contribution to the absorbance at 280 nm (this value is provided in protocol) and 203,000 value is the molar extinction coefficient (ε) in cm-1 M-1 of a typical IgG at 280 nm.

Degree of labelling (DOL) = (Adye x dilution factor) / (εdye x protein concentration (M))

where εdye value is the approximate molar extinction coefficient of the specific dye (this value is provided in protocol).

4.3.3 Single EV analysis by ExoView

Single EV analysis was used as an approach to validate expression of uEVs proteins between the two analysed cohorts. In addition, it was used as an additional method to characterise uEVs based on the tetraspanin vesicular markers. The ExoView platform utilizes single-particle interferometric reflectance imaging sensor (SP-IRIS) technology to directly analyse the size, quantity, and protein characteristics of small EVs (>50 nm) in biofluids. EVs are captured by EV-specific membrane protein markers, such as tetraspanins (CD63, CD81, and CD9) antibodies, on microarray chips. They are then imaged individually and characterized using established fluorochrome-conjugated antibodies. In addition to tetraspanins, the co-expression of three different proteins can be analysed by probing the captured EVs with additional fluorescent antibodies (Daaboul et al., 2016; Bachurski et al., 2019). Urine pools consisting of 20 individual cell-free urine samples per cohort were made by taking equal volume from each individual sample and centrifuged at 5,000 x g for 5 min to pellet debris. Chips from Leprechaun Exosome Human Tetraspanin Kit (251-1044, UnChained Labs) were placed in the specific chip holder called chunk and pre-scanned by ExoView R200 reader with sizing thresholds 50 to 200 nm diameter, using ExoView Scanner acquisition software according to manufacturer instructions. This involved imputing chips information data, available on the USB stick provided with the kit, and creating a pre-scan folder where the data from the chip pre-scanning would be saved. Next, the numerical label of the chip selected for the analysis was matched with the right chip position where it was placed in the chunk.

4.3.3.1. Validation of candidate uEVs protein biomarkers by ExoView

Single EV analysis by ExoView can be useful approach to validate vesicular protein biomarkers detected by mass spectrometry (Crescitelli et al., 2021). For this purpose, urine samples were diluted 1:2 using 1x incubation buffer from the kit. With such dilution chips get saturated, so EV quantification is not the most accurate, however it is sufficient dilution to detect signal of the rare potential biomarkers. 70 µl of samples, which is the maximal volume that can be applied on the chip, was loaded on top of the already pre-scanned chips which were placed in 24-well plate on a bench free of vibrations. Sample incubation was performed overnight (17 h) at room temperature. The following day, chips were processed according to the ExoView Kit Assay Protocol for cargo and surface membrane immuno-fluorescence staining which can detect proteins located both on the surface of EVs and inside the EVs. The protocol involved three washing steps with 1x wash solution A for 3 min on the orbital shaker at ~200 rpm, before and in-between of 10-minute incubations of the chips in permeabilization solutions C and D after which antibody mixture was applied. Each conjugated antibody (for the analysed protein) was replaced with one of the tetraspanin antibodies. So even if all EVs were captured based on CD63, CD81 and CD9 probes, signal of the captured EVs was detected either by corresponding tetraspanins or antibodies conjugated with compatible fluorophores. In three independent experiments, vesicular cargo protein syntenin was used as a permeabilization control by replacing CD81 antibody. Antibodies of the analysed proteins were diluted in blocking buffer 1:30, with the final dilution 1:60 when added to the chips, syntenin was diluted 1:200 with a final dilution of 1:400, and regular tetraspanins 1:500

which became 1:1000 in a solution with chips. Plate was covered from light and incubated for 1 hour on orbital shaker, which was followed by a series of washing steps with 1x solution A, 1x solution B, and finally with fresh MiliQ water. Chips were then removed from 24-well plate in a 10-cm Petri dish filled with MiliQ water, moved back and forth to circulate the water but without exposing the chips to the air, leaned to a ~45° angle and removed from the water in one move without shaking. Similar as with pre-scanning, dry chips were placed in the chunk and imaged with an ExoView R200 reader using the Exoview scanner acquisition software. The pre-scan information file was imputed in the software and the fluorescence channels were activated.

The acquired images were processed in the ExoView Analyzer software where the fluorescence cutoff values for each analysed antibody were equally applied to each sample, in order to remove the peak of non-specific MIgG fluorescence. Data were further analysed in Excel and GraphPad prism.

Chips needed to be handled very carefully in order not to damage the antibodies on their surface (Deng et al., 2022): chips were held with EMS style tweezers with carbon fiber tips, fine tip when added to either chunk or 24-well plate, the centre of the chips was never touched, only corners. Furthermore, chips were placed in the centre of the wells of the 24-well plate ensuring they do not touch the edges of the well walls. After adding the samples to the chip surface, 24-well plate was carefully sealed ensuring an airtight seal is created so that chips to not dry out by sample evaporation. Square/flat tip tweezers were used to move chips from 24-well plate to the Petri dish in order to keep the chips in horizontal position and prevent them to dry out. Straight strong point Boley

style tweezers were used to lean the chip to ~45° angle and remove it from water so that water can quickly repel off the chip surfaces and the chips can get dry in a proper way.

4.3.3.2. Characterisation of uEVs by ExoView

ExoView was also used to characterize uEVs based on vesicular tetraspanin markers, which is typically a more common application of this platform (Breitwieser et al., 2022). The principle and procedure were the same as explained earlier in 4.3.3.1 with a few changes: since tetraspanins are abundant markers in EVs, urine dilution in 1x incubation solution was 1:75 instead of 1:2, also since tetraspanins are known to be localized on the surface of EVs, chips were processed following the ExoView Kit Assay Protocol for surface membrane immuno-fluorescence staining. Without the need for vesicle permeabilization step, the 10-min incubation steps with solutions C and D were omitted, so immediately after initial three washed in 1x solution A, chips were incubated with tetraspanin antibody mix. All three tetraspanin antibodies were diluted in blocking buffer 1:500 with a final dilution 1:1000.

4.4 Results

4.4.1 Discovery of uEVs candidate biomarkers of DN progression

Candidate progression biomarkers were searched by comparing uEVs proteomes from stable and progressive DN patients. A quantitative mass spectrometry approach was used to detect differentially expressed proteins in progressive and stable DN uEVs fractions. Patient samples, 20 from each cohort (19 from diabetic group) had characteristics shown in Table 4.2. In particular, eGFR loss was comparable as reported in Chapter 3 (Table 3.1) which includes these samples (2.22 and 2.25 ml/min/year in stable, -8.26 and -9.53 ml/min/year in progressive).

Table 4.2: Clinical information of patient samples used for protein biomarker discovery

	Stable DN	Progressive DN	Diabetic	Healthy
Number of subjects	20	20	19	20
Gender (Female/Male)	4/16	3/17	9/10	7/4 (ND=9)
Age (mean ± SD)	72.1 ± 9.2	65.7 ± 10.5 (ND=4)	56.3 ± 14.1 (ND=10)	41.9 ± 27.4 (ND=8)
BMI (mean ± SD)	28.8 ± 4.9 (ND=1)	28.6 ± 4.3 (ND=9)	29.5 ± 6.8 (ND=10)	25.9 ± 4.2 (ND=10)
Serum creatinine (mg/dL) (mean ± SD)	1.83 ± 0.2 (ND=1)	2.09 ± 0.3 (ND=4)	0.94 ± 0.1 (ND=10)	0.8 ± 0.2 (ND=10)
eGFR (ml/min) (mean ± SD)	37.05 ± 4.7	33.9 ± 4.9	84.1 ± 9.7 (ND=10)	ND
eGFR change (ml/min/year) (mean ± SD)	2.22 ± 3.3	-8.26 ± 2.8	NA	NA
CKD stage	CKD 3b	CKD 3b	NA	NA

*ND = not determined (not provided information), NA = not applicable

To understand what sample size would be needed to achieve experimental power of 95%, power analysis was performed with GPower v3.1.9.7 (Kang, H., 2021) as described in the Methods 2.2.7 (Chapter 2) using the effect size determined from the pilot experiment in Chapter 3 where proteomics from 4 stable and 4 progressive uEVs samples was compared. At confidence level above 65%, the sample size required for 95% power was shown to be 20 per cohort.

The proteomic workflow was developed as illustrated in Figure 4.1: urine samples were individually processed to isolate small and large uEVs which were then combined in a common fraction, resuspended and lysed in RIPA as described in the Methods 3.3.5.3 (Chapter 3). Equal protein amount of 40 µg uEVs lysate was digested and cleared of detergents ("S-trap" method). The obtained peptides from the four cohorts (stable DN, progressive DN, diabetic with no CKD, healthy) were then analysed by RP-HPLC-ESI-MS/MS for qualitative and quantitative proteomic analysis.

Currently accepted normalization methods in proteomic studies of EVs include normalization by total protein amount, the volume of the starting material, or the particle count from which proteins were digested and injected for mass spectrometry analysis (Welsh et al., 2024). In this project, data were normalized in two ways; by equal protein amount and equal volume of starting urine used to isolate EVs. The rational for this dual analysis was that healthy urines are not rich in proteins so normalizing to equal amount could result in either "artificial" protein overloading from healthy samples or underloading from the disease group. Therefore, a "posteriori" data correction was applied to correct MS intensity values by EV total protein mass obtained from equal

starting volume of urine (5 ml) used to isolate EVs (as explained in the Methods 4.3.1.1).

"Equal amount" or "equal volume" data refer to these two approaches.
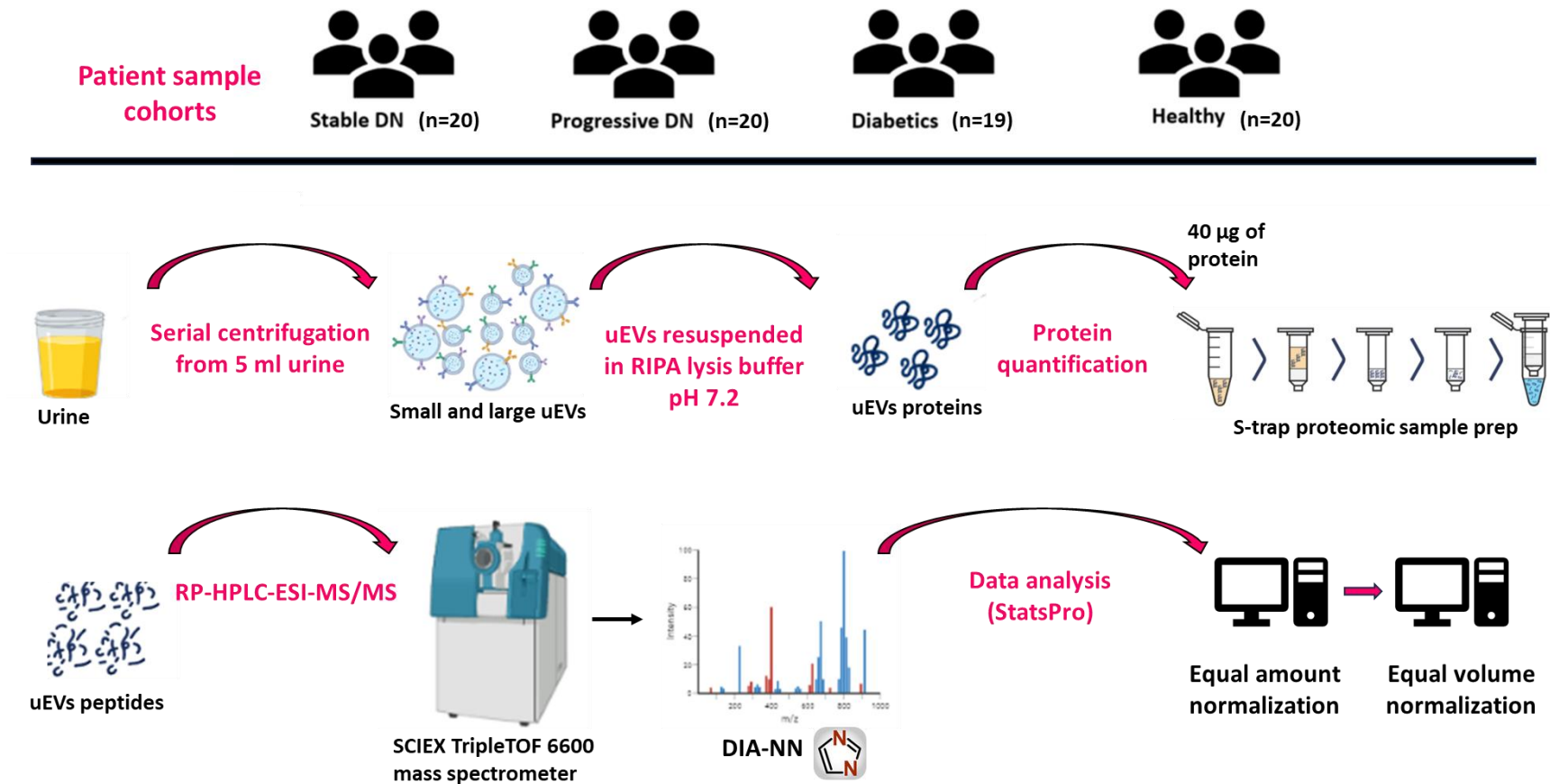
Figure 4.1 Proteomic workflow used for the discovery of uEVs protein biomarkers. Urine samples from all patients (n=79) were individually processed including uEVs isolation, uEVs protein quantification, generation of peptides for MS followed by MS run, and data analysis. Total uEVs were analysed (large and small uEVs). Figure was created in Biorender and PowerPoint.

4.4.1.1 Qualitative proteomics

In order to find new uEVs protein candidate biomarkers of DN progression, uEVs proteins from stable and progressive DN cohorts, and from diabetic and healthy control cohorts were screened using "library-free" SWATH/DIA mass spectrometry which led to a detection of 2017 proteins in total from all four cohorts. The spectral library was not generated as in the "OneOmics" approach shown in Chapter 3, instead, proteins present in the analysed samples were identified by searching against the Swissprot human database as described in the Methods 4.3.1. The number of identified proteins between the four cohorts was compared as shown in Figure 4.2. When the proteome from 20 individual samples was combined, 1669 proteins were detected in the progressive DN group, 1493 proteins in the stable DN, 1483 proteins in healthy individuals, and 1720 proteins in the diabetic with no CKD. In terms of shared proteome, 54% proteins were present in all four cohorts, with only ~4% of unique proteins found in progressive DN, ~4% of unique proteins in the diabetic group, ~1% in the stable DN and ~2% in the healthy group.
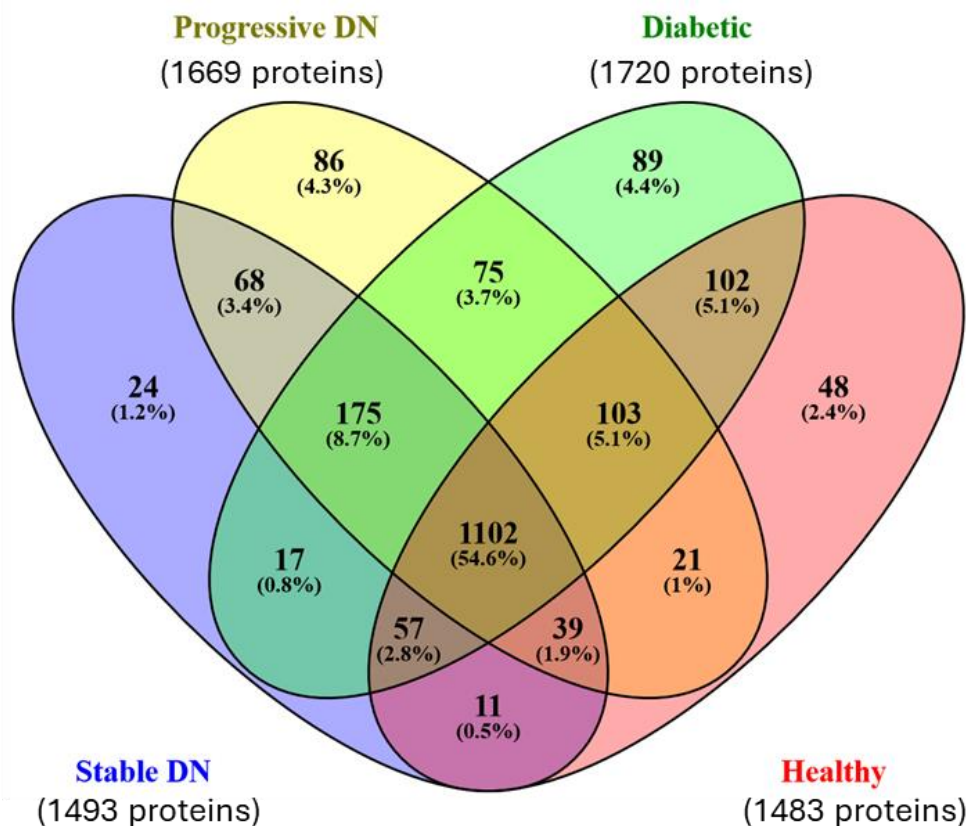
Figure 4.2: Qualitative proteomics showing number of proteins identified in each of the four analysed cohorts consisting of 20 individual samples (or 19 in diabetic group), based on library-free DIANN approach. Total uEVs (large and small) were isolated from 5 ml of urine. Out of 2017 detected proteins, 54% were present in all four cohorts. Venn diagram was created using Venny 2.1 online tool.

When the progressive DN cohort was compared only to stable DN (Figure 4.3A), 77.8% proteins were present in both group and 16% of proteins were unique in the progressive DN. Similarly, 75.2% of progressive DN proteins were common to diabetic group and 11.1% were unique proteins in progressive DN (Figure 4.3B). In a comparison of healthy and progressive DN cohort, 67% were common and 21.4% were unique to progressive DN group (Figure 4.3C).
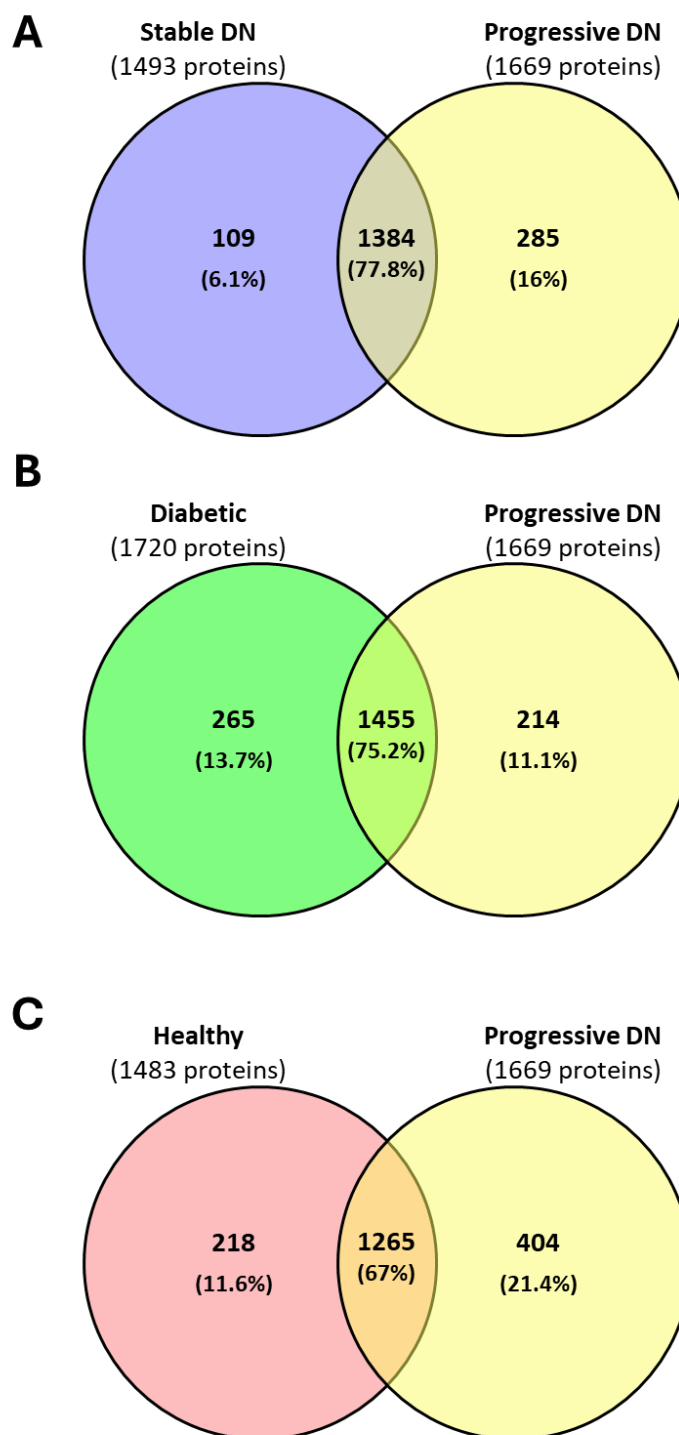
Figure 4.3: Qualitative proteomics showing comparison in the number of proteins identified between progressive DN and stable DN (A), diabetic (B) and healthy (C) groups based on library-free DIANN approach. More than 77% proteins were common to stable and progressive DN, about 75% proteins were common to diabetic and progressive DN, and 67% to healthy and porgressive DN. Venn diagrams were created in PowerPoint.

4.4.1.2 Quantitative proteomics

Following qualitative proteomics, quantitative SWATH/MS was carried out to explore significantly differentially expressed proteins in progressive DN progression.

Comparative proteomics was carried out in 20 progressive and 20 stable, however 3 progressive and 1 stable sample were excluded post MS processing due to lack of signal. Therefore, quantitative proteomics data were obtained from 17 progressive DN and 19 stable DN samples.

Proteins were considered statistically differentially expressed if p-value from Limma statistical test, adjusted according to Benjamini Hochberg, was < 0.05, and with fold change threshold of 1.5 meaning that the absolute logarithmic fold changes with base 2 |Log2(FCs)| was > 0.585.

Since the main focus of this chapter was DN progression, data here present proteomic comparison between progressive DN and stable DN stage, however significantly differentially changed proteins between progressive DN and diabetics with no CKD are shown in Result section 4.4.4.

Differential expression analysis of proteins that were present in at least 60% of biological replicas in both stable and progressive groups included 15% of proteins (305 out of 2017). Of them, 72 proteins were significantly differentially expressed in progressive DN (n=17) compared to stable DN (n=19): 29 upregulated (Table 4.3) and 43 downregulated (Table 4.4). Most of the highly upregulated proteins were abundant plasma proteins such as apolipoprotein, hemopexin, vitronectin, and also complement component C9, histidine rich glycoprotein and albumin. In general, majority of upregulated proteins fell

in the category of classic abundant plasma proteins, with the exception of thromboxane-A synthase, serine protease HTRA4, pigment epithelium derived factor, and ETS domain-containing transcription factor ERF-like. The most highly downregulated proteins in the progressive group (Table 4.4) were vasorin, podocalyxin, and mucin 1 which are not plasma proteins.

Table 4.3: Significantly differentially <u>upregulated</u> proteins in uEVs from progressive (n=17) vs stable DN (n=19) in dataset normalized to equal protein amount, listed according to fold change (Prog /Stab)

	Protein ID	Protein name	FC (Prog / Stab)	Adj. p-value (BH)
	APOA1_HUMAN	Apolipoprotein A-I	6.290	2.67E-05
	HEMO_HUMAN	Hemopexin	4.672	0.00093
	VTNC_HUMAN	Vitronectin	4.417	0.000569
	CO9_HUMAN	Complement component C9	4.408	0.001672
	HRG_HUMAN	Histidine-rich glycoprotein	4.219	0.001721
	ALBU_HUMAN	Albumin	4.036	0.004574
*	VTDB_HUMAN	Vitamin D-binding protein	3.975	0.001721
*	THAS_HUMAN	Thromboxane-A synthase	3.753	0.002016
*	HTRA4_HUMAN	Serine protease HTRA4	3.608	0.002108
	ANT3_HUMAN	Antithrombin-III	3.519	0.003294
	TTHY_HUMAN	Transthyretin	3.446	0.012877
	TRFE_HUMAN	Serotransferrin	3.247	0.009066
	HEP2_HUMAN	Heparin cofactor 2	3.154	0.016021
	FIBG_HUMAN	Fibrinogen gamma chain	3.074	0.012541
	FIBB_HUMAN	Fibrinogen beta chain	2.998	0.01383
	APOA4_HUMAN	Apolipoprotein A-IV	2.977	0.0184
	PLMN_HUMAN	Plasminogen	2.930	0.016021
	ITIH2_HUMAN	Inter-alpha-trypsin inhibitor heavy chain H2	2.926	0.01383
	IGHG1_HUMAN	Immunoglobulin heavy constant gamma 1	2.892	0.0184
	ITIH1_HUMAN	Inter-alpha-trypsin inhibitor heavy chain H1	2.862	0.019568
*	KAIN_HUMAN	Kallistatin	2.854	0.018581
	IGHG3_HUMAN	Immunoglobulin heavy constant gamma 3	2.742	0.016656
	THRB_HUMAN	Prothrombin	2.641	0.016656
	APOH_HUMAN	Beta-2-glycoprotein 1	2.594	0.022769
*	PEDF_HUMAN	Pigment epithelium-derived factor	2.592	0.044009
	CO2_HUMAN	Complement C2	2.547	0.048569
	CO4A_HUMAN	Complement C4-A	2.547	0.047608
*	ERFL_HUMAN	ETS domain-containing transcription factor ERF-like	2.525	0.031597
	CO4B_HUMAN	Complement C4-B	2.408	0.035983

p value adjusted to Benjamini-Hochberg (BH) procedure

* represent proteins that are not in the category of plasma proteins

Table 4.4: Significantly differentially <u>downregulated</u> proteins in uEVs from progressive (n=17) vs stable DN (n=19) in dataset normalized to equal protein amount, listed according to fold change (Prog /Stab)

Protein ID	Protein name	FC (Prog / Stab)	Adj. p-value (BH)
VASN_HUMAN	Vasorin	-6.101	0.00013
PODXL_HUMAN	Podocalyxin	-5.419	0.000569
MUC1_HUMAN	Mucin-1	-4.46	0.001721
AMPE_HUMAN	Glutamyl aminopeptidase	-3.972	0.001721
PSCA_HUMAN	Prostate stem cell antigen	-3.961	0.001721
MXRA8_HUMAN	Matrix remodeling-associated protein 8	-3.64	0.007266
CTL2_HUMAN	Choline transporter-like protein 2	-3.605	0.001785
SAP3_HUMAN	Ganglioside GM2 activator	-3.543	0.004241
IPSP_HUMAN	Plasma serine protease inhibitor	-3.274	0.004574
ANAG_HUMAN	Alpha-N-acetylglucosaminidase	-3.272	0.007013
EGF_HUMAN	Pro-epidermal growth factor	-3.059	0.01383
CD59_HUMAN	CD59 glycoprotein	-3.008	0.01242
CD81_HUMAN	CD81 antigen	-2.872	0.012541
BROX_HUMAN	BRO1 domain-containing protein BROX	-2.854	0.01242
NID1_HUMAN	Nidogen-1	-2.84	0.00862
CUBN_HUMAN	Cubilin	-2.828	0.013185
ALDOB_HUMAN	Fructose-bisphosphate aldolase B	-2.791	0.012541
SLUR2_HUMAN	Secreted Ly-6/uPAR domain-containing protein 2	-2.764	0.048569
PLS1_HUMAN	Phospholipid scramblase 1	-2.761	0.021666
SCTM1_HUMAN	Secreted and transmembrane protein 1	-2.755	0.016643
6PGL_HUMAN	6-phosphogluconolactonase	-2.749	0.023685
LG3BP_HUMAN	Galectin-3-binding protein	-2.742	0.01383
CPVL_HUMAN	Probable serine carboxypeptidase CPVL	-2.736	0.016134
NAPSA_HUMAN	Napsin-A	-2.732	0.021808
CPNE3_HUMAN	Copine-3	-2.73	0.024766
CHM2B_HUMAN	Charged multivesicular body protein 2b	-2.678	0.021808
TSN1_HUMAN	Tetraspanin-1	-2.667	0.016021
UROM_HUMAN	Uromodulin	-2.626	0.023685
LMAN2_HUMAN	Vesicular integral-membrane protein VIP36	-2.603	0.026247
UPK2_HUMAN	Uroplakin-2	-2.601	0.016825
PTGDS_HUMAN	Prostaglandin-H2 D-isomerase	-2.565	0.019441
VPS4A_HUMAN	Vacuolar protein sorting-associated protein 4A	-2.497	0.023685
NEP_HUMAN	Neprilysin	-2.483	0.016825
PDCD6_HUMAN	Programmed cell death protein 6	-2.483	0.02653
GGT1_HUMAN	Glutathione hydrolase 1 proenzyme	-2.433	0.024766
ASSY_HUMAN	Argininosuccinate synthase	-2.408	0.02653
XPP2_HUMAN	Xaa-Pro aminopeptidase 2	-2.4	0.024081
HACD1_HUMAN	Very-long-chain (3R)-3-hydroxyacyl-CoA dehydratase 1	-2.39	0.025552
TPP1_HUMAN	Tripeptidyl-peptidase 1	-2.382	0.04121
UPK1A_HUMAN	Uroplakin-1a	-2.373	0.024766
DPEP1_HUMAN	Dipeptidase 1	-2.329	0.039177
A2GL_HUMAN	Leucine-rich alpha-2-glycoprotein	-2.075	0.047528
AMPN_HUMAN	Aminopeptidase N	-2.063	0.047608

*p value adjusted to Benjamini-Hochberg (BH) procedure; all proteins are of cellular origin

Differential expression of proteins was visualized by volcano plot as shown in Figure 4.4 where blue dots on the left-hand side represent all significantly downregulated proteins (in progressive DN), while red dots on the right-hand side represent all significantly upregulated proteins. Grey dots instead, which are below red line indicating significance with adjusted $p<0.05$, are proteins included in differential expression analysis but not being significantly changed in progressive vs stable DN group. The most highly significantly changed proteins in progressive compared to stable DN were above the green line which indicates the highest significance of adjusted $p<0.001$. The most significantly changed proteins were apolipoprotein A-1, vitronectin and hemopexin which were upregulated, and vasorin and podocalyxin which were downregulated in progressive DN.
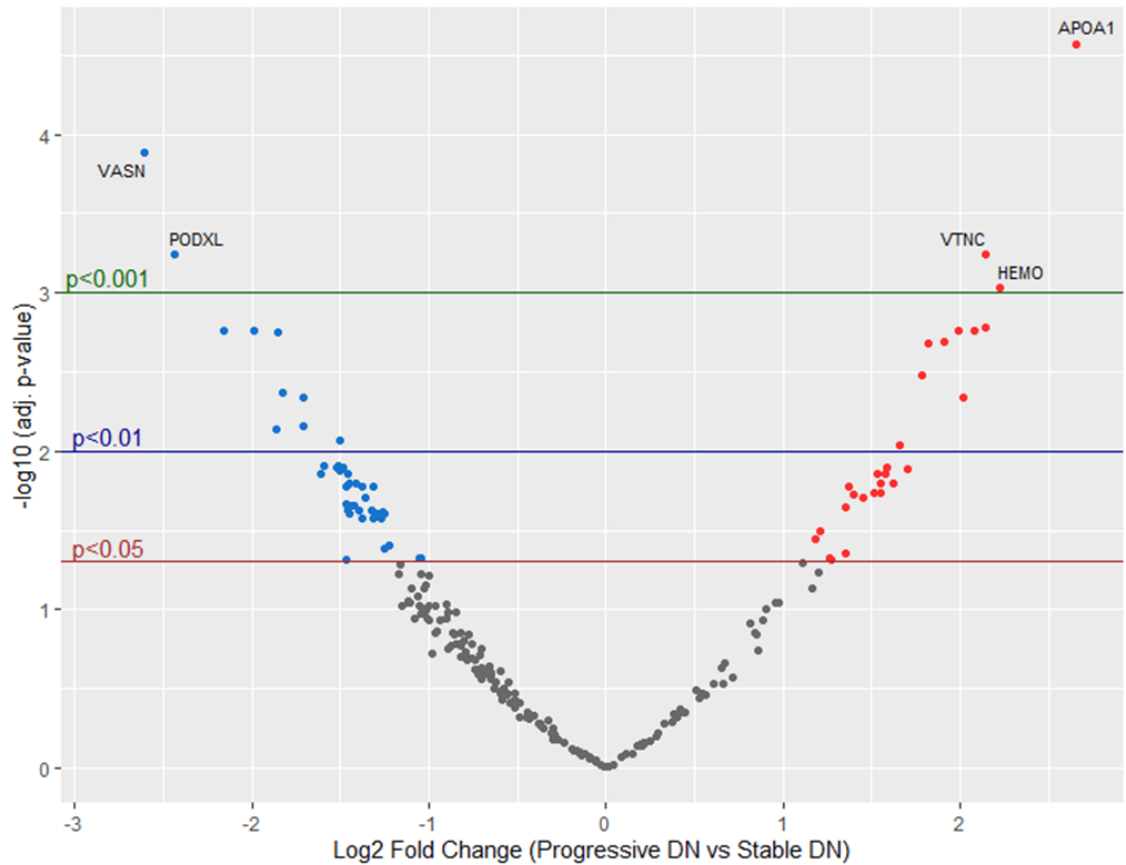
Figure 4.4: Proteins significantly differentially expressed in uEVs from progressive DN (n=17) compared to stable DN (n=19) cohorts from the dataset normalized to equal protein amount. Differential expression of proteins was expressed as fold change (progressive DN/stable DN) which was transformed into log base 2. Out of 2017 detected proteins, 305 proteins (15%) were eligible for quantification according to criterion to be present in at least 60% of patient samples as explained in 2.2.6.5 Methods. Of them, 72 were significantly differentially expressed: 29 upregulated (red dots) and 43 downregulated (blue dots).

Furthermore, a heat map was generated to visualize the expression of each significantly changed protein per single stable and progressive individual (Figure 4.5). As with the volcano plot, the blue colour was given to low expression in progressive DN, and the red colour to high expression in progressive DN. For most plasma proteins such as apolipoprotein A-I, vitronectin, hemopexin, complement component C9, serine protease HTRA4 or antithrombin-III there was a clear prevalence of bright red among progressive DN individuals and bright blue or lighter red in stable DN individuals. On the other hand, cellular proteins vasorin, podocalyxin, mucin-1, glutamyl aminopeptidase, CD59 glycoprotein and BRO1 domain-containing protein BROX all showed a consistent bright blue / light red in progressive individuals and a brighter red in stable DN patients. However, there are also proteins less consistent in their presence across individuals per group, such as complement C4-A, secreted Ly-6/uPAR domain-containing protein 2, or complement C2. In the progressive patient labelled in heat map as P_6 (corresponding to PDN138), a consistent very high expression of nearly all proteins was observed even though this was not the most progressive patient (eGFR loss of -7.53 ml/min/year).

Figure 4.5: Heat map showing significantly differentially changed proteins in progressive vs stable DN from the dataset normalized to equal protein amount, in each patient sample. Proteins are listed from the most significant on top to the least significant at the bottom, according to the adjusted p-values. Blue colour represents low expression and red high expression in progressive DN. S=stable, P=progressive. Heat map was created in Morpheus.

Significantly differentially expressed proteins between progressive and stable DN were also shown in histograms on Figure 4.6 where proteins are listed from most differentially expressed according to log2FC on top to the least changed at the bottom. Again, blue histograms represent downregulated proteins in progressive DN, and red histograms represent upregulated proteins in progressive DN.
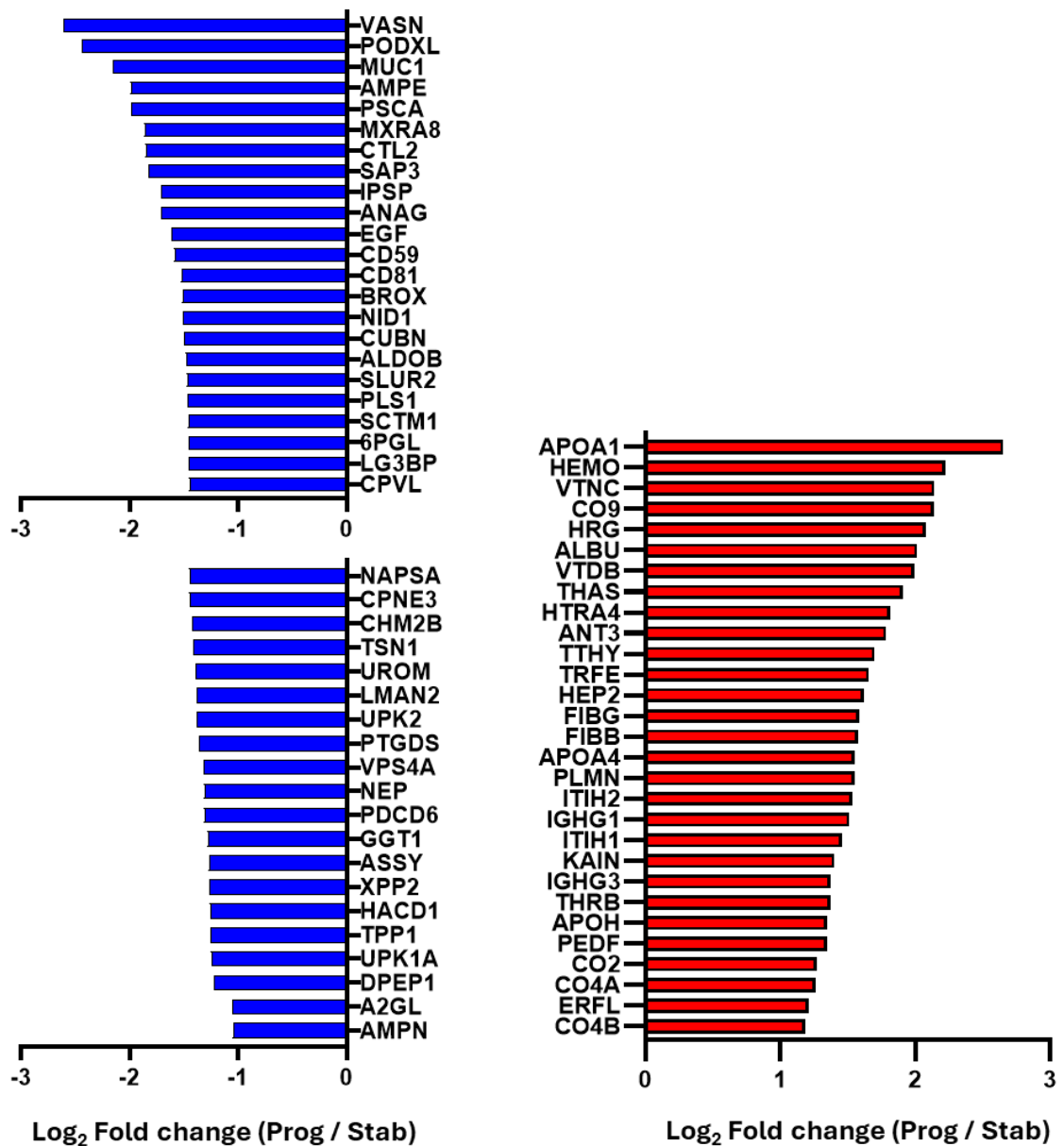
Figure 4.6: List of proteins significantly downregulated (blue, n=43) and upregulated (red, n=29) in uEVs from progressive DN (n=17) compared to stable DN (n=19) cohorts, from the dataset normalized to equal protein amount. Proteins are listed according to log$_2$ fold change ratios from the most differentially expressed on top to the least differentially expressed at the bottom.

Having analysed differential expression in dataset normalized to equal protein amount, a further analysis was performed using dataset normalized to equal uEVs volume, as explained in Methods 4.3.1.1. Out of 335 quantified proteins, 46 proteins (14%) were found significantly differentially deregulated in progressive vs stable DN: 32 were upregulated in progressive DN (Table 4.5) and 14 were downregulated (Table 4.6). Protein findings were very similar between the two analysed datasets (normalized for equal protein amount and normalized to equal uEVs volume), with 26 proteins (81%) being the same as those identified in the equal amount dataset. Upregulated proteins that were newly found in equal volume dataset were complement C3, which was the most overexpressed protein in progressive DN vs stable DN, complement component C8 beta chain, alpha-2-macroglobulin, immunoglobulin heavy constant gamma 2, complement component C7 and afamin. Of the 14 downregulated proteins, 78.6% (11 proteins) was the same as reported in the previous analysis. Three new proteins emerged as significantly downregulated in progressive vs stable DN in this new analysis and these were apolipoprotein D, keratin and charged multivesicular body protein 2a.

Table 4.5: Significantly differentially <u>upregulated</u> proteins in uEVs from progressive (n=17) vs stable DN (n=19) in dataset normalized to equal volume of uEVs, listed according to fold change (Prog /Stab).

	Protein ID	Protein name	FC (Prog / Stab)	Adj. p-value (BH)
+	CO3_HUMAN	Complement C3	9.600	0.000135
	APOA1_HUMAN	Apolipoprotein A-I	7.797	1.36E-05
	CO9_HUMAN	Complement component C9	6.152	0.00047
	VTNC_HUMAN	Vitronectin	5.840	0.000287
	HRG_HUMAN	Histidine-rich glycoprotein	5.396	0.000705
	ALBU_HUMAN	Albumin	5.191	0.002148
	VTDB_HUMAN	Vitamin D-binding protein	5.088	0.000705
	THAS_HUMAN	Thromboxane-A synthase	4.843	0.000705
	HTRA4_HUMAN	Serine protease HTRA4	4.541	0.000742
	ANT3_HUMAN	Antithrombin-III	4.448	0.00185
	TTHY_HUMAN	Transthyretin	4.176	0.008128
	TRFE_HUMAN	Serotransferrin	4.053	0.004031
	HEP2_HUMAN	Heparin cofactor 2	3.953	0.007763
	FIBG_HUMAN	Fibrinogen gamma chain	3.869	0.005686
	FIBB_HUMAN	Fibrinogen beta chain	3.842	0.007081
	PLMN_HUMAN	Plasminogen	3.776	0.005686
	ITIH2_HUMAN	Inter-alpha-trypsin inhibitor heavy chain H2	3.732	0.007763
	IGHG1_HUMAN	Immunoglobulin heavy constant gamma 1	3.671	0.011681
	ITIH1_HUMAN	Inter-alpha-trypsin inhibitor heavy chain H1	3.453	0.008077
	KAIN_HUMAN	Kallistatin	3.408	0.007823
	IGHG3_HUMAN	Immunoglobulin heavy constant gamma 3	3.333	0.008128
	THRB_HUMAN	Prothrombin	3.333	0.007823
	PEDF_HUMAN	Pigment epithelium-derived factor	3.258	0.024475
	CO2_HUMAN	Complement C2	3.057	0.02529
	CO4A_HUMAN	Complement C4-A	3.027	0.023654
	CO4B_HUMAN	Complement C4-B	2.936	0.016893
+	CO8B_HUMAN	Complement component C8 beta chain	2.932	0.029379
	ERFL_HUMAN	ETS domain-containing transcription factor ERF-like	2.918	0.008977
+	A2MG_HUMAN	Alpha-2-macroglobulin	2.874	0.035577
+	IGHG2_HUMAN	Immunoglobulin heavy constant gamma 2	2.780	0.023861
+	CO7_HUMAN	Complement component C7	2.535	0.045889
+	AFAM_HUMAN	Afamin	2.507	0.032899

p value adjusted to Benjamini-Hochberg (BH) procedure

+ represent proteins that were newly found in this analysis

Table 4.6: Significantly differentially <u>downregulated</u> proteins in uEVs from progressive (n=17) vs stable DN (n=19) in dataset normalized to equal volume of uEVs, listed according to fold change (Prog /Stab)

	Protein ID	Protein name	FC (Prog / Stab)	Adj. p-value (BH)
	VASN_HUMAN	Vasorin	-4.780	0.000705
	PODXL_HUMAN	Podocalyxin	-4.213	0.00275
+	APOD_HUMAN	Apolipoprotein D	-3.950	0.00234
	MUC1_HUMAN	Mucin-1	-3.456	0.007326
	PSCA_HUMAN	Prostate stem cell antigen	-3.097	0.008977
	AMPE_HUMAN	Glutamyl aminopeptidase	-3.091	0.008123
+	K2C1_HUMAN	Keratin, type II cytoskeletal 1	-3.029	0.021284
	MXRA8_HUMAN	Matrix remodeling-associated protein 8	-2.807	0.040846
	SAP3_HUMAN	Ganglioside GM2 activator	-2.755	0.015216
	CTL2_HUMAN	Choline transporter-like protein 2	-2.689	0.017349
	ANAG_HUMAN	Alpha-N-acetylglucosaminidase	-2.597	0.030373
	IPSP_HUMAN	Plasma serine protease inhibitor	-2.546	0.024824
	CD59_HUMAN	CD59 glycoprotein	-2.486	0.02529
+	CHM2A_HUMAN	Charged multivesicular body protein 2a	-2.344	0.040846

p value adjusted to Benjamini-Hochberg (BH) procedure

+ represent proteins that were newly found in this analysis

The distribution of significantly upregulated and downregulated proteins, as well as not significantly changed proteins, in progressive vs stable DN were again shown by volcano plot (Figure 4.7). It can be seen that vasorin, apolipoprotein A-1 and vitronectin were again among the most significantly changed proteins in progressive DN, which appear above green line representing p<0.001, with six extra proteins: complement C3, complement C9, thromboxane-A synthase, histidine-rich glycoprotein, vitamin D-binding protein, and serine protease HTRA4.
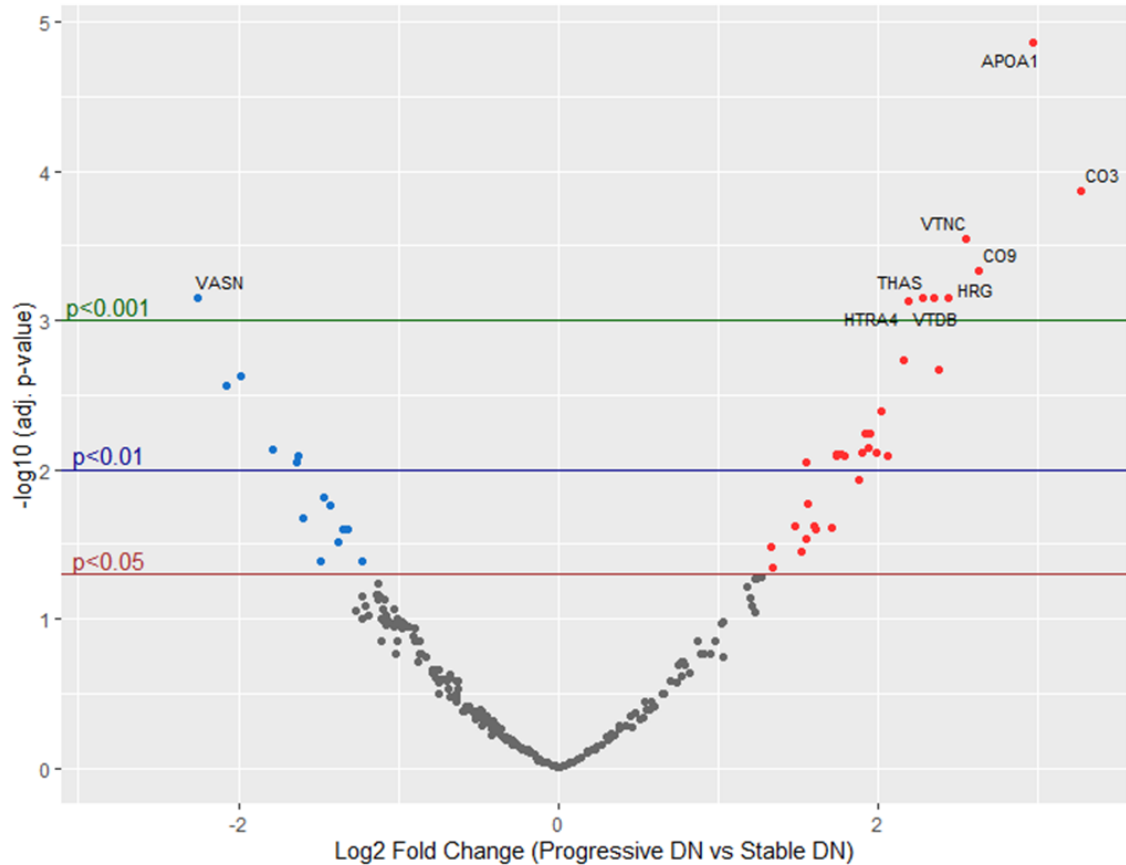
Figure 4.7: Proteins significantly differentially expressed in uEVs from progressive DN (n=17) compared to stable DN (n=19) cohorts from the dataset normalized to equal volume of uEVs. Differential expression of proteins was expressed as fold change (progressive DN/stable DN) which was transformed into log base 2. Out of 2017 detected proteins, 334 proteins (17%) were eligible for quantification according to criterion to be present in at least 60% of patient samples as explained in 2.2.6.5 Methods. Of them, 46 were significantly differentially expressed: 32 upregulated (red dots) and 14 downregulated (blue dots).

Same as with equal amount dataset, the heat map was generated to visualize the expression of each significantly changed protein per single stable and progressive individual (Figure 4.8). By observing the heat maps from equal amount and equal volume datasets, the broader difference in the progressive vs stable DN patients is visualized, meaning that protein expression is more uniform among individuals in each cohort. For example, the top significantly upregulated proteins apolipoprotein A-I, complement C3, vitronectin, complement component C9 and vitamin D-binding protein showed the prevalence in red colour (high expression) in progressive individuals and the prevalence in blue colour (low expression) in stable individuals. On the other hand, cellular proteins vasorin, apolipoprotein D, podocalyxin or mucin-1, showed consistent low expression in progressive individuals (blue) and high expression in stable individuals (red).

Furthermore, similar as in equal amount dataset where one progressive patient had consistently very high expression of nearly all proteins, in this analysis one stable patient labelled as S_1 (corresponding to PDN232) had consistently very low expression of majority of proteins. Agan, according to the eGFR loss value (-0.24 ml/min/year) this was not one of the most stable patient samples.
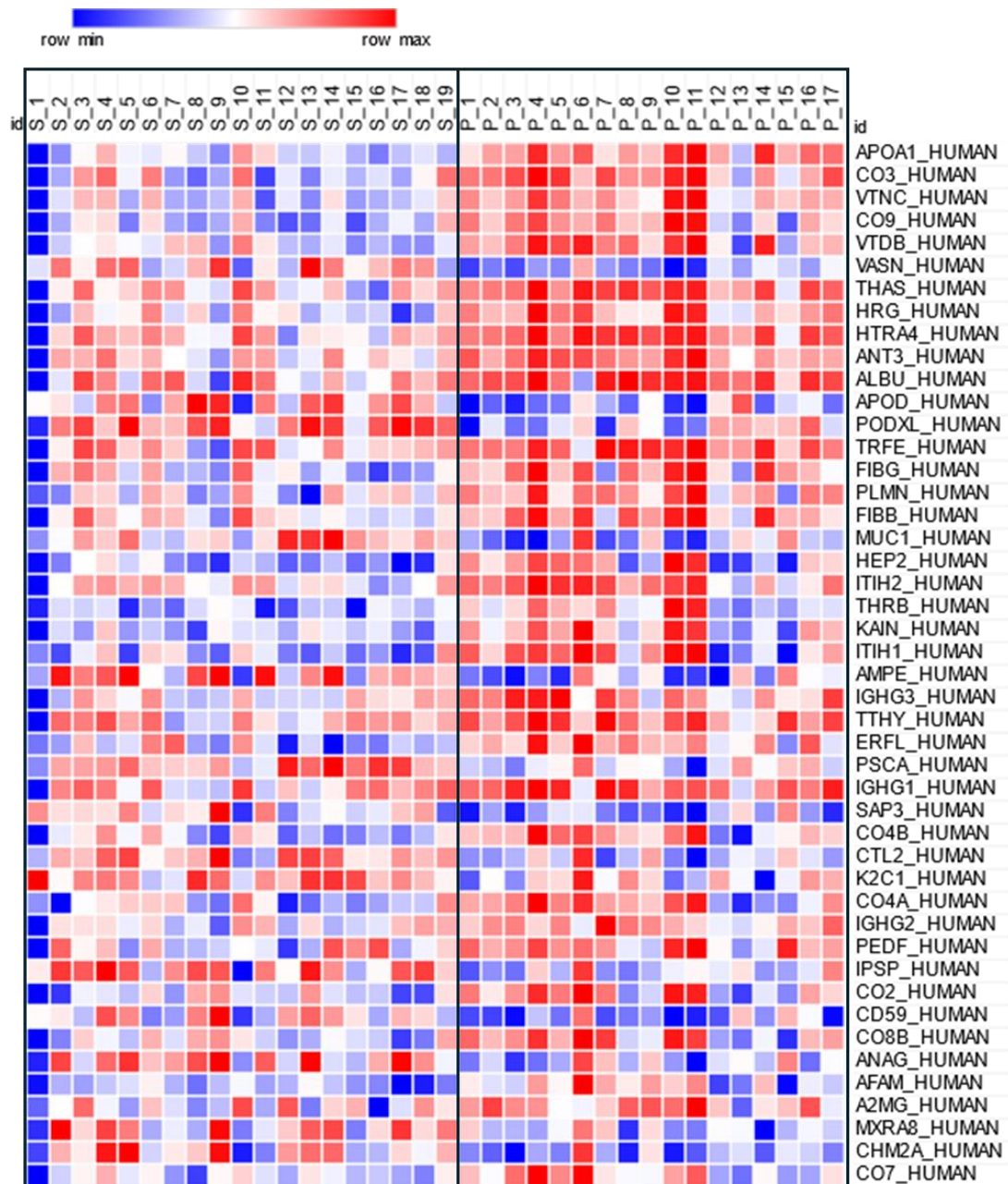
Figure 4.8: Heat map showing significantly differentially changed proteins in progressive vs stable DN from the dataset normalized to equal volume of uEVs, in each patient sample. Proteins are listed from the most significant on top to the least significant at the bottom, according to the adjusted p-values. Blue colour represents low expression and red high expression in progressive DN. S=stable, P=progressive. Heat map was created in Morpheus.

Finally, histograms of the significantly downregulated (blue) and upregulated (red) proteins in progressive DN were created from the equal volume dataset as shown in Figure 4.9.
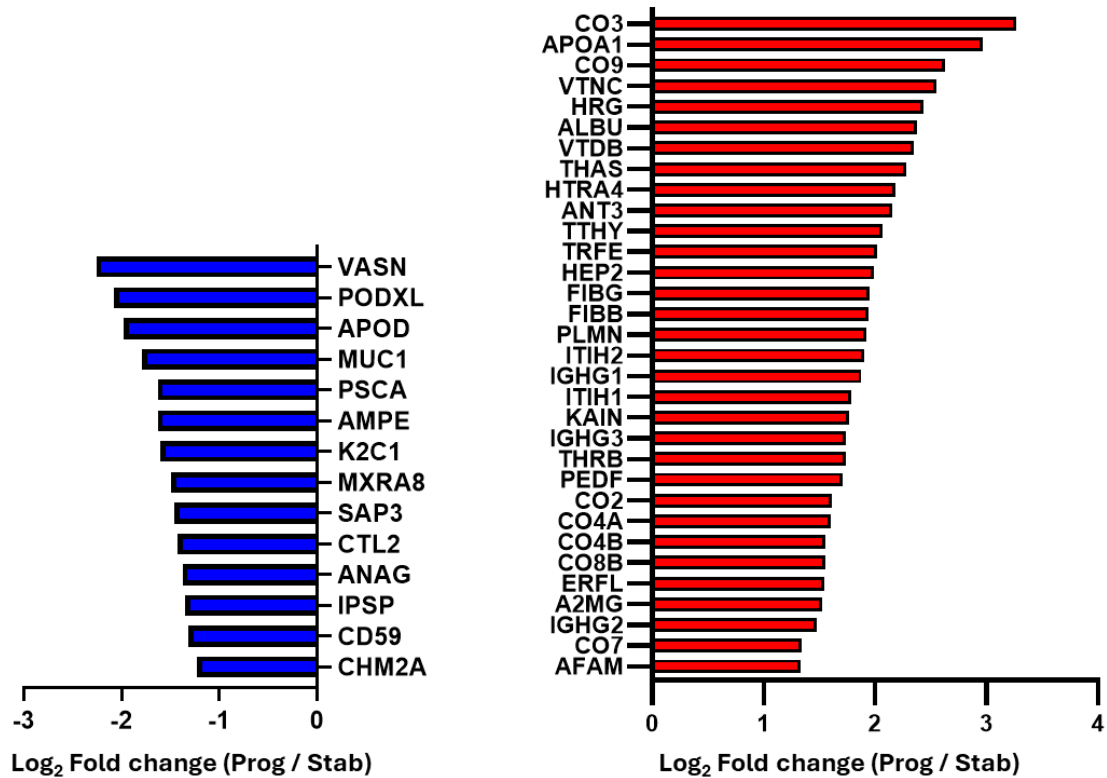
Figure 4.9: List of proteins significantly downregulated (blue, n=14) and upregulated (red, n=32) in uEVs from progressive DN (n=17) compared to stable DN (n=19) cohorts, from the dataset normalized to equal volume of uEVs. Proteins are listed according to log$_2$ fold change ratios from the most differentially expressed on top to the least differentially expressed at the bottom.

To classify proteins based on their subcellular localization, GeneCards (The Human Gene database) was used focusing on compartments with 5 and 4 level of confidence, as explained in Methods 4.3.1.2. Proteins were grouped in five subcellular localization categories: intracellular proteins, extracellular proteins, proteins that are localized intracellular / plasma membrane / extracellular proteins, proteins localized at plasma membrane / extracellular proteins, plasma proteins (Anderson, 2002).

Pie charts representation of subcellular localization for all significantly changed proteins (up- and down-regulated) in progressive vs stable DN from both normalization-based datasets are shown in Figure 4.10. The CKD progression proteins in uEVs were prevalently of plasma origin and proteins with either intracellular or extracellular location of which fraction the plasma membrane / extracellular proteins were more represented. The "equal volume" dataset, however, was characterised by more plasma origin proteins compared to the "equal amount" dataset, suggesting that the "equal amount" analysis is more suitable for detection of cell-origin uEVs biomarkers of progression.
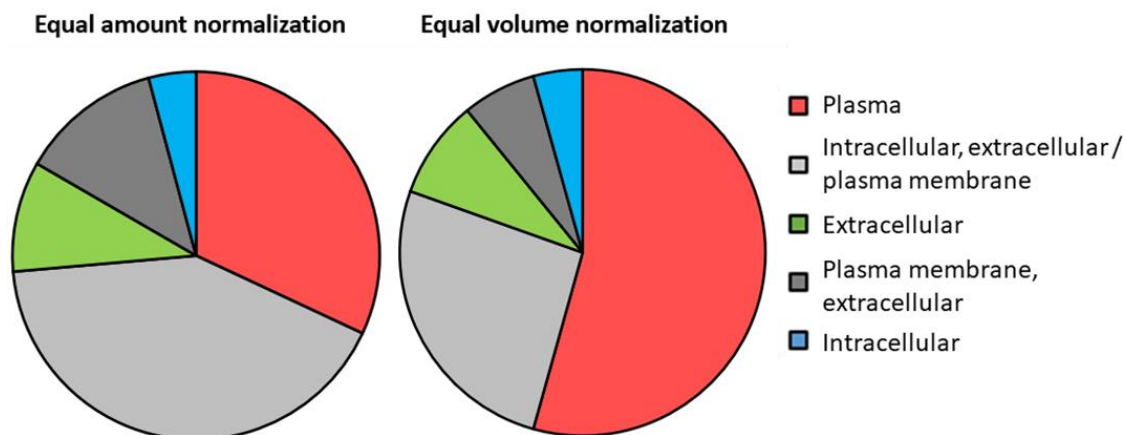
Figure 4.10: Localization of significantly differentially expressed proteins in uEVs from progressive compared to stable DN cohort from datasets normalized based on equal protein amount and based on equal volume of uEVs. Proteins were grouped in five categories: 1. intracellular proteins (blue), 2. extracellular proteins (green), 3. proteins that are localized intracellularly but also at the plasma membrane and/or extracellularly (light grey), 4. proteins that are localized at plasma membrane and extracellularly (dark grey), and 5. plasma proteins (red). Categories were made according to the Localization section within GeneCards focusing only on compartments with 5 and 4 level of confidence. Category of plasma proteins was created based on the human plasma protein list published in Anderson, 2002, Mol Cell Proteomics. Pie charts were created in Excel.

To explore if significantly changed proteins make clusters and interactions, protein-protein interaction networks of both upregulated and downregulated proteins combined were visualized by String v12.0: Functional protein association network as described in the Methods 4.3.1.2. Protein-protein interaction showed a network of 70 proteins and 325 interactions (equal amount dataset) (Figure 4.11), or 43 proteins and 286 interactions (equal volume dataset) (Figure 4.12) depending on the dataset. Networks from both datasets formed clusters of proteins involved in biological processes related to vesicular trafficking (proteins labelled with red circles) and response to wounding (proteins labelled with blue circles). When the networks were divided into upregulated and downregulated proteins, the enrichments in biological processes were associated solely with the proteins that were significantly upregulated. It is known that in kidney fibrosis, production of vesicles is increased (Liu, X., et al., 2020), and subsequent vesicular trafficking and vesicle-mediated cell-to-cell communication play a role in fibroblast activation and fibrosis development. Production of vesicles is also associated with the process of wound healing (Zhou, X., et al., 2017). Therefore, it is not surprising that the enrichment of biological processes regulating vesicle-mediated transport and/or response to wounding appeared in proteins that were significantly upregulated in uEVs from progressive DN.
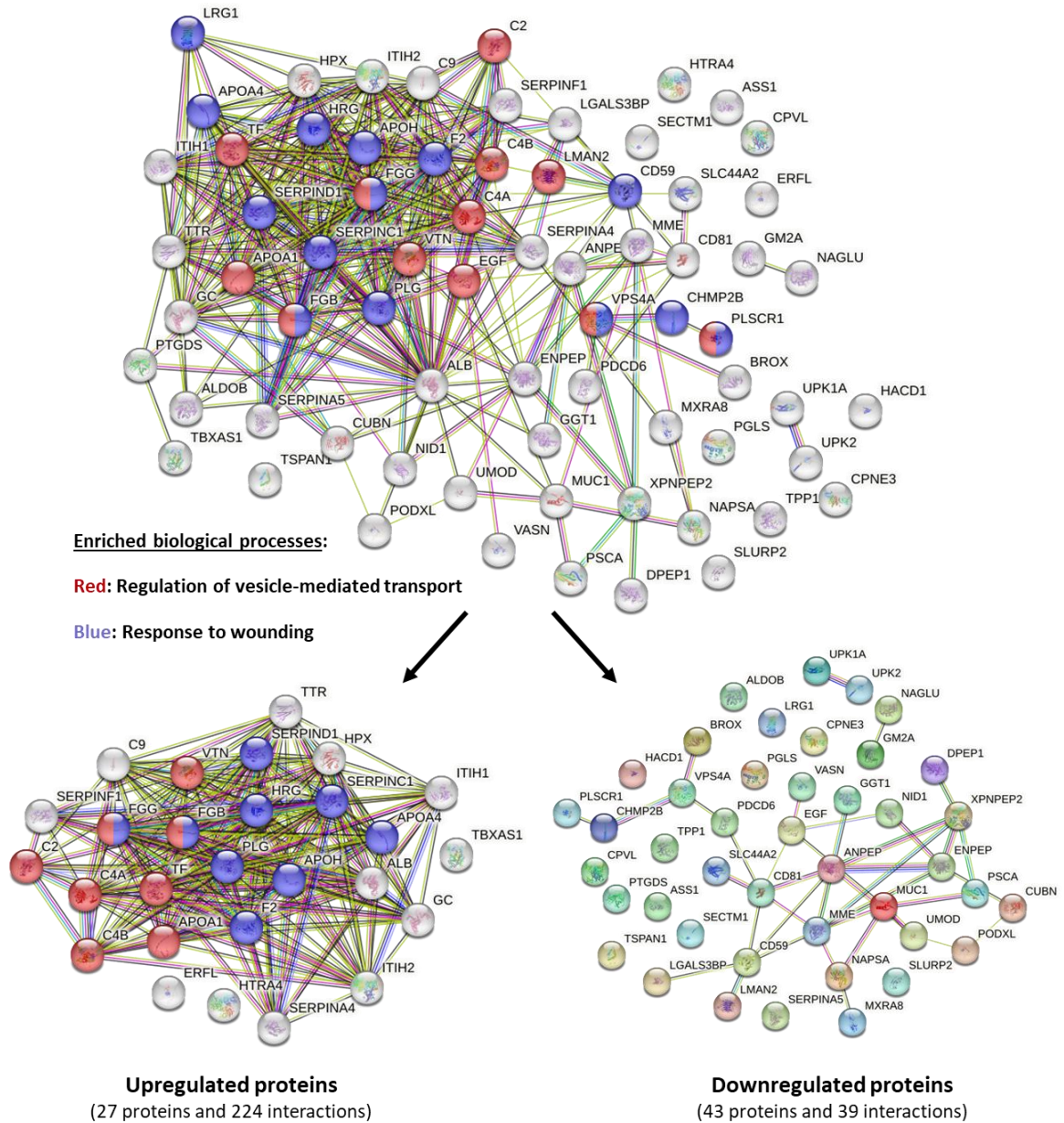
Figure 4.11: Protein-protein interaction network and enriched biological processes of significantly differentially expressed proteins in uEVs from progressive DN compared to stable DN from "equal amount" dataset. Protein network consisted of 70 proteins and 325 interactions. The upregulated uEVs proteins associated with DN progression were related with vesicular trafficking and regulation of wounding. Network analysis was done in String v12 with confidence level of 0.4 (default) based on known and predicted interactions.

235
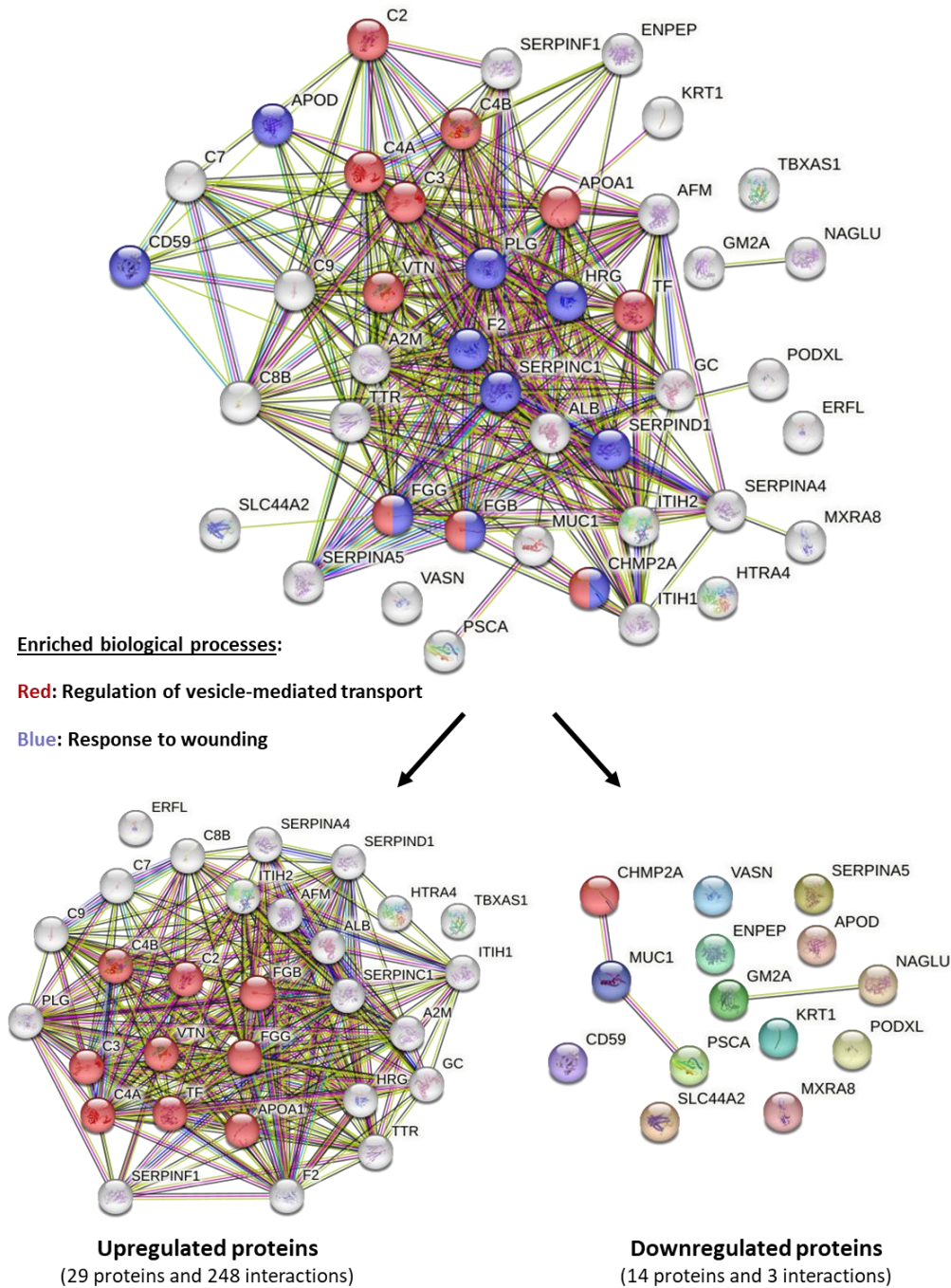
Figure 4.12: Protein-protein interaction network and enriched biological processes of significantly differentially expressed proteins in uEVs from progressive DN compared to stable DN from "equal volume" dataset. Protein network of this dataset consisted of 43 proteins and 286 interactions. The upregulated uEVs proteins associated with DN progression were enriched in biological processes related with vesicular trafficking but not response to wounding. Network analysis was done in String v12 with confidence level of 0.4 (default) based on known and predicted interactions.

4.4.2 Selection of uEVs candidate biomarkers for validation

A selection of proteins significantly differentially expressed in progressive DN compared to stable DN were validated by single EV quantification. Plasma proteins were excluded to focus on proteins originating from kidney cells, which are more likely to reflect on pathophysiological condition and possibly underlying mechanisms of disease. In particular, proteins which resulted significantly changed in progressive DN from both analyses were included in the validation. The only exception was protein argininosuccinate synthase (ASSY) which was found significantly downregulated in uEVs from progressive DN in one analysis (equal amount), however it was also found downregulated in DN progressive uEVs in an independent mass spectrometry experiment carried out by a post-doc in the Verderio's team (Tonoli et al., unpublished data).

Overall, twelve uEVs proteins associated with progression were selected for validation based on significance level (equal amount dataset) (Figure 4.13). Of them, thromboxane-A synthase (THAS) and pigment epithelium-derived factor (PEDF) were upregulated in progressive DN (Table 4.3), while the others (vasorin, podocalyxin, mucin-1, glutamyl aminopeptidase, choline transporter-like protein 2, ganglioside GM2 activator, plasma serine protease inhibitor, alpha-N-acetylglucosaminidase, CD59 glycoprotein, argininosuccinate synthase) were downregulated (Table 4.4).
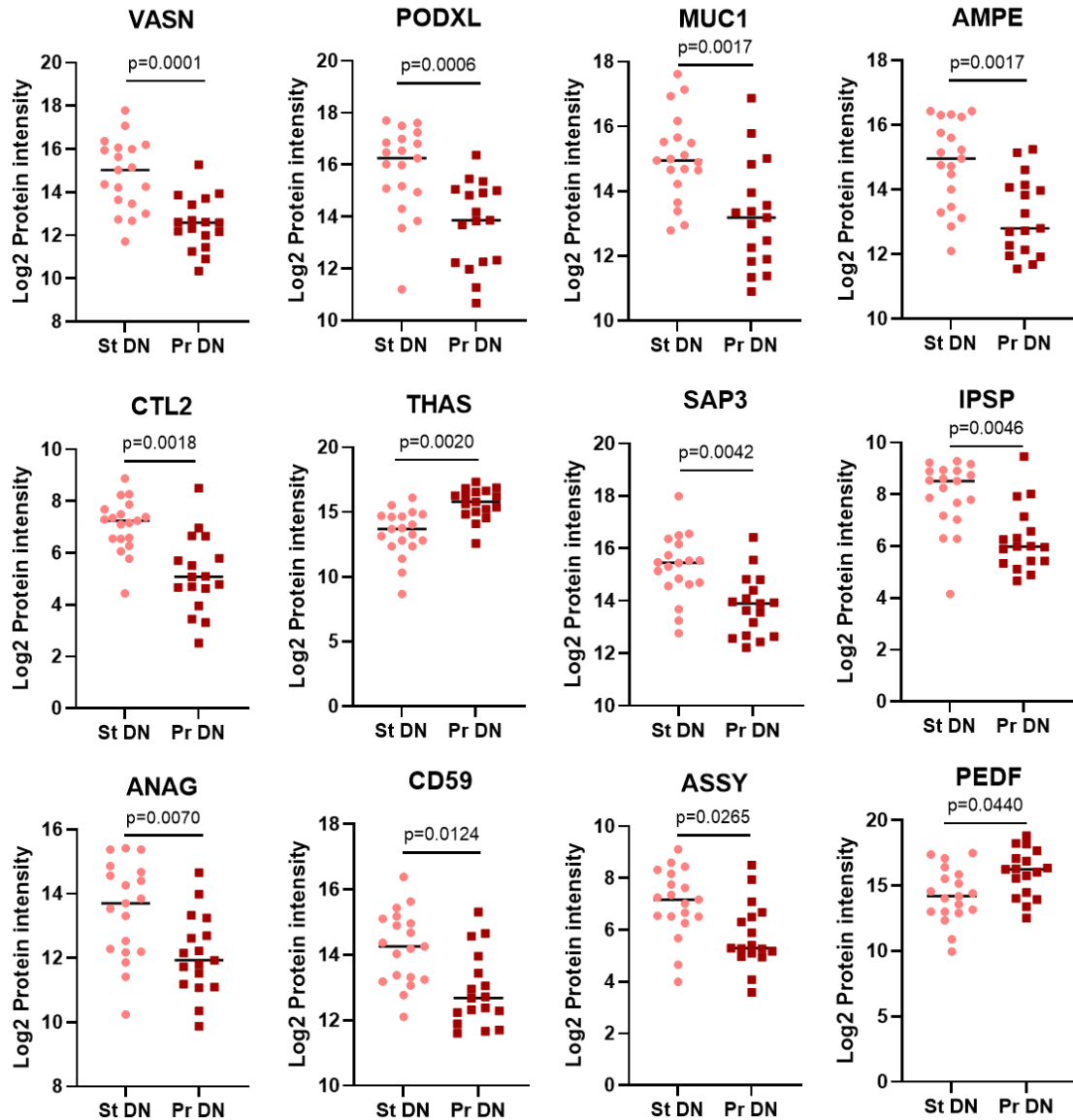
Figure 4.13: Top uEVs protein biomarker candidates that were considered for validation step to confirm their potential to predict DN progression. Each dot represents protein intensity of individual patient sample, either stable (St DN) or progressive (Pr DN). Proteins were listed according to the significance, from the most significant to the least significant based on the adj. p-values from the equal protein amount dataset (Limma statistical test with Benjamini-Hochberg correction). Graphs were created in Graph-Pad Prism.

Table 4.7 summarised the selected putative DN progression uEVs biomarkers and showed their known function.

Vasorin (VASN) is a single-pass transmembrane glycoprotein predominantly expressed in vascular smooth muscle cells (Bonnet et al., 2018). VASN was reported to directly bind to TGF-β and attenuate its signalling (Ikeda et al., 2004), while its degradation increased TGF-β activity (Pintus et al., 2018). It showed to have critical role in physiology since its deletion affects vascular smooth muscle cell phenotype, angiotensin II levels, nitric oxide signalling and intracellular calcium homeostasis altogether leading to premature death (Louvet et al., 2022). Podocalyxin (PODXL) is a single-pass transmembrane sialomucin which is expressed in the kidneys on the surface of podocytes and vascular endothelial cells (Refaeli et al., 2020). Its function is to increase the adhesion of cells to immobilized ligands and increase the rate of migration and intercellular contacts through integrin-dependent mechanisms (Larrucea et al., 2008). However, its opposite function has been demonstrated recently showing an anti-adhesive and impermeable role in epithelium (Heng et al., 2021). Mucin-1 (MUC1) is a multifunctional transmembrane protein expressed on the apical surface of most epithelial cells but also hematopoietic cells. One of its main functions is to provide a protective barrier to prevent pathogen access to the cell surface (Dhar and McAuley, 2019), however it is also involved in the renewal and differentiation of the epithelium, in the modulation of cell adhesion and in cell signalling (von Mensdorff-Pouilly et al., 2000). Glutamyl aminopeptidase (AMPE) is a zinc metallopeptidase that is the dominant enzyme for the degradation of angiotensin II in the glomerulus, highly expressed in kidney tissues, especially in podocytes and tubular

epithelium. Its deficiency has shown to affect glomerular integrity and to lead to increased susceptibility to glomerular injury (Marahrens et al., 2021). Choline transporter-like protein 2 (CTL2) mainly functions in the mitochondria where it acts as ethanolamine/proton antiporter and is responsible for the extracellular uptake and intracellular balance of ethanolamine (Taylor et al., 2021). It has been shown that CTL deficiency results in abnormal production of mitochondrial reactive oxygen species and decrease in ATP in platelets (Bennett et al., 2020). Furthermore, using mouse model it has been shown that CTL2 is expressed and highly glycosylated in kidney tissue, specifically in glomeruli in the lining of Bowman's capsule (Kommareddi et al., 2010). Thromboxane-A synthase (THAS) is a membrane protein structurally similar to the cytochrome P450 family and is particularly abundant in peripheral blood leukocytes, spleen, lung, and liver, but it is also expressed in the kidney, placenta, and thymus (Miyata et al., 1994). It functions to metabolize prostaglandin H2, a cyclooxygenase product, into thromboxane A2, which is a stimulator of vasoconstriction and platelet secretion and aggregation (Hsu et al., 1999). Ganglioside GM2 activator (SAP3) is one of the lysosomal proteins with function to mediate intermembrane cholesterol transfer (Babalola et al., 2007). It might be responsible for the development of obesity-related disorders since it was shown to accelerate insulin secretion and impair insulin signal transductions through its ligand-binding domain (Higashi et al., 2011). Plasma serine protease inhibitor (IPSP), also known as protein C inhibitor (PCI), is a member of the serine protease inhibitor (SERPIN) superfamily and procoagulant and proinflammatory factor with function to inhibit serine proteases such as plasminogen activator, thrombin, factor Xa, factor XIa,

kallikrein etc (España et al., 1995; Hayashi et al., 2004). IPSP was found in urine and shown to be expressed in renal tubular cells (Radtke et al., 1994). Alpha-N-acetylglucosaminidase (ANAG) is a lysosomal enzyme responsible for lysosomal degradation of heparan sulphate by hydrolysing the α-linked *N*-acetylglucosamine residues in heparan sulphate (Meikle et al., 2005). CD59 glycoprotein (CD59) is a transmembrane protein with the function of complement activity regulation, which is achieved by binding to the C5-8 complex and inhibiting the assembly of C9 monomers into the complement terminal complex, thereby protecting cells from complement-mediated damage (Meri et al., 1990). Argininosuccinate synthase (ASSY) is a urea cycle enzyme that catalyses the conversion of citrulline and aspartate to form argininosuccinate in arginine biosynthesis (Berning et al., 2008). Pigment epithelium-derived factor (PEDF) is a glycoprotein, neurite-promoting factor and a member of the serine protease inhibitor (serpin) family with neurotrophic activity (Becerra et al., 1995). Furthermore, PEDF was reported to have anti-fibrotic functions through downregulation of TGFβ1, reduction in extracellular matrix accumulation, regulation of endothelial-to-mesenchymal transition, and inhibition of Wnt signalling pathway (Xi, 2020). In kidney, it was shown to be expressed mostly in glomerulus where it functions as endogenous inhibitor of TGF-β expression and fibronectin production (Wang, J., et al., 2005).

Table 4.7: Summary of localizations and functions of uEVs proteins considered for validation to confirm their potential as biomarkers of DN progression (listed according to significance)

Candidate biomarker	Cellular localisation	Function
Vasorin (VASN)	Lysosome, plasma membrane, extracellular	Inhibition of TGF-beta signalling (Ikeda et al., 2004)
Podocalyxin (PODXL)	Nucleus, cytoskeleton, plasma membrane, extracellular	Regulation of cell adhesion and cell morphology (Larrucea et al., 2008)
Mucin 1 (MUC1)	Nucleus, plasma membrane, extracellular	Regulation of cell adhesion, providing a protective layer on epithelial cells, modulation of cell signalling (Dhar and McAuley, 2019; von Mensdorff-Pouilly et al., 2000)
Glutamyl aminopeptidase (AMPE) *	Plasma membrane, extracellular	Maintenance of glomerular structure and intrarenal homeostasis of angiotensin peptides, regulation of central hypertension (Marahrens et al., 2021)
Choline transporter-like protein 2 (CTL2)	Mitochondrion, plasma membrane, lysosome, extracellular	Ethanolamine transport and phosphatidylethanolamine synthesis (Taylor et al., 2021)
Thromboxane–A synthase (THAS)	Endoplasmic reticulum, cytosol	Catalysis of the conversion of prostaglandin H2 into thromboxane A2 (Hsu et al., 1999)
Ganglioside GM2 activator (SAP3) *	Lysosome, cytosol, plasma membrane, extracellular	Mediating intermembrane transfer of cholesterol (Babalola et al., 2007)
Plasma serine protease inhibitor (IPSP)	Plasma membrane, extracellular	Inactivation of serine proteases by binding irreversibly to their serine activation site (Espana et al., 1995; Hayashi et al., 2004)
Alpha-N-acetylglucosaminidase (ANAG) *	Lysosome, extracellular	Degradation of heparan sulphate (Meikle et al., 2005)
CD59 glycoprotein (CD59) *	Plasma membrane, extracellular	Regulation of complement activity (Meri et al., 1990)
Argininosuccinate synthase (ASSY) *	Cytosol, nucleus, mitochondrion, extracellular	Catalization of the condensation of citrulline and aspartate to argininosuccinate (Berning et al., 2008)
Pigment epithelium-derived factor (PEDF) *	Extracellular	Neurotrophic activity, inhibition of angiogenesis, inhibition of TGF-β expression and fibronectin production (Becerra et al., 1995; Wang et al., 2005)

* Proteins that were already detected as uEVs biomarkers of DN progression in unpublished work by the Verderio's group

Out of 12 listed proteins that met the criteria to be considered for validation, seven were selected and validated by single vesicle analysis ExoView: vasorin (VASN), podocalyxin (PODXL), mucin-1 (MUC1), glutamyl aminopeptidase (AMPE), thromboxane-A synthase (THAS), ganglioside GM2 activator (SAP3), and argininosuccinate synthase (ASSY). While VASN, PODXL, MUC1 and AMPE were selected because these were the top significantly changed proteins, THAS was interested because it was one of the two upregulated proteins in progressive DN and compared to PEDF with higher significance. Among the first 5 selected proteins, only AMPE was already found significantly differentially expressed in uEVs from progressive vs stable DN in an independent experiment done by this group, in particular by this thesis author as shown in Chapter 3. Therefore, the interest for the next two proteins was among such proteins already found by this group. Of these, SAP3 was selected as the next most significantly changed protein after AMPE, and ASSY was selected as it was found downregulated by Verderio's post-doc who used different stable and progressive DN cohorts (Tonoli et al., unpublished work), therefore it is a strong confirmation of its deregulated expression in progressive DN.

However, the future work plan is to validate also the remaining five proteins: choline transporter-like protein 2 (CTL2), plasma serine protease inhibitor (IPSP), alpha-N-acetylglucosaminidase (ANAG), CD59 glycoprotein (CD59), and pigment epithelium-derived factor (PEDF).

4.4.3 Validation of uEVs candidate biomarkers of DN progression

Having selected a set of uEVs proteins for validation of their expression in progressive and stable DN cohorts, proteins were validated by single EV analysis of the biofluid with methods suitable for the detection of both surface and intra EV proteins, as described in Methods 4.3.3.1. An intravesicular marker syntenin was used as a positive control of successful EV permeabilization (Supplementary Figure 2). Urine pools from 20 stable and 20 progressive DN individuals were applied on the chips without prior uEV isolation, as explained in the Methods 4.3.3.

The number of uEVs immobilised by each of the three tetraspanins (CD63, CD81, CD9), the wide EV markers, was significantly higher in progressive compared to stable DN group, with very low binding to generic mouse IgG (MIgG) (Figure 4.14A). In particular, total CD63-captured uEVs were 2.4 times more abundant in progressive vs stable DN cohort. Furthermore, to explore distribution and colocalization of the tetraspanin EV markers in captured uEVs from stable and progressive DN cohort, colocalization analysis was performed. As shown in Figure 4.14B, CD63 tetraspanin (red) was the most abundant uEVs marker in both stable and progressive DN cohort, respectively present in 44% (stable) and 57% (progressive) uEVs followed by CD9 (blue), whose expression was 40% in stable and 22% in progressive DN. The least expressed tetraspanin in uEVs from DN patients was CD81 (green), 4% in stable and 2.7% in progressive. Colocalization of CD63 and CD9 (purple) was the highest meaning that most uEVs display these tetraspanins.
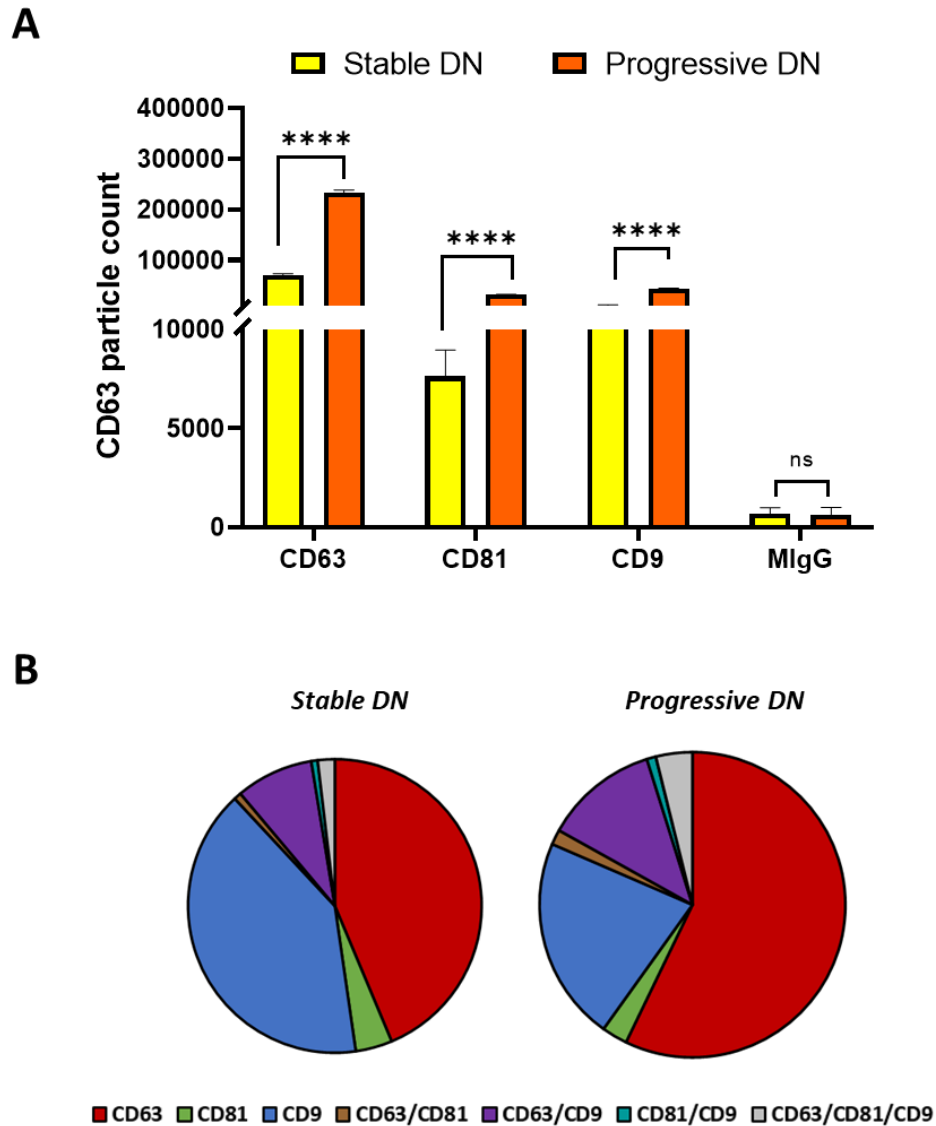
Figure 4.14: Signal of EV markers tetraspanins CD63, CD81, CD9 in stable DN (n=20) and progressive DN (n=20) groups in vesicles captured by CD63 capture. Bar-chart showing significantly higher signal of all three tetraspanins in uEVs from progressive vs stable DN, that, as well as very low unspecific signal from MIgG capture. Graph shows mean±SD (A). Pie charts showing distribution and colocalization of the three tetraspanins in uEVs from stable and progressive DN, captured by CD63 capture (B). Statistics: Two-way ANOVA with Sidak's multiple comparison test. ****$p < 0.0001$.

Next, pools of urine from stable DN (n=20) and progressive DN (n=20) individuals were employed for validation of the selected uEVs progression markers (Table 4.9) directly in the biofluids.

Validation of Vasorin by ExoView confirmed its significantly decreased expression in uEVs from progressive DN vs stable DN, found by mass spectrometry (Figure 4.15). Overall, the total VASN-containing particle count (captured by all tetraspanins) was 29 times lower in stable DN and 261 times lower in progressive DN compared to particle count detected by the well-established EV markers such as CD63. With >20 times or even >200 times less vesicles detected, VASN signal is closer to the signal of unspecific MIgG. However, this does not rule out the high possibility that the vesicles captured by tetraspanins which are well-known EV markers, and detected by VASN (or other protein validated as candidate biomarker) are not specific signal. Therefore, VASN-containing uEVs count was significantly decreased in progressive DN when captured by each of the three tetraspanin probes: 3-fold decrease in CD63 capture, and 2-fold decrease in CD81 and CD9 captures (Figure 4.15A). When total VASN-containing uEVs were normalized to total particle count, a significant 3.5-fold decrease in VASN signal in DN progressive was present compared to stable (Figure 4.15B).

Validation of Vasorin (VASN)
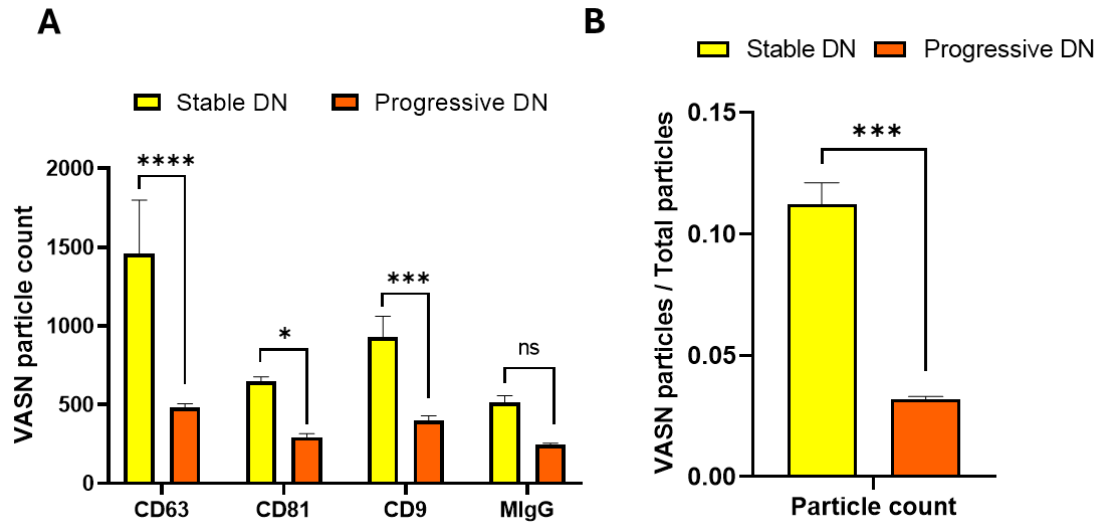
Figure 4.15: Validation of VASN in uEVs from stable DN (n=20) and progressive DN (n=20) pools, by ExoView. VASN-containing uEVs captured by each tetraspanin capture (A), and total VASN uEVs normalized to total uEVs (B). Graphs were created in Graph-Pad Prism and show mean±SD. Statistics applied was Two-way ANOVA with Sidak's multiple comparison test, and two-tailed unpaired t-test. ****$p < 0.0001$, ***$p < 0.001$, *$p < 0.05$

Podocalyxin was found to be significantly increased in uEVs from progressive DN compared to stable DN when captured by CD63 tetraspanin (0.74-fold increase), contrary to the MS data (Figure 4.16A). Capture of PODXL-positive uEVs was about 2 times lower in CD81 and CD9 tetraspanin captures compared to CD63, therefore only PODXL signal in uEVs captured by CD63 capture was considered as a reliable signal. When PODXL-containing uEVs captured by CD63 were normalized to total uEVs captured by CD63, a significant 1.7-fold decrease in PODXL signal was found in uEVs from progressive DN compared to stable DN group, as was also found by MS (Figure 4.16B).

Knowing that progressive DN contains significantly more total uEVs, smaller changes, for example less than 1.5-fold difference, in PODXL signal as shown in graph A might be affected by total particle count being significantly higher in progressive DN, however normalization to total particles as shown in graph B reflect more accurately on the real difference in PODXL signal in uEVs from the stable and progressive DN group.

Validation of Podocalyxin (PODXL)
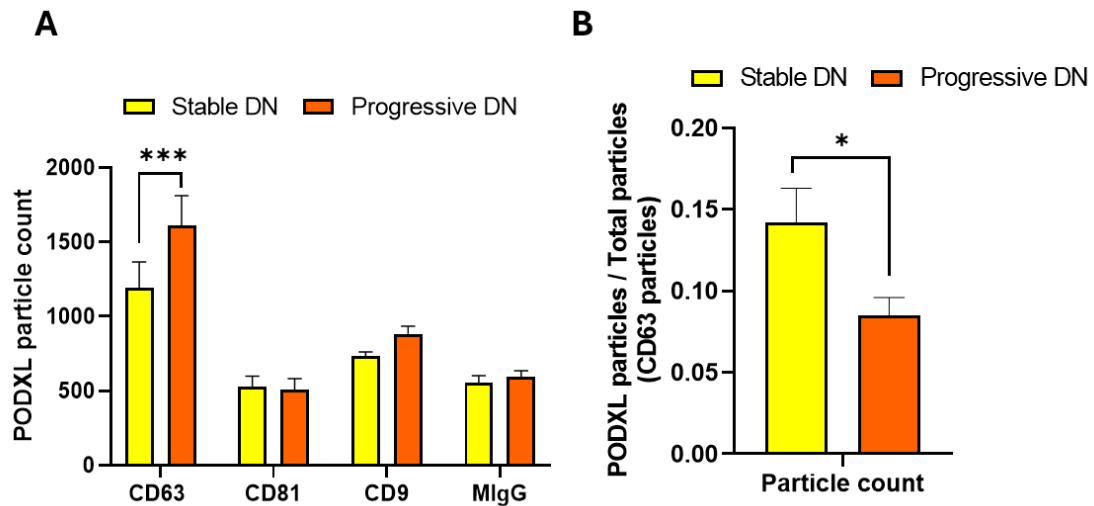
Figure 4.16: Validation of PODXL in uEVs from stable DN (n=20) and progressive DN (n=20) pools, by ExoView. PODXL-containing uEVs captured by each tetraspanin capture (A), and PODXL uEVs (from CD63) normalized to total uEVs (from CD63) (B). Graphs show mean±SD and statistics applied was Two-way ANOVA with Sidak's multiple comparison test, and two-tailed unpaired t-test ***$p < 0.001$, *$p < 0.05$

Mucin 1 showed the highest expression in uEVs captured by CD9 tetraspanin capture which was 4.3 times higher than in CD63 and 7.7 times higher than in CD81 from stable DN, and 2.9 times and 5.3 times higher in progressive DN, respectively (Figure 4.17A). Therefore, the MUC1 signal in uEVs captured by CD9 was deemed reliable, showing a significant 1.2-fold decrease in MUC1 signal in progressive versus stable DN, a result that confirmed finding by MS analysis (Figure 4.17A). Normalization of MUC1 particles captured by CD9 to total particles captured by CD9 confirmed significant 1.5-fold decrease in progressive vs stable DN (Figure 4.17B).

Validation of Mucin 1 (MUC1)
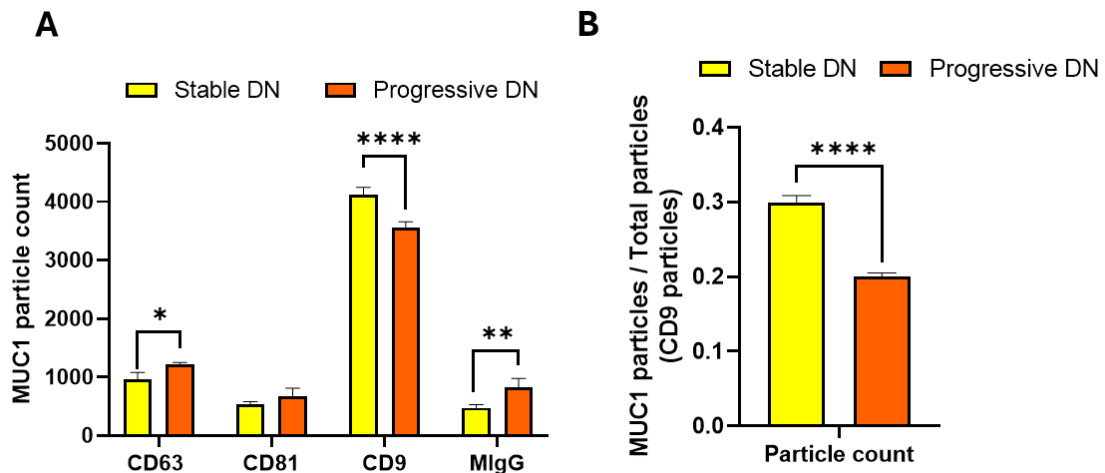
Figure 4.17: Validation of MUC1 in uEVs from stable DN (n=20) and progressive DN (n=20) pools, by ExoView. MUC1-containing uEVs captured by each tetraspanin capture (A), and MUC1 uEVs (from CD9) normalized to total uEVs (from CD9) (B). Graphs show mean±SD and statistics applied was Two-way ANOVA with Sidak's multiple comparison test, and two-tailed unpaired t-test. ****$p < 0.0001$, **$p < 0.01$, *$p < 0.05$

The validation of glutamyl aminopeptidase (AMPE) did not confirm the MS results. As shown in Figure 4.18A, the AMPE signal was highest in CD63 capture, with a significant 1.4-fold increase in the progressive versus stable DN group. Similar to PODXL, only CD63-captured vesicles were considered for the reliable AMPE signal. However, unlike the PODXL case, after normalizing the AMPE particles captured by CD63 to the total particles captured by CD63, a significant 1.4-fold increase in AMPE remained evident in the progressive DN group (Figure 4.18B).

Validation of Glutamyl aminopeptidase (AMPE)
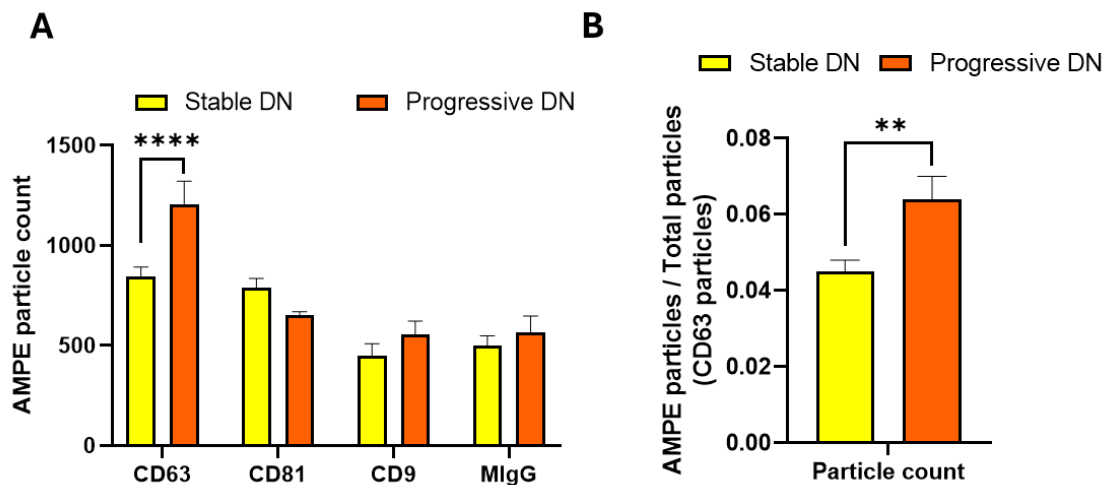
Figure 4.18: Validation of AMPE in uEVs from stable DN (n=20) and progressive DN (n=20) pools, by ExoView. AMPE-containing uEVs captured by each tetraspanin capture (A), and total AMPE uEVs (from CD63) normalized to total uEVs (from CD63) (B). Graphs show mean±SD and statistics applied was Two-way ANOVA with Sidak's multiple comparison test, and two-tailed unpaired t-test. ****$p < 0.0001$, **$p < 0.01$

Thromboxane-A synthase (THAS) expression was significantly increased in the progressive DN group, with a 2-fold increase observed in each of the three tetraspanin captures (Figure 4.19A). However, a significant change in the THAS signal was observed even in MIgG, with THAS levels 1.8-fold higher in the progressive DN. Even if significantly higher expression of THAS was found in progressive uEVs compared to stable DN by MS, after normalization of total THAS particles to total particles, there was no significant difference in THAS expression between stable and progressive DN (Figure 4.19B).

Validation of Thromboxane–A synthase (THAS)
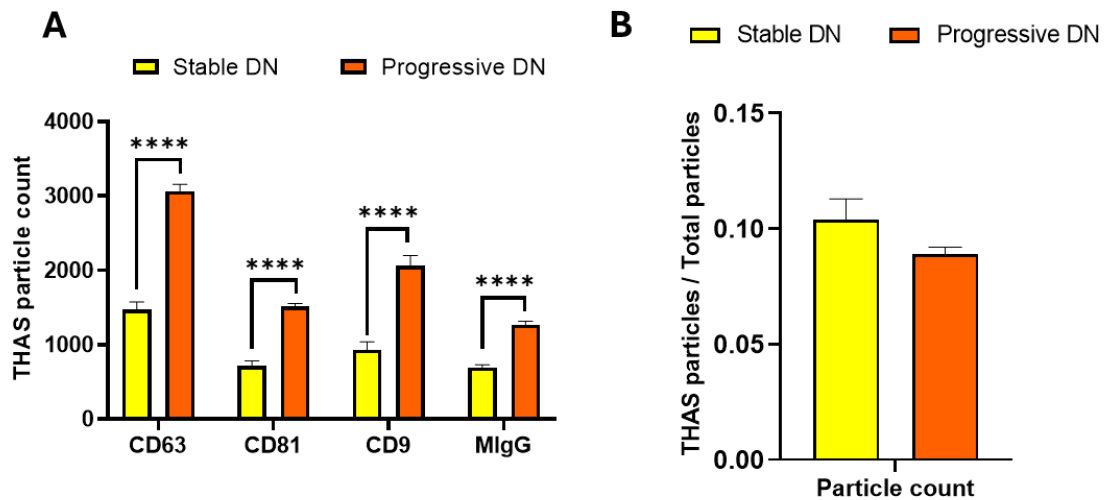
Figure 4.19: Validation of THAS in uEVs from stable DN (n=20) and progressive DN (n=20) pools, by ExoView. THAS-containing uEVs captured by each tetraspanin capture (A), and THAS uEVs normalized to total uEVs (B). Graphs show mean±SD and statistics applied was Two-way ANOVA with Sidak's multiple comparison test, and two-tailed unpaired t-test. ****p < 0.0001

Expression of ganglioside GM2 activator (SAP3) was not significantly changed between stable and progressive DN groups when captured by any of the tetraspanins (Figure 4.20A). However, when SAP3 particles captured by CD63, which showed about 1.6 times higher expression in stable DN and 1.8 times higher expression in progressive DN compared to CD81 and CD9, were normalized to total particles captured by CD63, SAP3 expression was significantly downregulated by 1.8-fold in the progressive DN compared to the stable DN group, which confirmed the MS results (Figure 4.20B)

Validation of Ganglioside GM2 activator (SAP3)
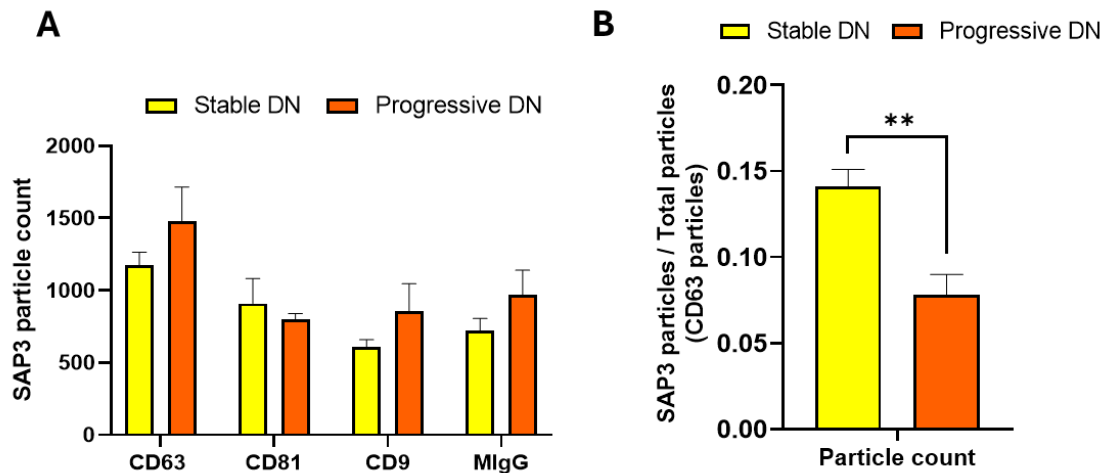
Figure 4.20: Validation of SAP3 in uEVs from stable DN (n=20) and progressive DN (n=20) pools, by ExoView. SAP3-containing uEVs captured by each tetraspanin capture (A), and total SAP3 uEVs (from CD63) normalized to total uEVs (from CD63) (B). Graphs show mean±SD and statistics applied was Two-way ANOVA with Sidak's multiple comparison test, and two-tailed unpaired t-test. **$p < 0.01$

Validation of argininosuccinate synthase (ASSY) confirmed result of MS both before and after normalization to total particle count. As shown in Figure 4.21A, uEVs captured by CD63 and CD81 exhibited a significant approximately 1.5-fold decrease in ASSY signal in the progressive DN compared to the stable DN group. In CD9 capture difference was not significant but the decreasing trend was still evident. Since expression of ASSY was the highest in vesicles captured by CD63 tetraspanin (1.5 times higher in stable, 1.6 times higher in progressive compared to CD81 and CD9 tetraspanin captures), ASSY signal from CD63 was normalized to total CD63-captured vesicles which showed significant 2-fold decrease in progressive vs stable DN group (Figure 4.21B).

Validation of Argininosuccinate synthase (ASSY)
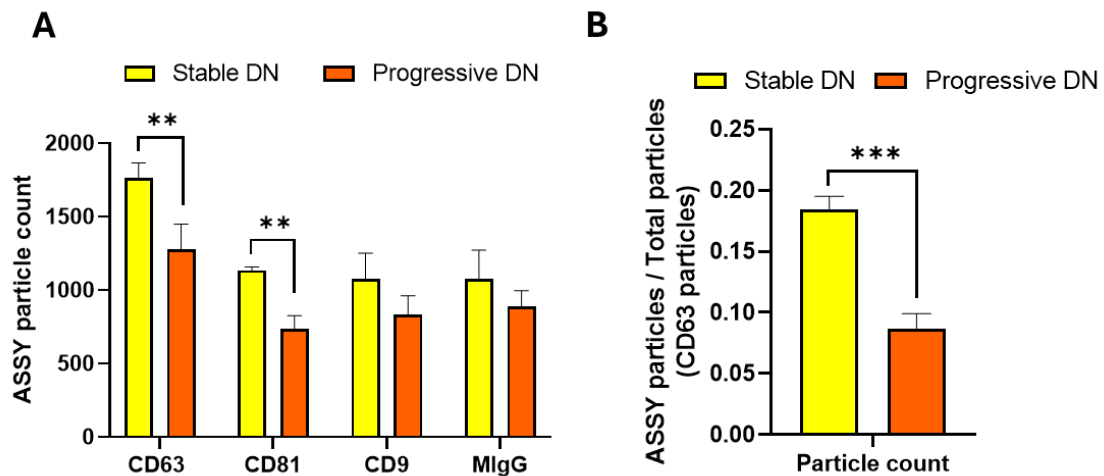
Figure 4.21: Validation of ASSY in uEVs from stable DN (n=20) and progressive DN (n=20) pools, by ExoView. ASSY-containing uEVs captured by each tetraspanin capture (A), and total ASSY uEVs (from CD63) normalized to total uEVs (from CD63) (B). Graphs show mean±SD and statistics applied was Two-way ANOVA with Sidak's multiple comparison test, and two-tailed unpaired t-test. ***$p < 0.001$, **$p < 0.01$

After validation of the seven out of twelve proteins which are discovered as potential uEVs candidate biomarkers of DN progression, it can be concluded that for five of them: VASN, PODXL, MUC1, SAP3, and ASSY a significant deregulation of their expression in progressive compared to stable DN was confirmed by single vesicle analysis. All of the five proteins were significantly downregulated in progressive DN group. THAS showed a significant increase in progressive DN in uEVs captured by CD63 and CD81 capture, which is the same expression direction as showed by MS, however after normalization, significance was lost. AMPE was found to be significantly increased in progressive DN contrary to the MS data which showed its significant decrease in progressive DN.

A summary of the differential expression data from discovery phase by MS and validation phase by ExoView, from the seven uEVs protein candidate biomarkers of DN progression is shown in Table 4.8.

Table 4.8: Summary of the validated uEVs candidate biomarkers of DN progression showing expression by MS in both equal amount and equal volume datasets expressed as log$_2$ fold change (progressive vs stable DN), and expression by ExoView in stable and progressive DN cohorts after normalization to total particle count.

Candidate biomarker	Expression by MS (eq amount)	Expression by MS (eq volume)	Expression by ExoView in prog DN	Expression by ExoView in stab DN
	Expressed as Log$_2$ Fold change (Progressive DN / Stable DN)		Signal after normalization to total particle count	
Vasorin (VASN)	-2.609 (adj.p = 0.0001)	-2.257 (adj.p = 0.0007)	0.032 ± 0.001	0.112 ± 0.009
Podocalyxin (PODXL)	-2.438 (adj.p = 0.0006)	-2.075 (adj.p = 0.0027)	(CD63 capture) 0.078 ± 0.012	(CD63 capture) 0.141 ± 0.01
Mucin 1 (MUC1)	-2.157 (adj.p = 0.0017)	-1.789 (adj.p = 0.0073)	(CD9 capture) 0.200 ± 0.005	(CD9 capture) 0.300 ± 0.009
Glutamyl aminopeptidase (AMPE)	-1.990 (adj.p = 0.0017)	-1.628 (adj.p = 0.0081)	(CD63 capture) 0.064 ± 0.006	(CD63 capture) 0.045 ± 0.003
Thromboxane–A synthase (THAS)	1.908 (adj.p = 0.0020)	2.276 (adj.p = 0.0007)	0.101 ± 0.003	0.111 ± 0.008
Ganglioside GM2 activator (SAP3)	-1.825 (adj.p = 0.0042)	-1.462 (adj.p = 0.0152)	(CD63 capture) 0.078 ± 0.012	(CD63 capture) 0.141 ± 0.010
Argininosuccinate synthase (ASSY)	-1.268 (adj.p = 0.0265)	-0.872 (adj.p = 0.1695)	(CD63 capture) 0.087 ± 0.012	(CD63 capture) 0.184 ± 0.011

4.4.4 Identification of uEVs candidate biomarkers of DN

In addition to identifying candidate biomarkers for DN progression, proteins that were significantly differentially expressed in progressive DN compared to both the diabetic group without CKD and healthy subjects were investigated as potential markers of DN. As analysed in the previous results section 4.4.1 where progressive DN protein markers were explored, two normalization approaches "equal amount" and "equal volume" were applied in these analyses. In the equal amount analysis, thirteen proteins emerged as significantly increased in DN vs diabetes, of which only pigment epithelium growth factor and titin were not of plasma origin (Table 4.9). Titin, a highly abundant protein in striated muscle (van Wijk et al., 2022), was the only protein that was not found earlier as marker of progression. On the other hand, a total of 44 proteins were significantly reduced in DN compared to the diabetic condition, with 54% of these not previously identified as markers of DN progression (Table 4.10). The heat map demonstrates the uniform expression of proteins across individual patient samples, with blue representing low expression and red representing high expression (Figure 4.22). The only exceptions are the progressive DN sample labelled P6, which exhibits unusually high expression of all proteins, including those that should be downregulated in progressive DN compared to diabetes, and the diabetic sample D11, which displays a pattern more similar to the progressive DN cohort than the diabetic cohort.

Table 4.9: Significantly <u>upregulated</u> proteins in uEVs from progressive DN (n=17) vs diabetic (n=14) in dataset normalized to <u>equal amount</u>, listed according to fold change (Prog / Diab)

	Protein ID	Protein name	FC (Prog / Diab)	Adj. p-value (BH)
*	PEDF_HUMAN	Pigment epithelium-derived factor	9.388	0.00069
	IGHG2_HUMAN	Immunoglobulin heavy constant gamma 2	8.494	0.000675
	CERU_HUMAN	Ceruloplasmin	8.350	0.001626
	TTHY_HUMAN	Transthyretin	7.162	0.001626
*	TITIN_HUMAN	Titin	6.486	0.001674
	ANT3_HUMAN	Antithrombin-III	6.115	0.003533
	HPT_HUMAN	Haptoglobin	5.790	0.008977
	IGHG3_HUMAN	Immunoglobulin heavy constant gamma 3	5.263	0.008985
	HV434_HUMAN	Immunoglobulin heavy variable 4-34	4.092	0.026938
	ITIH2_HUMAN	Inter-alpha-trypsin inhibitor heavy chain H2	4.051	0.049088
	CO4A_HUMAN	Complement C4-A	3.937	0.048133
	IGLL5_HUMAN	Immunoglobulin lambda-like polypeptide 5	3.795	0.0341
	IGK_HUMAN	Immunoglobulin kappa light chain	3.786	0.028782

* represent proteins that are not in the category of plasma proteins

Table 4.10: Significantly <u>downregulated</u> proteins in uEVs from progressive DN (n=17) vs diabetic (n=14) in dataset normalized to <u>equal amount</u>, listed according to fold change (Prog / Diab)

	Protein ID	Protein name	FC (Prog / Diab)	Adj. p-value (BH)
	MUC1_HUMAN	Mucin-1	-14.616	0.000675
#	LDHC_HUMAN	L-lactate dehydrogenase C chain	-9.544	0.001626
	VASN_HUMAN	Vasorin	-9.121	0.001674
	CTL2_HUMAN	Choline transporter-like protein 2	-8.047	0.001626
	IPSP_HUMAN	Plasma serine protease inhibitor	-7.481	0.001626
#	RHCG_HUMAN	Ammonium transporter Rh type C	-7.356	0.001626
#	RAI3_HUMAN	Retinoic acid-induced protein 3	-7.053	0.005228
#	MBNL1_HUMAN	Muscleblind-like protein 1	-6.867	0.002757
#	GNA13_HUMAN	Guanine nucleotide-binding protein subunit alpha-13	-6.672	0.002757
	LG3BP_HUMAN	Galectin-3-binding protein	-6.652	0.001626
#	THY1_HUMAN	Thy-1 membrane glycoprotein	-6.483	0.002559
	BROX_HUMAN	BRO1 domain-containing protein BROX	-6.476	0.004366
	VPS4A_HUMAN	Vacuolar protein sorting-associated protein 4A	-6.381	0.004446
#	ES8L2_HUMAN	Epidermal growth factor receptor kinase substrate 8-like protein 2	-6.325	0.015648
	PSA_HUMAN	Puromycin-sensitive aminopeptidase	-6.275	0.008985
	CD59_HUMAN	CD59 glycoprotein	-5.885	0.006095
#	GBB2_HUMAN	Guanine nucleotide-binding protein G(I)/G(S)/G(T) subunit beta-2	-5.829	0.009876
	GGT1_HUMAN	Glutathione hydrolase 1 proenzyme	-5.790	0.008985
#	AQP1_HUMAN	Aquaporin-1	-5.610	0.011419
#	TS101_HUMAN	Tumor susceptibility gene 101 protein	-5.544	0.008985
#	MAL2_HUMAN	Protein MAL2	-5.452	0.026099
	XPP2_HUMAN	Xaa-Pro aminopeptidase 2	-5.203	0.015648
	PSCA_HUMAN	Prostate stem cell antigen	-5.146	0.01565
#	VTA1_HUMAN	Vacuolar protein sorting-associated protein VTA1 homolog	-5.058	0.014897
#	GBB1_HUMAN	Guanine nucleotide-binding protein G(I)/G(S)/G(T) subunit beta-1	-5.035	0.01565
	HACD1_HUMAN	Very-long-chain (3R)-3-hydroxyacyl-CoA dehydratase 1	-5.023	0.015648
	CHM2B_HUMAN	Charged multivesicular body protein 2b	-5.011	0.029765
	PODXL_HUMAN	Podocalyxin	-4.989	0.030243
	PLS1_HUMAN	Phospholipid scramblase 1	-4.979	0.029114
#	ANXA7_HUMAN	Annexin A7	-4.952	0.028008
	PDCD6_HUMAN	Programmed cell death protein 6	-4.782	0.014828
	CD44_HUMAN	CD44 antigen	-4.780	0.038278
#	VMO1_HUMAN	Vitelline membrane outer layer protein 1 homolog	-4.742	0.035088
#	PEF1_HUMAN	Peflin	-4.730	0.031609
#	CHM4B_HUMAN	Charged multivesicular body protein 4b	-4.610	0.042549
#	GGH_HUMAN	Gamma-glutamyl hydrolase	-4.539	0.038973
#	UPK2_HUMAN	Uroplakin-2	-4.484	0.030116
	CPVL_HUMAN	Probable serine carboxypeptidase CPVL	-4.358	0.046775
#	UPK1A_HUMAN	Uroplakin-1a	-4.239	0.031609
	VPS4B_HUMAN	Vacuolar protein sorting-associated protein 4B	-4.167	0.041266
#	CHMP5_HUMAN	Charged multivesicular body protein 5	-4.149	0.0329
#	CD14_HUMAN	Monocyte differentiation antigen CD14	-3.951	0.0341
#	EZRI_HUMAN	Ezrin	-3.941	0.049649
#	PROM1_HUMAN	Prominin-1	-3.871	0.04267

represent proteins that were newly identified as markers of DN, but not DN progression

Figure 4.22: Heat map showing significantly differentially changed proteins in progressive DN vs diabetic group from the dataset normalized to <u>equal amount</u>, in each patient sample. Proteins are listed from the most significant on top to the least significant at the bottom, according to the adjusted p-values. Blue colour represents low expression and red high expression in progressive DN. D=diabetic, P=progressive.

In contrast to the "equal amount" analysis, the "equal volume" analysis identified a much smaller number of proteins with significant changes between the progressive DN and diabetic groups. No proteins were found to be significantly upregulated, and only six proteins were significantly downregulated in DN compared to diabetes (Table 4.11). Notably, apolipoprotein D was newly detected in this analysis, whereas it was not identified in the previously analysed dataset. The heat map from the "equal volume" analysis again revealed consistent protein expression across individuals within each cohort, with the same two outliers, progressive DN sample P6 and diabetic sample D11, showing distinct patterns compared to the rest of the population.

Table 4.11: Significantly <u>downregulated</u> proteins in uEVs from progressive DN (n=17) vs diabetic (n=14) in dataset normalized to <u>equal volume</u>, listed according to fold change (Prog / Diab)

	Protein ID	Protein name	FC (Prog / Diab)	Adj. p-value (BH)
	LDHC_HUMAN	L-lactate dehydrogenase C chain	-34.583	4.47E-05
+	APOD_HUMAN	Apolipoprotein D	-10.666	0.000403
	VASN_HUMAN	Vasorin	-6.409	0.027245
	CTL2_HUMAN	Choline transporter-like protein 2	-6.212	0.027245
	MBNL1_HUMAN	Muscleblind-like protein 1	-7.413	0.027245
	IPSP_HUMAN	Plasma serine protease inhibitor	-5.453	0.034029

+ represent proteins that were newly found in this analysis
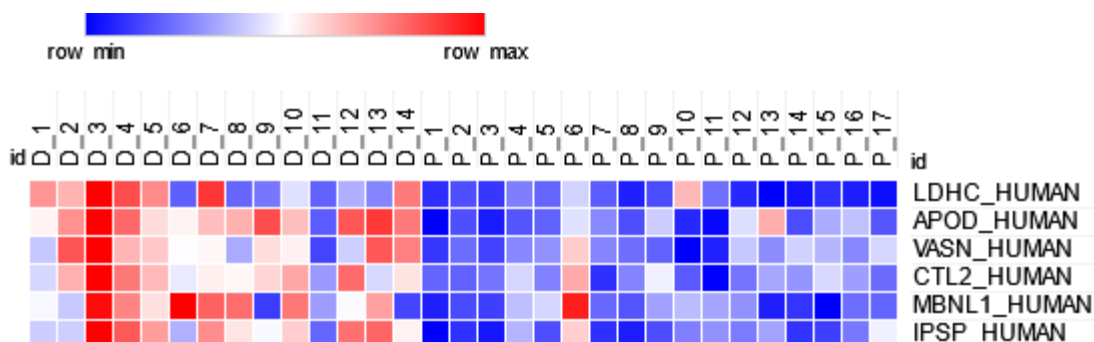
Figure 4.23: Heat map showing significantly changed proteins in progressive DN vs diabetics from the dataset normalized to <u>equal volume</u>. Proteins are listed from the most significant on top to the least significant at the bottom. Blue colour represents low expression and red high expression in progressive DN. D=diabetic, P=progressive.

Focusing on the proteins identified in both analyses, only two proteins were common and found to be significantly downregulated in the progressive DN group compared to the diabetic group: L-lactate dehydrogenase C chain (LDHC) and Muscleblind-like protein 1 (MBNL1). Both proteins are of cellular origin, predominantly expressed in cytosol and nucleus (Miller et al., 2000; de Mateo et al., 2011). LDHC protein is found in embryonic and germ cells, and although its functions are not completely understood, LDHC may play a role in cell proliferation, differentiation role and motility (Tang et al., 2024). While LDH-A and LDH-B were known to be implicated in CKD, for LDHC there are no reports. MBNL1 is an important RNA binding protein with function to regulate alternative splicing of specific pre-mRNAs such as cardiac troponin T and insulin receptor in pathology of myotonic dystrophy (Ho et al., 2004). Two recent studies have indicated that MBNL1 plays a role in the pathology of DN (Jiang et al., 2020; Wang et al., 2023).

In summary, when relying on the two normalization approaches for MS data analysis, two proteins, LDHC and MBNL1, were identified as potential uEVs markers for DN. Both

were significantly downregulated in the progressive DN cohort compared to the diabetic

cohort.

Proteins that showed significant changes between the progressive DN and the healthy

controls, and stable DN and the diabetic group, as well as between stable DN and the

healthy group, can be found in the Appendix (Supplementary table 3-5).

4.5 Discussion

Discovery of protein candidate markers of DN progression in uEVs and validation of strong candidates have provided a new non-invasive fingerprint of DN progression presented in this chapter.

uEVs are becoming an attractive source of biomarkers of all types of CKD (Tepus et al., 2023) due to their non-invasive nature, role in inter-cellular communication and hence potential to reflect on pathophysiological changes in kidney cell types. Although many proteins have been identified and reported as potential uEV biomarkers for CKD, markers specifically associated with DN progression and CKD progression in general remain relatively unexplored (Chu et al., 2020; Kammer et al., 2023; E et al., 2024). This is, however, a critical area of research, as CKD progression marks a stage that essentially leads to a rapid decline in kidney function, kidney fibrosis, and eventual kidney failure (Zhong et al., 2017). This project was focused on DN as the commonest type of CKD often resulting in ESKD. By studying alterations in the uEVs-protein profile using an above-average cohort size with the expected experimental power of 95% and sensitive robust technologies such as SWATH-MS and single EV analysis, a panel of uEVs proteins was discovered and validated, and offered as fingerprint of DN progression. Five uEVs proteins were all significantly downregulated in progressive DN as shown by MS and single EV quantifications: vasorin (Figure 4.15B), podocalyxin (Figure 4.16B), mucin-1 (Figure 4.17B), ganglioside GM2 activator (Figure 4.20B) and argininosuccinate synthase (Figure 4.21B).

Literature research revealed that each one of the five proteins was involved in some CKD forms before. For example, VASN was suggested as a potential therapeutic target for vascular calcification during CKD (Luong et al., 2019). Even if VASN showed anti-fibrotic effects, its expression was upregulated in plasma of DN patients (Ahn et al., 2010), and in uEVs from TBMN compared to normal group (Moon et al., 2011). It was also proposed as one of the seven biomarkers of MN from kidney biopsy sample (Caza et al., 2023).

Mutations in *PODXL* were shown to be associated with human kidney disease, for example deletion of *PODXL* gene was linked to development of a severe congenital nephrotic syndrome characterized by FSGS and proteinuria in mice model (Refaeli et al., 2020). Immunohistochemical expression of PODXL was reduced in podocytopathies compared to healthy control (Kavoura et al., 2011). Its expression was also found significantly decreased in uEVs from patients with FSGS and proteinuria (Cheruvanky et al., 2007). Interestingly, the number of PODXL-positive cells in combination with other urinary cell types showed potential to detect kidney transplant rejection (Goerlich et al., 2020).

Furthermore, mutations in MUC1 were reported to cause medullary cystic kidney disease (Kirby et al., 2013) and result in progressive chronic kidney failure (Bleyer et al., 2014). Persistent abnormal induction of MUC1 has been reported to be associated with failed epithelial repair, chronic inflammation, and renal fibrosis. In addition, in renal ischemia-reperfusion injury MUC1 had a protective role in early phase but pro-fibrotic role in later phase of disease (Gibier et al., 2017). Furthermore, it has been reported to play a role in DN by activating STAT-β-catenin signalling pathway consequently promoting kidney

fibrosis (Tao et al., 2021). Urinary MUC1 subunit α was suggested as a biomarker associated with renal dysfunction (Zhang, Z., et al., 2017).

Protein SAP3 was detected as uEVs marker of DN progression, being significantly downregulated in progressive DN, in both Chapter 3 (Figure 3.13C) and Chapter 4 (Figure 4.20B), whereas in the literature its expression was found upregulated in association to CKD conditions. For example, a meta-analysis on transcriptome signature in glomerular diseases found SAP3 (gene *GM2A*) significantly upregulated in various diabetic kidney disorders (Tryggvason et al., 2013). Furthermore, urinary SAP3 in combination with other 4 urinary proteins were found significantly increased in urine from DKD patients with poor prognosis compared to DKD patients with good prognosis and showed prediction potential in type 2 diabetes (Ahn et al., 2020). In addition, SAP3 can be potential indicator of severe parenchymal damage extending to the cortical area (Blanco-Gozalo et al., 2024). These findings suggest SAP3 may be an upregulated marker of CKD or AKI, but this chapter shows its significant downregulation in CKD progression, particularly in DN. Additionally, the cited studies were not based on uEVs, which better reflect kidney tissue pathology than urine (Wu et al., 2021; van Heugten et al., 2022; Khoo et al., 2024).

Finally, ASSY expression was found significantly reduced in human and mice kidney tissue from ADPKD (Trott et al., 2018). Renal ASSY abundance was also decreased in puromycin aminonucleoside-induced rat model of CKD (Chen, G., et al., 2012). On the other hand, in kidneys from mice model of tuberous sclerosis complex kidney disease, ASSY expression was significantly increased (Amleh et al., 2023).

Existing literature highlights the importance of the identified uEVs proteins in the development of various types of CKD. However, the data from this chapter extend their role by focusing on their involvement in the progression of DN pathology, particularly when they are carried as uEV cargo.

In addition to these five proteins suggested to form a panel of DN progression, two more proteins, glutamyl aminopeptidase (AMPE) and thromboxane-A synthase (THAS), were validated, however their expression was not confirmed in single EV validations without uEVs isolation. AMPE expression was found downregulated in progressive DN cohort (Figure 4.6, Figure 4.9), but significantly upregulated in the validation analysis (Figure 4.19B). THAS, on the other hand, was found upregulated in progressive DN when analysed by MS (Figure 4.6, Figure 4.9), but not significantly changed in validation by single EV analysis (Figure 4.20B). This inconsistency may be due to differences in the approach of the two techniques. Tetraspanins, used as captures in single EV analysis, are common markers of EV from all sources (Lozano-Andrés et al., 2019; Mizenko et al., 2021; Kumar et al., 2024), however there are other markers of EVs which might be more abundant in urinary EVs (Erdbrügger et al., 2021). By capturing only uEVs that contain CD63, CD81, and CD9 tetraspanins, validation of candidate protein biomarkers is limited only to such vesicles, whereas in the MS approach, protein expression was measured in all the vesicles, not only the tetraspanin-positive. The use of custom-made chips such as with the captures containing antibodies for the proteins that are being validated instead of generic tetraspanins could be useful but outside the resources in this project. For example, capturing uEVs with THAS would likely result in much higher vesicle count and

more reliable validation of its expression. Another consideration may be made that single EV quantification is designed for capturing vesicles in size range of 50-200, but tetraspanin EV markers are known to be markers of both small EVs but also larger EVs (Lischnig et al., 2022; Musante et al., 2020), although in a less prominent way (Rai et al., 2021; Lischnig et al., 2022). Therefore, validation of the candidate uEVs biomarkers of DN progression was limited only to small EV fraction, whereas in MS analysis fractions of both small and large uEVs were included. Despite these technical limitations, single EV analysis was selected as a validation approach because it is more sensitive technique compared to western blot, offering stronger detection and requiring less starting urine volume. At the time of this thesis writing, Anfaiha-Sanchez et al. (2024) used the same validation in a recent article.

AMPE and THAS were also reported to play a role in CKD. A decrease in AMPE expression was reported to be associated with the development of glomerulosclerosis (Velez et al., 2017). However, in uEVs from cisplatin-induced nephrotoxicity in the rat model, expression of AMPE was significantly increased, and its increased expression was associated with renal dysfunction (Quesada et al., 2017). THAS expression was observed in kidney specimens from 42% IgAN patients while in healthy control its expression was absent. Those THAS-positive patients had significantly reduced GFR and increased levels of serum creatinine and serum beta 2-microglobulin, therefore was suggested that THAS expression is associated with progression of IgAN (Endoh et al., 1997). Long term blockage of THAS showed prolonged survival in lupus nephritis murine model (Salvati et al., 1995). More recently, it has been discovered that THAS expression was associated

with increased oxidative stress in hypertensive glomerular injury, using mice model (Nakano et al., 2019).

In addition to the seven validated proteins, five extra protein candidates are planned to be validated as part of the future work, after which some of them might be added to the suggested uEVs panel of DN progression. Unlike pigment epithelium-derived factor (PEDF) which was significantly upregulated in progressive DN, choline transporter-like protein 2 (CTL2), plasma serine protease inhibitor (IPSP), alpha-N-acetylglucosaminidase (ANAG), and CD59 glycoprotein (CD59) were significantly downregulated in progressive DN (Figure 4.13). While for the CTL2 no literature was found in association with kidney disease, and for IPSP only one study reported that mutations in gene coding for IPSP was associated with severe AKI (Vilander et al., 2017), the other three unvalidated proteins were reported to be involved in kidney disease.

PEDF levels were shown to be significantly decreased at both transcriptomic and proteomic level in a rat model of DN (Wang, J., et al., 2005), and protective role against diabetes and AGE-stimulated diabetic retinopathy were shown (Yamagishi et al., 2006). On the other hand, Chen, H. et al (2010) showed that urinary PEDF was overexpressed in DN patients compared to controls, but also in kidney of diabetic rat model. Moreover, the urinary PEDF expression correlated with moderate albuminuria (Chen, H., et al., 2010), while its elevated plasma levels were closely related to the stages of CKD (Hui et al., 2014). More recently, urinary PEDF was suggested as biomarker of kidney fibrosis levels (Schmidt et al., 2021).

Transcriptomic expression of ANAG was documented to be elevated in a mouse model of FSGS with progressive proteinuria (Nielsen et al., 2013), whereas its proteomic expression was significantly downregulated in advanced stages of IgAN compared to early stages of IgAN (Niu et al., 2023).

High expression of CD59 in urine was discovered to be associated with a lower risk of ESKD in type 2 diabetes (Vaisar et al., 2019). In addition, protein abundance of urinary CD59 was negatively correlated with 24h proteinuria in CKD (Gaipov et al., 2022). In a mice model of ADPKD, expression of CD59 in kidney tissues was decreased (Bin et al., 2024). Furthermore, CD59 was detected as cargo of EVs derived from bone marrow endothelial progenitor cells, which were showed to have protective effect in complement-mediated mesangial injury in the experimental model of anti-Thy1.1 glomerulonephritis (Cantaluppi et al., 2015).

The supporting literature searches have revealed a role in CKD for all the uEVs markers of DN progression here validated, as well as most of those still unvalidated. Apart from PEDF, none of these uEVs proteins were recognised to be associated with disease progression. Therefore, in this context the uEVs DN progression markers emerged from this chapter may confidently represent novel disease progression fingerprint. Their combination as a multi-protein might strengthen the potential to accurately detect progressing DN patients, as already suggested by others (Fliser et al., 2007; Fan et al., 2021; Bienaimé et al., 2023). Future validations in alternative cohorts will ultimately confirm their prognostic value.

In addition to uEVs markers of DN progression, this chapter also identified uEVs markers significantly altered in progressive DN compared to diabetes. Two cellular proteins, L-lactate dehydrogenase C chain (LDHC) and Muscleblind-like protein 1 (MBNL1), were found downregulated in progressive DN in both MS analyses applied (Figure 4.22, Figure 4.23). Of them, MBNL1 was found to be implicated in DN (Jiang et al., 2020; Wang et al., 2023). Identifying stable uEV markers of DN could be clinically relevant, as biopsy remains the only reliable method for accurately distinguishing DN from other diabetes-associated conditions, such as non-diabetic kidney disease (NDKD), in patients with diabetes mellitus (Anders et al., 2018).

CHAPTER 5:

Discovery of uEVs miRNA markers of DN progression

5.1 Introduction

5.1.1 micro RNAs (miRNAs)

MicroRNAs (miRNAs) are small, approximately 22 nucleotide long RNA molecules that play a key role in post-transcriptional regulation of gene expression. Their biogenesis is a multi-step process that starts in the nucleus from non-protein-coding genes, which can be monocistronic coding for one miRNA, or polycistronic coding for several miRNAs (Bartel, D.P., 2004). Inside the nucleus, primary transcripts (pri-miRNA) are processed into precursor transcripts (pre-miRNA), which are transported to the cytoplasm where mature and functional miRNAs are generated. Single-stranded miRNAs, incorporated in the RNA-Induced Silencing Complex (RISC), target messenger RNA (mRNA) and bind to their active site – the 3' untranslated region (3'UTR) based on perfect or imperfect complementarity (Bernstein, E., *et al*., 2001). In the outcome of perfect complementarity, the target mRNA is degraded by endonuclease Argonaute from the RISC complex, while in the scenario of imperfect base pairing, mRNA translation is repressed (van den Berg et al., 2008). In this way, miRNAs are involved in numerous physiological processes with an impact on fundamental cellular functions such as proliferation, differentiation, migration, apoptosis. Therefore, their deregulation (increased or decreased expression levels) can lead to various pathological events, for example renal fibrosis and CKD. By manipulating miRNA expression levels, using miRNA mimics (Chorn, G., *et al.*, 2012) or modified anti-miRNA oligonucleotides (Weiler, J., *et al.,* 2006), candidate miRNA

biomarkers can serve as specific therapeutic tools for the treatment of a certain pathology.

5.1.2 miRNA in uEVs as markers of DN

Various studies have identified miRNAs in uEVs which are biomarker candidates of DN due to their dysregulated expression in DN but also often correlation of their expression with DN-associated parameters such as serum creatinine, eGFR, ACR, BMI etc. (Table 5.1). For example, miR-130a and miR-145 were found to be enriched in uEVs of early-stage DN patients, while miR-155 and miR-424 were downregulated (Barutta et al., 2013). Furthermore, miR-192, miR-194, and miR-215 were found significantly increased in uEVs from the T2DM-linked DN patients with moderate albuminuria when compared to the group with mild albuminuria and healthy controls but were decreased in the DN group with severe albuminuria (Jia et al., 2016). UEVs' miR-15b, miR-34a, and miR-636, which belong to a unique genetic cluster and share functions related to renal diseases and diabetes mellitus, were upregulated in patients with severe albuminuria compared to patients with mild albuminuria and healthy control group (Eissa et al., 2016). Further research (Delić et al., 2016) detected over 300 miRNAs in a small sample size of DN patients, healthy controls and non-CKD subjects, and singled out miR-320c and miR-6068 as the most upregulated miRNAs. In addition, miR-320c expression showed a significant positive correlation with urinary ACR, and a negative correlation with eGFR (Delić et al., 2016). MiR-877-3p was identified as a uEVs' candidate biomarker for DN in a small-scale study showing its significant upregulation in DN patients compared to diabetic

individuals (Xie et al., 2017). More recently, Zhao et al. (2020) discovered 14 miRNAs significantly upregulated in uEVs from type 2 DN patients compared to diabetic controls, however only miR-4687-3p, miR-4534, and miR-5007-3p emerged as significantly upregulated in DN after validation phase. Of them, miR-4534 positively correlated with moderate albuminuria in DN (Zhao et al., 2020).

Many miRNAs from uEVs have been discovered to be dysregulated in DN and therefore have diagnostic and/or prognostic potential, however, the novelty that this chapter aimed to bring is discovery of the panel of miRNAs from uEVs which can be used as markers of DN progression, the stage of rapid decline in renal function, accompanied with renal fibrosis and often ending in ESKD. Moreover, unlike all published studies that used Taqman microarrays and RT-qPCR, here full miRNA sequencing and digital miRNA profiling were utilized as more robust and sensitive techniques (Tam et al., 2014).

In addition to DN type of CKD, many studies reported on miRNAs in uEVs that can differentiate other types of CKD from control groups, summary of which is shown in Supplementary Table 6.

Table 5.1: miRNAs from uEVs proposed as candidate markers of DN

uEV miRNA biomarkers	CKD type	Expression in DN vs CTL	Sample size	Method of analysis	Source
miR-155	DN	↓	Moderate albuminuria=12 Mild albuminuria=12	Human TaqMan miRNA Array A	Barutta et al., 2013, Plos One
miR-424					
miR-130a					
miR-145		↑	Control=10		
miR-192	DN	↑	Mild albuminuria=30 Moderate albuminuria=30 Severe albuminuria=20 Control=10	RT-qPCR	Jia et al., 2016, J Diabetes Res
miR-194					
miR-215					
miR-15b	DN	↑	Severe albuminuria=90 Mild albuminuria=46 Control=44	SYBR green based custom miScript miRNA PCR Array	Eissa et al., 2016, J Diabetes Complicat
miR-34a					
miR-636					
miR-320c	DN	↑	DN=8 Diabetes=8 Control=8	Agilent microarrays	Delić et al., 2016, Plos One
miR-877-3p	DN	↑	DKD=5 Diabetes=5	miRCURY LNA Array	Xie et al., 2017, J Diabetes Res
miR-4687-3p	DN	↑	DKD=3 Diabetes=3	Exiqon's microRNA array	Zhao et al., 2020, Front Endocrinol
miR-4534					
miR-5007-3p					

↑ - increased expression; ↓ - decreased expression; DN - Diabetic Nephropathy; CTL - control

5.2 Aims of the chapter

As in the previous chapter, where proteins from uEVs were investigated as markers of DN progression, a stage of CKD that frequently leads to ESKD and kidney failure, this chapter shifts the focus to miRNAs from uEVs in relation to DN progression. Therefore, the specific aims of this chapter were:

1) To discover uEVs miRNA markers of DN progression by miRNA sequencing and digital miRNAs profiling.

2) To validate a set of uEVs miRNAs markers of DN progression by TaqMan RT-qPCR.

5.3 Methods

5.3.1 Total RNA purification from uEVs

Urinary EVs were isolated by differential ultracentrifugation as explained in 3.3.2. Total RNA was purified by the spin column chromatography-based Plasma/Serum RNA Purification Mini kit (55000, Norgen) following the manufacturer's supplementary protocol for Exosomal RNA Purification from Exosomes Already Purified. In brief, small and large uEVs pellets were resuspended in 1x particle-free PBS and vortexed, followed by the addition of provided lysis buffer containing guanidinium salts known to have strong denaturing properties of proteins, including nucleases, therefore, protecting nucleic acids from denaturation (Chomczynski and Sacchi, 1987; Thatcher, 2015). After mixing samples with lysis buffer, 96-100% (v/v) ethanol was added in a 1 to 1 ratio to sample (PBS and lysis buffer). The entire lysate was applied to spin columns using Norgen's patented proprietary silicon carbide resin on a silica sheet as the separation matrix to bind RNA. After the initial centrifugation at 3,500 x g for 1 min, the flowthrough was discarded, and the procedure was followed by three washing steps using supplied wash solution involving centrifugation at 14,000 x g for 1 min, which was followed by an "empty" run for 2 minutes to thoroughly dry the resin. Nuclease-free water, used as elution buffer, was incubated with the resin for 2 minutes, fully incorporated in the resin by gentle centrifugation at 200 x g for 2 minutes, and RNA was eluted by the final centrifugation at 14,000 x g for 1 min (total volume of eluted RNA is 10 µl).

Concentration and quality of purified RNA was assessed by NanoDrop 8000 spectrophotometer (absorbance for nucleic acids at 260 nm). The 260/280 ratio values between 1.6-1.8 and 260/230 ratio values between 0.7-1.2 are characteristic for RNA from uEVs (Tataruch-Weinert et al., 2016), even if are under the threshold values considered "pure".

5.3.2 RNA precipitation

If necessary, RNA preparations were concentrated by precipitation in 0.3 M sodium acetate, pH 5.2 (Figure 5.9). In particular, 3 M sodium acetate solution was freshly prepared from sodium acetate trihydrate powder ($CH_3COONa.3H_2O$) (Fisher Scientific) and resuspended in RNAase-free water (10977-035, Invitrogen). pH was adjusted to 5.2 with glacial acetic acid (10394970, A/0360/PB17, Fisher Scientific) using EutechTM Elite pH Spear (Thermo Scientific). Solution was then filter-sterilized using 0.2 μm PES syringe filter (E4780-1226, Star Lab). The 3 M sodium acetate solution was added to each sample, 1/10 volume, followed by 2.5 volumes of cold 100% ethanol molecular biology grade (BP2818-500, Fisher Scientific). Samples were incubated at -20°C for 17 h, after which RNA was recovered by centrifugation for 25 min at 13000 rpm at 4°C. The supernatant was removed and washed with 500 μl of cold 70% v/v ethanol. The pellet was recovered by centrifugation at the same speed for 10 min. Pellets were air dried and resuspended in 13 μl of RNAase-free water. Precipitated RNAs were quantified by NanoDrop 8000 spectrophotometer.

5.3.3 Small RNA sequencing

Small RNA sequencing or miRNA sequencing was performed by Source Bioscience (Cambridge). UEVs were isolated from 5 ml of cell-free urines from 3 stable DN, 3 progressive DN, 2 diabetic, and 2 healthy individuals.

The libraries were prepared by Source Bioscience (Cambridge) using the QIAseq miRNA Library Preparation Kit (331505, Qiagen). Specially designed 3' preadenylated DNA adapters and 5' RNA adapters were ligated to mature miRNAs. Ligated miRNAs were then reverse transcribed to cDNAs using reverse transcription primers containing integrated unique molecular identifiers, short sequences used as molecular barcodes, to uniquely tag each molecule in a sample library. Before library amplification, cDNA cleanup was performed using a magnetic bead method. The amplification occured directly in the index plate using QIAseq Illumina HT Plate indices (331565, Qiagen), after which magnetic bead-based cleanup of the amplified miRNA library was performed.

The prepared libraries were quantified by fluorometric method using the Invitrogen Qubit dsDNA assay and qualified using electrophoretic separation on the Agilent BioAnalyzer 2100. Concentration and sizing information has been used to calculate the molarity of each sample (Table 5.2). The libraries have passed the standard library preparation QC metrics and proceeded to sequencing.

Table 5.2: Concentration, size and molarity of cDNA samples after library creation

Cohort	Sample ID	Concentration (ng/µl)	Size (average bp)	nM
Stable DN	PDN127	12.6	186	101.61
Stable DN	SKI410	21.1	201	157.46
Stable DN	SKI470	14.6	209	104.78
Progressive DN	PDN22	6.34	191	49.79
Progressive DN	SKI837	10.7	184	87.23
Progressive DN	SKI1001	5.67	179	47.51
Diabetic no CKD	SKI1014	17.4	243	107.41
Diabetic no CKD	SKI1020	17.1	199	128.89
Healthy	SKI574	24	203	177.34
Healthy	SKI922	18.5	197	140.86

Created cDNA library was sequenced by Illumina NGS system using NovaSeq 6000. Sequencing was done in a paired-end mode with the read length (the length of individual nucleotide sequences) of 150 bp and the read depth of 50 M reads per sample. Paired end sequencing mode provides information from both 5' and 3' ends of RNA.

Sequence of the forward adapter was AACTGTAGGCACCATCAAT, and the reverse adapter was GTTCAGAGTTCTACAGTCCGACGATC.

5.3.3.1 Bioinformatic analysis of miRNA sequencing data

Bioinformatics analysis of the raw miRNAseq data in Fastq format was carried out by the team of General Bioinformatics Limited (Reading, UK). The latest Ensembl Homo sapiens GRCh38 genome was downloaded and indexed using Bowtie v1.3.1 alignment programme. First two bases from the start of the sequences were removed using Cutadapt v4.2 (Martin, 2011). The 'mapper.pl' from mirDeep2 v2.0.1.2, which is a pipeline that incorporates Bowtie and thus predicts the presence of known and novel candidate miRNAs from deep-sequencing data (Friedländer et al., 2012; Williamson et

al., 2013), was then used for adapter removal, trimming of reads, conversion of trimmed.fq files to .fasta files, and mapping the reads to the reference genome. A subset of the putative miRNAs was then checked and confirmed to be miRNAs in the miRbase database. miRDeep2.pl was run using the hsa_mature and hsa_hairpin reference databases from miRbase, with no optional parameters and no similar species, to identify and quantify known and novel miRNA in the fasta files resulting from mapping to the human genome. Differential expression analysis was run on unique mature and precursor read count values only. Differential expression analysis was done by DESEQ2 on the count files from miRDeep2. Differential expression data was expressed as fold change (or log2 fold change), and the change was considered significant if the adjusted p-value (according to Benjamini-Hochberg) was < 0.05.

One limitation of the bioinformatic analysis is that DESeq program used for the differential expression analysis works in expected miRNA counts rather than real miRNA counts meaning that zero values (meaning no miRNA expression in certain sample) are still used to perform the comparison between two groups considering that potential sequencing to a greater depth would lead to more expected miRNA reads appearing in the samples with values of zero. Therefore, the mean value of the cohort can be sometimes based only on the one expression value even if other replicates in the cohort had no expression from certain miRNA, which can consequently lead to artefacts.

5.3.4 miRNA expression profiling from uEVs by NanoString

Digital profiling of miRNAs was utilised using the nCounter Human v3 miRNA panel from NanoString (Seattle, WA). This technology enables direct single molecule counting using fluorescent molecular barcodes to label individual gene/miRNA transcripts. Gene expression is quantified by directly counting each barcode bound on the slide surface in an enzyme-free process, with no reverse transcription or RNA amplification (Geiss et al., 2008; M'Boutchou and van Kempen, 2016). The principle of the method is shown in Figure 5.1. The assay contains two DNA oligo probes: a miRNA-specific capture probe and a miRNA-specific reporter probe. Each probe contains hybridization region of ~50 bases that is designed to be specific to a miRNA of interest. Capture probe contains biotin at the 3' end and its purpose is to bind to and capture the miRNA and immobilize it on the streptavidin-coated slide where it can be counted. Reporter probe contains molecular barcode on its 5' consisting of 4 colours in 6 positions. Each miRNA to be quantified is assigned a distinct colour combination. The assay simply counts the molecular barcodes which are equivalent to each miRNA target.

The proprietary "Human v3 miRNA panel" used in this study consists of 800 miRNAs, 5 non-mammalian spike-in miRNA probes, 5 internal reference genes (housekeeping genes ACTB, B2M, GAPDH, RPL19, RPLP0), 8 negative RNA controls, 5 positive RNA controls, 3 ligation positive miRNA controls, and 3 ligation negative miRNA controls (Crossland et al., 2023).

5.3.4.1. miRNA sample preparation

nCounter Human miRNA Expression Assay kit (NanoString, Seattle, WA) was used for miRNA sample processing according to manufacturer's instructions with some modifications. All available RNA from stable DN (48.5 ng), progressive DN (63.1 ng), diabetic (24.4 ng), and healthy cohort (65 ng) was used, although assay recommends using 100 ng total RNA in 3 µl from each analysed sample as input for miRNA preparation procedure, however RNA samples from uEVs from all cohort had less RNA according to NanoDrop quantification.

The procedure of miRNA sample preparation started with annealing of the specific oligonucleotide tags provided by the kit, used to extend small miRNAs and allow them to be detected, to the target miRNAs via target specific bridge oligo. Annealed miRNA-specific tags were then ligated through creation of phosphodiester bonds to generate products known as "CodeSet targets" (Figure 5.1). Ligation was followed by enzymatic purification of unligated tags, and denaturation of miRNA samples which was done by sample incubation at 85°C for 5 min and quick-cool at 4°C. After denaturation, hybridization of the reporter and capture probes to the specific CodeSet targets was performed at 65°C for 20 hours, followed by the post-hybridization processing by nCounter FLEX analysis system (Prep-Station and Digital Analyzer) (Eastel et al., 2019).

The Prep Station is multi-channel pipetting robot that purifies and immobilizes samples in a sample cartridge for data collection on the Digital Analyzer. In the first step, the miRNA-probe complexes did bind to the magnetic beads complementary to the

sequences on capture probes, followed by the washing step where excess reporter probes were removed. Then, capture probes and miRNA-probe complexes were eluted off the beads and hybridized to magnetic beads complementary to sequences on the reporter probes. Washing step was performed again to remove excess capture probes after which the purified target-probe complexes are eluted off the beads and immobilized on the cartridge by biotin-streptavidin reaction. Once immobilized, the instrument applied an electric current (fluidic flow) across the slide, causing the molecules to align flat against the surface, oriented in the same direction, and also elongating them. Then a fixative was applied to the slide to prepare it for the next step of taking images of the slide surface creating a picture used for single molecule counting and data collection.

The Digital Analyzer is multichannel epifluorescence scanner that collects data by taking images of the immobilized fluorescent reporters in the sample cartridge with a CCD camera through a microscope objective lens. The number of images taken corresponds to the number of reporters counted. Images were processed internally, producing reporter code count (RCC) files which were then downloaded via USB flash drive and imported into the nSolver Analysis Software for quality control and analysis (Eastel et al., 2019).
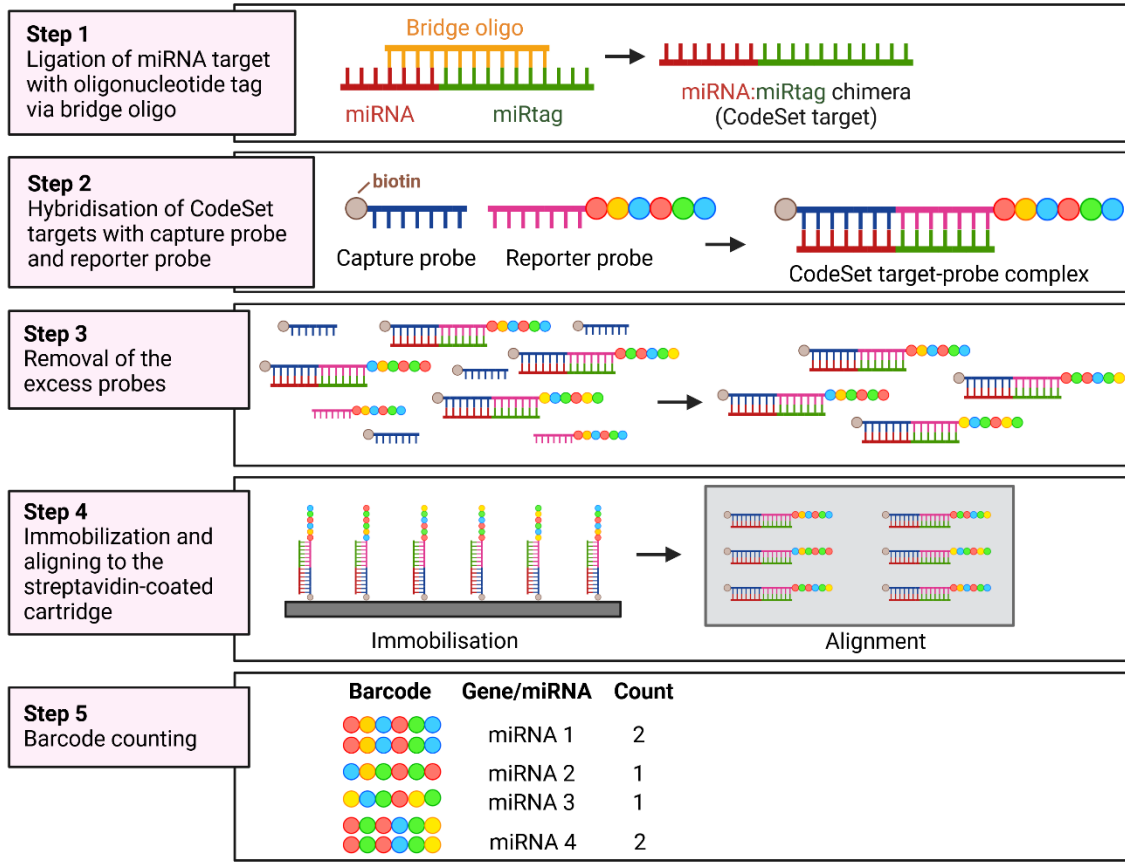
Figure 5.1: Principle of digital profiling of miRNAs by NanoString. Figure was created in BioRender

5.3.4.2 Data analysis

Data were analysed by nSolver Analysis Software v4.0 (NanoString Technologies). Firstly, the threshold count value was determined according to the manual recommendations in order to estimate systemic non-specific background counts. This consisted of 1) calculation of the mean plus standard deviation of negative control probes, eight reporters for which no transcript is supplied, 2) multiplication of the standard deviation by two and added to the mean value. According to the calculation, the threshold count value of 10 was applied to the software.

Four raw data normalization approaches were used, with three of them based on methodologies provided by the nSolver software, while the final approach was non-custom:

1) Normalization based on positive controls

Positive controls, consisting of six probes that recognize synthetic mRNA targets that are included in the assay at specified concentrations, were used for technical standardization to assess overall efficiency of hybridization and recovery. This approach is used to normalize any platform-related sources of variation, including those from automated purification and hybridization conditions. Default settings were applied: geometric mean used to compute normalization factor, and the appearance of flag lanes (warnings) if normalization factor is outside of the 0.3-3 range (NanoString technologies, 2017).

2) Normalization based on positive controls and CodeSet content involving top 100 miRNAs

In addition to positive control normalization, normalization to CodeSet content (or miRNA content) corrects for differences in sample input between assays and is typically performed after positive control normalization. CodeSet content involving top 100 miRNA targets is a recommended normalization method for cell- and tissue-derived miRNA data, or even miRNAs data from biofluids if there are more than 100 miRNA targets detected above the threshold.

Again, default settings were applied including the normalisation flagging outside the normalisation factor range 0.1-10 for CodeSet content normalization (NanoString technologies, 2017).

3) Normalization based on positive controls and CodeSet content involving all miRNAs

When CodeSet content normalization to top 100 miRNA targets is not appropriate, normalization to total miRNA is the next recommended approach. It normalizes data to the geometric mean of all the miRNAs that are expressed robustly above the background. However, this method can be less robust if relatively few targets are expressed above background.

Default settings were selected as explained above and reported in Crossland et al., 2023.

4) Normalization based on positive controls and equal RNA amount (non-custom)

The positive control normalization was calculated manually in excel following the steps from the nCounter Expression Data Analysis guide.

Micro RNA counts of each sample were divided by the RNA amount used as input for the experiment, so that the miRNA counts ratios reflect the scenario as if equal amount instead of equal volume of RNA was used as input in the analysis.

Fold change (FC) expression differences were calculated using nSolver ratio data, based on normalized count data.

5.3.5 Relative miRNA expression by TaqMan real-time PCR

TaqMan reverse transcription quantitative real time polymerase chain reaction (RT-qPCR) was performed to validate the expression of the miRNAs identified (by miRNA sequencing and NanoString). RNA was extracted from combined fraction of small and large uEVs coming from stable DN (n=20) and progressive DN (n=20) urine pools (Table 5.12). Because there is no known RNA from uEVs that can be used as endogenous housekeeping gene, custom-made spike-in miRNA cel-miR-39-3p (sequence: 5'-UCACCGGGUGUAAAUCAGCUUG-3') with 5'phosporilation (10620310, Invitrogen) was used as an exogenous reference gene. Equal concentration of 5 pM was added in both stable and progressive uEVs prior to RNA purification. Purified RNA was eluted in 15 µl elution solution, quantified by Nanodrop 8000 spectrophotometer and stored at -80°C until the next day (~ 18 hours).

Equal amount of total RNA (9 ng) from uEVs was converted to cDNA using TaqMan Advanced miRNA cDNA Synthesis Kit (A28007, Applied Biosystems) on a T100 Thermal Cycler (Bio Rad) according to the TaqMan Advanced miRNA Assays user guide involving five steps as demonstrated in Figure 5.2: 1) poly-A tailing reaction where poly(A) polymerase adds 3'adenosine tail to the mature miRNAs, 2) adaptor ligation reaction where an adaptor is added to the 5' of miRNA with poly-A tail, and this adaptor is used as forward primer binding site for the miR-Amplification reaction, 3) reverse transcription reaction where universal reverse-transcription primer binds to poly-A tail and all modified miRNAs are reverse transcribed, 4) miR-Amplification reaction where universal forward and reverse primers increase the number of cDNA molecules, and 5) real-time PCR reaction (Vautrot and Behm-Ansmant, 2020).
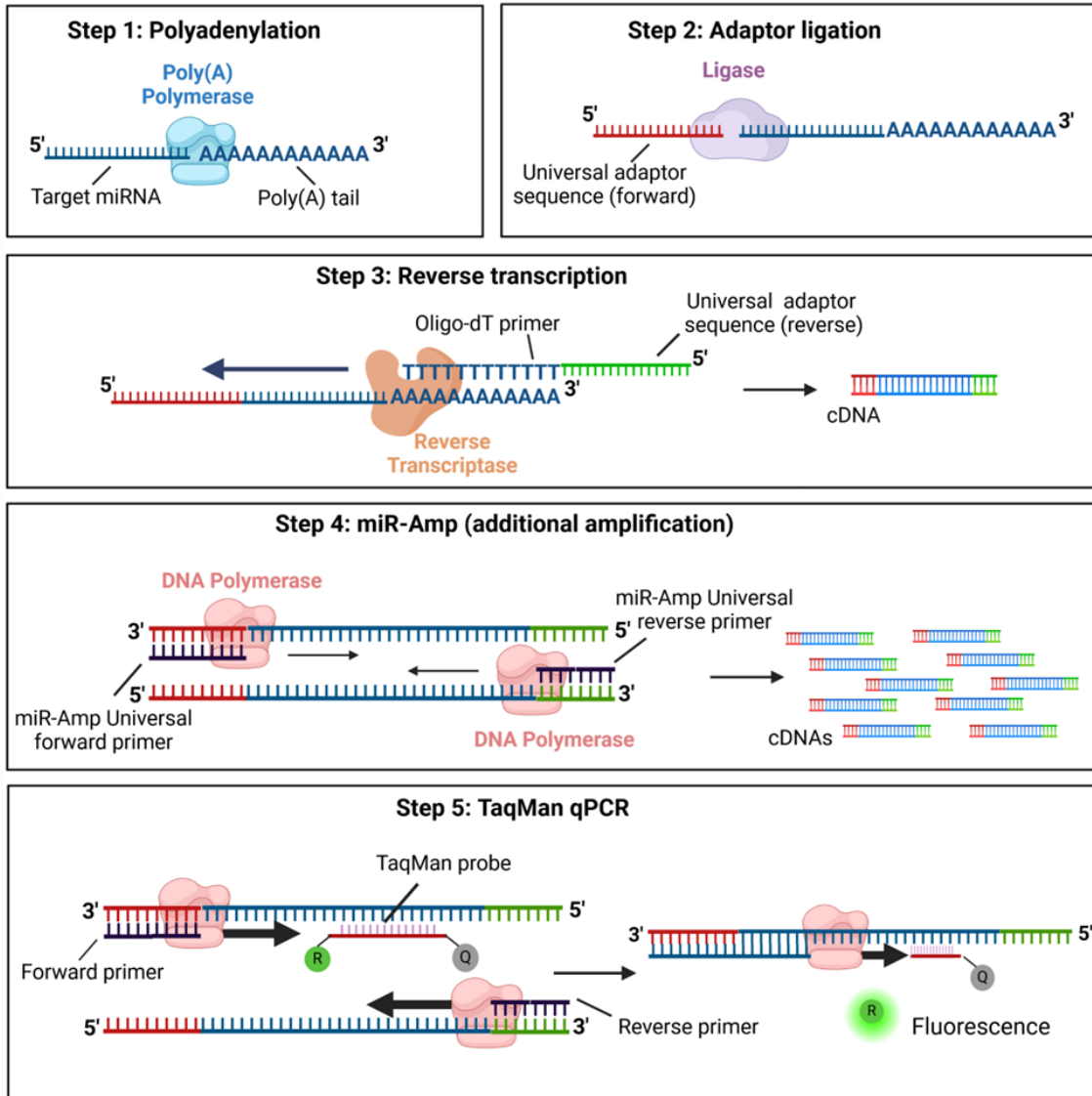
Figure 5.2: Principle of TaqMan Advanced RT-qPCR. Figure was created in BioRender.

5.3.5.1 Poly-A tailing reaction

Poly(A) Reaction mix was prepared according to the Table 5.3. Total volume of reaction was 5 µl of which 3 µl was reaction mix and 2 µl was RNA sample. The reaction mix was vortexed and spun down after which tubes were placed in a thermal cycler and incubated at 37°C for 45 min (polyadenylation), followed by incubation at 65°C for 10 min (stop reaction), and held at 4°C.

Table 5.3. Components and corresponding volumes per reaction of the poly-A reaction

Component	Volume
10x Poly(A) Buffer	0.5 µl
ATP (10 mM)	0.5 µl
Poly(A) Enzyme (5U/µl)	0.3 µl
RNase-free water	1.7 µl
RNA sample (9 ng)	2.0 µl
Total reaction volume	**5.0 µl**

5.3.5.2 Adaptor ligation reaction

Ligation reaction mix was prepared as shown in Table 5.4. 10 µl of the ligation mixture was added to a tube containing 5 µl of the poly(A) tailing reaction product, making the total adaptor ligation reaction volume 15 µl. After vortexing and briefly centrifuging the tubes, the ligation reaction was performed by incubating samples at 16°C for 60 min in the thermal cycler. At the end of ligation, the samples were kept at 4°C.

Table 5.4. Components and corresponding volumes per reaction of the adaptor ligation reaction

Component	Volume
5x DNA Ligase Buffer	3 µl
50% PEG 8000	4.5 µl
25x Ligation Adaptor	0.6 µl
RNA Ligase (10 U/µl)	1.5 µl
RNase-free water	0.4 µl
Poly(A) tailing reaction product	5.0 µl
Total reaction volume	**15.0 µl**

5.3.5.3 Reverse transcription (RT) reaction

Reaction mixture for reverse transcription was prepared according to the Table 5.5. The prepared 15 µl of the reverse transcription mix was transferred to the tubes containing 15 µl of the adaptor ligation reaction product, which made the total volume of the reverse transcription reaction 30 µl. The thermocycler settings for the reverse transcription included incubation at 42°C for 15 min (reverse transcription), followed by incubation at 85°C for 5 min (stop reaction), and held at 4°C.

Table 5.5. Components and corresponding volumes per reaction of the reverse transcription reaction

Component	Volume
5x RT Buffer	6 µl
dNTP Mix (25 mM each)	1.2 µl
20x Universal RT Primer	1.5 µl
10x RT enzyme mix	3 µl
RNase-free water	3.3 µl
Adaptor ligation reaction product	15.0 µl
Total reaction volume	**30.0 µl**

5.3.5.4 miR-Amplification reaction

The final step of cDNA synthesis was miR-amplification reaction. The sufficient reaction mix was prepared as listed in Table 5.6. The total volume of the reaction was 50 µl and thermal cycler settings were as follows: incubation at 95°C for 5 min (enzyme activation), 17 cycles of denaturation at 95°C for 3 sec and annealing / extending at 60°C for 30 sec, incubation at 99°C for 10 min (stop reaction) and upon finishing samples were kept at 4°C.

Table 5.6. Components and corresponding volumes per reaction of the miR-Amplification reaction

Component	Volume
2x miR-Amp Master Mix	25 µl
20x miR-Amp Primer Mix	2.5 µl
RNase-free water	17.5 µl
RT reaction product	5.0 µl
Total reaction volume	**50.0 µl**

5.3.5.5 Real Time PCR

The resulting cDNAs from stable and progressive DN cohorts were used in quadruplicates to quantify the expression levels of miR-99a-5p (Assay ID: 478519 mir), miR-223-3p (Assay ID: 477983 mir), miR-184 (Assay ID: 477938 mir), miR-3613-5p (Assay ID: 479424 mir) and spike-in cel-miR-39-3p (Assay ID: 478293 mir) using TaqMan Fast Advanced Master Mix, no UNG (A44359, Applied Biosystems) on a QuantStudio 5 (Applied Biosystems).

Real Time PCR Master Mix was prepared according to the Table 5.7 In each well of the PCR reaction plate (96-well plate), 15 µl of Master Mix was added together with 5 µl of 1:10 dilution of cDNA (diluted in nuclease-free water).

Real-time PCR run was set up for the 20 µl reactions in fast-cycling mode by following steps: enzyme activation at 95°C for 20 sec, 40 cycles of denaturation at 95°C for 1 sec and annealing / extending at 60°C for 20 sec.

Table 5.7. Components and corresponding volumes per reaction of the Real-Time PCR reaction

Component	Volume
TaqMan Fast Advanced Master Mix (2x)	10 µl
TaqMan Advanced miRNA Asay (20x)	1 µl
RNase-free water	4 µl
Diluted 1/10 cDNA	5.0 µl
Total reaction volume	**20.0 µl**

All working materials were UV-sterilized and working surfaces were cleaned with 70% isopropanol and RNaseZAP cleaning agent for removing RNase.

TaqMan chemistry was the method of choice because it is usually less likely to detect non-specific amplification compared to SYBR green. In particular, TaqMan probes contain a reporter dye (5') and a quencher dye (3') that are in close proximity and therefore reporter fluorescence is suppressed, primarily by Förster-type energy transfer (FRET) (Navarro et al., 2015). However, when the Taqman probe is complementary to the target sequence and anneals between the forward and reverse primers, the DNA polymerase cleaves the reporter dye from the probe and such separation of the reporter dye from the quencher dye results in increased fluorescence of the reporter dye. The more copies of the template created, the stronger the fluorescent signal (Holland et al., 1991; Lech and Anders, 2014). In addition, technology of TaqMan advanced microRNA assays includes a pre-amplification step to increase the initial pool of cDNA needed for the

qPCR. This is advantageous in case of limited miRNA amount from sample types such as uEVs.

5.3.5.6 qPCR Data analysis

Livak method was used for relative quantification of human miRNAs (Livak and Schmittgen, 2001), using cel-miR-39-3p as a reference.

ΔCt was calculated using formula:

ΔCt = mean Ct (target gene) - mean Ct (reference gene), where target gene was miRNA of interest (miR-99a-5p, miR-223-3p, miR-184, or miR-3613-5p), and reference gene was spike-in miRNA (cel-miR-39-3p).

ΔΔCt was calculated using formula:

ΔΔCt = ΔCt (target sample) - ΔCt (reference sample), where target sample was progressive DN, and reference sample was stable DN.

To calculate fold change between the two groups, exponential value was converted to linear value following formula: $2^{-\Delta\Delta Ct}$

5.4 Results

5.4.1 Discovery of uEVs miRNA markers of DN progression by miRNA sequencing

5.4.1.1 Screening of uEVs miRNAs of DN progression by miRNA sequencing

For the screening of miRNAs from uEVs that may be candidate markers of DN progression, uEVs RNA samples were obtained from patients in stable DN (n=3), progressive DN (n=3), diabetes with no CKD (n=2) and healthy control (n=2) (Table 5.8).

Table 5.8: Clinical information of patient samples used for miRNA sequencing from uEVs

Sample ID	Cohort	eGFR collection point [ml/min]	eGFR slope [ml/min/year]	Mean eGFR slope [ml/min/year]	Age	Gender	Serum creatinine [mg/dL]
SKI410	Stable DN	40	2.75		74	Female	1.3
SKI470	Stable DN	40	-1.68	0.53±2.2	54	Male	1.9
PDN127	Stable DN	35	0.53		56	Female	1.6
SKI1001	Progressive DN	40	-5.43		ND	Female	ND
SKI837	Progressive DN	33	-5.32	-7.52±3.7	ND	Female	ND
PDN22	Progressive DN	26	-11.82		78	Male	2.6
SKI1020	Diabetic	ND	NA		ND	Male	ND
SKI1014	Diabetic	ND	NA		ND	Female	ND
SKI574	Healthy	ND	NA		ND	ND	ND
SKI922	Healthy	ND	NA		ND	ND	ND

ND = not determined, NA = not applicable

The workflow of the miRNA sequencing procedure is shown in Figure 5.3, as explained in Methods 5.3.3. uEVs were isolated and RNA extracted as described in the Methods 5.3.1. For miRNA sequencing and bioinformatic analysis this project relied on external professional services as described in the Methods 5.3.3.
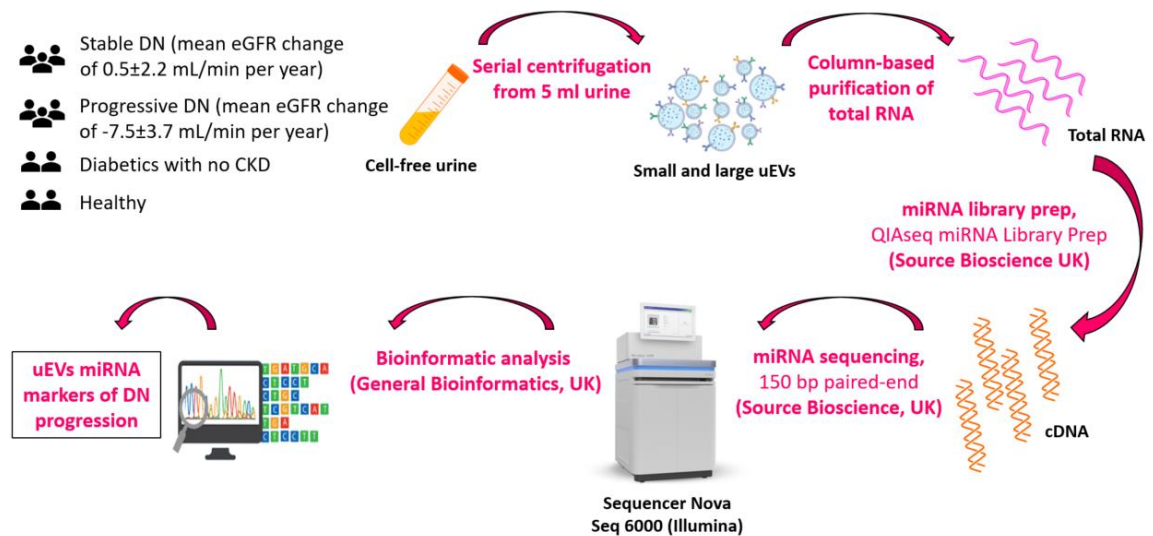
Figure 5.3 Workflow used for the discovery of uEVs' miRNA markers of DN progression by miRNA sequencing. uEVs RNA samples were isolated at NTU and then sequenced by Source Bioscience, UK company and bioinformatic analysis of the raw sequencing data was performed by General Bioinformatics, UK company.

The total number of detected miRNAs was compared between each of the four analysed groups. As shown in Figure 5.4, 44% of the detected miRNAs, corresponding to 512 miRNAs (highlighted with a red circle), was in common to all the groups: progressive DN (yellow circle), stable DN (blue circle), diabetic (green circle), and healthy (red circle). The diabetic group was the richest in the number of detected miRNAs with 14.7% of miRNA being unique. In progressive DN, instead, only 2% of miRNA, corresponding to 23 miRNAs, was unique when compared to all the other groups.
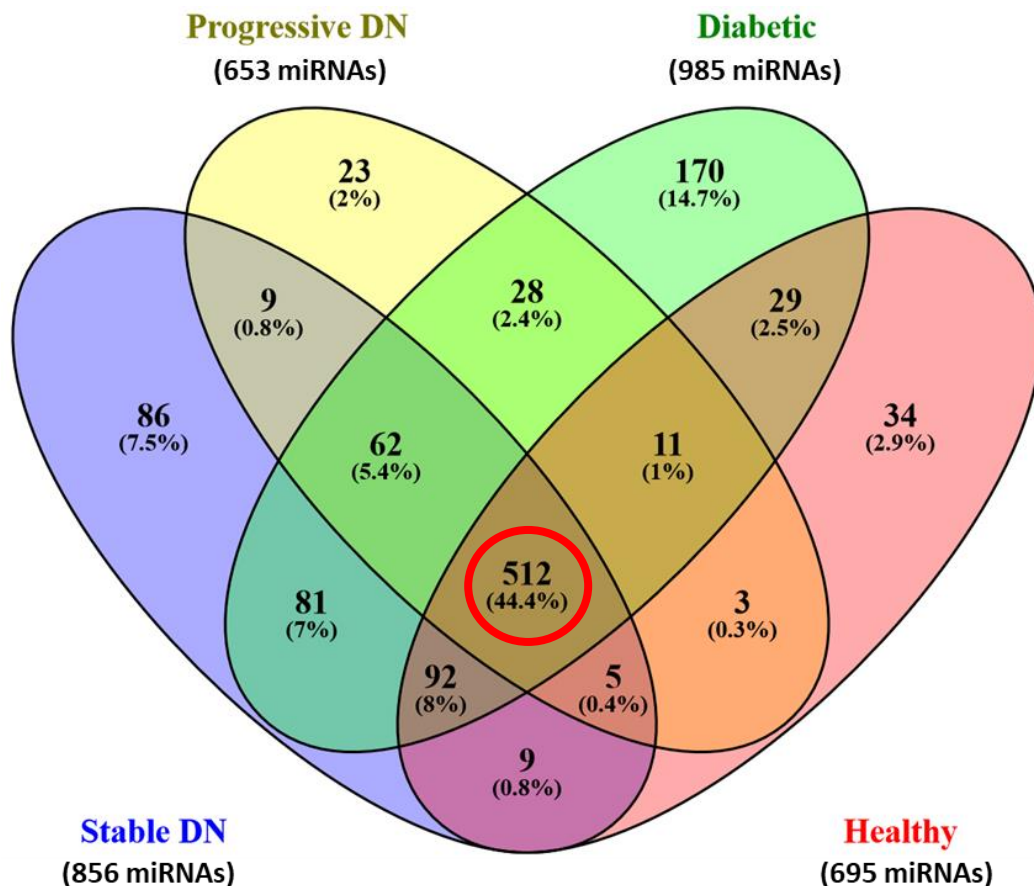
Figure 5.4: miRNAs from uEVs in the four analysed cohorts, detected by miRNA sequencing. Numbers of detected miRNAs were derived from all the miRNAs with read count > 0, in progressive DN (n=3), stable DN (n=3), diabetic (n=2) and healthy (n=2) cohorts. Venn diagram was created using Venny v2.1.0.

As the focus was on DN progression, the number of detected uEVs miRNAs was compared between progressive DN with the other three cohorts individually (Figure 5.5). About 60% of miRNAs was in common when progressive DN was compared to stable DN (A), diabetic (B), and healthy (C) groups. However, in all the three comparisons, the progressive DN group had the lowest number of detected miRNAs, and therefore a smaller number of uniquely found miRNAs.
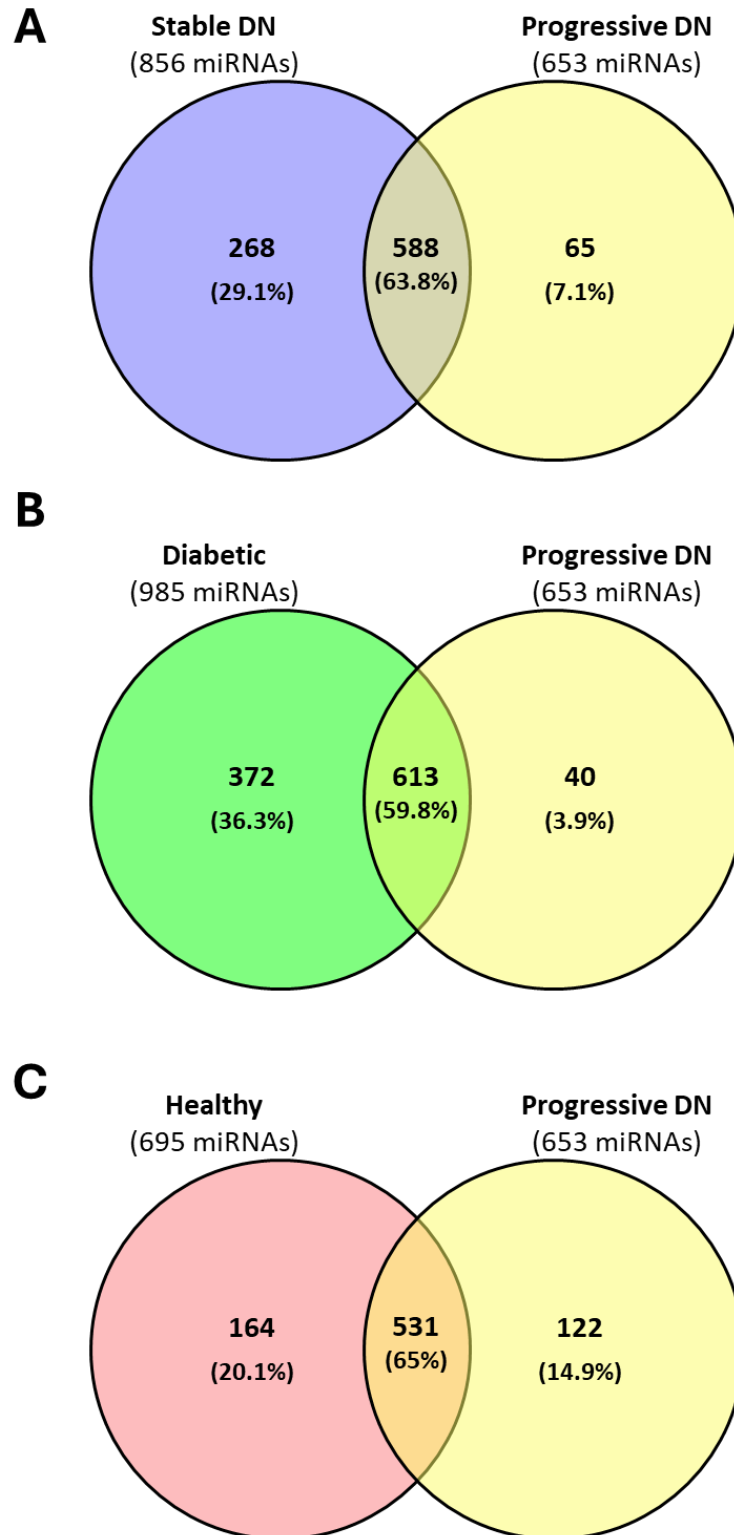
Figure 5.5: Dimension of detected miRNAs in uEVs from progressive DN when compared to stable DN (A), diabetic (B) or healthy (C) groups. Data were used in the same way as explained earlier in Figure 5.2. Venn diagrams were created in PowerPoint.

Furthermore, to discover what miRNAs are statistically significantly changed in progressive DN condition, differential expression analysis between progressive DN (n=3) and stable DN (n=3) was carried out (Table 5.9). Three miRNAs resulted as significantly deregulated in progressive DN compared to stable DN: miR-875-3p and miR-3613-5p that were significantly upregulated, and miR-184 which was significantly downregulated. Differential expression analysis was expressed as fold change ("Progressive DN vs Stable DN").

The volcano plot in Figure 5.6 shows all differentially expressed miRNAs distribution. Out of 647 miRNAs included in differential expression analysis, only three miRNAs were significantly differentially expressed in progressive vs stable DN according to the adjusted p-value and were labelled above the red line indicating significance of $p<0.05$. Two upregulated miRNAs (miR-3613-5p and miR-875-3p) were shown in red dots and one downregulated miRNA (miR-184) was shown as a blue dot. The rest of 644 miRNAs were not significantly changed and were shown as grey dots. Due to its extremely high fold change and extremely low significance, miR-875-3p stands out from the other miRNAs.
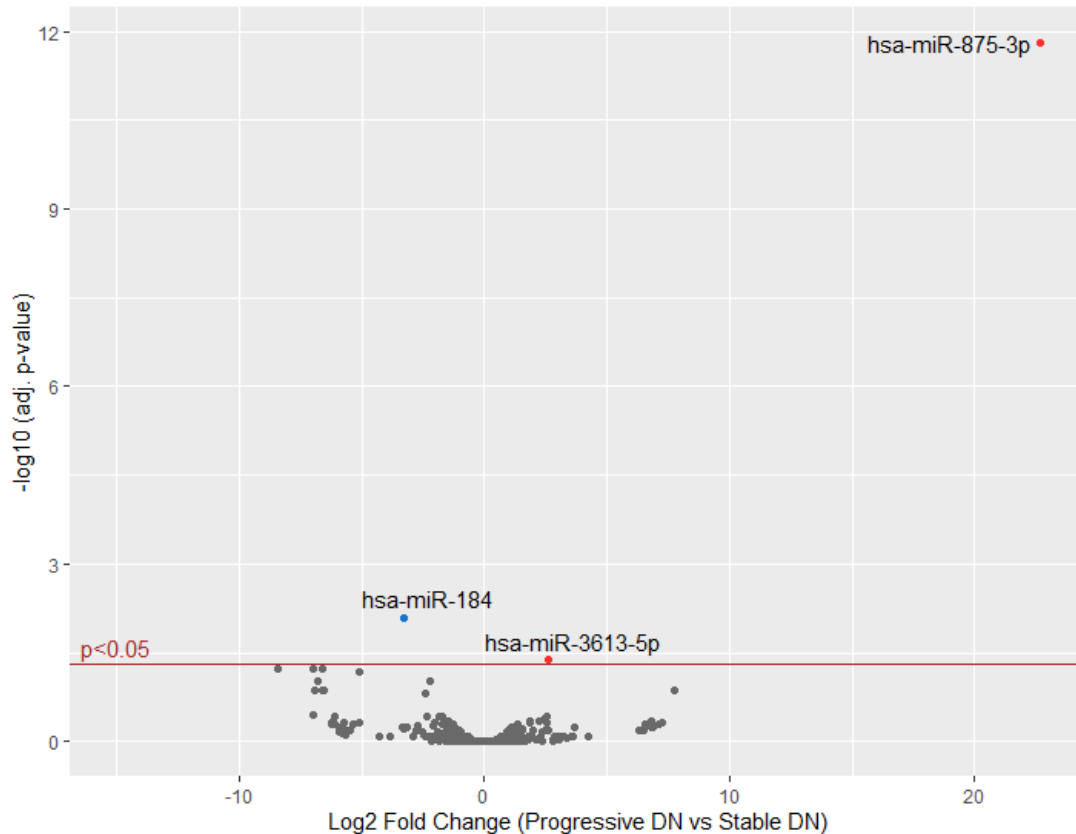
Figure 5.6: Differential expression of miRNAs from uEVs in progressive DN (n=3) compared to stable DN (n=3). Differential expression was expressed as fold change (progressive DN / stable DN) transformed into log2 (x-axis), and significance was expressed as adjusted p-values based on Benjamini Hochberg, transformed into log10 (y-axis). Out of 647 miRNAs included in differential expression analysis, only three miRNAs were significantly differentially expressed in progressive vs stable DN: two upregulated (red dots) and one downregulated (blue dot), while all the grey dots represent no significantly changed miRNAs.

While miR-184 was found 9.5-fold downregulated in progressive DN and miR-3613-5p was found 6-fold upregulated in progressive DN, the most significantly changed miR-875-3p showed > 6 million upregulation in progressive DN (Table 5.9).

Table 5.9: Significantly differentially expressed miRNAs from uEVs in progressive DN (n=3) versus stable DN (n=3) based on Wald test p-value adjusted according to Benjamini-Hochberg method. RNA samples were sequenced by Source Bioscience, UK, and bioinformatic analysis was performed by General Bioinformatics, UK.

miRNA	Fold change (Progressive DN / Stable DN)	Adjusted p-value
miR-875-3p	6739686.245	1.52E-12
miR-3613-5p	6.036	0.041612
miR-184	-9.607	0.007972

In order to explore the expression of the three significantly changed miRNAs (miR-875-3p, miR-3613-5p and miR-184) per single patient sample in stable and progressive DN cohorts, a heat map was created (Figure 5.7). In this way it can be appreciated that miR-875-3p, the most significantly changed miRNAs in progressive DN, was highly expressed in only one out of three progressive samples, shown as red square representing high expression as opposed to bright blue squares showing low expression or no expression. Because of this, miR-875-3p is considered as an artefact of the bioinformatic programme, as explained in Methods 5.3.3.1 (personal communication by General Bioinformatics, UK), it was not considered as a strong candidate marker of DN progression and thus was not included in the further analysis. On the other hand, miR-184 showed consistent decrease in progressive DN cohort represented as the prevalence

of red and bright red colour in stable DN subjects (showing high expression) and uniform

prevalence of bright blue colour in progressive DN subjects (showing low expression).

The miR-3613-5p was significantly upregulated in progressive DN as the uniform

appearance of the bright blue colour in stable DN subjects revealed low expression,

while the light blue, white and red colours in progressive DN individuals revealed higher

expression than in the stable DN for miR-3613-5p (Figure 5.7).
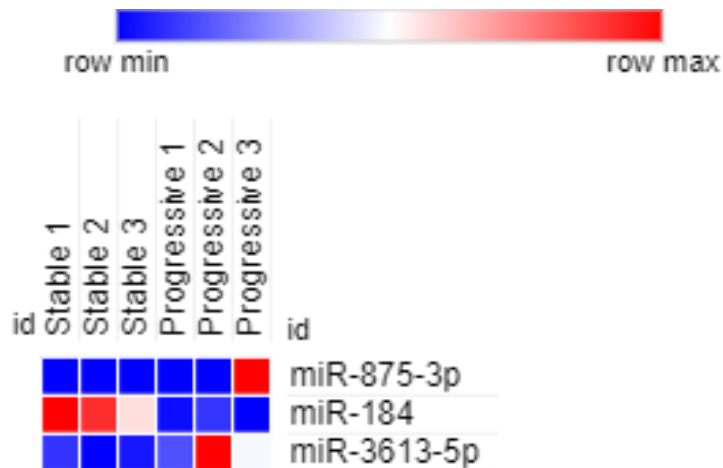
Figure 5.7: Significantly differentially expressed miRNAs from uEVs in progressive DN (n=3) versus stable DN (n=3), per individual sample. Data used to create the heat map were raw read counts of each of the significantly changed miRNA in each stable and progressive DN subject. Heat map was created in Morpheus, https://software.broadinstitute.org/morpheus.

In conclusion, three miRNAs were significantly differentially expressed in progressive vs

stable DN. Of them, two miRNAs (miR-184 and miR-3613-5p) showed consistent

expression pattern among the cohorts and were therefore further validated.

5.4.1.2 Involvement of miR-184 and miR-3613-5p with CKD

Literature searches revealed that miR-3613-5p had no known previous association with CKD but was proposed as a possible prediction factor of the progression of renal clear cell carcinoma (Qin et al., 2019; Zhan et al., 2021).

MiR-184 was reported to be associated with CKD before. It was significantly upregulated in a rat model of DN (Zanchi et al., 2017) and transfection of tubular epithelial cells with miR-184 mimic promoted a pro-fibrotic phenotype (Zanchi et al., 2017). Its significant upregulation was also shown in peripheral blood mononuclear cells from patients with IgAN, when screened by miRNA sequencing (Wang et al., 2020). Furthermore, downregulation of miR-184 was proven to be protective against pancreatic β-cell apoptosis and dysfunction in T2DM, via CREB regulated transcription coactivator 1 (CRTC1) upregulation (Grieco et al., 2022).

5.4.1.3 Screening of uEVs miRNAs as markers of DN by miRNA sequencing

The differential expression of miRNAs, comparing progressive DN (n=3) and diabetes (n=2) to explore uEVs miRNAs as potential markers of DN, is presented in Table 5.10. The miR-875-3p was once again identified as significantly upregulated; however, as mentioned earlier, it was dismissed as an artifact. The remaining findings included four novel downregulated miRNAs in uEVs from DN (miR-891a-5p, miR-432-5p, miR-890 and miR-892a). The heat map in Figure 5.8 indicates that all detected miRNAs were expressed solely in diabetes, with their expression absent in the DN condition. A literature search revealed that miR-891-5p was significantly changed in uEVs samples

from mesangial proliferative glomerulonephritis, showing downregulation when analysed by sequencing (Dai et al., 2023). However, its qRT-PCR validation did not confirm this finding. Furthermore, miR-432-5p has been reported to have detrimental effects in moderate CKD as it is involved in atherosclerosis and inflammation (Mansouri et al., 2017). No literature reports were found for the other two miRNAs (miR-890, miR-892a) in association with CKD.

Table 5.10: Significantly differentially expressed miRNAs from uEVs in progressive DN (n=3) versus diabetic (n=2). MiRNAs are sorted from top upregulated to top downregulated

miRNA	Fold change (Progressive DN / Diabetic)	Adjusted p-value
hsa-miR-875-3p	3443036.394	2.88E-08
hsa-miR-891a-5p	-60.352	0.041486
hsa-miR-432-5p	-202.908	0.006597
hsa-miR-890	-344.779	0.006597
hsa-miR-892a	-657.898	4.91E-05
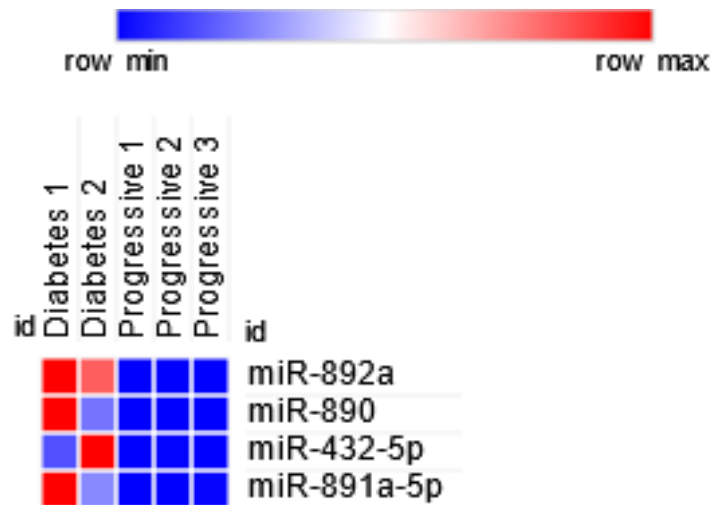
Figure 5.8: Significantly differentially expressed miRNAs from uEVs in progressive DN (n=3) versus diabetes (n=2), per individual sample.

Furthermore, Table 5.11 shows all miRNAs in uEVs which were significantly altered in progressive DN (n=3) compared to the healthy cohort (n=2).

After excluding miR-875-3p, which was considered an artefact, the comparison between progressive DN and the healthy cohort revealed five upregulated miRNAs and eight downregulated miRNAs in DN. Among these, miR-891-5p and miR-892a were repeated from the previous analysis comparing DN with diabetes (Table 5.11).

Table 5.11: Significantly differentially expressed miRNAs from uEVs in progressive DN (n=3) versus healthy (n=2)

miRNA	Fold change (Progressive DN / Healthy)	Adjusted p-value
hsa-miR-875-3p	2324549.956	2.36E-07
hsa-miR-23b-5p	230.128	0.038054
hsa-miR-146a-5p	66.397	0.000162
hsa-miR-150-5p	59.596	0.014793
hsa-miR-3613-5p	8.169	0.028856
hsa-miR-500a-3p	-6.429	0.047981
hsa-miR-362-5p	-14.868	0.027155
hsa-miR-891a-5p	-53.651	0.014793
hsa-miR-766-3p	-354.704	0.019652
hsa-miR-1469	-449.389	0.019652
hsa-miR-892a	-787.557	3.71E-05
hsa-miR-4508	-9231284.647	2.90E-16
hsa-miR-4492	-13848246.746	8.01E-06

Further analyses including stable DN cohort, as well as diabetes versus healthy, are shown in Appendix (Supplementary tables 7-9).

5.4.2 Discovery of uEVs miRNA markers of DN progression by NanoString

5.4.2.1 Screening of uEVs miRNAs by miRNA digital profiling

In addition to miRNA sequencing, screening for miRNA candidate biomarkers of DN progression from uEVs was done in pool by NanoString digital profiling as explained in Methods 5.3.4.1. RNA was purified from the uEVs isolated from the same patient samples used for the proteomic biomarker profiling in Chapter 4, with the exception of the patient samples involved with miRNA sequencing. For clarification, clinical information of samples from four cohorts is shown in Table 5.12.

Due to the limited amount of RNA from uEVs, total RNA samples were pooled together in each cohort consisting of 17 subjects per cohort or 18 in healthy group (Figure 5.9). Workflow of the sample preparation for the downstream NanoString analysis is shown in Figure 5.9 as explained in the Methods 5.3.4.

Table 5.12: Clinical information of patient samples used for miRNA digital profiling from uEVs

	Stable DN	Progressive DN	Diabetic	Healthy
Number of subjects	17	17	17	18
Gender (Female/Male)	2/15	1/16	8/9	7/4 (ND=7)
Age (mean ± SD)	72.1±9.2	65.7±10.5 (ND=4)	56.6±14.2 (ND=10)	41.9±27.4 (ND=8)
BMI (mean ± SD)	28.8±4.9 (ND=1)	28.6±4.3 (ND=9)	30.4±7.0 (ND=10)	25.9±4.2 (ND=10)
Serum creatinine (mg/dL) (mean ± SD)	1.82±0.2 (ND=1)	2.09±0.3 (ND=4)	1±0.2 (ND=10)	0.8±0.2 (ND=10)
eGFR (ml/min) (mean ± SD)	37.05 ± 4.7	33.9 ± 4.9	80.2 ± 16.3 (ND=10)	ND
eGFR change (ml/min/year) (mean ± SD)	2.22 ± 3.3	-8.26 ± 2.8	NA	NA
CKD stage	CKD 3b	CKD 3b	NA	NA

*ND = not determined (not provided information), NA = not applicable
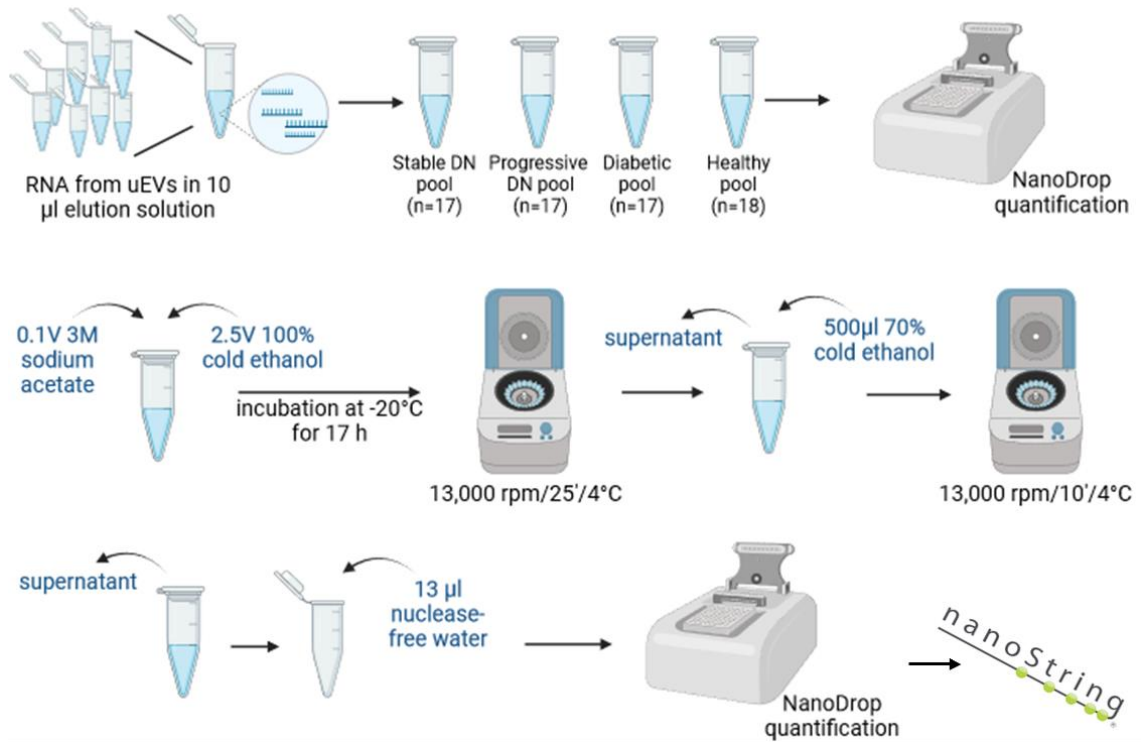
Figure 5.9: Workflow of the total RNA sample preparation for downstream NanoString digital profiling analysis.

RNA samples from pools of 17 patients in stable DN, progressive DN, and diabetic cohort, and 18 patients in healthy cohort were quantified as shown in Table 5.13. Healthy group had the highest concentration of RNA, while diabetic group was the least enriched in RNA. Quality control of RNA samples was similar in all the cohorts.

Table 5.13: RNA concentration and quality control from concentrated RNA samples (pools of 17-18 subject per cohort) from uEVs, by NanoDrop 8000 spectrophotometer

	Concentration (ng/µl)	260/280	260/230
Stable DN	16.61	1.62	0.79
	15.72	1.6	0.75
Progressive DN	23.85	1.75	0.87
	18.2	1.78	0.93
Diabetic with no CKD	8.306	1.66	0.76
	7.96	1.62	0.69
Healthy	57.01	1.64	0.87
	41.95	1.72	1.17

The distribution of detected uEVs' miRNAs obtained by digital profiling was compared among the four cohorts (Figure 5.10). Only miRNAs which were consistently detected in all three technical replicas of each cohort were included in the comparison. About 14% of the detected miRNAs (shown in red circle) was in common to all the compared groups. The diabetic group (green circle) had the highest number of detected miRNAs (39 miRNAs), followed by the healthy (red circle, 26 miRNAs), progressive DN (yellow circle, 17 miRNAs) and stable DN (blue circle, 13 miRNAs) group.

Figure 5.11 shows comparison in total number of detected miRNAs from uEVs in progressive DN vs stable DN (A), diabetic (B), or healthy (C) groups. About 30% of miRNAs were in common between progressive DN and any of the other comparing group.

Figure 5.10: Number of miRNAs from uEVs identified in each cohort, detected by NanoString digital profiling. The comparison in total number of detected miRNAs included only miRNAs whose expression was above threshold (as explained in Methods 5.3.4.3) in all three technical replicas of each cohort: stable DN (n=17), progressive DN (n=17), diabetic (n=17) and healthy (n=18).
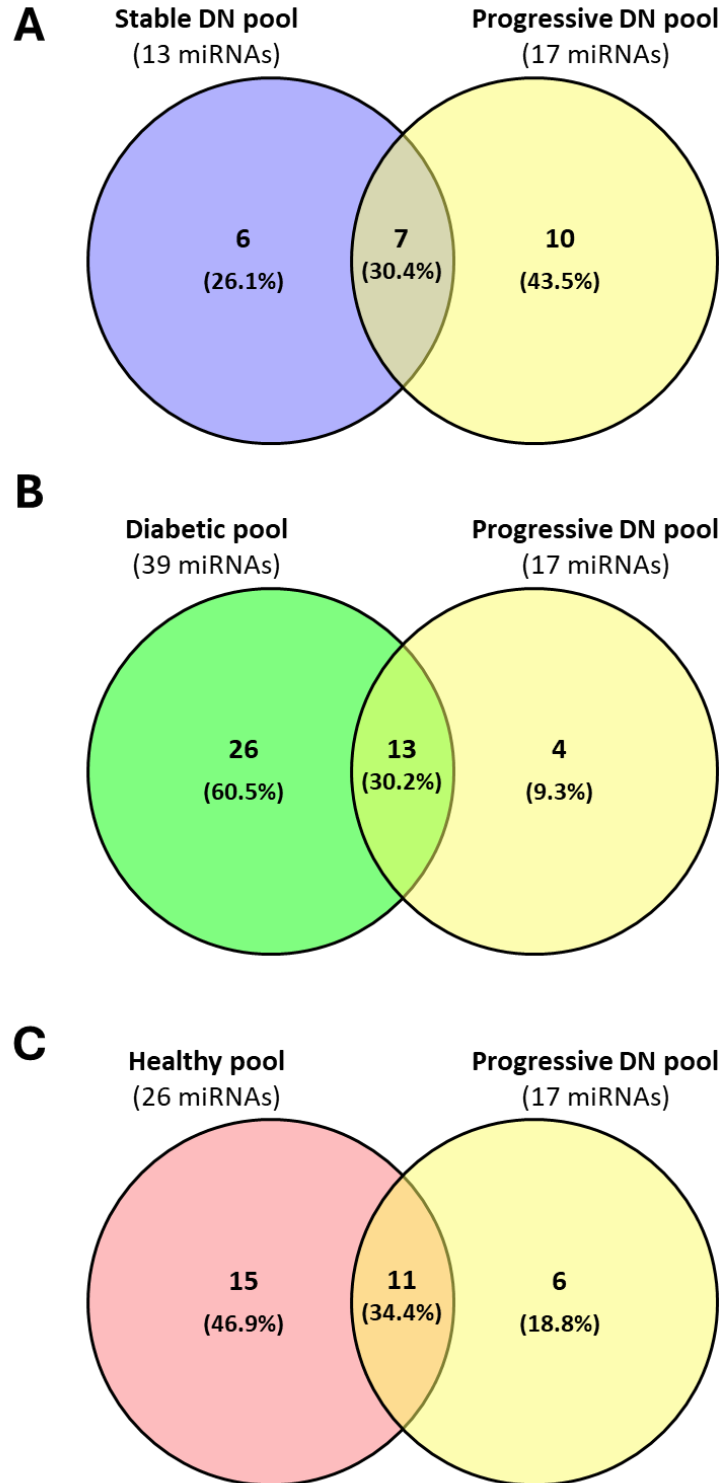
Figure 5.11: Number of detected miRNAs in uEVs from progressive DN when compared to stable DN (A), diabetic (B) or healthy (C) groups. Data were used in the same way as explained in Figure 5.7. Venn diagrams were created in PowerPoint.

Having shown the dimension of detected uEVs miRNAs in each cohort, the next question was to explore which miRNAs were significantly differentially changed in progressive compared to stable DN.

Data were analysed in four different ways, as explained in the Methods 5.3.4.3. Therefore, study from the four datasets of differentially changed miRNAs between stable and progressive DN were generated: (1) dataset normalized only to positive controls shown in Table 5.14; (2) dataset normalized to positive controls and miRNA content considering top 100 miRNAs (Table 5.15); (3) dataset normalized to positive controls and miRNA content considering total miRNAs (Table 5.16); and (4) dataset manually normalized to positive controls and corrected for differences in RNA amounts (Table 5.17).

Differential expression analysis was expressed as ratio between "progressive DN and stable DN groups", and the change was considered significant if p-value was < 0.05. In all four normalization datasets, two miRNAs were consistently significantly changed in progressive DN (Tables 5.14-5.17 and Figure 5.12): miR-99a-5p which was significantly upregulated in progressive DN (purple bars), and miR-223-3p which was significantly downregulated in progressive DN (pink bars). Due to their consistent detection, these two uEVs miRNAs were considered for the validation phase as candidate markers of DN progression.

The two miRNAs that emerged as significantly changed in miRNA sequencing (miR-184 and miR-3613-5p) were below threshold in NanoString datasets, therefore were not included in differential expression analysis.

Table 5.14: Significantly differentially expressed miRNAs from uEVs in progressive versus stable DN from dataset normalized to positive controls. Highlighted miRNAs were repetitive in all datasets (Tables 5.14-5.17). Significance was based on p-value according to Welch's t-test.

miRNA	Ratio (Prog / Stab)	P-value
hsa-miR-99a-5p	1.87	0.00323516
hsa-miR-223-3p	-1.33	0.01266719
hsa-miR-30a-5p	2.04	0.01321228
hsa-miR-4286	1.45	0.02386335
hsa-miR-4454+hsa-miR-7975	2.39	0.04285717
hsa-let-7b-5p	2.51	0.04401151

Table 5.15: Dataset normalized to positive controls and miRNA content considering top 100 miRNAs.

miRNA	Ratio (Prog / Stab)	P-value
hsa-miR-223-3p	-1.97	0.00667235
hsa-miR-191-5p	1.81	0.01164113
hsa-miR-922	-1.45	0.03825467
hsa-miR-451a	3.03	0.0390115
hsa-let-7b-5p	1.79	0.04433684
hsa-miR-99a-5p	1.59	0.04571871

Table 5.16: Dataset normalized to positive controls and miRNA content considering total miRNAs.

miRNA	Ratio (Prog / Stab)	P-value
hsa-miR-99a-5p	1.72	0.00134784
hsa-miR-30a-5p	1.87	0.01205544
hsa-miR-223-3p	-1.52	0.01397574
hsa-miR-4286	1.4	0.02990278
hsa-let-7b-5p	2.18	0.04787946

Table 5.17: Dataset manually normalized to positive controls and corrected for differences in RNA amount (ng). Significance was based on p-value according to two-tailed t-test.

miRNA	Ratio (Prog / Stab)	P-value
hsa-miR-223-3p	-2.03	0.008136885
hsa-miR-9-5p	-1.77	0.00850251
hsa-miR-194-5p	3.46	0.00895195
hsa-miR-451a	6.26	0.028914748
hsa-miR-526a+hsa-miR-518c-5p+hsa-miR-518d-5p	-1.91	0.033616417
hsa-miR-191-5p	2.0	0.037857611
hsa-miR-99a-5p	1.71	0.039841629
hsa-miR-25-5p	-1.55	0.042395575
hsa-miR-764	-1.80	0.043912778
hsa-miR-598-3p	-1.73	0.049656787
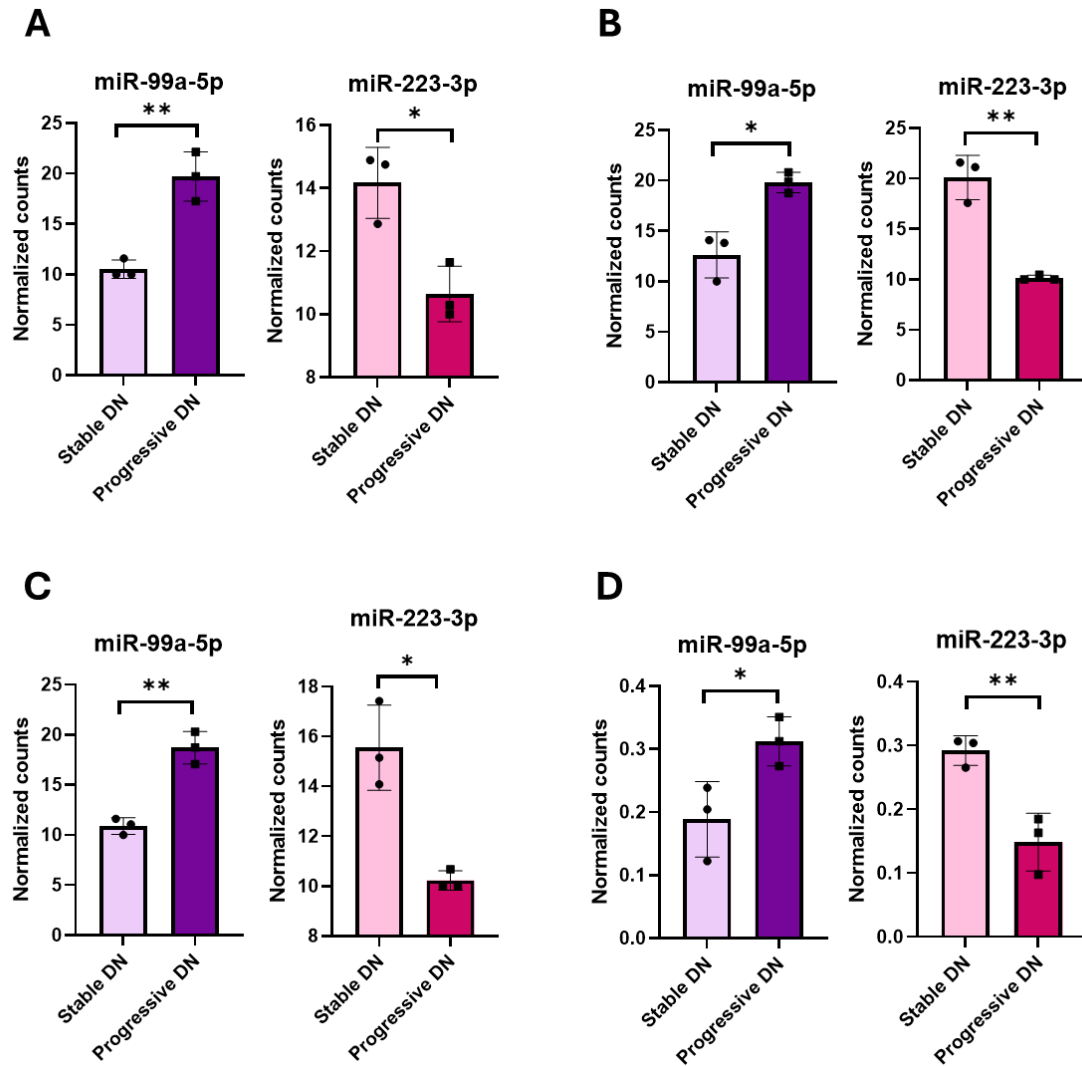
Figure 5.12: Significantly changed uEVs' miRNA in progressive compared to stable DN: upregulated miR-99a-5p (purple) and downregulated miR-223-3p (pink), analysed by NanoString digital profiling. Dataset normalized to positive controls (A), dataset normalized to positive controls and top 100 miRNAs (B), dataset normalized to positive controls and total miRNAs (C), and dataset normalized to positive controls and corrected to differences in miRNA amount (D). Graphs were created in GraphPad prism. Significance applied was t-test. **p < 0.01, *p < 0.05

5.4.2.2 Involvement of miR-99a-5p and miR-223-3p with CKD

MiR-99a-5p was found upregulated in plasma EVs from DN patients with severe albuminuria compared to moderate or mild albuminuria (Uil et al., 2021). In addition, miR-99a-5p expression showed protective effects to podocyte injury through downregulating one of its downstream targets mTOR (Uil et al., 2021). It was also investigated in uEVs from patients with ANCA-associated vasculitis, where it was identified as part of a panel of upregulated miRNAs compared to controls (Frydlova et al., 2022).

MiR-223-3p was found associated with kidney stone disease showing significant overexpression in EV derived from human kidney epithelial cell (HK2)-model of calcium oxalate stone disease (Yang et al., 2023) and in uEVs from patients with kidney stone compared to the healthy control (Yang et al., 2022). It was also found elevated in CD4+ splenic T cells from SLE patients, however, its deletion resulted in an aggravated lupus phenotype suggesting its compensatory role in the pathogenesis of LN (Hiramatsu-Asano et al., 2021). In AKI, miR-223-3p was downregulated in bone marrow mesenchymal stem cells-derived EVs, and its expression was shown to have an effect on reduced AKI-associated apoptosis, pyroptosis and inflammation (Xie et al., 2023).

5.4.2.3 Enrichment network of the uEVs miRNA candidate biomarkers of DN progression

The hypothesis was that the differentially changed miRNAs in uEVs from progressive DN, by miRNA sequencing (miR-184 and miR-3613-5p) and digital profiling (miR-99a-5p and miR-223-3p) could belong to functional pathways relevant to CKD or CKD progression. To investigate this, a network map involving the four miRNAs was built using miRNet 2.0 online database (Figure 5.13). The network showed that the four miRNAs (labelled with blue square nodes) do not cluster together making connections with each other. While miR-99a-5p and miR-184 interact with all the other three miRNAs through one or more common genes (purple circular nodes), miR-3613-5p and miR-223-3p do not interact with each other. The strongest connection was visible between miR-223-3p and miR-184, both downregulated in progressive DN, connected through five common genes, of which three act as transcription factors labelled in yellow nodes (E2F1, TP53 and STAT3). Furthermore, miR-99a-5p (upregulated in progressive DN) was connected to miR-184 through AKT1 and AGO2 genes. Enrichment of diseases (red nodes) was shown only in relation to miR-184. Nine diseases were associated with CKD (diabetic nephropathy, glomerulonephritis, diabetic retinopathy, renal fibrosis, wound healing, diabetes mellitus type 2, lupus nephritis, systemic lupus erythematosus, and Fabry disease). Most of remaining diseases were cancer-related diseases (104).
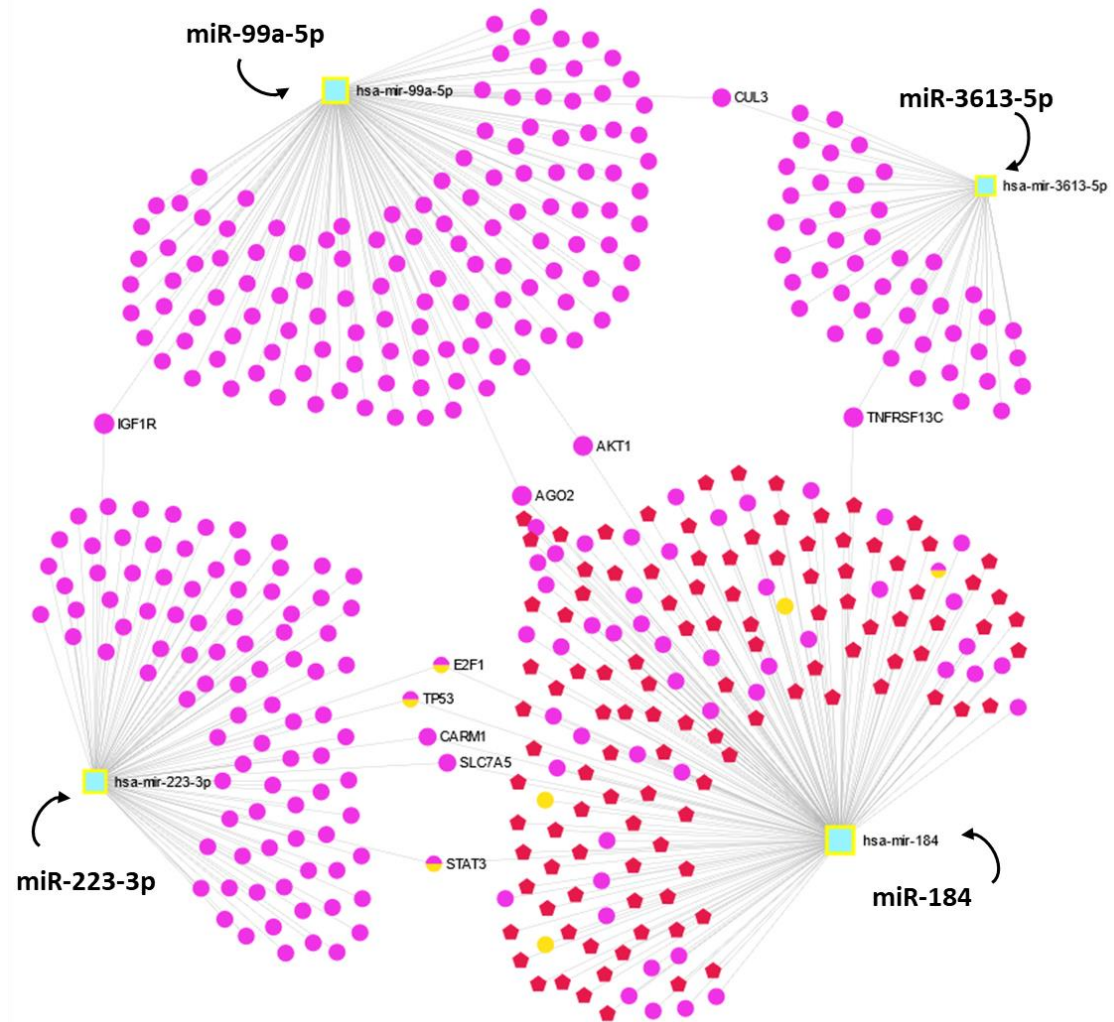
Figure 5.13: Enrichment network of the four miRNA uEVs candidate biomarkers of DN progression: miR-184 and miR-3613-5p detected by miRNA sequencing, and miR-99a-5p and miR-223-3p detected by NanoString. The miRNA network involves miRNAs (blue nodes), genes (purple nodes), transcription factors (yellow nodes) and diseases (red nodes). Network map and analysis was done by miRNet 2.0 online database.

As shown in Figure 5.13, miR-223-3p and miR-184 interact through five common genes: E2F transcription factor 1 (E2F1), tumour protein p53 (TP53), co-activator associated arginine methyltransferase 1 (CARM1), solute carrier family 7 member 5 (SLC7A5), and signal transducer and activator of transcription 3 (STAT3).

E2F1 is a cell cycle-related protein which was reported to be overexpressed in DKD inducing senescence of tubular epithelial cells, fibrosis and DNA damage under high glucose conditions (Liang et al., 2022). A connection between E2F1 and TP53 was reported in an interactive pathway involved in mediating apoptosis (Wu and Levine, 1994). By regulating the expression of various genes, TP53 plays a key role in processes such as apoptosis, DNA repair, cell cycle arrest, and cell metabolism, and was shown to be implicated in tubular cell necrosis and apoptosis following ischemic renal injury (Ying et al., 2014). TP53 is also linked to CARM1, where the collaborative actions of CARM1 along with the co-activators PRMT1 and p300 have been shown to regulate p53-dependent transcription (An et al., 2004). CARM1 plays a key role in mammalian autophagy through promoting histone methylation (Hu et al., 2020). In CKD its downregulation resulted in reduced skeletal muscle autophagy and oxidative stress (Hu et al., 2020), while its degradation through ubiquitination promoted podocyte apoptosis and loss in DN (Kim et al., 2014). STAT3 has been found dysregulated in multiple types of CKD (Pace et al., 2019). Interestingly, STAT3 activation can affect the progression from AKI to CKD by mediating apoptosis and fibrosis (Park et al., 2022). SLC7A5 is an amino acid transporter that has been implicated in mediating renal damage in SLE, with its expression being upregulated in circulating T and B lymphocytes (Tian et al., 2022).

Considering association of the genes common to miR-223-3p and miR-184 with cell cycle arrest and cell death, either through apoptosis or autophagy, it can be suggested that these genes and/or transcription factors together with miR-223-3p and miR-184 may constitute a novel mechanism related to cell aging and cell death in DN.

Furthermore, the connection of miR-99a-5p and miR-184 was made only through Akt serine/threonine kinase (AKT1) and Argonaute RISC catalytic component 2 genes (AGO2). It has been reported that AKT-mediated phosphorylation of AGO2 coordinates Ago2-mediated activities of endonucleolytic cleavage and translational repression of target mRNAs (Horman et al., 2013). AGO2 has function in RNA interference and gene silencing. It can be important in stabilizing urinary miRNAs by protecting them from RNase degradation and therefore increasing potential of miRNAs as biomarkers of CKD (Beltrami et al., 2015; Scullion et al., 2021). AKT1, also known as protein kinase B, is stimulated by cytokines or growth factors such as EGF, PDGF or TGFβ1 and once activated has wide roles associated with metabolism, proliferation, survival, angiogenesis etc (Lan and Du, 2015). In association to kidney disease, both pro-fibrotic (Lan and Du, 2015; Kim et al., 2023) and anti-fibrotic (Hanatani et al., 2014) activities of AKT1 have been reported. In conclusion, miR-99a-5p and miR-184 interaction may suggest that these two miRNAs are involved in a common signalling pathway being involved in modulating fibrosis and gene silencing-related functions.

Taken together, the networks involving miR-99a-5p and miR-184, as well as miR-223-2p and miR-184, may potentially be part of the functional pathways linked to kidney disease, as previously hypothesized.

5.4.3 Validation of uEVs miRNA candidate markers of DN progression

From the screening phase of uEVs miRNAs candidate markers of DN progression, four miRNAs were detected as significantly differentially changed in progressive compared to stable DN. Even if miRNA sequencing and NanoString are powerful methods which do not necessary require validation (Lopez et al., 1015; Veldman-Jones et al., 2015; Almenar-Pérez et al., 2020), Taqman Advanced RT-qPCR was employed to confirm the changes.

As shown in Figure 5.14, miR-99a-5p (A, D) and miR-223-3p (B, E) changes could be confirmed by Taqman Advanced RT-qPCR. Data are expressed as $2^{-(Ct)}$ to show the difference in expression of each miRNA from the raw Ct values, and as $2^{-(\Delta\Delta Ct)}$ to show expression relative to the reference miRNA (cel-miR-39-3p). An increasing miR-99a-5p (Figure 5.14A) and a decreasing miR-223-3p (Figure 5.14B) in progressive DN confirmed the miRNA digital profiling (NanoString) data. Furthermore, miR-3613-5p showed a trend of increase in progressive DN (Figure 5.14C, F), which is the same expression direction as found by miRNA sequencing. Ct values from miR-184 were very high, but also too variable among quadruplicate measurements in progressive DN suggesting too low expression and therefore data were not plotted for this miRNA.

Figure 5.14: Validation of candidate uEVs miRNA markers of DN progression by TaqMan Advanced RT-qPCR. Data represent a single experiment done in quadruplicates from stable DN (N=20) and progressive DN (N=20) pools. Equal RNA amount (9 ng) was used from each pool. Expression of each miRNA was analysed from raw Ct values (A-C) plotted as 2^-(Ct), and relative to the reference miRNA cel-miR-39-3p (D-F) plotted as 2^-(ΔΔCt). Graphs were created in GraphPad Prism v9. **$p < 0.01$, *$p < 0.05$

To ensure that spike-in miRNA (exogenous miRNAs) cel-miR-39-3p is a good reference for relative qPCR quantification, difference in its expression between stable and progressive DN groups was tested by two-tailed t-test. Table 5.18 shows no significant change between stable and progressive DN groups, which means that it is applicable as a reference miRNA in this RT-qPCR.

Table 5.18: Expression of spike-in miRNA cel-miR-39-3p, used as a reference miRNA, between uEVs from stable DN (n=20) and progressive DN (n=20) pools, in three independent experiments, by TaqMan Advanced RT-qPCR.

Spike-in miRNA (cel-miR-39-3p) *Reference gene*					
Sample	Ct value	Mean Ct	SD	2^-Ct	T test
Stable DN pool_1	23.168	24.211	0.77	1.1E-07	**0.823457**
Stable DN pool_2	24.188			5.2E-08	
Stable DN pool_3	24.966			3.1E-08	
Stable DN pool_4	24.524			4.1E-08	
Progressive DN pool_1	24.416	23.994	0.45	4.5E-08	
Progressive DN pool_2	24.301			4.8E-08	
Progressive DN pool_3	23.835			6.7E-08	
Progressive DN pool_4	23.425			8.9E-08	

To sum up, in this chapter, four miRNAs from uEVs were detected as candidate markers of DN progression: miR-184 and miR-3613-5p discovered by miRNA sequencing and miR-99a-5p and miR-223-3p discovered by NanoString digital profiling. Validation by TaqMan confirmed the same expression trends found by transcriptomics for miR-99a-5p, miR-223-3p and miR-3613-5p, while miR-184 expression was too low in progressive DN.

5.5 Discussion

This chapter aimed to discover a panel of miRNAs from uEVs that can be used as markers of DN progression. To purify RNAs from uEVs, the Norgen kit was chosen because it efficiently isolates exosomal RNAs, allows elution in just 10 µl with good recovery, making samples with limited RNA more concentrated. Besides, this kit does not involve phenol/chloroform compounds which are often used in nucleic acid extraction protocols but are known to be hazardous and to potentially affect sensitive downstream applications such as next-generation RNA sequencing (Arfin et al, 2019; Joshi and Adhikari, 2019).

The high-throughput discovery analyses done by miRNA sequencing and NanoString digital profiling identified four uEVs miRNAs dysregulated in progressive stage of DN compared to stable DN: miR-184 and miR-223-3p which were significantly downregulated, and miR-3613-5p and miR-99a-5p which were significantly upregulated in progressive DN (Figure 5.6 and Figure 5.12).

There are a number of miRNAs previously reported to play a role in CKD (Kato et al., 2009; Akkina and Becker; Sun and Lerman, 2019), among which three are the same reported as significant in this chapter. While miR-3613-5p has never been associated with CKD, miR-184 was reported to be dysregulated in DN (Zanchi et al., 2017) and IgAN (Wang et al., 2020), miR-99a-5p in DN (Uil et al., 2021) and ANCA-associated vasculitis (Frydlova et al., 2022), and miR-223-3p in SLE (Hiramatsu-Asano et al., 2021).

Among the miRNAs from uEVs reported as candidate biomarkers of CKD (Table 5.1-5.2), only miR-99a-5p was found significantly upregulated in ANCA-associated vasculitis (Frydlova et al., 2022), a systemic autoimmunity condition which can progress to CKD and ESKD in the absence of an immediate treatment (Moiseev et al., 2017).

However, even if the research on uEVs miRNA biomarkers of CKD has progressed considerably in the last decade, there is limited information on miRNA markers of DN progression. Dysregulation of miRNAs at different stages of CKD (Magayr et al., 2020), for example between mild and severe albuminuria have been reported in urine or uEVs (Barutta et al., 2013; Jia et al., 2016; Eissa et al., 2016). However, severe albuminuria despite being often correlated with progressive decline in eGFR (Nichols et al., 2020), has limitations when used alone as it does not always include longitudinal measurements of the patients to clearly show progression over the years. Coestimator of eGFR instead as done in this project can clearly indicate rapid decline in kidney function based on longitudinal follow-up (Levey et al., 2022; MacIsaac et al., 2014). Furthermore, stable albuminuria may be found in patients experiencing a decline in eGFR, while kidney function could be preserved in patients with elevated albuminuria, suggesting that combination of both eGFR decline and albuminuria measures is a stronger predictor of progression (Oshima et al., 2021; MacIsaac et al., 2014).

Results from this chapter have shown that miR-99a-5p, miR-223-3p, miR-184 and miR-3613-5p can significantly distinguish progressive from stable DN condition when analysed in uEVs patients stratified based on eGFR decline over time, with stable DN condition having slow eGFR decline or even showing improvements (small rises in eGFR),

and progressive condition having rapid and irreversible eGFR loss (Zhong et al., 2017). Even if these four miRNAs do not form cluster by miRNet analysis, an interaction was found between miR-184 and miR-99a-5p through two genes (AKT1 and AGO2) suggesting their shared roles in gene-silencing and fibrosis modulation (Figure 5.13). Another interaction was shown between miR-184 and miR-223-3p through five genes (E2F1, TP53, CARM1, SLC7A5, and STAT3) suggesting involvement in the pathways associated with cell aging and cell death (Figure 5.13). Despite not forming a common cluster and not being involved in the same signalling pathways, the four miRNAs could form a panel used to detect progressive DN, because a multi-marker miRNA panel has been shown to have greater accuracy in diagnosing CKD compared to a single miRNA biomarker (Garmaa et al., 2024).

Furthermore, a panel of four miRNAs in uEVs differentiating DN from diabetes was identified by miRNA sequencing (Table 5.10). All four miRNAs were significantly downregulated (or showed no expression) in DN compared to diabetes (miR-891a-5p, miR-432-5p, miR-890, miR-892a). Of them, miR-891a-5p and miR-432-5p have been reported to be involved in CKD (Dai et al., 2023; Mansouri et al., 2017). However, for this analysis, only two biological samples were available in the diabetic group, which makes these data less robust.

Few limitations of this chapter need to be addressed. Firstly, a small sample size was used in discovery phase done by miRNA sequencing (n=10), which, considering variability in biological samples might lead to less reproducible findings. miR-184 and miR-3613-5p did not emerge as significantly changed when analysed by NanoString profiling which

include larger number of clinical samples, however these were analysed in pool. Using pooled samples instead of individual ones in transcriptomic analysis can be another disadvantage, as potential outliers may go undetected, yet they can significantly impact the overall results. Moreover, unequal RNA amount from the four compared cohorts were used for digital transcriptomics due to limited RNA amounts in uEVs samples, however the same approach of equal volume loading (3 µl) instead of equal RNA amount from uEVs or biofluid sample type analysed by nCounter microRNA human panel was reported in Gheinani et al. (2018) and Hong et al. (2021).

The validation phase by RT-qPCR showed the expression trends of miR-99a-5p, miR-223-3p, and miR-3613-5p confirming the discovery findings by digital transcriptomics and miRNA sequencing, but it should be repeated on more biological replicas in order to confidently state that validation phase confirmed findings from the transcriptomics profiling, and to be able to apply statistical analysis.

In conclusion, in this chapter four miRNA from uEVs were suggested as markers of DN progression, and validation showed the same trends for the three miRNAs (miR-99a-5p, miR-223-3p and miR-3613-5p).

CHAPTER 6:

Do the uEVs miRNA DN markers control the

uEVs DN proteome?

6.1 Introduction

6.1.1 miRNA regulation of gene expression

As explained earlier in 5.1.1 (Chapter 5), miRNAs are well-known for their canonical mechanism of gene expression regulation, which takes place in the cytoplasm and involves the complementary pairing of the miRNA seed region with its target mRNA in the 3'UTR region (Bartel, 2004). However, recent studies have shown that miRNA regulation can extend beyond the canonical mechanism (Pu et al., 2019; Chipman and Pasquinelli, 2019).

In addition to 3'UTR region of mRNA targets, miRNAs have been discovered to suppress protein translation by binding to the coding regions of target mRNA, as well as 5'UTR. For example, miR-181a was shown to directly bind to the coding sequence of zinc finger genes, suppressing their expression (Huang et al., 2010), while miR-24 was found to inhibit c-Jun activation domain-binding protein-1 subunit CSN5 (Jab1/CSN5) expression by directly targeting both 3'UTR and 5'UTR sites (Wang et al., 2016). Interestingly, targeting 5'UTR region can lead to the activation of protein translation or stabilization of target mRNA showing that miRNAs can be implicated in both negative and positive regulation of gene expression (Ørom et al., 2008; Shimakami et al., 2012).

Moreover, numerous studies have shown that miRNAs not only function as regulators of gene expression in the cytoplasm (as part of the canonical mechanism), but also in the nucleus (Hwang et al., 2007; Huang and Li, 2012). Nuclear miRNAs have been found to

induce transcriptional gene silencing (Kim et al., 2008; Roberts, 2014; Miao et al., 2016) or activation (Place et al., 2008) by binding to gene promoter regions.

Furthermore, not only miRNAs can regulate gene expression by targeting a single region within mRNA, but miRNA regulation can be even enhanced through synergistic co-regulation of a target via multiple pathways (Pu et al., 2019). For example, it has been found that miRNAs can suppress gene expression by targeting its 3'UTR together with acting on transcriptional factors, such as miR-491-3p which downregulates its target ATP-dependent translocase ABCB1 (ABCB1) at the post-transcriptional level by directly binding to its 3' UTR, but also at the transcriptional level by binding to its transcription factor Sp3, thereby indirectly inhibiting ABCB1 expression (Zhao et al., 2017). A further example of miRNA co-regulation is via signalling cascades, such as miR-20 that inhibits cyclin-dependent kinase (CDK) inhibitor p21 directly through binding to its 3'UTR, and indirectly by blocking the TGF-β-induced transactivation of p21 promoter (Sokolova et al., 2018), or miR-338-5p which inhibits translation of ABCB1 via canonical mechanism and also through blocking EGFR/ERK1/2 signalling pathway which regulates ABCB1 expression (Zhao et al., 2018). Moreover, miR-215-5p has been shown to co-regulate its target Protocadherin-9 (PCDH9) by simultaneously binding to both its 3' UTR and promoter (Wang, C. et al., 2017).

6.1.2 MiRNA regulation in renal fibrosis and CKD

A growing number of studies have reported the roles of miRNAs in CKD, demonstrating either profibrotic or antifibrotic effects (Gluba-Sagr et al., 2023).

Profibrotic miR-214 and miR-21 were found to have a common target phosphatase and tensin homolog (PTEN). MiR-214-PTEN regulation resulted in delayed apoptosis and increased survival and invasion of monocytes contributing to the increased inflammation in kidney (Li, L. et al., 2011), while miR-21-mediated inhibition of PTEN promoted TGF-β1-induced EMT by modulating the expression of α-SMA and E-cadherin (Luo et al., 2019). Another direct target of miR-21 is peroxisome proliferator-activated receptor-α (Pparα), a transcription factor responsible for regulation of lipid metabolism that showed protective effects in renal fibrosis (Chau et al., 2012). Furthermore, other two pro-fibrotic miRNAs, miR-199a and miR-34a, both target Klotho, which is an endogenous inhibitor of renal fibrosis. MiR-199a-5p overexpression, induced by the high-glucose environment, caused suppression of Klotho which subsequently led to the activation of the toll-like receptor-4/nuclear factor κB p65/neutrophil gelatinase associated lipocalin (TLR4/NF-κB p65/NGAL) signalling pathway which then promoted development of kidney fibrosis and inflammation by increasing expression of fibrotic (fibronectin, connective tissue growth factor) and inflammation (monocyte chemoattractant protein 1, chemokine C-X-C motif ligand 5) factors (Wu et al., 2015).

On the other hand, overexpression of miR-34a was found to be stimulated by TGF-β, which then directly targets Klotho at 3'UTR and consequently promotes EMT (Liu et al.,

2019). In addition, miR-34a was found to increase profibrotic effects of TGF-β by directly targeting NAD-dependent protein deacetylase sirtuin-1 (SIRT1) (Xue et al., 2018). Next, miR-23a and miR-130-3p both target Ski-related novel protein N (SnoN), TGF-β1/Smad transcription co-repressor and a critical negative regulator of TGF-β1/Smad signalling pathway. Both miRNAs directly target 3'UTR of SnoN and suppress its expression (Xu et al., 2018), however, miR-130-3p can also suppress SnoN at transcriptional level (Ai et al., 2020). Furthermore, miR-192, miR-433 and miR-132 were all discovered as activators of TGF-β/Smad signalling, therefore contributing to progression of kidney fibrosis (Chung et al., 2010a; Li et al., 2013; Bijkerk et al., 2016). Pro-fibrotic miR-324-3p was found to target the 3'UTR of prolyl endopeptidase (Prep). Its downregulation contributed to fibrosis development by reducing the synthesis of the antifibrotic peptide N-acetyl-seryl-aspartyl-lysyl-proline (Ac-SDKP) and increasing collagen deposition (Macconi et al., 2012). Another miRNA, miR-299a-5p, was reported to be implicated in renal fibrosis development through targeting an antifibrotic protein follistatin (Mehta et al., 2021). Moreover, miR-671-5p has been shown to induce podocyte injury, proteinuria and renal fibrotic lesions by targeting Wilms tumour 1 (WT1) and mediating Wnt/β-Catenin pathway (Wang, C., et al., 2022). Other two miRNAs were found dysregulated in CKD and involved in CKD development: downregulated miR-3607-3p and upregulated miR-4709-3p, both of which participate in the reorganization of the actin cytoskeleton (Yu et al., 2019). MiR-3607-3p suppressed actin fibre assembly and cell motility by targeting integrin beta-8 (ITGB8), whereas miR-4709-3p enhanced these processes by targeting calmodulin 3 (CALM3).

One of the anti-fibrotic miRNAs is miR-29, which inhibits TGF-β/Smad3-mediated fibrosis. However, its expression is also downregulated by Smad3-induced TGF-β signalling, which binds to the miR-29 promoter (Qin et al., 2011). Next, both miR-26a and miR-30c have been shown to target CTGF, leading to reduced ECM production, diminished EMT, and lower activation of ERK1/2 and p38 MAPK (Zheng et al., 2016). Moreover, miR-30e was reported to ameliorate fibrosis by targeting mitochondrial uncoupling protein 2 (UCP2) (Jiang et al., 2013). Furthermore, members of the miR-200 family have been shown to protect TECs from EMT by inhibiting zinc finger E-box-binding homeobox (ZEB) 1 and ZEB2, which are transcriptional repressors of E-cadherin (Xiong et al., 2012; Tang et al., 2013). Another anti-fibrotic miRNA is miR-27b-3p which targets signal transducers and activators of transcription 1 (STAT1) thus decreasing EMT and apoptosis (Bai et al., 2021).

Knowing that impaired expression and regulation of miRNAs can be implicated in CKD, but with no findings observed regarding miRNA regulation mechanisms at the uEVs level that could contribute to DN and/or its progression, the aim of this chapter was to explore potential crosstalk/modulation between uEVs miRNAs and uEVs proteins, discovered as deregulated in DN and/or DN progression, in order to identify a potential novel pathway involved in DN development and/or progression.

6.2 Aims of the chapter

In previous chapters, miRNAs in uEVs (miR-99a-5p, miR-223-3p, miR-184 and miR-3613-5p) were identified as being significantly altered in progressive DN, along with a list of uEV proteins that are deregulated in both DN and DN progression.

The hypothesis was that the uEVs miRNA markers of progression (DN) regulate the expression of uEVs protein markers of DN, thereby playing a role in modulating the development or progression of DN.

To test this hypothesis, the following is planned:

1) To identify mRNA targets of the four miRNAs: miR-99a-5p, miR-223-3p, miR-184, and miR-3613-5p, which were detected as uEVs markers of DN progression.

2) To design and amplify primers for the 3'UTR sequence of the target gene(s) which was predicted to be target of analysed miRNAs.

3) To analyse uEVs miRNA-protein regulation.

6.3 Methods

6.3.1 miRNA target prediction

To predict miRNA targets for miR-99a-5p, miR-223-3p, miR-184, and miR-3613-5p, four target-prediction online tools were used: TargetScan, miRDB, miRWalk, and mirDIP which were selected based on their popularity (TargetScan, miRDB), inclusion of different gene regions that can be targeted by miRNAs (miRWalk) or incorporation of multiple single target-prediction databases resulting in stronger prediction scores (mirDIP). MiRWalk is an extended target prediction platform which uses random-forest-based approach software TarPmiR to search for target genes considering complete transcript sequences: 5'-UTR, coding sequence (CDS) and 3'-UTR. Moreover, it integrates results from other three databases: TargetScan, mirDB, and miRTarBase, which were selected based on their popularity and accuracy in predictions. It extracts information on mRNA sequences from NCBI database, and miRNA sequences from miRBase (Sticht et al., 2018). MirDIP database is a comprehensive and reliable tool that integrates 30 independent miRNA-target prediction resources (Tokar et al., 2018). Using the predictions from the individual sources, mirDIP provides a statistical information of integrative score for each miRNA-target match. The higher the score the stronger the target is. An integrative score from the mirDIP database gives more accurate predictions than any individual target prediction database, without accumulating prediction biases associated with specific biological processes or pathways (Tokar et al., 2018).

The lists of gene targets obtained from TargetScan, miRDB, miRWalk and mirDIP prediction tools for each analysed miRNA were compared to the list of proteins detected from uEVs as candidate markers of DN progression, using Venny 2.1 online tool.

6.3.2 Primer design for 3'UTR region of mRNA target

Primers were designed for the 3'UTR sequence of the MBNL1 gene which was predicted to be a target of miRNA-99a-5p and miR-223-3p. The purpose was to amplify the 3'UTR fragment for the downstream 3'UTR luciferase reporter assay. The NCBI (National Center for Biotechnology Information) website was used to find the full sequence of the MBNL1 gene from the Homo sapiens species (Accession: NM_021038) and focusing on the transcript variant 1. The full sequence in FASTA format was copied to the Word document. Next, the Ensembl website was used to detect and download only the 3'UTR part from the total transcript sequence (name of transcript: MBNL1-204), which was then highlighted within the total FASTA sequence in the word document from the previous step. TargetScanHuman 8.0 was used to check the length of the MBNL1 3'UTR sequence and to see where the binding sites of the targeting miRNAs (miR-99a-5p and miR-223-3p) are (Agarwal et al., 2015). Binding sites of both miRNAs were then highlighted within the 3'UTR sequence in the word document to be able to design primers which would include these binding regions.

Primer pairs were generated by using Primer3 v.0.4.0 where the product size of the 3'UTR sequence of MBNL1 gene was adjusted to 1000-3400 range in order to cover both miRNA binding sites within 3'UTR sequence. For that purpose, each pair of primers was checked

within the FASTA sequence to see where they are positioned. The reverse primers needed to be manually converted to complementary bases in order to be detectable within the FASTA sequence. Forward and reverse primers were then copy-pasted into the UCSC In-Silico PCR browser to assess if the length of the resulting sequence output matches with the length of the final product for the selected primer pair predicted by Primer3.

Since the downstream application of the designed primers was molecular cloning of the amplified 3'UTR fragment into a reporter plasmid (schematically shown in Figure 6.5A), primers needed to contain the sequences for the binding sites of the two restriction enzymes. To find suitable restriction enzymes, 3'UTR sequence from the beginning of the forward primer to the end of the reverse primer was pasted into NEBcutter v.3.0.17 tool. After submitting the sequence, the search was restricted to 0 cutters which are the restriction enzymes that do not cut the submitted 3'UTR sequence. From the obtained list of restriction enzymes, two were selected: *Not*I and *Xho*I that were compatible with the multiple cloning region of the reporter plasmid vector psiCHECK-2 (C8021, Promega) as shown in Figure 6.1.
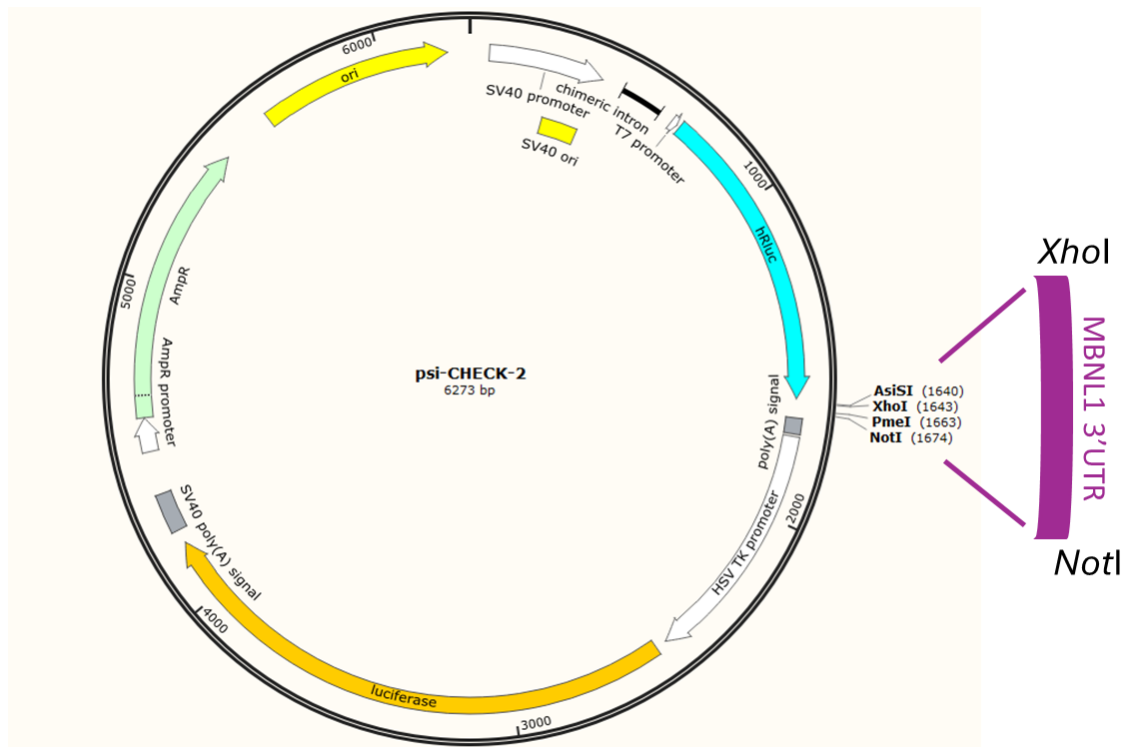
Figure 6.1: Plasmid map of the reporter psiCHECK-2 (Promega) with the marked location of the multiple cloning region downstream of the Renilla luciferase where the MBNL1 3'UTR insert can be cloned. Image was created and modified using SnapGene Viewer 5.2.2.

The binding site sequences for the selected restriction enzymes were manually added in front of both forward and reverse primers (in 5'→3' direction), *Not*I for the forward and *Xho*I for the reverse. In addition, two-three extra bases (dummy bases) were added in front of the restriction enzyme sequence (Table 6.1).

Designed primers were ordered from Sigma Aldrich, UK.

Table 6.1: Oligonucleotide primers for 3'-UTR sequence of MBNL1 with restriction enzymes *Not*I **(GCGGCCGC) and** *Xho*I **(CTCGAG) for molecular cloning**

Target name	Forward sequence (5'→3')	Reverse sequence (5'→3')	Product size (bp)
3'UTR MBNL1 (Acc: NM_021038)	ATAGCGGCCGCAGTTCCTCAGCCA CAAGA	CTCTCGAGAGATTTGGCCCCATG GAGTT	2618

6.3.3 Recombinant plasmid DNA sequencing

Recombinant plasmid DNA from two miniprep preparations, selected based on the highest DNA concentration were sequenced by PlasmidsNG (Birmingham, UK) to verify the recombinant sequence. DNA samples were diluted in nuclease-free water to a final concentration of 100 ng/µl. The sequence was obtained by the Oxford Nanopore R10.4 long-read sequencing (Sereika et al., 2022; Zhang, T. et al., 2023a), which is a direct sequencing based on nanopores. As described in Lin et al. (2021), the reaction is carried out in a flow cell which contains membrane with nanopores. On each side of the membrane is solution with applied cathode or anode. DNA molecules are placed in the side with a cathode and after applying electrophoretic force, DNA passes through the nanopores. Single nucleotides are captured and analysed on a computer-linked tools.

SnapGene Viewer 5.2.2 software was used to open and download the DNA sequence which was in fasta format. This was aligned to the original sequence of the 3'UTR MBNL1 insert using BLAST NCBI online tool to check for the potential mutations within 3'UTR insert.

6.3.4 3'UTR Luciferase reporter assay

To explore if miR-99a-5p and miR-223-3p bind to the 3'UTR region of MBNL1 and repress its translation, 3'UTR luciferase reporter assay was performed using the Dual-Glo luciferase assay system (E2920, Promega) according to the manual and as schematically illustrated in Figure 6.5B. The principle is based on the bioluminescent reactions involving two structurally distinct luciferase enzymes: Firefly (*Photinus pyralis*) and Renilla (*Renilla reniformis*, or sea pansy). Firefly luciferase uses the substrate beetle luciferin, along with oxygen, ATP, and Mg^{2+}, to produce light, along with the byproducts oxyluciferin, AMP, PPi, and CO_2. In contrast, Renilla luciferase does not require ATP. It catalyses a luminescent reaction using the substrate coelenterazine and oxygen to produce light, along with the byproducts coelenteramide and CO_2 (Sherf et al., 1996).

In brief, 75 µl of Luciferase assay reagent (which is the same volume as the cell media already present in the wells with adherent cells) was added directly to the 96-wells with tubular epithelial cells (HK-2 cell line) in DMEM/F12 media containing 10% FBS and 1% GlutaMAX and incubated for 15 minutes. This reagent lyses the cells and provides the substrate (beetle luciferin) for Firefly luciferase. The cell lysate was transferred into luminescent plate and Firefly luminescence was measured at 580 λ. Firefly luciferase measurement was followed by addition of 75 µl of Dual-Glo Stop & Glo reagent in the same wells of the luminescent plate. This reagent quenches the luminescence of Firefly and provides substrate (coelenterate-luciferin) for the Renilla luciferase. Renilla luminescence was read at 480 λ. Luminescence signals of both Firefly and Renilla

luciferases were measured by a ClarioStar plate reader (BMG LABTECH). Both luminescence data from miR-99a-5p and miR-223-3p were normalized to the miR-negative control (miR-NC) for both Firefly and Renilla signals, by dividing the relative light units (RLU) value of the analysed miRNA by the RLU of the miR-NC. Then mean values (from quadruplicate measurements) of Renilla and Firefly were used to calculate relative ratio of Renilla (experimental reporter) / Firefly (control reporter) for both miRNAs. Mean Renilla/Firefly ratios of the three independent experiments were plotted.

6.4 Results

6.4.1 Identification of gene targets of uEVs miRNA markers of DN progression

To find strong gene targets for the uEVs miRNAs of DN progression identified in this study, four target prediction databases were employed (TargetScan, miRDB, miRWalk and mirDIP), as described in Methods 6.3.1. As shown in Figure 6.2, gene targets of miR-99a-5p (A), miR-223-3p (B), miR-184 (C), and miR-3613-5p (D) extracted from each of the four databases were compared. Gene targets detected by all used databases (marked with red circle in the middle of Venn-diagrams in Figure 6.2), were 21 for miR-99a-5p, 75 for miR-223-3p, 9 for miR-184, and 8 for miR-3613-5p. These common gene targets by each of the four miRNAs were specified in Table 6.2, listed in alphabetical order.
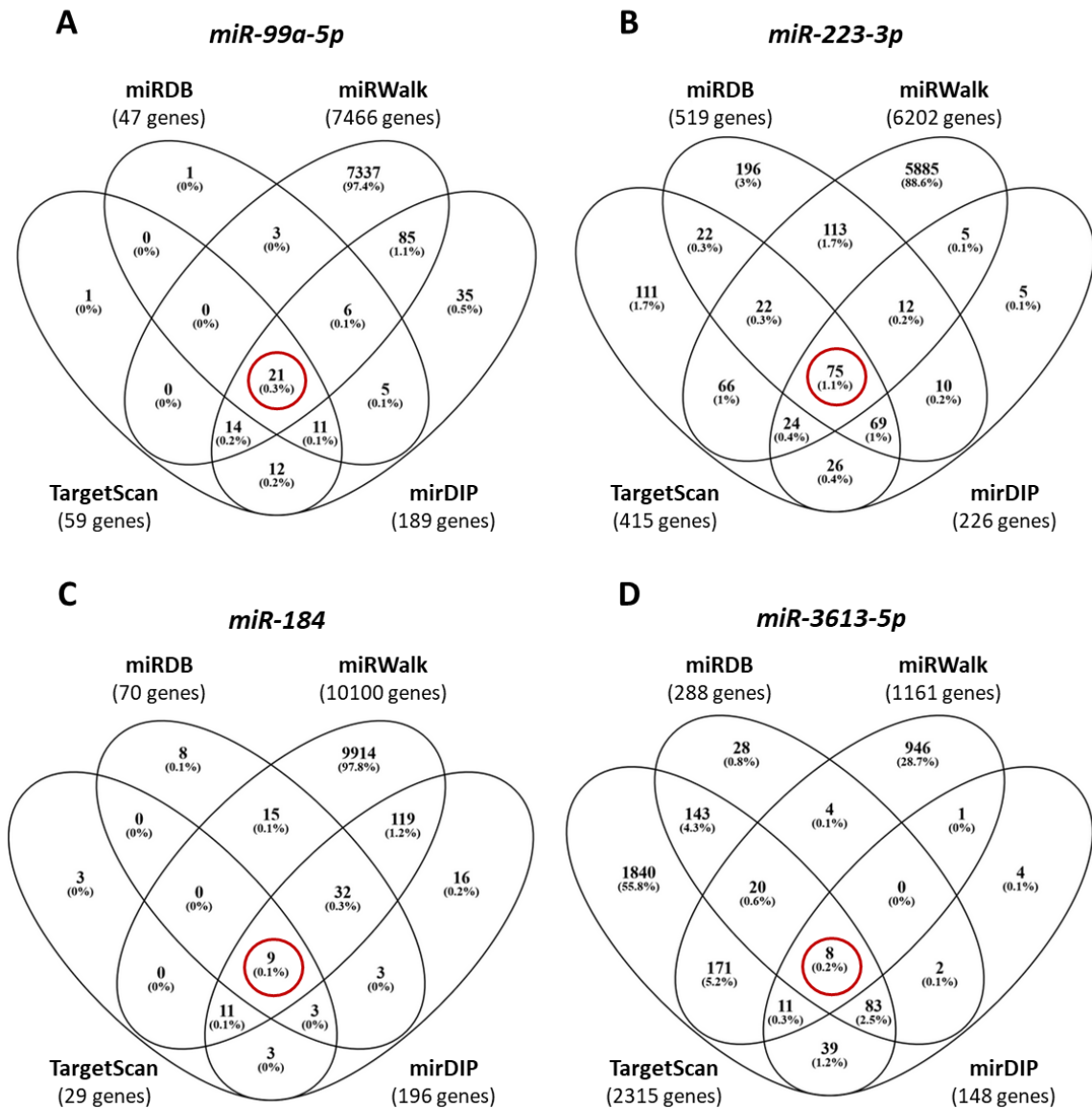
Figure 6.2: Gene target prediction of the uEVs miRNAs miR-99a-5p (A), miR-223-3p (B), miR-184 (C), and miR-3613-5p (D), detected as markers of DN progression, by four target-prediction databases: miRDB, TargetScan, miRWalk, and mirDIP. Common targets predicted by all used databases are marked with red circle. Venn diagrams were created in Venny 2.1.0

Table 6.2: Gene targets of miR-99a-5p (A), miR-223-3p (B), miR-184 (C) and miR-3613-5p (D) predicted by four target prediction databases: miRDB, TargetScan, miRWalk, and mirDIP

A	miR-99a-5p
Gene ID	**Gene name**
AGO2	Argonaute RISC Catalytic Component 2
BAZ2A	Bromodomain Adjacent To Zinc Finger Domain 2A
CDYL2	Chromodomain Y Like 2
EPDR1	Ependymin Related 1
FGFR3	Fibroblast Growth Factor Receptor 3
HES7	Hes Family BHLH Transcription Factor 7
HS3ST3B1	Heparan Sulfate-Glucosamine 3-Sulfotransferase 3B1
KBTBD8	Kelch Repeat And BTB Domain Containing 8
MBNL1	Muscleblind Like Splicing Regulator 1
MTMR3	Myotubularin Related Protein 3
MTOR	Mechanistic Target Of Rapamycin Kinase
NR6A1	Nuclear Receptor Subfamily 6 Group A Member 1
PPP3CA	Protein Phosphatase 3 Catalytic Subunit Alpha
RMND5A	Required For Meiotic Nuclear Division 5 Homolog A
SMARCA5	SWI/SNF Related, Matrix Associated, Actin Dependent Regulator Of Chromatin, Subfamily A, Member 5
ST6GALNAC4	ST6 N-Acetylgalactosaminide Alpha-2,6-Sialyltransferase 4
TRIB2	Tribbles Pseudokinase 2
TRIM71	Tripartite Motif Containing 71
TTC39A	Tetratricopeptide Repeat Domain 39A
ZNRF2	Zinc And Ring Finger 2
ZZEF1	Zinc Finger ZZ-Type And EF-Hand Domain Containing 1

B	miR-223-3p				
Gene ID #1	Gene name	Gene ID #2	Gene name	Gene ID #3	Gene name
ACSL3	Acyl-CoA Synthetase Long Chain Family Member 3	IL6ST	Interleukin 6 Cytokine Family Signal Transducer	RASA1	RAS P21 Protein Activator 1
ACVR2A	Activin A Receptor Type 2A	INPP4A	Inositol Polyphosphate-4-Phosphatase Type I A	RBPJ	Recombination Signal Binding Protein For Immunoglobulin Kappa J Region
ARID1A	AT-Rich Interaction Domain 1A	KPNA3	Karyopherin Subunit Alpha 3	RERG	RAS Like Estrogen Regulated Growth Inhibitor
ATP10D	ATPase Phospholipid Transporting 10D (Putative)	LMO2	LIM Domain Only	RPS6KB1	Ribosomal Protein S6 Kinase B1
ATP2B1	ATPase Plasma Membrane Ca2+ Transporting 1	MBNL1	Muscleblind Like Splicing Regulator 1	RSBN1L	Round Spermatid Basic Protein 1 Like
ATP7A	ATPase Copper Transporting Alpha	MID1IP1	MID1 Interacting Protein 1	SCAF8	SR-Related CTD Associated Factor 8
BRPF3	Bromodomain And PHD Finger Containing 3	MMP16	Matrix Metallopeptidase 16	SCN2A	Sodium Voltage-Gated Channel Alpha Subunit 2
CALML4	Calmodulin Like 4	MTSS1	MTSS I-BAR Domain Containing 1	SCN3A	Sodium Voltage-Gated Channel Alpha Subunit 3
CBLB	Cbl Proto-Oncogene B	MYH10	Myosin Heavy Chain 10	SDC2	Syndecan 2
CBX5	Chromobox 5	NAA50	N-Alpha-Acetyltransferase 50, NatE Catalytic Subunit	SIAH1	Siah E3 Ubiquitin Protein Ligase 1
CEP41	Centrosomal Protein 41	NFIA	Nuclear Factor I A	SLC37A3	Solute Carrier Family 37 Member 3
CLSTN1	Calsyntenin 1	NFIB	Nuclear Factor I B	SLC4A4	Solute Carrier Family 4 Member 4
CNOT2	CCR4-NOT Transcription Complex Subunit 2	NLRP3	NLR Family Pyrin Domain Containing 3	SLC8A1	Solute Carrier Family 8 Member A1
COPS2	COP9 Signalosome Subunit 2	NUP210	Nucleoporin 210	SMARCD1	SWI/SNF Related, Matrix Associated, Actin Dependent Regulator Of Chromatin, Subfamily D, Member 1
DENND5B	DENN Domain Containing 5B	NXF1	Nuclear RNA Export Factor 1	SORBS1	Sorbin And SH3 Domain Containing 1
FAT1	FAT Atypical Cadherin 1	OTUD4	OTU Deubiquitinase 4	SPTLC2	Serine Palmitoyltransferase Long Chain Base Subunit 2
FBXO8	F-Box Protein 8	PDE4D	Phosphodiesterase 4D	STIM1	Stromal Interaction Molecule 1
FBXW7	F-Box And WD Repeat Domain Containing 7	PDS5B	PDS5 Cohesin Associated Factor B	STK39	Serine/Threonine Kinase 39
FGFR2	Fibroblast Growth Factor Receptor 2	PHF20L1	PHD Finger Protein 20 Like 1	SYNCRIP	Synaptotagmin Binding Cytoplasmic RNA Interacting Protein
FOXO1	Forkhead Box O1	POU2F1	POU Class 2 Homeobox 1	TBC1D17	TBC1 Domain Family Member 17
FZD4	Frizzled Class Receptor 4	PRDM1	PR/SET Domain 1	TGFBR3	Transforming Growth Factor Beta Receptor 3
GALNT18	Polypeptide N-Acetylgalactosaminyltransferase 18	PTBP2	Polypyrimidine Tract Binding Protein 2	TSHZ3	Teashirt Zinc Finger Homeobox 3
GPM6B	Glycoprotein M6B	PURA	Purine Rich Element Binding Protein A	ULK2	Unc-51 Like Autophagy Activating Kinase 2
GTPBP8	GTP Binding Protein 8	RAB10	RAB10, Member RAS Oncogene Family	WASL	WASP Like Actin Nucleation Promoting Factor
HLF	HLF Transcription Factor, PAR BZIP Family Member	RAP2A	RAP2A, Member Of RAS Oncogene Family	WBP1L	WW Domain Binding Protein 1 Like

349

C	miR-184
Gene ID	**Gene name**
AGO2	Argonaute RISC Catalytic Component 2
CRISPLD2	Cysteine Rich Secretory Protein LCCL Domain Containing 2
CRTC1	CREB Regulated Transcription Coactivator 1
EPB41L5	Erythrocyte Membrane Protein Band 4.1 Like 5
FBXO28	F-Box Protein 28
NUS1	NUS1 Dehydrodolichyl Diphosphate Synthase Subunit
SF1	Splicing Factor 1
ZNF740	Zinc Finger Protein 740
ZNF865	Zinc Finger Protein 865

D	miR-3613-5p
Gene ID	**Gene name**
CLOCK	Clock Circadian Regulator
DLG5	Discs Large MAGUK Scaffold Protein 5
MEF2C	Myocyte Enhancer Factor 2C
MYB	MYB Proto-Oncogene, Transcription Factor
PLA2G12A	Phospholipase A2 Group XIIA
PPFIA2	PTPRF Interacting Protein Alpha 2
RGPD5	RANBP2 Like And GRIP Domain Containing 5
ZFAND5	Zinc Finger AN1-Type Containing 5

To explore if the four miRNAs' predicted gene targets are enriched in pathways related with kidney disease, pathways enrichment analysis was carried out using the Database for Annotation Visualization and Integrated Discovery (DAVID) with focus on KEGG and Reactome Pathway databases (Figure 6.3). From the 21 predicted gene targets of miR-99a-5p (Table 6.2A), ten significantly enriched pathways emerged (Figure 6.3A). Further, 23 significantly enriched pathways were detected from the 75 gene targets of miR-223-3p (Table 6.2B), with the bubble size representing the range of 3-14 genes involved in the pathways (Figure 6.3B). Two pathways were significantly enriched from targets of miR-3613-5p (Figure 6.3C) while no enrichment pathways were discovered from the miR-184 predicted gene targets.

Enriched pathways for both miR-99a-5p and miR-223-3p predicted targets included: PI3K/Akt/mTOR signalling (Margaria et al., 2020), calcium signalling (Lajdova et al., 2009), insulin signalling (Thomas et al., 2015) EPH-Ephrin signalling (Huang et al., 2021), C-type lectin receptor signalling (Lech et al., 2012), activin signalling (Williams et al., 2018; Cianciolo et al., 2021), ion transport and homeostasis (Wesson et al., 2020), mineral absorption (Floege and Drüeke, 2020), platelet homeostasis (Lutz et al., 2014), which are reported to be involved in CKD pathogenesis. This suggests that miR-99a-5p and miR-223-3p play a role in the pathogenesis of CKD by regulating the expression of their target genes.

A miR-99a-5p

- Adaptive Immune Systrem
- MicroRNAs in cancer
- PIP3 activates AKT signaling
- Antigen processing: ubiquitination & proteasome degradation
- Intracellular signaling by second messengers
- Central carbon metabolism in cancer
- Ca2+ pathway
- EGFR tyrosine kinase inhibitor resistance
- Class I MHC ,mediated antigen processing & presentation
- PD-L1 expression and PD-1 checkpoint pathway in cancer

-log10 (p-value)

B miR-223-3p

- Muscle contraction
- Cardiac conduction
- Insulin signaling pathway
- Platelet calcium homeostasis
- EPH-Ephrin signaling
- RNA Polymerase III Transcription
- RNA Polymerase III Abortive and Retractive Initiation
- EPHB-mediated forward signaling
- Gene expression (Transcription)
- Developmental Biology
- Ion homeostasis
- Ion transport by P-type ATPases
- Signaling pathways regulating pluripotency of stem cells
- Calcium signaling pathway
- Mineral absorption
- Axon guidelines
- Hepatocellular carcinoma
- Nervous system development
- Platelet homeostasis
- Reduction of cytosolic Ca++ levels
- Signaling by Activin
- C-type lectin receptor signaling pathway
- Nucleocytoplasmic transport

-log10 (p-value)

C miR-3613-5p

- Heme signaling
- Circadian Clock

-log10 (p-value)

Figure 6.3: Pathway enrichment analysis from the shortlisted predicted gene targets of miR-99a-5p (A), miR-223-3p (B), and miR-3613-5p (C). Pathways are listed from the most significantly enriched on top to the least significant at the bottom. Dimension of the bubble represents the number of genes included in the pathway (range 2-14). Analysis was performed using DAVID (https://davidbioinformatics.nih.gov/). Graphs were created in Excel.

Next, the list of predicted gene targets of each of the four analysed miRNAs were compared to both the uEVs proteins identified as markers of DN progression and markers of DN compared to diabetes with no kidney disease (Chapter 4) to investigate whether uEVs markers of DN are regulated by any of the uEVs miRNAs discovered as markers of DN progression (Figure 6.4). It was hypothesized that such regulation/connection play a role in the modulation of DN and or DN progression. One of the predicted targets for miR-99a-5p was also an identified marker of DN (Figure 6.4A). This gene was Muscleblind Like Splicing Regulator 1 (MBNL1), the expression of which was significantly decreased in progressive DN compared to diabetes with no CKD component, when analysed by quantitative proteomics. Two of the predicted targets for miR-223-3p were DN markers identified in this study (Figure 6.4B): one was MBNL1 and the other Ras-related protein Rab-10 (RAB10), the expression of which was significantly downregulated in progressive DN vs healthy subjects. Unlike for miR-99a-5p and miR-223-3p, there were no predicted gene targets for miR-184 (Figure 6.4C) and miR-3613-5p (Figure 6.4D) overlapped with the DN markers identified in this study.

In summary, by comparing predicted target genes for each of the four discovered uEVs miRNA markers of DN progression, with four prediction databases in order to obtain the strongest findings, one gene discovered as uEVs marker of DN – MBNL1 (Chapter 4,

Results 4.4.4) emerged as a common predicted target of the miR-99a-5p and miR-223-3p, therefore it was selected to explore if any of the two miRNAs could regulate the expression of MBNL1 by directly targeting its 3'UTR region.
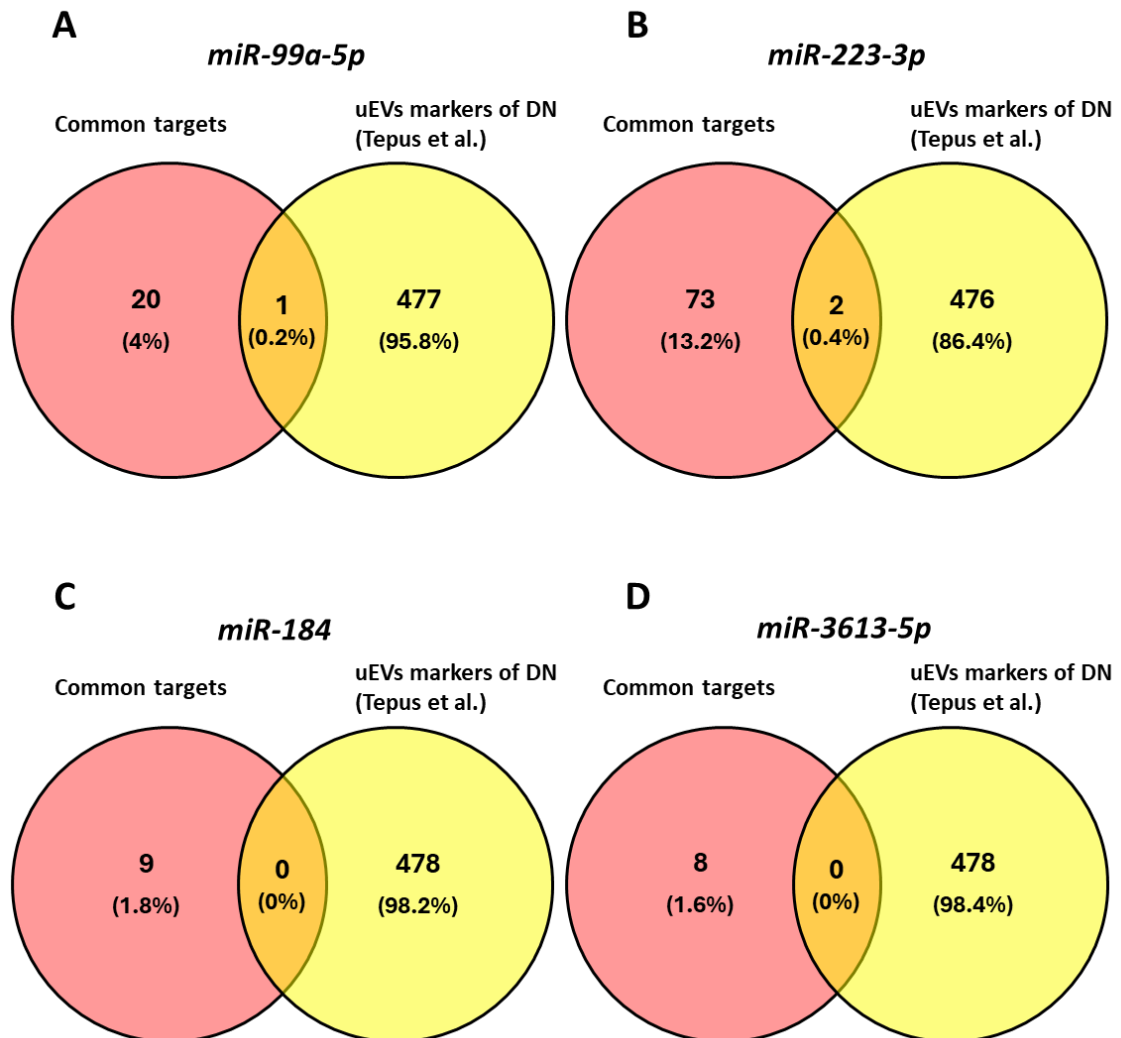
Figure 6.4: Comparison of the common predicted gene targets of the uEVs miRNAs miR-99a-5p (A), miR-223-3p (B), miR-184 (C), and miR-3613-5p based on the four target-prediction databases (miRDB, TargetScan, miRWalk, mirDIP) with discovered uEVs protein markers of DN (called Tepus et al.). All significantly changed proteins (up- and down-regulated) in DN vs healthy or diabetic groups were transferred into gene names. Venn diagrams were created in Venny 2.1.0

6.4.2 Molecular cloning of the MBNL1 3'UTR construct into reporter plasmid

In order to investigate whether uEVs miRNAs miR-99a-5p and miR-223-3p, suggested as markers of DN progression, interact with MBNL1 by directly targeting its 3'UTR region, primers were designed for the 3'UTR region of MBNL1 containing seeding sites of both miRNAs, to amplify it by end-point PCR and subclone it into a luciferase-gene expression reporter plasmid, as demonstrated in Figure 6.5A. The schematic of the MBNL1 mRNA transcript consisting of 5'UTR region, ten exons and 3'UTR region is shown in Figure 6.6.
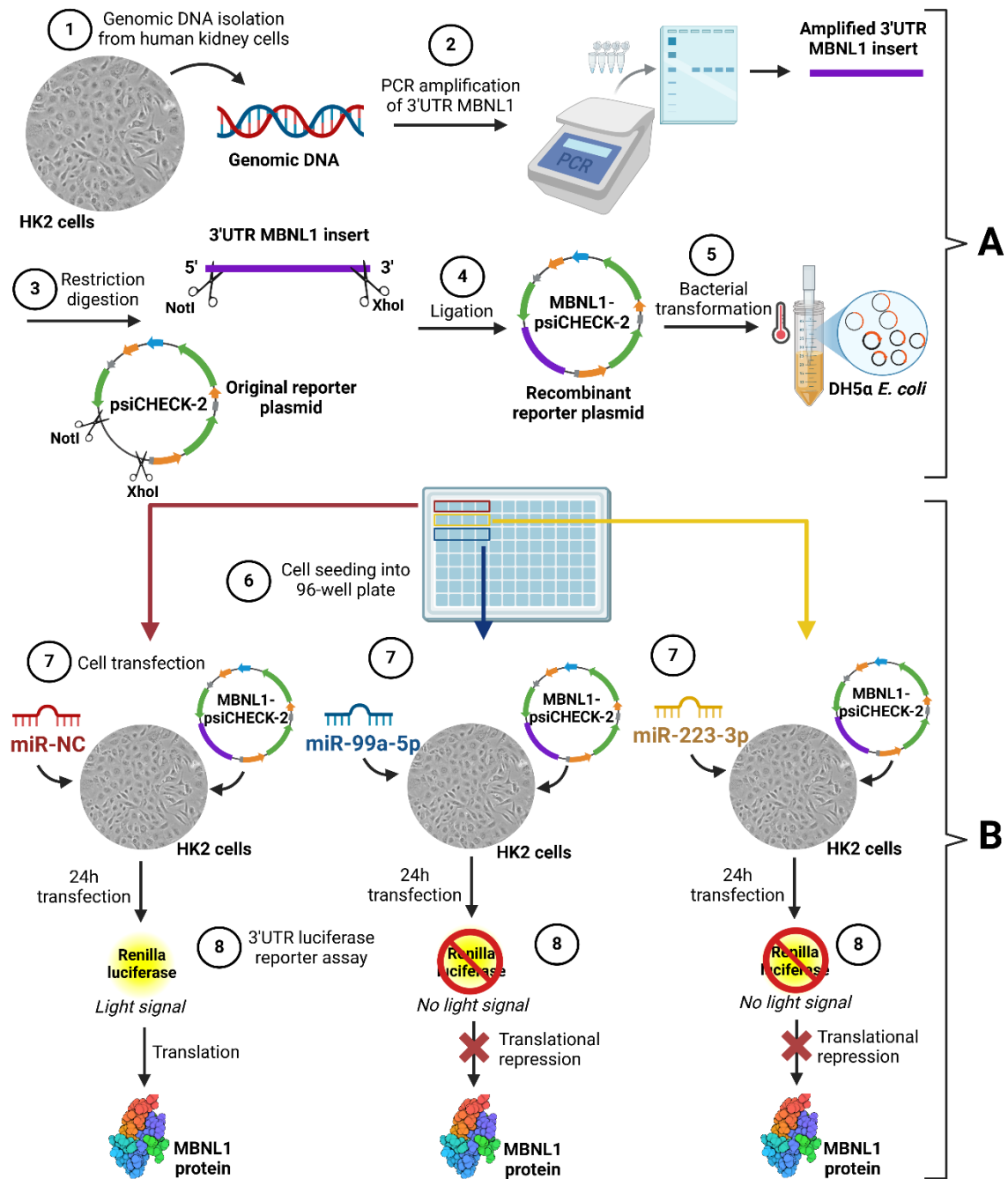
Figure 6.5: Workflow of the construction of the recombinant reporter plasmid containing the 3'UTR MBNL1 sequence (A) and of 3'UTR luciferase reporter assay (B) to study the hypothesis that miR-99a-5p and miR-223-3p interact with MBNL1 3'UTR and repress its translation into protein.

MBNL1 mRNA
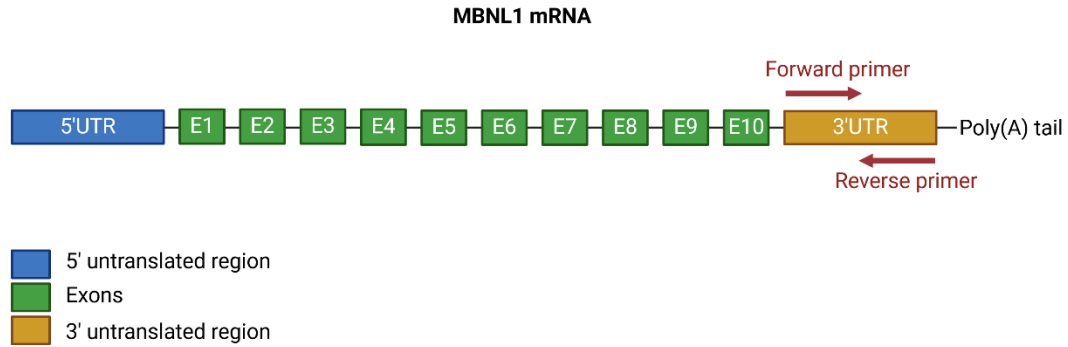
Figure 6.6: Schematic of MBNL1 transcript

The size of the designed 3'UTR MBNL1 insert was 2,618 bp and was amplified by end-point PCR as shown in Figure 6.7.
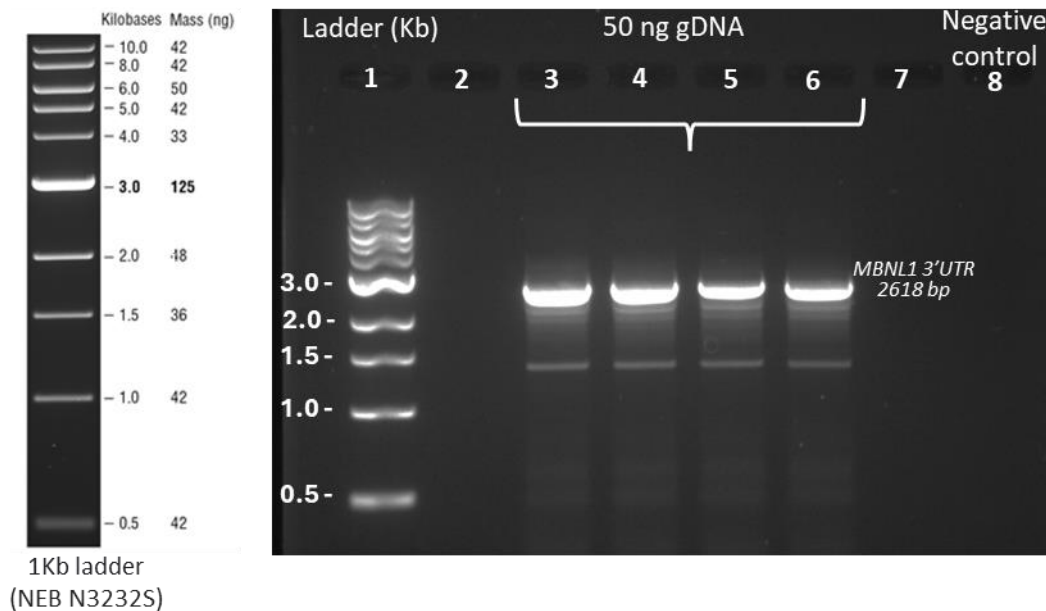
Figure 6.7: **PCR amplification of 3'UTR fragment of MBNL1.** The figure shows DNA ladder in lane 1 of the gel, PCR product of 3'UTR MBNL1 from 50 ng genomic DNA (from HK2 cells) in quadruplicates (lanes 3-6) and negative control where water was used instead of DNA in lane 8. Electrophoresis run on 1% agarose gel. The annealing temperature was set at 64°C. Four bends represent quadruplicates.

Both original reporter plasmid psiCHECK-2 (Promega) (1 μg) and amplified DNA fragments of 3'UTR MBNL1 (611 ng) were digested by restriction enzymes *Not*I and *Xho*I, (Figure 6.5A), in order to ligate the 3'UTR MBNL1 insert into the multiple cloning region of the psiCHECK-2 reporter plasmid as schematically shown in Figure 6.1. Concentration and quality of the DNA fragments were assessed by NanoDrop at each step showing consistently good quality of DNA (Table 6.3-6.5).

Following digestion, ligation and bacterial transformation reactions were performed as explained in Chapter 2 Methods 2.2.6.5-2.2.6.7, and eight colonies of transformed bacteria resistant to ampicillin were amplified and used for the downstream miniprep DNA extraction processing (according to Methods 2.2.6.8). Next, diagnostic digestion was carried out via agarose gel electrophoresis to confirm presence of the DNA fragment of empty reporter plasmid with expected size of 6,273 bp and DNA fragment of the insert with expected size of 2,618 bp (Figure 6.8) for all eight preparations of MBNL1-psiCHECK2. In addition, digested MBNL1-psiCHECK-2 of the two preparations used as example were analysed by agarose gel electrophoresis along with the uncut recombinant MBNL1-psiCHECK-2 plasmid showing expected size of 8,891 bp (Figure 6.9).

Table 6.3: Quality control and concentration measurement of gel-purified <u>PCR products </u>of MBNL1 3'UTR, by NanoDrop. The first elution was 20 µl (Elution 1), and second was 15 µl (Elution 2). NanoDrop assessment was done in triplicates (Elution1 1-3, Elution2 1-3).

MBNL1	Concentration (ng/µl)	Mean concentration	260/280	Mean 260/280	260/230	Mean 260/230	Yield (µg)	Mean yield (µg)
Elution1_1	36.5		1.75		0.76		0.621	
Elution1_2	20.52	25.30	1.82	1.82	1.13	1.03	0.349	0.430
Elution1_3	18.88		1.89		1.21		0.321	
Elution2_1	24.08		1.58		0.67		0.289	
Elution2_2	10.52	15.12	1.82	1.70	0.89	0.87	0.126	0.181
Elution2_3	10.76		1.71		1.04		0.129	

Table 6.4: NanoDrop measurements of gel-purified <u>digested</u> products of MBNL1 3'UTR insert and psiCHECK-2 reporter plasmid. Elution was in 20 µl. NanoDrop assessment was done in triplicates (Insert 1-3, Plasmid 1-3).

MBNL1	Concentration (ng/µl)	Mean concentration	260/280	Mean 260/280	260/230	Mean 260/230	Yield (µg)	Mean yield (µg)
Insert 1	14.81		1.7		0.4		0.252	
Insert 2	14.77	14.28	1.61	1.74	0.37	0.38	0.251	0.243
Insert 3	13.25		1.9		0.36		0.225	
Plasmid 1	38.19		1.77		0.93		0.649	
Plasmid 2	32.76	35.96	1.86	1.80	1.01	0.95	0.557	0.611
Plasmid 3	36.94		1.76		0.92		0.628	

Table 6.5: NanoDrop measurements of the MBNL1-psiCHECK-2 recombinant plasmid DNA after miniprep preparations from 8 colonies (MINI 1-8). Elution was in 50 µl.

	Concentration (ng/µl)	Mean concentration	260/280	Mean 260/280	260/230	Mean 260/230	Yield (µg)	Mean yield (µg)
MINI 1	575.4		1.87		2.16		27.04	
MINI 1	599.2	604.47	1.95	1.91	2.27	2.26	28.16	28.41
MINI 1	638.8		1.91		2.34		30.02	
MINI 2	521.5		1.83		2.21		24.51	
MINI 2	533.2	526.77	1.83	1.83	2.2	2.20	25.06	24.76
MINI 2	525.6		1.84		2.2		24.70	
MINI 3	577		1.9		2.29		27.12	
MINI 3	573.3	588.53	1.91	1.90	2.18	2.23	26.95	27.66
MINI 3	615.3		1.88		2.21		28.92	
MINI 4	479.8		1.84		2.2		22.55	
MINI 4	490	485.33	1.83	1.84	2.2	2.20	23.03	22.81
MINI 4	486.2		1.84		2.19		22.85	
MINI 5	504.9		1.85		2.21		23.73	
MINI 5	503.1	500.87	1.85	1.85	2.23	2.22	23.65	23.54
MINI 5	494.6		1.85		2.22		23.25	
MINI 6	547.4		1.83		2.21		25.73	
MINI 6	542.1	539.57	1.83	1.83	2.21	2.21	25.48	25.36
MINI 6	529.2		1.84		2.21		24.87	
MINI 7	508		1.95		2.45		23.88	
MINI 7	516.2	568.00	1.91	1.84	2.29	2.24	24.26	26.70
MINI 7	679.8		1.67		1.97		31.95	
MINI 8	481.7		1.84		2.23		22.64	
MINI 8	462.8	465.37	1.84	1.84	2.23	2.23	21.75	21.87
MINI 8	451.6		1.85		2.24		21.23	
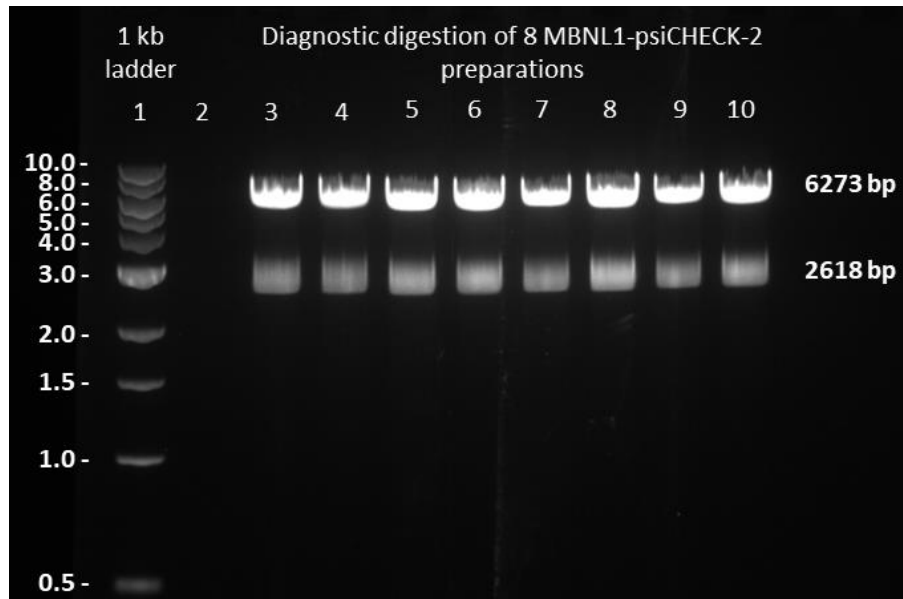
Figure 6.8: Diagnostic restriction digestion of 1 μg of recombinant MBNL1-psiCHECK-2 plasmid DNA containing 3'UTR insert of MBNL1 gene (2618 bp) and psiCHECK-2 plasmid vector (6273 bp). The electrophoresis was run on 1% agarose gel for ~2 h at 80-90 V.
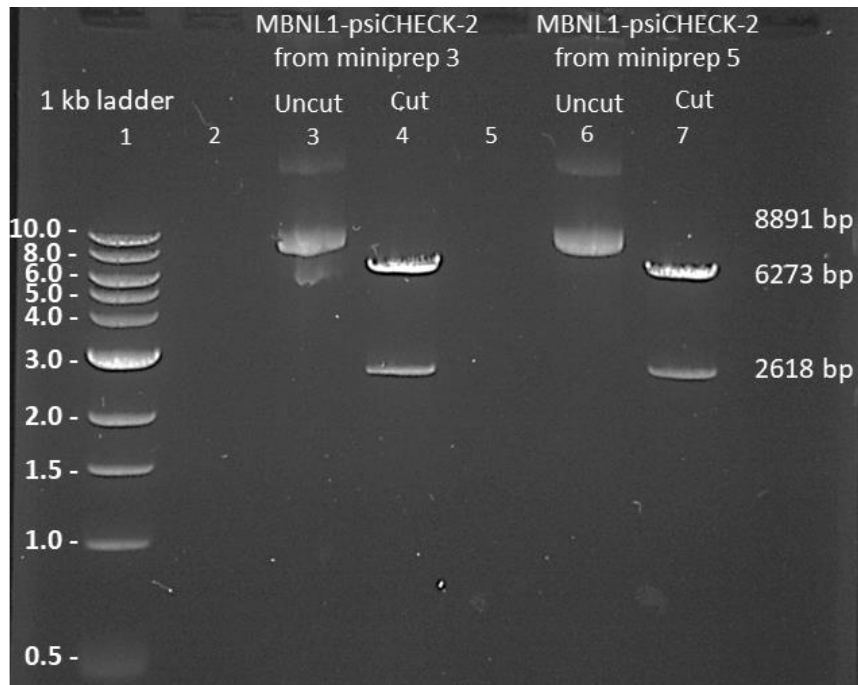
Figure 6.9: Electrophoresis of undigested (8891 bp) and digested recombinant MBNL1-psiCHECK-2 plasmid DNA (2618 bp of 3'UTR MBNL1 insert and 6273 bp of empty psiCHECK-2 plasmid) from two minipreps used as example. From each sample 200 ng of DNA was loaded on the 1% agarose gel and reaction run for ~2 h at 80-90 V.

Plasmid DNA sequencing confirmed the sequence of the recombinant MBNL1-psiCHECK-2 plasmid. As shown in Figure 6.10, recombinant MBNL1-psiCHECK-2 reporter plasmid contained both luciferase genes: Firefly used as a positive control and Renilla used as a reporter (green parts in the plasmid map), as well as the 3'UTR MBNL1 insert (purple part in plasmid) located downstream Renilla. The size of the sequenced MBNL1-psiCHECK-2 reporter plasmid was 8,868 bp which is close to the expected size of 8,891 bp.

To explore if the 3'UTR MBNL1 sequence within the recombinant MBNL1-psiCHECK-2 contained any mutations, especially within the seeding regions of the targeting miRNAs, the piece of the 3'UTR MBNL1 sequence (2618 bp) used as an insert was aligned to the sequence of the full MBNL1-psiCHECK-2 recombinant plasmid (8868 bp) using BLAST NCBI (https://blast.ncbi.nlm.nih.gov/Blast.cgi). As shown in Figure 6.11, no mutations occurred in the seeding regions within 3'UTR sequence of both miR-99a-5p (A) highlighted in green and miR-223-3p (B) highlighted in yellow. Regarding the remaining 3'UTR MBNL1 part of the MBNL1-psiCHECK-2 recombinant reporter plasmid, in both sequenced DNA preparations, two point mutations appeared: one mismatch type and one deletion type (Supplementary figure 3). Alignment of recombinant MBNL1-psiCHECK-2 plasmid with original psiCHECK-2 plasmid showed no mutations (Supplementary figure 4).
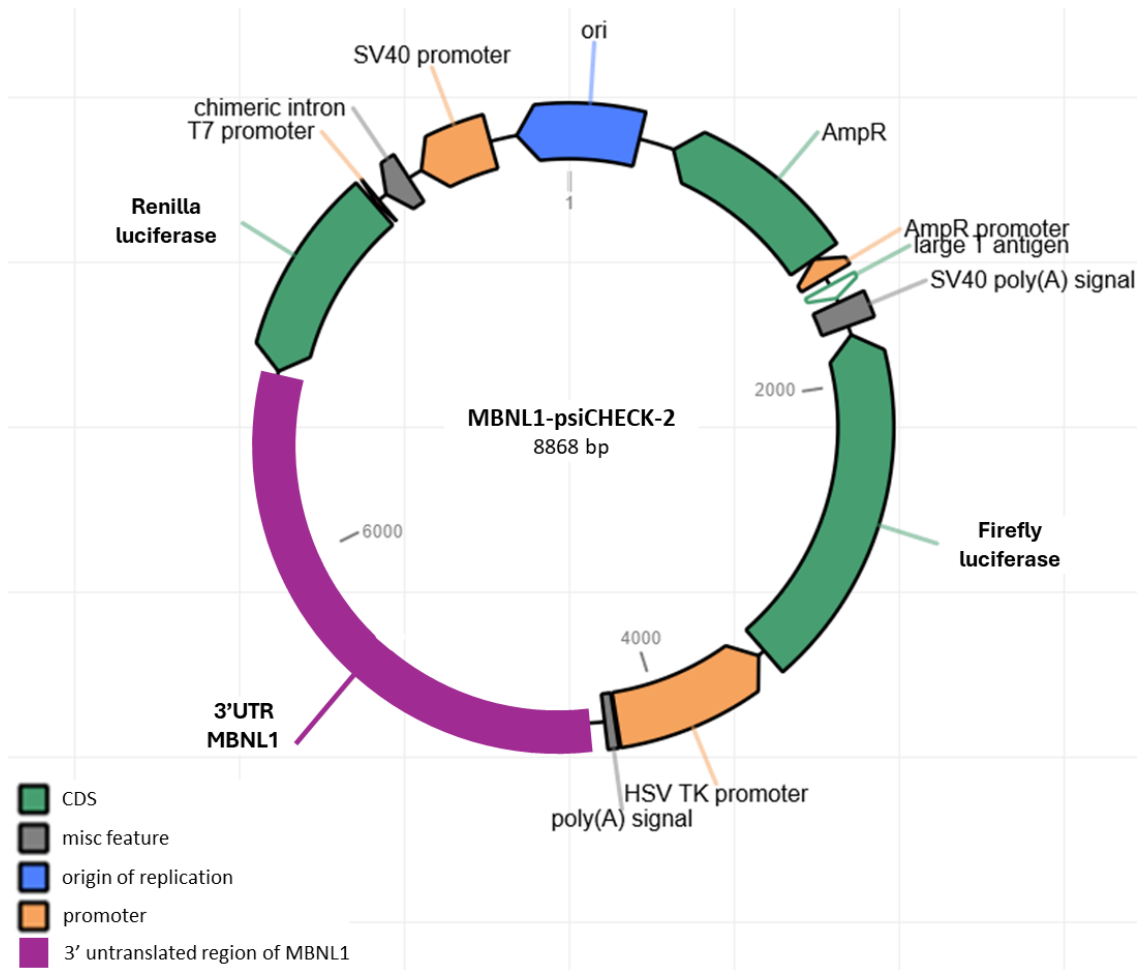
Figure 6.10: Recombinant MBNL1-psiCHECK-2 plasmid map. The plasmid consists of all the segments from the original reporter plasmid psiCHECK-2 (6273 bp) and the insert of 3'UTR MBNL1 (2618) labelled in purple. The figure was generated by modifying a PlasmidsNG map and is a representative recombinant plasmid map from one preparation out of two which were sequenced.

A

<div align="center">

miR-99a-5p

</div>

3'UTR MBNL1
1500-1559   GTACATCTATTAAAGCCTT`AGAT`TATTACAT`TACGGGT`TGGAACCCATACCAATGTAATT

||||||||||||||||||||||||||||||||||||||||||||||||||||||||||||

MBNL1-psiCHECK-2
5782-5841   GTACATCTATTAAAGCCTT`AGAT`TATTACAT`TACGGGT`TGGAACCCATACCAATGTAATT

<div align="center">

miR-99a-5p

</div>

B

<div align="center">

miR-223-3p

</div>

3'UTR MBNL1
2580-2618   AACCCTCATG`ACTGACA`AAAACTCCATGGGGCCAAATCT

|||||||||||||||||||||||||||||||||||||||

MBNL1-psiCHECK-2
6862-6900   AACCCTCATG`ACTGACA`AAAACTCCATGGGGCCAAATCT

<div align="center">

miR-223-3p

</div>

Figure 6.11: Sequence analysis of recombinant reporter plasmid (MBNL1-psiCHECK-2) against the 3'UTR MBNL1 sequence used as an insert showing intact seeding regions within 3'UTR sequence for both miR-99a-5p (green) (A) and miR-223-3p (yellow) (B). Sequences of the recombinant reporter plasmid (MBNL1-psiCHECK-2) (8868 bp) and the 3'UTR insert (2618) were aligned in BLASTN NCBI in order to check the match in the sequences. The figure is a representative alignment from one miniprep preparation out of two, however result was the same in both preparations.

6.4.3 Exploring miRNA regulation of MBNL1 expression via 3'UTR luciferase reporter assay

To study miRNA regulation of MBNL1 translation, the miRNA mimics (miR-99a-5p, miR-223-3p and miR-negative control (miR-NC)) together with recombinant reporter plasmid (MBNL1-psiCHECK-2) were transfected into human kidney epithelial cells HK2 using Lipofectamine 3000 (Figure 6.5B). Post 24h, no morphological changes were observed between cells transfected with MBNL1-psiCHECK-2 plasmid and miR-99a-5p (Figure 6.12A), miR-223-3p (B), miR-NC (C) or non-transfected wild-type cells (D).
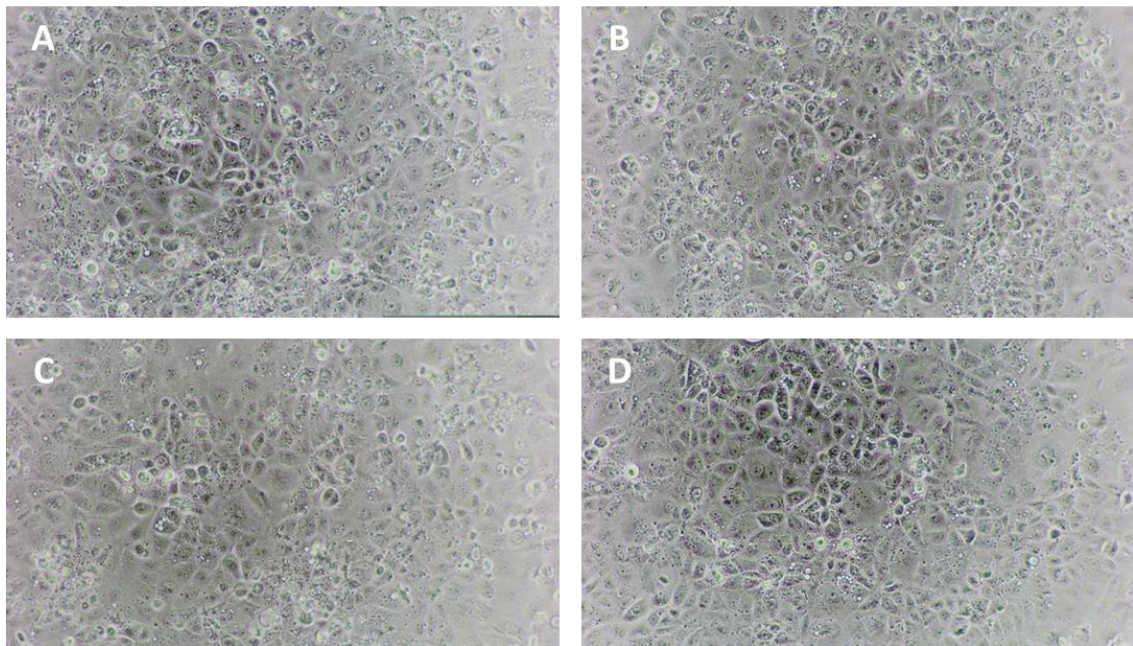
Figure 6.12: Images of HK2 cells 24h after transient transfection. Co-transfection with 5 nM miR-99a-5p mimic and 100 ng MBNL1-psiCHECK-2 recombinant reporter plasmid (A), 5 nM miR-223-3p mimic and 100 ng MBNL1-psiCHECK-2 (B), 5 nM miR-negative control mimic and 100 ng MBNL1-psiCHECK-2 (C) and wild-type cells (D). Seeding density (15,000 cells/well) was uniform in all the conditions. Images were taken with 10x magnification. Each image is a representative of the four images from different wells of 96-well plate of the same condition.

Upon 24 h transient transfection, the interactions between tested miRNAs and MBNL1 transcript were analysed by measuring the luminescent signals of luciferase genes from the MBNL1-psiCHECK-2 reporter plasmid from each well (4 wells per condition) (Figure 13). If MBNL1 3'UTR was regulated by miR-99a-5p or miR-223-3p it would be expected that luminescent signal by Renilla luciferase is decreased. The signal of Firefly luciferase acts as control for transfection efficiency. The ratios of the mean Renilla luminescence (used as reporter) / Firefly luminescence (used as normalizer) were calculated for each condition (miR-99a-5p, miR-223-3p, miR-NC) as described in Methods 6.3.4 after which Renilla/Firefly ratios of the tested miRNAs (miR-99a-5p and miR-223-3p) were normalised to the Renilla/Firefly ratio of miR-NC (Table 6.6). Therefore, values show that both miR-99a-5p (Figure 13A) and miR-223-3p (Figure 13B) bind to the 3'UTR region of MBNL1 transcript and downregulate MBNL1 expression.

Table 6.6: Renilla/Firefly ratios before and after normalisation to miR-NC for miR-99a-5p (A) and miR-223-3p (B). Ratios were calculated from the mean of quadruplicate Renilla and Firefly luciferase values.

A	Not normalised		Normalised to miR-NC	
	miR-99a-5p & MBNL1-psiCHECK-2	miR-NC & MBNL1-psiCHECK-2	miR-99a-5p & MBNL1-psiCHECK-2	miR-NC & MBNL1-psiCHECK-2
Experiment 1	1.415	2.038	0.694	1
Experiment 2	1.252	2.810	0.446	1
Experiment 3	2.470	3.918	0.630	1

B	Not normalised		Normalised to miR-NC	
	miR-223-3p & MBNL1-psiCHECK-2	miR-NC & MBNL1-psiCHECK-2	miR-223-3p & MBNL1-psiCHECK-2	miR-NC & MBNL1-psiCHECK-2
Experiment 1	1.094	1.442	0.759	1
Experiment 2	1.876	2.810	0.668	1
Experiment 3	2.797	3.918	0.714	1
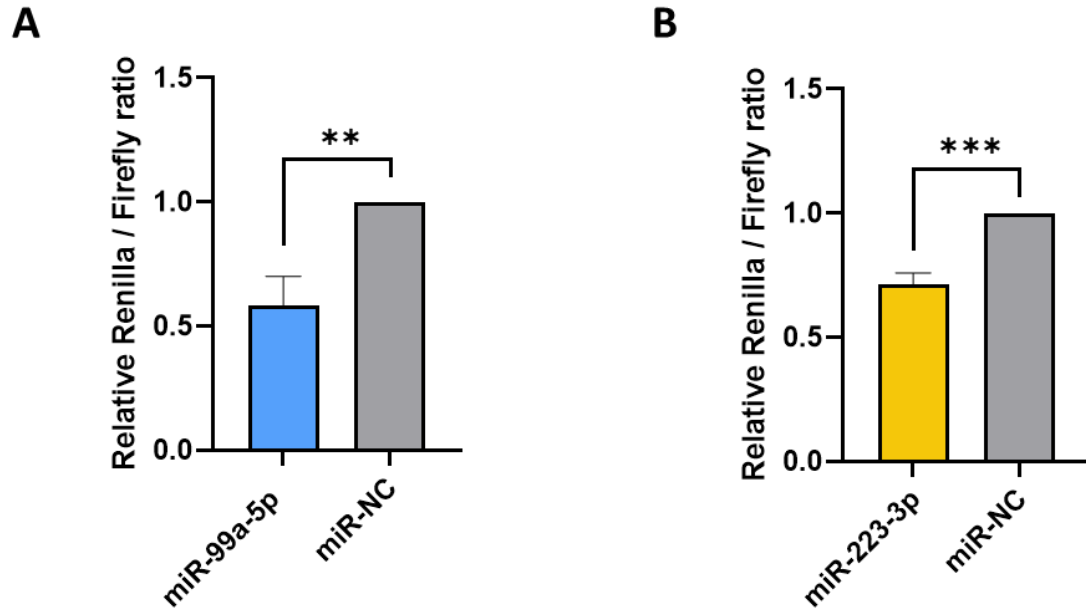
Figure 6.13: Interaction between miR-99a-5p (A) and miR-223-3p (B) with MBNL1 transcript by 3'UTR luciferase reporter assay. HK2 cells were co-transfected with recombinant reporter plasmid DNA (MBNL1-psiCHECK-2) and miR-99a-5p (A) and miR-223-3p (B) and miRNA negative control (miR-NC). Luminescent signals of the reporter plasmid were measured and data were expressed as Renilla/Firefly ratio where Renilla luciferase is reporter and Firefly normalizer. Renilla/Firefly ratios of analysed miRNAs were normalized to the ratio of miR-NC. Experiment was done in quadruplicates and repeated three independent times using three separate transfections. Statistics applied was two-tailed t-test. ***$p < 0.001$, **$p < 0.01$

In summary, these data support our hypothesis that both miR-99a-5p and miR-223-3p regulate MBNL1 expression by directly targeting MBNL1 3'UTR region (incorporated into the MBNL1-psiCHECK-2 reporter plasmid) and suppressing MBNL1 mRNA translation into protein which was here shown as a decrease in luciferase signal compared to the non-regulating miRNA-negative control.

6.5 Discussion

Having discovered a set of protein and miRNA markers of DN and DN progression (Chapters 4 and 5), this chapter aimed to identify potential crosstalk between uEVs miRNAs and proteins implicated in DN and/or DN progression in terms of miRNA regulation of gene expression and translation into proteins.

Gene targets of all four uEVs miRNAs that were found as markers of DN progression were explored using four different databases and only those genes that were predicted by all used sources were considered as stronger candidates (Table 6.2A-D). When these stronger candidates of each miRNA were compared to the list of uEVs proteins differentially expressed in DN, only one protein target appeared for miR-99a-5p and two for miR-223-3p, while no matches were found for the other two miRNAs: miR-184 and miR-3613-5p (Figure 6.4). Since MBNL1 was the common predicted target to both miR-99a-5p and miR-223-3p, it was selected for further experiments to explore whether it is a direct target of the two analysed miRNAs. The 3'UTR region of MBNL1 containing seed regions of both miRNAs was cloned into a reporter plasmid (Figure 6.5A) to create a recombinant reporter plasmid MBNL1-psiCHECK-2 (Figure 6.10). Data from the 3'UTR luciferase reporter assay suggested that MBNL1 is a direct target of both miR-99a-5p and miR-223-3p (Figure 6.13).

MBNL1 protein has been reported to play an important role in DN. A study on high glucose treated mouse mesangial cells showed decreased expression of MBNL1 as a result of its direct translational suppression by miR-452-5p (Wang et al., 2023). Upregulation of MBNL1 instead was associated with decreased levels of alpha-SMA,

fibronectin, and collagens type I and IV. Furthermore, MBNL1 was found to be downregulated in a diabetic mouse model compared to wild-type controls, while an increase in its expression reduced senescence in renal tubular epithelial cells through the MBNL1/miR-130a-3p/STAT3 pathway (Jiang et al., 2020). In this pathway, MBNL1 extended the half-life of miR-130a-3p, enabling its repression of downstream STAT3. These findings suggest that MBNL1 may hold promise as a therapeutic target for DN (Jiang et al., 2020). Consistent with the literature, MBNL1 was found to be downregulated in uEVs from progressive DN compared to diabetic controls, with its reduced expression contributing to the development and progression of DN. The data in this chapter reveal a novel regulatory pathway for MBNL1 expression, mediated by miR-99a-5p and miR-223-3p, both of which are dysregulated during DN progression. Furthermore, all three components potentially involved in this new regulatory mechanism—MBNL1, miR-99a-5p, and miR-223-3p—are uEVs markers of DN and DN progression. This is another key strength of the finding, as EVs are known to play a critical role in kidney diseases. Not only do EVs serve as carriers of biomarkers, but those derived from damaged kidney cells are also implicated in exacerbating kidney damage by mediating long-distance communication between different regions and cell types within the kidney (Grange et al., 2023; Li, B., et al., 2024). This suggests that a regulatory mechanism involving components associated with uEVs may have a more significant impact on CKD pathophysiology than conventional cellular signalling pathways.

This chapter, however, has few limitations. Firstly, a recombinant reporter plasmid with mutated seeded region of miRNAs would be a proper negative control, best to

recombinant reporter plasmid with wild-type 3'UTR regions. Secondly, transfection efficiency was not optimised which could be done by using some anti-luciferin antibodies, for example, to determine the degree of transfection in comparing conditions. Lastly, no studies on cell phenotype upon transfection with analysed miRNAs could be carried out in the available time.

As part of the future studies, it would be interesting to investigate whether wild-type cells transfected with miR-99a-5p (found upregulated in progressive DN) undergo a phenotypic shift towards a more fibrotic state, or if diabetic/fibrotic cell model transfected with miR-223-3p (found downregulated in progressive DN) can reverse some of the fibrotic characteristics. A more advanced approach could involve overexpressing miRNA mimics (miR-99a-5p and miR-223-3p) and isolating EVs from the transfected cells. These EVs could then be applied to wild-type cells transfected with a recombinant reporter plasmid, MBNL1-psiCHECK-2, to investigate whether miRNA transfer via EVs can replicate the effects of MBNL1 post-transcriptional repression. Alternatively, the transfer of enriched miRNAs via EVs could be studied for its potential impact on cell phenotype.

In conclusion, this chapter demonstrates that MBNL1, identified as a uEVs marker of DN, is a direct target of miR-99a-5p and miR-223-3p, which are uEVs markers of DN progression. This finding raises new research questions and offers the potential to uncover a novel pathway involved in the pathology and/or progression of DN.

CHAPTER 7:

Surface charge of urinary extracellular vesicles

Is it useful for patient stratification?

7.1 Introduction

As already mentioned in previous chapters, uEVs are an attractive source of biomarkers of renal diseases (Pisitkun et al., 2004; Van Niel et al., 2018; Tepus et al., 2023) mostly because their cargo can reflect physiological and pathophysiological conditions of the renal cells (Heijnen et al., 1999, Cocucci et al., 2015). However, apart from their biological properties depending on their cargo, EVs are commonly characterized based on their physical properties such as concentration, size, morphology, or even surface charge.

A popular method used to indicate EV surface charge is zeta potential (ZP), an indicator of colloidal stability based on the particle mobility within the applied electrical field (Tamrin et al., 2023). The net surface charge of nanoparticles in a disperse system can determine the stability of particle-particle and particle-medium interactions, including the tendency of particles to aggregate (Midekessa *et al.*, 2020). Although different factors such as pH and ion concentrations of different valences in a solution in which EVs are suspended can influence the measurement of ZP, EVs are known to carry a net negative charge under normal physiological conditions (pH 7.4) which can be due to molecules expressed at EV surface as well as their post-translational modifications. For example, glycoproteins such as mucin-1 and fibronectin-1, phospholipids such as phosphatidylinositol and phosphatidylserine, and proteins with negatively charged extracellular domains such as tetraspanins (Seigneuret *et al.*, 2001) are present at the membrane of EVs and contribute to the net-negative charge (Hallal *et al.*, 2022). We know that the presence of negatively charged glycans such as heparan sulphate (HS)

proteoglycan, which is a polyanionic glycoprotein containing long HS chains (40–300 sugar residues), sulphate groups, and uronic acids (Sarrazin *et al*., 2011), has an impact on the ZP of different populations of EVs which were shown to be negatively charged (Zhang, H., *et al*., 2018). In addition, glycosidase treatment, which causes glycan cleavage, reduces ZP towards neutrality without having a significant effect on EV size (Williams *et al.,* 2019). EVs with smaller ZP tend to aggregate, thus are considered less stable. The higher ZP is (either positive or negative), the greater the electrostatic repulsion between particles is too, which leads to a lower tendency of EVs to aggregate with increased stability (Beit-Yannai *et al*., 2017).

Changes in the zeta potential of EVs in association with pathophysiological conditions and potential diagnosis is not well explored area and only few studies were found reporting on changes in zeta potential related to a pathological condition such as in SLE (Losada et al., 2024) where EVs from patients showed significantly reduced electronegative surface charge compared to controls, then in breast cancer where zeta potential of plasma EVs was associated with clinical characteristics of patients such as visceral fat and weight (Mendivil-Alvarado *et al*., 2023). Furthermore, in Myalgic Encephalomyelitis/Chronic Fatigue Syndrome, plasma EVs from patients were significantly more negatively charged compared to EVs from healthy controls (Almenar-Pérez *et al*., 2020), and similar finding was reported in pathology of gastric cancer where EVs from patients had also significantly more negative zeta potential than healthy controls (Baran *et al*., 2010). However, no study has investigated whether ZP could help stratify patients with diabetes and diabetes with kidney disease.

Therefore, the goal of this work was to assess whether physical properties of zeta potential, concentration and size of urinary small and large EVs change between pathological conditions of DN and diabetes compared to the healthy controls.

7.2 Aims of the chapter

In the previous chapters, the uEVs cargo was investigated as a tool for stratifying DN and DN progression by identifying uEVs biomarkers. In this final chapter, the hypothesis is that physical properties of uEVs, such as surface charge, size, or concentration, could also be useful in differentiating between diabetes and DN conditions. To test this hypothesis, the aims of this chapter were:

1) To explore whether surface charge known as zeta potential (ZP) of uEVs change in diabetes and DN cohorts compared to healthy.

2) To explore whether size distribution and concentration of uEVs change in diabetes and DN cohorts compared to healthy.

3) To assess whether change in ZP of uEVs correlate with the uEVs concentration.

7.3 Methods

7.3.1 Nanoparticle tracking analysis (NTA)

Size distribution, concentration, and particle surface charge also known as zeta potential (ZP) of the isolated uEVs were analysed by nanoparticle tracking analyser ZetaView PMX 120 (Particle Metrix, Germany) and corresponding ZetaView 8.04.02 software on the same day of uEVs isolation. 100 µl preparations of native uEVs (non-denaturated) were resuspended in particle-free PBS (LZBE17-516F, Lonza / 15313581, Corning) and diluted to reach the number of 50-200 detected particles per frame which is the ideal range for particle measurements. If the sample is too concentrated and the number of detected particles too high, particle-particle interactions can disturb the particle distribution and thus the measurements. However sometimes the large fractions of uEVs had very low particle concentration even with minimal dilution, so measurements were made with 10-50 particles in the cell channel. Prior to sample analysis, the cell channel was filled with distilled water followed by the autoalignment dispersion of 100 nm sized polystyrene latex particles (1:300,000) for the cell quality and over-all instrument condition check (concentration range, autofocus of the microscope, electrophoresis symmetry). For each size and concentration measurement, the manufacturer's default software settings for EVs protocol were applied; 11 cell positions were scanned in two cycles meaning that each position was measured twice, capturing 30 frames per position (medium video resolution). The zeta potential was measured at two stationary layers in the cell, in three cycles capturing 60 frames per position (high video resolution) under the pulsed electric

field which is the recommendation when the conductivity of the medium is above 2 ms/cm. Cell temperature during all the measurements was set at 24°C, and pH about 7.4.

The principle of EVs characterisation by NTA is based on documenting the characteristic Brownian motion, of individual particles in a defined solution, such as PBS. This movement of the particles is visualized by the charge-coupled camera that captures the scatter light upon illumination of the particles with a laser. The size of each monitored particle is calculated by the Stokes-Einstein equation, while the particle concentration is determined by the number of individual particles relative to the cell volume (Bachurski, D., *et al.*, 2019). Zeta potential is calculated from the velocity of the charged particles under the applied electric field, measured and expressed as electrophoretic mobility, which is converted into zeta potential through Henry equation or Smoluchowski equation (Kaszuba, M., *et al.*, 2010).

The Stokes-Einstein equation (Dragovic *et al.*, 2011):

$$<x, y>^2 = \frac{K_B T_{ts}}{3\pi\eta d_h}$$

$<x,y>^2$ = mean squared displacement; K_B = Boltzmann's constant; T = temperature of the solvent in Kelvin; t_s = sampling time, η = viscosity; d_h = hydrodynamic diameter

The Smoluchowski's equation (Chapter 3. Electrophoretic mobility of rigid colloidal particles, 2006):

$$\mu = \frac{\epsilon_r \epsilon_0}{\eta} \zeta$$

μ = electrophoretic mobility; ϵ_r = relative permittivity under an applied electric field; ϵ_0 = vacuum permittivity; η = viscosity; ζ = zeta potential

7.4 Results

7.4.1 Can zeta potential of uEVs distinguish and stratify diabetes, stable and progressive DN and healthy conditions?

To study physical properties of uEVs between diabetes, DN and healthy cohorts, nanoparticle tracking analysis (NTA) was applied using ZetaView PMX 120 instrument. Urine samples used for this chapter were selected from the same cohorts shown in Table 4.3 from the Chapter 4 in this thesis, based on the sample availability. Therefore, 18 samples from stable DN, progressive DN, and healthy DN, and 16 samples from diabetes DN groups had enough volume to isolate uEVs and were used for NTA experiments. Clinical characteristics of these slightly reduced cohorts are shown in Table 7.1.

In order to understand what cohort size would be needed to achieve a 95% experimental power, the *A priori* power analysis was conducted using the G*Power 3.1 software and applying the One-way ANOVA statistical test. The effect size values were calculated for small and large uEVs fractions separately, based on the data from a small cohort size pilot experiment where ZP of uEVs from healthy, stable DN, and progressive DN cohorts (n=3 per cohort) was measured (data not showed). According to the calculated effect sizes, sample sizes of 35 samples per cohort for small uEVs fraction and 19 samples per cohort for large uEVs fraction were determined which would give the actual power of 95%. However, due to the limited availability to patient samples, the *Post hoc* power analysis was applied with the effect sizes calculated from the present experiment's data to determine the actual power of the present experiment. By using the maximum available

sample size of 16 urine samples from diabetes cohort, and 18 samples from other three

cohorts, the experimental power for small uEVs was 32% and for large uEVs was 78%.

Table 7.1: Clinical information of patient samples from stable DN, progressive DN and diabetes cohorts, and healthy control individuals used for studying differences in uEVs physical properties between the cohorts, by NTA

	Stable DN	Progressive DN	Diabetic	Healthy
Number of individual samples	18	18	16	18
Gender (Female/Male)	3/15	3/15	8/8	7/4 (ND=7)
Age (mean ± SD)	72.4±8.5	64.7±10.6 (ND=4)	55±16.1 (ND=10)	34.5±12.8 (ND=8)
BMI (mean ± SD)	26.4±3.3 (ND=9)	28.7±4.6 (ND=9)	30.1±8 (ND=10)	25.9±4.2 (ND=8)
Serum creatinine (mg/dL) (mean ± SD)	1.84±0.2	2.05±0.3	0.93±0.1 (ND=10)	0.8±0.2 (ND=8)
eGFR (ml/min) (mean ± SD)	37.11 ± 4.9	34.11 ± 4.6	84.67 ± 12.2 (ND=10)	ND
eGFR change (ml/min/year) (mean ± SD)	2.46 ± 3.4	-8.39 ± 2.9	NA	NA
CKD stage	CKD 3b	CKD 3b	NA	NA

*ND = not determined (not provided information), NA = not applicable

The explored hypothesis before measuring ZP of uEVs from four cohorts was that uEVs surface charge changes in diabetes pathophysiological conditions. To test this hypothesis, ZP was investigated in each uEVs sample from the four cohorts (diabetes, DN stable, DN progressive and healthy control). As shown in Figure 7.1, the mean ZP was negative in all groups of uEVs, however the ZP of large uEVs fraction was significantly different in the diabetes group (n=16, shown in green dots) compared to the healthy group (n=18, shown in blue dots) being less negative than in the healthy controls (Figure 7.1A). This suggests that the metabolic changes associated with the diabetes status modify the molecular composition at the uEVs surface and this may distinguish between diabetes status and control status. When the ZP of the healthy control group was compared to that of the DN (beige dots), a smaller change in ZP was still observed in the DN group which however was no longer significantly different from the healthy group (Figure 7.1B). Interestingly, the DN ZP was significantly lower than that of diabetes uEVs suggesting that the kidney disease component associated with diabetes status changes the uEVs charge moving it accordingly from the healthy group (Figure 7.1C).

When the DN group uEVs were analysed based on the diabetes kidney disease progression, the uEVs from progressive DN were significantly different from the diabetes group and not the stable DN (Figure 7.1C). This suggests that molecular events associated with kidney disease progression such as worsening of kidney fibrosis / extracellular matrix accumulation modify uEVs surface charge, therefore the ZP of large uEVs can be used to distinguish patients with diabetes and perhaps with active, progressive diabetes nephropathy.

When ZP of small uEVs was investigated, the uEVs ZP was smaller than found in the large uEVs (less negative). However, no significant differences in ZP could be measured among the healthy, diabetes, and DN states in the four cohorts (Figure 7.1D-F). Considering the different biogenesis of small and large uEVs fraction (van Niel et al., 2018), these data suggest that the surface charge of the large uEVs, which originate from the budding of the plasma membrane, better reflect the status of the cell from which they are secreted. Because of the endosomal origin of the small EVs, these are less likely to mimic the surface charge of the host cell.
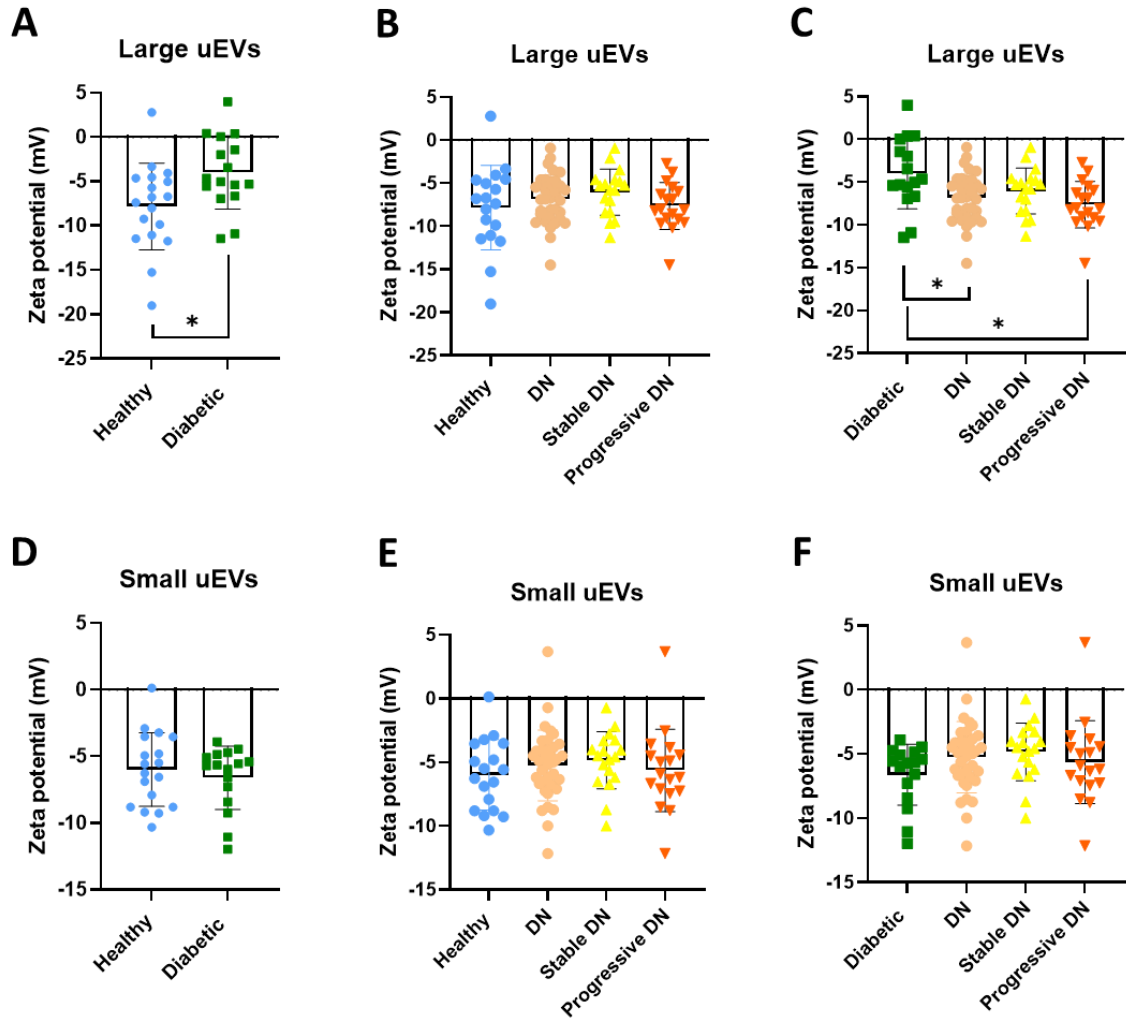
Figure 7.1: Zeta potential of large and small uEVs fraction by nanoparticle tracking analysis revealed potential of large uEVs to distinguish non-CKD diabetes from healthy and DN conditions. Zeta potential of large uEVs from diabetes subjects (n=16) was significantly less negative than from healthy (n=18) (A) while DN status (n=36) did not significantly change from healthy controls (B). Zeta potential of large uEVs from diabetes samples was significantly less negative compared to DN status (n=36), especially progressive stage of DN (n=18) (C). In small uEVs no significant differences in zeta potential were reported between healthy or diabetes status (D), nor between healthy and DN status (E), or DN and diabetes status (F). Data are expressed as mean + SD. Statistical differences were calculated by one-way ANOVA with Tukey's multiple comparisons test. *p < 0.05

7.4.2 Does uEVs size and concentration differ between diabetes, stable and progressive DN and healthy conditions?

Having established that surface charge of large, but not small uEVs, significantly changes between diabetes and DN status, or diabetes and healthy control, the next question was whether size distribution or concentration of uEVs also changes in the diabetes-related conditions.

The size of the small and the large uEVs was measured in all uEVs samples, in every cohort. As shown in Figure 7.2, NTA revealed the mean size of 152.4 ± 5.2 for small uEVs and of 209.8 ± 10.0 for large uEVs. There was no significant difference in uEVs size among the four cohorts, suggesting that the pathological conditions of DN and diabetes do not affect size distribution of uEVs, even if uEVs in different pathological states can contain different composition and number of biomolecules on their surface, which apparently significantly affects their surface charge as shown earlier in Figure 7.1.
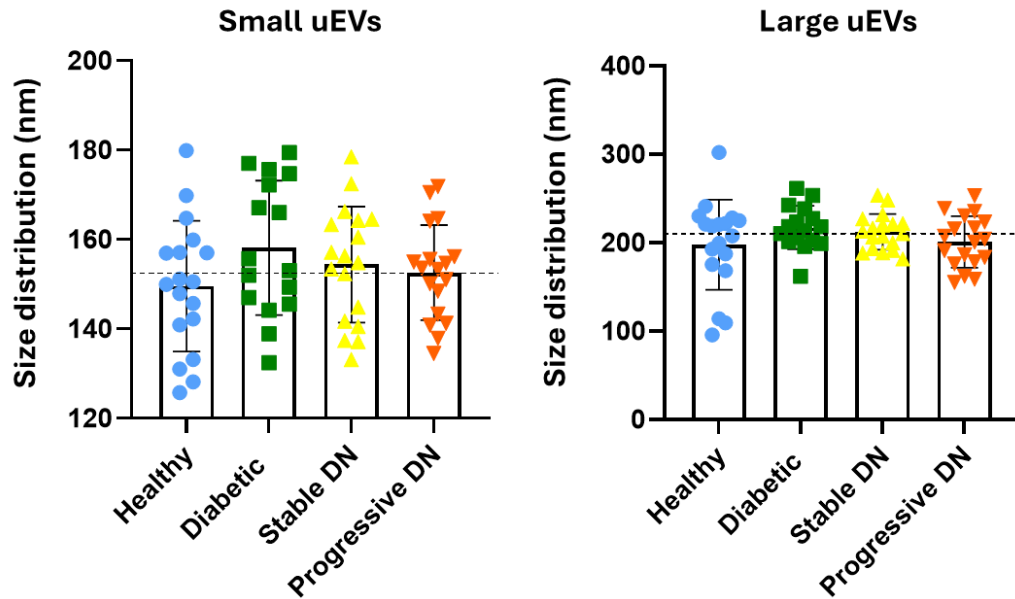
Figure 7.2: Size distribution of small and large uEVs fraction by nanoparticle tracking analysis (NTA) showing no significant difference in particle size between diabetes (n=16), stable DN (n=18), progressive DN (n=18) and healthy control (n=18) conditions. Data are expressed as mean + SD. Statistics applied was one-way ANOVA with Tukey's multiple comparisons test.

Particle concentration, on the other hand, of both small and large uEVs was significantly increased in progressive stage of DN compared to stable DN (Figure 7.3). Moreover, progressive DN had significantly higher concentration of large, but not small, uEVs compared to diabetic and healthy cohort (Figure 7.3B, 7.3D). However, uEVs concentration was not significantly different between the diabetes state and the healthy control group, nor when each of these groups was compared with DN (Figure 7.3A, 7.3C). This suggests that significant increase in particle concentration is associated with progression of diabetes kidney disease.
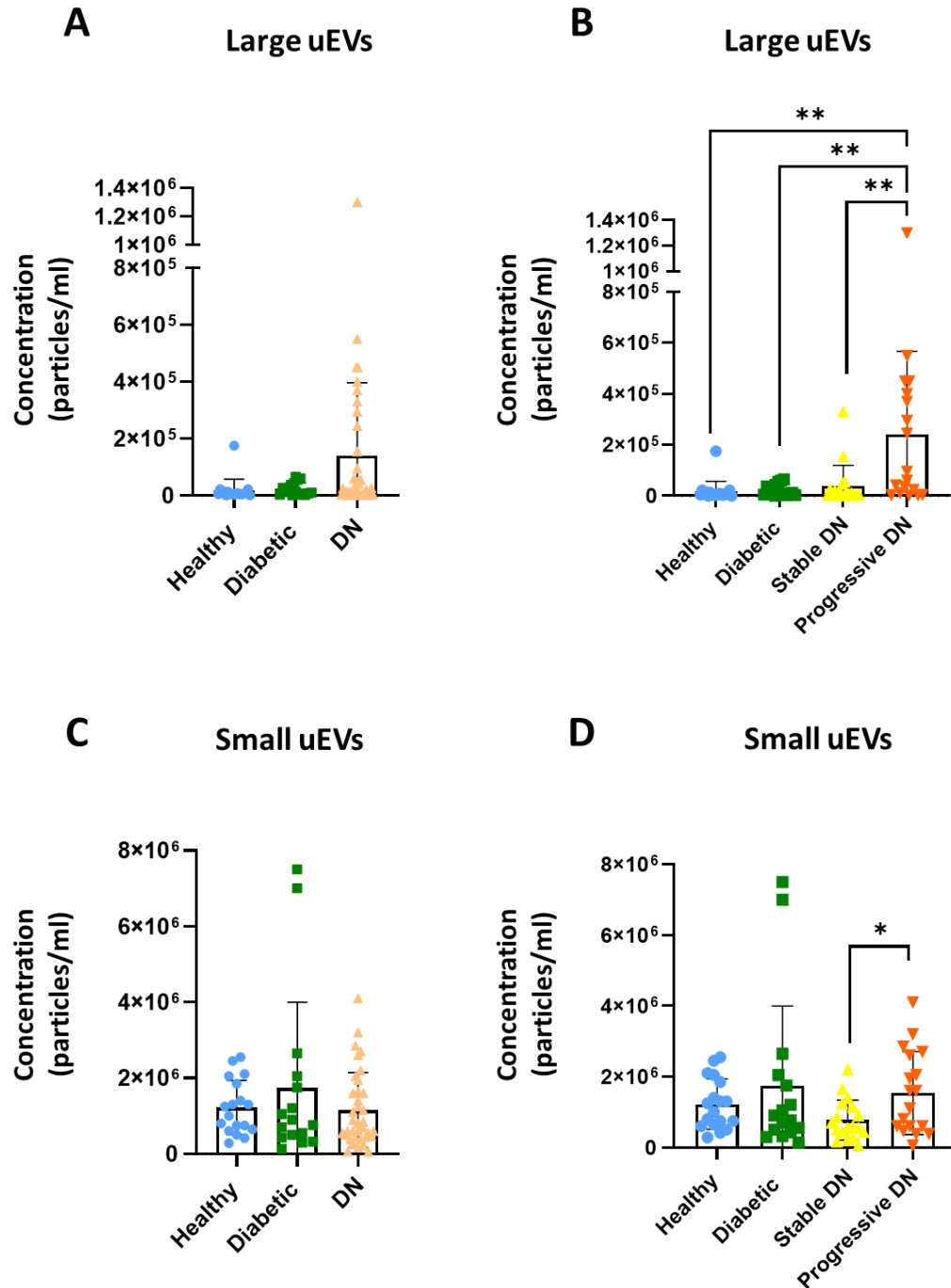
Figure 7.3: Concentration of uEVs between diabetes, DN and healthy conditions, measured by NTA. Concentration of large and small uEVs did not significanlty change between DN, diabetes and healthy condition (A, C), however progressive DN cohort showed significantly higher concentration of large uEVs compared to all other conditions (B). Both large (B) and small (D) uEVs were significantly more concentrated in progressive DN compared to stable DN. Data are expressed as mean + SD. Statistics applied was one-way ANOVA with Tukey's multiple comparisons test. *$**p < 0.01$, $*p < 0.05$*.

7.4.3 Is there a correlation between ZP and particle count?

Having seen that ZP of large uEVs from DN and healthy is more negative than in diabetes with no kidney component, and that particle concentration was significantly enriched in progressive DN compared to stable DN, diabetes and healthy cohorts, next it was investigated whether significantly higher ZP is influenced by significantly higher concentration of particles in the cohort. Including data from all four cohorts, no correlation between ZP and particle concentration was found (Figure 7.4), suggesting that ZP of uEVs can distinguish diabetes conditions independently of particle concentration.
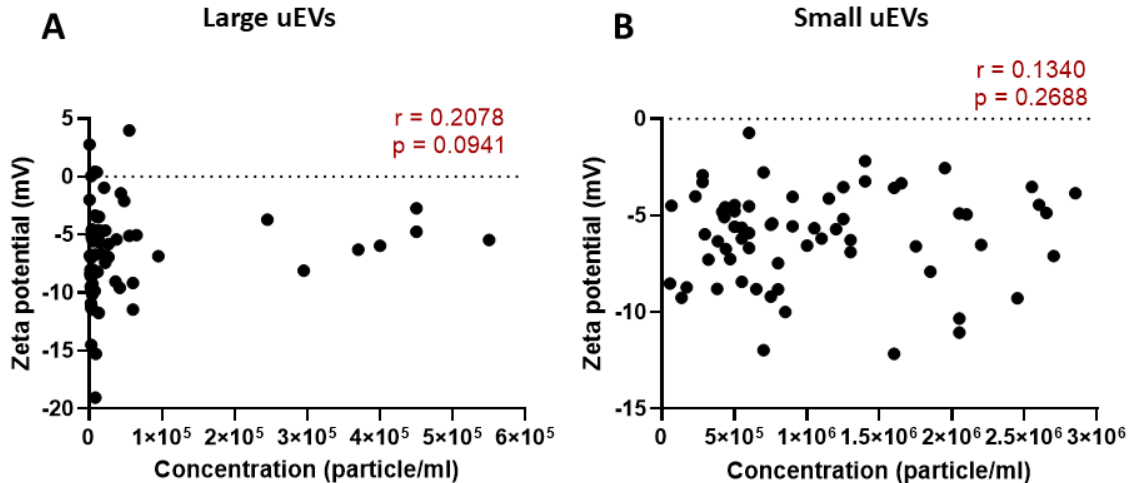
Figure 7.4: Zeta potential and concentration of both large uEVs (A) and small uEVs (B) showed no significant correlation. Data from all four analysed cohorts were included. Statistics applied was Spearman correlation test.

7.5 Discussion

There is a growing interest in studying uEVs as a tool for diagnosing various forms of kidney disease as uEVs cargo can reflect on cellular events during the pathophysiological conditions (Tepus et al., 2023), however, no reports on differences in physical properties such as surface charge, of uEVs during kidney disease was found.

In this chapter, for the first time, it has been analysed the surface charge (ZP) of uEVs isolated from subjects with metabolic disorders such as diabetes and DN at different stages of severity. The aim was to investigate whether uEVs charge, which depends on the naturally occurring negatively charged proteins and proteoglycans on the EV surface as well as the degree of carbohydrate post translational modification be correlated with a dysmetabolic status in urines. In particular, in this chapter was explored if the uEVs charge could be discriminative between diabetes and diabetes with progressive nephropathy.

Analysis of uEVs surface charge revealed a negative zeta potential which is consistent with previous reports (Zhang, H., et al., 2018; Losada et al., 2024) showing that EVs treated and untreated with glycosidases displayed the presence of glycans affecting the surface charge of EVs towards a negative value (Williams et al., 2019). For example, the glomerular endothelial cell surface is rich in negatively charged glycoproteins, glycolipids, and proteoglycans, which are important for restricting the glomerular protein passage and thus maintaining the normal filtration barrier (Singh et al., 2007).

In this study was found that the large uEVs zeta potential was significantly less negative in diabetes compared to healthy group.

This may be explained considering the endothelial glycocalyx, a coat covering vascular endothelial cells consisting of membrane-bound negatively charged proteoglycans, glycoproteins, glycolipids and glycosaminoglycans. The glycocalyx constitutes the material required for a solid and efficient vascular endothelium. Dysmetabolisms such as diabetes, chronic kidney disease (CKD) and inflammatory disorders are often associated with a dysfunction of the glycocalyx (Nieuwdorp et al., 2006; Salmon et al., 2012; Khramova et al., 2021). The nephrosis inducing agent puromycin amino nucleo-side has been shown to favour the downregulation of proteoglycan expression and the development of proteinuria (Bjornson et al, 2005). In diabetes patients the systemic endothelial glycocalyx volume is reduced compared to normal subjects, which is more severe in the presence of moderate albuminuria (Nieuwdorp et al., 2006). Reduction/alteration of endothelial glycocalyx was also reported in CKD (Salmon et al., 2012). The change in zeta potential reported in the diabetes group compared to healthy was only evident in the large EVs and not in the small uEVs fraction, which can be explained by the different biogenesis of small and large uEVs. While large uEVs originate from outward budding plasma membrane, small uEVs do not have direct contact with the plasma membrane, as they are formed within the endosomes by inward budding of endosomal membrane (Cocucci and Meldolesi, 2015), therefore the small uEVs are less likely to reflect cell surface changes as large uEVs do.

We hypothesize that reduced glycan coating on the endothelium surface may be reflected on endothelium-derived uEVs.

The surface of cancer derived EVs was shown to contain transmembrane proteoglycan betaglycan which is capable of binding TGFβ1 and subsequently inducing differentiation of fibroblast into myofibroblast (Weber et al., 2010). Cleavage of betaglycans from the EV surface led to decreased α-SMA production and fibroblast differentiation. Furthermore, the presence of HS side chains was reported to be present on the surface of EVs from prostate cancer cell line (Webber et al., 2015). The loss of HS chains from the EV surface was associated with attenuated SMAD-dependent TGFβ signalling. Even if these changes were associated with prostate cancer pathology, TGFβ signalling, fibroblast differentiation to myofibroblast and production of α-SMA are features also characteristic to fibrosis in kidney disease, suggesting that even surface of EVs from progressive fibrotic patients might be enriched in negatively charged proteoglycans.

The zeta potential of the large uEVs in the DN cohort was significantly more negative compared to that of the diabetes cohort with no CKD. We explain this by the fact that, unlike diabetes, DN is characterised by the development of kidney fibrosis, the progression of which is associated with increased accumulation of extracellular matrix components such as collagen, fibronectin, HS proteoglycan (Zhang, L. et al., 2020; Burhan et al., 2016), but also post-translational modifications such as increased 6-O-sulfation of HS (Alhasan et al., 2014), as well as 2-O-sulfation of HS accompanied with an increased expression of HS enzyme heparan sulphate 2-O sulfotransferase strongly correlating with the amount of fibrosis (Ferreras et al., 2019). Since accumulation of ECM components

and their post-translational modifications have negative charge, this can consequently increase the negative charge of large uEVs therefore partially compensating the drop in zeta potential measured in diabetes. Therefore, based on these findings the zeta potential of the large uEVs could differentiate diabetes subjects with no CKD from diabetes with fast progressing CKD (loss of eGFR> 5 ml/min/year) and thus help predict the disease course in a non-invasive way.

Since electrostatic forces between negatively charged EVs and lipid cell membrane affect EVs adsorption influencing EV-mediated intercellular communication (Ridolfi et al., 2023), the physical properties of EVs may be exploited to determine the evolution of other pathological condition and provide improvement in current diagnosis, prognosis and/or prediction of disease.

The limitation of this study is that the cohort size of patient samples is not large enough to give an experimental power of 95%. Furthermore, as evident even in previous chapters, there are some missing clinical information about patient samples in different cohorts for example for age, BMI, and serum creatinine parameters, but also some information was not provided such as albuminuria level.

In conclusion, the data in this chapter demonstrated that ZP of large uEVs can distinguish between diabetes, DN and healthy conditions, as graphically summarised in Figure 7.5.
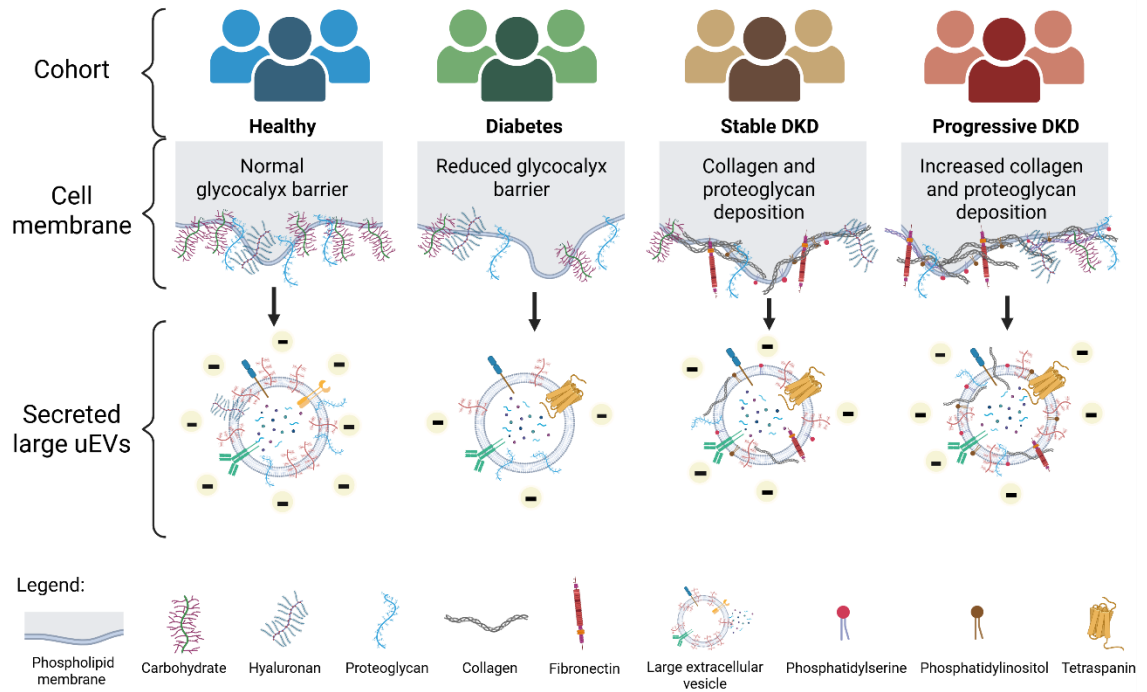
Figure 7.5: Graphical summary. Large uEVs reflect the state of the phospholipid membrane of their origin cells. In healthy condition, cell membrane and hence uEVs membrane is rich in negatively charged glycocalyx barrier so the ZP of large uEVs is negative. In diabetes condition, glycocalyx barrier is damaged which is reflected in large uEVs having a smaller negative charge. DN is linked with kidney fibrosis characterised by the overproduction of negatively charged components of ECM such as collagens, fibronectins, proteoglycans, and therefore large uEVs have higher negative charge than in diabetes, which is even more increased in progressive DN stage.

CHAPTER 8:

General discussion

8.1 General discussion

Urinary EVs hold promise as a source of kidney disease biomarkers, as they are secreted by kidney cells, facilitate intercellular communication, and contain molecular cargo that reflects underlying pathophysiological conditions (Lu et al., 2020). This thesis presents a number of novel findings that emphasize the potential role of uEVs "multi-omics" approach in determining the progression of DN, which is a common form of CKD, and differences between diabetes and diabetes kidney disease (DKD). Starting from the finding that uEVs proteome is larger than full urine proteome, the cargo of uEVs was analysed to identify markers (protein and miRNA) associated with DN progression. A mechanistic link was also established between a miRNA dysregulated in progressive DN and new protein marker of DN severity, the expression of which can be controlled by the miRNA. For the first time, the uEVs surface charge was also explored and this showed significant changes between diabetes and diabetes with CKD (DN). Consistent with the idea that uEVs cargo is distinct between diabetes and DN and uEVs profiling leads to CKD stratification. The key results are summarised in Figure 8.1.

Data from the proteomic analysis of uEVs and full urine in Chapter 3 revealed that uEVs are a more robust source of biomarkers compared to urine due to their larger proteome, which contains proteins of cellular origin that are rarely found in unfractionated urine. These data extend the findings of Gudehithlu et al. (2016), who demonstrated that the uEVs protein markers ceruloplasmin and gelatinase more accurately reflect the underlying protein changes in the DKD kidney compared to full urine samples. The new

panel of uEVs-derived cellular proteins reported in Chapter 4 (vasorin, podocalyxin, mucin 1, ganglioside GM2 activator, and argininosuccinate synthase) can discriminate between progressive and stable DN (<2 ml/min/year eGFR loss in stable DN and >5 ml/min/year eGFR loss in progressive DN). Validation on a different cohort of stable and progressive DN patients will reveal the potential of this new DN progression fingerprint to be translated into clinics. There is a pressing need for biomarkers to track the progression of DN (Hirakawa et al., 2022; Huang et al., 2022). To monitor the progression of DN, current model approaches based on urinary proteins propose to distinguish between diabetes and DN, between DN stages (stage 3 and stage 4), or detect early signs of DN (Fan et al., 2021). One study has proposed complement proteins (especially complement factor H (CFAH) and decay-accelerating factor (DAF)) as able to predict ESKD in DN progression (Zhao, L., et al., 2021). However, the majority of the protein composition in these models consists of excreted plasma proteins, but it is recognised that the key characteristics of a "good biomarker" is its biological reliability and ability to offer insights into the underlying pathological mechanisms of a disease (Bennett and Devarajan, 2017). The five uEVs proteins proposed here as DN progression markers are likely of kidney cell origin, rather than plasma. Based on the identified uEVs protein that are known to track the uEVs cell origin according to considerations from Turco et al. (2016) and Erdbrugger et al. (2021), the likely cell types are podocytes (podocalyxin), tubular epithelial cells (complement C3 and C9) in proximal tubule (aminopeptidase N, cubilin), Henle's loop (uromodulin), or collecting duct (mucin 1).

Chapter 5 uncovered the miRNAs significantly differentially changed in progressive DN compared to stable condition (miR-184, miR-3613-5p, miR-99a-5p, and miR-223-3p). Validation of miR-99a-5p, miR-223-3p and miR-3616-5p showed promising results with expression trends consistent with those observed by profiling. Inclusion of these three miRNAs in the uEVs panel of DN progression could strengthen the diagnostic power of the panel in detecting DN severity. Additionally, the suggested panel of protein and miRNA uEVs markers, which have the potential to indicate DN progression, could serve as an alternative to biopsy. The advantage of this approach is its non-invasive nature, greater stability and, therefore, increased reliability of markers within membranous uEVs compared to markers found in full urine, and the possibility for longitudinal monitoring. Biomarker studies utilizing various omics analyses hold significant potential for disease diagnosis, prediction, progression, and monitoring treatment responses, as omics platforms generate large, unbiased datasets from biological samples (Barutta et al., 2021). Moreover, multi-marker panels are recognized for their superior performance compared to single biomarkers. Multi-omics approaches and the integration of various omics data has grown significantly because the pathogenesis of a disease, in this case DKD, is complex, involving various mechanisms as part of metabolic, fibrotic, or inflammatory pathways that interact with one another. Therefore, a biomarker panel composed of multiple types of molecules could provide a more comprehensive understanding of the diverse dysregulated molecular mechanisms, enhancing both diagnostic and prognostic potential (Scamporrino et al., 2023).

Apart from the progression protein markers, Chapter 4 and Chapter 5 also presented uEVs candidate protein and miRNA markers for DN compared to diabetes without CKD (L-lactate dehydrogenase C chain, muscleblind-like protein 1, miR-891a-5p, miR-432-5p, miR-890, miR-892a) all of which were downregulated in DN. Not all patients with DKD experience renal dysfunction solely due to diabetes, as some may have nondiabetic kidney disease (NDKD) or a combination of DKD and NDKD (Anders et al., 2018). Therefore, identifying novel markers to distinguish DN from other similar conditions is crucial, especially since many diabetic patients do not undergo biopsy, the only definitive test. Validating these markers in larger cohorts could be valuable for clinical application, as these might help meet the medical need of differentiating diabetes-related kidney conditions.

Furthermore, data from Chapter 6 demonstrated that miRNAs dysregulated during DN progression (miR-99a-5p and miR-223-3p) directly repress the translation of MBNL1, which was found to be dysregulated in DN compared to diabetes. This is particularly noteworthy given that epigenetic modifications such as miRNA posttranscriptional regulation of gene expression are also involved in the pathogenesis of CKD (Liu et al., 2023). Epigenetic modifications, including miRNA posttranscriptional regulation of gene expression, play a role in the inhibition or activation of various pathogenic signalling pathways, which may contribute to the development and progression of DN. The findings regarding miR-99a-5p-MBNL1 and miR-223-3p-MBNL1 regulations open new research avenues and the potential to identify novel signalling pathways involved in the development and progression of DN. Therefore, a mechanism of posttranscriptional

regulation of gene expression involving uEVs components, which may play a role in the development or progression of DN is proposed.

Because uEVs, originating from damaged kidney cells, play a role in exacerbating kidney damage by facilitating long-distance communication between different regions and cell types within the kidney (Grange et al., 2023; Li, B., et al., 2024), this mechanism of regulation of uEVs markers (miR-99a-5p, miR-223-3p and MBNL1) may have an impact on DN pathophysiology and was not described before. In particular, miRNA-mRNA regulation takes place at the cellular level, however these miRNAs can be transported through uEVs and inhibit translation of certain proteins in recipient cells. The downregulation of such proteins may then be observable in the uEVs secreted from these cells. In this manner, uEVs provide insight into the mechanisms occurring at the cellular level.

In addition to the uEVs protein and miRNA cargo, which reflect DN pathology and progression, our data from Chapter 7 demonstrated for the first time that the surface charge, also known as zeta potential, of the large uEVs population can differentiate between diabetes and progressive DN conditions in comparison to healthy volunteers. Given that the presence of glycans can influence the surface charge of EVs, making it more negative (Williams et al., 2019), our data suggest that the less negative zeta potential of large uEVs in diabetes results from damage to the glomerular endothelial surface layer, acting as a barrier to protein permeability, which leads to a reduction in negatively charged proteoglycans, glycoproteins and glycolipids. In contrast to diabetes, large uEVs from progressive DN had more negative zeta potential and we propose that

the increased deposition of negatively charged ECM components, along with a rise in negatively charged albumin in progressive fibrotic DN, may result in a more negative zeta potential of large uEVs, reflecting changes in the cell membrane from which they originate. To date, only one study has reported a change in zeta potential between CKD and healthy conditions, specifically in Systemic Lupus Erythematosus (Losada et al., 2024). This study found that EVs from patients exhibited a significantly reduced electronegative surface charge compared to controls. The scarcity of published studies in this area underscores the novelty of utilizing the physical properties of uEVs for diagnostic and/or prognostic applications.

In conclusion, this PhD project demonstrated the significant potential of uEVs as a source of biomarkers. For clinical relevance, additional validation steps are needed for the proposed biomarkers of DN progression. However, all the findings pave the way for new research opportunities in this area.
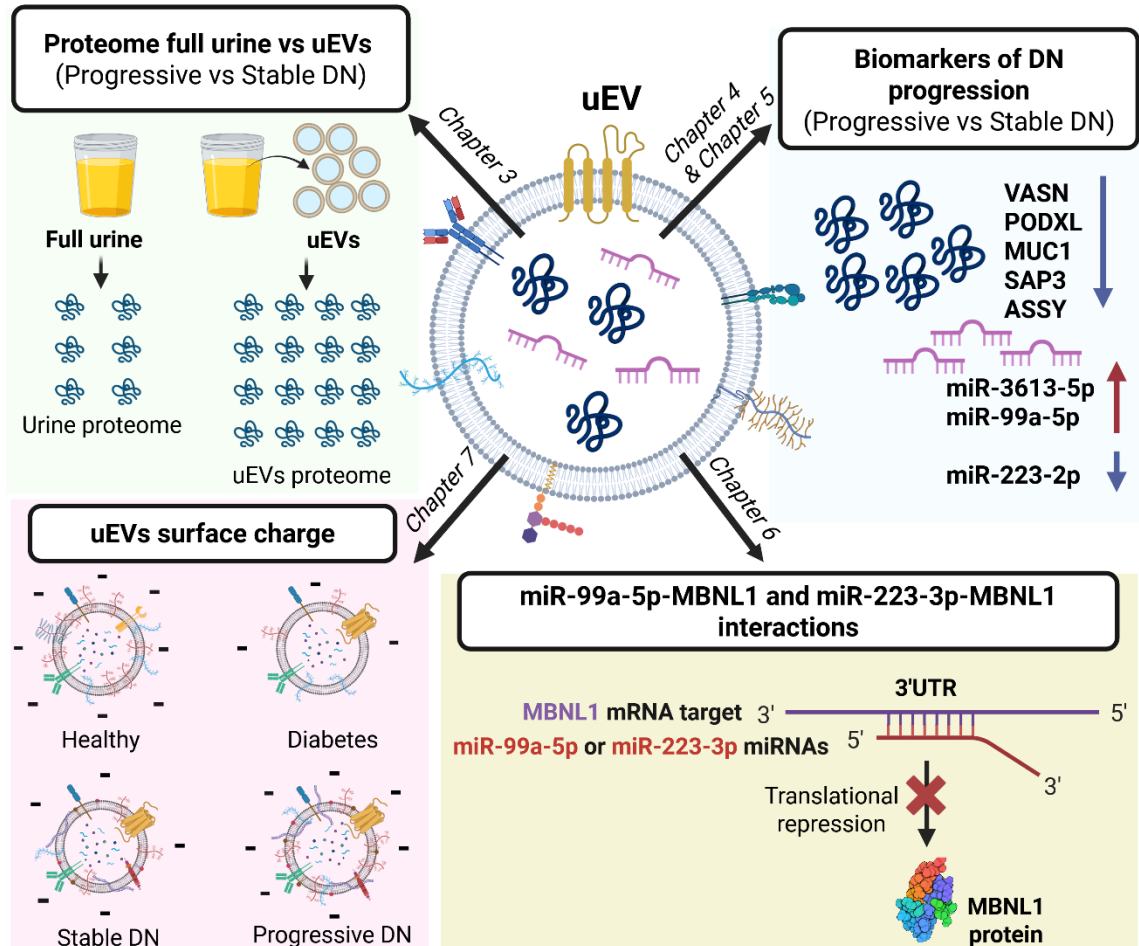
Figure 8.1: DN progression panel emerged from urinary EV multi-OMICs. 1) uEVs are enriched in proteome size compared to full urine. 2) uEVs offer a multi-marker panel (proteins and miRNAs) of DN progression. 3) differentially expressed miRNAs in uEVs (Pr vs St DN) directly regulate expression of MBNL1 (differentially expressed in uEVs from Pr DN vs diabetes). 4) uEVs surface charge significantly distinguish diabetic from healthy and progressive DN condition.

8.2 Future directions

To demonstrate a clear improvement of the diagnostic potential of DN progression, comparing the discovered uEVs signature to that of what is already being used currently (albumin-to-creatinine ratio and/or the kidney failure risk equation), the expression of the candidate protein and miRNA biomarkers of DN progression would need to be validated in the second independent cohorts. Such cohorts should be of significant sizes, ideally consisting of 100 to 200 patients. Additionally, this study introduced a biomarker cocktail comprising 5 proteins and 3 miRNAs. However, a few additional proteins have been shortlisted for validation, and their inclusion could further enhance the current biomarker panel. Although the primary focus of this PhD work was on detecting DN progression, a set of proteins and miRNAs with potential to diagnose early or stable stages of DN was also identified. Therefore, it would be valuable to validate and further investigate markers for both DN progression and non-progressive stages of the disease.

Furthermore, this work emphasizes the importance of identifying cellular markers of kidney disease, mainly because of their potential to provide insights into the underlying pathological mechanisms. Therefore, the next step in future research would be to explore the role of the proposed markers in DN and DN progression. One approach could involve overexpressing a wild-type human kidney cell model with the markers found to be upregulated in DN/DN progression and investigating whether this leads to a fibrotic phenotype in the cells. Likewise, it would be interesting to explore whether a fibrotic human kidney cell model (induced by TGF-β, high glucose, or advanced glycation end products) could revert to a healthier phenotype when transfected with markers that

were discovered to be downregulated in DN/DN progression. A more elegant approach would involve isolating EVs from human kidney cells after overexpressing specific markers of DN/DN progression and applying these EVs to recipient cells to demonstrate that the pathological or protective effects are mediated through EV-based transport and communication. In addition, the expression of the biomarker panel could be analysed in tissue biopsies from DN patients using spatial transcriptomics. This approach would enable the identification of the more precise kidney regions and/or cell types where these markers are expressed, as well as the extent of their expression. Finally, through target prediction, one protein (MBNL1) was experimentally shown to be targeted by the two miRNAs (miR-99a-5p and miR-223-3p). This aspect of the work could be expanded by investigating other potential miRNA targets involved in CKD pathology or progression. By examining existing proteomic studies on human kidney cell types, additional candidates could be identified. Discovering and evaluating more targets could provide further insights into the associated signalling pathways.

APPENDIX

Supplementary table 1: Stable (n=28) and progressive (n=25) DN patient samples with individual eGFR (ml/min) and eGFR slope (ml/min/year) values. Samples are listed according to eGFR slope with the most stable or most progressive on top. Red values are the patients from who urines were not yet used.

Stable IDs	eGFR	eGFR slope	Progressive IDs	eGFR	eGFR slope
SKI1004	37	13.21	SKI801	34	-25.65
SKI453	34	9.62	PDN33	31	-15.08
SKI535	30	7.52	PDN194	31	-14.62
PDN423	30	6.49	PDN291	37	-13.19
SKI425	40	5.8	SKI398	35	-12.6
PDN13	44	4.41	PDN46	38	-11.91
SKI581	34	4.36	PDN22	26	-11.82
SKI613	33	3.39	PDN348	29	-11.34
PDN10	44	3.07	SKI901	32	-11.18
SKI417	35	3.06	PDN261	32	-10.68
SKI594	37	3.05	PDN154	42	-9.05
SKI410	40	2.75	PDN382	30	-8.22
SKI643	33	2.56	PDN436	39	-8.2
SKI961	36	1.98	PDN282	42	-8.14
SKI730	43	1.37	PDN138	33	-7.53
PDN299	33	0.65	SKI662	30	-7.51
PDN127	35	0.53	SKI441	33	-6.46
PDN164	41	0.27	PDN51	32	-6.4
PDN157	44	-0.14	SKI657	33	-5.97
PDN266	38	-0.22	PDN17	25	-5.92
PDN232	37	-0.24	PDN216	38	-5.53
SKI848	32	-0.77	SKI1001	40	-5.43
PDN162	32	-1.35	SKI837	33	-5.32
SKI812	32	-1.38	SKI857	35	-5.32
PDN300	42	-1.64	PDN414	38	-5.08
SKI470	40	-1.68			
PDN209	31	-1.75			
SKI907	40	-1.86			

A

EVs proteins from Vesiclepedia
(8452 proteins)

uEVs proteins in DN from DDA library
(751 proteins)

7784 (91.2%) **668** (7.8%) **83** (1%)

89% of proteins in uEVs from DN

B

uEVs proteins from Vesiclepedia
(4836 proteins)

uEVs proteins in DN from DDA library
(751 proteins)

4206 (84.8%) **630** (12.7%) **121** (2.4%)

84% of proteins in uEVs from DN
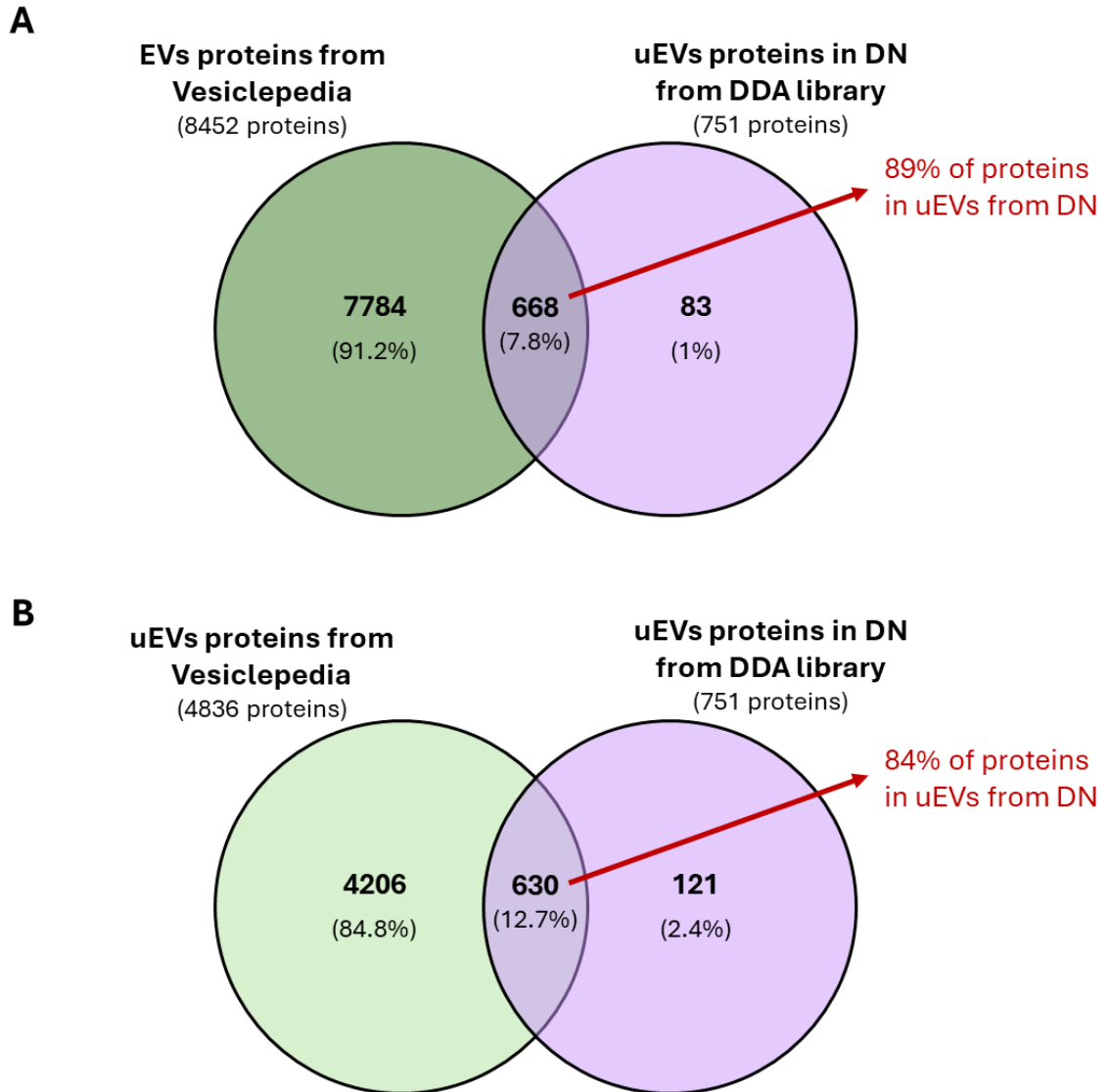
Supplementary figure 1: Number of proteins detected by DDA in uEVs from DN that match to the list of protein reported in EVs exported from the Vesiclepedia database. A) Vesiclepedia proteins compared to proteins in uEVs from DN, B) Vesiclepedia proteins reported only in urinary EVs compared to proteins in uEVs from DN. Comparison was done using Venny 2.1, and venn diagrams were created using PowerPoint.

Supplementary table 2: Proteins isolated from human uEV, proposed to be biomarkers of non-DN CKD

uEV protein	CKD type	Expression in CKD vs CTL	Sample size	Method of analysis	So62urce
Osteoprotegerin (OPG)	DN ADPKD	↑	CKD = 14 Control = 4	LC-MS/MS + SRM QQQ-LC/MS	Benito-Martin et al., 2013, PLoS ONE
Periplakin Envoplakin Villin-1 Complement C3 Complement C9	ADPKD	↑	ADPKD = 6 Control = 6	LC-MS/MS + Immunoblotting	Salih et al., 2016, JASN
*Ceruloplasmin *α-1-antitrypsin	IgAN	↑	IgAN = 5		Moon et al., 2011, Proteomics
Aminopeptidase N		↑	TBMN = 7	LC-MS/MS	
*Vasorin	TBMN	↑	Control = 7		
CCL2 mRNA	IgAN	↑	IgAN = 6 Control = 6	Real-time RT-PCR	Feng et al., 2018, Am J Pathol
*Ceruloplasmin		↑	IgAN = 16		Farzamikia et al., 2024, Bioimpacts
*Vasorin	IgAN	↓	MGN = 16 Control = 16	Immunoblotting	
*Ceruloplasmin	IgAN MN FSGS LN	↑	MN = 9 IgAN = 7 FSGS = 10 LN = 10 Control = 15	Sandwich ELISA	Gudehithlu et al., 2019, Clin Exp Nephrol
Dipeptidase 1 (DPEP1)	FSGS	↓	CKD = 12		Stokman et al., 2019, Journal of Proteomics
Protocadherin Fat 4 (FAT4)	Nephronophthisis	↓		LC-MS/MS	
Versican core protein (VCAN)	CKD pool	↑	Control = 12		
CD2AP mRNA	CKD pool	↓	CKD = 32 Control = 7	Real-time RT-PCR	Lv et al., 2014, Clinica Chimica Acta
CD133	CKD pool	↓	CKD = 12 Control = 7	Cytofluorimetric analysis	Dimuccio et al., 2020, Am J Physiol Renal Physiol
Aquaporin 1 (AQP1), AQP2	CKD	↓	CKD = 62 Control = 15	Immunoblotting	Oshikawa-Hori et al., 2021, Physiol. Rep.

↑ - increased expression; ↓ - decreased expression; * - found in different studies; ADPKD - autosomal dominant polycystic kidney disease; IgAN - Immunoglobulin A nephropathy; TBMN - thin basement membrane nephropathy; MGN - membranous glomerulonephritis; MN - membranous nephropathy; FSGS - Focal Segmental Glomerulosclerosis; LN - lupus nephritis; CTL - control

Supplementary table 3: Significantly <u>upregulated</u> proteins in uEVs from progressive DN (n=17) vs healthy (n=18) in dataset normalized to equal volume, listed according to fold change (Prog / Healt)

	Protein ID	Protein name	FC (Prog / Healt)	Adj. p-value (BH)
	ALBU_HUMAN	Albumin	110.049	1.17E-16
	TRFE_HUMAN	Serotransferrin	77.601	2.90E-16
	HEMO_HUMAN	Hemopexin	69.744	1.71E-14
	CO3_HUMAN	Complement C3	58.770	1.35E-12
	A1AT_HUMAN	Alpha-1-antitrypsin	29.651	1.70E-11
	CERU_HUMAN	Ceruloplasmin	27.322	6.31E-10
	CO9_HUMAN	Complement component C9	24.522	1.38E-08
	ANT3_HUMAN	Antithrombin-III	19.535	3.18E-08
	HPT_HUMAN	Haptoglobin	19.346	1.53E-09
	IGHG3_HUMAN	Immunoglobulin heavy constant gamma 3	18.961	3.45E-08
*	PEDF_HUMAN	Pigment epithelium-derived factor	18.392	8.88E-08
	PLMN_HUMAN	Plasminogen	18.328	9.83E-08
	APOA1_HUMAN	Apolipoprotein A-I	16.610	1.12E-07
	A1AG1_HUMAN	Alpha-1-acid glycoprotein 1	14.825	7.56E-08
	TTHY_HUMAN	Transthyretin	14.825	1.08E-07
	FIBG_HUMAN	Fibrinogen gamma chain	12.924	1.84E-06
	IGHG4_HUMAN	Immunoglobulin heavy constant gamma 4	12.519	1.26E-06
	APOA4_HUMAN	Apolipoprotein A-IV	12.109	8.20E-06
	VTNC_HUMAN	Vitronectin	11.696	4.05E-06
	A2MG_HUMAN	Alpha-2-macroglobulin	11.496	3.77E-06
	A1BG_HUMAN	Alpha-1B-glycoprotein	11.243	1.11E-06
	ZA2G_HUMAN	Zinc-alpha-2-glycoprotein	10.282	1.66E-06
	CFAB_HUMAN	Complement factor B	9.822	1.07E-05
	IGLL5_HUMAN	Immunoglobulin lambda-like polypeptide 5	9.019	3.77E-06
*	ZGRF1_HUMAN	Protein ZGRF1	8.640	0.000583
	IGLC3_HUMAN	Immunoglobulin lambda constant 3	8.580	2.71E-05
	IGK_HUMAN	Immunoglobulin kappa light chain	8.503	6.81E-06
	LV147_HUMAN	Immunoglobulin lambda variable 1-47	8.474	3.60E-05
	FIBB_HUMAN	Fibrinogen beta chain	8.468	5.76E-05
	HEP2_HUMAN	Heparin cofactor 2	8.415	0.000284
*	HTRA4_HUMAN	Serine protease HTRA4	8.157	1.03E-05
	IGKC_HUMAN	Immunoglobulin kappa constant	7.770	5.05E-05
*	THAS_HUMAN	Thromboxane-A synthase	7.501	4.49E-05
	CO4B_HUMAN	Complement C4-B	7.170	0.000174
	ITIH2_HUMAN	Inter-alpha-trypsin inhibitor heavy chain H2	7.160	0.000185
	ANGT_HUMAN	Angiotensinogen	6.760	0.000544
	CO4A_HUMAN	Complement C4-A	6.681	0.000403
	KV37_HUMAN	Probable non-functional immunoglobulin kappa variable 3-7	6.485	0.000179
	KV311_HUMAN	Immunoglobulin kappa variable 3-11	6.480	0.000134
	THRB_HUMAN	Prothrombin	6.312	0.000398

* represent proteins that are not in the category of plasma proteins

Supplementary table 3: Continuation

	Protein ID	Protein name	FC (Prog / Healt)	Adj. p-value (BH)
	HV434_HUMAN	Immunoglobulin heavy variable 4-34	6.080	0.00037
*	AMBP_HUMAN	Protein AMBP	6.050	0.000544
*	TITIN_HUMAN	Titin	6.034	0.019321
	HV307_HUMAN	Immunoglobulin heavy variable 3-7	5.564	0.00154
	ITIH1_HUMAN	Inter-alpha-trypsin inhibitor heavy chain H1	5.348	0.003058
*	CDC5L_HUMAN	Cell division cycle 5-like protein	5.195	0.001367
	KV320_HUMAN	Immunoglobulin kappa variable 3-20	4.874	0.001327
	A1AG2_HUMAN	Alpha-1-acid glycoprotein 2	4.810	0.002997
	CO5_HUMAN	Complement C5	4.770	0.00822
*	BGH3_HUMAN	Transforming growth factor-beta-induced protein ig-h3	4.688	0.002312
	FRIL_HUMAN	Ferritin light chain	4.601	0.005265
	APOH_HUMAN	Beta-2-glycoprotein 1	4.566	0.010945
	HV323_HUMAN	Immunoglobulin heavy variable 3-23	4.547	0.007652
*	CBG_HUMAN	Corticosteroid-binding globulin	4.506	0.003009
	FETUA_HUMAN	Alpha-2-HS-glycoprotein	4.179	0.010945
*	LBP_HUMAN	Lipopolysaccharide-binding protein	4.150	0.012859
	IGG1_HUMAN	Immunoglobulin gamma-1 heavy chain	4.141	0.009735
	HV601_HUMAN	Immunoglobulin heavy variable 6-1	3.842	0.023769
	HV374_HUMAN	Immunoglobulin heavy variable 3-74	3.737	0.028664
	LV319_HUMAN	Immunoglobulin lambda variable 3-19	3.575	0.042161
	KV401_HUMAN	Immunoglobulin kappa variable 4-1	3.511	0.02518
	A2GL_HUMAN	Leucine-rich alpha-2-glycoprotein	3.432	0.028664

Supplementary table 4: Significantly <u>downregulated</u> proteins in uEVs from progressive DN (n=17) vs healthy (n=18) in dataset normalized to equal volume, listed according to fold change (Prog / Healt)

Protein ID	Protein name	FC (Prog / Healt)	Adj. p-value (BH)
EGF_HUMAN	Pro-epidermal growth factor	-14.420	4.82E-08
VASN_HUMAN	Vasorin	-10.868	1.18E-06
MUC1_HUMAN	Mucin-1	-10.133	1.49E-06
IPSP_HUMAN	Plasma serine protease inhibitor	-6.593	7.93E-05
RHCG_HUMAN	Ammonium transporter Rh type C	-6.092	0.000174
APOD_HUMAN	Apolipoprotein D	-5.602	0.000746
THY1_HUMAN	Thy-1 membrane glycoprotein	-5.529	0.000737
CTL2_HUMAN	Choline transporter-like protein 2	-5.252	0.000851
GTR5_HUMAN	Solute carrier family 2, facilitated glucose transporter member 5	-4.482	0.010643
UROM_HUMAN	Uromodulin	-4.252	0.018655
CYBR1_HUMAN	Plasma membrane ascorbate-dependent reductase CYBRD1	-3.923	0.03336
BROX_HUMAN	BRO1 domain-containing protein BROX	-3.834	0.012918
UEVLD_HUMAN	Ubiquitin-conjugating enzyme E2 variant 3	-3.605	0.047573
VPS4A_HUMAN	Vacuolar protein sorting-associated protein 4A	-3.533	0.025623
HACD1_HUMAN	Very-long-chain (3R)-3-hydroxyacyl-CoA dehydratase 1	-3.385	0.04878
CHM2A_HUMAN	Charged multivesicular body protein 2a	-3.371	0.036577
CHMP5_HUMAN	Charged multivesicular body protein 5	-3.352	0.038806
XPP2_HUMAN	Xaa-Pro aminopeptidase 2	-3.326	0.044546
RAI3_HUMAN	Retinoic acid-induced protein 3	-3.276	0.044323

Supplementary table 5: Significantly upregulated (red) and downregulated (blue) proteins in uEVs from stable DN (n=19) vs healthy (n=18) in dataset normalized to equal volume, listed according to fold change (Stab / Healt)

Protein ID	Protein name	FC (Stab / Healt)	Adj. p-value (BH)
ALBU_HUMAN	Albumin	21.200	7.56E-11
TRFE_HUMAN	Serotransferrin	19.186	7.56E-11
ZA2G_HUMAN	Zinc-alpha-2-glycoprotein	13.529	2.92E-09
CERU_HUMAN	Ceruloplasmin	12.987	4.45E-08
A1AT_HUMAN	Alpha-1-antitrypsin	12.897	5.77E-09
B2MG_HUMAN	Beta-2-microglobulin	10.303	1.08E-06
HPT_HUMAN	Haptoglobin	8.299	5.71E-06
A1BG_HUMAN	Alpha-1B-glycoprotein	7.260	3.06E-05
A1AG1_HUMAN	Alpha-1-acid glycoprotein 1	6.984	3.10E-05
IGLC3_HUMAN	Immunoglobulin lambda constant 3	6.950	3.19E-05
AMBP_HUMAN	Protein AMBP	6.883	4.69E-05
IGHG3_HUMAN	Immunoglobulin heavy constant gamma 3	6.566	4.81E-05
SAP3_HUMAN	Ganglioside GM2 activator	6.539	4.76E-05
KV320_HUMAN	Immunoglobulin kappa variable 3-20	6.298	4.49E-05
IGKC_HUMAN	Immunoglobulin kappa constant	6.160	8.89E-05
KV311_HUMAN	Immunoglobulin kappa variable 3-11	6.013	5.01E-05
LV147_HUMAN	Immunoglobulin lambda variable 1-47	5.728	0.000166
CFAB_HUMAN	Complement factor B	5.724	0.000159
CO9_HUMAN	Complement component C9	5.622	0.000287
PEDF_HUMAN	Pigment epithelium-derived factor	5.598	0.000523
KV37_HUMAN	Probable non-functional immunoglobulin kappa variable 3-7	5.567	9.33E-05
CO3_HUMAN	Complement C3	5.498	0.000946
PLMN_HUMAN	Plasminogen	5.289	0.000946
ANGT_HUMAN	Angiotensinogen	5.070	0.000677
IGHG4_HUMAN	Immunoglobulin heavy constant gamma 4	4.959	0.001007
IGLL5_HUMAN	Immunoglobulin lambda-like polypeptide 5	4.652	0.001104
IGK_HUMAN	Immunoglobulin kappa light chain	4.503	0.001766
CDC5L_HUMAN	Cell division cycle 5-like protein	4.208	0.002917
HV434_HUMAN	Immunoglobulin heavy variable 4-34	4.193	0.003475
TITIN_HUMAN	Titin	4.067	0.010167
A2GL_HUMAN	Leucine-rich alpha-2-glycoprotein	3.931	0.00389
TTHY_HUMAN	Transthyretin	3.891	0.014362
A2MG_HUMAN	Alpha-2-macroglobulin	3.774	0.018408
KVD20_HUMAN	Immunoglobulin kappa variable 3D-20	3.724	0.010167
ANT3_HUMAN	Antithrombin-III	3.509	0.031479
FIBG_HUMAN	Fibrinogen gamma chain	3.359	0.039193
CBG_HUMAN	Corticosteroid-binding globulin	3.242	0.030297
Protein ID	Protein name	FC (Prog / Healt)	Adj. p-value (BH)
EGF_HUMAN	Pro-epidermal growth factor	-6.548	5.67E-05
GPC5B_HUMAN	G-protein coupled receptor family C group 5 member B	-4.532	0.001321
GTR5_HUMAN	Solute carrier family 2, facilitated glucose transporter member 5	-3.308	0.046253
RHCG_HUMAN	Ammonium transporter Rh type C	-3.151	0.045766

Supplementary table 6: miRNAs from uEVs proposed as candidate markers of different CKD types

uEV miRNA biomarkers	CKD type	Expression in CKD vs CTL	Sample size	Method of analysis	Source
miR-1225-5p	FSGS	↑ (MCD)	FSGS=16	MiRNA expression microarrays	Ramezani et al., 2015, Eur J Clin Invest
miR-1915		↓ (FSGS)	MCD=5		
miR-663	MCD				
*miR-155		↑ (FSGS)	Control=5		
miR-335	SLE	↑	SLE=28	RT-qPCR	Perez-Hernandez et al., 2015, Plos One
miR-302d					
miR-200c			Control=12		
miR-146a					
miR-26a	LN	↑	LN=13	RT-qPCR	Ichii et al., 2014, Plos One
			Control=8		
miR-3135b	LNIV	↑	Active LNIV=5	miRNA sequencing	Li, Y., et al., 2018, J Biol Res (Thessalon)
miR-654-5p	LNIV-CC	↑	Active LNIV-CC=5		
			Inactive LNIV=4		
			Control=3		
miR-21, miR-150, miR-29c	Renal fibrosis in LN	↑	LN=45	miRCURY LNA Universal RT microRNA PCR	Sole et al. 2019, Cells
			Control=20		
let-7a	LN	↓	Active LN=3	RT-qPCR	Tangtanatakul et al., 2019, Asian Pac J Allergy Immunol
*miR-21			Inactive LN=3		
*miR-194-5p	Paediatric NS	↑	NS=5 (pool of 25)	High-throughput Illumina sequencing	Chen et al., 2019, EBioMedicine
miR-146b-5p					
miR-378a-3p			Control=4 (pool of 20)		
miR-23b-3p					
*miR-30a-5p					
*miR-192-5p	ADPKD	↓	Early ADPKS=7	miRNA sequencing	Magayr et al., 2020, Kidney Int
*miR-194-5p			Late ADPKD=9		
*miR-30a-5p					
miR-30d-5p			Control=6		
miR-30e-5p					
*miR-150	IgAN	↑	IgAN=22	NanoString nCounter miRNA Expression Assay	Szeto et al., 2019, BMC Nephrology
miR-204		↓	Control=6		
miR-555					
*miR-29	Renal fibrosis	↓	CKD=32	RT-qPCR	Lv, L.L., et al., 2013, Am J Physiol Renal Physiol
miR-200			Control=7		
miR-181a	CKD pool	↓	CKD=15	Total RNA NGS	Khurana et al., 2017, RNA
			Control=10		
*miR-21	CKD pool	↑	CKD=41	RT-qPCR	Lange et al., 2019, J Cell Mol Med
			Control=5		
*miR-21-5p	CKD pool	↑	CKD=14	PCR panels	Zang et al., 2019, Sientific Reports
miR-30b-5p		↓	Diabetes=15		
miR-451	CKD pool	↑	CKD=48	RT-qPCR	Kumari et al., 2020, Front Physiol
			Control=23		

↑ - increased expression; ↓ - decreased expression; * - found in different studies; FSGS - Focal Segmental Glomerulosclerosis; MCD - minimal change disease; SLE - systemic lupus erythematosus; LN - lupus nephritis; NS - nephrotic syndrome; ADPKD - autosomal dominant polycystic kidney disease; IgAN - Immunoglobulin A nephropathy; CTL - control

Supplementary table 7: Significantly differentially expressed miRNAs from uEVs in stable DN (n=3) versus diabetic (n=2) based on Wald test p-value adjusted according to Benjamini-Hochberg. MiRNAs are sorted from the most downregulated on top

miRNA	Log$_2$ FC (Stable DN / Diabetic)	Adjusted p-value
hsa-miR-890	-9.25525	3.97E-05
hsa-miR-891b	-8.20019	0.006833
hsa-miR-888-5p	-4.43028	3.13E-05
hsa-miR-891a-5p	-3.87225	0.001323

Supplementary table 8: Significantly differentially expressed miRNAs from uEVs in stable DN (n=3) versus healthy (n=2) based on Wald test p-value adjusted according to Benjamini-Hochberg. MiRNAs are sorted from top upregulated to top downregulated

miRNA	Log$_2$ FC (Stable DN / Healthy)	Adjusted p-value
hsa-miR-23b-5p	7.344903	0.042524
hsa-miR-216a-5p	7.316232	0.045274
hsa-miR-888-5p	-3.36034	0.003515
hsa-miR-891a-5p	-3.71101	0.003515
hsa-miR-891b	-8.19614	0.026714

Supplementary table 9: Significantly differentially expressed miRNAs from uEVs in diabetic (n=2) versus healthy (n=2) based on Wald test p-value adjusted according to Benjamini-Hochberg

miRNA	Log$_2$ FC (Diabetic / Healthy)	Adjusted p-value
miR-216a-5p	8.895839	0.000342
miR-409-3p	7.574742	0.048795

A
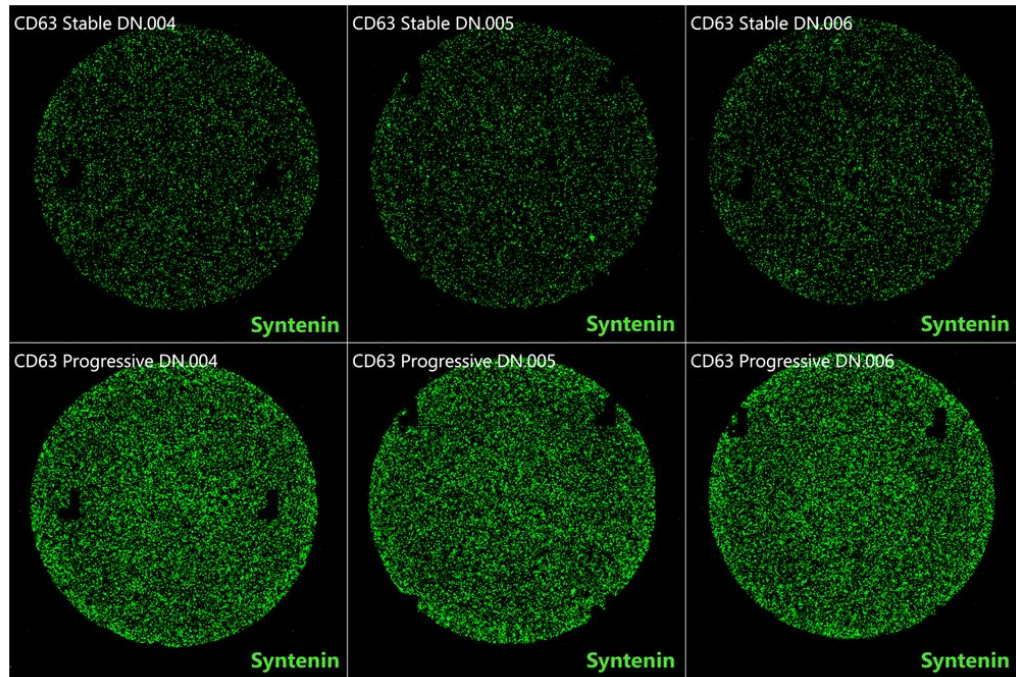
B
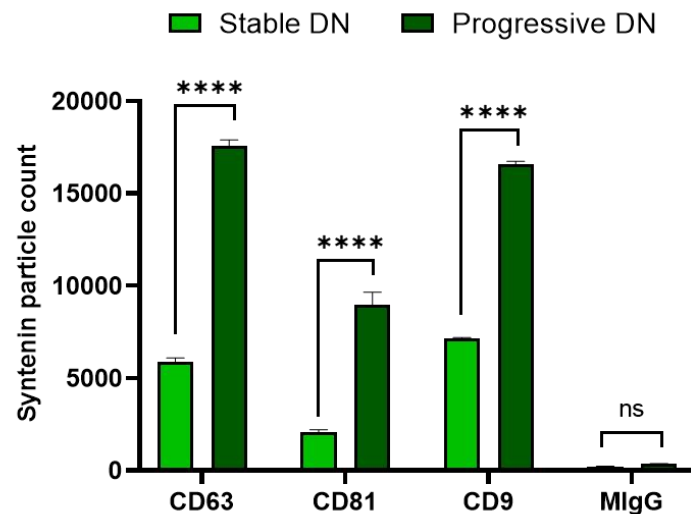
Supplementary Figure 2: Signal of intravesicular syntenin in stable DN (n=20) and progressive DN (n=20) groups showing uEVs permeabilization. Image of chips with three positions for stable DN (top row) and progressive DN (bottom row) showing vesicles captured by CD63 probe which were positive for syntenin labelled with green (A). Bar-chart showing significantly higher signal of syntenin in uEVs from progressive vs stable DN, captured by CD63, CD81, and CD9 tetraspanin, as well as very low unspecific signal from mouse IgG capture. Graph shows mean±SD (B). Figure represents one experiment, which was however repeated three independent times. Statistics: Two-way ANOVA with Sidak's multiple comparison test. ****$p < 0.0001$.

Query: Recombinant MBNL1-psiCHECK-2 plasmid, length 8868 bp
Subject: Original sequence of 3'UTR MBNL1 insert, length 2618 bp

Score:4824 bits(2612), Expect:0.0,
Identities:2617/2619(99%), Gaps:1/2619(0%), Strand: Plus/Plus

```
Query  4282   AGTTCCTCAGCCACAAGACATCCACATATTGCATGTTAACCAGAAGAAAAGACAACATTT
4341
              |||||||||||||||||||||||||||||||||||||||||||||||||||||||||||
Sbjct  1      AGTTCCTCAGCCACAAGACATCCACATATTGCATGTTAACCAGAAGAAAAGACAACATTT
60


Query  4342   TCCGGAAATCCACTGCACACTGTTGCCTATACACTTTGTACATTTAATTGATATTTGTGC
4401
              |||||||||||||||||||||||||||||||||||||||||||||||||||||||||||
Sbjct  61     TCCGGAAATCCACTGCACACTGTTGCCTATACACTTTGTACATTTAATTGATATTTGTGC
120


Query  4402   TGAGGTGATATTCCTGTCTAAAAGAACAACATTGTCTTTCTTTTCTAGCACAGAGTTATG
4461
              |||||||||||||||||||||||||||||||||||||||||||||||||||||||||||
Sbjct  121    TGAGGTGATATTCCTGTCTAAAAGAACAACATTGTCTTTCTTTTCTAGCACAGAGTTATG
180


Query  4462   CATTCAAAGATGCATACCTAGTTAGTTTCCTATATATTCATGCCATCTTGAAAAGACAGA
4521
              |||||||||||||||||||||||||||||||||||||||||||||||||||||||||||
Sbjct  181    CATTCAAAGATGCATACCTAGTTAGTTTCCTATATATTCATGCCATCTTGAAAAGACAGA
240


Query  4522   CTATGGTGTAACCATGATTCTATTATGTATTGGTACGTCTGTAGACCAAGATATAATTTT
4581
              |||||||||||||||||||||||||||||||||||||||||||||||||||||||||||
Sbjct  241    CTATGGTGTAACCATGATTCTATTATGTATTGGTACGTCTGTAGACCAAGATATAATTTT
300


Query  4582   TTAAAAATAAGTTTATTTCTTTCAAGGTTTACAAATAACAAAGGTGCACCTTGTATTTAA
4641
              |||||||||||||||||||||||||||||||||||||||||||||||||||||||||||
Sbjct  301    TTAAAAATAAGTTTATTTCTTTCAAGGTTTACAAATAACAAAGGTGCACCTTGTATTTAA
360


Query  4642   AATTGCCATTATAGATGAGAGCGTGCATGCACAGTCATTTTTGTTTAAGAGTAATATTTT
4701
              |||||||||||||||||||||||||||||||||||||||||||||||||||||||||||
Sbjct  361    AATTGCCATTATAGATGAGAGCGTGCATGCACAGTCATTTTTGTTTAAGAGTAATATTTT
420


Query  4702   TAATGTAATAGATTGTAAGACGTGGTGAGGGAGGGAT T TGACAGAGATGAATGTGCCAAG
4761
              ||||||||||||||||||||||||||||||||||||| |||||||||||||||||||||
Sbjct  421    TAATGTAATAGATTGTAAGACGTGGTGAGGGAGGGAT C TGACAGAGATGAATGTGCCAAG
480
```

```
Query  4762   CAAAACCACAACTGTGTATATTTTAAAGCACATCATGGCTTTAAGTACCATGTTGTTAAG
4821
              |||||||||||||||||||||||||||||||||||||||||||||||||||||||||||
Sbjct  481    CAAAACCACAACTGTGTATATTTTAAAGCACATCATGGCTTTAAGTACCATGTTGTTAAG
540

Query  4822   GATTCTCATGAAGTGCCATAGACTGTACATCAAATTAGAGTATTATTTCTTCAGTGTTAT
4881
              |||||||||||||||||||||||||||||||||||||||||||||||||||||||||||
Sbjct  541    GATTCTCATGAAGTGCCATAGACTGTACATCAAATTAGAGTATTATTTCTTCAGTGTTAT
600

Query  4882   TGTTTTCAGAGCCACATTTTGTTGCATATTTGCTAGTACTAATCAGTCAAAGGGCACCAT
4941
              |||||||||||||||||||||||||||||||||||||||||||||||||||||||||||
Sbjct  601    TGTTTTCAGAGCCACATTTTGTTGCATATTTGCTAGTACTAATCAGTCAAAGGGCACCAT
660

Query  4942   TCttttttttttttttttGAAACCAAAGCTGTCTCAGAAATGGCCAATTTAACTTTACAG
5001
              ||  |||||||||||||||||||||||||||||||||||||||||||||||||||||||
Sbjct  661    TC-TTTTTTTTTTTTTTTGAAACCAAAGCTGTCTCAGAAATGGCCAATTTAACTTTACAG
719

Query  5002   TAACAATAGACAGCACAACACAAACTCTCTCAATACAGATAAACTCACACATACTGGAGa
5061
              |||||||||||||||||||||||||||||||||||||||||||||||||||||||||||
Sbjct  720    TAACAATAGACAGCACAACACAAACTCTCTCAATACAGATAAACTCACACATACTGGAGA
779

Query  5062   tatatatataatagatatatataAAATTATTTTAATGCATTGTAGTGTAATATTTATGCA
5121
              |||||||||||||||||||||||||||||||||||||||||||||||||||||||||||
Sbjct  780    TATATATATAATAGATATATATAAAAATTATTTTAATGCATTGTAGTGTAATATTTATGCA
839

Query  5122   TACTATACTGTATAACATGTTATTCAAAAGGGATTGCCATTTCTGAGACACAGTAACaaa
5181
              |||||||||||||||||||||||||||||||||||||||||||||||||||||||||||
Sbjct  840    TACTATACTGTATAACATGTTATTCAAAAGGGATTGCCATTTCTGAGACACAGTAACAAA
899

Query  5182   aaaaTGAGGAAATTATTTTGCTTCTATTTATAGCCTCTGTCAAAAGTCAAAAGACTATAA
5241
              |||||||||||||||||||||||||||||||||||||||||||||||||||||||||||
Sbjct  900    AAAATGAGGAAATTATTTTGCTTCTATTTATAGCCTCTGTCAAAAGTCAAAAGACTATAA
959

Query  5242   ATGCTTTGCAAAAATGGTTTCACGTTTGCTTAAATGCTTCATCACAGTCACATTCAAAAT
5301
              |||||||||||||||||||||||||||||||||||||||||||||||||||||||||||
Sbjct  960    ATGCTTTGCAAAAATGGTTTCACGTTTGCTTAAATGCTTCATCACAGTCACATTCAAAAT
1019
```

415

```
Query  5302  AGTGACTCTAAACAAAGAAGAAAGCAGCACTGTCATCAGATGCATGATAAACCAAAATAT
5361
             ||||||||||||||||||||||||||||||||||||||||||||||||||||||||||||
Sbjct  1020  AGTGACTCTAAACAAAGAAGAAAGCAGCACTGTCATCAGATGCATGATAAACCAAAATAT
1079


Query  5362  GAAAATGGGAAATGTTTAATTAACCTAGTAATTGGGTGGGTTAAGTACATGGGTGAATTT
5421
             ||||||||||||||||||||||||||||||||||||||||||||||||||||||||||||
Sbjct  1080  GAAAATGGGAAATGTTTAATTAACCTAGTAATTGGGTGGGTTAAGTACATGGGTGAATTT
1139


Query  5422  TATATGTGAtttttgttttgttttgttttgttCAGATTAACTGCTTATAGCCTTAGAAAG
5481
             ||||||||||||||||||||||||||||||||||||||||||||||||||||||||||||
Sbjct  1140  TATATGTGATTTTTGTTTTGTTTTGTTTTGTTCAGATTAACTGCTTATAGCCTTAGAAAG
1199


Query  5482  CCTTTTACAAAATTaaaaaaaaaaTAGATGTGCATTCAGTTTTTAAGAATGGAATCATCC
5541
             ||||||||||||||||||||||||||||||||||||||||||||||||||||||||||||
Sbjct  1200  CCTTTTACAAAATTAAAAAAAAAATAGATGTGCATTCAGTTTTTAAGAATGGAATCATCC
1259


Query  5542  AAAGGAATTCCttttttttGAGGTTTGGATGTTGCAGCTAGTAAAGGATATTTTTGCTCTG
5601
             ||||||||||||||||||||||||||||||||||||||||||||||||||||||||||||
Sbjct  1260  AAAGGAATTCCTTTTTTTTGAGGTTTGGATGTTGCAGCTAGTAAAGGATATTTTTGCTCTG
1319


Query  5602  TTCAGCAGTTCTAAAAATTGCTGAAGTAGGGGCCAGGTCACTGGTAGTTATAGTATGGAA
5661
             ||||||||||||||||||||||||||||||||||||||||||||||||||||||||||||
Sbjct  1320  TTCAGCAGTTCTAAAAATTGCTGAAGTAGGGGCCAGGTCACTGGTAGTTATAGTATGGAA
1379


Query  5662  TGGGAGAAGTGAAAGTTCAGTTATAGAACTTTCCATACTTCCAAGTTTACTGCAAGTTTT
5721
             ||||||||||||||||||||||||||||||||||||||||||||||||||||||||||||
Sbjct  1380  TGGGAGAAGTGAAAGTTCAGTTATAGAACTTTCCATACTTCCAAGTTTACTGCAAGTTTT
1439


Query  5722  TATGCTTGAGAGAGATGCTTTCTAATATAAGACTGATGTGTTGATTTTACTGATTGTACT
5781
             ||||||||||||||||||||||||||||||||||||||||||||||||||||||||||||
Sbjct  1440  TATGCTTGAGAGAGATGCTTTCTAATATAAGACTGATGTGTTGATTTTACTGATTGTACT
1499


Query  5782  GTACATCTATTAAAGCCTTAGATTATTACATTACGGGTTGGAACCCATACCAATGTAATT
5841
             ||||||||||||||||||||||||||||||||||||||||||||||||||||||||||||
Sbjct  1500  GTACATCTATTAAAGCCTTAGATTATTACATTACGGGTTGGAACCCATACCAATGTAATT
1559
```

416

```
Query  5842  TCAATCGTGTTAAGAAAGTAATGGTGACTTCACATGTTATTGTAGTTAGTTACATTATAG
5901
             ||||||||||||||||||||||||||||||||||||||||||||||||||||||||||||
Sbjct  1560  TCAATCGTGTTAAGAAAGTAATGGTGACTTCACATGTTATTGTAGTTAGTTACATTATAG
1619


Query  5902  AATATTACTTATTTTTCTTGTTAAAATGTAGTTTTTCATTTCCTACATTTATTAGATTTT
5961
             ||||||||||||||||||||||||||||||||||||||||||||||||||||||||||||
Sbjct  1620  AATATTACTTATTTTTCTTGTTAAAATGTAGTTTTTCATTTCCTACATTTATTAGATTTT
1679


Query  5962  CATTTTCTATTAACAATTGAATACCATTTCAGTTTATAGACTTGTTTTATTAGATTTTAC
6021
             ||||||||||||||||||||||||||||||||||||||||||||||||||||||||||||
Sbjct  1680  CATTTTCTATTAACAATTGAATACCATTTCAGTTTATAGACTTGTTTTATTAGATTTTAC
1739


Query  6022  CAATGAATTTTTCAAAATACaaaaaaaaGTAGTTTTTCCTTCATAACATACTCAGTTTTG
6081
             ||||||||||||||||||||||||||||||||||||||||||||||||||||||||||||
Sbjct  1740  CAATGAATTTTTCAAAATACAAAAAAAAGTAGTTTTTCCTTCATAACATACTCAGTTTTG
1799


Query  6082  AATTACATGTAGTGTCACATGAATATTCGTATTGTTAACTAAATGATTTATATTTTACTG
6141
             ||||||||||||||||||||||||||||||||||||||||||||||||||||||||||||
Sbjct  1800  AATTACATGTAGTGTCACATGAATATTCGTATTGTTAACTAAATGATTTATATTTTACTG
1859


Query  6142  ATTTAATATTACAGTGTAAGAATGTCAGTCATTGTTAGTTCTTGTCTAGTTTTCATTAAA
6201
             ||||||||||||||||||||||||||||||||||||||||||||||||||||||||||||
Sbjct  1860  ATTTAATATTACAGTGTAAGAATGTCAGTCATTGTTAGTTCTTGTCTAGTTTTCATTAAA
1919


Query  6202  AGAACAAAGATCTTTTATATGGATATCTTATAAATATATAATCATTGCTAAGTAAGAAGT
6261
             ||||||||||||||||||||||||||||||||||||||||||||||||||||||||||||
Sbjct  1920  AGAACAAAGATCTTTTATATGGATATCTTATAAATATATAATCATTGCTAAGTAAGAAGT
1979


Query  6262  TAAGTTGTTGCTATCGCAACAATCCTGGCAGACAATTGAGTAATATTTTGATGATTTATT
6321
             ||||||||||||||||||||||||||||||||||||||||||||||||||||||||||||
Sbjct  1980  TAAGTTGTTGCTATCGCAACAATCCTGGCAGACAATTGAGTAATATTTTGATGATTTATT
2039


Query  6322  TTGTTTGTAATTAGTTATTATAAGAAGATCTAGATCCTAGATATTAGAATAAAATTTATT
6381
             ||||||||||||||||||||||||||||||||||||||||||||||||||||||||||||
Sbjct  2040  TTGTTTGTAATTAGTTATTATAAGAAGATCTAGATCCTAGATATTAGAATAAAATTTATT
2099
```

417

```
Query  6382   TTCTACTGTATCCATTTCAAATGTTAAAATATTGTTTAATATTTTTGAAATCCCTGAGTA
6441
              ||||||||||||||||||||||||||||||||||||||||||||||||||||||||||||
Sbjct  2100   TTCTACTGTATCCATTTCAAATGTTAAAATATTGTTTAATATTTTTGAAATCCCTGAGTA
2159


Query  6442   TCAGGCCTTGTTATAAATAAGCTGCATAATCAATAAATAGAACAAGGGACTTTTTGTTGA
6501
              ||||||||||||||||||||||||||||||||||||||||||||||||||||||||||||
Sbjct  2160   TCAGGCCTTGTTATAAATAAGCTGCATAATCAATAAATAGAACAAGGGACTTTTTGTTGA
2219


Query  6502   TAATCCAAATACTCAAAGTTTACGTAATGAAAATTATAGCGTGTGTGCAAACTCTTGAGG
6561
              ||||||||||||||||||||||||||||||||||||||||||||||||||||||||||||
Sbjct  2220   TAATCCAAATACTCAAAGTTTACGTAATGAAAATTATAGCGTGTGTGCAAACTCTTGAGG
2279


Query  6562   GTTGATTATGCTGCAATTTAGCATGTTGGAACGTCTAGGGAGAAGGTTGACTTTTTGCAC
6621
              ||||||||||||||||||||||||||||||||||||||||||||||||||||||||||||
Sbjct  2280   GTTGATTATGCTGCAATTTAGCATGTTGGAACGTCTAGGGAGAAGGTTGACTTTTTGCAC
2339


Query  6622   TTCTGTATATAGTCAAAAGAGAGAAACCTGTATAATAGTAAGATCTTATTTTGAATAAAA
6681
              ||||||||||||||||||||||||||||||||||||||||||||||||||||||||||||
Sbjct  2340   TTCTGTATATAGTCAAAAGAGAGAAACCTGTATAATAGTAAGATCTTATTTTGAATAAAA
2399


Query  6682   ACGTCTATAATTACAAGGAGTTTTGTTAAGGCTAATACAATGACAGACTGAGCAAAATTG
6741
              ||||||||||||||||||||||||||||||||||||||||||||||||||||||||||||
Sbjct  2400   ACGTCTATAATTACAAGGAGTTTTGTTAAGGCTAATACAATGACAGACTGAGCAAAATTG
2459


Query  6742   CTTGCAAAAGTGGCACAGAGTTAGCACTCCATACCCCTTCAAACATGTTGCTTTGCTTTC
6801
              ||||||||||||||||||||||||||||||||||||||||||||||||||||||||||||
Sbjct  2460   CTTGCAAAAGTGGCACAGAGTTAGCACTCCATACCCCTTCAAACATGTTGCTTTGCTTTC
2519


Query  6802   TTGTGGACAGCTTGTAGTTTGCCAGGATTTTTTCAGCTGGAAAGATACGCCATCCTTTCA
6861
              ||||||||||||||||||||||||||||||||||||||||||||||||||||||||||||
Sbjct  2520   TTGTGGACAGCTTGTAGTTTGCCAGGATTTTTTCAGCTGGAAAGATACGCCATCCTTTCA
2579


Query  6862   AACCCTCATGACTGACAAAAACTCCATGGGGCCAAATCT   6900
              |||||||||||||||||||||||||||||||||||||||
Sbjct  2580   AACCCTCATGACTGACAAAAACTCCATGGGGCCAAATCT   2618
```

Supplementary Figure 3: Full sequence alignment of recombinant plasmid (MBNL1-psiCHECK-2) against 3'UTR MBNL1 insert. Two mutations are highlighted in blue. Alignment analysis was done in BLASTN NCBI.

Query: Recombinant MBNL1-psiCHECK-2 plasmid, length: 8868
Subject: Original sequence of psiCHECK-2 plasmid, length: 6273

Score:7906 bits(4281), Expect:0.0,
Identities:4281/4281(100%), Gaps:0/4281(0%), Strand: Plus/Minus

```
Query  1     GTGCACGAACCCCCCGTTCAGCCCGACCGCTGCGCCTTATCCGGTAACTATCGTCTTGAG
60
             ||||||||||||||||||||||||||||||||||||||||||||||||||||||||||||
Sbjct  5953  GTGCACGAACCCCCCGTTCAGCCCGACCGCTGCGCCTTATCCGGTAACTATCGTCTTGAG
5894


Query  61    TCCAACCCGGTAAGACACGACTTATCGCCACTGGCAGCAGCCACTGGTAACAGGATTAGC
120
             ||||||||||||||||||||||||||||||||||||||||||||||||||||||||||||
Sbjct  5893  TCCAACCCGGTAAGACACGACTTATCGCCACTGGCAGCAGCCACTGGTAACAGGATTAGC
5834


Query  121   AGAGCGAGGTATGTAGGCGGTGCTACAGAGTTCTTGAAGTGGTGGCCTAACTACGGCTAC
180
             ||||||||||||||||||||||||||||||||||||||||||||||||||||||||||||
Sbjct  5833  AGAGCGAGGTATGTAGGCGGTGCTACAGAGTTCTTGAAGTGGTGGCCTAACTACGGCTAC
5774


Query  181   ACTAGAAGAACAGTATTTGGTATCTGCGCTCTGCTGAAGCCAGTTACCTTCGGAAAAAGA
240
             ||||||||||||||||||||||||||||||||||||||||||||||||||||||||||||
Sbjct  5773  ACTAGAAGAACAGTATTTGGTATCTGCGCTCTGCTGAAGCCAGTTACCTTCGGAAAAAGA
5714


Query  241   GTTGGTAGCTCTTGATCCGGCAAACAAACCACCGCTGGTAGCGGTGGtttttttGTTTGC
300
             ||||||||||||||||||||||||||||||||||||||||||||||||||||||||||||
Sbjct  5713  GTTGGTAGCTCTTGATCCGGCAAACAAACCACCGCTGGTAGCGGTGGTTTTTTTGTTTGC
5654


Query  301   AAGCAGCAGATTACGCGCAGaaaaaaaGGATCTCAAGAAGATCCTTTGATCTTTTCTACG
360
             ||||||||||||||||||||||||||||||||||||||||||||||||||||||||||||
Sbjct  5653  AAGCAGCAGATTACGCGCAGAAAAAAAGGATCTCAAGAAGATCCTTTGATCTTTTCTACG
5594


Query  361   GGGTCTGACGCTCAGTGGAACGAAAACTCACGTTAAGGGATTTTGGTCATGAGATTATCA
420
             ||||||||||||||||||||||||||||||||||||||||||||||||||||||||||||
Sbjct  5593  GGGTCTGACGCTCAGTGGAACGAAAACTCACGTTAAGGGATTTTGGTCATGAGATTATCA
5534


Query  421   AAAAGGATCTTCACCTAGATCCTTTTAAATTAAAAATGAAGTTTTAAATCAATCTAAAGT
480
             ||||||||||||||||||||||||||||||||||||||||||||||||||||||||||||
Sbjct  5533  AAAAGGATCTTCACCTAGATCCTTTTAAATTAAAAATGAAGTTTTAAATCAATCTAAAGT
5474
```

```
Query   481    ATATATGAGTAAACTTGGTCTGACAGTTACCAATGCTTAATCAGTGAGGCACCTATCTCA
540
               ||||||||||||||||||||||||||||||||||||||||||||||||||||||||||||
Sbjct   5473   ATATATGAGTAAACTTGGTCTGACAGTTACCAATGCTTAATCAGTGAGGCACCTATCTCA
5414


Query   541    GCGATCTGTCTATTTCGTTCATCCATAGTTGCCTGACTCCCCGTCGTGTAGATAACTACG
600
               ||||||||||||||||||||||||||||||||||||||||||||||||||||||||||||
Sbjct   5413   GCGATCTGTCTATTTCGTTCATCCATAGTTGCCTGACTCCCCGTCGTGTAGATAACTACG
5354


Query   601    ATACGGGAGGGCTTACCATCTGGCCCCAGTGCTGCAATGATACCGCGAGACCCACGCTCA
660
               ||||||||||||||||||||||||||||||||||||||||||||||||||||||||||||
Sbjct   5353   ATACGGGAGGGCTTACCATCTGGCCCCAGTGCTGCAATGATACCGCGAGACCCACGCTCA
5294


Query   661    CCGGCTCCAGATTTATCAGCAATAAACCAGCCAGCCGGAAGGGCCGAGCGCAGAAGTGGT
720
               ||||||||||||||||||||||||||||||||||||||||||||||||||||||||||||
Sbjct   5293   CCGGCTCCAGATTTATCAGCAATAAACCAGCCAGCCGGAAGGGCCGAGCGCAGAAGTGGT
5234


Query   721    CCTGCAACTTTATCCGCCTCCATCCAGTCTATTAATTGTTGCCGGGAAGCTAGAGTAAGT
780
               ||||||||||||||||||||||||||||||||||||||||||||||||||||||||||||
Sbjct   5233   CCTGCAACTTTATCCGCCTCCATCCAGTCTATTAATTGTTGCCGGGAAGCTAGAGTAAGT
5174


Query   781    AGTTCGCCAGTTAATAGTTTGCGCAACGTTGTTGCCATTGCTACAGGCATCGTGGTGTCA
840
               ||||||||||||||||||||||||||||||||||||||||||||||||||||||||||||
Sbjct   5173   AGTTCGCCAGTTAATAGTTTGCGCAACGTTGTTGCCATTGCTACAGGCATCGTGGTGTCA
5114


Query   841    CGCTCGTCGTTTGGTATGGCTTCATTCAGCTCCGGTTCCCAACGATCAAGGCGAGTTACA
900
               ||||||||||||||||||||||||||||||||||||||||||||||||||||||||||||
Sbjct   5113   CGCTCGTCGTTTGGTATGGCTTCATTCAGCTCCGGTTCCCAACGATCAAGGCGAGTTACA
5054


Query   901    TGATCCCCCATGTTGTGCAAAAAAGCGGTTAGCTCCTTCGGTCCTCCGATCGTTGTCAGA
960
               ||||||||||||||||||||||||||||||||||||||||||||||||||||||||||||
Sbjct   5053   TGATCCCCCATGTTGTGCAAAAAAGCGGTTAGCTCCTTCGGTCCTCCGATCGTTGTCAGA
4994


Query   961    AGTAAGTTGGCCGCAGTGTTATCACTCATGGTTATGGCAGCACTGCATAATTCTCTTACT
1020
               ||||||||||||||||||||||||||||||||||||||||||||||||||||||||||||
Sbjct   4993   AGTAAGTTGGCCGCAGTGTTATCACTCATGGTTATGGCAGCACTGCATAATTCTCTTACT
4934
```

```
Query  1021   GTCATGCCATCCGTAAGATGCTTTTCTGTGACTGGTGAGTACTCAACCAAGTCATTCTGA
1080
              ||||||||||||||||||||||||||||||||||||||||||||||||||||||||||||
Sbjct  4933   GTCATGCCATCCGTAAGATGCTTTTCTGTGACTGGTGAGTACTCAACCAAGTCATTCTGA
4874


Query  1081   GAATAGTGTATGCGGCGACCGAGTTGCTCTTGCCCGGCGTCAATACGGGATAATACCGCG
1140
              ||||||||||||||||||||||||||||||||||||||||||||||||||||||||||||
Sbjct  4873   GAATAGTGTATGCGGCGACCGAGTTGCTCTTGCCCGGCGTCAATACGGGATAATACCGCG
4814


Query  1141   CCACATAGCAGAACTTTAAAAGTGCTCATCATTGGAAAACGTTCTTCGGGGCGAAAACTC
1200
              ||||||||||||||||||||||||||||||||||||||||||||||||||||||||||||
Sbjct  4813   CCACATAGCAGAACTTTAAAAGTGCTCATCATTGGAAAACGTTCTTCGGGGCGAAAACTC
4754


Query  1201   TCAAGGATCTTACCGCTGTTGAGATCCAGTTCGATGTAACCCACTCGTGCACCCAACTGA
1260
              ||||||||||||||||||||||||||||||||||||||||||||||||||||||||||||
Sbjct  4753   TCAAGGATCTTACCGCTGTTGAGATCCAGTTCGATGTAACCCACTCGTGCACCCAACTGA
4694


Query  1261   TCTTCAGCATCTTTTACTTTCACCAGCGTTTCTGGGTGAGCAAAAACAGGAAGGCAAAAT
1320
              ||||||||||||||||||||||||||||||||||||||||||||||||||||||||||||
Sbjct  4693   TCTTCAGCATCTTTTACTTTCACCAGCGTTTCTGGGTGAGCAAAAACAGGAAGGCAAAAT
4634


Query  1321   GCCGCAAAAAAGGGAATAAGGGCGACACGGAAATGTTGAATACTCATACTCTTCCTTTTT
1380
              ||||||||||||||||||||||||||||||||||||||||||||||||||||||||||||
Sbjct  4633   GCCGCAAAAAAGGGAATAAGGGCGACACGGAAATGTTGAATACTCATACTCTTCCTTTTT
4574


Query  1381   CAATATTATTGAAGCATTTATCAGGGTTATTGTCTCATGAGCGGATACATATTTGAATGT
1440
              ||||||||||||||||||||||||||||||||||||||||||||||||||||||||||||
Sbjct  4573   CAATATTATTGAAGCATTTATCAGGGTTATTGTCTCATGAGCGGATACATATTTGAATGT
4514


Query  1441   ATTTAGAAAAATAAACAAATAGGGGTTCCGCGCACATTTCCCCGAAAAGTGCCACCTGGA
1500
              ||||||||||||||||||||||||||||||||||||||||||||||||||||||||||||
Sbjct  4513   ATTTAGAAAAATAAACAAATAGGGGTTCCGCGCACATTTCCCCGAAAAGTGCCACCTGGA
4454


Query  1501   TCCTTATCGATTTTACCACATTTGTAGAGGTTTTACTTGCTTTAAAAAACCTCCCACACC
1560
              ||||||||||||||||||||||||||||||||||||||||||||||||||||||||||||
Sbjct  4453   TCCTTATCGATTTTACCACATTTGTAGAGGTTTTACTTGCTTTAAAAAACCTCCCACACC
4394
```

```
Query  1561  TCCCCCTGAACCTGAAACATAAAATGAATGCAATTGTTGTTGTTAACTTGTTTATTGCAG
1620
             ||||||||||||||||||||||||||||||||||||||||||||||||||||||||||||
Sbjct  4393  TCCCCCTGAACCTGAAACATAAAATGAATGCAATTGTTGTTGTTAACTTGTTTATTGCAG
4334

Query  1621  CTTATAATGGTTACAAATAAAGCAATAGCATCACAAATTTCACAAATAAAGCAtttttttt
1680
             ||||||||||||||||||||||||||||||||||||||||||||||||||||||||||||
Sbjct  4333  CTTATAATGGTTACAAATAAAGCAATAGCATCACAAATTTCACAAATAAAGCATTTTTTT
4274

Query  1681  CACTGCATTCTAGTTGTGGTTTGTCCAAACTCATCAATGTATCTTATCATGTCTGCTCGA
1740
             ||||||||||||||||||||||||||||||||||||||||||||||||||||||||||||
Sbjct  4273  CACTGCATTCTAGTTGTGGTTTGTCCAAACTCATCAATGTATCTTATCATGTCTGCTCGA
4214

Query  1741  AGCGGCCGGCCGCCCCGACTCTAGAATTATTACACGGCGATCTTGCCGCCTTTCTTAGCC
1800
             ||||||||||||||||||||||||||||||||||||||||||||||||||||||||||||
Sbjct  4213  AGCGGCCGGCCGCCCCGACTCTAGAATTATTACACGGCGATCTTGCCGCCTTTCTTAGCC
4154

Query  1801  TTGATCAGGATCTCGCGGATCTTGCGGGCGTCCAGCTTGCCGGTCAGGCCCTTGGGCACC
1860
             ||||||||||||||||||||||||||||||||||||||||||||||||||||||||||||
Sbjct  4153  TTGATCAGGATCTCGCGGATCTTGCGGGCGTCCAGCTTGCCGGTCAGGCCCTTGGGCACC
4094

Query  1861  TCGTCCACGAACACCACTCCGCCGCGCAGCTTCTTGGCGGTTGTCACCTGGCTGGCCACA
1920
             ||||||||||||||||||||||||||||||||||||||||||||||||||||||||||||
Sbjct  4093  TCGTCCACGAACACCACTCCGCCGCGCAGCTTCTTGGCGGTTGTCACCTGGCTGGCCACA
4034

Query  1921  TAGTCCACGATCTCCTTCTCGGTCATGGTCTTGCCGTGTTCCAGCACGACGACGGCGGCA
1980
             ||||||||||||||||||||||||||||||||||||||||||||||||||||||||||||
Sbjct  4033  TAGTCCACGATCTCCTTCTCGGTCATGGTCTTGCCGTGTTCCAGCACGACGACGGCGGCA
3974

Query  1981  GGCAGCTCGCCGGCATCGTCGTCGGGCAGGCCGGCCACTCCGGCGTCGAAAATGTTAGGG
2040
             ||||||||||||||||||||||||||||||||||||||||||||||||||||||||||||
Sbjct  3973  GGCAGCTCGCCGGCATCGTCGTCGGGCAGGCCGGCCACTCCGGCGTCGAAAATGTTAGGG
3914

Query  2041  TGCTGCAGCAGGATAGACTCCAGCTCGGCTGGGGCCACCTGGTAGCCCTTGTACTTGATC
2100
             ||||||||||||||||||||||||||||||||||||||||||||||||||||||||||||
Sbjct  3913  TGCTGCAGCAGGATAGACTCCAGCTCGGCTGGGGCCACCTGGTAGCCCTTGTACTTGATC
3854
```

```
Query  2101  AGAGACTTCAGGCGGTCCACGATGAAGAAGTGCTCGTCCTCGTCCCAGTAGGCAATGTCG
2160
             ||||||||||||||||||||||||||||||||||||||||||||||||||||||||||||
Sbjct  3853  AGAGACTTCAGGCGGTCCACGATGAAGAAGTGCTCGTCCTCGTCCCAGTAGGCAATGTCG
3794


Query  2161  CCAGAGTGCAGCCAGCCGTCCTTGTCGATCAGGGCGTTTGTGGCCTCAGGGTTATTCACG
2220
             ||||||||||||||||||||||||||||||||||||||||||||||||||||||||||||
Sbjct  3793  CCAGAGTGCAGCCAGCCGTCCTTGTCGATCAGGGCGTTTGTGGCCTCAGGGTTATTCACG
3734


Query  2221  TAGCCGGACATAATCATAGGGCCGCGCACACACAGCTCGCCGCGCTGGTTCACTCCCAGG
2280
             ||||||||||||||||||||||||||||||||||||||||||||||||||||||||||||
Sbjct  3733  TAGCCGGACATAATCATAGGGCCGCGCACACACAGCTCGCCGCGCTGGTTCACTCCCAGG
3674


Query  2281  GTCTTGCCGGTGTCCAGGTCCACCACCTTGGCCTCGAAGAATGGCACCACCTTGCCCACG
2340
             ||||||||||||||||||||||||||||||||||||||||||||||||||||||||||||
Sbjct  3673  GTCTTGCCGGTGTCCAGGTCCACCACCTTGGCCTCGAAGAATGGCACCACCTTGCCCACG
3614


Query  2341  GCGCCAGGCTTGTCGTCGCCCTCTGGGGTAATCAGAATGGCGCTGGTTGTCTCGGTCAGG
2400
             ||||||||||||||||||||||||||||||||||||||||||||||||||||||||||||
Sbjct  3613  GCGCCAGGCTTGTCGTCGCCCTCTGGGGTAATCAGAATGGCGCTGGTTGTCTCGGTCAGG
3554


Query  2401  CCGTAGCCCTGGCGGATGCCTGGCAGATGAAAGCGCTTGGCCACGGCTTCGCCCACCTCC
2460
             ||||||||||||||||||||||||||||||||||||||||||||||||||||||||||||
Sbjct  3553  CCGTAGCCCTGGCGGATGCCTGGCAGATGAAAGCGCTTGGCCACGGCTTCGCCCACCTCC
3494


Query  2461  TTAGACAGTGGGGCGCCGCCAGAGGCAATCTCGTGCAGGTTAGACAGGTCGTACTTGTCG
2520
             ||||||||||||||||||||||||||||||||||||||||||||||||||||||||||||
Sbjct  3493  TTAGACAGTGGGGCGCCGCCAGAGGCAATCTCGTGCAGGTTAGACAGGTCGTACTTGTCG
3434


Query  2521  ATCAGGGTGCTCTTAGCGAAGAAGCTGAACAGGGTTGGCACCAGCAGGGCAGACTGAATT
2580
             ||||||||||||||||||||||||||||||||||||||||||||||||||||||||||||
Sbjct  3433  ATCAGGGTGCTCTTAGCGAAGAAGCTGAACAGGGTTGGCACCAGCAGGGCAGACTGAATT
3374


Query  2581  TTGTAGTCTTGCAGGCTGCGCAGGAACAGCTCCTCCTCGAAGCGGTACATCAGCACCACC
2640
             ||||||||||||||||||||||||||||||||||||||||||||||||||||||||||||
Sbjct  3373  TTGTAGTCTTGCAGGCTGCGCAGGAACAGCTCCTCCTCGAAGCGGTACATCAGCACCACC
3314
```

```
Query  2641  CGAAAGCCGCAAATCAGGTAGCCCAGGGTGGTGAACATGCCGAAGCCGTGGTGGAATGGC
2700

             ||||||||||||||||||||||||||||||||||||||||||||||||||||||||||||
Sbjct  3313  CGAAAGCCGCAAATCAGGTAGCCCAGGGTGGTGAACATGCCGAAGCCGTGGTGGAATGGC
3254


Query  2701  ACCACGCTCAGAATAGCGGTGTCGGGGATGATCTGGTTGCCGAAAATAGGGTCGCGGGCG
2760

             ||||||||||||||||||||||||||||||||||||||||||||||||||||||||||||
Sbjct  3253  ACCACGCTCAGAATAGCGGTGTCGGGGATGATCTGGTTGCCGAAAATAGGGTCGCGGGCG
3194


Query  2761  TGAGAGAAGCGCACACAGGCGGTGCGATGAGGCAGGGCCACGCCCTTAGGCAGGCCGGTA
2820

             ||||||||||||||||||||||||||||||||||||||||||||||||||||||||||||
Sbjct  3193  TGAGAGAAGCGCACACAGGCGGTGCGATGAGGCAGGGCCACGCCCTTAGGCAGGCCGGTA
3134


Query  2821  GACCCAGAGCTGTTCATGATCAGGGCAATGGTTTTGTCCCTGTCGAAAGACTCTGGCACG
2880

             ||||||||||||||||||||||||||||||||||||||||||||||||||||||||||||
Sbjct  3133  GACCCAGAGCTGTTCATGATCAGGGCAATGGTTTTGTCCCTGTCGAAAGACTCTGGCACG
3074


Query  2881  AAGTCGTACTCGTTGAAGCCAGGAGGCAGATGAGATGTCACGAATGTGTACATGCTCTGG
2940

             ||||||||||||||||||||||||||||||||||||||||||||||||||||||||||||
Sbjct  3073  AAGTCGTACTCGTTGAAGCCAGGAGGCAGATGAGATGTCACGAATGTGTACATGCTCTGG
3014


Query  2941  AAGCCCTGGTAGTCGGTCTTAGAGTCCATGATGATGATCTTCTGGATGATAGGCAGCTTC
3000

             ||||||||||||||||||||||||||||||||||||||||||||||||||||||||||||
Sbjct  3013  AAGCCCTGGTAGTCGGTCTTAGAGTCCATGATGATGATCTTCTGGATGATAGGCAGCTTC
2954


Query  3001  TTCTGCACGTTCAGGATCTTCTGCAGGCCCTTCTTAGACACGAACACCACGGTAGGCTGA
3060

             ||||||||||||||||||||||||||||||||||||||||||||||||||||||||||||
Sbjct  2953  TTCTGCACGTTCAGGATCTTCTGCAGGCCCTTCTTAGACACGAACACCACGGTAGGCTGA
2894


Query  3061  GAAATGCCCATGCTGTTCAGCAGCTCGCGCTCGTTGTAAATGTCGTTAGCAGGGGCCACG
3120

             ||||||||||||||||||||||||||||||||||||||||||||||||||||||||||||
Sbjct  2893  GAAATGCCCATGCTGTTCAGCAGCTCGCGCTCGTTGTAAATGTCGTTAGCAGGGGCCACG
2834


Query  3121  GCCACTCCGATGAACAGGGCGCCCAGCACTGGCATGAAGAACTGCAGAGAGTTCTCAGAG
3180

             ||||||||||||||||||||||||||||||||||||||||||||||||||||||||||||
Sbjct  2833  GCCACTCCGATGAACAGGGCGCCCAGCACTGGCATGAAGAACTGCAGAGAGTTCTCAGAG
2774
```

```
Query  3181   CACACCACGATGCGGTGGTTGGTGTTCAGGCCGTACCTCTTCATGGCCTCGGCCAGGCGC
3240
              ||||||||||||||||||||||||||||||||||||||||||||||||||||||||||||
Sbjct  2773   CACACCACGATGCGGTGGTTGGTGTTCAGGCCGTACCTCTTCATGGCCTCGGCCAGGCGC
2714


Query  3241   ACAGACATCTCGAAGTACTCGGCATAGGTGATGTCCACCTCAATGTGGGCATCGGTGAAG
3300
              ||||||||||||||||||||||||||||||||||||||||||||||||||||||||||||
Sbjct  2713   ACAGACATCTCGAAGTACTCGGCATAGGTGATGTCCACCTCAATGTGGGCATCGGTGAAG
2654


Query  3301   GCAATGGTGCCAGGCACCAGGGCATACCTCTTCATGGCCTTGTGCAGCTGCTCGCCAGCG
3360
              ||||||||||||||||||||||||||||||||||||||||||||||||||||||||||||
Sbjct  2653   GCAATGGTGCCAGGCACCAGGGCATACCTCTTCATGGCCTTGTGCAGCTGCTCGCCAGCG
2594


Query  3361   GTGCCATCCTCCAGAGGGTAGAAGGGAGCAGGGCCCTTCTTAATGTTCTTAGCATCGGCC
3420
              ||||||||||||||||||||||||||||||||||||||||||||||||||||||||||||
Sbjct  2593   GTGCCATCCTCCAGAGGGTAGAAGGGAGCAGGGCCCTTCTTAATGTTCTTAGCATCGGCC
2534


Query  3421   ATGGTGGCTTTACCAACAGTACCGGAATGCCAAGCTTTTAAGCGGGTCGCTGCAGGGTCG
3480
              ||||||||||||||||||||||||||||||||||||||||||||||||||||||||||||
Sbjct  2533   ATGGTGGCTTTACCAACAGTACCGGAATGCCAAGCTTTTAAGCGGGTCGCTGCAGGGTCG
2474


Query  3481   CTCGGTGTTCGAGGCCACACGCGTCACCTTAATATGCGAAGTGGACCTGGGACCGCGCCG
3540
              ||||||||||||||||||||||||||||||||||||||||||||||||||||||||||||
Sbjct  2473   CTCGGTGTTCGAGGCCACACGCGTCACCTTAATATGCGAAGTGGACCTGGGACCGCGCCG
2414


Query  3541   CCCCGACTGCATCTGCGTGTTCGAATTCGCCAATGACAAGACGCTGGGCGGGGTTTGTGT
3600
              |||||||||||||||||||||||||||||||||||||||||||||||||||||||||||
Sbjct  2413   CCCCGACTGCATCTGCGTGTTCGAATTCGCCAATGACAAGACGCTGGGCGGGGTTTGTGT
2354


Query  3601   CATCATAGAACTAAAGACATGCAAATATATTTCTTCCGGGGACACCGCCAGCAAACGCGA
3660
              ||||||||||||||||||||||||||||||||||||||||||||||||||||||||||||
Sbjct  2353   CATCATAGAACTAAAGACATGCAAATATATTTCTTCCGGGGACACCGCCAGCAAACGCGA
2294


Query  3661   GCAACGGGCCACGGGGATGAAGCAGCTGCGCCACTCCCTGAAGCTCCTGCAGTCCCTCGC
3720
              ||||||||||||||||||||||||||||||||||||||||||||||||||||||||||||
Sbjct  2293   GCAACGGGCCACGGGGATGAAGCAGCTGCGCCACTCCCTGAAGCTCCTGCAGTCCCTCGC
2234
```

425

```
Query  3721   GCCTCCGGGTGACAAGATAGTGTACCTGTGCCCCGTCCTGGTGTTTGTCGCCCAACGGAC
3780

              ||||||||||||||||||||||||||||||||||||||||||||||||||||||||||||
Sbjct  2233   GCCTCCGGGTGACAAGATAGTGTACCTGTGCCCCGTCCTGGTGTTTGTCGCCCAACGGAC
2174


Query  3781   GCTCCGCGTCAGCCGCGTGACCCGGCTCGTCCCGCAGAAGGTCTCCGGTAATATCACCGC
3840

              ||||||||||||||||||||||||||||||||||||||||||||||||||||||||||||
Sbjct  2173   GCTCCGCGTCAGCCGCGTGACCCGGCTCGTCCCGCAGAAGGTCTCCGGTAATATCACCGC
2114


Query  3841   AGTCGTGCGGATGCTCCAGAGCCTGTCCACGTATACGGTCCCCATGGAGCCTAGGACCCA
3900

              ||||||||||||||||||||||||||||||||||||||||||||||||||||||||||||
Sbjct  2113   AGTCGTGCGGATGCTCCAGAGCCTGTCCACGTATACGGTCCCCATGGAGCCTAGGACCCA
2054


Query  3901   GCGAGCCCGTCGCCGCCGCGGCGGCGCCGCCCGGGGGTCTGCGAGCAGACCGAAAAGGTC
3960

              ||||||||||||||||||||||||||||||||||||||||||||||||||||||||||||
Sbjct  2053   GCGAGCCCGTCGCCGCCGCGGCGGCGCCGCCCGGGGGTCTGCGAGCAGACCGAAAAGGTC
1994


Query  3961   ACACTCTGGGGCGCGCGACCCGCCCGAGTCAGCGGCCCGCCAGTTACCACCCGCCGACCA
4020

              ||||||||||||||||||||||||||||||||||||||||||||||||||||||||||||
Sbjct  1993   ACACTCTGGGGCGCGCGACCCGCCCGAGTCAGCGGCCCGCCAGTTACCACCCGCCGACCA
1934


Query  4021   AACCCCCGCCTCCACGGAGGGCgggggggTGCTTAAGAGGATCGCGGCGCTCTTCTGCGT
4080

              ||||||||||||||||||||||||||||||||||||||||||||||||||||||||||||
Sbjct  1933   AACCCCCGCCTCCACGGAGGGCGGGGGGGGTGCTTAAGAGGATCGCGGCGCTCTTCTGCGT
1874


Query  4081   GCCCGTGGCCACCAAGACCAAACCCCGAGCCGCCTCCGAATGAGAGTGTTTCGTTCCTTc
4140

              ||||||||||||||||||||||||||||||||||||||||||||||||||||||||||||
Sbjct  1873   GCCCGTGGCCACCAAGACCAAACCCCGAGCCGCCTCCGAATGAGAGTGTTTCGTTCCTTC
1814


Query  4141   cccctcccccccGCGTCAGACAAACCCTAACCACCGCTTAAGCGGCCCCCGCGAGGTCCGA
4200

              ||||||||||||||||||||||||||||||||||||||||||||||||||||||||||||
Sbjct  1813   CCCCTCCCCCCCGCGTCAGACAAACCCTAACCACCGCTTAAGCGGCCCCCGCGAGGTCCGA
1754


Query  4201   AGACTCATTTAGATCCTCACACAAAAAACCAACACACAGATGTAATGAAAATAAAGATAT
4260

              ||||||||||||||||||||||||||||||||||||||||||||||||||||||||||||
Sbjct  1753   AGACTCATTTAGATCCTCACACAAAAAACCAACACACAGATGTAATGAAAATAAAGATAT
1694
```

```
Query  4261  TTTATTGCGGCCAGCGGCCGC  4281
             |||||||||||||||||||||
Sbjct  1693  TTTATTGCGGCCAGCGGCCGC  1673
```

Range 2: 1 to 1648

Score:3044 bits(1648), Expect:0.0,
Identities:1648/1648(100%), Gaps:0/1648(0%), Strand: Plus/Minus

```
Query  6901  CTCGAGCGATCGCCTAGAATTACTGCTCGTTCTTCAGCACGCGCTCCACGAAGCTCTTGA
6960
             ||||||||||||||||||||||||||||||||||||||||||||||||||||||||||||
Sbjct  1648  CTCGAGCGATCGCCTAGAATTACTGCTCGTTCTTCAGCACGCGCTCCACGAAGCTCTTGA
1589

Query  6961  TGTACTTACCCATTTCATCTGGAGCGTCCTCCTGGCTGAAGTGGAGGCCCTTCACCTTCA
7020
             ||||||||||||||||||||||||||||||||||||||||||||||||||||||||||||
Sbjct  1588  TGTACTTACCCATTTCATCTGGAGCGTCCTCCTGGCTGAAGTGGAGGCCCTTCACCTTCA
1529

Query  7021  CGAACTCGGTGTTAGGGAACTTCTTAGCTCCCTCGACAATAGCGTTGGAAAAGAACCCAG
7080
             ||||||||||||||||||||||||||||||||||||||||||||||||||||||||||||
Sbjct  1528  CGAACTCGGTGTTAGGGAACTTCTTAGCTCCCTCGACAATAGCGTTGGAAAAGAACCCAG
1469

Query  7081  GGTCGGACTCGATGAACATCTTAGGCAGATCGTCGCTGGCCCGAAGGTAGGCGTTGTAGT
7140
             ||||||||||||||||||||||||||||||||||||||||||||||||||||||||||||
Sbjct  1468  GGTCGGACTCGATGAACATCTTAGGCAGATCGTCGCTGGCCCGAAGGTAGGCGTTGTAGT
1409

Query  7141  TGCGGACAATCTGGACGACGTCGGGCTTGCCTCCCTTAACGAGAGGGATCTCGCGAGGCC
7200
             ||||||||||||||||||||||||||||||||||||||||||||||||||||||||||||
Sbjct  1408  TGCGGACAATCTGGACGACGTCGGGCTTGCCTCCCTTAACGAGAGGGATCTCGCGAGGCC
1349

Query  7201  AGGAGAGGGTAGGCCGTCTAACCTCGCCCTTCTCCTTGAATGGCTCCAGGTAGGCAGCGA
7260
             ||||||||||||||||||||||||||||||||||||||||||||||||||||||||||||
Sbjct  1348  AGGAGAGGGTAGGCCGTCTAACCTCGCCCTTCTCCTTGAATGGCTCCAGGTAGGCAGCGA
1289

Query  7261  ACTCCTCAGGCTCCAGTTTCCGCATGATCTTGCTTGGGAGCATGGTCTCGACGAAGAAGT
7320
             ||||||||||||||||||||||||||||||||||||||||||||||||||||||||||||
Sbjct  1288  ACTCCTCAGGCTCCAGTTTCCGCATGATCTTGCTTGGGAGCATGGTCTCGACGAAGAAGT
1229
```

```
Query  7321  TATTCTCAAGCACCATTTTCTCGCCCTCTTCGCTCTTGATCAGGGCGATATCCTCCTCGA
7380
             ||||||||||||||||||||||||||||||||||||||||||||||||||||||||||||
Sbjct  1228  TATTCTCAAGCACCATTTTCTCGCCCTCTTCGCTCTTGATCAGGGCGATATCCTCCTCGA
1169

Query  7381  TGTCAGGCCACTCGTCCCAGGACTCGATCACGTCCACGACACTCTCAGCATGGACGATGG
7440
             ||||||||||||||||||||||||||||||||||||||||||||||||||||||||||||
Sbjct  1168  TGTCAGGCCACTCGTCCCAGGACTCGATCACGTCCACGACACTCTCAGCATGGACGATGG
1109

Query  7441  CCTTGATCTTGTCTTGGTGCTCGTAGGAGTAGTGAAAGGCCAGACAAGCCCCCCAGTCGT
7500
             ||||||||||||||||||||||||||||||||||||||||||||||||||||||||||||
Sbjct  1108  CCTTGATCTTGTCTTGGTGCTCGTAGGAGTAGTGAAAGGCCAGACAAGCCCCCCAGTCGT
1049

Query  7501  GGCCCACAAAGATGATTTTCTTTGGAAGGTTCAGCAGCTCGAACCAAGCGGTGAGGTACT
7560
             ||||||||||||||||||||||||||||||||||||||||||||||||||||||||||||
Sbjct  1048  GGCCCACAAAGATGATTTTCTTTGGAAGGTTCAGCAGCTCGAACCAAGCGGTGAGGTACT
989

Query  7561  TGTAGTGATCCAGGAGGCGATATGAGCCATTCCCGCTCTTGCCGGACTTACCCATTCCGA
7620
             ||||||||||||||||||||||||||||||||||||||||||||||||||||||||||||
Sbjct  988   TGTAGTGATCCAGGAGGCGATATGAGCCATTCCCGCTCTTGCCGGACTTACCCATTCCGA
929

Query  7621  TCAGATCAGGGATGATGCATCTAGCCACGGGCTCGATGTGAGGCACGACGTGCCTCCACA
7680
             ||||||||||||||||||||||||||||||||||||||||||||||||||||||||||||
Sbjct  928   TCAGATCAGGGATGATGCATCTAGCCACGGGCTCGATGTGAGGCACGACGTGCCTCCACA
869

Query  7681  GGTAGCTGGAGGCAGCGTTACCATGCAGAAAAATCACGGCGTTCTCGGCGTGCTTCTCGG
7740
             ||||||||||||||||||||||||||||||||||||||||||||||||||||||||||||
Sbjct  868   GGTAGCTGGAGGCAGCGTTACCATGCAGAAAAATCACGGCGTTCTCGGCGTGCTTCTCGG
809

Query  7741  AATCATAGTAGTTGATGAAGGAGTCCAGCACGTTCATTTGCTTGCAGCGAGCCCACCACT
7800
             ||||||||||||||||||||||||||||||||||||||||||||||||||||||||||||
Sbjct  808   AATCATAGTAGTTGATGAAGGAGTCCAGCACGTTCATTTGCTTGCAGCGAGCCCACCACT
749

Query  7801  GAGGCCCAGTGATCATGCGTTTGCGTTGCTCGGGGTCGTACACCTTGGAAGCCATGGTGG
7860
             ||||||||||||||||||||||||||||||||||||||||||||||||||||||||||||
Sbjct  748   GAGGCCCAGTGATCATGCGTTTGCGTTGCTCGGGGTCGTACACCTTGGAAGCCATGGTGG
689
```

```
Query  7861  CTAGCCTATAGTGAGTCGTATTAAGTACTCTAGCCTTAAGAGCTGTAATTGAACTGGGAG
7920
             ||||||||||||||||||||||||||||||||||||||||||||||||||||||||||||
Sbjct  688   CTAGCCTATAGTGAGTCGTATTAAGTACTCTAGCCTTAAGAGCTGTAATTGAACTGGGAG
629


Query  7921  TGGACACCTGTGGAGAGAAAGGCAAAGTGGATGTCAGTAAGACCAATAGGTGCCTATCAG
7980
             ||||||||||||||||||||||||||||||||||||||||||||||||||||||||||||
Sbjct  628   TGGACACCTGTGGAGAGAAAGGCAAAGTGGATGTCAGTAAGACCAATAGGTGCCTATCAG
569


Query  7981  AAACGCAAGAGTCTTCTCTGTCTCGACAAGCCCAGTTTCTATTGGTCTCCTTAAACCTGT
8040
             ||||||||||||||||||||||||||||||||||||||||||||||||||||||||||||
Sbjct  568   AAACGCAAGAGTCTTCTCTGTCTCGACAAGCCCAGTTTCTATTGGTCTCCTTAAACCTGT
509


Query  8041  CTTGTAACCTTGATACTTACCTGCCCAGTGCCTCACGACCAACTTCTGCAGCTTAAGTTC
8100
             ||||||||||||||||||||||||||||||||||||||||||||||||||||||||||||
Sbjct  508   CTTGTAACCTTGATACTTACCTGCCCAGTGCCTCACGACCAACTTCTGCAGCTTAAGTTC
449


Query  8101  GAGACTGTTGTGTCAGAAGAATCAAGCTTTTTGCAAAAGCCTAGGCCTCCAAAAAAGCCT
8160
             ||||||||||||||||||||||||||||||||||||||||||||||||||||||||||||
Sbjct  448   GAGACTGTTGTGTCAGAAGAATCAAGCTTTTTGCAAAAGCCTAGGCCTCCAAAAAAGCCT
389


Query  8161  CCTCACTACTTCTGGAATAGCTCAGAGGCCGAGGCGGCCTCGGCCTCTGCATAAATaaaa
8220
             ||||||||||||||||||||||||||||||||||||||||||||||||||||||||||||
Sbjct  388   CCTCACTACTTCTGGAATAGCTCAGAGGCCGAGGCGGCCTCGGCCTCTGCATAAATAAAA
329


Query  8221  aaaaTTAGTCAGCCAtggggcggagaatgggcggaactgggcggagttaggggcgggatg
8280
             ||||||||||||||||||||||||||||||||||||||||||||||||||||||||||||
Sbjct  328   AAAATTAGTCAGCCATGGGGCGGAGAATGGGCGGAACTGGGCGGAGTTAGGGGCGGGATG
269


Query  8281  ggcggagttaggggcgggaCTATGGTTGCTGACTAATTGAGATGCATGCTTTGCATACTT
8340
             ||||||||||||||||||||||||||||||||||||||||||||||||||||||||||||
Sbjct  268   GGCGGAGTTAGGGGCGGGACTATGGTTGCTGACTAATTGAGATGCATGCTTTGCATACTT
209


Query  8341  CTGCCTGCTGGGGAGCCTGGGGACTTTCCACACCTGGTTGCTGACTAATTGAGATGCATG
8400
             ||||||||||||||||||||||||||||||||||||||||||||||||||||||||||||
Sbjct  208   CTGCCTGCTGGGGAGCCTGGGGACTTTCCACACCTGGTTGCTGACTAATTGAGATGCATG
149
```

```
Query  8401   CTTTGCATACTTCTGCCTGCTGGGGAGCCTGGGGACTTTCCACACCCTAACTGACACACA
8460
              ||||||||||||||||||||||||||||||||||||||||||||||||||||||||||||
Sbjct  148    CTTTGCATACTTCTGCCTGCTGGGGAGCCTGGGGACTTTCCACACCCTAACTGACACACA
89


Query  8461   TTCCACAGCTGGTTCTTTCCGCCTCAGAAGGTACCTAACCAAGTTCCTCTTTCAGAGGTT
8520
              ||||||||||||||||||||||||||||||||||||||||||||||||||||||||||||
Sbjct  88     TTCCACAGCTGGTTCTTTCCGCCTCAGAAGGTACCTAACCAAGTTCCTCTTTCAGAGGTT
29


Query  8521   ATTTCAGGCCATGGTGCTGCGCAGATCT   8548
              ||||||||||||||||||||||||||||
Sbjct  28     ATTTCAGGCCATGGTGCTGCGCAGATCT   1
```

Range 3: 5954 to 6273

Score:592 bits(320), Expect:3e-171,
Identities:320/320(100%), Gaps:0/320(0%), Strand: Plus/Minus

```
Query  8549   GTCGAGCCATGTGAGCAAAAGGCCAGCAAAAGGCCAGGAACCGTAAAAAGGCCGCGTTGC
8608
              ||||||||||||||||||||||||||||||||||||||||||||||||||||||||||||
Sbjct  6273   GTCGAGCCATGTGAGCAAAAGGCCAGCAAAAGGCCAGGAACCGTAAAAAGGCCGCGTTGC
6214


Query  8609   TGGCGTTTTTCCATAGGCTCCGCCCCCCTGACGAGCATCACAAAAATCGACGCTCAAGTC
8668
              ||||||||||||||||||||||||||||||||||||||||||||||||||||||||||||
Sbjct  6213   TGGCGTTTTTCCATAGGCTCCGCCCCCCTGACGAGCATCACAAAAATCGACGCTCAAGTC
6154


Query  8669   AGAGGTGGCGAAACCCGACAGGACTATAAAGATACCAGGCGTTTCCCCCTGGAAGCTCCC
8728
              ||||||||||||||||||||||||||||||||||||||||||||||||||||||||||||
Sbjct  6153   AGAGGTGGCGAAACCCGACAGGACTATAAAGATACCAGGCGTTTCCCCCTGGAAGCTCCC
6094


Query  8729   TCGTGCGCTCTCCTGTTCCGACCCTGCCGCTTACCGGATACCTGTCCGCCTTTCTCCCTT
8788
              ||||||||||||||||||||||||||||||||||||||||||||||||||||||||||||
Sbjct  6093   TCGTGCGCTCTCCTGTTCCGACCCTGCCGCTTACCGGATACCTGTCCGCCTTTCTCCCTT
6034


Query  8789   CGGGAAGCGTGGCGCTTTCTCATAGCTCACGCTGTAGGTATCTCAGTTCGGTGTAGGTCG
8848
              ||||||||||||||||||||||||||||||||||||||||||||||||||||||||||||
Sbjct  6033   CGGGAAGCGTGGCGCTTTCTCATAGCTCACGCTGTAGGTATCTCAGTTCGGTGTAGGTCG
5974
```

```
Query  8849  TTCGCTCCAAGCTGGGCTGT  8868
             ||||||||||||||||||||
Sbjct  5973  TTCGCTCCAAGCTGGGCTGT  5954
```

Range 4: 103 to 174

Score:134 bits(72), Expect:2e-33,
Identities:72/72(100%), Gaps:0/72(0%), Strand: Plus/Minus

```
Query  8303  TGGTTGCTGACTAATTGAGATGCATGCTTTGCATACTTCTGCCTGCTGGGGAGCCTGGGG
8362
             ||||||||||||||||||||||||||||||||||||||||||||||||||||||||||||
Sbjct  174   TGGTTGCTGACTAATTGAGATGCATGCTTTGCATACTTCTGCCTGCTGGGGAGCCTGGGG
115

Query  8363  ACTTTCCACACC  8374
             ||||||||||||
Sbjct  114   ACTTTCCACACC  103
```

Range 5: 175 to 246

Score:134 bits(72), Expect:2e-33,
Identities:72/72(100%), Gaps:0/72(0%), Strand: Plus/Minus

```
Query  8375  TGGTTGCTGACTAATTGAGATGCATGCTTTGCATACTTCTGCCTGCTGGGGAGCCTGGGG
8434
             ||||||||||||||||||||||||||||||||||||||||||||||||||||||||||||
Sbjct  246   TGGTTGCTGACTAATTGAGATGCATGCTTTGCATACTTCTGCCTGCTGGGGAGCCTGGGG
187

Query  8435  ACTTTCCACACC  8446
             ||||||||||||
Sbjct  186   ACTTTCCACACC  175
```

Supplementary Figure 4: Full sequence alignment of recombinant plasmid (MBNL1-psiCHECK-2) against the original psiCHECK-2 reporter plasmid. Alignment analysis was done in BLASTN NCBI.

431

LIST OF REFERENCES

Abedini, A., Zhu, Y.O., Chatterjee, S., Halasz, G., Devalaraja-Narashimha, K., Shrestha, R., Balzer, M.S., Park, J., Zhou, T., Ma, Z., Sullivan, K.M., Hu, H., Sheng, X., Liu, H., Wei, Y., Boustany-Kari, C.M., Patel, U., Almaani, S., Palmer, M., Townsend, R., Blady, S., Hogan, J., Morton, L. and Susztak, K., 2021. Urinary Single-Cell Profiling Captures the Cellular Diversity of the Kidney. Journal of the American Society of Nephrology, 32 (3), 614-627. Afkarian, M., Sachs, M.C., Kestenbaum, B., Hirsch, I.B., Tuttle, K.R., Himmelfarb, J. and De Boer, I.H., 2013. Kidney Disease and Increased Mortality Risk in Type 2 Diabetes. *Journal of the American Society of Nephrology,* 24 (2), 302-308.

Aebersold, R. and Mann, M., 2003. Mass spectrometry-based proteomics. *Nature,* 422, 198–207.

Afkarian, M., Sachs, M.C., Kestenbaum, B., Hirsch, I.B., Tuttle, K.R., Himmelfarb, J. and De Boer, I.H., 2013. Kidney Disease and Increased Mortality Risk in Type 2 Diabetes. *Journal of the American Society of Nephrology,* 24 (2), 302-308.

Agarwal, V., Bell, G.W., Nam, J. and Bartel, D.P., 2015. Predicting effective microRNA target sites in mammalian mRNAs. *eLife*, 4, e05005.

Ahn, H., Kim, J.H., Jeong, H., Yu, J., Yeom, J., Song, S.H., Kim, S.S., Kim, I.J. and Kim, K., 2020. Differential Urinary Proteome Analysis for Predicting Prognosis in Type 2 Diabetes Patients with and without Renal Dysfunction. *International Journal of Molecular Sciences,* 21 (12), 4236.

Ahn, J., Kim, B., Yu, M., Lee, I. and Cho, J., 2010. Identification of diabetic nephropathy-selective proteins in human plasma by multi-lectin affinity chromatography and LC-MS/MS. *PROTEOMICS – Clinical Applications,* 4 (6-7), 644–653.

Ai, K., Zhu, X., Kang, Y., Li, H. and Zhang, L., 2020. miR-130a-3p inhibition protects against renal fibrosis in vitro via the TGF-β1/Smad pathway by targeting SnoN. *Experimental and Molecular Pathology,* 112, 104358.

Akinc, A., Zumbuehl, A., Goldberg, M., Leshchiner, E.S., Busini, V., Hossain, N., Bacallado, S.A., Nguyen, D.N., Fuller, J., Alvarez, R., Borodovsky, A., Borland, T., Constien, R., de Fougerolles, A., Dorkin, J.R., Narayanannair Jayaprakash, K., Jayaraman, M., John, M., Koteliansky, V., Manoharan, M., Nechev, L., Qin, J., Racie, T., Raitcheva, D., Rajeev, K.G., Sah, D.W.Y., Soutschek, J., Toudjarska, I., Vornlocher, H., Zimmermann, T.S., Langer, R. and Anderson, D.G., 2008. A combinatorial library of lipid-like materials for delivery of RNAi therapeutics. *Nature Biotechnology,* 26 (5), 561–569.

Akkina, S., and Becker, B.N., 2011. MicroRNAs in kidney function and disease. *Translational Research,* 157 (4), 236–240.

Al-Amoudi, M.S., Salman, M., Al-Majthoub, M.M., Adam, A.M.A., Alshanbari, N.A. and Refat, M.S., 2015. Spectral studies to increase the efficiency and stability of laser dyes by charge-transfer reactions for using in solar cells: charge-transfer complexes of Ponceau S with p-chloranil, chloranilic and picric acids. *Research on Chemical Intermediates,* 41 (5), 3089-3108.

Alhasan, A.A., Spielhofer, J., Kusche-Gullberg, M., Kirby, J.A. and Ali, S., 2014. Role of 6-O-Sulfated Heparan Sulfate in Chronic Renal Fibrosis. *Journal of Biological Chemistry,* 289 (29), 20295–20306.

Alicic, R.Z., Rooney, M.T. and Tuttle, K.R., 2017. Diabetic Kidney Disease: Challenges, Progress, and Possibilities. *Clinical Journal of the American Society of Nephrology,* 12 (12), 2032-2045.

Alkadi, M.M., Abuhelaiqa, E.A., Thappy, S.B., Eltayeb, F.B., Murshed, K.A., Akhtar, M., Almokdad, O.I., Al-Malki, H.A., Hamad, A.I., Hamdi, A.F., Fituri, O.M., Ashour, A.M., Nauman, A., Tohid, H., Singh, R. and Asim, M., 2022. Kidney Biopsy in Patients With Markedly Reduced Kidney Function. *Kidney International Reports,* 7 (11), 2505-2508.

Allan, D., Billah, M.M., Finean, J.B. and Michell, R.H., 1976. Release of diacylglycerol-enriched vesicles from erythrocytes with increased intracellular [Ca 2+]. *Nature (London),* 261 (5555), 58-60.

Almenar-Pérez, E., Sarría, L., Nathanson, L. and Oltra, E., 2020. Assessing diagnostic value of microRNAs from peripheral blood mononuclear cells and extracellular vesicles in Myalgic Encephalomyelitis/Chronic Fatigue Syndrome. *Scientific Reports,* 10 (1), 2064.

AlQudah, M., Hale, T.M. and Czubryt, M.P., 2020. Targeting the renin-angiotensin-aldosterone system in fibrosis. *Matrix Biology,* 91-92, 92-108.

Alsaad, K.O., and Herzenberg, A.M., 2007. Distinguishing diabetic nephropathy from other causes of glomerulosclerosis: an update. *Journal of Clinical Pathology,* 60 (1), 18-26.

Akhmetshina, A., Palumbo, K., Dees, C., Bergmann, C., Venalis, P., Zerr, P., Horn, A., Kireva, T., Beyer, C., Zwerina, J., Schneider, H., Sadowski, A., Riener, M., MacDougald, O.A., Distler, O., Schett, G. and Distler, J.H.W., 2012. Activation of canonical Wnt signalling is required for TGF-β-mediated fibrosis. *Nature Communications,* 3 (1), 735.

Amleh, A., Chen, H.P., Watad, L., Abramovich, I., Agranovich, B., Gottlieb, E., Ben-Dov, I.Z., Nechama, M. and Volovelsky, O., 2023. Arginine depletion attenuates renal cystogenesis in tuberous sclerosis complex model. *Cell Reports Medicine,* 4 (6), 101073.

Amoah, E., Glickman, J.L., Malchoff, C.D., Sturgill, B.C., Kaiser, D.L. and Bolton, K., 1988. Clinical Identification of Nondiabetic Renal Disease in Diabetic Patients with Type I and Type II Disease Presenting with Renal Dysfunction. *American Journal of Nephrology,* 8 (3), 204-211.

An, W., Kim, J. and Roeder, R.G., 2004. Ordered Cooperative Functions of PRMT1, p300, and CARM1 in Transcriptional Activation by p53. *Cell,* 117 (6), 735–748.

Anders, H., Huber, T.B., Isermann, B. and Schiffer, M., 2018. CKD in diabetes: diabetic kidney disease versus nondiabetic kidney disease. *Nature Reviews. Nephrology,* 14 (6), 361–377.

Anderson, N.L., and Anderson, N.G., 2002. The human plasma proteome: history, character, and diagnostic prospects. *Molecular & Cellular Proteomics,* 1 (11), 845–867.

Anderson, R.G.W., 1998. THE CAVEOLAE MEMBRANE SYSTEM. *Annual Review of Biochemistry,* 67 (1), 199-225.

Andreev, E., Koopman, M. and Arisz, L., 1999. A rise in plasma creatinine that is not a sign of renal failure: which drugs can be responsible? *Journal of Internal Medicine,* 246 (3), 247-252.

Andreu, Z., and Yáñez-Mó, M., 2014. Tetraspanins in extracellular vesicle formation and function. *Frontiers in Immunology,* 5, 442.

Anfaiha-Sanchez, M., Santiago-Hernandez, A., Lopez, J.A., Lago-Baameiro, N., Pardo, M., Martin-Blazquez, A., Vazquez, J., Ruiz-Hurtado, G., Barderas, M.G., Segura, J., Ruilope, L.M., Martin-Lorenzo, M. and Alvarez-Llamas, G., 2024. Urinary extracellular vesicles as a monitoring tool for renal damage in patients not meeting criteria for chronic kidney disease. *Journal of Extracellular Biology,* 3 (9), e170–n/a.

Arfin, T., Sonawane and Arshiya Tarannum, K., 2019. Review on Detection of Phenol in Water. Advanced Materials Letters, 10 (11), 753-785.

Arai, H., Sato, Y. and Yanagita, M., 2021. Fibroblast heterogeneity and tertiary lymphoid tissues in the kidney. *Immunological Reviews,* 302 (1), 196-210.

Arya, S.B., Collie, S.P. and Parent, C.A., 2024. The ins-and-outs of exosome biogenesis, secretion, and internalization. *Trends in Cell Biology,* 34 (2), 90–108.

Asada, N., Takase, M., Nakamura, J., Oguchi, A., Asada, M., Suzuki, N., Yamamura, K., Nagoshi, N., Shibata, S., Rao, T.N., Fehling, H.J., Fukatsu, A., Minegishi, N., Kita, T., Kimura, T., Okano, H., Yamamoto, M. and Yanagita, M., 2011. Dysfunction of fibroblasts of extrarenal origin underlies renal fibrosis and renal anemia in mice. *The Journal of Clinical Investigation,* 121 (10), 3981-3990.

Asao, H., Sasaki, Y., Arita, T., Tanaka, N., Endo, K., Kasai, H., Takeshita, T., Endo, Y., Fujita, T. and Sugamura, K., 1997. Hrs is associated with STAM, a signal-transducing adaptor molecule. Its suppressive effect on cytokine-induced cell growth. *The Journal of Biological Chemistry,* 272 (52), 32785-32791.

Asghar, M.S., Denic, A. and Rule, A.D., 2024. Morphometric analysis of chronicity on kidney biopsy: a useful prognostic exercise. *Clinical Kidney Journal,* 17 (2), sfad226.

Babalola, J.O., Wendeler, M., Breiden, B., Arenz, C., Schwarzmann, G., Locatelli-Hoops, S. and Sandhoff, K., 2007. Development of an assay for the intermembrane transfer of cholesterol by Niemann-Pick C2 protein. *Biological Chemistry,* 388 (6), 617–626.

Babst, M., 2005. A Protein's Final ESCRT. *Traffic (Copenhagen, Denmark),* 6 (1), 2-9.

Babst, M., Katzmann, D.J., Estepa-Sabal, E.J., Meerloo, T. and Emr, S.D., 2002. Escrt-III: An endosome-associated heterooligomeric protein complex required for mvb sorting. *Developmental Cell,* 3 (2), 271-282.

Babst, M., Katzmann, D.J., Snyder, W.B., Wendland, B. and Emr, S.D., 2002. Endosome-Associated Complex, ESCRT-II, Recruits Transport Machinery for Protein Sorting at the Multivesicular Body. *Developmental Cell,* 3 (2), 283-289. a

Babst, M., Sato, T.K., Banta, L.M. and Emr, S.D., 1997. Endosomal transport function in yeast requires a novel AAA-type ATPase, Vps4p. *The EMBO Journal,* 16 (8), 1820-1831.

Babst, M., Wendland, B., Estepa, E.J. and Emr, S.D., 1998. Vps4p AAA ATPase regulates membrane association of a Vps protein complex required for normal endosome function. *The EMBO Journal,* 17 (11), 2982-2993.

Babuke, T., Ruonala, M., Meister, M., Amaddii, M., Genzler, C., Esposito, A. and Tikkanen, R., 2009. Hetero-oligomerization of reggie-1/flotillin-2 and reggie-2/flotillin-1 is required for their endocytosis. *Cellular Signalling,* 21 (8), 1287-1297.

Bache, K.G., Brech, A., Mehlum, A. and Stenmark, H., 2003. Hrs Regulates Multivesicular Body Formation via ESCRT Recruitment to Endosomes. *The Journal of Cell Biology,* 162 (3), 435-442.

Bachurski, D., Schuldner, M., Nguyen, P., Malz, A., Reiners, K.S., Grenzi, P.C., Babatz, F., Schauss, A.C., Hansen, H.P., Hallek, M. and Pogge Von Strandmann, E., 2019. Extracellular vesicle measurements with nanoparticle tracking analysis - An accuracy and repeatability comparison between NanoSight NS300 and ZetaView. *Journal of Extracellular Vesicles*, 8 (1).

Badenas, C., Praga, M., Davila, S., Mila, M., Antignac, C., Darnell, A., Torra, R., Tazon, B., Heidet, L., Arrondel, C., Armengol, A., Andres, A., Morales, E., Camacho, J.A. and Lens, X., 2002. Mutations in the COL4A4 and COL4A3 genes cause familial benign hematuria. *Journal of the American Society of Nephrology*, 13 (5), 1248-1254.

Bai, L., Lin, Y., Xie, J., Zhang, Y., Wang, H. and Zheng, D., 2021. MiR-27b-3p inhibits the progression of renal fibrosis via suppressing STAT1. *Human Cell,* 34 (2), 383–393.

Ballermann, B.J., Nyström, J. and Haraldsson, B., 2021. The Glomerular Endothelium Restricts Albumin Filtration. *Frontiers in Medicine,* 8, 766689.

Balzer, M.S., Rohacs, T. and Susztak, K., 2022. How Many Cell Types Are in the Kidney and What Do They Do? *Annual Review of Physiology,* 84 (1), 507-531. Baxmann, A.C., Ahmed, M.S., Marques, N.C., Menon, V.B., Pereira, A.B., Kirsztajn, G.M. and Heilberg, I.P., 2008. Influence of Muscle Mass and Physical Activity on Serum and Urinary Creatinine and Serum Cystatin C. *Clinical Journal of the American Society of Nephrology,* 3 (2), 348-354.

Barrès, C., Blanc, L., Bette-Bobillo, P., André, S., Mamoun, R., Gabius, H. and Vidal, M., 2010. Galectin-5 is bound onto the surface of rat reticulocyte exosomes and modulates vesicle uptake by macrophages. *Blood,* 115 (3), 696-705.

Bartel, D.P., 2004. MicroRNAs: Genomics, Biogenesis, Mechanism, and Function. *Cell*, 116 (2), 281-297.

Barutta, F., Bellini, S., Canepa, S., Durazzo, M. and Gruden, G., 2021. Novel biomarkers of diabetic kidney disease: current status and potential clinical application. *Acta diabetologica*, 58 (7), 819–830. 10.1007/s00592-020-01656-9.

Barutta, F., Tricarico, M., Corbelli, A., Annaratone, L., Pinach, S., Grimaldi, S., Bruno, G., Cimino, D., Taverna, D., Deregibus, M.C., Rastaldi, M.P., Perin, P.C., and Gruden, G., 2013. Urinary Exosomal MicroRNAs in Incipient Diabetic Nephropathy. *Plos One*, 8 (11), e73798.

Becerra, S.P., Sagasti, A., Spinella, P. and Notario, V., 1995. Pigment Epithelium-derived Factor Behaves Like a Noninhibitory Serpin. *Journal of Biological Chemistry,* 270 (43), 25992–25999.

Bello-Reuss, E., Holubec, K. and Rajaraman, S., 2001. Angiogenesis in autosomal-dominant polycystic kidney disease. *Kidney International,* 60 (1), 37-45.

Bellucci, L., Montini, G., Collino, F. and Bussolati, B., 2021. Mesenchymal Stromal Cell-Derived Extracellular Vesicles Pass through the Filtration Barrier and Protect Podocytes in a 3D Glomerular Model under Continuous Perfusion. *Jo'jig Gonghag Gwa Jaesaeng Uihag,* 18 (4), 549–560.

Beltrami, C., Clayton, A., Newbury, L.J., Corish, P., Jenkins, R.H., Phillips, A.O., Fraser, D.J. and Bowen, T., 2015. Stabilization of Urinary MicroRNAs by Association with Exosomes and Argonaute 2 Protein. *Non-Coding RNA,* 1 (2), 151–166.

Benito-Martin, A., Ucero, A.C., Zubiri, I., Posada-Ayala, M., Fernandez-Fernandez, B., Cannata-Ortiz, P., Sanchez-Nino, M.D., Ruiz-Ortega, M., Egido, J., Alvarez-Llamas, G. and Ortiz, A., 2013. Osteoprotegerin in Exosome-Like Vesicles from Human Cultured Tubular Cells and Urine. *PloS One,* 8 (8), e72387.

Bennett, J.A., Mastrangelo, M.A., Ture, S.K., Smith, C.O., Loelius, S.G., Berg, R.A., Shi, X., Burke, R.M., Spinelli, S.L., Cameron, S.J., Carey, T.E., Brookes, P.S., Gerszten, R.E., Sabater-Lleal, M., de Vries, P.S., Huffman, J.E., Smith, N.L., Morrell, C.N. and Lowenstein, C.J., 2020. The choline transporter Slc44a2 controls platelet activation and thrombosis by regulating mitochondrial function. *Nature Communications,* 11 (1), 3479.

Bennett, M.R., and Devarajan, P., 2017, Chapter One - Characteristics of an Ideal Biomarker of Kidney Diseases. *In:* Chapter One - Characteristics of an Ideal Biomarker of Kidney Diseases. *Biomarkers of Kidney Disease.* Second Edition ed. United States: Elsevier Inc, 2017, pp. 1–20.

Berning, C., Bieger, I., Pauli, S., Vermeulen, T., Vogl, T., Rummel, T., Höhne, W., Koch, H.G., Rolinski, B., Gempel, K. and Häberle, J., 2008. Investigation of citrullinemia type I variants by in vitro expression studies. *Human Mutation,* 29 (10), 1222–1227.

Bernstein, E., Caudy, A.A., Hammond, S.M. and Hannon, G.J., 2001. Role for a bidentate ribonuclease in the initiation step of RNA interference. *Nature*, 409 (6818), p.363.

Betancourt, L.H., Sanchez, A., Pla, I., Kuras, M., Zhou, Q., Andersson, R. and Marko-Varga, G., 2018. Quantitative Assessment of Urea In-Solution Lys-C/Trypsin Digestions Reveals Superior

Performance at Room Temperature over Traditional Proteolysis at 37 °C. *Journal of Proteome Research,* 17 (7), 2556–2561.

Bhensdadia, N.M., Hunt, K.J., Lopes-Virella, M.F., Michael Tucker, J., Mataria, M.R., Alge, J.L., Neely, B.A., Janech, M.G. and Arthur, J.M., 2013. Urine haptoglobin levels predict early renal functional decline in patients with type 2 diabetes. *Kidney International,* 83 (6), 1136-1143.

Bienaimé, F., Muorah, M., Metzger, M., Broeuilh, M., Houiller, P., Flamant, M., Haymann, J., Vonderscher, J., Mizrahi, J., Friedlander, G., Stengel, B., Terzi, F., Vrtovsnik, F., Daugas, E., Flamant, M., Vidal-Petiot, E., Jacquot, C., Karras, A., Roueff, S., Thervet, E., Houillier, P., Courbebaisse, M., Eladari et Gérard Maruani, D., Urena-Torres, P., Boffa, J., Ronco, P., Fessi, H., Rondeau, E., Letavernier, E., Tabibzadeh, N. and Haymann, J., 2023. Combining robust urine biomarkers to assess chronic kidney disease progression. *EBioMedicine*, 93, 104635.

Bijkerk, R., de Bruin, R.G., van Solingen, C., van Gils, J.M., Duijs, J.M.G.J., van der Veer, E.P., Rabelink, T.J., Humphreys, B.D. and van Zonneveld, A.J., 2016. Silencing of microRNA-132 reduces renal fibrosis by selectively inhibiting myofibroblast proliferation. *Kidney International,* 89 (6), 1268–1280.

Bikbov, B., Purcell, C.A., Abebe, M., Adebayo, O.M., Afarideh, M., Agarwal, S.K., Agudelo-Botero, M., Alipour, V., Al-Raddadi, R.M., Alvis-Guzman, N., Andualem, Z., Asmelash, D., Atout, M.M.W., Bakhtiari, A., Ballew, S.H., Balouchi, A., Basu, S., Bedi, N., Bijani, A., Boloor, A., Cámera, L.A., Carrero, J.J., Chin, K.L., Cirillo, M., Cousin, E., Dandona, L., Daryani, A., Demeke, F.M., Demoz, G.T., Desta, D.M., Do, H.P., Eftekhari, A., Esteghamati, A., Fernandes, J.C., Fernandes, E., Geta, B., Ghafourifard, M., Haj-Mirzaian, A., Hasan, M., Hasanzadeh, A., Hassen, H.Y., Herteliu, C., Hoang, C.L., Jafari Balalami, N., James, S.L., Jassal, S.K., Kassa, T.D., Khalilov, R., Khan, E.A., Kuate Defo, B., Lopez, A.D., Majeed, A., Meheretu, H.A.A., Mirica, A., Moazen, B., Mohammed, S., Mokdad, A.H., Morales, L., Mukhopadhyay, S., Nadkarni, G.N., Natarajan, G., Nazari, J., Negoi, R.I., Nowak, C., Olagunju, A.T., Ortiz, A., Owolabi, M.O., Palladino, R., Pathak, M., Poustchi, H., Prasad, N., Rafiei, A., Raju, S.B., Rawal, L., Reiner, R.C., Rezapour, A., Rothenbacher, D., Rwegerera, G.M., Saadatagah, S., Safari, S., Santos, I.S., Sawhney, M., Schaeffner, E., Sharafi, Z., Sharif, M., Silva, D.A.S., Singh, J.A., Singh, N.P., Sisay, M.M.M., Sutradhar, I., Tesfay, B.e., Teshome, G.F., Thakur, J.S., Vos, T., Yamada, T., Yusefzadeh, H., Zaman, S.B., Zamora, N., Zarghi, A., Ärnlöv, J. and Murray, C.J.L., 2020. Global, regional, and national burden of chronic kidney disease, 1990–2017: a systematic analysis for the Global Burden of Disease Study 2017. *The Lancet,* 395 (10225), 709-733.

Bimboim, H.C., and Doly, J., 1979. A rapid alkaline extraction procedure for screening recombinant plasmid DNA. *Nucleic Acids Research,* 7 (6), 1513–1523.

Bin, S., Yoo, M., Molinari, P., Gentile, M., Budge, K., Cantarelli, C., Khan, Y., La Manna, G., Baldwin, W.M., Dvorina, N., Cravedi, P. and Gusella, G.L., 2024. Reduced decay-accelerating factor expression promotes complement-mediated cystogenesis in murine ADPKD. *JCI Insight,* 9 (12).

Biomarkers Definitions Working Group, Atkinson Jr, A.J., Colburn, W.A., DeGruttola, V.G., DeMets, D.L., Downing, G.J., Hoth, D.F., Oates, J.A., Peck, C.C. and Schooley, R.T., 2001. Biomarkers and surrogate endpoints: preferred definitions and conceptual framework. *Clinical Pharmacology & Therapeutics,* 69 (3), 89–95.

Biomarkers on a roll. 2010. *Nature Biotechnology,* 28 (5), 431.

Blanco-Gozalo, V., Quiros, Y., Vicente-Vicente, L., Casanova, A.G., Sancho-Martínez, S.M. and López-Hernández, F.J., 2024. Urinary GM2AP coincides with renal cortical damage and grades cisplatin nephrotoxicity severity in rats. *Toxicology (Amsterdam),* 508, 153919.

Bleyer, A. J., Kidd, K., Živná, M., and Kmoch, S. (2017). Autosomal dominant tubulointerstitial kidney disease. Adv. Chronic Kidney Dis. 24 (2), 86–93. doi:10.1053/j.ackd.2016.11.012

Bleyer, A.J., Kmoch, S., Antignac, C., Robins, V., Kidd, K., Kelsoe, J.R., Hladik, G., Klemmer, P., Knohl, S.J., Scheinman, S.J., Vo, N., Santi, A., Harris, A., Canaday, O., Weller, N., Hulick, P.J., Vogel, K., Rahbari-Oskoui, F.F., Tuazon, J., Deltas, C., Somers, D., Megarbane, A., Kimmel, P.L., Sperati, C.J., Orr-Urtreger, A., Ben-Shachar, S., Waugh, D.A., McGinn, S., Hodaňová, K., Vylet'al, P., Živná, M., Hart, T.C. and Hart, P.S., 2014. Variable Clinical Presentation of an MUC1 Mutation Causing Medullary Cystic Kidney Disease Type 1. *Clinical Journal of the American Society of Nephrology,* 9 (3), 527–535.

Blijdorp, C.J., and Hoorn, E.J., 2019. Urinary extracellular vesicles: the mothership connection. *American Journal of Physiology. Renal Physiology,* 317 (3), F648–F649.

Blijdorp, C.J., Hartjes, T.A., Wei, K., Heugten, M.H., Bovée, D.M., Budde, R.P.J., Wetering, J., Hoenderop, J.G.J., Royen, M.E., Zietse, R., Severs, D. and Hoorn, E.J., 2022. Nephron mass determines the excretion rate of urinary extracellular vesicles. *Journal of Extracellular Vesicles,* 11 (1), e12181–n/a.

Bonnet, A., Chaussain, C., Broutin, I., Rochefort, G.Y., Schrewe, H. and Gaucher, C., 2018. From Vascular Smooth Muscle Cells to Folliculogenesis: What About Vasorin? *Frontiers in Medicine,* 5, 335.

Boor, P., Ostendorf, T. and Floege, J., 2010. Renal fibrosis: novel insights into mechanisms and therapeutic targets. *Nature Reviews.Nephrology*, 6 (11), 643-656.

Borges, F.T., Melo, S.A., Özdemir, B.C., Kato, N., Revuelta, I., Miller, C.A., Gattone II, V.H., LeBleu, V.S. and Kalluri, R., 2013. TGF-β1-Containing exosomes from injured epithelial cells activate fibroblasts to initiate tissue regenerative responses and fibrosis. *Journal of the American Society of Nephrology,* 24 (3), 385-392.

Bradford, M.M., 1976. A rapid and sensitive method for the quantitation of microgram quantities of protein utilizing the principle of protein-dye binding. Analytical Biochemistry, 72 (1), 248-254.

Bradham, D.M., Igarashi, A., Potter, R.L. and Grotendorst, G.R., 1991. Connective tissue growth factor: a cysteine-rich mitogen secreted by human vascular endothelial cells is related to the

SRC-induced immediate early gene product CEF-10. *The Journal of Cell Biology,* 114 (6), 1285-1294.

Breitwieser, K., Koch, L.F., Tertel, T., Proestler, E., Burgers, L.D., Lipps, C., Adjaye, J., Fürst, R., Giebel, B. and Saul, M.J., 2022. Detailed Characterization of Small Extracellular Vesicles from Different Cell Types Based on Tetraspanin Composition by ExoView R100 Platform. *International Journal of Molecular Sciences,* 23 (15), 8544.

Bright, N.A., Lindsay, M.R., Stewart, A. and Luzio, J.P., 2001. The Relationship Between Lumenal and Limiting Membranes in Swollen Late Endocytic Compartments Formed After Wortmannin Treatment or Sucrose Accumulation. *Traffic (Copenhagen, Denmark),* 2 (9), 631-642.

Brod, J., and Sirota, J.H., 1948. THE RENAL CLEARANCE OF ENDOGENOUS "CREATININE" IN MAN. *The Journal of Clinical Investigation,* 27 (5), 645-654.

Bruno, S., Grange, C., Collino, F., Deregibus, M.C., Cantaluppi, V., Biancone, L., Tetta, C. and Camussi, G., 2012. Microvesicles Derived from Mesenchymal Stem Cells Enhance Survival in a Lethal Model of Acute Kidney Injury. *PLoS ONE,* 7 (3), e33115.

Bruno, S., Grange, C., Tetta, C., Camussi, G., Chiara Deregibus, M., Calogero, R.A., Saviozzi, S., Collino, F., Morando, L., Busca, A., Falda, M. And Bussolati, B., 2009. Mesenchymal Stem Cell-Derived Microvesicles Protect Against Acute Tubular Injury. *Journal of the American Society of Nephrology,* 20 (5), 1053-1067.

Burhan, I., Furini, G., Lortat-Jacob, H., Atobatele, A.G., Scarpellini, A., Schroeder, N., Atkinson, J., Maamra, M., Nutter, F.H., Watson, P., Vinciguerra, M., Johnson, T.S. and Verderio, E.A.M., 2016. Interplay between transglutaminases and heparan sulphate in progressive renal scarring. *Scientific Reports*, 6 (1), 31343.

Burrello, J., Monticone, S., Burrello, A., Bolis, S., Cristalli, C.P., Comai, G., Corradetti, V., Grange, C., Orlando, G., Bonafè, M., La Manna, G., Barile, L. and Bussolati, B., 2023. Identification of a serum and urine extracellular vesicle signature predicting renal outcome after kidney transplant. *Nephrology, Dialysis, Transplantation,* 38 (3), 764–777.

Butler, M.J., Down, C.J., Foster, R.R. and Satchell, S.C., 2020. The Pathological Relevance of Increased Endothelial Glycocalyx Permeability. *The American Journal of Pathology,* 190 (4), 742–751.

Campanholle, G., Ligresti, G., Gharib, S.A. and Duffield, J.S., 2013. Cellular Mechanisms of Tissue Fibrosis. 3. Novel mechanisms of kidney fibrosis. *American Journal of Physiology-Cell Physiology,* 304 (7), 591.

Cantaluppi, V., Medica, D., Mannari, C., Stiaccini, G., Figliolini, F., Dellepiane, S., Quercia, A.D., Migliori, M., Panichi, V., Giovannini, L., Bruno, S., Tetta, C., Biancone, L. and Camussi, G., 2015. Endothelial progenitor cell-derived extracellular vesicles protect from complement-mediated mesangial injury in experimental anti-Thy1.1 glomerulonephritis. *Nephrology, Dialysis, Transplantation,* 30 (3), 410–422.

Cao, S., Pan, Y., Terker, A.S., Arroyo Ornelas, J.P., Wang, Y., Tang, J., Niu, A., Kar, S.A., Jiang, M., Luo, W., Dong, X., Fan, X., Wang, S., Wilson, M.H., Fogo, A., Zhang, M. and Harris, R.C., 2023. Epidermal growth factor receptor activation is essential for kidney fibrosis development. *Nature Communications,* 14 (1), 7357.

Caza, T.N., Storey, A.J., Hassen, S.I., Herzog, C., Edmondson, R.D., Arthur, J.M., Kenan, D.J. and Larsen, C.P., 2023. Discovery of seven novel putative antigens in membranous nephropathy and membranous lupus nephritis identified by mass spectrometry. *Kidney International,* 103 (3), 593–606.

Chairoungdua, A., Smith, D.L., Pochard, P., Hull, M. and Caplan, M.J., 2010. Exosome release of β-catenin: a novel mechanism that antagonizes Wnt signaling. *The Journal of Cell Biology,* 190 (6), 1079-1091.

Chang, T.I., Park, J.T., Kim, J., Kim, S.J., Oh, H.J., Yoo, D.E., Han, S.H., Yoo, T. and Kang, S., 2011. Renal outcomes in patients with type 2 diabetes with or without coexisting non-diabetic renal disease. *Diabetes Research and Clinical Practice,* 92 (2), 198-204.

Chapter 3. Electrophoretic mobility of rigid colloidal particles. 2006, In: Chapter 3. Electrophoretic mobility of rigid colloidal particles. Interface Science and Technology. *Elsevier Science & Technology*, 2006, pp. 56-110.

Chau, B.N., Xin, C., Hartner, J., Ren, S., Castano, A.P., Linn, G., Li, J., Tran, P.T., Kaimal, V., Huang, X., Chang, A.N., Li, S., Kalra, A., Grafals, M., Portilla, D., MacKenna, D.A., Orkin, S.H. and Duffield, J.S., 2012. MicroRNA-21 Promotes Fibrosis of the Kidney by Silencing Metabolic Pathways. *Science Translational Medicine,* 4 (121), 121ra18–121ra18.

Chebib, F.T., MD, and Torres, Vicente E., MD, PhD, 2015. Autosomal Dominant Polycystic Kidney Disease: Core Curriculum 2016. *American Journal of Kidney Diseases*, 67 (5), 792-810.

Chebotareva, N.V., Vinogradov, A., Brzhozovskiy, A.G., Kashirina, D.N., Indeykina, M.I., Bugrova, A.E., Lebedeva, M., Moiseev, S., Nikolaev, E.N. and Kononikhin, A.S., 2022. Potential Urine Proteomic Biomarkers for Focal Segmental Glomerulosclerosis and Minimal Change Disease. *International Journal of Molecular Sciences,* 23 (20), 12607.

Chen, G., Moningka, N.C., Sasser, J.M., Zharikov, S., Cunningham, J., Mark, Tain, Y., Schwartz, I.F. and Baylis, C., 2012. Arginine and Asymmetric Dimethylarginine in Puromycin Aminonucleoside-Induced Chronic Kidney Disease in the Rat. *American Journal of Nephrology,* 35 (1), 40–48.

Chen, H., Zheng, Z., Li, R., Lu, J., Bao, Y., Ying, X., Zeng, R. and Jia, W., 2010. Urinary Pigment Epithelium-Derived Factor as a Marker of Diabetic Nephropathy. *American Journal of Nephrology,* 32 (1), 47–56.

Chen, J., Chen, J. and Harris, R.C., 2015. EGF Receptor Deletion in Podocytes Attenuates Diabetic Nephropathy. *Journal of the American Society of Nephrology,* 26 (5), 1115-1125.

Chen, J., Chen, J., Nagai, K., Plieth, D., Tan, M., Lee, T., Threadgill, D.W., Neilson, E.G. and Harris, R.C., 2012. EGFR Signaling Promotes TGFβ-Dependent Renal Fibrosis. *Journal of the American Society of Nephrology,* 23 (2), 215-224.

Chen, M., Lin, S., Zhou, C., Cui, D., Haick, H. and Tang, N., 2023. From Conventional to Microfluidic: Progress in Extracellular Vesicle Separation and Individual Characterization (Adv. Healthcare Mater. 8/2023). *Advanced Healthcare Materials,* 12 (8), n/a.

Chen, S., and Chiaramonte, R., 2019. Estimating Creatinine Clearance in the Nonsteady State: The Determination and Role of the True Average Creatinine Concentration. *Kidney Medicine,* 1 (4), 207-216.

Chen, S., Zhang, M., Li, J., Huang, J., Zhou, S., Hou, X., Ye, H., Liu, X., Xiang, S., Shen, W., Miao, J., Hou, F.F., Liu, Y. and Zhou, L., 2022. β-catenin-controlled tubular cell-derived exosomes play a key role in fibroblast activation via the OPN-CD44 axis. *Journal of Extracellular Vesicles,* 11 (3), e12203-n/a.

Chen, T., Wang, C., Yu, H., Ding, M., Zhang, C., Lu, X., Zhang, C. and Zhang, C., 2019. Increased urinary exosomal microRNAs in children with idiopathic nephrotic syndrome. *EBioMedicine*, 39, 552-561.

Chen, Y.M., and Liapis, H., 2015. Focal segmental glomerulosclerosis: molecular genetics and targeted therapies. *BMC Nephrology,* 16 (1), 101.

Chernomordik, L.V., and Kozlov, M.M., 2008. Mechanics of membrane fusion. *Nature Structural & Molecular Biology,* 15 (7), 675-683.

Cheruvanky, A., Hua Zhou, Pisitkun, T., Kopp, J.B., Knepper, M.A., Yuen, P.S.T. and Star, R.A., 2007. Rapid isolation of urinary exosomal biomarkers using a nanomembrane ultrafiltration concentrator. *American Journal of Physiology. Renal Physiology,* 61 (5).

Chipman, L.B., and Pasquinelli, A.E., 2019. miRNA Targeting: Growing beyond the Seed. *Trends in Genetics,* 35 (3), 215–222.

Choi, Y.J., Halbritter, J., Braun, D.A., Schueler, M., Schapiro, D., Rim, J.H., Nandadasa, S., Choi, W., Widmeier, E., Shril, S., Körber, F., Sethi, S.K., Lifton, R.P., Beck, B.B., Apte, S.S., Gee, H.Y. and Hildebrandt, F., 2019. Mutations of ADAMTS9 Cause Nephronophthisis-Related Ciliopathy. *American Journal of Human Genetics*, 104 (1), 45-54.

Chomczynski, P., and Sacchi, N., 1987. Single-Step Method of RNA Isolation by Acid Guanidinium Thiocyanate–Phenol–Chloroform Extraction. *Analytical Biochemistry,* 162 (1), 156-159.

Chorn, G., Klein-McDowell, M., Zhao, L., Saunders, M.A., Flanagan, W.M., Willingham, A.T. and Lim, L.P., 2012. Single-stranded microRNA mimics. *Rna,* 18 (10), 1796–1804.

Christianson, H.C., and Belting, M., 2014. Heparan sulfate proteoglycan as a cell-surface endocytosis receptor. *Matrix Biology,* 35 (Oct 18), 51–55.

Christianson, H.C., Svensson, K.J., van Kuppevelt, T.H., Li, J. and Belting, M., 2013. Cancer cell exosomes depend on cell-surface heparan sulfate proteoglycans for their internalization and functional activity. *Proceedings of the National Academy of Sciences - PNAS,* 110 (43), 17380-17385.

Chu, C.D., McCulloch, C.E., Banerjee, T., Pavkov, M.E., Burrows, N.R., Gillespie, B.W., Saran, R., Shlipak, M.G., Powe, N.R., Tuot, D.S., Shahinian, V., Heung, M., Gillespie, B., Morgenstern, H., Herman, W., Zivin, K., Bragg-Gresham, J., Steffick, D., Han, Y., Zhang, X., Li, Y., Kurtz, V., Wyncott, A., Powe, N., Hsu, C., Crews, D., Hsu, R., Johansen, K., Shlipak, M., Canela, J., Burrows, N.R., Eberhardt, M., Mondesire, J., Patel, P., Pavkov, M., Rolka, D., Saydah, S., Shrestha, S. and Waller, L., 2020. CKD Awareness Among US Adults by Future Risk of Kidney Failure. *American Journal of Kidney Diseases,* 76 (2), 174–183.

Chung, A.C., Huang, X.R., Meng, X. and Lan, H.Y., 2010. miR-192 mediates TGF-β/Smad3-driven renal fibrosis. *Journal of the American Society of Nephrology,* 21 (8), 1317–1325.a

Chung, A.C.K., Haiyan Zhang, Kong, Y., Tan, J., Huang, X.R., Kopp, J.B. and Lan, H.Y., 2010. Advanced Glycation End-Products Induce Tubular CTGF via TGF-β–Independent Smad3 Signaling. *Journal of the American Society of Nephrology,* 21 (2), 249-260.b

Cianciolo, G., La Manna, G., Capelli, I., Gasperoni, L., Galassi, A., Ciceri, P. and Cozzolino, M., 2021. The role of activin: the other side of chronic kidney disease–mineral bone disorder? *Nephrology, Dialysis, Transplantation,* 36 (6), 966–974.

Ciftci, E., Bozbeyoglu, N., Gursel, I., Korkusuz, F., Bakan Misirlioglu, F. and Korkusuz, P., 2023. Comparative analysis of magnetically activated cell sorting and ultracentrifugation methods for exosome isolation. *PloS One*, 18 (2), e0282238.

Coca, S.G., Nadkarni, G.N., Huang, Y., Moledina, D.G., Rao, V., Zhang, J., Ferket, B., Crowley, S.T., Fried, L.F. and Parikh, C.R., 2017. Plasma Biomarkers and Kidney Function Decline in Early and Established Diabetic Kidney Disease. *Journal of the American Society of Nephrology,* 28 (9), 2786-2793.

Cockcroft, D.W., and Gault, H., 1976. Prediction of Creatinine Clearance from Serum Creatinine. *Nephron,* 16 (1), 31-41.

Cocucci, E., and Meldolesi, J., 2015. Ectosomes and exosomes: shedding the confusion between extracellular vesicles. *Trends in Cell Biology,* 25 (6), 364-372.

Colombo, M., Moita, C., van Niel, G., Kowal, J., Vigneron, J., Benaroch, P., Manel, N., Moita, L.F., Théry, C. and Raposo, G., 2013. Analysis of ESCRT functions in exosome biogenesis, composition and secretion highlights the heterogeneity of extracellular vesicles. *Journal of Cell Science,* 126 (Pt 24), 5553-5565.

Colombo, M., Raposo, G. and Théry, C., 2014. Biogenesis, Secretion, and Intercellular Interactions of Exosomes and Other Extracellular Vesicles. *Annual Review of Cell and Developmental Biology,* 30 (1), 255-289.

Comper, W.D., Vuchkova, J. and McCarthy, K.J., 2022. New insights into proteinuria/albuminuria. *Frontiers in Physiology,* 13, 991756.

Conner, S.D., and Schmid, S.L., 2003. Regulated portals of entry into the cell. *Nature (London),* 422 (6927), 37-44.

Connor, D.E., Exner, T., Ma, D.D.F. and Joseph, J.E., 2010. The majority of circulating platelet-derived microparticles fail to bind annexin V, lack phospholipid-dependent procoagulant activity and demonstrate greater expression of glycoprotein Ib. *Thrombosis and Haemostasis,* 103 (5), 1044-1052.

Cravedi, P., Kopp, J.B., and Remuzzi, G., 2013. Recent progress in the pathophysiology and treatment of FSGS recurrence. *American Journal of Transplantation*, 13 (2), 266-274.

Crescitelli, R., Lässer, C. and Lötvall, J., 2021. Isolation and characterization of extracellular vesicle subpopulations from tissues. *Nature Protocols,* 16 (3), 1548-1580.

Cricrì, G., Bellucci, L., Montini, G. and Collino, F., 2021. Urinary Extracellular Vesicles: Uncovering the Basis of the Pathological Processes in Kidney-Related Diseases. *International Journal of Molecular Sciences,* 22 (12), 6507.

Critselis, E., and Lambers Heerspink, H., 2016. Utility of the CKD273 peptide classifier in predicting chronic kidney disease progression. *Nephrology, Dialysis, Transplantation,* 31 (2), 249–254.

Crossland, R.E., Albiero, A., Sanjurjo-Rodríguez, C., Reis, M., Resteu, A., Anderson, A.E., Dickinson, A.M., Pratt, A.G., Birch, M., McCaskie, A.W., Jones, E. and Wang, X., 2023. MicroRNA profiling of low concentration extracellular vesicle RNA utilizing NanoString nCounter technology. *Journal of Extracellular Biology*, 2 (1), e72–n/a.

Da Silva Lodge, M., Pullen, N., Pereira, M. and Johnson, T.S., 2022. Urinary levels of pro-fibrotic transglutaminase 2 (TG2) may help predict progression of chronic kidney disease. *PloS One,* 17 (1), e0262104.

Daaboul, G.G., Gagni, P., Benussi, L., Bettotti, P., Ciani, M., Cretich, M., Freedman, D.S., Ghidoni, R., Ozkumur, A.Y., Piotto, C., Prosperi, D., Santini, B., Ünlü, M.S. and Chiari, M., 2016. Digital Detection of Exosomes by Interferometric Imaging. *Scientific Reports,* 6 (1), 37246.

D'Agati, V.D., Fogo, A.B., Bruijn, J.A. and Jennette, J.C., 2004. Pathologic classification of focal segmental glomerulosclerosis: a working proposal. *American Journal of Kidney Diseases,* 43 (2), 368-382.

Dai, R., Zhang, L., Jin, H., Wang, D., Cheng, M., Xu, Y., Zhang, H. and Wang, Y., 2023. Differential expression profile of urinary exosomal microRNAs in patients with mesangial proliferative glomerulonephritis. *Aging (Albany, NY.),* 15 (3), 866–880.

Dattani, R., Corbett, R.W., Galliford, J., Hill, P., Cairns, T., Cook, H.T., Roufosse, C. and Ashby, D.R., 2020. The Effect of Kidney Biopsy on Glomerular Filtration Rate: A Frequent Patient Concern. *American Journal of Nephrology,* 51 (11), 903-906.

de Mateo, S., Castillo, J., Estanyol, J.M., Ballescà, J.L. and Oliva, R., 2011. Proteomic characterization of the human sperm nucleus. *PROTEOMICS,* 11 (13), 2714–2726.

De, S., Kuwahara, S., Hosojima, M., Ishikawa, T., Kaseda, R., Sarkar, P., Yoshioka, Y., Kabasawa, H., Iida, T., Goto, S., Toba, K., Higuchi, Y., Suzuki, Y., Hara, M., Kurosawa, H., Narita, I., Hirayama, Y., Ochiya, T. and Saito, A., 2017. Exocytosis-mediated urinary full-length megalin excretion is linked with the pathogenesis of diabetic nephropathy. *Diabetes,* 66 (5), 1391–1404.

De Vriese, A.S., Tilton, R.G., Elger, M., Stephan, C.C., Kriz, W. and Lameire, N.H., 2001. Antibodies against Vascular Endothelial Growth Factor Improve Early Renal Dysfunction in Experimental Diabetes. *Journal of the American Society of Nephrology,* 12 (5), 993-1000.

Deatherage, B.L., and Cookson, B.T., 2012. Membrane Vesicle Release in Bacteria, Eukaryotes, and Archaea: a Conserved yet Underappreciated Aspect of Microbial Life. *Infection and Immunity,* 80 (6), 1948-1957.

del Conde, I., Shrimpton, C.N., Thiagarajan, P. and López, J.A., 2005. Tissue-factor–bearing microvesicles arise from lipid rafts and fuse with activated platelets to initiate coagulation. *Blood,* 106 (5), 1604-1611.

Delić, D., Eisele, C., Schmid, R., Baum, P., Wiech, F., Gerl, M., Zimdahl, H., Pullen, S.S. and Urquhart, R., 2016. Urinary exosomal miRNA signature in type II diabetic nephropathy patients. *PloS One,* 11 (3), e0150154.

Demichev, V., Messner, C.B., Vernardis, S.I., Lilley, K.S. and Ralser, M., 2020. DIA-NN: neural networks and interference correction enable deep proteome coverage in high throughput. *Nature Methods,* 17 (1), 41-44.

Deng, F., Ratri, A., Deighan, C., Daaboul, G., Geiger, P.C. and Christenson, L.K., 2022. Single-Particle Interferometric Reflectance Imaging Characterization of Individual Extracellular Vesicles and Population Dynamics. *Journal of Visualized Experiments,* (179).

Desnick Robert, J., Ioannou Yiannis, A. and Eng Christine, M., 2001, α-Galactosidase A Deficiency: Fabry Disease. In: Scriver CR, Beaudet AL, Sly WS, Valle D, ed., *The Metabolic and Molecular Bases of Inherited Disease*, 8th edn. New York: McGraw-Hill, 2001, pp. 37–74.

Dhar, P., and McAuley, J., 2019. The Role of the Cell Surface Mucin MUC1 as a Barrier to Infection and Regulator of Inflammation. *Frontiers in Cellular and Infection Microbiology,* 9, 117.

Dimuccio, V., Peruzzi, L., Brizzi, M.F., Cocchi, E., Fop, F., Boido, A., Gili, M., Gallo, S., Biancone, L., Camussi, G. and Bussolati, B., 2020. Acute and chronic glomerular damage is associated with reduced CD133 expression in urinary extracellular vesicles. *American Journal of Physiology. Renal Physiology,* 318 (2), F486–F495.

Ding, H., Zhou, D., Hao, S., Zhou, L., He, W., Nie, J., Hou, F.F. and Liu, Y., 2012. Sonic Hedgehog Signaling Mediates Epithelial–Mesenchymal Communication and Promotes Renal Fibrosis. *Journal of the American Society of Nephrology,* 23 (5), 801-813.

Dische, F.E., Anderson, V.E., Keane, S.J., Taube, D., Bewick, M. and Parsons, V., 1990. Incidence of thin membrane nephropathy: morphometric investigation of a population sample. *Journal of Clinical Pathology*, 43 (6), 457-460.

Dixson, A.C., Dawson, T.R., Di Vizio, D. and Weaver, A.M., 2023. Context-specific regulation of extracellular vesicle biogenesis and cargo selection. *Nature Reviews Molecular Cell Biology,* 24 (7), 454–476.

Djudjaj, S., Chatziantoniou, C., Raffetseder, U., Guerrot, D., Dussaule, J., Boor, P., Kerroch, M., Hanssen, L., Brandt, S., Dittrich, A., Ostendorf, T., Floege, J., Zhu, C., Lindenmeyer, M., Cohen, C. and Mertens, P., 2012. Notch-3 receptor activation drives inflammation and fibrosis following tubulointerstitial kidney injury. *The Journal of Pathology,* 228 (3), 286-99.

Domon, B., and Aebersold, R., 2006. Mass Spectrometry and Protein Analysis. *Science,* 312 (5771), 212-217.

Dragovic, R.A., Gardiner, C., Brooks, A.S., Tannetta, D.S., Ferguson, D.J., Hole, P., Carr, B., Redman, C.W., Harris, A.L. and Dobson, P.J., 2011. Sizing and phenotyping of cellular vesicles using Nanoparticle Tracking Analysis. *Nanomedicine: Nanotechnology, Biology and Medicine,* 7 (6), 780–788.

Dube, J., Girouard, J., Leclerc, P. and Douville, P., 2005. Problems with the estimation of urine protein by automated assays. *clinical Biochemistry,* 38 (5), 479-485.

E, J., Liu, S., Ma, D., Zhang, G., Cao, S., Li, B., Lu, X., Luo, H., Bao, L., Lan, X., Fu, R. and Zheng, Y., 2024. Nanopore-based full-length transcriptome sequencing for understanding the underlying molecular mechanisms of rapid and slow progression of diabetes nephropathy. BMC Medical Genomics, 17 (1), 246–16.

Eastel, J.M., Lam, K.W., Lee, N.L., Lok, W.Y., Tsang, A.H.F., Pei, X.M., Chan, A.K.C., Cho, W.C.S. and Wong, S.C.C., 2019. Application of NanoString technologies in companion diagnostic development. *Expert Review of Molecular Diagnostics,* 19 (7), 591–598.

Eddy, A.A., and Symons, J.M., 2003. Nephrotic syndrome in childhood. *The Lancet (British Edition),* 362 (9384), 629-639.

Edeling, M., Ragi, G., Huang, S., Pavenstädt, H. and Susztak, K., 2016. Developmental signalling pathways in renal fibrosis: the roles of Notch, Wnt and Hedgehog. *Nature Reviews. Nephrology,* 12 (7), 426-439.

Eissa, S., Matboli, M., Aboushahba, R., Bekhet, M.M., Soliman, Y., 2016. Urinary exosomal microRNA panel unravels novel biomarkers for diagnosis of type 2 diabetic kidney disease. *Journal of Diabetes and its Complications*, 30 (8), 1585-1592.

Elwood, C.M., and Sigman, E.M., 1967. The Measurement of Glomerular Filtration Rate and Effective Renal Plasma Flow in Man by Iothalamate ^{125}I and Iodopyracet ^{131}I. *Circulation,* 36 (3), 441. ENDOH, M., KASHEM, A., YAMAUCHI, F., YANO, N., NOMOTO, Y., SAKAI, H. and KUROKAWA, K., 1997. Expression of thromboxane synthase in kidney tissues from patients with IgA nephropathy. *Clinical Nephrology,* 47 (3), 168–175.

Endoh, M., Kashem, A., Yamauchi, F., Yano, N., Nomoto, Y., Sakai, H. and Kurokawa, K., 1997. Expression of thromboxane synthase in kidney tissues from patients with IgA nephropathy. *Clinical Nephrology,* 47 (3), 168–175.

Engel, J.E., Williams, E., Williams, M.L., Bidwell, G.L. and Chade, A.R., 2019. Targeted VEGF (Vascular Endothelial Growth Factor) Therapy Induces Long-Term Renal Recovery in Chronic Kidney Disease via Macrophage Polarization. *Hypertension,* 74 (5), 1113–1123.

Erdbrügger, U., and Le, T.H., 2016. Extracellular vesicles in renal diseases: More than novel biomarkers? *Journal of the American Society of Nephrology,* 27 (1), 12-26.

Erdbrügger, U., Blijdorp, C.J., Bijnsdorp, I.V., Borràs, F.E., Burger, D., Bussolati, B., Byrd, J.B., Clayton, A., Dear, J.W., Falcón-Pérez, J.M., Grange, C., Hill, A.F., Holthöfer, H., Hoorn, E.J., Jenster, G., Jimenez, C.R., Junker, K., Klein, J., Knepper, M.A., Koritzinsky, E.H., Luther, J.M., Lenassi, M., Leivo, J., Mertens, I., Musante, L., Oeyen, E., Puhka, M., van Royen, M.E., Sánchez, C., Soekmadji, C., Thongboonkerd, V., van Steijn, V., Verhaegh, G., Webber, J.P., Witwer, K., Yuen, P.S.T., Zheng, L., Llorente, A. and Martens-Uzunova, E.S., 2021. Urinary extracellular vesicles: A position paper by the Urine Task Force of the International Society for Extracellular Vesicles. *Journal of Flood Risk Management,* 10 (7), e12093-n/a.

Erdfelder, E., Faul, F. and Buchner, A., 1996. GPOWER: A general power analysis program. *Behavior Research Methods, Instruments & Computers.,* 28 (1), 1–11.

Erozenci, L.A., Piersma, S.R., Pham, T.V., Bijnsdorp, I.V. and Jimenez, C.R., 2021. Longitudinal stability of urinary extracellular vesicle protein patterns within and between individuals. *Scientific Reports,* 11 (1), 15629.

Escher, C., Reiter, L., MacLean, B., Ossola, R., Herzog, F., Chilton, J., MacCoss, M.J. and Rinner, O., 2012. Using iRT, a normalized retention time for more targeted measurement of peptides. *Proteomics,* 12 (8), 1111-1121.

Escrevente, C., Keller, S., Altevogt, P. and Costa, J., 2011. Interaction and uptake of exosomes by ovarian cancer cells. *BMC Cancer,* 11 (1), 108.

España, F., Fink, E., Sanchez-Cuenca, J., Gilabert, J., Estellés, A. and Witzgall, K., 1995. Complexes of Tissue Kallikrein with Protein C Inhibitor in Human Semen and Urine. *European Journal of Biochemistry,* 234 (2), 641–649.

Essawy, M., Soylemezoglu, O., Muchaneta-kubara, E.C., Shortland, J., Brown, C.B. and El Nahas, A.M., 1997. Myofibroblasts and the progression of diabetic nephropathy. *Nephrology Dialysis Transplantation,* 12 (1), 43-50.

Fabian, S.L., Penchev, R.R., St-Jacques, B., Rao, A.N., Sipilä, P., West, K.A., McMahon, A.P. and Humphreys, B.D., 2012. Hedgehog-Gli Pathway Activation during Kidney Fibrosis. *The American Journal of Pathology,* 180 (4), 1441-1453.

Falke, L.L., Gholizadeh, S., Goldschmeding, R., Kok, R.J. and Nguyen, T.Q., 2015. Diverse origins of the myofibroblast—implications for kidney fibrosis. *Nature Reviews Nephrology,* 11 (4), 233-244.

Fan, G., Gong, T., Lin, Y., Wang, J., Sun, L., Wei, H., Yang, X., Liu, Z., Li, X., Zhao, L., Song, L., He, J., Liu, H., Li, X., Liu, L., Li, A., Lu, Q., Zou, D., Wen, J., Xia, Y., Wu, L., Huang, H., Zhang, Y., Xie, W., Huang, J., Luo, L., Wu, L., He, L., Liang, Q., Chen, Q., Chen, G., Bai, M., Qin, J., Ni, X., Tang, X. and Wang, Y., 2021. Urine proteomics identifies biomarkers for diabetic kidney disease at different stages. *Clinical Proteomics,* 18 (1), doi: 10.1186/s12014-021-09338-6

Farzamikia, N., Hejazian, S.M., Mostafavi, S., Baradaran, B., Zununi Vahed, S. and Ardalan, M., 2024. Podocyte-specific proteins in urinary extracellular vesicles of patients with IgA nephropathy: Vasorin and ceruloplasmin. *BioImpacts : BI,* 14 (3), 29981–8.

Feng, D., Zhao, W., Ye, Y., Bai, X., Liu, R., Chang, L., Zhou, Q. and Sui, S., 2010. Cellular Internalization of Exosomes Occurs Through Phagocytosis. *Traffic (Copenhagen, Denmark),* 11 (5), 675-687.

Feng, Y., Huo, Q., Li, B. and Yokota, H., 2023. Unveiling the Dichotomy of Urinary Proteins: Diagnostic Insights into Breast and Prostate Cancer and Their Roles. *Proteomes,* 12 (1), 1.

Feng, Y., Lv, L., Wu, W., Li, Z., Chen, J., Ni, H., Zhou, L., Tang, T., Wang, F., Wang, B., Chen, P., Crowley, S.D. and Liu, B., 2018. Urinary Exosomes and Exosomal CCL2 mRNA as Biomarkers of Active Histologic Injury in IgA Nephropathy. *The American Journal of Pathology,* 188 (11), 2542–2552.

Fenta, E.T., Eshetu, H.B., Kebede, N., Bogale, E.K., Zewdie, A., Kassie, T.D., Anagaw, T.F., Mazengia, E.M. and Gelaw, S.S., 2023. Prevalence and predictors of chronic kidney disease among type 2 diabetic patients worldwide, systematic review and meta-analysis. *Diabetology and Metabolic Syndrome,* 15 (1), 1-245.

Ferreras, L., Moles, A., Situmorang, G.R., el Masri, R., Wilson, I.L., Cooke, K., Thompson, E., Kusche-Gullberg, M., Vivès, R.R., Sheerin, N.S. and Ali, S., 2019. Heparan sulfate in chronic kidney diseases: Exploring the role of 3-O-sulfation. *Biochimica Et Biophysica Acta. General Subjects,* 1863 (5), 839–848.

Ferretti, C., and La Cava, A., 2016, Chapter 8 - Overview of the Pathogenesis of Systemic Lupus Erythematosus. *In:* Chapter 8 - Overview of the Pathogenesis of Systemic Lupus Erythematosus. *Systemic Lupus Erythematosus.* Elsevier Inc, 2016, pp. 55-62.

Filip, S., Vougas, K., Zoidakis, J., Latosinska, A., Mullen, W., Spasovski, G., Mischak, H., Vlahou, A., Jankowski, J. and Martens, L., 2015. Comparison of Depletion Strategies for the Enrichment of Low-Abundance Proteins in Urine. *PLoS ONE,* 10 (7).

Fitzner, D., Schnaars, M., van Rossum, D., Krishnamoorthy, G., Dibaj, P., Bakhti, M., Regen, T., Hanisch, U. and Simons, M., 2011. Selective Transfer of Exosomes From Oligodendrocytes to Microglia by Macropinocytosis. *J. Cell Science,* 124 (Pt 3), 447-458.

Fliser, D., Novak, J., Thongboonkerd, V., Argiles, A., Jankowski, V., Girolami, M.A., Jankowski, J. and Mischak, H., 2007. Advances in Urinary Proteome Analysis and Biomarker Discovery. *Journal of the American Society of Nephrology,* 18 (4), 1057-1071.

Floege, J., and Drüeke, T.B., 2020. Mineral and bone disorder in chronic kidney disease: pioneering studies. *Kidney International,* 98 (4), 807–811.

Flyvbjerg, A., Dagnaes-hansen, F., De Vriese, A.S., Schrijvers, B.F., Tilton, R.G. and Rasch, R., 2002. Amelioration of Long-Term Renal Changes in Obese Type 2 Diabetic Mice by a Neutralizing Vascular Endothelial Growth Factor Antibody. *Diabetes,* 51 (10), 3090-3094.

Foreman, K.J., Marquez, N., Dolgert, A., Fukutaki, K., Fullman, N., McGaughey, M., Pletcher, M.A., Smith, A.E., Tang, K., Yuan, C., Brown, J.C., Friedman, J., He, J., Heuton, K.R., Holmberg, M., Patel, D.J., Reidy, P., Carter, A., Cercy, K., Chapin, A., Douwes-Schultz, D., Frank, T., Goettsch, F., Liu, P.Y., Nandakumar, V., Reitsma, M.B., Reuter, V., Sadat, N., Sorensen, R.J.D., Srinivasan, V., Updike, R.L., York, H., Lopez, A.D., Lozano, R., Lim, S.S., Mokdad, A.H., Vollset, S.E. and Murray, C.J.L., 2018. Forecasting life expectancy, years of life lost, and all-cause and cause-specific mortality for 250 causes of death: reference and alternative scenarios for 2016–40 for 195 countries and territories. *The Lancet,* 392 (10159), 2052-2090.

Frazier, K., Williams, S., Kothapalli, D., Klapper, H. and Grotendorst, G.R., 1996. Stimulation of Fibroblast Cell Growth, Matrix Production, and Granulation Tissue Formation by Connective Tissue Growth Factor. *Journal of Investigative Dermatology,* 107 (3), 404-411.

Frick, M., Bright, N.A., Riento, K., Bray, A., Merrified, C. and Nichols, B.J., 2007. Coassembly of Flotillins Induces Formation of Membrane Microdomains, Membrane Curvature, and Vesicle Budding. *Current Biology,* 17 (13), 1151-1156.

Friedländer, M.R., Mackowiak, S.D., Li, N., Chen, W. and Rajewsky, N., 2012. miRDeep2 accurately identifies known and hundreds of novel microRNA genes in seven animal clades. *Nucleic Acids Research,* 40 (1), 37–52.

Frydlova, J., Zednikova, I., Satrapova, V., Pazourkova, E., Santorova, S., Hruskova, Z., Tesar, V., Vokurka, M., Prikryl, P. and Korabecna, M., 2022. Analysis of microRNAs in Small Urinary

Extracellular Vesicles and Their Potential Roles in Pathogenesis of Renal ANCA-Associated Vasculitis. *International Journal of Molecular Sciences,* 23 (8), 4344.

Frühbeis, C., Fröhlich, D., Kuo, W.P., Amphornrat, J., Thilemann, S., Saab, A.S., Kirchhoff, F., Möbius, W., Goebbels, S., Nave, K., Schneider, A., Simons, M., Klugmann, M., Trotter, J. and Krämer-Albers, E., 2013. Neurotransmitter-Triggered Transfer of Exosomes Mediates Oligodendrocyte–Neuron Communication. *PLoS Biology,* 11 (7), e1001604.

Furini, G., Schroeder, N., Huang, L., Boocock, D., Scarpellini, A., Coveney, C., Tonoli, E., Ramaswamy, R., Ball, G., Verderio, C., Johnson, T.S. and Verderio, E.A.M., 2018. Proteomic Profiling Reveals the Transglutaminase-2 Externalization Pathway in Kidneys after Unilateral Ureteric Obstruction. *Journal of the American Society of Nephrology,* 29 (3), 880-905.

Furness, P.N., and Taub, N., 2001. International variation in the interpretation of renal transplant biopsies: Report of the CERTPAP Project. *Kidney International,* 60 (5), 1998-2012.

Futter, C.E., Collinson, L.M., Backer, J.M. and Hopkins, C.R., 2001. Human VPS34 Is Required for Internal Vesicle Formation within Multivesicular Endosomes. *The Journal of Cell Biology,* 155 (7), 1251-1263.

Gaipov, A., Makhammajanov, Z., Dauyey, Z., Markhametova, Z., Mussina, K., Nogaibayeva, A., Kozina, L., Auganova, D., Tarlykov, P., Bukasov, R., Utegulov, Z., Turebekov, D., Soler, M.J., Ortiz, A. and Kanbay, M., 2022. Urinary Protein Profiling for Potential Biomarkers of Chronic Kidney Disease: A Pilot Study. *Diagnostics (Basel),* 12 (11), 2583.

Garmaa, G., Nagy, R., Kói, T., To, U.N.D., Gergő, D., Kleiner, D., Csupor, D., Hegyi, P. and Kökény, G., 2024. Panel miRNAs are potential diagnostic markers for chronic kidney diseases: a systematic review and meta-analysis. *BMC Nephrology,* 25 (1), 261–14.

Gaspari, F., Perico, N., Ruggenenti, P., Mosconi, L., Amuchastegui, C.S., Guerini, E., Daina, E. and Remuzzi, G., 1995. Plasma clearance of nonradioactive iohexol as a measure of glomerular filtration rate. *Journal of the American Society of Nephrology,* 6 (2), 257-263.

Geiss, G.K., Bumgarner, R.E., Birditt, B., Dahl, T., Dowidar, N., Dunaway, D.L., Fell, H.P., Ferree, S., George, R.D., Grogan, T., James, J.J., Maysuria, M., Mitton, J.D., Oliveri, P., Osborn, J.L., Peng, T., Ratcliffe, A.L., Webster, P.J., Davidson, E.H., Hood, L. and Dimitrov, K., 2008. Direct multiplexed measurement of gene expression with color-coded probe pairs. *Nature Biotechnology,* 26 (3), 317–325.

Gheinani, A.H., Vögeli, M., Baumgartner, U., Vassella, E., Draeger, A., Burkhard, F.C. and Monastyrskaya, K., 2018. Improved isolation strategies to increase the yield and purity of human urinary exosomes for biomarker discovery. *Scientific Reports*, 8 (1), 3945–17.

Ghossoub, R., Lembo, F., Rubio, A., Gaillard, C.B., Bouchet, J., Vitale, N., Slavík, J., Machala, M. and Zimmermann, P., 2014. Syntenin-ALIX exosome biogenesis and budding into multivesicular bodies are controlled by ARF6 and PLD2. *Nature Communications,* 5 (1), 3477.

Gibier, J., Hémon, B., Fanchon, M., Gaudelot, K., Pottier, N., Ringot, B., Van Seuningen, I., Glowacki, F., Cauffiez, C., Blum, D., Copin, M., Perrais, M. and Gnemmi, V., 2017. Dual role of MUC1 mucin in kidney ischemia-reperfusion injury: Nephroprotector in early phase, but pro-fibrotic in late phase. *Biochimica Et Biophysica Acta. Molecular Basis of Disease,* 1863 (6), 1336–1349.

Gildea, J.J., Seaton, J.E., Victor, K.G., Reyes, C.M., Bigler Wang, D., Pettigrew, A.C., Courtner, C.E., Shah, N., Tran, H.T., Van Sciver, R.E., Carlson, J.M. and Felder, R.A., 2014. Exosomal transfer from human renal proximal tubule cells to distal tubule and collecting duct cells. *Clinical Biochemistry,* 47 (15), 89-94.

Gillet, L.C., Navarro, P., Tate, S., Röst, H., Selevsek, N., Reiter, L., Bonner, R. and Aebersold, R., 2012. Targeted Data Extraction of the MS/MS Spectra Generated by Data-independent Acquisition: A New Concept for Consistent and Accurate Proteome Analysis. *Molecular & Cellular Proteomics,* 11 (6), O111.-O111.016717.

Gluba-Sagr, A., Franczyk, B., Rysz-Górzyńska, M., Ławiński, J. and Rysz, J., 2023. The Role of miRNA in Renal Fibrosis Leading to Chronic Kidney Disease. *Biomedicines,* 11 (9), 2358.

Goerlich, N., Brand, H.A., Langhans, V., Tesch, S., Schachtner, T., Koch, B., Paliege, A., Schneider, W., Grützkau, A., Reinke, P. and Enghard, P., 2020. Kidney transplant monitoring by urinary flow cytometry: Biomarker combination of T cells, renal tubular epithelial cells, and podocalyxin-positive cells detects rejection. *Scientific Reports,* 10 (1), 796.

Gomes, F.A., Souza Junior, D.R., Massafera, M.P. and Ronsein, G.E., 2024. Robust assessment of sample preparation protocols for proteomics of cells and tissues. *Biochimica Et Biophysica Acta. Proteins and Proteomics,* 1872 (5), 141030.

Gonzales, P.A., Pisitkun, T., Hoffert, J.D., Tchapyjnikov, D., Star, R.A., Kleta, R., Wang, N.S. and Knepper, M.A., 2009. Large-Scale Proteomics and Phosphoproteomics of Urinary Exosomes. Journal of the American Society of Nephrology, 20 (2), 363-379.

Good, D.M., Zürbig, P., Argilés, À, Bauer, H.W., Behrens, G., Coon, J.J., Dakna, M., Decramer, S., Delles, C., Dominiczak, A.F., Ehrich, J.H.H., Eitner, F., Fliser, D., Frommberger, M., Ganser, A., Girolami, M.A., Golovko, I., Gwinner, W., Haubitz, M., Herget-Rosenthal, S., Jankowski, J., Jahn, H., Jerums, G., Julian, B.A., Kellmann, M., Kliem, V., Kolch, W., Krolewski, A.S., Luppi, M., Massy, Z., Melter, M., Neusüss, C., Novak, J., Peter, K., Rossing, K., Rupprecht, H., Schanstra, J.P., Schiffer, E., Stolzenburg, J., Tarnow, L., Theodorescu, D., Thongboonkerd, V., Vanholder, R., Weissinger, E.M., Mischak, H. and Schmitt-Kopplin, P., 2010. Naturally Occurring Human Urinary Peptides for Use in Diagnosis of Chronic Kidney Disease. *Molecular & Cellular Proteomics,* 9 (11), 2424–2437.

Goto, Y., Uchio-Yamada, K., Anan, S., Yamamoto, Y., Ogura, A. and Manabe, N., 2005. Transforming growth factor-β1 mediated up-regulation of lysyl oxidase in the kidneys of hereditary nephrotic mouse with chronic renal fibrosis. *Virchows Archiv : An International Journal of Pathology,* 447 (5), 859-868.

Grange, C., and Bussolati, B., 2022. Extracellular vesicles in kidney disease. *Nature Reviews. Nephrology,* 18 (8), 499–513.

Grange, C., Dalmasso, A., Cortez, J.J., Spokeviciute, B. and Bussolati, B., 2023. Exploring the role of urinary extracellular vesicles in kidney physiology, aging, and disease progression. *American Journal of Physiology: Cell Physiology,* 325 (6), C1439–C1450.

Graumann, J., Scheltema, R.A., Zhang, Y., Cox, J. and Mann, M., 2012. A Framework for Intelligent Data Acquisition and Real-Time Database Searching for Shotgun Proteomics. *Molecular & Cellular Proteomics,* 11 (3), M111.013185.

Grieco, G.E., Brusco, N., Fignani, D., Nigi, L., Formichi, C., Licata, G., Marselli, L., Marchetti, P., Salvini, L., Tinti, L., Po, A., Ferretti, E., Sebastiani, G. and Dotta, F., 2022. Reduced miR-184-3p expression protects pancreatic β-cells from lipotoxic and proinflammatory apoptosis in type 2 diabetes via CRTC1 upregulation. *Cell Death Discovery*, 8 (1), 340.

Griep, R.J., and Nelp, W.B., 1969. Mechanism of Excretion of Radioiodinated Sodium Iothalamate. *Radiology,* 93 (4), 807-811.

Groop Per-Henrik, Thomas Merlin C., Moran John L., Wadèn Johan, Thorn Lena M., Mäkinen Ville-Petteri, Rosengård-Bärlund Milla, Saraheimom Markku, Hietala Kustaa, Heikkilä Outi and Forsblom Carol, 2009. The Presence and Severity of Chronic Kidney Disease Predicts All-Cause Mortality in Type 1 Diabetes. *Diabetes,* 58 (7), 1651-1658.

Grubb, A., Simonsen, O., Sturfelt, G., Truedsson, L. And Thysell, H., 1985. Serum Concentration of Cystatin C, Factor D and β2-Microglobulin as a Measure of Glomerular Filtration Rate. *Acta Medica Scandinavica,* 218 (5), 499-503.

Gudehithlu, K.P., Hart, P., Joshi, A., Garcia-Gomez, I., Cimbaluk, D.J., Dunea, G., Arruda, J.A.L. and Singh, A.K., 2019. Urine exosomal ceruloplasmin: a potential early biomarker of underlying kidney disease. *Clinical and Experimental Nephrology,* 23 (8), 1013–1021.

Gudehithlu, K.P., Garcia-Gomez, I., Vernik, J., Brecklin, C., Kraus, M., Cimbaluk, D.J., Hart, P., Dunea, G., Arruda, J.A.L. and Singh, A.K., 2016. In Diabetic Kidney Disease Urinary Exosomes Better Represent Kidney Specific Protein Alterations Than Whole Urine. *American Journal of Nephrology,* 42 (6), 418–424.

Guerra, F., and Bucci, C., 2016. Multiple Roles of the Small GTPase Rab7. *Cells (Basel, Switzerland),* 5 (3), 34.

Guo, Z., Zhang, Y., Zou, L., Wang, D., Shao, C., Wang, Y., Sun, W. and Zhang, L., 2015. A Proteomic Analysis of Individual and Gender Variations in Normal Human Urine and Cerebrospinal Fluid Using iTRAQ Quantification. *Plos One,* 10 (7), e0–e0133270.

Haas, M., 2006. Thin glomerular basement membrane nephropathy: incidence in 3471 consecutive renal biopsies examined by electron microscopy. *Archives of Pathology & Laboratory Medicine,* 130 (5), 699-706.

Hanatani, S., Izumiya, Y., Araki, S., Rokutanda, T., Kimura, Y., Walsh, K. and Ogawa, H., 2014. Akt1-Mediated Fast/Glycolytic Skeletal Muscle Growth Attenuates Renal Damage in Experimental Kidney Disease. *Journal of the American Society of Nephrology,* 25 (12), 2800–2811.

Harpole, M., Davis, J. and Espina, V., 2016. Current state of the art for enhancing urine biomarker discovery. *Expert Review of Proteomics,* 13 (6), 609-626.

Harris, J.I., 1956. Effect of Urea on Trypsin and Alpha-Chymotrypsin. *Nature (London),* 177 (4506), 471-473.

Hayashi, T., Nishioka, J., Kamada, H., Asanuma, K., Kondo, H., Gabazza, E.C., Ido, M. and Suzuki, K., 2004. Characterization of a novel human protein C inhibitor (PCI) gene transgenic mouse useful for studying the role of PCI in physiological and pathological conditions. *Journal of Thrombosis and Haemostasis,* 2 (6), 949–961.

Heijnen, H.F.G., Schiel, A.E., Fijnheer, R., Geuze, H.J. and Sixma, J.J., 1999. Activated Platelets Release Two Types of Membrane Vesicles: Microvesicles by Surface Shedding and Exosomes Derived From Exocytosis of Multivesicular Bodies and α-Granules. *Blood,* 94 (11), 3791-3799.

Helm, B., Hansen, P., Lai, L., Schwarzmuller, L., Clas, S.M., Richter, A., Ruwolt, M., Liu, F., Frey, D., Dalessandro, L.A., Lehmann, W.D., Schilling, M., Helm, D., Fiedler, D. and Klingmuller, U., 2024. *Lysis buffer selection guidance for mass spectrometry-based global proteomics including studies on the intersection of signal transduction and metabolism.* Cold Spring Harbor: Cold Spring Harbor Laboratory Press.

Heng, S., Samarajeewa, N., Wang, Y., Paule, S.G., Breen, J. and Nie, G., 2021. Podocalyxin promotes an impermeable epithelium and inhibits pro-implantation factors to negatively regulate endometrial receptivity. *Scientific Reports,* 11 (1), 24016.

Henne, W.M., Stenmark, H. and Emr, S.D., 2013. Molecular mechanisms of the membrane sculpting ESCRT pathway. *Cold Spring Harbor Perspectives in Biology,* 5 (9), a016766.

Herman-Edelstein, M., Scherzer, P., Tobar, A., Levi, M. and Gafter, U., 2014. Altered renal lipid metabolism and renal lipid accumulation in human diabetic nephropathy. *Journal of Lipid Research,* 55 (3), 561-572.

Higashi, K., Kubo, H., Watanabe, H., Fujimori, K., Mikami, T. and Kaneko, H., 2011. Adipokine ganglioside GM2 activator protein stimulates insulin secretion. *FEBS Letters,* 585 (16), 2587–2591.

Hildebrandt, F., and Zhou, W., 2007. Nephronophthisis-associated ciliopathies. *Journal of the American Society of Nephrology: JASN*, 18 (6), 1855-1871.

Himmelfarb, J., and Tuttle, K.R., 2013. New Therapies for Diabetic Kidney Disease. *The New England Journal of Medicine,* 369 (26), 2549–2550.

Hirakawa, Y., Yoshioka, K., Kojima, K., Yamashita, Y., Shibahara, T., Wada, T., Nangaku, M. and Inagi, R., 2022. Potential progression biomarkers of diabetic kidney disease determined using comprehensive machine learning analysis of non-targeted metabolomics. *Scientific Reports,* 12 (1), 16287.

Hiramatsu-Asano, S., Sunahori-Watanabe, K., Zeggar, S., Katsuyama, E., Mukai, T., Morita, Y. and Wada, J., 2021. Deletion of Mir223 Exacerbates Lupus Nephritis by Targeting S1pr1 in Faslpr/lpr Mice. *Frontiers in Immunology,* 11, 616141.

Ho, T.H., Charlet-B, N., Poulos, M.G., Singh, G., Swanson, M.S. and Cooper, T.A., 2004. Muscleblind proteins regulate alternative splicing. *EMBO Journal,* 23 (15), 3103–3112.

Holland, P.M., Abramson, R.D., Watson, R. and Gelfand, D.H., 1991. Detection of specific polymerase chain reaction product by utilizing the 5'----3' exonuclease activity of Thermus aquaticus DNA polymerase. *Proceedings of the National Academy of Sciences,* 88 (16), 7276–7280.

Hogan, J.J., Owen, J.G., Blady, S.J., Almaani, S., Avasare, R.S., Bansal, S., Lenz, O., Luciano, R.L., Parikh, S.V., Ross, M.J., Sharma, D., Szerlip, H., Wadhwani, S., Townsend, R.R., Palmer, M.B., Susztak, K. and Mottl, A.K., 2020. The Feasibility and Safety of Obtaining Research Kidney Biopsy Cores in Patients with Diabetes: An Interim Analysis of the TRIDENT Study. *Clinical Journal of the American Society of Nephrology,* 15 (7), 1024-1026.

Hogan, M.C., Johnson, K.L., Zenka, R.M., Cristine Charlesworth, M., Madden, B.J., Mahoney, D.W., Oberg, A.L., Huang, B.Q., Leontovich, A.A., Nesbitt, L.L., Bakeberg, J.L., McCormick, D.J., Robert Bergen, H. and Ward, C.J., 2014. Subfractionation, characterization, and in-depth proteomic analysis of glomerular membrane vesicles in human urine. *Kidney International,* 85 (5), 1225–1237.

Hong, L.Z., Zhou, L., Zou, R., Khoo, C.M., Chew, A.L.S., Chin, C. and Shih, S., 2021. Systematic evaluation of multiple qPCR platforms, NanoString and miRNA-Seq for microRNA biomarker discovery in human biofluids. *Scientific Reports,* 11 (1), 4435.

Horder, E.G., 1899. BLOOD DUST OR BLOOD GRANULES: A NEW CONSTITUENT OF THE BLOOD? *Lancet,* 154 (3972), 1015.

Horibe, S., Tanahashi, T., Kawauchi, S., Murakami, Y. and Rikitake, Y., 2018. Mechanism of recipient cell-dependent differences in exosome uptake. *BMC Cancer,* 18 (1), 47–47.

Horman, S., Janas, M., Litterst, C., Wang, B., MacRae, I., Sever, M., Morrissey, D., Graves, P., Luo, B., Umesalma, S., Qi, H., Miraglia, L., Novina, C. and Orth, A., 2013. Akt-Mediated Phosphorylation of Argonaute 2 Downregulates Cleavage and Upregulates Translational Repression of MicroRNA Targets. *Molecular Cell,* 50 (3), 356–367.

Hovind, P., Rossing, P., Tarnow, L., Smidt, U.M. and Parving, H., 2001. Progression of diabetic nephropathy. *Kidney International,* 59 (2), 702–709.

Howey, J.E., Browning, M.C. and Fraser, C.G., 1989. Biologic Variation of Urinary Albumin: Consequences for Analysis, Specimen Collection, Interpretation of Results, and Screening Programs. *American Journal of Kidney Diseases,* 13 (1), 35-37.

Hoyer, J.R., and Seiler, M.W., 1979. Pathophysiology of Tamm-Horsfall protein. *Kidney International,* 16 (3), 279-289.

Hsu, P., Tsai, A., Kulmacz, R.J. and Wang, L., 1999. Expression, Purification, and Spectroscopic Characterization of Human Thromboxane Synthase. *Journal of Biological Chemistry,* 274 (2), 762–769.

Hu, R., Wang, M., Liu, L., You, H., Wu, X., Liu, Y., Wang, Y., Lu, L., Xiao, W. and Wei, L., 2020. Calycosin inhibited autophagy and oxidative stress in chronic kidney disease skeletal muscle atrophy by regulating AMPK/SKP2/CARM1 signalling pathway. *Journal of Cellular and Molecular Medicine,* 24 (19), 11084–11099.

Huang, Q., Fei, X., Zhong, Z., Zhou, J., Gong, J., Chen, Y., Li, Y. and Wu, X., 2022. Stratification of diabetic kidney diseases via data-independent acquisition proteomics–based analysis of human kidney tissue specimens. *Frontiers in Endocrinology,* 13, 995362.

Huang, S., Wu, S., Ding, J., Lin, J., Wei, L., Gu, J. and He, X., 2010. MicroRNA-181a modulates gene expression of zinc finger family members by directly targeting their coding regions. *Nucleic Acids Research,* 38 (20), 7211–7218.

Huang, V., and Li, L., 2012. miRNA goes nuclear. *RNA Biology,* 9 (3), 269–273.

Huang, W., Zhu, X., Lerman, A. and Lerman, L.O., 2022. Extracellular Vesicles as Theranostic Tools in Kidney Disease. *Clinical Journal of the American Society of Nephrology,* 17 (9), 1418–1429.

Huang, X.R., Chung, A.C.K., Wang, X.J., Lai, K.N. and Lan, H.Y., 2008. Mice overexpressing latent TGF-beta1 are protected against renal fibrosis in obstructive kidney disease. *American Journal of Physiology. Renal Physiology,* 295 (1), F118-F127.

Huang, Z., Liu, S., Tang, A., Al-Rabadi, L., Henkemeyer, M., Mimche, P.N. and Huang, Y., 2021. Key role for EphB2 receptor in kidney fibrosis. *Clinical Science,* 135 (17), 2127–2142.

Hull, K.L., Adenwalla, S.F., Topham, P. and Graham-Brown, M.P., 2022. Indications and considerations for kidney biopsy: an overview of clinical considerations for the non-specialist. *Clinical Medicine (London, England),* 22 (1), 34-40.

Hung, P., Lu, Y., Chen, Y., Chou, H., Lyu, P., Lee, Y. and Chan, H., 2011. Proteomic identification of plasma biomarkers in type 2 diabetic nephropathy. *Journal of Integrated OMICS,* 1 (1).

Hunger-Glaser, I., Fan, R.S., Perez-Salazar, E. and Rozengurt, E., 2004. PDGF and FGF induce focal adhesion kinase (FAK) phosphorylation at Ser-910: Dissociation from Tyr-397 phosphorylation and requirement for ERK activation. *Journal of Cellular Physiology,* 200 (2), 213-222.

Hwang, H., Wentzel, E.A. and Mendell, J.T., 2007. Hexanucleotide Element Directs MicroRNA Nuclear Import. *Science,* 315 (5808), 97–100.

Ichii, O., Otsuka-Kanazawa, S., Horino, T., Kimura, J., Nakamura, T., Matsumoto, M., Toi, M. and Kon, Y., 2014. Decreased miR-26a expression correlates with the progression of podocyte injury in autoimmune glomerulonephritis. *PloS One*, 9 (10), e110383.

Ikeda, Y., Imai, Y., Kumagai, H., Nosaka, T., Morikawa, Y., Hisaoka, T., Manabe, I., Maemura, K., Nakaoka, T., Imamura, T., Miyazono, K., Komuro, I., Nagai, R., Kitamura, T. and Yanagisawa, M., 2004. Vasorin, a Transforming Growth Factor β-Binding Protein Expressed in Vascular Smooth Muscle Cells, Modulates the Arterial Response to Injury in vivo. *Proceedings of the National Academy of Sciences - PNAS,* 101 (29), 10732–10737.

Inker, L. A., Astor, B. C., Fox, C. H., Isakova, T., Lash, J. P., Peralta, C. A., et al. (2014). KDOQI US commentary on the 2012 KDIGO clinical practice guideline for the evaluation and management of CKD. Am. J. Kidney Dis. Official J. Natl. Kidney Found. 63 (5), 713–735. doi:10.1053/j.ajkd.2014.01.416

Inker, L.A., Eneanya, N.D., Coresh, J., Tighiouart, H., Wang, D., Sang, Y., Crews, D.C., Doria, A., Estrella, M.M., Froissart, M., Grams, M.E., Greene, T., Grubb, A., Gudnason, V., Gutiérrez, O.M., Kalil, R., Karger, A.B., Mauer, M., Navis, G., Nelson, R.G., Poggio, E.D., Rodby, R., Rossing, P., Rule, A.D., Selvin, E., Seegmiller, J.C., Shlipak, M.G., Torres, V.E., Yang, W., Ballew, S.H., Couture, S.J., Powe, N.R. and Levey, A.S., 2021. New Creatinine- and Cystatin C–Based Equations to Estimate GFR without Race. *The New England Journal of Medicine,* 385 (19), 1737-1749.

Inker, L.A., Schmid, C.H., Tighiouart, H., Eckfeldt, J.H., Feldman, H.I., Greene, T., Kusek, J.W., Manzi, J., Van Lente, F., Zhang, Y.L., Coresh, J. and Levey, A.S., 2012. Estimating Glomerular Filtration Rate from Serum Creatinine and Cystatin C. *The New England Journal of Medicine,* 367 (1), 20-29.

Inker, L.A., and Titan, S., 2021. Measurement and Estimation of GFR for Use in Clinical Practice: Core Curriculum 2021. *American Journal of Kidney Diseases,* 78 (5), 736-749.

Ito, Y., Aten, J., Bende, R.J., Oemar, B.S., Rabelink, T.J., Weening, J.J., and Goldschmeding, R., 1998. Expression of connective tissue growth factor in human renal fibrosis. *Kidney International,* 53 (4), 853-861.

Itoh, S., Itoh, F., Goumans, M. and ten Dijke, P., 2000. Signaling of transforming growth factor-β family members through Smad proteins. *European Journal of Biochemistry,* 267 (24), 6954-6967.

Jacobsen, F.K., Christensen, C.K., Mogensen, C.E., Andreasen, F. and Heilskov, N.S., 1979. Pronounced increase in serum creatinine concentration after eating cooked meat. *Bmj,* 1 (6170), 1049-1050.

Jahn, R., and Scheller, R.H., 2006. SNAREs - engines for membrane fusion. *Nature Reviews. Molecular Cell Biology,* 7 (9), 631-643.

Jeanmard, N., Bissanum, R., Sriplung, H., Charoenlappanit, S., Roytrakul, S. and Navakanitworakul, R., 2023. Proteomic profiling of urinary extracellular vesicles differentiates breast cancer patients from healthy women. *PloS One,* 18 (11), e0291574.

Jha, V., Prof, Garcia-Garcia, G., Prof, Iseki, K., Prof, Li, Z., MD, Naicker, S., Prof, Plattner, B., MD, Saran, R., Prof, Wang, A.Y., Prof and Yang, C., Prof, 2013. Chronic kidney disease: global dimension and perspectives. *The Lancet,* 382 (9888), 260-272.

Jia, Y., Guan, M., Zheng, Z., Zhang, Q., Tang, C., Xu, W., Xiao, Z., Wang, L., and Xue, Y., 2016. miRNAs in Urine Extracellular Vesicles as Predictors of Early-Stage Diabetic Nephropathy. *Journal of Diabetes Research*, 2016 (7932765).

Jiang, L., Qiu, W., Zhou, Y., Wen, P., Fang, L., Cao, H., Zen, K., He, W., Zhang, C., Dai, C. and Yang, J., 2013. A microRNA-30e/mitochondrial uncoupling protein 2 axis mediates TGF-β1-induced tubular epithelial cell extracellular matrix production and kidney fibrosis. *Kidney International,* 84 (2), 285–296.

Jiang, X., Qin, L., Wei, J., Su, G., Su, X., Lu, A., Huang, J., Lu, F., Lu, T., Huang, P. and Su, B., 2022. Urine Cystatin C Determination in the Establishment of Reference Interval in the Diagnosis and Treatment of Renal Injury. *Natural Science (Irvine, Calif.),* 14 (1), 13-17.

Jiang, X., Ruan, X., Xue, Y., Yang, S., Shi, M. and Wang, L., 2020. Metformin reduces the senescence of renal tubular epithelial cells in diabetic nephropathy via the MBNL1/miR-130a-3p/STAT3 pathway. *Oxidative Medicine and Cellular Longevity,* 2020 (1), 8708236.

Jimenez, J.J., Jy, W., Mauro, L.M., Soderland, C., Horstman, L.L. and Ahn, Y.S., 2003. Endothelial cells release phenotypically and quantitatively distinct microparticles in activation and apoptosis. *Thrombosis Research,* 109 (4), 175-180.

Jin, D., Tu, X., Xu, W., Zheng, H., Zeng, J., Bi, P., Yang, R., Li, Y., Ni, J., Zhu, C., Chen, H., Yu, D. and Wan, F., 2024. Identification and validation of diagnostic markers related to immunogenic cell death and infiltration of immune cells in diabetic nephropathy. *International Immunopharmacology,* 143 (Pt 1), 113236.

Jin, J., Ku, Y.H., Kim, Y., Kim, Y., Kim, K., Lee, J.Y., Cho, Y.M., Lee, H.K., Park, K.S. and Kim, Y., 2012. Differential Proteome Profiling Using iTRAQ in Microalbuminuric and Normoalbuminuric Type 2 Diabetic Patients. *Experimental Diabetes Research,* 2012, 168602–31.

Johannes, L., Wunder, C. and Shafaq-Zadah, M., 2016. Glycolipids and Lectins in Endocytic Uptake Processes. *Journal of Molecular Biology,* 428 (24), 4792–4818.

Johnson, T.S., El-Koraie, A.F., Skill, N.J., Baddour, N.M., El Nahas, A.M., Njloma, M., Adam, A.G. and Griffin, M., 2003. Tissue Transglutaminase and the Progression of Human Renal Scarring. *Journal of the American Society of Nephrology,* 14 (8), 2052-2062.

Johnstone, R.M., Adam, M., Hammond, J.R., Orr, L. and Turbide, C., 1987. Vesicle formation during reticulocyte maturation. Association of plasma membrane activities with released vesicles (exosomes). *The Journal of Biological Chemistry,* 262 (19), 9412-9420.

Joshi, D.R., and Adhikari, N., 2019. An Overview on Common Organic Solvents and Their Toxicity. *Journal of Pharmaceutical Research International*, 28 (3), 1-18.

Kagami, S., Border, W.A., Miller, D.E. and Noble, N.A., 1994. Angiotensin II stimulates extracellular matrix protein synthesis through induction of transforming growth factor-beta expression in rat glomerular mesangial cells. *The Journal of Clinical Investigation,* 93 (6), 2431-2437.

Kalani, A., Mohan, A., Godbole, M.M., Bhatia, E., Gupta, A., Sharma, R.K. and Tiwari, S., 2013. Wilm's Tumor-1 Protein Levels in Urinary Exosomes from Diabetic Patients with or without Proteinuria. *PloS One,* 8 (3), e60177.

Kammer, M., Heinzel, A., Hu, K., Meiselbach, H., Gregorich, M., Busch, M., Duffin. K., Gomez, M., Eckardt, K.U. and Oberbauer, R., 2023. Different roles of protein biomarkers predicting eGFR trajectories in people with chronic kidney disease and diabetes mellitus: a nationwide retrospective cohort study. *Cardiovascular diabetology*, 22 (1), 74–74.

Kang, H., 2021. Sample size determination and power analysis using the GPower software. *Journal of Educational Evaluation for Health Professions, 18(0),* 18, 17.

Kang, H.M., Ahn, S.H., Choi, P., Ko, Y., Han, S.H., Chinga, F., Park, A.S.D., Tao, J., Sharma, K. and Pullman, J., 2015. Defective fatty acid oxidation in renal tubular epithelial cells has a key role in kidney fibrosis development. *Nature Medicine,* 21 (1), 37–46.

Kaszuba, M., Corbett, J., Watson, F.M. and Jones, A., 2010. High-concentration zeta potential measurements using light-scattering techniques. Philosophical Transactions of the Royal Society of London. Series A: Mathematical, Physical, and Engineering Sciences, 368 (1927), 4439-4451.

Kato, M., Arce, L. and Natarajan, R., 2009. MicroRNAs and Their Role in Progressive Kidney Diseases. *Clinical Journal of the American Society of Nephrology,* 4 (7), 1255–1266.

Katzmann, D.J., Babst, M. and Emr, S.D., 2001. Ubiquitin-Dependent Sorting into the Multivesicular Body Pathway Requires the Function of a Conserved Endosomal Protein Sorting Complex, ESCRT-I. *Cell,* 106 (2), 145-155.

Kavoura, E., MD, Gakiopoulou, Hariklia, MD, PhD, Paraskevakou, Helen, MD, PhD, Marinaki, S., MD, Agrogiannis, G., MD, Stofas, A., MD, Boletis, I., MD, Patsouris, Efstratios, MD, PhD and Lazaris, Andreas C., MD, PhD, 2011. Immunohistochemical evaluation of podocalyxin expression in glomerulopathies associated with nephrotic syndrome. *Human Pathology,* 42 (2), 227–235.

Kayhan, M., Vouillamoz, J., Rodriguez, D.G., Bugarski, M., Mitamura, Y., Gschwend, J., Schneider, C., Hall, A., Legouis, D., Akdis, C.A., Peter, L., Rehrauer, H., Gewin, L., Wenger, R.H. and Khodo, S.N., 2023. Intrinsic TGF-β signaling attenuates proximal tubule mitochondrial injury and inflammation in chronic kidney disease. *Nature Communications,* 14 (1), 3236.

Ke, C., Liang, J., Liu, M., Liu, S. and Wang, C., 2022. Burden of chronic kidney disease and its risk-attributable burden in 137 low-and middle-income countries, 1990–2019: results from the global burden of disease study 2019. *BMC Nephrology,* 23 (1), 17.

Keane, W.F., and Eknoyan, G., 1999. Proteinuria, albuminuria, risk, assessment, detection, elimination (parade) : A position paper of the National Kidney Foundation. *American Journal of Kidney Diseases,* 33 (5), 1004-1010.

Kelly, J.D., Haldeman, B.A., Grant, F.J., Murray, M.J., Seifert, R.A., Bowen-pope, D.F., Cooper, J.A. and Kazlauskas, A., 1991. Platelet-derived growth factor (PDGF) stimulates PDGF receptor subunit dimerization and intersubunit trans-phosphorylation. *The Journal of Biological Chemistry,* 266 (14), 8987-8992.

Kerr, M.C., and Teasdale, R.D., 2009. Defining Macropinocytosis. *Traffic (Copenhagen, Denmark),* 10 (4), 364-371.

Khoo, A., Govindarajan, M., Qiu, Z., Liu, L.Y., Ignatchenko, V., Waas, M., Macklin, A., Keszei, A., Neu, S., Main, B.P., Yang, L., Lance, R.S., Downes, M.R., Semmes, O.J., Vesprini, D., Liu, S.K., Nyalwidhe, J.O., Boutros, P.C. and Kislinger, T., 2024. Prostate cancer reshapes the secreted and extracellular vesicle urinary proteomes. *Nature Communications,* 15 (1), 5069–16.

Khurana, R., Ranches, G., Schafferer, S., Lukasser, M., Rudnicki, M., Mayer, G. and Hüttenhofer, A., 2017. Identification of urinary exosomal noncoding RNAs as novel biomarkers in chronic kidney disease. *RNA (Cambridge),* 23 (2), 142-152.

Kim, D., Lim, S., Park, M., Choi, J., Kim, J., Han, H., Yoon, K., Kim, K., Lim, J. and Park, S., 2014. Ubiquitination-dependent CARM1 degradation facilitates Notch1-mediated podocyte apoptosis in diabetic nephropathy. *Cellular Signalling,* 26 (9), 1774–1782.

Kim, D.H., Sætrom, P., Snøve, O.J. and Rossi, J.J., 2008. MicroRNA-directed transcriptional gene silencing in mammalian cells. *Proceedings of the National Academy of Sciences,* 105 (42), 16230–16235.

Kim, I.Y., Song, S.H., Seong, E.Y., Lee, D.W., Bae, S.S. and Lee, S.B., 2023. Akt1 is involved in renal fibrosis and tubular apoptosis in a murine model of acute kidney injury-to-chronic kidney disease transition. *Experimental Cell Research,* 424 (2), 113509.

Kim, K.E., Onesti, G., Ramirez, O., Brest, A.N. and Swartz, C., 1969. Creatinine clearance in renal disease. A reappraisal. *Bmj,* 4 (5674), 11-14.

Kirby, A., Gnirke, A., Jaffe, D.B., Barešová, V., Pochet, N., Blumenstiel, B., Ye, C., Aird, D., Stevens, C., Robinson, J.T., Cabili, M.N., Gat-Viks, I., Kelliher, E., Daza, R., DeFelice, M., Hůlková, H., Sovová, J., Vylet'al, P., Antignac, C., Guttman, M., Handsaker, R.E., Perrin, D., Steelman, S.,

Sigurdsson, S., Scheinman, S.J., Sougnez, C., Cibulskis, K., Parkin, M., Green, T., Rossin, E., Zody, M.C., Xavier, R.J., Pollak, M.R., Alper, S.L., Lindblad-Toh, K., Gabriel, S., Hart, P.S., Regev, A., Nusbaum, C., Kmoch, S., Bleyer, A.J., Lander, E.S. and Daly, M.J., 2013. Mutations causing medullary cystic kidney disease type 1 lie in a large VNTR in MUC1 missed by massively parallel sequencing. *Nature Genetics,* 45 (3), 299–303.

Klessens, C.Q.F., Woutman, T.D., Veraar, K.A.M., Zandbergen, M., Valk, E.J.J., Rotmans, J.I., Wolterbeek, R., Bruijn, J.A. and Bajema, I.M., 2016. An autopsy study suggests that diabetic nephropathy is underdiagnosed. *Kidney International,* 90 (1), 149-156.

Knight, E.L., Verhave, J.C., Spiegelman, D., Hillege, H.L., De Zeeuw, D., Curhan, G.C. and De Jong, P.E., 2004. Factors influencing serum cystatin C levels other than renal function and the impact on renal function measurement. *Kidney International,* 65 (4), 1416-1421.

Kobayashi, T., Stang, E., Fang, K.S., de Moerloose, P., Parton, R.G. and Gruenberg, J., 1998. A lipid associated with the antiphospholipid syndrome regulates endosome structure and function. *Nature (London),* 392 (6672), 193.

Kolb, A., Gallacher, P.J., Campbell, J., O'Neill, M., Smith, J.R., Bell, S., Conway, B.R., Metcalfe, W., Joss, N., Dey, V., Alfonzo, A., Kelly, M., Shah, S., McQuarrie, E., Geddes, C., Traynor, J. and Hunter, R.W., 2021. A National Registry Study of Patient and Renal Survival in Adult Nephrotic Syndrome. *Kidney International Reports,* 6 (2), 449-459.

Komatsu, S., Kato, N., Kitai, H., Funahashi, Y., Noda, Y., Tsubota, S., Tanaka, A., Sato, Y., Maeda, K., Saito, S., Furuhashi, K., Ishimoto, T., Kosugi, T., Maruyama, S. and Kadomatsu, K., 2024. Detecting and exploring kidney-derived extracellular vesicles in plasma. *Clinical and Experimental Nephrology,* 28 (7), 617–628.

Kommareddi, P.K., Nair, T.S., Thang, L.V., Galano, M.M., Babu, E., Ganapathy, V., Kanazawa, T., McHugh, J.B. and Carey, T.E., 2010. Isoforms, Expression, Glycosylation, and Tissue Distribution of CTL2/SLC44A2. *The Protein Journal,* 29 (6), 417–426.

Kramer, H.J., Nguyen, Q.D., Curhan, G. and Hsu, C., 2003. Renal Insufficiency in the Absence of Albuminuria and Retinopathy Among Adults With Type 2 Diabetes Mellitus. *JAMA : The Journal of the American Medical Association,* 289 (24), 3273-3277.

Krolewski, A.S., Niewczas, M.A., Skupien, J., Gohda, T., Smiles, A., Eckfeldt, J.H., Doria, A. and Warram, J.H., 2014. Early Progressive Renal Decline Precedes the Onset of Microalbuminuria and Its Progression to Macroalbuminuria. *Diabetes Care,* 37 (1), 226-234.

Kumar, M.A., Baba, S.K., Sadida, H.Q., Marzooqi, S.A., Jerobin, J., Altemani, F.H., Algehainy, N., Alanazi, M.A., Abou-Samra, A., Kumar, R., Al-Shabeeb Akil, A.S., Macha, M.A., Mir, R. and Bhat, A.A., 2024. Extracellular vesicles as tools and targets in therapy for diseases. *Signal Transduction and Targeted Therapy,* 9 (1), 27.

Kumari, M., Mohan, A., Ecelbarger, C.M., Gupta, A., Prasad, N. and Tiwari, S., 2020. miR-451 Loaded Exosomes Are Released by the Renal Cells in Response to Injury and Associated With Reduced Kidney Function in Human. *Frontiers in Physiology*, 11, 234.

Kuppe, C., Ibrahim, M.M., Kranz, J., Zhang, X.T., Ziegler, S., Perales-Paton, J., Jansen, J., Reimer, K.C., Smith, J.R., Dobie, R., Wilson-Kanamori, J.R., Halder, M., Xu, Y.X., Kabgani, N., Kaesler, N., Klaus, M., Gernhold, L., Puelles, V.G., Huber, T.B., Boor, P., Menzel, S., Hoogenboezem, R., Bindels, E., Steffens, J., Floege, J., Schneider, R., Saez-Roiguez, J., Henderson, N.C. and Kramann, R., 2021. Decoding myofibroblast origins in human kidney fibrosis. *Nature (London),* 589 (7841), 281-286.

Kyhse-Andersen, J., Schmidt, C., Nordin, G., Andersson, B., Nilsson-Ehle, P., Lindstrom, V. and Grubb, A., 1994. Serum cystatin C, determined by a rapid, automated particle-enhanced turbidimetric method, is a better marker than serum creatinine for glomerular filtration rate. *Clinical Chemistry (Baltimore, Md.),* 40 (10), 1921-1926.

LAEMMLI, U.K., 1970. Cleavage of Structural Proteins during the Assembly of the Head of Bacteriophage T4. Nature (London), 227 (5259), 680-685.

Lai, K.N., Leung, J.C.K., Chan, L.Y.Y., Saleem, M.A., Mathieson, P.W., Tam, K.Y., Xiao, J., Lai, F.M. and Tang, S.C.W., 2009. Podocyte injury induced by mesangial-derived cytokines in IgA nephropathy. *Nephrology, Dialysis, Transplantation*, 24 (1), 62-72.

Lajdova, I., Spustova, V., Oksa, A., Chorvatova, A., Chorvat, D. and Dzurik, R., 2009. Intracellular calcium homeostasis in patients with early stagesof chronic kidney disease: effects of vitamin D3 supplementation. *Nephrology, Dialysis, Transplantation,* 24 (11), 3376–3381.

Lambert, J., Ivosev, G., Couzens, A.L., Larsen, B., Taipale, M., Lin, Z., Zhong, Q., Lindquist, S., Vidal, M., Aebersold, R., Pawson, T., Bonner, R., Tate, S. and Gingras, A., 2013. Mapping differential interactomes by affinity purification coupled with data-independent mass spectrometry acquisition. Nature Methods, 10 (12), 1239–1245.

Lan, A., and Du, J., 2015. Potential role of Akt signaling in chronic kidney disease. *Nephrology, Dialysis, Transplantation,* 30 (3), 385–394.

Lan, H.Y., 2011. Diverse Roles of TGF-β/Smads in Renal Fibrosis and Inflammation. *International Journal of Biological Sciences,* 7 (7), 1056-1067.

Lange, T., Artelt, N., Kindt, F., Stracke, S., Rettig, R., Lendeckel, U., Chadjichristos, C.E., Kavvadas, P., Chatziantoniou, C., Endlich, K., Endlich, N., 2019. MiR-21 is up-regulated in urinary exosomes of chronic kidney disease patients and after glomerular injury. *Journal of Cellular and Molecular Medicine*, 23 (7), 4839-4843.

LaRochelle, W.J., Jeffers, M., McDonald, W.F., Chillakuru, R.A., Giese, N.A., Lokker, N.A., Sullivan, C., Boldog, F.L., Yang, M., Vernet, C., Burgess, C.E., Fernandes, E., Deegler, L.L., Rittman, B.,

Shimkets, J., Shimkets, R.A., Rothberg, J.M. and Lichenstein, H.S., 2001. PDGF-D, a new protease-activated growth factor. *Nature Cell Biology,* 3 (5), 517-521.

Larrucea, S., Butta, N., Arias-Salgado, E.G., Alonso-Martin, S., Ayuso, M.S. and Parrilla, R., 2008. Expression of podocalyxin enhances the adherence, migration, and intercellular communication of cells. *Experimental Cell Research,* 314 (10), 2004–2015.

LeBleu, V.S., Taduri, G., O'Connell, J., Teng, Y., Cooke, V.G., Woda, C., Sugimoto, H. and Kalluri, R., 2013. Origin and function of myofibroblasts in kidney fibrosis. *Nature Medicine,* 19 (8), 1047-1053.

Lech, M., and Anders, H., 2013. The Pathogenesis of Lupus Nephritis. *Journal of the American Society of Nephrology,* 24 (9), 1357-1366.

Lech, M., and Anders, H., 2014, Expression Profiling by Real-Time Quantitative Polymerase Chain Reaction (RT-qPCR). *In:* Expression Profiling by Real-Time Quantitative Polymerase Chain Reaction (RT-qPCR). *Innate DNA and RNA Recognition.* New York, NY: Springer New York, 2014, pp. 133–142.

Lech, M., Susanti, H., Römmele, C., Gröbmayr, R., Günthner, R. and Anders, H., 2012. Lech, M., et al., Quantitative Expression of C-Type Lectin Receptors in Humans and Mice. Int. J. Mol. Sci. 2012, 13, 10113-10131. *International Journal of Molecular Sciences,* 13 (12), 17294.

Lee, C.H., and Lam, K.S.L., 2015. Biomarkers of progression in diabetic nephropathy: The past, present and future. *Journal of Diabetes Investigation,* 6 (3).

Levey, A.S., Bosch, J.P., Lewis, J.B., Greene, T., Rogers, N. and Roth, D., 1999. A More Accurate Method To Estimate Glomerular Filtration Rate from Serum Creatinine: A New Prediction Equation. *Annals of Internal Medicine,* 130 (6), 461-470.

Levey, A.S., Coresh, J., Greene, T., Stevens, l.A., Zhang, Y., Hendriksen, S., Kusek, J.W. and Van Lente, F., 2006. Using Standardized Serum Creatinine Values in the Modification of Diet in Renal Disease Study Equation for Estimating Glomerular Filtration Rate. *Annals of Internal Medicine,* 145 (4), 247-254.

Levey, A.S., Grams, M.E. and Inker, L.A., 2022. Uses of GFR and Albuminuria Level in Acute and Chronic Kidney Disease. *New England Journal of Medicine,* 386 (22), 2120–2128.

Levey, A.S., Stevens, L.A., Coresh, J., Schmid, C.H., Zhang, Y., Castro, A.F., Feldman, H.I., Kusek, J.W., Eggers, P., Van Lente, F. and Greene, T., 2009. A New Equation to Estimate Glomerular Filtration Rate. *Annals of Internal Medicine,* 150 (9), 604-612.

Levin, A., Stevens, P.E., Bilous, R.W., Coresh, J., De Francisco, A.L.M., De Jong, P.E., Griffith, K.E., Hemmelgarn, B.R., Iseki, K., Lamb, E.J., Levey, A.S., Riella, M.C., Shlipak, M.G., Wang, H., White, C.T. and Winearls, C.G., 2013. Kidney disease: Improving global outcomes (KDIGO) CKD work group. KDIGO 2012 clinical practice guideline for the evaluation and management of chronic

kidney disease. *Kidney International Supplements*, 3 (1), 1-150.
https://doi.org/10.1038/kisup.2012.73

Li, B., Antonyak, M.A., Zhang, J. and Cerione, R.A., 2012. RhoA triggers a specific signaling pathway that generates transforming microvesicles in cancer cells. *Oncogene,* 31 (45), 4740-4749.

Li, B., Qi, C., Zhang, Y., Shi, L., Zhang, J., Qian, H. and Ji, C., 2024. Frontier role of extracellular vesicles in kidney disease. *Journal of Nanobiotechnology,* 22 (1), 583–25.

Li, H., Lu, W., Wang, A., Jiang, H. and Lyu, J., 2021. Changing epidemiology of chronic kidney disease as a result of type 2 diabetes mellitus from 1990 to 2017: Estimates from Global Burden of Disease 2017. *Journal of Diabetes Investigation,* 12 (3), 346-356.

Li, J.H., Huang, X.R., Zhu, H., Oldfield, M., Cooper, M., Truong, L.D., Johnson, R.J. and Lan, H.Y., 2004. Advanced glycation end products activate Smad signaling via TGF-β-dependent and -independent mechanisms: implications for diabetic renal and vascular disease. *The FASEB Journal,* 18 (1), 176-178.

Li, L., Hou, D., Guo, Y., Yang, J., Liu, Y., Zhang, C. and Zen, K., 2011. Role of MicroRNA-214–Targeting Phosphatase and Tensin Homolog in Advanced Glycation End Product-Induced Apoptosis Delay in Monocytes. *The Journal of Immunology,* 186 (4), 2552–2560.

Li, L., Liu, Q., Shang, T., Song, W., Xu, D., Allen, T.D., Wang, X., Jeong, J., Lobe, C.G. and Liu, J., 2021. Aberrant Activation of Notch1 Signaling in Glomerular Endothelium Induces Albuminuria. *Circulation Research,* 128 (5), 602-618.

Li, R., Chung, A.C.K., Dong, Y., Yang, W., Zhong, X. and Lan, H.Y., 2013. The microRNA miR-433 promotes renal fibrosis by amplifying the TGF-β/Smad3-Azin1 pathway. *Kidney International,* 84 (6), 1129–1144.

Li, Y., Xu, X., Tang, X., Bian, X., Shen, B., Zhao, H., Luo, S., Chen, Z. and Zhang, K., 2018. MicroRNA expression profile of urinary exosomes in Type IV lupus nephritis complicated by cellular crescent. *Journal of Biological Research (Thessalonikē, Greece)*, 25 (1), 1-13.

Liang, D., Li, Z., Feng, Z., Yuan, Z., Dai, Y., Wu, X., Zhang, F., Wang, Y., Zhou, Y., Liu, L., Shi, M., Xiao, Y. and Guo, B., 2022. Metformin Improves the Senescence of Renal Tubular Epithelial Cells in a High-Glucose State Through E2F1. *Frontiers in Pharmacology,* 13, 926211.

Lim, A.K.H., and Tesch, G.H., 2012. Inflammation in Diabetic Nephropathy. *Mediators of Inflammation,* 2012 (2012), 1–12.

Lin, B., Hui, J. and Mao, H., 2021. Nanopore Technology and Its Applications in Gene Sequencing. *Biosensors,* 11 (7), 214.

Lin, S., Kisseleva, T., Brenner, D.A. and Duffield, J.S., 2008. Pericytes and Perivascular Fibroblasts Are the Primary Source of Collagen-Producing Cells in Obstructive Fibrosis of the Kidney. *The American Journal of Pathology,* 173 (6), 1617-1627.

Lischnig, A., Bergqvist, M., Ochiya, T. and Lässer, C., 2022. Quantitative Proteomics Identifies Proteins Enriched in Large and Small Extracellular Vesicles. *Molecular & Cellular Proteomics*, 21 (9), 100273.

Liu, S., Qiu, C., Li, W., Li, X., Liu, F. and Hu, G., 2024. Blood urea nitrogen to serum albumin ratio as a new prognostic indicator in type 2 diabetes mellitus patients with chronic kidney disease. *Scientific Reports,* 14 (1), 8002-9.

Liu, R., Das, B., Xiao, W., Li, Z., Li, H., Lee, K. and He, J.C., 2017. A Novel Inhibitor of Homeodomain Interacting Protein Kinase 2 Mitigates Kidney Fibrosis through Inhibition of the TGF-β1/Smad3 Pathway. *Journal of the American Society of Nephrology,* 28 (7), 2133–2143.

Liu, X., Miao, J., Wang, C., Zhou, S., Chen, S., Ren, Q., Hong, X., Wang, Y., Hou, F.F., Zhou, L. and Liu, Y., 2020. Tubule-derived exosomes play a central role in fibroblast activation and kidney fibrosis. *Kidney International,* 97 (6), 1181–1195.

Liu, Y., and Wang, C., 2023. A review of the regulatory mechanisms of extracellular vesicles-mediated intercellular communication. *Cell Communication and Signaling,* 21 (1), 77.

Liu, Y., Bi, X., Xiong, J., Han, W., Xiao, T., Xu, X., Yang, K., Liu, C., Jiang, W., He, T., Yu, Y., Li, Y., Zhang, J., Zhang, B. and Zhao, J., 2019. MicroRNA-34a Promotes Renal Fibrosis by Downregulation of Klotho in Tubular Epithelial Cells. *Molecular Therapy,* 27 (5), 1051–1065.

Liu, Z., Huang, X.R., Chen, H., Penninger, J.M. and Lan, H.Y., 2012. Loss of angiotensin-converting enzyme 2 enhances TGF-β/Smad-mediated renal fibrosis and NF-κB-driven renal inflammation in a mouse model of obstructive nephropathy. *Laboratory Investigation,* 92 (5), 650-661.

Liu, Z., Liu, J., Wang, W., An, X., Luo, L., Yu, D. and Sun, W., 2023. Epigenetic modification in diabetic kidney disease. *Frontiers in Endocrinology,* 14, 1133970.

Livak, K.J., and Schmittgen, T.D., 2001. Analysis of relative gene expression data using real-time quantitative PCR and the 2 method. *Methods (San Diego, Calif.),* 25 (4), 402–408.

Lopez, J.P., Diallo, A., Cruceanu, C., Fiori, L.M., Laboissiere, S., Guillet, I., Fontaine, J., Ragoussis, J., Benes, V., Turecki, G. and Ernst, C., 2015. Biomarker discovery: quantification of microRNAs and other small non-coding RNAs using next generation sequencing. *BMC Medical Genomics,* 8 (1), 35–35.

Lottridge, J.M., Flannery, A.R., Vincelli, J.L. and Stevens, T.H., 2006. Vta1p and Vps46p regulate the membrane association and ATPase activity of Vps4p at the yeast multivesicular body. *Proceedings of the National Academy of Sciences - PNAS,* 103 (16), 6202-6207.

Louvet, L., Lenglet, G., Krautzberger, A.M., Mentaverri, R., Hague, F., Kowalewski, C., Mahtal, N., Lesieur, J., Bonnet, A., Andrique, C., Gaucher, C., Gomila, C., Schrewe, H., Tharaux, P., Kamel, S., Chaussain, C. and Six, I., 2022. Vasorin plays a critical role in vascular smooth muscle cells and arterial functions. *Journal of Cellular Physiology,* 237 (10), 3845–3859.

Lozano-Andrés, E., Libregts, S.F., Toribio, V., Royo, F., Morales, S., López-Martín, S., Valés-Gómez, M., Reyburn, H.T., Falcón-Pérez, J.M., Wauben, M.H., Soto, M. and Yáñez-Mó, M., 2019. Tetraspanin-decorated extracellular vesicle-mimetics as a novel adaptable reference material. *Journal of Extracellular Vesicles,* 8 (1), 1573052–n/a.

Lu, Y. Liu, D., Feng, Q. and Liu, Z., 2020. Diabetic Nephropathy: Perspective on Extracellular Vesicles. *Frontiers in immunology*, 11, 943–943. 10.3389/fimmu.2020.00943.

Luo, C., Zhou, S., Zhou, Z., Liu, Y., Yang, L., Liu, J., Zhang, Y., Li, H., Liu, Y., Hou, F.F. and Zhou, L., 2018. Wnt9a Promotes Renal Fibrosis by Accelerating Cellular Senescence in Tubular Epithelial Cells. *Journal of the American Society of Nephrology,* 29 (4), 1238-1256.

Luo, Q., Cai, Z., Tu, J., Ling, Y., Wang, D. and Cai, Y., 2019. Total flavonoids from Smilax glabra Roxb blocks epithelial-mesenchymal transition and inhibits renal interstitial fibrosis by targeting miR-21/PTEN signaling. *Journal of Cellular Biochemistry,* 120 (3), 3861–3873.

Luong, T.T.D., Estepa, M., Boehme, B., Pieske, B., Lang, F., Eckardt, K., Voelkl, J. and Alesutan, I., 2019. Inhibition of vascular smooth muscle cell calcification by vasorin through interference with TGFβ1 signaling. *Cellular Signalling,* 64, 109414.

Lutz, J., Menke, J., Sollinger, D., Schinzel, H. and Thürmel, K., 2014. Haemostasis in chronic kidney disease. *Nephrology, Dialysis, Transplantation,* 29 (1), 29–40.

Lv, L.L., Cao, Y.H., Ni, H.F., Xu, M., Liu, D., Liu, H., Chen, P.S., and Liu, B.C., 2013. MicroRNA-29c in urinary exosome/microvesicle as a biomarker of renal fibrosis. *American Journal of Physiology – Renal Physiology*, 305 (8), 1220-1227.

Lv, L., Cao, Y., Pan, M., Liu, H., Tang, R., Ma, K., Chen, P. and Liu, B., 2014. CD2AP mRNA in urinary exosome as biomarker of kidney disease. *Clinica Chimica Acta,* 428, 26–31.

Lv, L., Feng, Y., Wen, Y., Wu, W., Ni, H., Li, Z., Zhou, L., Wang, B., Zhang, J., Crowley, S.D. and Liu, B., 2018. Exosomal CCL2 from Tubular Epithelial Cells Is Critical for Albumin-Induced Tubulointerstitial Inflammation. *Journal of the American Society of Nephrology,* 29 (3), 919–935.

Ma, L., Li, Y., Peng, J., Wu, D., Zhao, X., Cui, Y., Chen, L., Yan, X., Du, Y. and Yu, L., 2015. Discovery of the migrasome, an organelle mediating release of cytoplasmic contents during cell migration. Cell Research, 25 (1), 24-38.

Ma, Y., Li, T., Zhao, L., Zhou, D., Dong, L., Xu, Z., Wang, Y., Yao, X. and Zhao, K., 2023. Isolation and characterization of extracellular vesicle-like nanoparticles derived from migrasomes. The FEBS Journal, 290 (13), 3359-3368.

Macconi, D., Tomasoni, S., Benigni, A., Romagnani, P., Trionfini, P., Sangalli, F., Mazzinghi, B., Rizzo, P., Lazzeri, E., Abbate, M. and Remuzzi, G., 2012. MicroRNA-324-3p Promotes Renal Fibrosis and Is a Target of ACE Inhibition. *Journal of the American Society of Nephrology,* 23 (9), 1496–1505.

MacIsaac, R.J., Ekinci, E.I. and Jerums, G., 2014. Progressive diabetic nephropathy. How useful is microalbuminuria?: contra. *Kidney International,* 86 (1), 50–57.

Magayr, T.A., Song, X., Streets, A.J., Vergoz, L., Chang, L., Valluru, M.K., Yap, H.L., Lannoy, M., Haghighi, A., Simms, R.J., Tam, F.W.K., Pei, Y. and Ong, A.C.M., 2020. Global microRNA profiling in human urinary exosomes reveals novel disease biomarkers and cellular pathways for autosomal dominant polycystic kidney disease. *Kidney International,* 98 (2), 420–435.

Magliano, D.J., and Boyko, E.J., 2021, Global picture. *In:* Global picture. *IDF DIABETES ATLAS [Internet]. 10th edition.* International Diabetes Federation, 2021.

Mak, S.K., Gwi, E., Chan, K.W., Wong, P.N., Lo, K.Y., Lee, K.F. and Wong, A.K.M., 1997. Clinical predictors of non-diabetic renal disease in patients with non-insulin dependent diabetes mellitus. *Nephrology, Dialysis, Transplantation,* 12 (12), 2588-2591.

Mansouri, L., Lundwall, K., Moshfegh, A., Jacobson, S.H., Lundahl, J. and Spaak, J., 2017. Vitamin D receptor activation reduces inflammatory cytokines and plasma MicroRNAs in moderate chronic kidney disease – a randomized trial. *Bmc Nephrology,* 18 (1), 161.

Marahrens, B., Schulze, A., Wysocki, J., Lin, M., Ye, M., Kanwar, Y.S., Bader, M., Velez, J.C.Q., Miner, J.H. and Batlle, D., 2021. Knockout of aminopeptidase A in mice causes functional alterations and morphological glomerular basement membrane changes in the kidneys. *Kidney International,* 99 (4), 900–913.

Margaria, J.P., Campa, C.C., De Santis, M.C., Hirsch, E. and Franco, I., 2020. The PI3K/Akt/mTOR pathway in polycystic kidney disease: A complex interaction with polycystins and primary cilium. *Cellular Signalling,* 66, 109468.

Mariani, L.H., Eddy, S., AlAkwaa, F.M., McCown, P.J., Harder, J.L., Nair, V., Eichinger, F., Martini, S., Ademola, A.D., Boima, V., Reich, H.N., El Saghir, J., Godfrey, B., Ju, W., Tanner, E.C., Vega-Warner, V., Wys, N.L., Adler, S.G., Appel, G.B., Athavale, A., Atkinson, M.A., Bagnasco, S.M., Barisoni, L., Brown, E., Cattran, D.C., Coppock, G.M., Dell, K.M., Derebail, V.K., Fervenza, F.C., Fornoni, A., Gadegbeku, C.A., Gibson, K.L., Greenbaum, L.A., Hingorani, S.R., Hladunewich, M.A., Hodgin, J.B., Hogan, M.C., Holzman, L.B., Jefferson, J.A., Kaskel, F.J., Kopp, J.B., Lafayette, R.A., Lemley, K.V., Lieske, J.C., Lin, J., Menon, R., Meyers, K.E., Nachman, P.H., Nast, C.C., O'Shaughnessy, M.M., Otto, E.A., Reidy, K.J., Sambandam, K.K., Sedor, J.R., Sethna, C.B., Singer, P., Srivastava, T., Tran, C.L., Tuttle, K.R., Vento, S.M., Wang, C., Ojo, A.O., Adu, D., Gipson, D.S., Trachtman, H. and Kretzler, M., 2023. Precision nephrology identified tumor necrosis factor activation variability in minimal change disease and focal segmental glomerulosclerosis. *Kidney International,* 103 (3), 565-579.

Martin, M., 2011. CUTADAPT removes adapter sequences from high-throughput sequencing reads. *EMBnet.Journal,* 17 (1), 10–12.

Mathieu, M., Martin-Jaular, L., Lavieu, G. and Théry, C., 2019. Specificities of secretion and uptake of exosomes and other extracellular vesicles for cell-to-cell communication. *Nature Cell Biology,* 21 (1), 9–17.

Matsui, T., Osaki, F., Hiragi, S., Sakamaki, Y. and Fukuda, M., 2021. ALIX and ceramide differentially control polarized small extracellular vesicle release from epithelial cells. *EMBO Reports,* 22 (5), e51475–n/a.

Mavrogeorgis, E., Mischak, H., Latosinska, A., Siwy, J., Jankowski, V. and Jankowski, J., 2021. Reproducibility Evaluation of Urinary Peptide Detection Using CE-MS. *Molecules (Basel, Switzerland),* 26 (23), 7260.

Mayersohn, M., Conrad, K. and Achari, R., 1983. The influence of a cooked meat meal on creatinine plasma concentration and creatinine clearance. *British Journal of Clinical Pharmacology,* 15 (2), 227-230.

M'Boutchou, M., and van Kempen, L.C., 2016, Analysis of the Tumor Microenvironment Transcriptome via NanoString mRNA and miRNA Expression Profiling. *In:* Analysis of the Tumor Microenvironment Transcriptome via NanoString mRNA and miRNA Expression Profiling. *Methods in molecular biology (Clifton, N.J.).* New York, NY: Springer New York, 2016, pp. 291–310.

McElderry, L.A., Tarbit, I.F. and Cassells-Smith, A.J., 1982. Six methods for urinary protein compared. *Clinical Chemistry (Baltimore, Md.),* 28 (2), 356-360.

Mehta, N., Li, R., Zhang, D., Soomro, A., He, J., Zhang, I., MacDonald, M., Gao, B. and Krepinsky, J.C., 2021. miR299a-5p promotes renal fibrosis by suppressing the antifibrotic actions of follistatin. *Scientific Reports,* 11 (1), 88.

Meikle, P.J., Fuller, M. and Hopwood, J.J., 2005, Chapter 10 - Lysosomal Degradation of Heparin and Heparan Sulfate. *In:* Chapter 10 - Lysosomal Degradation of Heparin and Heparan Sulfate. *Chemistry and Biology of Heparin and Heparan Sulfate.* Elsevier Ltd, 2005, pp. 285–311.

Meltzer, J.S., 2019, 40 - Renal Physiology. *In:* 40 - Renal Physiology. *Pharmacology and Physiology for Anesthesia.* Second Edition ed. Elsevier Inc, 2019, pp. 782–794.

Meng, X., Nikolic-Paterson, D.J. and Lan, H.Y., 2016. TGF-β: the master regulator of fibrosis. *Nature Reviews. Nephrology,* 12 (6), 325-338.

Merchant, M.L., Rood, I.M., Deegens, J.K.J. and Klein, J.B., 2017. Isolation and characterization of urinary extracellular vesicles: implications for biomarker discovery. *Nature Reviews. Nephrology,* 13 (12), 731-749.

Meri, P., Morgan, B.P., Davies, A., Daniels, R.H., Olavesen, M.G., Waldmann, H. and Lachmann, P.J., 1990. Human protectin (CD59), an 18,000-20,000 MW complement lysis restricting factor, inhibits C5b-8 catalysed insertion of C9 into lipid bilayers. *Immunology,* 71 (1), 1–9.

Miao, L., Yao, H., Li, C., Pu, M., Yao, X., Yang, H., Qi, X., Ren, J. and Wang, Y., 2016. A dual inhibition: microRNA-552 suppresses both transcription and translation of cytochrome P450 2E1. *Biochimica Et Biophysica Acta (BBA)-Gene Regulatory Mechanisms,* 1859 (4), 650–662.

Miller, J.W., Urbinati, C.R., Teng-Umnuay, P., Stenberg, M.G., Byrne, B.J., Thornton, C.A. and Swanson, M.S., 2000. Recruitment of human muscleblind proteins to (CUG)(n) expansions associated with myotonic dystrophy. *The EMBO Journal,* 19 (17), 4439–4448.

Miller, W.G., Bruns, D.E., Bunk, D.M., Curhan, G.C., Narva, A.S., Hortin, G.L., Sandberg, S., Aakre, K.M., Mcqueen, M.J., Itoh, Y., Lieske, J.C., Seccombe, D.W. and Jones, G., 2009. Current Issues in Measurement and Reporting of Urinary Albumin Excretion. *Clinical Chemistry,* 55 (1), 24-38.

Miller, W.G., Kaufman, H.W., Levey, A.S., Straseski, J.A., Wilhelms, K.W., Yu, H., Klutts, J.S., Hilborne, L.H., Horowitz, G.L., Lieske, J., Ennis, J.L., Bowling, J.L., Lewis, M.J., Montgomery, E., Vassalotti, J.A. and Inker, L.A., 2022. National Kidney Foundation Laboratory Engagement Working Group Recommendations for Implementing the CKD-EPI 2021 Race-Free Equations for Estimated Glomerular Filtration Rate: Practical Guidance for Clinical Laboratories. *Clinical Chemistry (Baltimore, Md.),* 68 (4), 511-520.

Minciacchi, V.R., Freeman, M.R. and Di Vizio, D., 2015. Extracellular Vesicles in Cancer: Exosomes, Microvesicles and the Emerging Role of Large Oncosomes. *Seminars in Cell & Developmental Biology,* 40, 41-51.

Mise, A.D., Tamma, G., Ranieri, M., Centrone, M., Heuvel, L. P. W. J. van den, Mekahli, D., Levtchenko, E.N. and Valenti, G., 2018. Activation of Calcium-Sensing Receptor increases intracellular calcium and decreases cAMP and mTOR in PKD1 deficient cells. *Scientific Reports*, 8 (1), 1-14.

Mitchell, H.R. and Kline, W.B., 2006. CORE CURRICULUM IN NEPHROLOGY. Renal function testing *Am J Kidney Dis,* 47 (1), 174-83.

Miyata, A., Yokoyama, C., Ihara, H., Bandoh, S., Takeda, O., Takahashi, E. and Tanabe, T., 1994. Characterization of the Human Gene (TBXAS1) Encoding Thromboxane Synthase. *European Journal of Biochemistry,* 224 (2), 273–279.

Mizenko, R.R., Brostoff, T., Rojalin, T., Koster, H.J., Swindell, H.S., Leiserowitz, G.S., Wang, A. and Carney, R.P., 2021. Tetraspanins are unevenly distributed across single extracellular vesicles and bias sensitivity to multiplexed cancer biomarkers. *Journal of Nanobiotechnology,* 19 (1), 250.

Mobius, W., Ohno-Iwashita, Y., van Donselaar, E.G., Oorschot, V.M.J., Shimada, Y., Fujimoto, T., Heijnen, H.F.G., Geuze, H.J. and Slot, J.W., 2002. Immunoelectron Microscopic Localization of

Cholesterol Using Biotinylated and Non-cytolytic Perfringolysin O. *The Journal of Histochemistry and Cytochemistry,* 50 (1), 43-55.

Moiseev, S., Novikov, P., Jayne, D. and Mukhin, N., 2017. End-stage renal disease in ANCA-associated vasculitis. *Nephrology, Dialysis, Transplantation,* 32 (2), 248–253.

Montecalvo, A., Larregina, A.T., Shufesky, W.J., Beer Stolz, D., Sullivan, M.L.G., Karlsson, J.M., Baty, C.J., Gibson, G.A., Erdos, G., Wang, Z., Milosevic, J., Tkacheva, O.A., Divito, S.J., Jordan, R., Lyons-Weiler, J., Watkins, S.C. and Morelli, A.E., 2012. Mechanism of transfer of functional microRNAs between mouse dendritic cells via exosomes. *Blood,* 119 (3), 756-766.

Moon, P., Lee, J., You, S., Kim, T., Cho, J., Kim, I., Kwon, T., Kim, C., Park, S., Hwang, D., Kim, Y. and Baek, M., 2011. Proteomic analysis of urinary exosomes from patients of early IgA nephropathy and thin basement membrane nephropathy. *Proteomics,* 11 (12), 2459–2475.

Morelli, A.E., Larregina, A.T., Shufesky, W.J., Sullivan, M.L.G., Stolz, D.B., Papworth, G.D., Zahorchak, A.F., Logar, A.J., Wang, Z., Watkins, S.C., Falo, L.D. and Thomson, A.W., 2004. Endocytosis, intracellular sorting, and processing of exosomes by dendritic cells. *Blood,* 104 (10), 3257-3266.

Mulcahy, L.A., Pink, R.C. and Carter, D.R.F., 2014. Routes and mechanisms of extracellular vesicle uptake. *Journal of Extracellular Vesicles,* 3 (1), 1-n/a.

Munroe, Melissa E., and James, Judith A., 2015. Genetics of Lupus Nephritis: Clinical Implications. *Seminars in Nephrology,* 35 (5), 396-409.

Muralidharan-Chari, V., Clancy, J., Plou, C., Romao, M., Chavrier, P., Raposo, G. and D'Souza-Schorey, C., 2009. ARF6-regulated shedding of tumor cell-derived plasma membrane microvesicles. *Current Biology,* 19 (22), 1875-1885.

Murata, M., Peranen, J., Schreiner, R., Wieland, F., Kurzchalia, T.V. and Simons, K., 1995. VIP21/Caveolin is a Cholesterol-Binding Protein. *Proceedings of the National Academy of Sciences - PNAS,* 92 (22), 10339-10343.

Murea, M., Park, J., Sharma, S., Kato, H., Gruenwald, A., Niranjan, T., Si, H., Thomas, D.B., Pullman, J.M., Melamed, M.L. and Susztak, K., 2010. Expression of Notch pathway proteins correlate with albuminuria, glomerulosclerosis, and renal function. *Kidney International,* 78 (5), 514-522.

Musante, L., Tataruch, D., Gu, D., Liu, X., Forsblom, C., Groop, P. and Holthofer, H., 2015. Proteases and protease inhibitors of urinary extracellular vesicles in diabetic nephropathy. *Journal of Diabetes Research,* 2015 (1), 289734.

Nabi, I.R., and Le, P.U., 2003. Caveolae/Raft-Dependent Endocytosis. *The Journal of Cell Biology,* 161 (4), 673-677.

Nagaraj, N., and Mann, M., 2011. Quantitative Analysis of the Intra- and Inter-Individual Variability of the Normal Urinary Proteome. *Journal of Proteome Research,* 10 (2), 637–645.

Nakano, Y., Nakatani, Y., Takami, M., Taniyama, Y. and Arima, S., 2019. Diverse associations between oxidative stress and thromboxane A2 in hypertensive glomerular injury. *Hypertension Research,* 42 (4), 450–458.

Nakase, I., Kobayashi, N.B., Takatani-Nakase, T. and Yoshida, T., 2015. Active macropinocytosis induction by stimulation of epidermal growth factor receptor and oncogenic Ras expression potentiates cellular uptake efficacy of exosomes. *Scientific Reports,* 5 (1), 10300.

Nanbo, A., Kawanishi, E., Yoshida, R. and Yoshiyama, H., 2013. Exosomes Derived from Epstein-Barr Virus-Infected Cells Are Internalized via Caveola-Dependent Endocytosis and Promote Phenotypic Modulation in Target Cells. *Journal of Virology,* 87 (18), 10334-10347.

NanoString technologies, 2017. Gene expression data analysis guidelines. Available from: https://nanostring.com/wp-content/uploads/Gene_Expression_Data_Analysis_Guidelines.pdf. [Last accessed on 13 Jan 2025].

National Kidney Foundation, 2002. K/DOQI clinical practice guidelines for chronic kidney disease: evaluation, classification, and stratification. *American Journal of Kidney Diseases,* 39, S1-266.

Navarro, E., Serrano-Heras, G., Castaño, M.J. and Solera, J., 2015. Real-time PCR detection chemistry. *Clinica Chimica Acta,* 439, 231–250.

Nazarenko, I., Rana, S., Baumann, A., McAlear, J., Hellwig, A., Trendelenburg, M., Lochnit, G., Preissner, K.T. and Zoller, M., 2010. Cell Surface Tetraspanin Tspan8 Contributes to Molecular Pathways of Exosome-Induced Endothelial Cell Activation. *Cancer Research,* 70 (4), 1668-1678.

Newman, D.J., Thakkar, H., Edwards, R.G., Wilkie, M., White, T., Grubb, A.O. and Price, C.P., 1995. Serum cystatin C measured by automated immunoassay: A more sensitive marker of changes in GFR than serum creatinine. *Kidney International,* 47 (1), 312-318.

Newman, D.J., Thakkar, H., Medcalf, E.A., Gray, M.R. and Price, C.P., 1995. Use of urine albumin measurement as a replacement for total protein. *Clinical Nephrology,* 43 (2), 104-109.

Newton, A.J., Kirchhausen, T. and Murthy, V.N., 2006. Inhibition of Dynamin Completely Blocks Compensatory Synaptic Vesicle Endocytosis. *Proceedings of the National Academy of Sciences - PNAS,* 103 (47), 17955-17960.

Nichols, G.A., Déruaz-Luyet, A., Brodovicz, K.G., Kimes, T.M., Rosales, A.G. and Hauske, S.J., 2020. Kidney disease progression and all-cause mortality across estimated glomerular filtration rate and albuminuria categories among patients with vs. without type 2 diabetes. *BMC Nephrology,* 21 (1), 167.

Nielsen, R., Mollet, G., Esquivel, E.L., Weyer, K., Nielsen, P.K., Antignac, C. and Christensen, E.I., 2013. Increased lysosomal proteolysis counteracts protein accumulation in the proximal tubule during focal segmental glomerulosclerosis. *Kidney International,* 84 (5), 902–910.

Ning, J., Xiang, Z., Xiong, C., Zhou, Q., Wang, X. and Zou, H., 2020. Alpha1-Antitrypsin in Urinary Extracellular Vesicles: A Potential Biomarker of Diabetic Kidney Disease Prior to Microalbuminuria. *Diabetes, Metabolic Syndrome and Obesity,* 13, 2037–2048.

Niu, X., Zhang, S., Shao, C., Guo, Z., Wu, J., Tao, J., Zheng, K., Ye, W., Cai, G., Sun, W. and Li, M., 2023. Urinary complement proteins in IgA nephropathy progression from a relative quantitative proteomic analysis. *PeerJ,* 11, e15125.

Nørgård, M.Ø, Steffensen, L.B., Hansen, D.R., Füchtbauer, E., Engelund, M.B., Dimke, H., Andersen, D.C. and Svenningsen, P., 2022. A new transgene mouse model using an extravesicular EGFP tag enables affinity isolation of cell-specific extracellular vesicles. *Scientific Reports,* 12 (1), 496.

Obita, T., Saksena, S., Ghazi-tabatabai, S., Grill, D.J., Perisic, O., Emr, S.D. and Williams, R.L., 2007. Structural basis for selective recognition of ESCRT-III by the AAA ATPase Vps4. *Nature,* 449 (7163), 735-739.

Ogurtsova, K., da Rocha Fernandes, J.D., Huang, Y., Linnenkamp, U., Guariguata, L., Cho, N.H., Cavan, D., Shaw, J.E. and Makaroff, L.E., 2017. IDF Diabetes Atlas: Global estimates for the prevalence of diabetes for 2015 and 2040. *Diabetes Research and Clinical Practice,* 128, 40-50.

Ohshima, K., Nojima, S., Tahara, S., Kurashige, M., Hori, Y., Hagiwara, K., Okuzaki, D., Oki, S., Wada, N., Ikeda, J., Kanai, Y. and Morii, E., 2017. Argininosuccinate Synthase 1-Deficiency Enhances the Cell Sensitivity to Arginine through Decreased DEPTOR Expression in Endometrial Cancer. *Scientific Reports,* 7 (1), 45504–45504.

Oksa, H., Pasternack, A. and Pasanen, M., 1987. Serum urea-creatinine ratio as a prognostic index in hemodialysis patients. *Clinical Nephrology,* 27 (3), 125-130.

Ong, A.C.M., Devuyst, O., Knebelmann, B., Walz, G., 2015. Autosomal dominant polycystic kidney disease: the changing face of clinical management. *The Lancet*, 385 (9981), 1993-2002.

Ørom, U.A., Nielsen, F.C. and Lund, A.H., 2008. MicroRNA-10a Binds the 5'UTR of Ribosomal Protein mRNAs and Enhances Their Translation. *Molecular Cell,* 30 (4), 460–471.

Orth, J.D., Krueger, E.W., Cao, H. and McNiven, M.A., 2002. The Large GTPase Dynamin Regulates Actin Comet Formation and Movement in Living Cells. *Proceedings of the National Academy of Sciences - PNAS,* 99 (1), 167-172.

Oshikawa-Hori, S., Yokota-Ikeda, N., Sonoda, H., Sasaki, Y. and Ikeda, M., 2021. Reduced urinary release of AQP1- and AQP2-bearing extracellular vesicles in patients with advanced chronic kidney disease. *Physiological Reports,* 9 (17), e15005–n/a.

Oshima, M., Toyama, T., Hara, A., Shimizu, M., Kitajima, S., Iwata, Y., Sakai, N., Furuichi, K., Haneda, M., Babazono, T., Yokoyama, H., Iseki, K., Araki, S., Ninomiya, T., Hara, S., Suzuki, Y., Iwano, M., Kusano, E., Moriya, T., Satoh, H., Nakamura, H., Makino, H. and Wada, T., 2021. Combined changes in albuminuria and kidney function and subsequent risk for kidney failure in type 2 diabetes. *BMJ Open Diabetes Research & Care,* 9 (1), e.

Osicka, T.M., Houlihan, C.A., Chan, J.G., Jerums, G. and Comper, W.D., 2000. Albuminuria in patients with type 1 diabetes is directly linked to changes in the lysosome-mediated degradation of albumin during renal passage. *Diabetes,* 49 (9), 1579–1584.

Ostendorf, T., Kunter, U., Eitner, F., Loos, A., Regele, H., Kerjaschki, D., Henninger, D.D., Janjic, N. and Floege, J., 1999. VEGF165 mediates glomerular endothelial repair. *The Journal of Clinical Investigation,* 104 (7), 913-923.

Ota, K., Ota, Z., Shikata, K. and Makino, H., 1995. The ultrastructural disruption of the glomerular basement membrane in diabetic nephropathy revealed by "tissue negative staining method". *Journal of Diabetes and its Complications,* 9 (4), 285–287.

Pace, J., Paladugu, P., Das, B., He, J.C. and Mallipattu, S.K., 2019. Targeting STAT3 signaling in kidney disease. *American Journal of Physiology-Renal Physiology,* 316 (6), 1151.

Pan, B.T., and Johnstone, R., 1984. Selective externalization of the transferrin receptor by sheep reticulocytes in vitro. Response to ligands and inhibitors of endocytosis. *The Journal of Biological Chemistry,* 259 (15), 9776-9782.

Pan, B., and Johnstone, R.M., 1983. Fate of the transferrin receptor during maturation of sheep reticulocytes in vitro: Selective externalization of the receptor. *Cell,* 33 (3), 967-978.

Pap, E., Pállinger, É, Pásztói, M. and Falus, A., 2009. Highlights of a new type of intercellular communication: microvesicle-based information transfer. *Inflammation Research,* 58 (1), 1-8.

Park, J.Y., Yoo, K.D., Bae, E., Kim, K.H., Lee, J.W., Shin, S.J., Lee, J.S., Kim, Y.S. and Yang, S.H., 2022. Blockade of STAT3 signaling alleviates the progression of acute kidney injury to chronic kidney disease through antiapoptosis. *American Journal of Physiology. Renal Physiology,* 322 (5), F553–F572.

Parolini, I., Federici, C., Raggi, C., Lugini, L., Palleschi, S., De Milito, A., Coscia, C., Iessi, E., Logozzi, M., Molinari, A., Colone, M., Tatti, M., Sargiacomo, M. and Fais, S., 2009. Microenvironmental pH Is a Key Factor for Exosome Traffic in Tumor Cells. *The Journal of Biological Chemistry,* 284 (49), 34211-34222.

Parving, H., Gall, M., Skøtt, P., Jørgensen, H.E., Løkkegaard, H., Jørgensen, F., Nielsen, B. and Larsen, S., 1992. Prevalence and causes of albuminuria in non-insulin-dependent diabetic patients. *Kidney International,* 41 (4), 758-762.

Parving, H., Hommel, E., Mathiesen, E., Skøtt, P., Edsberg, B., Bahnsen, M., Lauritzen, M., Hougaard, P. and Lauritzen, E., 1988. Prevalence of microalbuminuria, arterial hypertension, retinopathy, and neuropathy in patients with insulin dependent diabetes. *Bmj,* 296 (6616), 156-160.

Pascual, M., Steiger, G., Sadallah, S., Paccaud, J.-., Carpentier, J.-., James, R. and Schifferli, J.-., 1994. Identification of membrane bound CR1 (CD35) in human urine: evidence for its release by glomerular podocytes. *The Journal of Experimental Medicine,* 179 (3), 889-899.

Pasquet, J., Dachary-Prigent, J. and Nurden, A.T., 1996. Calcium Influx is a Determining Factor of Calpain Activation and Microparticle Formation in Platelets. *European Journal of Biochemistry,* 239 (3), 647-654.

Pastor-Soler, N.M., Sutton, T.A., Mang, H.E., Kinlough, C.L., Gendler, S.J., Madsen, C.S., Bastacky, S.I., Ho, J., Al-Bataineh, M.M., Hallows, K.R., Singh, S., Monga, S.P., Kobayashi, H., Haase, V.H. and Hughey, R.P., 2015. Muc1 is protective during kidney ischemia-reperfusion injury. *American Journal of Physiology. Renal Physiology,* 308 (12), F1452-F1462.

Perez-Hernandez, J., Forner, M.J., Pinto, C., Chaves, F.J., Cortes, R. and Redon, J., 2015. Increased urinary exosomal micrornas in patients with systemic lupus erythematosus. *PloS One,* 10 (9), e0138618.

Pergande, M., and Jung, K., 1993. Sandwich enzyme immunoassay of cystatin C in serum with commercially available antibodies. *Clinical Chemistry (Baltimore, Md.),* 39 (9), 1885-1890.

Perrone, R.D., Madias, N.E. and Levey, A.S., 1992. Serum creatinine as an index of renal function: new insights into old concepts. *Clinical Chemistry (Baltimore, Md.),* 38 (10), 1933-1953.

Perry, H.M., Görldt, N., Sung, S.J., Huang, L., Rudnicka, K.P., Encarnacion, I.M., Bajwa, A., Tanaka, S., Poudel, N., Yao, J., Rosin, D.L., Schrader, J. and Okusa, M.D., 2019. Perivascular CD73 + cells attenuate inflammation and interstitial fibrosis in the kidney microenvironment. *American Journal of Physiology. Renal Physiology,* 317 (3), F658-F669.

Piccin, A., Murphy, W.G. and Smith, O.P., 2007. Circulating microparticles: pathophysiology and clinical implications. *Blood Reviews,* 21 (3), 157-171.

Pintus, G., Giordo, R., Wang, Y., Zhu, W., Kim, S.H., Zhang, L., Ni, L., Zhang, J., Telljohann, R., McGraw, K.R., Monticone, R.E., Ferris, C., Liu, L., Wang, M. and Lakatta, E.G., 2018. Reduced vasorin enhances angiotensin II signaling within the aging arterial wall. *Oncotarget,* 9 (43), 27117–27132.

Pisitkun, T., Shen, R., Knepper, M.A. and Sly, W.S., 2004. Identification and Proteomic Profiling of Exosomes in Human Urine. *Proceedings of the National Academy of Sciences,* 101 (36), 13368-13373.

Place, R.F., Li, L., Pookot, D., Noonan, E.J. and Dahiya, R., 2008. MicroRNA-373 Induces Expression of Genes with Complementary Promoter Sequences. *Proceedings of the National Academy of Sciences - PNAS,* 105 (5), 1608–1613.

Poggio, E.D., McClelland, R.L., Blank, K.N., Hansen, S., Bansal, S., Bomback, A.S., Canetta, P.A., Khairallah, P., Kiryluk, K., Lecker, S.H., McMahon, G.M., Palevsky, P.M., Parikh, S., Rosas, S.E., Tuttle, K., Vazquez, M.A., Vijayan, A. and Rovin, B.H., 2020. Systematic Review and Meta-Analysis of Native Kidney Biopsy Complications. *Clinical Journal of the American Society of Nephrology,* 15 (11), 1595-1602.

Pomatto, M.A.C., Gai, C., Bussolati, B. and Camussi, G., 2017. Extracellular Vesicles in Renal Pathophysiology. *Frontiers in Molecular Biosciences,* 4, 37.

Pontillo, C., Jacobs, L., Staessen, J.A., Schanstra, J.P., Rossing, P., Heerspink, H.J.L., Siwy, J., Mullen, W., Vlahou, A., Mischak, H., Vanholder, R., Zürbig, P. and Jankowski, J., 2017. A urinary proteome-based classifier for the early detection of decline in glomerular filtration. *Nephrology, Dialysis, Transplantation,* 32 (9), 1510–1516.

Porrini, E., Ruggenenti, P., Luis-Lima, S., Carrara, F., Jiménez, A., de Vries, A.P.J., Torres, A., Gaspari, F. and Remuzzi, G., 2019. Estimated GFR: time for a critical appraisal. *Nature Reviews. Nephrology,* 15 (3), 177–190.

Pottel, H., Delanaye, P. and Cavalier, E., 2024. Exploring Renal Function Assessment: Creatinine, Cystatin C, and Estimated Glomerular Filtration Rate Focused on the European Kidney Function Consortium Equation. *Annals of Laboratory Medicine,* 44 (2), 135-143.

Prajczer, S., Heidenreich, U., Pfaller, W., Kotanko, P., Lhotta, K. and Jennings, P., 2010. Evidence for a role of uromodulin in chronic kidney disease progression. *Nephrology, Dialysis, Transplantation,* 25 (6), 1896–1903.

Prat-Duran, J., De Araujo, I.B.B.A., Juste, N., Pinilla, E., Rios, F.J., Montezano, A.C., Touyz, R.M., Simonsen, U., Nørregaard, R. and Buus, N.H., 2024. Pharmacological modulation of transglutaminase 2 in the unilateral ureteral obstruction mouse model. *European Journal of Pharmacology,* 984, 177037.

Prat-Duran, J., Pinilla, E., Nørregaard, R., Simonsen, U. and Buus, N.H., 2021. Transglutaminase 2 as a novel target in chronic kidney disease – Methods, mechanisms and pharmacological inhibition. *Pharmacology & Therapeutics,* 222, 107787.

Prekeris, R., Yang, B., Oorschot, V., Klumperman, J. and Scheller, R.H., 1999. Differential Roles of Syntaxin 7 and Syntaxin 8 in Endosomal Trafficking. *Molecular Biology of the Cell,* 10 (11), 3891-3908.

Prikryl, P., Satrapova, V., Frydlova, J., Hruskova, Z., Zima, T., Tesar, V. and Vokurka, M., 2021. Mass spectrometry-based proteomic exploration of the small urinary extracellular vesicles in ANCA-associated vasculitis in comparison with total urine. *Journal of Proteomics,* 233, 104067.

Pu, M., Chen, J., Tao, Z., Miao, L., Qi, X., Wang, Y. and Ren, J., 2019. Regulatory network of miRNA on its target: coordination between transcriptional and post-transcriptional regulation of gene expression. *Cellular and Molecular Life Sciences,* 76 (3), 441–451.

Qian, Y., Feldman, E., Pennathur, S., Kretzler, M. and Brosius, F.C., 2008. Mechanisms of Glomerulosclerosis in Diabetic Nephropathy. *Diabetes (New York, N.Y.),* 57 (6), 1439-1445.

Qin, S., Shi, X., Wang, C., Jin, P. and Ma, F., 2019. Transcription Factor and miRNA Interplays Can Manifest the Survival of ccRCC Patients. *Cancers,* 11 (11), 1668.

Qin, W., Chung, A.C., Huang, X.R., Meng, X., Hui, D.S., Yu, C., Sung, J.J. and Lan, H.Y., 2011. TGF-β/Smad3 signaling promotes renal fibrosis by inhibiting miR-29. *Journal of the American Society of Nephrology,* 22 (8), 1462–1474.

Quesada, A., Segarra, A.B., Montoro-Molina, S., de Gracia, M.D.C., Osuna, A., O'Valle, F., Gómez-Guzmán, M., Vargas, F. and Wangensteen, R., 2017. Glutamyl aminopeptidase in microvesicular and exosomal fractions of urine is related with renal dysfunction in cisplatin-treated rats. *PloS One,* 12 (4), e0175462.

Quesenberry, P.J., Goldberg, L.R., Aliotta, J.M., Dooner, M.S., Pereira, M.G., Wen, S. and Camussi, G., 2014. Cellular Phenotype and Extracellular Vesicles: Basic and Clinical Considerations. *Stem Cells and Development,* 23 (13), 1429-1436.

Radford, M.G., Donadio, J.V., Bergstralh, E.J. and Grande, J.P., 1997. Predicting renal outcome in IgA nephropathy. *Journal of the American Society of Nephrology*, 8 (2), 199-207.

Radtke, K.P., Fernández, J.A., Greengard, J.S., Tang, W.W., Wilson, C.B., Loskutoff, D.J., Scharrer, I. and Griffin, J.H., 1994. Protein C inhibitor is expressed in tubular cells of human kidney. *Journal of Clinical Investigation,* 94 (5), 2117–2124.

Rai, A., Fang, H., Claridge, B., Simpson, R.J. and Greening, D.W., 2021. Proteomic dissection of large extracellular vesicle surfaceome unravels interactive surface platform. *Journal of Extracellular Vesicles,* 10 (13), e12164–n/a.

Ramezani, A., Devaney, J.M., Cohen, S., Wing, M.R., Scott, R., Knoblach, S., Singhal, R., Howard, L., Kopp, J.B. and Raj, D.S., 2015. Circulating and urinary microRNA profile in focal segmental glomerulosclerosis: a pilot study. *European Journal of Clinical Investigation,* 45 (4), 394–404.

Rana, S., Claas, C., Kretz, C.C., Nazarenko, I. and Zoeller, M., 2011. Activation-induced internalization differs for the tetraspanins CD9 and Tspan8: Impact on tumor cell motility. *The International Journal of Biochemistry & Cell Biology,* 43 (1), 106-119.

Rana, S., Yue, S., Stadel, D. and Zöller, M., 2012. Toward tailored exosomes: The exosomal tetraspanin web contributes to target cell selection. *The International Journal of Biochemistry & Cell Biology,* 44 (9), 1574-1584.

Ranghino, A., Dimuccio, V., Papadimitriou, E. and Bussolati, B., 2015. Extracellular vesicles in the urine: Markers and mediators of tissue damage and regeneration. *Clinical Kidney Journal,* 8 (1), 23-30.

Rayego-Mateos, S., Morgado-Pascual, J.L., Rodrigues-Diez, R.R., Rodrigues-Diez, R., Falke, L.L., Mezzano, S., Ortiz, A., Egido, J., Goldschmeding, R. and Ruiz-Ortega, M., 2018. Connective tissue growth factor induces renal fibrosis via epidermal growth factor receptor activation. *The Journal of Pathology,* 244 (2), 227–241.

Reddy, V.S., Madala, S.K., Trinath, J. and Reddy, G.B., 2018. Extracellular small heat shock proteins: exosomal biogenesis and function. *Cell Stress & Chaperones,* 23 (3), 441-454.

Rehling, M., Møller, M.L., Thamdrup, B., Lund, J.O. and Trap-Jensen, J., 1984. Simultaneous Measurement of Renal Clearance and Plasma Clearance of 99mTc-Labelled Diethylenetriaminepenta-Acetate, 51Cr-Labelled Ethylenediaminetetra-Acetate and Inulin in Man. *Clinical Science (1979),* 66 (5), 613-619.

Ricciardi, C.A., and Gnudi, L., 2020. The endoplasmic reticulum stress and the unfolded protein response in kidney disease: Implications for vascular growth factors. *Journal of Cellular and Molecular Medicine,* 24 (22), 12910–12919.

Ridolfi, A., Cardellini, J., Gashi, F., van Herwijnen, M.J.C., Trulsson, M., Campos-Terán, J., H. M. Wauben, M., Berti, D., Nylander, T. and Stenhammar, J., 2023. Electrostatic interactions control the adsorption of extracellular vesicles onto supported lipid bilayers. *Journal of Colloid and Interface Science,* 650 (Pt A), 883–891.

Riento, K., Frick, M., Schafer, I. and Nichols, B.J., 2009. Endocytosis of flotillin-1 and flotillin-2 is regulated by Fyn kinase. *Journal of Cell Science,* 122 (7), 912-918.

Ritchie, M.E., Phipson, B., Wu, D., Hu, Y., Law, C.W., Shi, W. and Smyth, G.K., 2015. Limma Powers Differential Expression Analyses for RNA-Sequencing and Microarray Studies. *Nucleic Acids Research,* 43 (7), e47.

Roberts, I.S., Burrows, C., Shanks, J.H., Venning, M. and McWilliam, L.J., 1997. Interstitial myofibroblasts: predictors of progression in membranous nephropathy. *Journal of Clinical Pathology,* 50 (2), 123-127.

Roberts, T.C., 2014. The MicroRNA Biology of the Mammalian Nucleus. *Molecular Therapy - Nucleic Acids,* 3 (8), e188–e188.

Robinson, D.G., Ding, Y. and Jiang, L., 2016. Unconventional protein secretion in plants: a critical assessment. *Protoplasma,* 253 (1), 31-43.

Robinson, L.J., Aniento, F. and Gruenberg, J., 1997. NSF is required for transport from early to late endosomes. *Journal of Cell Science,* 110 (17), 2079-2087.

Rodrigues, J.C., Haas, M. and Reich, H.N., 2017. IgA Nephropathy. *Clinical Journal of the American Society of Nephrology: CJASN*, 12 (4), 677-686.

Rodríguez-Ortiz, M.E., Pontillo, C., Rodríguez, M., Zürbig, P., Mischak, H. and Ortiz, A., 2018. Novel Urinary Biomarkers For Improved Prediction Of Progressive eGFR Loss In Early Chronic Kidney Disease Stages And In High Risk Individuals Without Chronic Kidney Disease. *Scientific Reports,* 8 (1), 15940–11.

Roscioni, S.S., de Zeeuw, D., Hellemons, M.E., Mischak, H., Zürbig, P., Bakker, S.J.L., Gansevoort, R.T., Reinhard, H., Persson, F., Lajer, M., Rossing, P. and Heerspink, H.J.L., 2013. A urinary peptide biomarker set predicts worsening of albuminuria in type 2 diabetes mellitus. *Diabetologia,* 56 (2), 259–267.

Rosenberg, A.Z., and Kopp, J.B., 2017. Focal segmental glomerulosclerosis. *Clinical Journal of the American Society of Nephrology*, 12 (3), 502-517.

Rothberg, K.G., Heuser, J.E., Donzell, W.C., Ying, Y., Glenney, J.R. and Anderson, R.G.W., 1992. Caveolin, a protein component of caveolae membrane coats. *Cell,* 68 (4), 673-682.

Russo, L.M., Sandoval, R.M., McKee, M., Osicka, T.M., Collins, A.B., Brown, D., Molitoris, B.A. and Comper, W.D., 2007. The normal kidney filters nephrotic levels of albumin retrieved by proximal tubule cells: Retrieval is disrupted in nephrotic states. *Kidney International,* 71 (6), 504–513.

Rybin, V., Ullrich, O., Rubino, M., Alexandrov, K., Simon, I., Seabra, M.C., Goody, R. and Zerial, M., 1996. GTPase activity of Rab5 acts as a timer for endocytic membrane fusion. *Nature (London),* 383 (6597), 266.

Saad, S., Stevens, V.A., Wassef, L., Poronnik, P., Kelly, D.J., Gilbert, R.E. and Pollock, C.A., 2005. High glucose transactivates the EGF receptor and up-regulates serum glucocorticoid kinase in the proximal tubule. *Kidney International,* 68 (3), 985-997.

Sabaratnam, R., Geertsen, L., Skjødt, K., Højlund, K., Dimke, H., Lund, L. and Svenningsen, P., 2019. In human nephrectomy specimens, the kidney level of tubular transport proteins does not correlate with their abundance in urinary extracellular vesicles. *American Journal of Physiology. Renal Physiology,* 317 (3), F560–F571.

Sabbisetti, V.S., Waikar, S.S., Antoine, D.J., Smiles, A., Wang, C., Ravisankar, A., Ito, K., Sharma, S., Ramadesikan, S., Lee, M., Briskin, R., De Jager, P.L., Ngo, T.T., Radlinski, M., Dear, J.W., Park, K.B., Betensky, R., Krolewski, A.S. and Bonventre, J.V., 2014. Blood Kidney Injury Molecule-1 Is a Biomarker of Acute and Chronic Kidney Injury and Predicts Progression to ESRD in Type I Diabetes. *Journal of the American Society of Nephrology,* 25 (10), 2177-2186.

Said, S.M., and Nasr, S.H., 2016. Silent diabetic nephropathy. *Kidney International,* 90 (1), 24-26.

Sakurai, A., Ono, H., Ochi, A., Matsuura, M., Yoshimoto, S., Kishi, S., Murakami, T., Tominaga, T., Nagai, K., Abe, H. and Doi, T., 2019. Involvement of Elf3 on Smad3 activation-dependent injuries in podocytes and excretion of urinary exosome in diabetic nephropathy. *PLoS ONE,* 14 (5), e0216788.

Salih, M., Demmers, J.A., Bezstarosti, K., Leonhard, W.N., Losekoot, M., van Kooten, C., Gansevoort, R.T., Peters, D.J.M., Zietse, R. and Hoorn, E.J., 2016. Proteomics of Urinary Vesicles Links Plakins and Complement to Polycystic Kidney Disease. *Journal of the American Society of Nephrology,* 27 (10), 3079–3092.

Salvati, P., Lamberti, E., Ferrario, R., Ferrario, R.G., Scampini, G., Pugliese, F., Barsotti, P. and Patrono, C., 1995. Long-term thromboxane-synthase inhibition prolongs survival in murine lupus nephritis. *Kidney International,* 47 (4), 1168–1175.

Santiago-Hernandez, A., Martin-Lorenzo, M., Gómez-Serrano, M., Lopez, J.A., Martin-Blazquez, A., Vellosillo, P., Minguez, P., Martinez, P.J., Vázquez, J., Ruiz-Hurtado, G., Barderas, M.G., Sarafidis, P., Segura, J., Ruilope, L.M. and Alvarez-Llamas, G., 2024. The Urinary Glycopeptide Profile Differentiates Early Cardiorenal Risk in Subjects Not Meeting Criteria for Chronic Kidney Disease. *International Journal of Molecular Sciences,* 25 (13), 7005.

Santiago-Hernandez, A., Martin-Lorenzo, M., Martínez, P.J., Gómez-Serrano, M., Lopez, J.A., Cannata, P., Esteban, V., Heredero, A., Aldamiz-Echevarria, G., Vázquez, J., Ruiz-Hurtado, G., Barderas, M.G., Segura, J., Ruilope, L.M. and Alvarez-Llamas, G., 2021. Early renal and vascular damage within the normoalbuminuria condition. *Journal of Hypertension,* 39 (11), 2220–2231.

Sato, M., Muragaki, Y., Saika, S., Roberts, A.B. and Ooshima, A., 2003. Targeted disruption of TGF-β1/Smad3 signaling protects against renal tubulointerstitial fibrosis induced by unilateral ureteral obstruction. *The Journal of Clinical Investigation,* 112 (10), 1486-1494.

Scamporrino, A., Di Mauro, S., Filippello, A., Di Marco, G., Di Pino, A., Scicali, R., Di Marco, M., Martorana, E., Malaguarnera, R., Purrello, F. and Piro, S., 2023. Identification of a New RNA and Protein Integrated Biomarker Panel Associated with Kidney Function Impairment in DKD: Translational Implications. *International Journal of Molecular Sciences,* 24 (11), 9412.

Scarpellini, A., Linghong Huang, Burhan, I., Schroeder, N., Funck, M., Johnson, T.S. and Verderio, E.A.M., 2014. Syndecan-4 Knockout Leads to Reduced Extracellular Transglutaminase-2 and Protects against Tubulointerstitial Fibrosis. *Journal of the American Society of Nephrology,* 25 (5), 1013-1027.

Schiessl, I.M., Grill, A., Fremter, K., Steppan, D., Hellmuth, M. and Castrop, H., 2018. Renal Interstitial Platelet-Derived Growth Factor Receptor- β Cells Support Proximal Tubular Regeneration. *Journal of the American Society of Nephrology,* 29 (5), 1383-1396.

Schmidt, I.M., Colona, M.R., Kestenbaum, B.R., Alexopoulos, L.G., Palsson, R., Srivastava, A., Liu, J., Stillman, I.E., Rennke, H.G., Vaidya, V.S., …, and Arora, T, 2021. Cadherin-11, Sparc-related modular calcium binding protein-2, and Pigment epithelium-derived factor are promising non-invasive biomarkers of kidney fibrosis. *Kidney International,* 100 (3), 672–683.

Schrauben, S.J., Shou, H., Zhang, X., Anderson, A.H., Bonventre, J.V., Chen, J., Coca, S., Furth, S.L., Greenberg, J.H., Gutierrez, O.M., Ix, J.H., Lash, J.P., Parikh, C.R., Rebholz, C.M., Sabbisetti, V., Sarnak, M.J., Shlipak, M.G., Waikar, S.S., Kimmel, P.L., Vasan, R.S., Feldman, H.I. and Schelling, J.R., 2021. Association of Multiple Plasma Biomarker Concentrations with Progression of Prevalent Diabetic Kidney Disease: Findings from the Chronic Renal Insufficiency Cohort (CRIC) Study. *Journal of the American Society of Nephrology,* 32 (1), 115-126.

Schrijvers, B.F., Flyvbjerg, A. and De Vriese, A.S., 2004. The role of vascular endothelial growth factor (VEGF) in renal pathophysiology. Kidney International, 65 (6), 2003-2017.

Scullion, K.M., Vliegenthart, A.D.B., Rivoli, L., Oosthuyzen, W., Farrah, T.E., Czopek, A., Webb, D.J., Hunter, R.W., Bailey, M.A., Dhaun, N. and Dear, J.W., 2021. Circulating argonaute-bound

microRNA-126 reports vascular dysfunction and treatment response in acute and chronic kidney disease. *iScience,* 24 (1), 101937.

Seki, M., Nakayama, M., Sakoh, T., Yoshitomi, R., Fukui, A., Katafuchi, E., Tsuda, S., Nakano, T., Tsuruya, K. and Kitazono, T., 2019. Blood urea nitrogen is independently associated with renal outcomes in Japanese patients with stage 3–5 chronic kidney disease: a prospective observational study. *BMC Nephrology,* 20 (1), 115.

Selby, N.M., and Taal, M.W., 2020. An updated overview of diabetic nephropathy: Diagnosis, prognosis, treatment goals and latest guidelines. *Diabetes, Obesity & Metabolism,* 22 (S1), 3-15.

Sereika, M., Kirkegaard, R.H., Karst, S.M., Michaelsen, T.Y., Sørensen, E.A., Wollenberg, R.D. and Albertsen, M., 2022. Oxford Nanopore R10.4 long-read sequencing enables the generation of near-finished bacterial genomes from pure cultures and metagenomes without short-read or reference polishing. *Nature Methods,* 19 (7), 823–826.

Shannon, J.A., and Smith, H.W., 1935. The excretion of inulin, xylose and urea by normal and phlorizinized man. *The Journal of Clinical Investigation,* 14 (4), 393-401.

Shao, C., Zhao, M., Chen, X., Sun, H., Yang, Y., Xiao, X., Guo, Z., Liu, X., Lv, Y., Chen, X., Sun, W., Wu, D. and Gao, Y., 2019. Comprehensive Analysis of Individual Variation in the Urinary Proteome Revealed Significant Gender Differences[S]. *Molecular & Cellular Proteomics,* 18 (6), 1110–1122.

Sharma, S.G., Bomback, A.S., Radhakrishnan, J., Herlitz, L.C., Stokes, M.B., Markowitz, G.S. and D'Agati, V.D., 2013. The Modern Spectrum of Renal Biopsy Findings in Patients with Diabetes. *Clinical Journal of the American Society of Nephrology,* 8 (10), 1718-1724.

Shemesh, O., Golbetz, H., Kriss, J.P. and Myers, B.D., 1985. Limitations of creatinine as a filtration marker in glomerulopathic patients. *Kidney International,* 28 (5), 830-838.

Sherf, B.A., Navarro, S.L., Hannah, R.R. and Wood, K.V., 1996. Dual-luciferase reporter assay: an advanced co-reporter technology integrating firefly and Renilla luciferase assays. *Promega Notes,* 57 (2), 2–8.

Shihabi, Z.K., Konen, J.C. and O'Connor, M.L., 1991. Albuminuria vs urinary total protein for detecting chronic renal disorders. *Clinical Chemistry (Baltimore, Md.),* 37 (5), 621-624.

Shikata, K., and Makino, H., 2013. Microinflammation in the pathogenesis of diabetic nephropathy. *Journal of Diabetes Investigation,* 4 (2), 142–149.

Shimakami, T., Yamane, D., Jangra, R.K., Kempf, B.J., Spaniel, C., Barton, D.J. and Lemon, S.M., 2012. Stabilization of hepatitis C virus RNA by an Ago2–miR-122 complex. *Proceedings of the National Academy of Sciences*, 109 (3), 941–946.

Smith, P.K., Krohn, R.I., Hermanson, G.T., Mallia, A.K., Gartner, F.H., Provenzano, M.D., Fujimoto, E.K., Goeke, N.M., Olson, B.J. and Klenk, D.C., 1985. Measurement of protein using bicinchoninic acid. Analytical Biochemistry, 150 (1), 76-85.

Sokolova, V., Fiorino, A., Zoni, E., Crippa, E., Reid, J.F., Gariboldi, M. and Pierotti, M.A., 2015. The Effects of miR-20a on p21: Two Mechanisms Blocking Growth Arrest in TGF-β-Responsive Colon Carcinoma. *Journal of Cellular Physiology,* 230 (12), 3105–3114.

Solé, C., Moliné, T., Vidal, M., Ordi-Ros, J. and Cortés-Hernández, J., 2019. An Exosomal Urinary miRNA Signature for Early Diagnosis of Renal Fibrosis in Lupus Nephritis. *Cells (Basel, Switzerland),* 8 (8), 773.

Spahr, C.S., Davis, M.T., McGinley, M.D., Robinson, J.H., Bures, E.J., Beierle, J., Mort, J., Courchesne, P.L., Chen, K., Wahl, R.C., Yu, W., Luethy, R. and Patterson, S.D., 2001. Towards defining the urinary proteome using liquid chromatography-tandem mass spectrometry. I. Profiling an unfractionated tryptic digest. *Proteomics (Weinheim),* 1 (1), 93–107.

Starkey, R.H., Cohen, S. and Orth, D.N., 1975. Epidermal growth factor: identification of a new hormone in human urine. *Science,* 189 (4205), 800-802.

Stenmark, H., and Raiborg, C., 2009. The ESCRT machinery in endosomal sorting of ubiquitylated membrane proteins. *Nature (London),* 458 (7237), 445-452.

Stevens, P.E., Ahmed, S.B., Carrero, J.J., Foster, B., Francis, A., Hall, R.K., Herrington, W.G., Hill, G., Inker, L.A., Kazancıoğlu, R., Lamb, E., Lin, P., Madero, M., McIntyre, N., Morrow, K., Roberts, G., Sabanayagam, D., Schaeffner, E., Shlipak, M., Shroff, R., Tangri, N., Thanachayanont, T., Ulasi, I., Wong, G., Yang, C., Zhang, L. and Levin, A., 2024. KDIGO 2024 Clinical Practice Guideline for the Evaluation and Management of Chronic Kidney Disease. *Kidney International,* 105 (4), S117-S314.

Stevens, L.A., Shastri, S. and Levey, A.S., 2010, CHAPTER 3 - Assessment of Renal Function. *In:* J. Floege, R.J. Johnson and J. Feehally, eds., *Comprehensive Clinical Nephrology (Fourth Edition).* Philadelphia: Mosby, 2010, pp. 31-38.

Sticht, C., De La Torre, C., Parveen, A. and Gretz, N., 2018. miRWalk: An online resource for prediction of microRNA binding sites. PloS One, 13 (10), e0206239.

Stokman, M.F., Bijnsdorp, I.V., Schelfhorst, T., Pham, T.V., Piersma, S.R., Knol, J.C., Giles, R.H., Bongers, E.M.H.F., Knoers, N.V.A.M., Lilien, M.R., Jiménez, C.R. and Renkema, K.Y., 2019. Changes in the urinary extracellular vesicle proteome are associated with nephronophthisis-related ciliopathies. *Journal of Proteomics,* 192, 27–36.

Stoorvogel, W., Strous, G.J., Geuze, H.J., Oorschot, V. and Schwartzt, A.L., 1991. Late endosomes derive from early endosomes by maturation. Cell, 65 (3), 417-427.

Street, J.M., Birkhoff, W., Menzies, R.I., Webb, D.J., Bailey, M.A. and Dear, J.W., 2011. Exosomal transmission of functional aquaporin 2 in kidney cortical collecting duct cells. *The Journal of Physiology,* 589 (24), 6119-6127.

Stuffers, S., Sem Wegner, C., Stenmark, H. and Brech, A., 2009. Multivesicular Endosome Biogenesis in the Absence of ESCRTs. *Traffic (Copenhagen, Denmark),* 10 (7), 925-937.

Su, J., Li, S.J., Chen, Z.H., Zeng, C.H., Zhou, H., Li, L.S., Liu, Z.H., 2010. Evaluation of podocyte lesion in patients with diabetic nephropathy: Wilms' tumor-1 protein used as a podocyte marker. Diabetes Research and Clinical Practice, 87 (2), 167-175.

Subedi, P., Schneider, M., Philipp, J., Azimzadeh, O., Metzger, F., Moertl, S., Atkinson, M.J. and Tapio, S., 2019. Comparison of methods to isolate proteins from extracellular vesicles for mass spectrometry-based proteomic analyses. *Analytical Biochemistry,* 584, 113390.

Sun, A., Deng, J., Guan, G., Chen, S., Liu, Y., Cheng, J., Li, Z., Zhuang, X., Sun, F. and Deng, H., 2012. Dipeptidyl peptidase-IV is a potential molecular biomarker in diabetic kidney disease. *Diabetes & Vascular Disease Research,* 9 (4), 301–308.

Sun, I.O., and Lerman, L.O., 2019. Urinary microRNA in kidney disease: utility and roles. *American Journal of Physiology. Renal Physiology,* 316 (5), F785–F793.

Suzuki, H., Kiryluk, K., Novak, J., Moldoveanu, Z., Herr, A.B., Renfrow, M.B., Wyatt, R.J., Scolari, F., Mestecky, J., Gharavi, A.G. and Julian, B.A., 2011. The pathophysiology of IgA nephropathy. *Journal of the American Society of Nephrology: JASN*, 22 (10), 1795-1803.

Svenningsen, P., Sabaratnam, R. and Jensen, B.L., 2020. Urinary extracellular vesicles: Origin, role as intercellular messengers and biomarkers; efficient sorting and potential treatment options. *Acta Physiologica,* 228 (1), e13346–n/a.

Svensson, K.J., Christianson, H.C., Wittrup, A., Bourseau-Guilmain, E., Lindqvist, E., Svensson, L.M., Mörgelin, M. and Belting, M., 2013. Exosome Uptake Depends on ERK1/2-Heat Shock Protein 27 Signaling and Lipid Raft-mediated Endocytosis Negatively Regulated by Caveolin-1. *The Journal of Biological Chemistry,* 288 (24), 17713-17724.

Sviridov, D., Drake, S.K. and Hortin, G.L., 2008. Reactivity of Urinary Albumin (Microalbumin) Assays with Fragmented or Modified Albumin. *Clinical Chemistry (Baltimore, Md.),* 54 (1), 61-68.

Szeto, C., Wang, G., Ng, J.K., Kwan, B.C., Mac-Moune Lai, F., Chow, K., Luk, C.C., Lai, K. and Li, P.K., 2019. Urinary miRNA profile for the diagnosis of IgA nephropathy. *BMC Nephrology*, 20 (1), 77.

Ta, C.M., Vien, T.N., Ng, L.C.T. and DeCaen, P.G., 2020. Structure and function of polycystin channels in primary cilia. *Cellular Signalling*, 72, 109626.

Takei, K., Mundigl, O., Daniell, L. and De Camilli, P., 1996. The Synaptic Vesicle Cycle: A Single Vesicle Budding Step Involving Clathrin and Dynamin. *The Journal of Cell Biology,* 133 (6), 1237-1250.

Takizawa, K., Ueda, K., Sekiguchi, M., Nakano, E., Nishimura, T., Kajiho, Y., Kanda, S., Miura, K., Hattori, M., Hashimoto, J., Hamasaki, Y., Hisano, M., Omori, T., Okamoto, T., Kitayama, H., Fujita, N., Kuramochi, H., Ichiki, T., Oka, A. and Harita, Y., 2022. Urinary extracellular vesicles signature for diagnosis of kidney disease. *iScience,* 25 (11), 105416.

Tam, S., de Borja, R., Tsao, M. and McPherson, J.D., 2014. Robust global microRNA expression profiling using next-generation sequencing technologies. *Laboratory Investigation,* 94 (3), 350–358.

Tanaka, S., Ninomiya, T., Taniguchi, M., Tokumoto, M., Masutani, K., Ooboshi, H., Kitazono, T. and Tsuruya, K., 2017. Impact of blood urea nitrogen to creatinine ratio on mortality and morbidity in hemodialysis patients: The Q-Cohort Study. *Scientific Reports,* 7 (1), 14901-9.

Tang, L., Yang, Q., Ma, R., Zhou, P., Peng, C., Xie, C., Liang, Q., Wu, T., Gao, W., Yu, H., Deng, G., Dai, Z., Mao, N. and Xiao, X., 2024. Association between lactate dehydrogenase and the risk of diabetic kidney disease in patients with type 2 diabetes. *Frontiers in Endocrinology (Lausanne),* 15, 1369968.

Tang, O., Chen, X., Shen, S., Hahn, M. and Pollock, C.A., 2013. MiRNA-200b represses transforming growth factor-β1-induced EMT and fibronectin expression in kidney proximal tubular cells. *American Journal of Physiology-Renal Physiology,* 304 (10), 1266.

Tang, W.W., Ulich, T.R., Lacey, D.L., Hill, D.C., Qi, M., Kaufman, S.A., Van, G.Y., Tarpley, J.E. and Yee, J.S., 1996. Platelet-derived growth factor-BB induces renal tubulointerstitial myofibroblast formation and tubulointerstitial fibrosis. *The American Journal of Pathology,* 148 (4), 1169-1180.

Tangtanatakul, P., Klinchanhom, S., Sodsai, P., Sutichet, T., Promjeen, C., Avihingsanon, Y. and Hirankarn, N., 2019. Down-regulation of let-7a and miR-21 in urine exosomes from lupus nephritis patients during disease flare. *Asian Pacific Journal of Allergy and Immunology,* 37 (4), 189–197.

Tao, Y., Han, J., Liu, W., An, L., Hu, W., Wang, N. and Yu, Y., 2021. MUC1 Promotes Mesangial Cell Proliferation and Kidney Fibrosis in Diabetic Nephropathy Through Activating STAT and β-Catenin Signal Pathway. *DNA and Cell Biology,* 40 (10), 1308–1316.

Tataruch-Weinert, D., Musante, L., Kretz, O. and Holthofer, H., 2016. Urinary extracellular vesicles for RNA extraction: optimization of a protocol devoid of prokaryote contamination. *Journal of Extracellular Vesicles,* 5 (1), 30281–n/a.

Taylor, A., Grapentine, S., Ichhpuniani, J. and Bakovic, M., 2021. Choline transporter-like proteins 1 and 2 are newly identified plasma membrane and mitochondrial ethanolamine transporters. *Journal of Biological Chemistry/˜The œJournal of Biological Chemistry,* 296, 100604.

Thatcher, S.A., 2015. DNA/RNA Preparation for Molecular Detection. *Clinical Chemistry,* 61 (1), 89-99.

Théry, C., Witwer, K.W., Aikawa, E., Andriantsitohaina, R., Baharvand, H., Bauer, N.N., Baxter, A.A., Beckham, C., Bielska, E., Boireau, W., Bongiovanni, A., Brisson, A., Broekman, M.L., Bryl-Górecka, P., Buch, S., Bussolati, B., Caruso, S., Clayton, A., Cocucci, E., de Candia, P., Demaret, T., Dourado, M.R., Falcón-Pérez, J.M., Försönits, A., Frelet-Barrand, A., Fuhrmann, G., Gabrielsson, S., Gámez-Valero, A., Gaudin, R., Handberg, A., Hegyesi, H., Hendrix, A., Hill, A.F., Inal, J.M., Ivanova, A., Jackson, H.K., Jayachandran, M., Jiang, L., Kalluri, R., Kaur, S., Kierulf, P., Kim, K.P., Krasemann, S., Kurochkin, I.V., Langevin, S.M., Lázaro-Ibáñez, E., Lee, Y.X.F., Libregts, S.F., Linē, A., Linnemannstöns, K., Lombard, C.A., Lukomska, B., Marcilla, A., Mathivanan, S., McVey, M.J., Mertens, I., Morhayim, J., Mullier, F., Nawaz, M., Nimrichter, L., Noren Hooten, N., Olivier, M., Ortiz, L.A., Ostrowski, M., Pegtel, D.M., Perut, F., Polakovicova, I., Pulliam, L., Regev-Rudzki, N., Rouschop, K.M., Rughetti, A., Saá, P., Saul, M.J., Schøyen, T.H., Shahaj, E., Sharma, S., Shekari, F., Siljander, P.R., Skowronek, A., Soares, R.P., Stoorvogel, W., Stott, S.L., Tixeira, R., Toh, W.S., Tomasini, R., van Herwijnen, M.J., van Niel, G., van Wijnen, A.J., Vasconcelos, M.H., Veit, T.D., Viñas, J.L., Visnovitz, T., Wehman, A.M., Weiss, D.J., Wheelock, A.M., Xagorari, A., Xander, P., Zhang, J., Zheutlin, A.R. and Zickler, A.M., 2018. Minimal information for studies of extracellular vesicles 2018 (MISEV2018): a position statement of the International Society for Extracellular Vesicles and update of the MISEV2014 guidelines. *Journal of Extracellular Vesicles,* 7 (1), 1535750-n/a.

Thomas, S.S., Zhang, L. and Mitch, W.E., 2015. Molecular mechanisms of insulin resistance in chronic kidney disease. *Kidney International,* 88 (6), 1233–1239.

Tian, J., Li, X., Jiang, Y., Gao, F., Ju, B., Chen, J., Zhu, W., He, L., Meng, L. and Lu, S., 2022. SLC7A5 expression is up-regulated in peripheral blood T and B lymphocytes of systemic lupus erythematosus patients, associating with renal damage. *Clinical Immunology (Orlando, Fla.),* 237, 108987.

Tian, T., Zhu, Y., Hu, F., Wang, Y., Huang, N. and Xiao, Z., 2013. Dynamics of exosome internalization and trafficking. *Journal of Cellular Physiology,* 228 (7), 1487-1495.

Tian, T., Zhu, Y., Zhou, Y., Liang, G., Wang, Y., Hu, F. and Xiao, Z., 2014. Exosome Uptake through Clathrin-mediated Endocytosis and Macropinocytosis and Mediating miR-21 Delivery. *The Journal of Biological Chemistry,* 289 (32), 22258-22267.

Tian, Y., Gong, M., Hu, Y., Liu, H., Zhang, W., Zhang, M., Hu, X., Aubert, D., Zhu, S., Wu, L. and Yan, X., 2020. Quality and efficiency assessment of six extracellular vesicle isolation methods by nano-flow cytometry. *Journal of Extracellular Vesicles*, 9 (1), 1-n/a.

Tobias, G.J., McLaughlin, R.F. and Hopper, J., 1962. Endogenous Creatinine Clearance. *The New England Journal of Medicine,* 266 (7), 317-323.

Tokar, T., Pastrello, C., Rossos, A.E.M., Abovsky, M., Hauschild, A., Tsay, M., Lu, R. and Jurisica, I., 2018. mirDIP 4.1-integrative database of human microRNA target predictions. Nucleic Acids Research, 46 (D1), D360-D370.

Tone, A., Shikata, K., Matsuda, M., Usui, H., Okada, S., Ogawa, D., Wada, J. and Makino, H., 2005. Clinical features of non-diabetic renal diseases in patients with type 2 diabetes. *Diabetes Research and Clinical Practice,* 69 (3), 237-242.

Torres, V.E., Sweeney, W.E., Wang, X., Qian, Q., Harris, P.C., Frost, P. and Avner, E.D., 2003. EGF receptor tyrosine kinase inhibition attenuates the development of PKD in Han:SPRD rats. *Kidney International,* 64 (5), 1573-1579.

Trajkovic, K., Hsu, C., Chiantia, S., Rajendran, L., Wenzel, D., Wieland, F., Schwille, P., Brügger, B. and Simons, M., 2008. Ceramide Triggers Budding of Exosome Vesicles into Multivesicular Endosomes. *Science,* 319 (5867), 1244-1247.

Trams, E.G., Lauter, C.J., Norman Salem, J. and Heine, U., 1981. Exfoliation of membrane ecto-enzymes in the form of micro-vesicles. *Biochimica Et Biophysica Acta,* 645 (1), 63-70.

Trott, J.F., Hwang, V.J., Ishimaru, T., Chmiel, K.J., Zhou, J.X., Shim, K., Stewart, B.J., Mahjoub, M.R., Jen, K., Barupal, D.K., Li, X. and Weiss, R.H., 2018. Arginine reprogramming in ADPKD results in arginine-dependent cystogenesis. *American Journal of Physiology. Renal Physiology,* 315 (6), F1855–F1868.

Tryggvason, K., and Patrakka, J., 2006. Thin Basement Membrane Nephropathy. *Journal of the American Society of Nephrology*, 17 (3), 813-822.

Tryggvason, S.H., Guo, J., Nukui, M., Norlin, J., Haraldsson, B., Jörnvall, H., Tryggvason, K. and He, L., 2013. A meta-analysis of expression signatures in glomerular disease. *Kidney International,* 84 (3), 591–599.

Tsalamandris, C., Allen, T.J., Gilbert, R.E., Sinha, A., Panagiotopoulos, S., Cooper, M.E. and Jerums, G., 1994. Progressive decline in renal function in diabetic patients with and without albuminuria. *Diabetes (New York, N.Y.),* 43 (5), 649-655.

Turco, A.E., Lam, W., Rule, A.D., Denic, A., Lieske, J.C., Miller, V.M., Larson, J.J., Kremers, W.K. and Jayachandran, M., 2016. Specific renal parenchymal-derived urinary extracellular vesicles identify age-associated structural changes in living donor kidneys. *Journal of Extracellular Vesicles,* 5 (1), 29642-n/a.

Uil, M., Hau, C.M., Ahdi, M., Mills, J.D., Kers, J., Saleem, M.A., Florquin, S., Gerdes, V.E.A., Nieuwland, R. and Roelofs, J.J.T.H., 2021. Cellular origin and microRNA profiles of circulating extracellular vesicles in different stages of diabetic nephropathy. *Clinical Kidney Journal,* 14 (1), 358–365.

Vaidya, V., Niewczas, M., Ficociello, L., Johnson, A., Collings, F., Warram, J., Krolewski, A. and Bonventre, J., 2011. Regression of microalbuminuria in type 1 diabetes is associated with lower levels of urinary tubular injury biomarkers, kidney injury molecule-1, and N-acetyl-[beta]-D-glucosaminidase. *Kidney International,* 79 (4), 464.

Vaisar, T., Durbin-Johnson, B., Whitlock, K., Babenko, I., Mehrotra, R., Rocke, D.M. and Afkarian, M., 2019. Erratum. Urine Complement Proteins and the Risk of Kidney Disease Progression and Mortality in Type 2 Diabetes. Diabetes Care 2018;41:2361–2369. *Diabetes Care,* 42 (6), 1155.

Van, J.A.D., Scholey, J.W. and Konvalinka, A., 2017. Insights into Diabetic Kidney Disease Using Urinary Proteomics and Bioinformatics. *Journal of the American Society of Nephrology,* 28 (4), 1050–1061.

van Heugten, M.H., Hoorn, E.J. and Fenton, R.A., 2022. Urinary extracellular vesicles: does cargo reflect tissue? *Current Opinion in Nephrology and Hypertension,* 31 (5), 464–470.

van Niel, G., Charrin, S., Simoes, S., Romao, M., Rochin, L., Saftig, P., Marks, M., Rubinstein, E. and Raposo, G., 2011. The Tetraspanin CD63 Regulates ESCRT-Independent and -Dependent Endosomal Sorting during Melanogenesis. *Developmental Cell,* 21 (4), 708-721.

van Acker, B.A.C., Koopman, M.G., Arisz, L., Koomen, G.C.M. and de Waart, D.R., 1992. Creatinine clearance during cimetidine administration for measurement of glomerular filtration rate. *The Lancet,* 340 (8831), 1326-1329.

van den Berg, A., Mols, J. and Han, J., 2008. RISC-target interaction: Cleavage and translational suppression. *Biochimica Et Biophysica Acta,* 1779 (11), 668–677.

van Niel, G., D'Angelo, G. and Raposo, G., 2018. Shedding light on the cell biology of extracellular vesicles. *Nature Reviews. Molecular Cell Biology,* 19 (4), 213-228.

van Reis, R., and Saksena, S., 1997. Optimization diagram for membrane separations. *Journal of Membrane Science*, 129 (1), 19-29.

van Reis, R., and Zydney, A., 2001. *Membrane separations in biotechnology*. England: Elsevier Ltd.

van Roeyen, C.R.C., Martin, I.V., Drescher, A., Schuett, K.A., Hermert, D., Raffetseder, U., Otten, S., Buhl, E.M., Braun, G.S., Kuppe, C., Liehn, E., Boor, P., Weiskirchen, R., Eriksson, U., Gross, O., Eitner, F., Floege, J. and Ostendorf, T., 2019. Identification of platelet-derived growth factor C as a mediator of both renal fibrosis and hypertension. *Kidney International,* 95 (5), 1103–1119.

van Timmeren, M.M., van den Heuvel, M.C., Bailly, V., Bakker, S., van Goor, H. and Stegeman, C.A., 2007. Tubular kidney injury molecule-1 (KIM-1) in human renal disease. *The Journal of Pathology,* 212 (2), 209–217.

van Wijk, S.W., Su, W., Wijdeveld, L.F.J.M., Ramos, K.S. and Brundel, B.J.J.M., 2022. Cytoskeletal Protein Variants Driving Atrial Fibrillation: Potential Mechanisms of Action. Cells (Basel, Switzerland), 11 (3), 416.

Vautrot, V., and Behm-Ansmant, I., 2020, Enhanced Probe-Based RT-qPCR Quantification of MicroRNAs Using Poly(A) Tailing and 5' Adaptor Ligation. *In:* Enhanced Probe-Based RT-qPCR Quantification of MicroRNAs Using Poly(A) Tailing and 5' Adaptor Ligation. *Methods in Molecular Biology.* New York, NY: Springer New York, 2020, pp. 39–54.

Vegas, A.J., and Anderson, D.G., 2012, 9.24 - High-Throughput Approaches. *In:* 9.24 - High-Throughput Approaches. *Polymer Science: A Comprehensive Reference, 10 Volume Set.* Elsevier B.V, 2012, pp. 457–484.

Veldman-Jones, M.H., Brant, R., Rooney, C., Geh, C., Emery, H., Harbron, C.G., Wappett, M., Sharpe, A., Dymond, M., Barrett, J.C., Harrington, E.A. and Marshall, G., 2015. Evaluating Robustness and Sensitivity of the NanoString Technologies nCounter Platform to Enable Multiplexed Gene Expression Analysis of Clinical Samples. *Cancer Research,* 75 (13), 2587–2593.

Velez, J.C.Q., Arif, E., Rodgers, J., Hicks, M.P., Arthur, J.M., Nihalani, D., Bruner, E.T., Budisavljevic, M.N., Atkinson, C., Fitzgibbon, W.R. and Janech, M.G., 2017. Deficiency of the Angiotensinase Aminopeptidase A Increases Susceptibility to Glomerular Injury. *Journal of the American Society of Nephrology,* 28 (7), 2119–2132.

Verderio, E.A.M., Furini, G., Burhan, I.W., and Johnson, T.S., 2016. Transglutaminases: Expression in Kidney and Relation to Kidney Fibrosis. In: *Transglutaminases: Multiple Functional Modifiers and Targets for New Drug Discovery*. Springer, 2016, 229-263.

Verkleij, A.J., Zwaal, R.F.A., Roelofsen, B., Comfurius, P., Kastelijn, D. and van Deenen, L.L.M., 1973. The asymmetric distribution of phospholipids in the human red cell membrane. A combined study using phospholipases and freeze-etch electron microscopy. *Biochimica Et Biophysica Acta,* 323 (2), 178-193.

Viau, A., El Karoui, K., Laouari, D., Burtin, M., Nguyen, C., Mori, K., Pillebout, E., Berger, T., Mak, T.W., Knebelmann, B., Friedlander, G., Barasch, J. and Terzi, F., 2010. Lipocalin 2 is essential for chronic kidney disease progression in mice and humans. *The Journal of Clinical Investigation,* 120 (11), 4065–4076.

Vilander, L.M., Kaunisto, M.A., Vaara, S.T. and Pettilä, V., 2017. Genetic variants in SERPINA4 and SERPINA5, but not BCL2 and SIK3 are associated with acute kidney injury in critically ill patients with septic shock. *Critical Care (London, England),* 21 (1), 47.

Vivekanandan-Giri, A., Slocum, J.L., Buller, C.L., Basrur, V., Ju, W., Pop-Busui, R., Lubman, D.M., Kretzler, M. and Pennathur, S., 2011. Urine Glycoprotein Profile Reveals Novel Markers for Chronic Kidney Disease. *International Journal of Proteomics,* 2011, 214715–18.

von Mensdorff-Pouilly, S., Snijdewint, F.G., Verstraeten, A.A., Verheijen, R.H. and Kenemans, P., 2000. Human MUC1 Mucin: A Multifaceted Glycoprotein. *The International Journal of Biological Markers,* 15 (4), 343–356.

Vos, T., Lim, S.S., Abbafati, C., Abbas, K.M., Abbasi, M., Abbasifard, M., Abbasi-Kangevari, M., Abbastabar, H., Abd-Allah, F., Abdelalim, A., …, 2020. Global burden of 369 diseases and injuries in 204 countries and territories, 1990–2019: a systematic analysis for the Global Burden of Disease Study 2019. *The Lancet,* 396 (10258), 1204–1222.

Waldek, S., Patel, M.R., Banikazemi, M., Lemay, R. and Lee, P., 2009. Life expectancy and cause of death in males and females with Fabry disease: findings from the Fabry Registry. *Genetics in Medicine*, 11 (11), 790-796.

Wang, C., Chen, Q., Li, S., Li, S., Zhao, Z., Gao, H., Wang, X., Li, B., Zhang, W., Yuan, Y., Ming, L., He, H., Tao, B. and Zhong, J., 2017. Dual inhibition of PCDH9 expression by miR-215-5p up-regulation in gliomas. *Oncotarget,* 8 (6), 10287–10297.

Wang, C., Liu, J., Zhang, X., Chen, Q., Bai, X., Hong, X., Zhou, L. and Liu, Y., 2022. Role of miRNA-671-5p in Mediating Wnt/β-Catenin-Triggered Podocyte Injury. *Frontiers in Pharmacology,* 12, 784489.

Wang, J.J., Zhang, S.X., Kangmo Lu, Ying Chen, Mott, R., Sato, S. and Ma, J., 2005. Decreased Expression of Pigment Epithelium-Derived Factor Is Involved in the Pathogenesis of Diabetic Nephropathy. *Diabetes (New York, N.Y.),* 54 (1), 243–250.

Wang, L., Rothberg, K.G. and Richard G. W. Anderson, 1993. Mis-Assembly of Clathrin Lattices on Endosomes Reveals a Regulatory Switch for Coated Pit Formation. *The Journal of Cell Biology,* 123 (5), 1107-1117.

Wang, Q., Zhu, Y., Dong, Q., Zhang, L. and Zhang, W., 2023. A Novel Circ_Arf3/miR-452-5p/Mbnl1 Axis Regulates Proliferation and Expression of Fibrosis-Related Proteins of Mouse Mesangial Cells Under High Glucose. *Diabetes, Metabolic Syndrome and Obesity,* 16, 2105–2116.

Wang, S., Pan, Y., Zhang, R., Xu, T., Wu, W., Wang, C., Huang, H., Calin, C.A., Yang, H. and Claret, F.X., 2016. Hsa-miR-24-3p increases nasopharyngeal carcinoma radiosensitivity by targeting both the 3'UTR and 5'UTR of Jab1/CSN5. *Oncogene,* 35 (47), 6096–6108.

Wang, W., Huang, X.R., Li, A.G., Liu, F., Li, J., Truong, L.D., Wang, X.J. and Lan, H.Y., 2005. Signaling mechanism of TGF-β1 in prevention of renal inflammation : Role of Smad7. *Journal of the American Society of Nephrology,* 16 (5), 1371-1383.

Wang, Z., Liao, Y., Wang, L., Lin, Y., Ye, Z., Zeng, X., Liu, X., Wei, F. and Yang, N., 2020. Small RNA deep sequencing reveals novel miRNAs in peripheral blood mononuclear cells from patients with IgA nephropathy. *Molecular Medicine Reports*, 22 (4), 3378-3386.

Webber, J.P., Spary, L.K., Sanders, A.J., Chowdhury, R., Jiang, W.G., Steadman, R., Wymant, J., Jones, A.T., Kynaston, H., Mason, M.D., Tabi, Z. and Clayton, A., 2015. Differentiation of tumour-promoting stromal myofibroblasts by cancer exosomes. *Oncogene,* 34 (3), 290–302.

Webber, J., Steadman, R., Mason, M.D., Tabi, Z. and Clayton, A., 2010. Cancer Exosomes Trigger Fibroblast to Myofibroblast Differentiation. *Cancer Research,* 70 (23), 9621–9630.

Webster, A.C., Nagler, E.V., Morton, R.L., and Masson, P., 2017. Chronic kidney disease. *Lancet*, 389(10075), 1238-52.

Wei, D., Zhan, W., Gao, Y., Huang, L., Gong, R., Wang, W., Zhang, R., Wu, Y., Gao, S. and Kang, T., 2021. RAB31 marks and controls an ESCRT-independent exosome pathway. *Cell Research,* 31 (2), 157–177.

Weiler, J., Hunziker, J. and Hall, J., 2006. Anti-miRNA oligonucleotides (AMOs): ammunition to target miRNAs implicated in human disease? *Gene Therapy,* 13 (6), 496–502.

Welsh, J.A., Goberdhan, D.C.I., O'Driscoll, L., Buzas, E.I., Blenkiron, C., Bussolati, B., Cai, H., Di Vizio, D., Driedonks, T.A.P., Erdbrügger, U., Falcon-Perez, J.M., Fu, Q.L., Hill, A.F., Lenassi, M., Lim, S.K., Mahoney, M.G., Mohanty, S., Möller, A., Nieuwland, R., Ochiya, T., Sahoo, S., Torrecilhas, A.C., Zheng, L., Zijlstra, A., Abuelreich, S., Bagabas, R., Bergese, P., Bridges, E.M., Brucale, M., Burger, D., Carney, R.P., Cocucci, E., Crescitelli, R., Hanser, E., Harris, A.L., Haughey, N.J., Hendrix, A., Ivanov, A.R., Jovanovic-Talisman, T., Kruh-Garcia, N.A., Ku'ulei-Lyn, F.V., Kyburz, D., Lässer, C., Lennon, K.M., Lötvall, J., Maddox, A.L., Martens-Uzunova, E.S., Mizenko, R.R., Newman, L.A., Ridolfi, A., Rohde, E., Rojalin, T., Rowland, A., Saftics, A., Sandau, U.S., Saugstad, J.A., Shekari, F., Swift, S., Ter-Ovanesyan, D., Tosar, J.P., Useckaite, Z., Valle, F., Varga, Z., van der Pol, E., van Herwijnen, M.J.C., Wauben, M.H.M., Wehman, A.M., Williams, S., Zendrini, A., Zimmerman, A.J., MISEV Consortium, Théry, C., and Witwer, W.K., 2024. Minimal information for studies of extracellular vesicles (MISEV2023): From basic to advanced approaches. *Journal of Extracellular Vesicles,* 13 (2), e12404-n/a.

Wesson, D.E., Buysse, J.M. and Bushinsky, D.A., 2020. Mechanisms of Metabolic Acidosis–Induced Kidney Injury in Chronic Kidney Disease. *Journal of the American Society of Nephrology,* 31 (3), 469–482.

White, I.J., Bailey, L.M., Aghakhani, M.R., Moss, S.E. and Futter, C.E., 2006. EGF stimulates annexin 1-dependent inward vesiculation in a multivesicular endosome subpopulation. *The EMBO Journal,* 25 (1), 1-12.

Whittier, W.L., and Korbet, S.M., 2004. Timing of Complications in Percutaneous Renal Biopsy. *Journal of the American Society of Nephrology,* 15 (1), 142-147.

Wiggins, R.C., Glatfelter, A., Kshirsagar, B. and Brukman, J., 1986. Procoagulant activity in normal human urine associated with subcellular particles. *Kidney International,* 29 (2), 591-597.

Williams, M.J., Sugatani, T., Agapova, O.A., Fang, Y., Gaut, J.P., Faugere, M., Malluche, H.H. and Hruska, K.A., 2018. The activin receptor is stimulated in the skeleton, vasculature, heart, and kidney during chronic kidney disease. *Kidney International,* 93 (1), 147–158.

Williamson, V., Kim, A., Xie, B., McMichael, G.O., Gao, Y. and Vladimirov, V., 2013. Detecting miRNAs in deep-sequencing data: a software performance comparison and evaluation. *Briefings in Bioinformatics,* 14 (1), 36–45.

Wolf, P., 1967. The Nature and Significance of Platelet Products in Human Plasma. *British Journal of Haematology,* 13 (3), 269-288.

Wu, C., Lv, C., Chen, F., Ma, X., Shao, Y. and Wang, Q., 2015. The function of miR-199a-5p/Klotho regulating TLR4/NF-κB p65/NGAL pathways in rat mesangial cells cultured with high glucose and the mechanism. *Molecular and Cellular Endocrinology,* 417, 84–93.

Wu, Q., Poulsen, S.B., Murali, S.K., Grimm, P.R., Su, X., Delpire, E., Welling, P.A., Ellison, D.H. and Fenton, R.A., 2021. Large-Scale Proteomic Assessment of Urinary Extracellular Vesicles

Highlights Their Reliability in Reflecting Protein Changes in the Kidney. *Journal of the American Society of Nephrology,* 32 (9), 2195–2209.

Wu, X., and Levine, A.J., 1994. p53 and E2F-1 cooperate to mediate apoptosis. *Proceedings of the National Academy of Sciences,* 91 (9), 3602–3606.

Xi, L., 2020. Pigment Epithelium-Derived Factor as a Possible Treatment Agent for Choroidal Neovascularization. *Oxidative Medicine and Cellular Longevity,* 2020 (2020), 1–11.

Xiao, L., Zhou, D., Tan, R.J., Fu, H., Zhou, L., Hou, F.F. and Liu, Y., 2016. Sustained Activation of Wnt/β-Catenin Signaling Drives AKI to CKD Progression. *Journal of the American Society of Nephrology,* 27 (6), 1727-1740.

Xiao, W., E, J., Bao, L., Fan, Y., Jin, Y., Wang, A., Bauman, D., Li, Z., Zheng, Y., Liu, R., Lee, K. and He, J.C., 2020. Tubular HIPK2 is a key contributor to renal fibrosis. *JCI Insight,* 5 (17).

Xiao, Z., Zhang, J., Peng, X., Dong, Y., Jia, L., Li, H. and Du, J., 2014. The Notch γ-secretase inhibitor ameliorates kidney fibrosis via inhibition of TGF-β/Smad2/3 signaling pathway activation. *The International Journal of Biochemistry & Cell Biology,* 55, 65-71.

Xie, Y., Jia, Y., Cuihua, X., Hu, F., Xue, M. and Xue, Y., 2017. Urinary exosomal microRNA profiling in incipient type 2 diabetic kidney disease. *Journal of Diabetes Research,* 2017 (1), 6978984.

Xie, Z., Tang, J., Chen, Z., Wei, L., Chen, J. and Liu, Q., 2023. Human bone marrow mesenchymal stem cell-derived extracellular vesicles reduce inflammation and pyroptosis in acute kidney injury via miR-223-3p/HDAC2/SNRK. *Inflammation Research,* 72 (3), 553–576.

Xiong, M., Jiang, L., Zhou, Y., Qiu, W., Fang, L., Tan, R., Wen, P. and Yang, J., 2012. The miR-200 family regulates TGF-β1-induced renal tubular epithelial to mesenchymal transition through Smad pathway by targeting ZEB1 and ZEB2 expression. *American Journal of Physiology-Renal Physiology,* 302 (3), 369.

Xu, H., Sun, F., Li, X. and Sun, L., 2018. Down-regulation of miR-23a inhibits high glucose-induced EMT and renal fibrogenesis by up-regulation of SnoN. *Human Cell,* 31 (1), 22–32.

Xu, Z., Li, W., Han, J., Zou, C., Huang, W., Yu, W., Shan, X., Lum, H., Li, X. and Liang, G., 2017. Angiotensin II induces kidney inflammatory injury and fibrosis through binding to myeloid differentiation protein-2 (MD2). *Scientific Reports,* 7 (1), 44911.

Xue, M., Li, Y., Hu, F., Jia, Y., Zheng, Z., Wang, L. and Xue, Y., 2018. High glucose up-regulates microRNA-34a-5p to aggravate fibrosis by targeting SIRT1 in HK-2 cells. *Biochemical and Biophysical Research Communications,* 498 (1), 38–44.

Yamagishi, S., Matsui, T., Nakamura, K., Takeuchi, M. and Imaizumi, T., 2006. Pigment epithelium-derived factor (PEDF) prevents diabetes- or advanced glycation end products (AGE)-elicited retinal leukostasis. *Microvascular Research,* 72 (1), 86–90.

Yang, F., Chung, A.C.K., Huang, X. R. and Lan, h.Y., 2009. Angiotensin II Induces Connective Tissue Growth Factor and Collagen I Expression via Transforming Growth Factor–β–Dependent and –Independent Smad Pathways. *Hypertension,* 54 (4), 877-884.

Yang, J., Antin, P., Berx, G., Blanpain, C., Brabletz, T., Bronner, M., Campbell, K., Cano, A., Casanova, J., Christofori, G., Dedhar, S., Derynck, R., Ford, H.L., Fuxe, J., García de Herreros, A., Goodall, G.J., Hadjantonakis, A., Huang, R.Y.J., Kalcheim, C., Kalluri, R., Kang, Y., Khew-Goodall, Y., Levine, H., Liu, J., Longmore, G.D., Mani, S.A., Massagué, J., Mayor, R., McClay, D., Mostov, K.E., Newgreen, D.F., Nieto, M.A., Puisieux, A., Runyan, R., Savagner, P., Stanger, B., Stemmler, M.P., Takahashi, Y., Takeichi, M., Theveneau, E., Thiery, J.P., Thompson, E.W., Weinberg, R.A., Williams, E.D., Xing, J., Zhou, B.P. and Sheng, G., 2020. Guidelines and definitions for research on epithelial–mesenchymal transition. *Nature Reviews Molecular Cell Biology,* 21 (6), 341–352.

Yang, Y., Hong, S., Wang, Q., Wang, S. and Xun, Y., 2023. Exosome-mediated crosstalk between epithelial cells amplifies the cell injury cascade in CaOx stone formation. *Journal of Biological Engineering,* 17 (1), 16.

Yang, Y., Wang, Q., Xun, Y., Li, C. and Wang, S., 2022. The Preliminary Exploration of What Role miRNAs Derived From Urinary Exosomes Play in Kidney Stone Formation. *Urology (Ridgewood, N.J.),* 166, 104–110.

Ying, Y., Kim, J., Westphal, S.N., Long, K.E. and Padanilam, B.J., 2014. Targeted Deletion of p53 in the Proximal Tubule Prevents Ischemic Renal Injury. *Journal of the American Society of Nephrology,* 25 (12), 2707–2716.

Yinon, J., 1990, Tandem Mass Spectrometry (MS/MS) and Collision Induced Dissociation (CID)—an Introduction. *In: Chemistry and Physics of Energetic Materials.* Springer, 1990, pp. 685-693.

Yu, J., Yu, C., Feng, B., Zhan, X., Luo, N., Yu, X. and Zhou, Q., 2019. Intrarenal microRNA signature related to the fibrosis process in chronic kidney disease: identification and functional validation of key miRNAs. *BMC Nephrology*, 20 (1), 336.

Yuan, Q., Tang, B. and Zhang, C., 2022. Signaling pathways of chronic kidney diseases, implications for therapeutics. *Signal Transduction and Targeted Therapy,* 7 (1), 182.

Zanchi, C., Macconi, D., Trionfini, P., Tomasoni, S., Rottoli, D., Locatelli, M., Rudnicki, M., Vandesompele, J., Mestdagh, P., Remuzzi, G., Benigni, A. and Zoja, C., 2017. MicroRNA-184 is a downstream effector of albuminuria driving renal fibrosis in rats with diabetic nephropathy. *Diabetologia*, 60 (6), 1114-1125.

Zang, J., Maxwell, A.P., Simpson, D.A., and McKay, G.J., 2019. Differential Expression of Urinary Exosomal MicroRNAs miR-21-5p and miR-30b-5p in Individuals with Diabetic Kidney Disease. *Scientific Reports*, 9 (1), 1-10.

Zhang, H., Freitas, D., Kim, H.S., Fabijanic, K., Li, Z., Chen, H., Mark, M.T., Molina, H., Martin, A.B., Bojmar, L., Fang, J., Rampersaud, S., Hoshino, A., Matei, I., Kenific, C.M., Nakajima, M., Mutvei, A.P., Sansone, P., Buehring, W., Wang, H., Jimenez, J.P., Cohen-Gould, L., Paknejad, N.,

Brendel, M., Manova-Todorova, K., Magalhães, A., Ferreira, J.A., Osório, H., Silva, A.M., Massey, A., Cubillos-Ruiz, J., Galletti, G., Giannakakou, P., Cuervo, A.M., Blenis, J., Schwartz, R., Brady, M.S., Peinado, H., Bromberg, J., Matsui, H., Reis, C.A. and Lyden, D., 2018. Identification of distinct nanoparticles and subsets of extracellular vesicles by asymmetric flow field-flow fractionation. *Nature Cell Biology,* 20 (3), 332-343.

Zhang, H., Unal, H., Desnoyer, R., Han, G.W., Patel, N., Katritch, V., Karnik, S.S., Cherezov, V. and Stevens, R.C., 2015. Structural Basis for Ligand Recognition and Functional Selectivity at Angiotensin Receptor. *The Journal of Biological Chemistry,* 290 (49), 29127-29139.

Zhang, K., Zheng, S., Wu, J., He, J., Ouyang, Y., Ao, C., Lang, R., Jiang, Y., Yang, Y., Xiao, H., Li, Y., Li, M., Wang, H., Li, C. and Wu, D., 2024. Human umbilical cord mesenchymal stem cell-derived exosomes ameliorate renal fibrosis in diabetic nephropathy by targeting Hedgehog/SMO signaling. *The FASEB Journal,* 38 (7), e23599–n/a.

Zhang, L., Xue, S., Wu, M. and Dong, D., 2022. Performance of urinary liver-type fatty acid-binding protein in diabetic nephropathy: A meta-analysis. *Frontiers in Medicine,* 9, 914587.

Zhang, M., Jin, K., Gao, L., Zhang, Z., Li, F., Zhou, F. and Zhang, L., 2018. Methods and Technologies for Exosome Isolation and Characterization. *Small Methods,* 2 (9), 1–n/a.

Zhang, Q., Higginbotham, J.N., Jeppesen, D.K., Yang, Y., Li, W., McKinley, E.T., Graves-Deal, R., Ping, J., Britain, C.M., Dorsett, K.A., Hartman, C.L., Ford, D.A., Allen, R.M., Vickers, K.C., Liu, Q., Franklin, J.L., Bellis, S.L. and Coffey, R.J., 2019. Transfer of Functional Cargo in Exomeres. *Cell Reports,* 27 (3), 940-954.e6.

Zhang, T., Li, H., Ma, S., Cao, J., Liao, H., Huang, Q. and Chen, W., 2023a. The newest Oxford Nanopore R10.4.1 full-length 16S rRNA sequencing enables the accurate resolution of species-level microbial community profiling. *Applied and Environmental Microbiology,* 89 (10), 1–e0060523.

Zhang, T., Yang, X., Zhang, M., Zhou, W., Jin, Y., Zhou, H., Zhou, Y., Wang, Q. and Mou, S., 2023b. Effects of receiving renal biopsy on the prognosis of chronic kidney disease patients with impaired renal function. *BMC Nephrology,* 24 (1), 56.

Zhang, W., Yuan, M., Hong, L., Zhou, Q., Chen, W., Yang, S., Yang, Q., Chen, W. and Yu, X., 2016(a). Clinical outcomes of lupus nephritis patients with different proportions of crescents. *Lupus,* 25 (14), 1532-1541.

Zhang, W., Zhou, X., Zhang, H., Yao, Q., Liu, Y. and Dong, Z., 2016(b). Extracellular vesicles in diagnosis and therapy of kidney diseases. *American Journal of Physiology. Renal Physiology,* 311 (5), F844-F851.

Zhang, X., Li, X., Zhou, W., Liu, X., Huang, J., Zhang, Y., Lindholm, B. and Yu, C., 2020. Serum Lysyl Oxidase Is a Potential Diagnostic Biomarker for Kidney Fibrosis. *American Journal of Nephrology,* 51 (11), 907-918.

Zhang, Z., Ravassa, S., Pejchinovski, M., Yang, W., Zürbig, P., López, B., Wei, F., Thijs, L., Jacobs, L., González, A., Voigt, J., Verhamme, P., Kuznetsova, T., Díez, J., Mischak, H. and Staessen, J.A., 2017. A Urinary Fragment of Mucin-1 Subunit α Is a Novel Biomarker Associated With Renal Dysfunction in the General Population. *Kidney International Reports,* 2 (5), 811–820.

Zhao, L., Zhang, Y., Liu, F., Yang, H., Zhong, Y., Wang, Y., Li, S., Su, Q., Tang, L., Bai, L., Ren, H., Zou, Y., Wang, S., Zheng, S., Xu, H., Li, L., Zhang, J., Chai, Z., Cooper, M.E. and Tong, N., 2021. Urinary complement proteins and risk of end-stage renal disease: quantitative urinary proteomics in patients with type 2 diabetes and biopsy-proven diabetic nephropathy. *Journal of Endocrinological Investigation,* 44 (12), 2709–2723.

Zhao, Y., Chen, J., Wei, W., Qi, X., Li, C. and Ren, J., 2018. The dual-inhibitory effect of miR-338-5p on the multidrug resistance and cell growth of hepatocellular carcinoma. *Signal Transduction and Targeted Therapy,* 3 (1), 3–10.

Zhao, Y., Qi, X., Chen, J., Wei, W., Yu, C., Yan, H., Pu, M., Li, Y., Miao, L., Li, C. and Ren, J., 2017. The miR-491-3p/Sp3/ABCB1 axis attenuates multidrug resistance of hepatocellular carcinoma. *Cancer Letters,* 408, 102–111.

Zhao, Y., Shen, A., Guo, F., Song, Y., Jing, N., Ding, X., Pan, M., Zhang, H., Wang, J., Wu, L., Ma, X., Feng, L. and Qin, G., 2020. Urinary Exosomal MiRNA-4534 as a Novel Diagnostic Biomarker for Diabetic Kidney Disease. *Frontiers in Endocrinology,* 11, 590.

Zheng, Z., Guan, M., Jia, Y., Wang, D., Pang, R., Lv, F., Xiao, Z., Wang, L., Zhang, H. and Xue, Y., 2016. The coordinated roles of miR-26a and miR-30c in regulating TGFβ1-induced epithelial-to-mesenchymal transition in diabetic nephropathy. *Scientific Reports,* 6 (1), 37492.

Zhong, J., Yang, H. and Fogo, A.B., 2017. A perspective on chronic kidney disease progression. *American Journal of Physiology. Renal Physiology,* 312 (3), F375-F384.

Zhou, D., Li, Y., Zhou, L., Tan, R.J., Xiao, L., Liang, M., Hou, F.F. and Liu, Y., 2014. Sonic Hedgehog Is a Novel Tubule-Derived Growth Factor for Interstitial Fibroblasts after Kidney Injury. *Journal of the American Society of Nephrology,* 25 (10), 2187-2200.

Zhou, X., Zhang, W., Yao, Q., Zhang, H., Dong, G., Zhang, M., Liu, Y., Chen, J. and Dong, Z., 2017. Exosome production and its regulation of EGFR during wound healing in renal tubular cells. *American Journal of Physiology. Renal Physiology,* 312 (6), F963–F970.

Zubiri, I., Posada-Ayala, M., Benito-Martin, A., Maroto, A.S., Martin-Lorenzo, M., Cannata-Ortiz, P., de la Cuesta, F., Gonzalez-Calero, L., Barderas, M.G., Fernandez-Fernandez, B., Ortiz, A., Vivanco, F. and Alvarez-Llamas, G., 2015. Kidney tissue proteomics reveals regucalcin downregulation in response to diabetic nephropathy with reflection in urinary exosomes. *Translational Research: The Journal of Laboratory and Clinical Medicine,* 166 (5), 474–484.e4.

Zubiri, I., Posada-Ayala, M., Sanz-Maroto, A., Calvo, E., Martin-Lorenzo, M., Gonzalez-Calero, L., de la Cuesta, F., Lopez, J.A., Fernandez-Fernandez, B., Ortiz, A., Vivanco, F. and Alvarez-Llamas,

G., 2014. Diabetic nephropathy induces changes in the proteome of human urinary exosomes as revealed by label-free comparative analysis. *Journal of Proteomics,* 96, 92–102.

Zürbig, P., Mischak, H., Menne, J. and Haller, H., 2019. CKD273 Enables Efficient Prediction of Diabetic Nephropathy in Nonalbuminuric Patients. *Diabetes Care,* 42 (1), e4–e5.